AD-A031 877 BOEING COMMERCIAL AIRPLANE CO SEATTLE WASH F/G 21/5
727/JT8D JET AND FAN NOISE FLIGHT EFFECTS STUDY.(U)
AUG 76 L F MUNOZ DOT-FA71WA-2637
UNCLASSIFIED D6-44145 FAA-RD-76-110 NL

1 OF 4
AD A031877

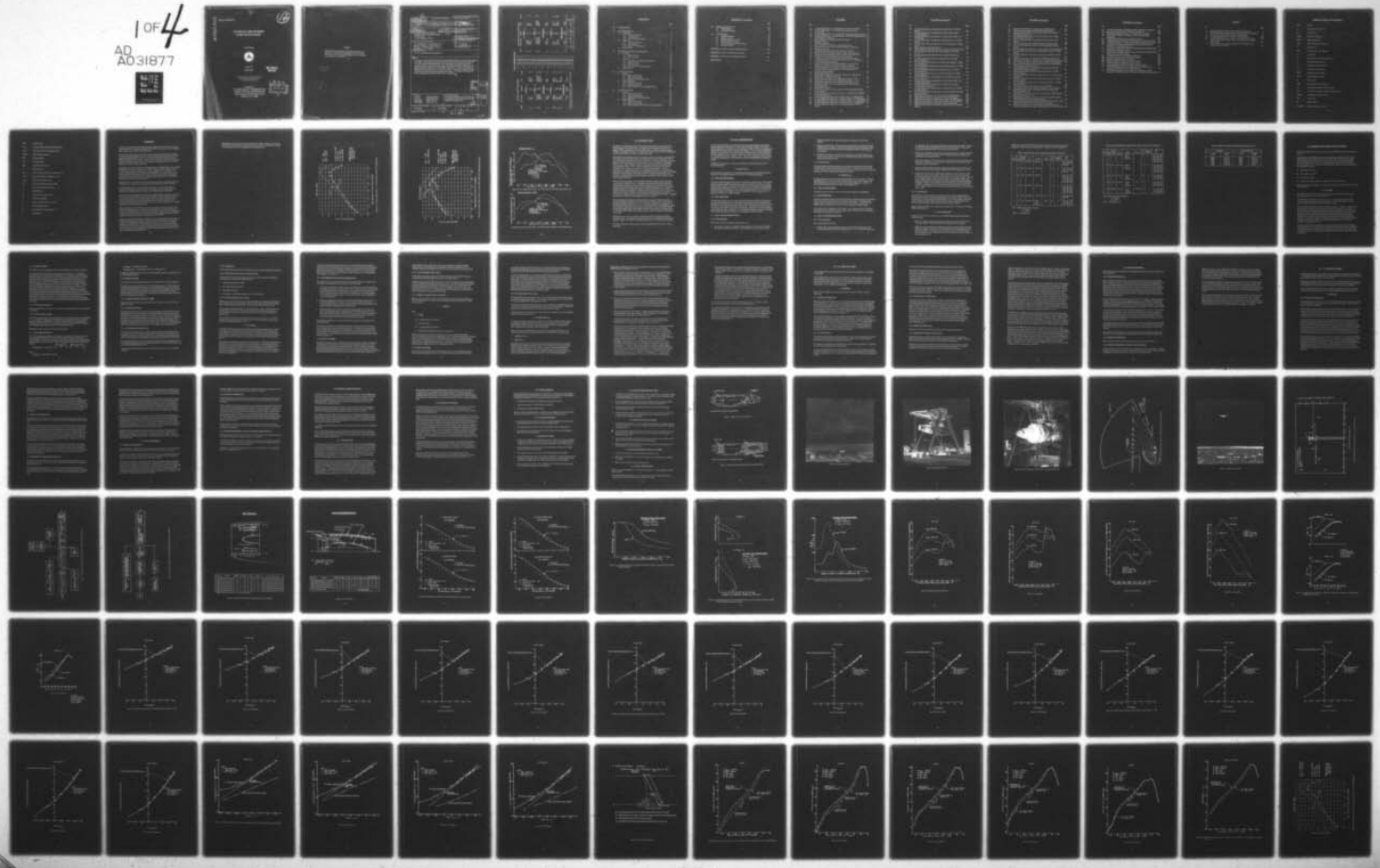

Report No. FAA-RD-76-110

12

# 727/JT8D JET AND FAN NOISE FLIGHT EFFECTS STUDY

Luis F. Munoz


August 1976

Final Report







Prepared for
U.S. DEPARTMENT OF TRANSPORTATION
FEDERAL AVIATION ADMINISTRATION
Systems Research and Development Service
Washington, D.C. 20590

## NOTICE

This document is disseminated under the sponsorship of the department of Transportation in the interest of information exchange. The United States Government assumes no liability for its contents or use thereof.

TECHNICAL REPORT STANDARD TITLE PAGE

| 1. Report No. | 2. Government Accession No. | 3. Recipient's Catalog No. |
|---|---|---|
| (18) FAA-RD-76-110 (19) | | |

**4. Title and Subtitle**
(6) 727/JT8D JET AND FAN NOISE FLIGHT EFFECTS STUDY,

**5. Report Date**
(11) AUG [redacted]76

**6. Performing Organization Code**

**7. Author(s)**
(10) Luis F. Munoz

(12) 295 p.

**8. Performing Organization Report No.**
(14) D6-44145

**9. Performing Organization Name and Address**
Boeing Commercial Airplane Company
P. O. Box 3707
Seattle, Washington 98124

**10. Work Unit No.**

**11. Contract or Grant No.**
(15) DOT-FA71WA-2637 Mod 12

**12. Sponsoring Agency Name and Address**
U.S. Department of Transportation
Federal Aviation Administration
Research and Development Service
Washington, D.C. 20590

**13. Type of Report and Period Covered**
(9) Final Report.

**14. Sponsoring Agency Code**

**15. Supplementary Notes**
H. C. True, DOT/FAA Technical Monitor

**16. Abstract**

A study was conducted to define specific ground-to-flight effects on the noise of a low-bypass-ratio engine. The analysis was based on acoustic data recorded during the FAA-sponsored 727 Noise Retrofit Feasibility Program. Two configurations, a baseline and an ejector suppressor nacelle, were included in the study. Noise flight effects were obtained by comparing JT8D ground static and 727/JT8D flight acoustic data. Procedures are defined for normalizing static and flight data to common conditions. The analysis considered both jet and fan noise characteristics for five engine power settings. The results of this study will provide a guideline for establishing flight effects technology.



**17. Key Words**
Jet noise
Fan noise
Flight effects
JT8D engine
Ejector suppressor
Installation effects
Flight noise data
Static noise data

**18. Distribution Statement**
Document is available to the public through the National Technical Information Service, Springfield, Virginia 22151.

| 19. Security Classif. (of this report) | 20. Security Classif. (of this page) | 21. No. of Pages | 22. Price |
|---|---|---|---|
| Unclassified | Unclassified | 296 | |

Form DOT F 1700.7 (8-69)



390 145

mt

# METRIC CONVERSION FACTORS

## Approximate Conversions to Metric Measures

| Symbol | When You Know | Multiply by | To Find | Symbol |
|---|---|---|---|---|
| | | **LENGTH** | | |
| in | inches | *2.5 | centimeters | cm |
| ft | feet | 30 | centimeters | cm |
| yd | yards | 0.9 | meters | m |
| mi | miles | 1.6 | kilometers | km |
| | | **AREA** | | |
| $in^2$ | square inches | 6.5 | square centimeters | $cm^2$ |
| $ft^2$ | square feet | 0.09 | square meters | $m^2$ |
| $yd^2$ | square yards | 0.8 | square meters | $m^2$ |
| $mi^2$ | square miles | 2.6 | square kilometers | $km^2$ |
| | acres | 0.4 | hectares | ha |
| | | **MASS (weight)** | | |
| oz | ounces | 28 | grams | g |
| lb | pounds | 0.45 | kilograms | kg |
| | short tons (2000 lb) | 0.9 | tonnes | t |
| | | **VOLUME** | | |
| tsp | teaspoons | 5 | milliliters | ml |
| Tbsp | tablespoons | 15 | milliliters | ml |
| fl oz | fluid ounces | 30 | milliliters | ml |
| c | cups | 0.24 | liters | l |
| pt | pints | 0.47 | liters | l |
| qt | quarts | 0.95 | liters | l |
| gal | gallons | 3.8 | liters | l |
| $ft^3$ | cubic feet | 0.03 | cubic meters | $m^3$ |
| $yd^3$ | cubic yards | 0.76 | cubic meters | $m^3$ |
| | | **TEMPERATURE (exact)** | | |
| °F | Fahrenheit temperature | 5/9 (after subtracting 32) | Celsius temperature | °C |

*1 in = 2.54 (exactly). For other exact conversions and more detailed tables, see NBS Misc. Publ. 286, Units of Weights and Measures, Price $2.25, SD Catalog No. C13.10:286.


## Approximate Conversions from Metric Measures

| Symbol | When You Know | Multiply by | To Find | Symbol |
|---|---|---|---|---|
| | | **LENGTH** | | |
| mm | millimeters | 0.04 | inches | in |
| cm | centimeters | 0.4 | inches | in |
| m | meters | 3.3 | feet | ft |
| m | meters | 1.1 | yards | yd |
| km | kilometers | 0.6 | miles | mi |
| | | **AREA** | | |
| $cm^2$ | square centimeters | 0.16 | square inches | $in^2$ |
| $m^2$ | square meters | 1.2 | square yards | $yd^2$ |
| $km^2$ | square kilometers | 0.4 | square miles | $mi^2$ |
| ha | hectares (10,000 $m^2$) | 2.5 | acres | |
| | | **MASS (weight)** | | |
| g | grams | 0.035 | ounces | oz |
| kg | kilograms | 2.2 | pounds | lb |
| t | tonnes (1000 kg) | 1.1 | short tons | |
| | | **VOLUME** | | |
| ml | milliliters | 0.03 | fluid ounces | fl oz |
| l | liters | 2.1 | pints | pt |
| l | liters | 1.06 | quarts | qt |
| l | liters | 0.26 | gallons | gal |
| $m^3$ | cubic meters | 35 | cubic feet | $ft^3$ |
| $m^3$ | cubic meters | 1.3 | cubic yards | $yd^3$ |
| | | **TEMPERATURE (exact)** | | |
| °C | Celsius temperature | 9/5 (then add 32) | Fahrenheit temperature | °F |

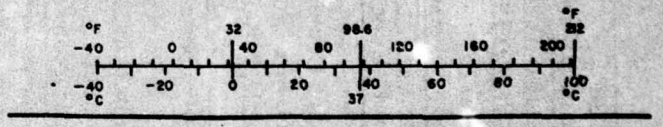

# CONTENTS

## CONTENTS (Concluded)

# FIGURES

## FIGURES (Continued)

## FIGURES (Continued)

## FIGURES (Concluded)

# TABLES

# ABBREVIATIONS AND SYMBOLS

| | |
|---|---|
| amb | ambient |
| $a_o$ | ambient speed of sound, ft/s |
| $D_j$ | jet diameter, ft |
| $D_{jPRI}$ | primary jet diameter, ft |
| DMT | digital magnetic tape |
| EPR | engine pressure ratio, $P_{T7}/P_{T2}$ |
| f | frequency, Hz |
| FAA | Federal Aviation Administration |
| $F_n$ | net thrust, lb |
| $f_o$ | static frequency (no Doppler effect), Hz |
| $F_1$ | first-stage fundamental tone |
| $F_2$ | second-stage fundamental tone |
| $2F_1$ | first-stage second harmonic |
| HGW | airplane heavy gross weight |
| LGW | airplane light gross weight |
| M | Mach number |
| NPR | nozzle pressure ratio, $P_{T7}/P_{amb}$ |
| N1 | low-pressure compressor rotor speed, rpm |
| N1C | corrected low-pressure compressor rotor speed, rpm |
| OASPL | overall sound pressure level, dB |
| O.B. | octave band |
| P | pressure, $lb/in^2$ |
| $P_{amb}$, $P_\infty$ | ambient static pressure, $lb/in^2$ |

| | |
|---|---|
| PRI | primary nozzle |
| $P_{T7}$ | primary exhaust nozzle total pressure, $lb/in^2$ |
| $P_{TF7}$ | fan exhaust nozzle total pressure, $lb/in^2$ |
| P&WA | Pratt & Whitney Aircraft |
| RH | relative humidity |
| SN | Strouhal number |
| SPL | sound pressure level, dB |
| T | temperature, °R |
| $T_{T7}$ | primary exhaust nozzle total temperature, °R |
| $T_{TF7}$ | fan exhaust nozzle total temperature, °R |
| $V_{A/P}$ | airplane true airspeed, ft/sec |
| $V_E$ | velocity of entrained ejector air, ft/sec |
| $V_j$ | ideal expanded jet velocity, ft/sec |
| X | axial distance, ft |
| $X_s$ | jet noise source axial location, ft |
| $\Gamma$ | acoustic angle, degrees |
| $\delta$ | altitude pressure ratio, $P/14.7\ lb/in^2$ |
| $\theta$ | directivity angle, degrees |
| $\theta_t$ | total temperature ratio, T/518.7 °R |
| $\lambda$ | wavelength, ft |

# SUMMARY

A study was conducted to define specific ground-to-flight effects on the jet and fan noise characteristics of a low-bypass-ratio engine for various power settings and for two configurations, a baseline and an ejector suppressor nacelle.

The experimental data selected as the basis of the study were the acoustic data recorded in a series of ground and flight noise tests conducted during the FAA-sponsored 727 Noise Retrofit Feasibility Program (1972). The low-bypass-ratio engine used was the P&WA JT8D that powered the 727 airplanes. The baseline configuration consisted of a production inlet and a production tailpipe. The ejector suppressor configuration consisted of a two-ring inlet and a 20-lobe ejector suppressor.

Noise flight effects were obtained by comparing the static and flight acoustic data, previously normalized to the following conditions: (1) 400-ft altitude, (2) three-engine noise levels, (3) 0° engine pitch angle, and (4) standard weather conditions (77°F, 70% RH). The measured flight noise data used were the data corresponding to the 400-ft target altitude flyovers and therefore required small corrections. The static noise data were measured at 100 ft or less and were extrapolated to 400-ft sideline, taking into account the spatial distribution of the jet and fan noise sources.

Noise flight effects are defined as the differences between the static and flight noise levels generated by the engines operating on the ground and in flight at the same conditions.

Jet noise flight effects are presented in plots of constant 1/3-octave-band frequency, where static and flight jet noise directivities are compared. Fan noise flight effects are shown for tones and broadband noise using 37.5-Hz bandwidth narrowband data.

Substantial reduction of baseline overall jet noise in flight is observed at angles closer to the jet axis. This reduction progressively decreases toward the forward angles where little or no reduction exists (fig. S-1). At a given flight velocity, the amount of peak jet noise reduction is dependent on power setting, which indicates a relative velocity effect. At forward angles, the baseline jet noise flight effects are a function of frequency, with a slight amplification observed at high frequencies.

Ejector suppressor jet noise flight effects at the same flight velocities show similar trends to that of the baseline (fig. S-2). Peak noise reductions, however, are lower than those observed for the baseline and vary little with power setting. Ejector suppressor flight effects are also a function of frequency at forward angles, but the amplification observed at high frequencies is larger, with crossover occurring between 70° and 90°.

Fan noise tone levels for the baseline configuration show substantial reduction at all power settings. The first-stage fan fundamental tone is reduced 10 to 20 dB at forward angles because of both flight effects and wing shielding (fig. S-3). This reduction is generally independent of power setting. The first-stage fan second harmonic shows an even larger reduction in level. The second-stage fan fundamental tone shows the least reduction of the three tones studied. Ejector suppressor tone levels, although observed in the static data, were not discernible in the flight spectra.

Broadband fan noise levels are reduced in flight for the baseline configurations (fig. S-4). The reduction is dependent on broadband frequency but not on power setting. A similar trend is observed for the ejector suppressor fan broadband noise.

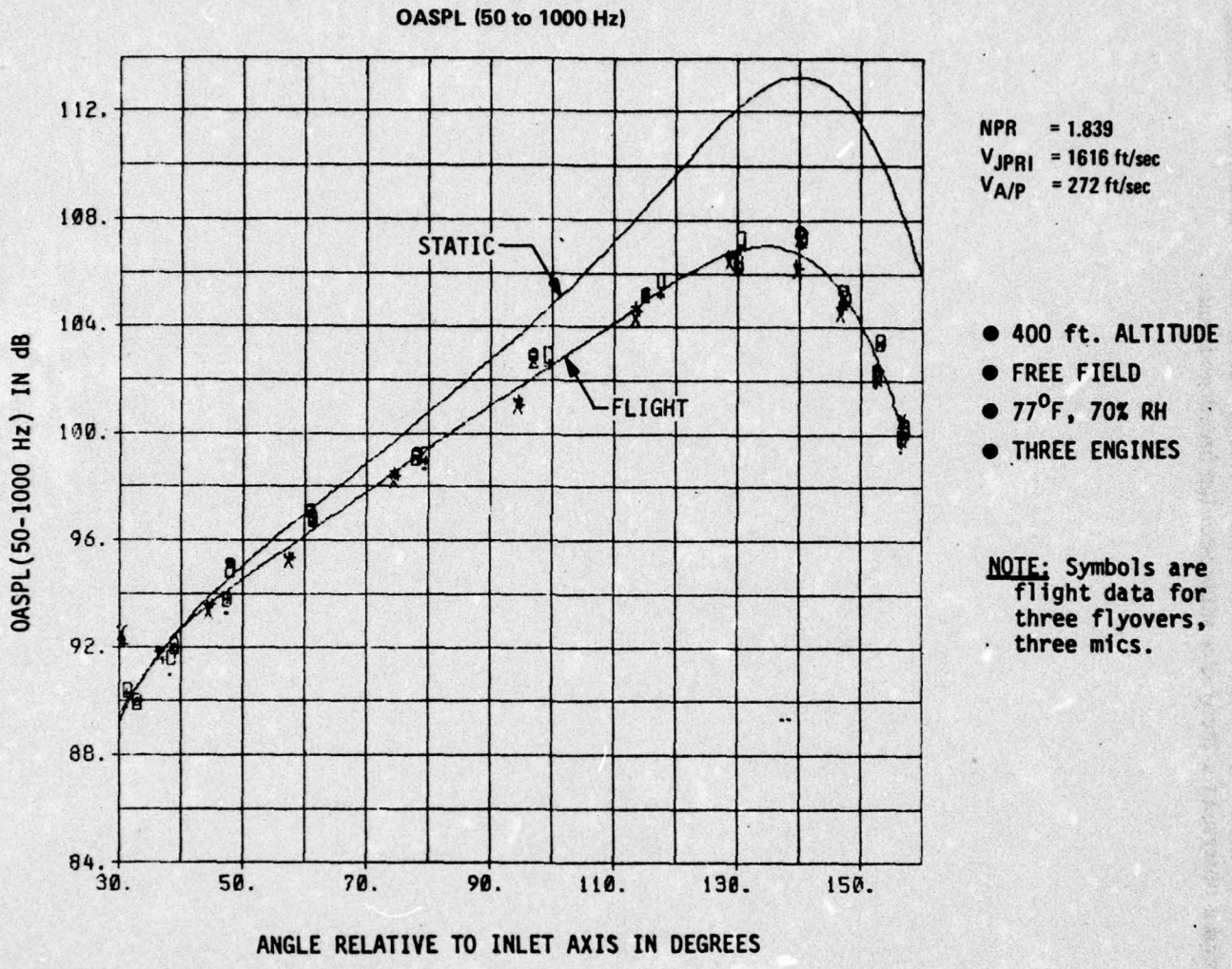


*Figure S-1.—Jet Noise Flight Effects at Cutback Power (HGW) 727/JT8D Baseline*

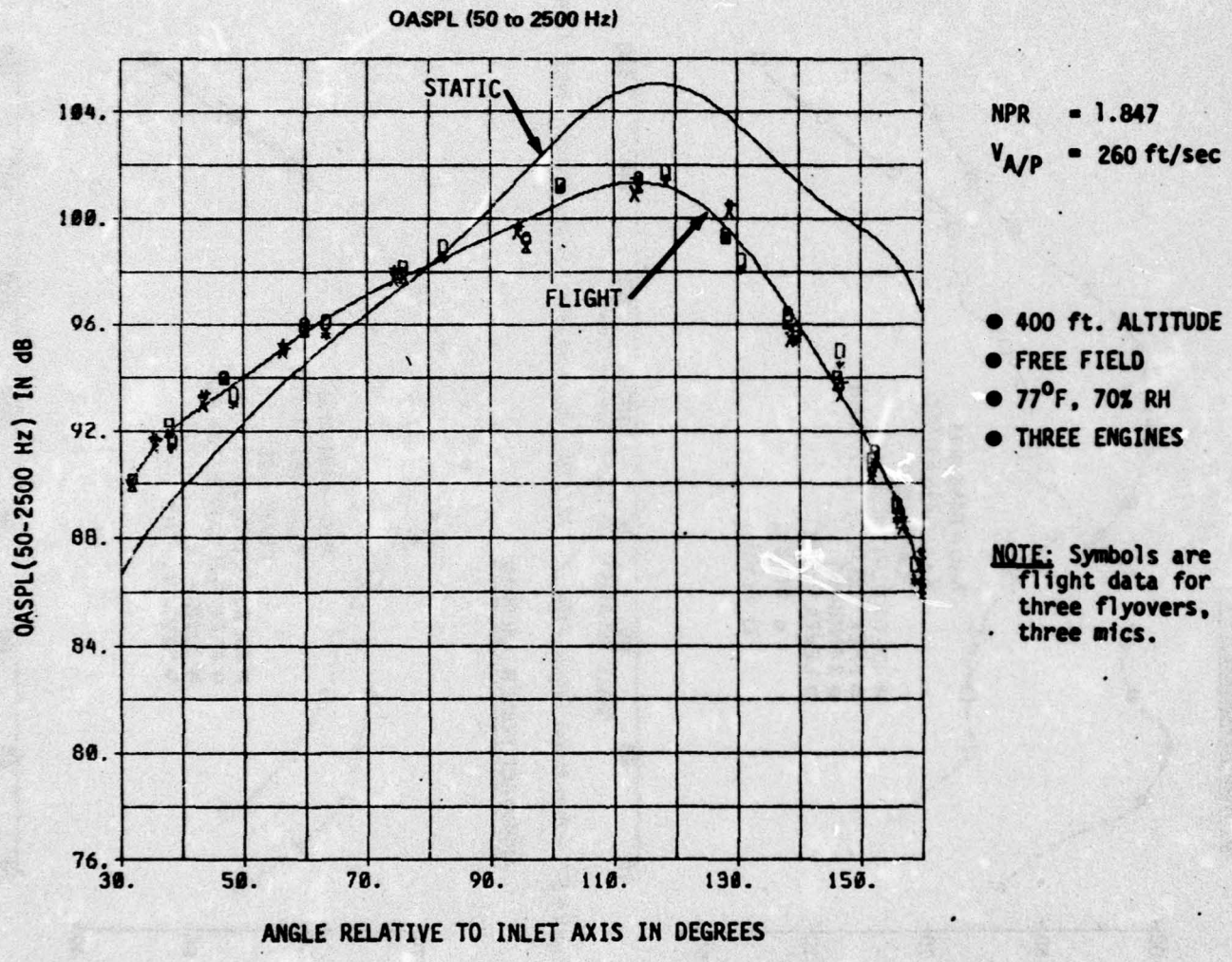


*Figure S-2.—Jet Noise Flight Effects at Cutback Power (HGW) 727/JT8D Ejector Suppressor*

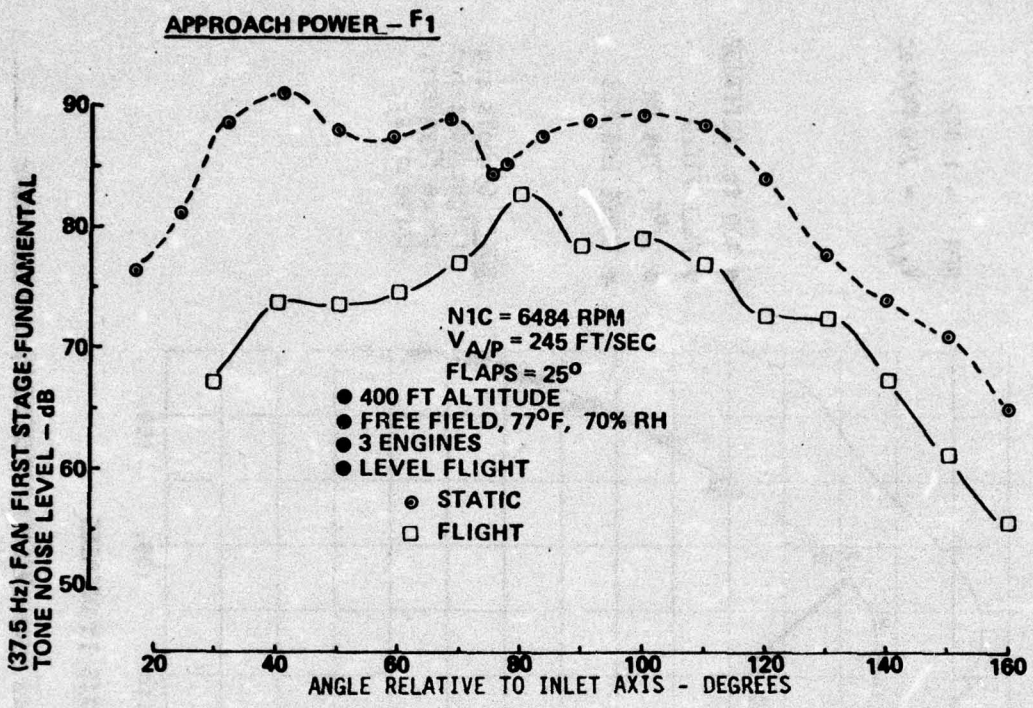


*Figure S-3.—Fan Noise Flight Effects, 727/JT8D Baseline, First-Stage Fundamental Tone*

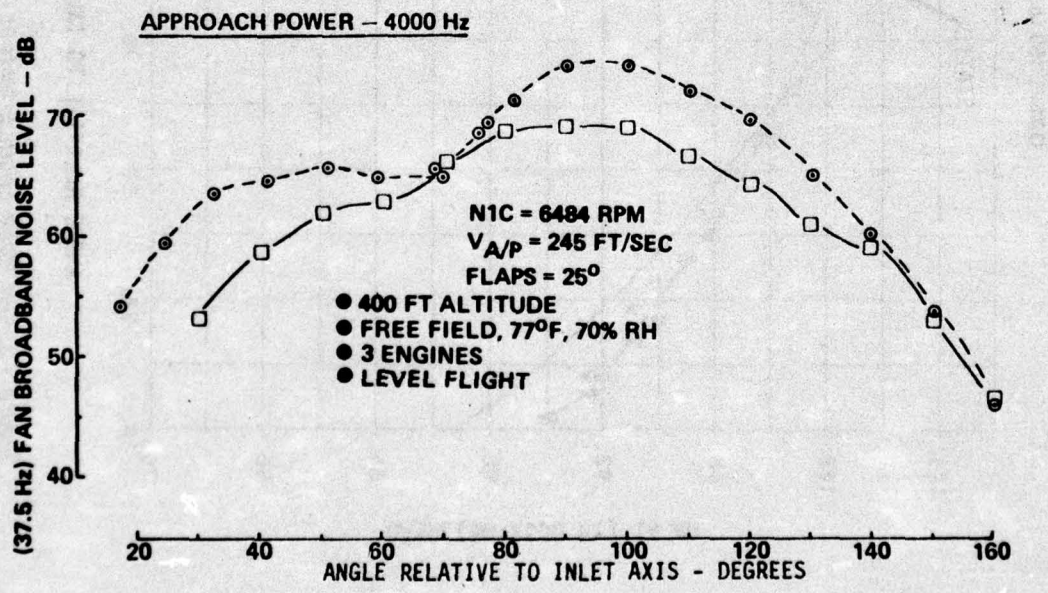


*Figure S-4.—Fan Noise Flight Effects, 727/JT8D Baseline, 4000-Hz Fan Broadband Noise*

# 1.0 INTRODUCTION

Development of efficient jet and fan noise suppression systems requires a detailed understanding of engine noise flight effects. Conclusions based on static tests of models or engines, without consideration of ground-to-flight effects, may result in improper design decisions. Consequently, there is a Government and industry-wide interest in understanding and defining the influence of flight on aircraft engine noise.

Noise flight effects technology is still in its preliminary stage. The industry lacks theoretical and empirical procedures to determine these effects with confidence. One reason is that they are not easily discernible. The most direct method to obtain flight effects is to compare flight and static noise data that had been corrected to the same conditions. This method, however, is very costly. Therefore, industry is searching for alternative techniques that could simulate noise flight effects. These techniques, such as wind-tunnel testing, free jet testing, rotary devices, ground vehicles, etc., have several advantages. They have lower costs, easy configuration changes, use of nonairworthy systems, and controlled and repeatable test conditions. However, the results given by these simulations must be comparable with those obtained in flight. This implies a need for a full-scale static and flight noise data base for unsuppressed and suppressed engine configurations that can be used to verify these simulation techniques.

Under the FAA sponsorship (727 Noise Retrofit Feasibility Program), ground and flight noise tests were conducted in 1972. The high-quality acoustic data recorded represent a unique body of information ideal for the study of flight effects. With this idea in mind, selected data were analyzed to compare static and flight noise measurements. Some of the problems existing in the comparison of static and flight measurement, such as presence of ground reflections, atmospheric conditions and distances, data scatter, etc., were already minimized in the test by using ground microphones, low flight altitudes, and repeated test conditions. Airplane spatial location and altitude were also precisely recorded. Additional problems were overcome by using appropriate analysis techniques.

The data acquisition techniques and instrumentation systems are reviewed in section 2. The general analysis method used to correct the static and flight jet and fan noise data to the same conditions is described in section 3. The static and flight noise comparisons are presented in sections 4 and 5 for the jet and fan noise, respectively. Comparisons are shown for two-engine configurations (unsuppressed and suppressed), at power settings covering the engine operational range. Noise installation effects characteristic of the airplane used for the flight test (727-100) are discussed in section 6. Section 7 presents the conclusions of this study.

Finally, three appendixes are included. Appendix A contains the engine and airplane performance data. Appendix B describes the methods used to determine the noise source locations. Appendix C describes the statistical characteristics of the jet and fan noise data.

The author would like to acknowledge the assistance provided by Dr. K. Chun in the fan noise study.

# 2.0 DATA DESCRIPTION

The data used in this study were taken from a series of ground and flight noise tests conducted under the FAA-sponsored 727 Noise Retrofit Feasibility Program. Two JT8D engine configurations, a baseline and a quiet nacelle, were tested. The baseline configuration consisted of a production inlet and a production tailpipe. The quiet nacelle configuration consisted of a two-ring inlet and a 20-lobe ejector suppressor nozzle. Detailed descriptions of these configurations can be found in references 1, 2, and 3. Schematic drawings of the two configurations are shown in figures 1 and 2. The second configuration will be referred to as the ejector suppressor to avoid confusion with other configurations also called quiet nacelles.

A description of the static and flight test sites and test operations is presented in the following paragraphs.

## 2.1 STATIC DATA

The static data were acquired at the Boeing Boardman (Oregon) test facility during Phase I (winter 1971) and Phase II (summer 1972) of the 727 Noise Retrofit Program.

### 2.1.1 TEST SITE DESCRIPTION

The test site terrain was relatively flat and free of reflecting surfaces (fig. 3). Test runs were made on an acoustic engine test stand which supported the engine 13 ft above the surface of pad B-2 (figs. 4 and 5). This stand was equipped with a thrust balance and all necessary instrumentation for propulsion analysis. The concrete surface of pad B-2 extended 225 ft radially from the test stand location and covered the angular range from 70° to 150° from the engine centerline. In addition, the forward quadrant was covered by concrete to a distance of 70 ft from the engine centerline.

### 2.1.2 TEST OPERATION

Test procedures were used to ensure that all required data were recorded and that all data accuracies were satisfied. Prior to engine start, each microphone system was calibrated. The engine was operated 3 minutes on-condition to allow propulsion parameters to stabilize. Acoustic as well as propulsion data were then recorded. The engine operating condition was changed and a similar test procedure was followed. Postcalibration of each microphone system, identical to the precalibration, was accomplished following completion of an engine run. Weather data during each engine operating condition were also recorded.

### 2.1.3 DATA AND INSTRUMENTATION

#### 2.1.3.1 Data Acquisition

Three types of data were obtained during the static tests:

1. Acoustic data: Nineteen ½-in. B&K 4134 microphones, located as shown in figure 6, were used to record the acoustic data. The microphones were positioned with the

diaphragm parallel to the concrete surface and at a distance ½-in. above this surface.

2. Engine performance data: The engine was fully instrumented to record the required propulsion data. In addition, during ejector suppressor runs, static pressures on plug and shroud surfaces and total pressure and temperature profiles at the shroud exit were obtained.

3. Weather data: Windspeed, wind direction, temperature, and relative humidity were recorded on strip charts. These data were monitored continuously to ensure weather conditions inside FAR 36 limits.

#### 2.1.3.2 Data Reduction

The analog magnetic tapes containing the raw acoustic data were spectral analyzed using a General Radio 1/3-octave-band analyzer (model 1921). An integration time of 32 sec was used. For the study of fan noise, the raw acoustic data were also reduced to narrowband spectra using a Nicolet Scientific Model 400A FFT analyzer.

## 2.2 FLIGHT DATA

The flight noise data were obtained during Phase III (Sept. 1972) of the FAA 727 Retrofit Feasibility Program. Tests were conducted with a Boeing-owned 727-100 airplane. The three-engined airplane was powered by two JT8D-9 engines (engines No. 1 and No. 2) and one JT8D-15 engine operated at JT8D-9 ratings (engine No. 3).

### 2.2.1 TEST SITE DESCRIPTION

The flight tests were conducted at Grant County Airport, Moses Lake, Washington.

### 2.2.2 TEST OPERATION

Level flyover tests were conducted to provide generalized noise-thrust-altitude characteristics of the 727-100 with baseline and ejector suppressor engines (fig. 7). The airplane flew straight and level along the runway over the range shown in figure 8, at 400-, 850-, and 1400-ft altitudes. Engine thrust levels were from low approach to takeoff ratings.

The external aircraft configuration was established by the drag requirements to maintain proper airspeed at the required thrust and altitude. Each condition was run a minimum of three times to obtain reliable noise levels.

### 2.2.3 DATA AND INSTRUMENTATION

#### 2.2.3.1 Data Acquisition

Four types of data were recorded:

1. Acoustic data: Twelve microphones were used to record the acoustic data, three of which were ground microphones designated as K1, L1, M1. The microphones were

1-in. B&K 4145 type. The three microphones were positioned horizontally 1 ft apart, on a flat metal plate that was placed on the paved runway extension. The location of the ground microphones at the test site can be seen in figure 8.

2. Weather data: Windspeed, wind direction, ambient temperature, and relative humidity were measured at 10 m above ground level. In addition, the relative humidity was recorded at 1.2 m above the ground.

   Upper air measurements were obtained from weather balloons launched hourly during test periods. Temperature, relative humidity, windspeed, and wind direction were obtained from these measurements.

3. Engine and airplane performance data: Engine and airplane performance data were obtained with a pulse code modulation (PCM) System, which sampled every 0.4 sec.

4. Airplane-space position data: Airplane-space position data were obtained by using an onboard camera system (APACS). This system uses a 35-mm camera mounted in a downward-looking position in the lower surface of the airplane fuselage. Surveyed pairs of targets arranged in parallel lines were used to obtain airplane altitude and position along all three axes by means of perspective geometry and photogrammetric techniques. Time and frame pulsing was provided by the data system code generator. In addition, airplane pitch, roll, and yaw were recorded by gyroscope sensors every 0.2 sec. Airplane distance above the ground was measured directly by a radio altimeter every 0.2 sec.

#### 2.2.3.2 Data Reduction

The analog tapes containing the flyover acoustic data were analyzed using the Boeing flyover digital acoustic noise analysis (DIANA) system. This system consists of an analog tape recorder, 1/3-octave-band General Radio Model 1921 real-time analyzer with twenty-four 1/3-octave-band filters, digital computer, teletype machine, digital magnetic tape recorder, time-code reader, and associated control and interface circuitry.

Engine, airplane performance, and airplane-space position data were reduced by the Boeing Flight Test Organization.

## 2.3 DATA SELECTION

Selection of the data used in the jet and fan noise flight effects study was based on the following criteria:

1. Static test: data from baseline and ejector suppressor runs with and without inlet or exhaust mufflers.—Those runs with mixed configurations were excluded.

2. Flight test: data corresponding to the lowest test altitude and recorded by the three ground microphones.—Experience shows that flight noise data scatter increases with flyover test altitude. Thus, data from runs at lowest test altitude (400 ft) provide the best overall accuracy. Reflection-free ground microphone data are best suited for jet noise study (ref. 4).

Tables 1 and 2 show the static Boardman baseline and ejector suppressor selected runs, respectively. Table 3 shows the selected flyover conditions for both configurations.

*Table 1.—Static Boardman Data—Selected Runs, Baseline Configuration*

| Phase | Run | Config-uration | Inlet | Tailpipe | Muffler | BG (a) | Number of conditions | NPR (b) |
|---|---|---|---|---|---|---|---|---|
| I | 4 | 501 | Production | Production | | 2 | 8 | 1.32, 1.39, 1.50, 1.61, 1.69, 1.81, 1.90, 2.01 |
| I | 15 | 501 | Production | Production | | 2 | 8 | 1.30, 1.40, 1.50, 1.60, 1.70, 1.80, 1.90, 2.01 |
| II | 24 | 501 | Production | Production | | 2 | 15 | 1.09, 1.18, 1.29, 1.39, 1.48, 1.59, 1.63, 1.69, 1.73, 1.78, 1.84, 1.89, 1.93, 1.98, 2.02 |
| II | 70 | 501 | Production | Production | | 2 | 15 | 1.1, 1.20, 1.30, 1.39, 1.49, 1.59, 1.65, 1.69, 1.74, 1.79, 1.84, 1.89, 1.96, 1.99, 2.03 |
| I | 16 | 502 | Production | Production | Inlet | 2 | 5 | 1.30, 1.38, 1.49, 1.59, 1.69 |
| II | 67 | 619 | Production | 20-lobe ejector suppressor | Exhaust | 19 | 9 | 1.14, 1.30, 1.40, 1.49, 1.60, 1.70, 1.80, 1.89, 2.03 |

[a]BG = P&WA acoustic treatment designation
- 2 untreated
- 19 treated

[b]NPR = Nozzle pressure ratio

*Table 2.—Static Boardman Data—Selected Runs, Ejector Suppressor Configuration*

| Phase | Run | Config-uration | Inlet | Tailpipe | Muffler | BG (a) | Number of conditions | NPR (b) |
|---|---|---|---|---|---|---|---|---|
| II | 49 | 611 | Two-ring | 20-lobe ejector suppressor | | 19 | 15 | 1.10, 1.20, 1.30, 1.40, 1.50, 1.59, 1.64, 1.69, 1.74, 1.80, 1.83, 1.90, 1.94, 2.00, 2.02 |
| II | 63 | 611 | Two-ring | 20-lobe ejector suppressor | | 19 | 15 | 1.10, 1.19, 1.30, 1.39, 1.49, 1.60, 1.65, 1.69, 1.75, 1.78, 1.84, 1.89, 1.93, 1.99, 2.02 |
| II | 68 | 611 | Two-ring | 20-lobe ejector suppressor | | 19 | 9 | 1.14, 1.30, 1.40, 1.51, 1.60, 1.69, 1.79, 1.90, 2.03 |
| II | 56 | 614 | Two-ring | 20-lobe ejector suppressor | Inlet | 19 | 9 | 1.14, 1.30, 1.40 1.50, 1.60, 1.70, 1.79, 1.90, 1.98 |
| II | 66 | 618 | Two-ring | 20-lobe ejector suppressor | Exhaust | 19 | 9 | 1.14, 1.30, 1.40 1.50, 1.60, 1.69, 1.79, 1.88, 2.03 |

[a]BG = P&WA acoustic treatment designation
- 2 untreated
- 19 treated

[b]NPR = Nozzle pressure ratio

*Table 3.—Phase III 727 Noise Test, 400-ft Altitude, Selected Runs*

| (a) Baseline | | (b) Ejector Suppressor | |
|---|---|---|---|
| $F_n$, target, lb | Condition number | $F_n$, target, lb | Condition number |
| 12 000 | 19, 20, 21 | 12 000 | 19, 20.1, 21 |
| 10 000 | 28, 29, 30 | 10 000 | 28, 29, 30 |
| 8 000 | 43, 44, 45 | 8 000 | 43, 44, 45 |
| 6 000 | 55, 56, 57.1 | 6 000 | 55, 56, 57 |
| 4 000 | 64, 65, 66 | 4 000 | 65, 66 |

# 3.0 METHOD FOR FLIGHT EFFECTS STUDY

The analysis sequence used in the study of jet and fan noise flight effects is described in this section.

In order to study noise flight effects from experimental data, comparison of two sets of data (static noise data and flight noise data) is required. Both sets of data were obtained under different test setups; therefore, the data must be reduced to the same conditions before the comparison can be made. This implies that the corrections must be applied to one or both sets of data. In the study reported herein, both sets of data were normalized to the following conditions:

- 400-ft altitude (sideline)
- Three-engine noise levels
- $0^{\circ}$ engine pitch angle
- Standard atmospheric conditions, FAR Part 36 ($77^{\circ}$F and 70% RH)

Selection of the above conditions was based on the criterion of causing a minimum correction to the flight data.

## 3.1 JET NOISE

The present study is based on a JT8D engine which is a low-bypass-ratio turbofan with a fan-to-primary velocity ratio ranging from 0.6 to 0.7.

The JT8D engine, configured as a baseline (fig. 1), is characterized by high primary jet velocities, which are responsible for its high jet noise level. Baseline JT8D jet noise has been found to correlate with the primary jet velocity, $V_{jPRI}$.

When the JT8D is equipped with an ejector suppressor (fig. 2), the primary and fan airflows are mixed inside the shroud with entrained ambient air. This results in lower exit jet velocities. Two jet noise generation regions are clearly distinguishable. One region, inside the ejector shroud, is characterized by high jet velocities and small jet length scales. The high-frequency noise produced in this region is referred to as premerged jet noise and correlates with the relative velocity between the primary airflow and the entrained air ($V_{jPRI} - V_E$). The other region, downstream of the shroud exit, is characterized by lower jet velocities and larger jet length scales producing low-frequency noise. This noise is referred to as postmerged jet noise.

Jet noise is generated by the mixing process of the turbulent jet with the surrounding air. Consequently, jet noise sources are spatially distributed in the turbulent efflux. Near-field jet noise is affected by the distribution of the noise sources. Therefore, knowledge of the noise source locations is necessary when extrapolation of the near-field data to the far-field is performed.

### 3.1.1 STATIC JET NOISE

The baseline and ejector suppressor static jet noise analysis network is shown in figure 9.

Acoustic data were first corrected to standard weather conditions (77°F, 70% RH) by using the actual test weather data and the ARP 866 (ref. 5) absorption coefficient curves. Engine performance parameters were obtained from the measured engine data. Jet noise data were plotted versus engine performance correlating parameter, and fourth-order regression curves were fitted to the data points. The nondimensional ideal primary jet velocity ($V_{jPRI}/a_o$) was used as the baseline engine performance correlating parameter while the nondimensional ideal primary relative velocity at lobe exit ($(V_{jPRI} - V_E)/a_o$) was used as the ejector suppressor performance correlating parameter. A study was performed to identify at which power settings the spectra were affected by core noise. The average static jet noise, corresponding to the flight power settings, was determined by using the static-flight jet noise engine performance matching parameter and the fourth-order regression curves. Extrapolation to 400-ft sideline was done, assuming jet noise sources as point sources distributed along the jet axis, downstream of the nozzle exit. The extrapolated noise levels (one engine) were corrected to the noise levels of three engines. Corrections to free-field values were done by subtracting 6 dB from the ground microphone noise levels.

#### 3.1.1.1 Static Engine Performance

Static engine performance parameters, used in the jet noise flight effects study, are included in appendix A.

#### 3.1.1.2 Jet Noise Source Locations

Noise source locations, used in the extrapolation of the static jet noise data, were determined for: (1) the baseline configuration, by using the Boeing Lu/Berman flow/noise analytical computer program; and (2) the ejector suppressor configuration, by using noise source location experimental data, from an ejector suppressor nozzle scale model (1/5), obtained in the Boeing Anechoic chamber using a multiple sideline technique.

Descriptions of these methods are presented in appendix B.

#### 3.1.1.3 Three-Engine Noise Levels

The 727-100 airplane is powered by three engines; two mounted on pods on the aft sides of the fuselage and the third, with an S-duct inlet, mounted in the aft center of the airplane fuselage. In order to obtain absolute noise levels comparable with the total airplane noise, correction of the static jet noise data to three engines was done using the following formula:

$$SPL_{3ENG}(\theta,f) = 10 \log \left[ 2 \times 10^{\left(\frac{SPL_{1ENG}(\theta,f)}{10}\right)} + 10^{\left(\frac{SPL_{ENG\ 2}(\theta,f)}{10}\right)} \right]$$

where

$SPL_{3ENG}$ = three-engine noise levels

$SPL_{1ENG}$ = one-engine noise level

$SPL_{ENG\ 2}(\theta, f)$ = center engine noise level = $SPL_{1ENG}(\theta', f)$

The different directivity angle, $\theta'$, is due to the center engine nozzle exit being located 196 in. behind the pod engines.

### 3.1.2 FLIGHT JET NOISE

The baseline and ejector suppressor flight jet noise analysis network is shown in figure 10.

The analog tapes were processed with a 1921 General Radio analyzer. The Boeing flyover noise analysis computer program was used to correct the flight noise data to the selected conditions. Statistical noise data averages were obtained by fitting eighth-order regression curves to noise data from three repeat flyovers and three microphones plotted versus directivity angle. Free-field noise values were obtained by subtracting 6 dB from the flight jet noise levels (ground microphones).

#### 3.1.2.1 Airplane and Engine Performance in Flight

Appendix A includes airplane and engine performance in-flight data used in the jet noise flight effects study.

#### 3.1.2.2 Airplane-Space Position

The imaginary intersection between the body station (BS) and waterline (WL) of the pod engines nozzle exit centers was defined as the airplane engines' position reference point. The relative position between the noise sources (engines) and the observers (microphones) was defined by the following parameters: (1) altitude of reference point, (2) overhead time of reference point, (3) airplane sideline deviation, and (4) airplane groundspeed. These parameters were obtained from the onboard camera system (APACS). The altitude and overhead time given by the camera, however, were referred to the airplane APACS reference point. Thus, these values were first corrected to the engines' position reference point.

#### 3.1.2.3 Data Reduction Integration Time

A conflicting situation is found in the flight noise data analysis. Long integration times are required to reduce the statistical uncertainties due to the random fluctuations of the noise signal. However, as a result of airplane motion, difficulties in correlating noise with airplane position increase as the integration time increases, thus giving rise to a bias error.

The uncertainty and bias error were minimized by selecting a 0.5-sec integration time, and by correlating the airplane noise with the airplane position at the time corresponding to the center of each integration time interval.

Appendix C presents a discussion on the uncertainty and bias error present in the flight noise data.

#### 3.1.2.4 Weather Data

Ground weather data were used in the baseline and ejector suppressor flight jet noise analysis.

#### 3.1.2.5 Boeing Flyover Noise Analysis Computer Program

The Boeing flyover noise analysis computer program was used to perform the following corrections to the "as measured" flight noise data:

1. Altitude normalization to 400 ft
2. Zero airplane sideline deviation
3. Zero engine pitch angle
4. Atmospheric conditions normalization to 77°F and 70% RH

#### 3.1.2.6 Statistical Flight Noise Data Average

Flight noise data for each of the power settings considered were averaged by fitting eighth-order regression curves to the noise data, from three repeat flyovers and three microphones (M1, L1, K1), plotted versus directivity angle at constant 1/3-octave-band frequency.

The three ground microphones (M1, L1, K1) were located 1 ft apart. Therefore, the noise signals cannot be considered statistically independent. Nevertheless, the inclusion of the three microphones' data on the average is expected to reduce the possible microphone system errors.

Of all the flight jet noise data considered 90% were observed to lie inside a ±1.7-dB band around the eighth-order regression curves; except for the low frequencies (50 Hz), where the 90% scatter band increased to ±2.5 dB

### 3.2 FAN NOISE

The baseline JT8D engine noise data show fan noise dominating the high-frequency region of the spectrum. The JT8D engine has 19 inlet guide vanes (IGV) and two fan stages of 27 and 40 blades, respectively. The ejector suppressor configuration is a modified JT8D engine with an acoustically treated inlet (two-ring), acoustically treated fan ducts, and a 20-lobe suppressor nozzle consisting of an acoustically lined centerbody and ejector shroud (fig. 11).

Some unique characteristics of fan noise to be considered are: (1) different noise generation mechanisms contribute to the total fan noise, which results in a broadband signal with a number of discrete tones superimposed; (2) noise generated by the fan propagates both forward (inlet fan noise) and rearward (aft fan noise); (3) fundamental and harmonic tone frequencies are functions of the fan rotor speed; and (4) Doppler effects, such as frequency shift and level amplification, occur to the broadband, as well as the tones, as the airplane flies over the microphones.

The first fan noise characteristic mentioned requires the identification of the different tones and associated noise generation mechanisms, as well as the broadband noise and tone relative levels. The second characteristic is important in defining the fan noise directivity pattern and, therefore, in the extrapolation of fan noise data as well. Fan noise sources were assumed to be located at the inlet plane for inlet fan noise and at the exhaust plane for aft fan noise. (See app. B.)

### 3.2.1 ONE-THIRD-OCTAVE-BAND FAN NOISE STUDY

The feasibility of using 1/3-octave-band data to obtain meaningful fan noise flight effects was studied. Several problems were identified and are listed below.

1. Fan noise subcomponents: One-third-octave-band data gives very little information on the different tones that are present in the fan noise. In the static data, for those power settings where the tones are dominating the fan noise, the 1/3-octave-band levels can be considered equal to the tone levels. In the flight data, the tone levels relative to the broadband are small, and the 1/3-octave-band levels are a clear combination of tones and broadband.

2. Split tones: Split tones are found in cases where the tone is close to one of the 1/3-octave-band limits (lower or upper). The 1/3-octave-band filters split the tone acoustic energy into the two contiguous bands resulting in noise levels associated with those bands that are meaningless for fan noise study.

3. Doppler frequency shift: Due to the Doppler frequency shift, a tone moves from one 1/3-octave-band to others, during the flyover. This shift could be as much as three bands. Since the frequency bandwidth of the 1/3-octave-bands is not constant, use of noise data from different bands requires bandwidth corrections, which can become complicated when both, tones and broadband, are present.

These problems suggest that 1/3-octave-band data are not suitable for the study of fan noise flight effects.

Narrowband data, however, has advantages which make it more suitable for the study of fan noise flight effects. Some of these advantages are: (1) different fan subcomponents, such as fundamentals and harmonics of each fan stage, can be easily identified; (2) tones and broadband can be separated readily; and (3) the narrowband spectra frequency bandwidth is constant. Thus, levels from two different bands can be compared directly, without bandwidth corrections.

### 3.2.2 FLIGHT FAN NOISE

Narrowband flight spectra were obtained by using the Nicolet FFT analyzer. Examination of baseline flight spectra, for five power settings and 14 directivity angles (30° to 160°), showed three fan tones distinctive enough for analysis. These fan tones were identified as the first-stage blade passage fundamental tone (F1), its second harmonic (2F1), and the second-stage blade passage fundamental tone (F2). Ejector suppressor flight spectra, however, showed no discernible tones through the entire range of directivity angles. Flight tones

and broadband levels were read from each spectrum, taking into account the Doppler frequency shift. The fan flight data were normalized to 400-ft level flight and 77°F, 70% RH. Correction of the flight fan noise data to free field was done by subtracting 6 dB.

### 3.2.2.1 Narrowband Flight Noise Analysis

The Boeing fast fourier transform system (Nicolet Scientific model 400A FFT analyzer) was selected for reducing the flight noise data in narrowband spectra.

Ensemble averaging of microphone M1 acoustic data for three repeat flyovers was performed in order to obtain noise data of good statistical accuracy. The effective frequency bandwidth and sample time used for the flight data narrowband analysis were 37.5 Hz and 0.27 sec, respectively (400 points and 8 averages per point). Together, the bandwidth and sample times selected produce the best compromise between the broadband noise confidence levels and the resolution of the airplane position in flight.

### 3.2.2.2 Flight Data Doppler Frequency Shift Study

Measured and calculated first-stage fundamental frequency shifts are compared in figure 12. The calculated values were obtained using the Doppler frequency shift formula for a single source in motion

$$f' = \frac{f_o}{1 - M \cos \Gamma}$$

where

$$f_o = \frac{N1 \bullet b}{60}$$

$N_1$ = average measured rotor speed

b = n° of fan blades

M = average airplane Mach number

$\Gamma$ = angle between the flight path and the acoustic path

Measured and calculated values agree relatively well, except at cutback power (HGW) and at the lowest power setting. The disagreement at these two power settings is not completely understood. Following are some factors that might have contributed to this disagreement: (1) the airplane is a multinoise source instead of a single source as reflected in the preceding equation, and (2) airplane performance, altitude, and sideline deviation probably suffered variation between repeat flyovers and even during each flyover.

## 3.2.3 STATIC FAN NOISE

Narrowband data were obtained with the Boeing FFT analyzer for two baseline static runs and two ejector suppressor static runs. Six conditions per run were reduced for corrected

rotor speed, ranging from 5500 to 8000 rpm. Fundamental first-stage, second-harmonic first-stage, and fundamental second-stage tone levels were obtained from the narrowband spectra, as well as the 2000-, 4000-, and 6000-Hz broadband noise levels.

The static narrowband data were corrected to standard weather conditions using ARP 866 curves. Corrected static fan data were plotted against corrected rotor speed for each microphone angle. Sixth-order regression curves were fitted to the data points. Static fan tones and broadband noise levels corresponding to the flight power settings (same corrected rotor speed) were determined using the regression curves. The effect of fan noise source locations (app. B) was considered for the extrapolation of the fan noise data to 400-ft sideline. The extrapolated noise levels (one engine) were corrected to airplane noise levels (three engines) by adding 4.8 dB (10 log number of engines). Correction to free field was made by subtracting 6 dB from the fan static noise data.

### 3.2.4 Narrowband Static Noise Analysis

The Boeing FFT analyzer was used to reduce the fan noise static data to narrowband spectra. An effective frequency bandwidth of 37.5 Hz and an integration time of 35 sec were selected for the analysis (400 points, 1024 averages per point).

The broadband noise 90% confidence interval, for this combination of bandwidth and integration time, is ±0.2 dB, which is well beyond the accuracy of the instrumentation. Appendix C includes a more detailed discussion on the statistical qualities of fan noise.

Agreement within 1% was found between the measured tone frequencies and those calculated using the measured rotor speed, N1.

## 3.3 FLIGHT EFFECTS

The preceding analysis method had, as its objective, correction of flight (727-100 airplane) and static (bare engine) noise data for differences in test conditions. In addition, noise level differences between the three-engine airplane (flight) and the bare engine (static) were accounted for by assuming noise intensity addition.

However, the static and flight noise data continue to show significant differences. The effects responsible for the remaining differences can be classified into two main groups:

1. Installation effects

2. Flight effects

Installation effects are due to the presence of finite boundary surfaces, such as wings and fuselage, in the propagation path of the sound waves. Therefore, these effects are present only in the flight noise data (727-100 airplane). Qualitative evaluations of installation effects are relatively simple but, because of the complexity of the various phenomena involved, quantitative results are, in general, difficult to obtain. Section 6 includes a discussion on the possible installation effects present in the 727-100 flight noise data.

Flight effects comprise those effects that are attributable to the airplane forward motion. Flight effects can be classified as follows:

1. Effects associated with the acoustics of a moving source: The relative motion between the noise source and the medium gives rise to a source intensity amplification. The magnitude of this amplification depends on the type of source, the relative Mach number, and the angular position between source and observer. Theoretical studies on the sound field from noise sources such as monopoles, dipoles, or quadrupoles in motion can be found in the literature (ref. 6, 7). These studies show that the noise intensity level of a moving source (relative to the medium) is amplified with respect to the noise intensity level of the source at rest in the forward angles and is reduced in the aft angles.

   Another phenomenon associated with the kinematics of the acoustic sources in motion is the well-known Doppler frequency shift. This Doppler change of frequency affects the noise intensity level received by the observer as explained in item 2.

2. Effects associated with the propagation of sound waves–Doppler frequency shift: Atmospheric absorption is a function of frequency. Because of the Doppler frequency shift associated with the airplane motion, atmospheric absorption values are thus different between static and flight, at the same source-observer relative position. Consequently, this creates differences between the static and flight noise intensity level received by the observer.

3. Effects associated with source alteration: Airplane motion modifies the strength of jet and fan noise sources. This alteration occurs by changing the noise generation mechanisms and by affecting the intensity of the source.

   Jet noise source intensity, for instance, depends on the mean and turbulent fluid mechanic properties of the jet flow. The presence of a freestream velocity alters these properties, thus modifying the strength of the jet noise sources.

   The freestream velocity affects the mean flow field of the jet by, for instance, stretching the potential core. The magnitude of the stretching is a function of jet diameter, temperature, pressure ratio, and freestream velocity. Figure 13 shows the primary core stretch due to a freestream velocity of 300 ft/sec. The data were obtained from a JT8D (dual-flow jet) simulation using the Boeing Lu/flow computer program (ref. 8). The turbulent properties in the jet are also affected by the presence of a freestream velocity. Using the data provided by the dual-flow jet simulation, the radial distribution, at two streamwise stations, of the normalized streamwise turbulent intensity $\sqrt{u^2}/V_{jPRI}$, is shown in figure 14 for the flight and static cases. At $X/D_j = 5$, the figure shows the turbulence intensity for the flight case substantially lower than for the static case. At $X/D_j = 15$, the maximum turbulence intensity is slightly higher in the flight case, but the jet width at this location is considerably larger for the static case. The far-field sound intensity is proportional to the fourth power of the turbulent fluctuation velocity, $u^2 \cdot u^2$. In order to show the effect of the freestream velocity on the noise source strength, the variation of the maximum of $u^2 \cdot u^2$ along the jet is shown in figure 15, again using the data given by the Lu/flow computer program.

The source alteration due to the airplane motion sometimes consists of a change in the dominant noise component. For instance, at low power settings, jet noise levels may be reduced in flight below core noise levels. Core noise then becomes the dominant noise component.

A similar thing happens to the fan tone fundamental noise source in going from static to flight. For engines with and without inlet guide vanes (IGV's), the fan tone fundamental static noise levels are attributed to the noise generated from the inlet turbulence interacting with the rotor (ref. 9). The high static inlet turbulence intensity levels can result from the following: (1) eddy stretching of large atmospheric disturbances as they are sucked into the engine, (2) flow separation inside the inlet, and (3) unsteady velocities in the inflow resulting from obstructions around the inlet. In flight, because of the absence of the phenomena just described, the turbulence intensity levels are considerably reduced. Consequently, the corresponding noise levels are reduced as well. Then, for engines with IGV's like the JT8D, the noise due to the IGV/rotor interaction becomes dominant in flight. In addition to the turbulence effects, ground vortex effects and fan loading changes may also be responsible for source alteration between static and flight.

The airplane forward motion also alters the installation effects. For instance, it gives rise to the wing wake which scatters the sound passing through it.

The location of the engine's nozzle exit in the 727-100 airplane suggests that jet and aft fan noise will suffer little or no installation effects. Differences between the static and flight levels of these two components can be considered to be due only to flight effects. However, the location of the engine inlets in the airplane suggests that propagation of the inlet fan noise will be affected by the presence of the fuselage and wings. Therefore, installation and flight effects should be included in the interpretation of the static and flight inlet fan noise differences.

# 4.0 727/JT8D JET NOISE

Jet noise flight effects for the baseline and ejector suppressor configurations are presented in this section.

Jet noise flight effects are shown in plots of constant 1/3-octave-band frequency, where static and flight jet noise directivities are compared. Five power settings, covering the engine operational range, are included for each configuration. Baseline jet noise spectra were limited to a 50- to 1000-Hz frequency range. Ejector suppressor jet noise spectra were limited to a 50- to 2500-Hz frequency range.

## 4.1 BASELINE

Baseline static and flight test runs, used in this study, are shown in tables 1 and 3(a), respectively.

### 4.1.1 STATIC JET NOISE DATA

Static noise spectra from baseline run 24, at three power settings and at four sideline angles, are shown in figure 16. Fan noise is shown dominating the high frequencies. At angles far from the jet axis and at low-moderate power settings, fan tones are present in the 2500-Hz 1/3-octave-band. Therefore, in order to guarantee the absence of fan noise in the data used for jet noise study, only the region of the spectra between 50 and 1000 Hz was considered. Overall sound pressure levels based on 14 (50 to 1000 Hz), 17 (50 to 2000 Hz), and 24 (50 to 10 000 Hz) bands are compared in figure 17.

Static noise data from four test runs at sideline microphones 90°, 120°, and 140° are shown as a function of engine power setting in figures 18 through 20. The data were plotted at constant 1/3-octave-band frequency. In order to remove the ambient condition differences between data points, 1/3-octave-band SPL's were first normalized to 77°F and 70% RH. The small data scatter observed in these figures indicates that the nondimensional ideal jet velocity $V_{jPRI}/a_o$ is an excellent noise-engine performance correlating parameter for the baseline configuration. The fourth-order regression curves, representing the static noise data average, are also shown in figures 18 through 20.

#### 4.1.1.1 Core Noise Study

Core noise can best be defined as the low-frequency "excess" noise that cannot be accounted for as jet noise. It includes the contribution of such components as combustion noise, swirl noise, internal boundary-layer separation noise, etc.

The presence of core noise in the JT8D baseline acoustic data was investigated by comparing jet and core noise predictions with measured data.

Jet noise was predicted using the latest proposed SAE dual-flow jet noise prediction method, developed by Rolls-Royce (ref. 10). The newest proposed SAE single-flow jet noise prediction, developed by Boeing (ref. 11), was used for the single-flow part of the Rolls-Royce prediction method.

Core noise was predicted using the Boeing core noise standard prediction method.

Comparison of prediction results and actual measured static noise data is presented in figure 21 at two angles, 90° and 120°, and at two frequencies, 315 and 400 Hz. The frequencies were selected as being representative of core noise, while the angles were in the region of peak noise radiation for this component. Core noise predicted values fall below the average regression curves, except at very low power settings. In this region, the average regression curve deviates from the characteristic jet noise curve observed at the high power settings. It is concluded that core noise becomes an important noise component in the static engine low-frequency noise only at power settings below NPR = 1.3 ($V_j/a_o$ = 0.9).

Static jet noise levels, corresponding to the flight average operating conditions, were obtained by using the fourth-order regression curves and the nondimensionalized primary jet velocities calculated at each flight condition. For the case of takeoff power, this represents an extrapolation beyond the static data base.

#### 4.1.1.2 Extrapolation to 400-ft Sideline

The static jet noise levels corresponding to the flight conditions were extrapolated by assuming jet noise sources distributed along the jet axis. The locations of these sources were obtained using the Boeing Lu/Berman flow/noise analytical computer program as shown in appendix B. The extrapolation was performed using the geometry shown in figure 22. The acoustic path was defined as a straight line passing through the noise source and the microphone position. It can be seen from this figure that the effect of considering the noise source as the origin of the extrapolation is to produce a change in directivity from $\theta_1$ to $\theta$. Figures 23 and 24 show the effects of noise source location on the extrapolation results at takeoff power. The dashed curves represent the extrapolation results assuming jet noise sources at nozzle exit. Differences between both curves are larger at low frequencies since corresponding noise sources are located farther downstream of the nozzle exit. Differences as much as 1.5 dB are observed at 90° angle for the OASPL (50- to 1000-Hz) curves.

### 4.1.2 FLIGHT JET NOISE DATA

Flight jet noise data were normalized using the procedure described in section 3.1.

### 4.1.3 BASELINE JET NOISE FLIGHT EFFECTS

Extrapolated static and corrected flight baseline jet noise directivities are compared in figures 25 through 29 for five power settings and frequencies from 50 to 1000 Hz. Spectral comparisons at four directivity angles are shown in figures 30 through 34.

Differences between static and flight levels represent the jet noise reduction due to flight. The possible explanations for these differences were described in section 3.3. However, installation effects are not considered to be present in the jet noise flight data.

Figures 25 through 29 clearly indicate that jet noise flight effects are a function of directivity angle. At angles closer to the jet axis, jet noise is reduced in flight at all power settings. This reduction is practically independent of frequency (figs. 30 through 34, $\theta = 140°$) but is dependent on power settings, with the reduction being larger at lower power settings. Since the airplane flight velocity was approximately the same for all power settings, it can be stated that, at the same flight velocity, the noise reduction decreases as the jet velocity increases.

Jet noise reduction decreases progressively toward the forward angle. At low forward angles (about 50°) and frequencies below 250 Hz, the static noise levels are higher than the flight levels at takeoff power, cutback power (high gross weight), and the lowest power setting. For the other power settings, static and flight levels are approximately the same. However, at frequencies above 250 Hz, flight noise levels are higher than the static levels at takeoff power, approach, and the lowest power setting. This apparent amplification of the jet noise in flight is relatively small (about 2 dB for the takeoff and approach power settings) and slightly higher (about 3 dB) for the lowest power setting. This indicates that the static and flight directivity curves cross over. The angle at which the crossover occurs is different at each of these power settings and remains relatively constant with frequency. No trend is observed in the dependency of the crossover angle with power setting. At both cutback powers, high gross weight and light gross weight, flight and static noise levels have approximately the same values at frequencies above 250 Hz. (See figs. 30 through 34, $\theta = 50°$.) In evaluating these flight effect differences, it should be remembered that the 90% confidence interval is ±1.7 dB for the 1/3-octave-band flight noise data (sec. 3.1.2.6).

The OASPL (50- to 1000-Hz) directivity figures also show large noise reductions at angles closer to the jet axis with the reduction decreasing progressively toward the forward angles. At takeoff power, crossover occurs around 60° and the flight noise levels are higher than the static levels by approximately 1 dB at forward angles. At cutback powers, crossover does not exist and the static and flight curves merge together at angles of about 40°. At approach power and at the lowest power setting, crossover is present at angles of about 70°. Further forward, the flight noise levels remain slightly higher than the static levels by less than 1 dB.

The shape of the OASPL flight directivity curves for the high power settings is that of typical jet noise; e.g., peak noise about 140°. However, at the lowest power setting ($V_{jPRI}$ = 1090 ft/sec), the OASPL flight directivity noise peaks at 110°, which is more typical of other low-frequency noise components such as core noise. Although core noise flight effects are not yet completely understood, core noise is expected to suffer less reduction in flight than jet noise. It is noted that a Doppler amplification effect is expected for core noise in going from static to flight conditions. The magnitude is equal to $(1 - M \cos \theta)^{-n}$ where n may be as high as 4. Because of the static jet and core noise relative levels at low jet velocities ($V_{jPRI} \simeq 1100$ ft/sec, fig. 21), jet noise reduction in flight would cause core noise to become the dominant low-frequency noise component.

## 4.2 EJECTOR SUPPRESSOR

Runs selected for ejector suppressor static and flight noise analysis are shown in tables 2 and 3(b), respectively.

### 4.2.1 STATIC JET NOISE DATA

Ejector suppressor run 49 static noise spectra at three power settings and at four sideline angles are shown in figure 35. The ejector suppressor spectra show the following characteristics: (1) premerged jet noise, generated inside the shroud, peaks at 800 to 1000 Hz and dominates the directivity angles around 110° to 120°; (2) postmerged jet noise, generated downstream of the shroud exit, peaks at 160 to 200 Hz and dominates the directivity angles closer to the jet axis; and (3) fan noise levels are dramatically reduced from those of the baseline engine. Figure 35 indicates that in order to cover the jet noise region and at the same time avoid the presence of fan noise, the ejector suppressor spectra should be limited to frequencies below 2500 Hz.

The two engine performance parameters—relative jet velocity, $(V_{jPRI} - V_E)/a_o$, and the jet velocity at the shroud exit, $V_{j\ MAX\ SHROUD\ EXIT}/a_o$—were investigated as noise-engine performance correlating parameters. Results indicated that the noise data correlated well with both parameters and were slightly better for the first parameter $(V_{jPRI} - V_E)$, even at low frequencies where the $V_{j\ MAX\ SHROUD\ EXIT}$ was expected to give a better correlation.

Static noise data from three test runs at sideline microphones 90°, 120°, and 140° are shown as a function of log $(V_{jPRI} - V_E)/a_o$ in figures 36 through 38. The data were plotted at constant 1/3-octave-band frequency. First, however, the ambient condition differences between data points were removed by normalizing the 1/3-octave-band SPL's to 77°F and 70% RH. The fourth-order regression curves, representing the static noise data average, are also shown in figures 36 through 38.

The in-flight engine parameter $P_{T7}/P_{amb}$ was used to calculate (using fig. A-5 in app. A) the corresponding static relative primary jet velocity at the lobe exit. With these values and the fourth-order regression curves, the static jet noise levels at in-flight engine conditions were obtained.

Extrapolation to 400-ft sideline was performed using the geometry shown in figure 22 and the jet noise sources location given in appendix B for the ejector suppressor configuration.

### 4.2.2 FLIGHT JET NOISE DATA

Flight jet noise data were normalized using the procedure described in section 3.1.

### 4.2.3 EJECTOR SUPPRESSOR JET NOISE FLIGHT EFFECTS

Extrapolated static and corrected flight ejector suppressor jet noise directivities are compared in figures 39 through 43 for five power settings and frequencies from 50 to 2500 Hz. Spectra comparisons at four directivity angles are shown in figures 44 through 48.

Flight effect results for this configuration are difficult to interpret because of a complex interaction of the internal sound field with both the nozzle and the internal and external flows. This problem has been addressed theoretically for an idealized situation in reference 12. In general, a Doppler amplification effect is possible for the jet noise generated inside the shroud in going from static to flight conditions, although direct verification of this behavior has not been obtained.

The static and flight OASPL (50- to 2500-Hz) directivities show crossover at angles around 70° for the high power settings and shift to around 90° for the low power settings. Noise reduction peak to peak changes little with power setting. The magnitude, about 3 dB, is smaller than observed in the baseline flight effects. At angles forward of the crossover angle, the flight noise levels are higher than static noise levels by 1 to 3 dB depending on power setting.

Several interesting characteristics are observed in the individual frequency directivities at all power settings. At low frequencies (50 to 250 Hz), crossover does not occur. At middle frequencies (250 to 630 Hz), crossover is shown at angles around 70° to 80°. At lower angles, flight noise levels are higher than static noise levels by 1 to 2 dB. At high frequencies (800 to 2500 Hz), crossover occurs at angles between 90° and 100°. The difference between the flight and static noise levels at the forward angles is now as high as 5 to 8 dB.

# 5.0 727/JT8D FAN NOISE

Fan noise flight effects for the baseline and ejector suppressor configurations are presented in this section. Static and flight tone and broadband noise directivities are compared, based on narrowband acoustic data of 37.5-Hz bandwidth.

Baseline fan tone flight effects are shown for the first-stage blade passage frequency ($F_1$), its second harmonic ($2F_1$), and the second-stage fundamental tone ($F_2$). Baseline broadband fan noise flight effects are shown for three frequencies: 2000, 4000, and 6000 Hz.

Ejector suppressor tone levels were not discernible in the flight spectra. Fan noise flight effects for this configuration are shown for 4000- and 6000-Hz broadband levels only.

## 5.1 BASELINE

### 5.1.1 FLIGHT FAN NOISE DATA

Narrowband spectra were obtained by ensemble averaging microphone M1 acoustic data for three repeat flyovers. Fourteen angles (30° to 160°) for each flyover were reduced. Five power settings were considered.

Baseline flight narrowband spectra at 40° and 100° directivity angles are shown in figures 49 through 53 for each of the five power settings studied. At the lowest power setting, the signature is clearly dominated by three tones, which were identified as the first-stage fundamental tone ($F_1$), its second harmonic ($2F_1$), and the second-stage fundamental tone ($F_2$). Underlying the tones is a spectrum of noise identified as the fan broadband noise.

As the power setting is increased, tones and braodband level differences decrease until, at takeoff power, the tones are no longer discernible from the rest of the spectra (fig. 53). Since at takeoff power jet noise is the dominant noise component, the broadband noise levels seen at the corresponding high-frequency region of the spectrum cannot be identified as only broadband fan noise. Consequently, the takeoff data were excluded from the fan noise study. At the other four power settings, the first-stage fundamental tone can be clearly identified above the broadband at all angles. However, its second harmonic and the second-stage fundamental tones are only distinctive at certain angles and power settings.

The first-stage fundamental blade passing frequency was obtained by reading the frequency value from each spectrum; therefore, these are the Doppler frequency shift values. At each spectrum, the first-stage second-harmonic frequency and the second-stage fundamental blade passage frequency were calculated by using the first-stage fundamental blade passing frequency. For example, the second-stage fundamental frequency was calculated by multiplying the first-stage fundamental frequency by the ratio of second- to first-stage number of blades. Afterward, the noise levels at these three frequencies were read at each spectrum.

The broadband noise levels corresponding to the 2000-, 4000-, and 6000-Hz unshifted frequencies were selected to study the broadband fan noise flight effects. The first-stage fundamental shift-to-unshift frequency ratio was used to calculate the Doppler frequency shift for each of the three selected broadband frequencies at each spectrum.

The tones and broadband flight noise levels were corrected to standard atmospheric conditions and altitude. Corrected flight noise data directivities are shown at approach power in figures 54 and 55 for the first-stage fundamental tone and the 4000-Hz broadband noise, respectively. Directivity levels shown in the figures are those of the actual airplane as it flies over the observer at an altitude of 400 ft and at a Mach number of M = 0.23. Therefore, the noise levels at each angle correspond to a different frequency (Doppler frequency shift). The frequencies at 30° and 160°, as well as the unshifted frequency (90°), are also shown in these figures.

### 5.1.2 STATIC FAN NOISE DATA

Narrowband spectra were obtained for two Boardman baseline static runs, 24 and 70. Six conditions per run were reduced for corrected rotor speed (N1C) ranging from 5500 to 8000 rpm.

Baseline static narrowband spectra for two microphone angles (40° polar and 100° sideline) at two power settings (approach and cutback) are shown in figures 56 and 57, respectively. Fan tone noise levels at first-stage fundamental frequency, second harmonic, and second-stage fundamental frequency as well as the fan broadband noise levels at 2000, 4000, and 6000 Hz were read from each spectra. The noise data, corrected to standard weather conditions, were plotted against corrected rotor speed for each microphone angle, as shown in figures 58 and 59. These figures show the first-stage fundamental tones and the 4000-Hz broadband noise data at two angles, 40° polar and 100° sideline. Also shown are the sixth-order regression curves used to fit the data.

Static fan tones and broadband noise levels corresponding to the in-flight power settings were determined from these curves and then extrapolated to 400-ft sideline using the noise source locations as described in appendix B. First-stage fundamental tone and 4000-Hz broadband directivities for the approach power are shown in figures 60 and 61, respectively. The directivity angles where uncertainty in the fan noise source locations exists are also indicated in these figures.

### 5.1.3 BASELINE FAN NOISE FLIGHT EFFECTS

Extrapolated static and corrected flight baseline fan noise directivities for three tones ($F_1$, $F_2$, and $2F_1$) and three broadband frequencies (2000, 4000, and 6000 Hz) are compared in figures 62 through 65.

Tones and broadband frequencies are constant with directivity angle for the static data, but the flight data have a Doppler frequency shift which results in the frequency decreasing from the forward angles to the aft angles. At 90°, the static and flight frequencies are the same.

Although the $F_2$ and $2F_1$ tones were not always clearly distinguishable in the flight spectra, the spectrum levels corresponding to their frequencies were read and used for the static and flight noise data comparisons. Symbols were used to indicate those angles at which the tone levels were at least 5 dB above the broadband levels.

Tone data show noise reductions when going from static to flight. The first-stage fan fundamental tone at approach and low power settings is reduced 10 to 20 dB in the forward and aft angles. At higher power settings, these large reductions are seen only at the forward angles. The first-stage fan second harmonic shows the largest reduction of the three tones, although the reduction disappears at large aft angles. This behavior is similar at all power settings. The second-stage fan fundamental tone shows a different behavior. The largest reductions, 10 to 15 dB, are observed at the aft angles while the forward angles show little or no reduction.

The first-stage fundamental tone static noise source is believed to have been dominated by the turbulence-rotor interaction. In flight, the inlet cleanup effect decreased the strength of this noise generation mechanism and resulted in lower inlet fan noise levels. Besides the turbulence effects, there were other fan noise sources which changed from static to flight and should not be ignored. (See sec. 3.3.) Furthermore, installation effects are expected to be present in the flight noise data in the forward angles (sec. 6.0) and should be included in the interpretations of the noise results observed at forward angles.

Broadband fan noise static and flight comparisons show smaller noise level reductions in flight than those observed for the fan tones. This reduction is largest at 6000 Hz and disappears at 2000 Hz, with the exception of certain aft arc radiation angles. At cutback power (HGW), the 2000-Hz flight noise levels are slightly higher than static, showing a small noise amplification.

## 5.2 EJECTOR SUPPRESSOR

### 5.2.1 FLIGHT FAN NOISE DATA

Narrowband spectra were obtained by ensemble averaging microphone M1 acoustic data for three repeat flyovers. Fourteen angles (30° to 160°) for each flyover were reduced.

Inspection of the flight narrowband spectra for five power settings indicated the absence of distinctive tones. Thus, only broadband fan noise was considered. Figure 66 shows the approach power flight noise spectra at two angles, 40° and 100°.

The broadband noise levels corresponding to the 4000- and 6000-Hz unshifted frequencies were selected to study the ejector suppressor fan noise flight effects. Unlike the baseline configuration, the 2000-Hz ejector suppressor broadband noise was believed to be dominated by jet noise and, therefore, was not considered in the ejector suppressor fan noise flight effects study. At directivity angles different from 90°, the Doppler shifted frequencies were calculated using the Doppler frequency shift formula for a single source in motion, $f/(1 - M \cos \Gamma)$ where $f$ takes the value of 4000 and 6000 Hz.

Broadband flight noise levels, determined from each spectrum using the appropriate frequencies, were corrected to standard atmospheric conditions and altitude.

### 5.2.2 STATIC FAN NOISE DATA

Narrowband spectra were obtained for two Boardman ejector suppressor static runs, 49 and 63. Six conditions per run were reduced for corrected rotor speeds ranging from 5500 to 8000 rpm.

Ejector suppressor static narrowband spectra for two microphone angles (40° polar and 100° sideline) at two power settings (approach and cutback) are shown in figures 67 and 68. Fan tone noise levels at first-stage fundamental frequency, second harmonic, and second-stage fundamental frequency as well as the fan broadband noise levels at 4000 and 6000 Hz were read from each spectra. The noise data, corrected to standard weather conditions, were plotted against corrected rotor speed for each microphone angle as shown in figures 69 and 70. These figures show the first-stage fundamental tones and the 4000-Hz broadband noise data at two angles, 40° polar and 100° sideline. Also shown are the sixth-order regression curves used to fit the data.

Static broadband noise levels at the in-flight power settings were determined, using the regression curves, and then extrapolated to 400-ft sideline, using the noise source locations as described in appendix B.

### 5.2.3 EJECTOR SUPPRESSOR NACELLE FAN NOISE FLIGHT EFFECTS

Static and flight ejector suppressor nacelle fan noise directivities for two broadband frequencies (4000 and 6000 Hz) are compared in figures 71 through 74.

At 4000 Hz, the flight noise levels are higher than the static levels at forward and aft angles but are similar at angles around 90°. The differences between static and flight levels at forward and aft angles increase with power setting.

At 6000 Hz, 5- to 15-dB noise reductions are observed in flight except at very high angles where noise amplification is seen.

# 6.0 INSTALLATION EFFECTS

The presence of finite boundary surfaces, such as fuselage and wings in the propagating path of the sound waves, gives rise to phenomena such as sound reflection, refraction, diffraction, and scattering. These effects are included in the measured flight noise data and, in some cases, may be responsible for part or all of the noise level differences between static (bare engine) and flight. This section presents a discussion of the installation effects on the 727/JT8D jet and fan flight noise data.

Qualitative evaluation of installation effects is relatively simple but, due to the complexity of the various phenomena involved, quantitative results are in general difficult to obtain. Reference 13 presents analytical and empirical models to predict these effects.

The location of the three engines' nozzle exits on the 727-100 airplane suggests that the jet flows would be relatively unobstructed and propagation of the jet and aft fan noise toward a ground observer under the airplane flightpath would suffer little or no installation effects. On the contrary, this also suggests that propagation of the inlet fan noise will be affected by the presence of the fuselage and wings.

The installation effects present in the inlet fan noise flight data are discussed in the following paragraphs.

The 727-100 airplane is powered by three engines, two mounted on pods on the aft sides of the fuselage and the third, with an S-duct inlet, mounted in the aft center of the airplane fuselage. The difference in location between the pod engines and the center engine suggests differences in noise installation effects.

## 6.1 CENTER ENGINE

The center engine inlet is located above the fuselage, ahead of the vertical tail leading edge. Consequently, during the airplane flyover, the line of sight between the inlet and the ground observer under the flightpath becomes blocked at all times. The propagation of the center engine inlet fan noise is affected by fuselage and wing diffraction and by wing wake scattering. Moreover, it is expected that the increase in inlet flow turbulence, due to the long S-shaped inlet duct, will increase the center engine inlet fan noise levels from those of the two pod engines. Nevertheless, it is reasonable to assume that the center engine inlet fan noise will be substantially reduced by the airframe shielding effects.

The most important factor limiting the amount of fuselage shielding is the diffraction of the sound waves by the fuselage. A theoretical procedure to calculate the sound attenuation caused by an infinite long cylindrical body shielding with sound diffraction is presented in reference 13. Figure 75 shows results obtained by applying this procedure to the 727 airplane in still air. Theoretically predicted noise reduction for a receiver located on a far-field line parallel to and directly underneath the flightpath can be obtained by using the curve in figure 75. At $\theta$ of 90° (fig. 75), inlet fan noise at frequencies higher than 250 Hz would suffer noise level reductions on the order of 24 dB or more. Substantiation of this

theoretical procedure has been partially made by using an anechoic room test. However, for the flight case, the credibility of the predicted large noise reduction has not been established. Surrounding airflow and associated turbulence scattering would reduce the shielding benefit to some extent. The theoretical result suggests that the airframe shielding is an important contributing factor in the inlet fan noise level differences between static and flight.

## 6.2 POD-MOUNTED ENGINES

A different situation exists for the inlet fan noise of the pod-mounted engines. The wing and trailing-edge flaps now obstruct the noise propagation in the forward angles. In addition, the noise propagation is also affected by the presence of the wing wake, which is directly in the propagation path.

Figure 76 presents two schematic drawings which depict the wing shielding effect at two flap settings, 5° and 25°. The wing and flaps can be assumed as solid sound barriers that are known to be effective in shielding the high-frequency noise when the barrier is near the source. In this case, the sound waves are diffracted at the edge of the barrier. Harris (ref. 14) and Dunn (ref. 13) present methods to calculate the associated noise reduction in the shadow zone. Figure 77 presents a schematic diagram of the geometry used in these methods. Assuming a point source and a half-plane barrier, the noise levels obtained in the shadow zone are functions of the deflection angle $\theta$ and the effective barrier height EF/$\lambda$, where EF is the perpendicular distance from the edge E to the line OM, and $\lambda$ is the wavelength of the incident sound wave. (See fig. 77.) Calculations based on these methods showed that a 3150-Hz frequency sound wave traveling in the 40° direction (measured from the inlet axis) from the inlet center ($\theta \simeq 20°$ and EF/$\lambda$ of 12) would be reduced in level about 20 dB because of the wing shielding.

With the surrounding air in motion (e.g., airplane in flight), the preceding analysis must be modified to include the effect of moving medium on diffraction as well as the effect of sound scattering caused by the turbulent wing wake. According to the study included in reference 13, scattering would substantially limit the noise reduction to be gained by wing shielding.

Peak noise reduction for the pod engines inlet fan noise, including the effects of diffraction with uniform flow and scattering by the wing wake, is estimated to be about 16 dB and corresponds to emission angle relative to the inlet around 28° (ref. 13).

# 7.0 CONCLUSIONS

The data included in this report represent a unique piece of information on actual engine full-scale jet and fan noise flight effects for a low-bypass-ratio engine with a suppressed and unsuppressed configuration. This information provides a data base for:

1. Development or improvement of flight effects prediction procedures

2. Verifying the adequacy of flight simulation techniques

3. Evaluation of jet noise theoretical work

Specific conclusions regarding analysis techniques and actual flight effects on engine noise, derived from observation of the data, are summarized in the following sections.

## 7.1 ANALYSIS TECHNIQUES

1. Several repeated flyovers (three or more) or ensemble averaging of statistically independent microphones is required to obtain meaningful results.

2. Narrowband spectral analysis is needed for the study of fan noise flight effects.

3. Jet and fan noise source locations must be taken into account when extrapolating static data to the aircraft altitude.

## 7.2 BASELINE JET NOISE

1. A reduction of OASPL (50 to 1000 Hz) occurs due to flight. The amount of reduction is substantial at angles near the jet axis (aft quadrant) and becomes progressively less at angles near the inlet axis (forward quadrant) where little or no reduction occurs.

2. At the same flight speed, the amount of peak OASPL noise reduction due to flight decreases as the jet velocity increases.

3. At aft angles, the noise reduction at low and high frequencies is comparable.

4. At forward angles, flight effects are a function of frequency. At low frequencies, below 250 Hz, noise reduction exists. At middle frequencies, 315 to 500 Hz, no reduction is observed. At higher frequencies, small noise amplification occurs in flight.

5. If source location corrections are not applied when extrapolating static data, greater noise amplification is observed at forward angles.

## 7.3 EJECTOR SUPPRESSOR JET NOISE

1. A reduction of peak OASPL (50 to 2500 Hz) and aft angle noise occurs because of flight. At forward angles, static and flight noise directivities show crossover, indicating a noise amplification in flight that depends on power setting.

2. At constant flight velocity, the amount of peak OASPL reduction changes little with power setting and is less than that observed for the baseline configuration.

3. At aft angles, the low-frequency postmerged noise is reduced more than the high-frequency premerged noise.

4. At forward angles, a small noise reduction occurs at low frequencies and is independent of power setting. However, a large amplification occurs at high frequencies and increases with decreasing power setting.

## 7.4 BASELINE NACELLE FAN NOISE

1. The fundamental first-stage tone shows a large reduction in flight. The largest reduction occurs at forward angles. The observed in-flight changes are the result of both flight and installation effects.

2. The second-harmonic first-stage tone shows the largest reduction of the three tones that were studied. The in-flight reduction decreases in the aft angles, and at high power settings crossover occurs.

3. The second-stage fundamental tone shows the largest reduction between 110° and 120° angles with less reduction forward and aft of this angle range.

4. Broadband fan noise for the baseline nacelle shows a smaller reduction than the tones. The reduction increases with frequency.

## 7.5 EJECTOR SUPPRESSOR NACELLE FAN NOISE

1. In flight, all tone levels were reduced below the broadband levels.

2. High-frequency broadband noise is reduced in flight at forward angles but is amplified at aft angles.

3. Flight effects are much smaller for low frequencies.

## 7.6 INSTALLATION EFFECTS

Forward arc fan noise flight data are affected by wing shielding, fuselage shielding, and wing wake scattering.

The conclusions listed can be directly used as guidelines for further flight effects studies, including the development of flight effects prediction procedures.

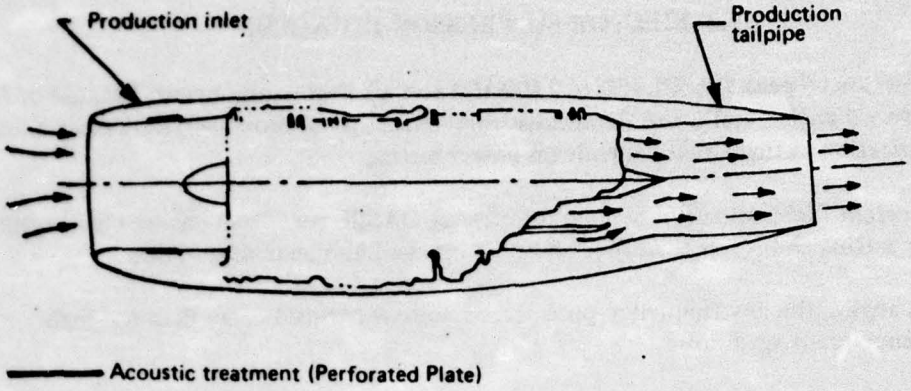


*Figure 1.—Baseline Engine Configuration*

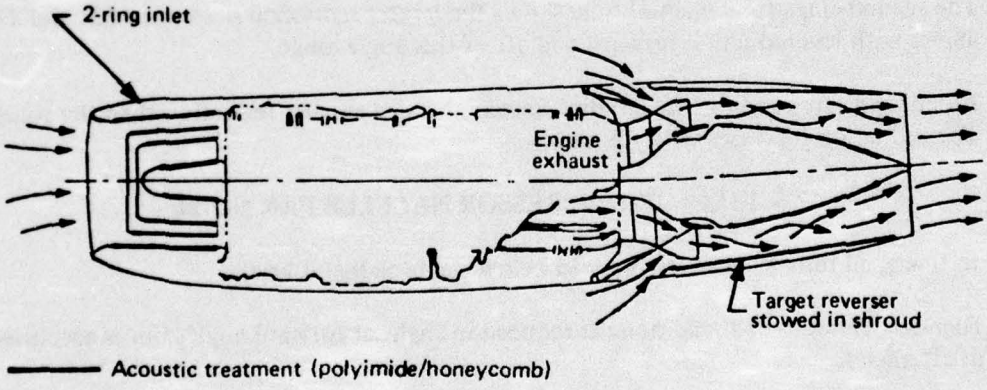


*Figure 2.—Ejector Suppressor Configuration (Suppression Mode)*

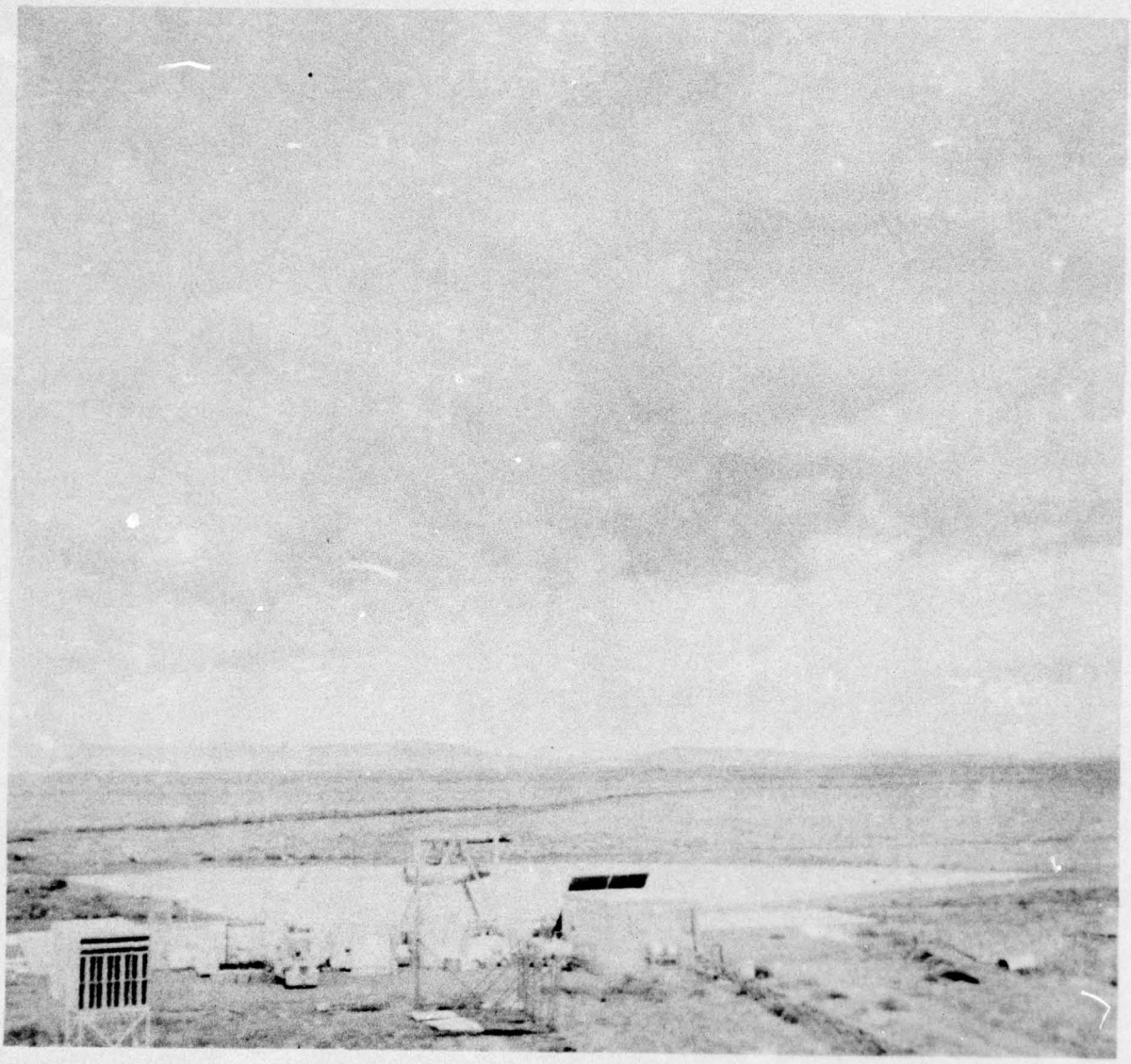

*Figure 3.—Boardman Test Site*

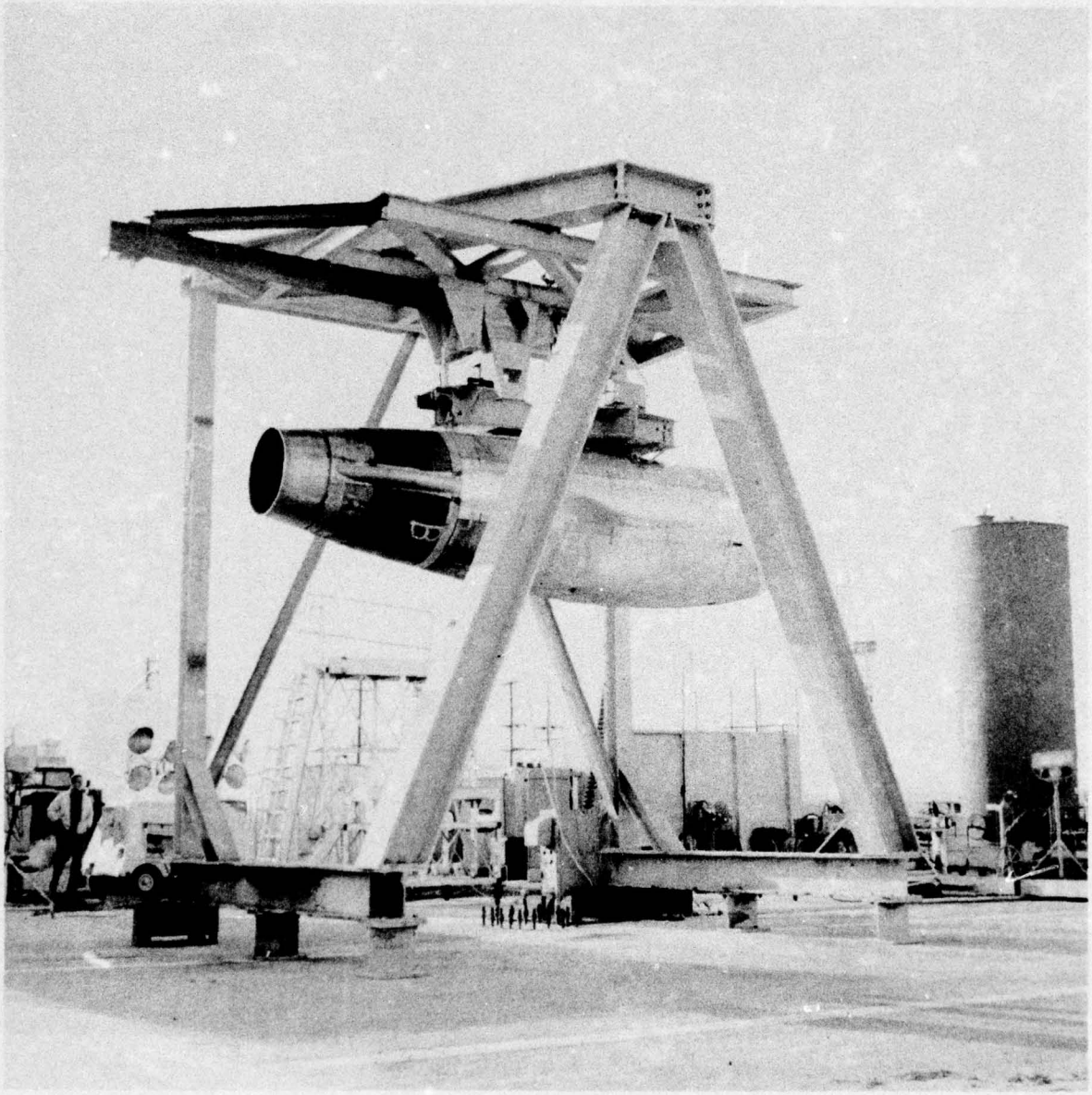

*Figure 4.—Boardman Test Stand*

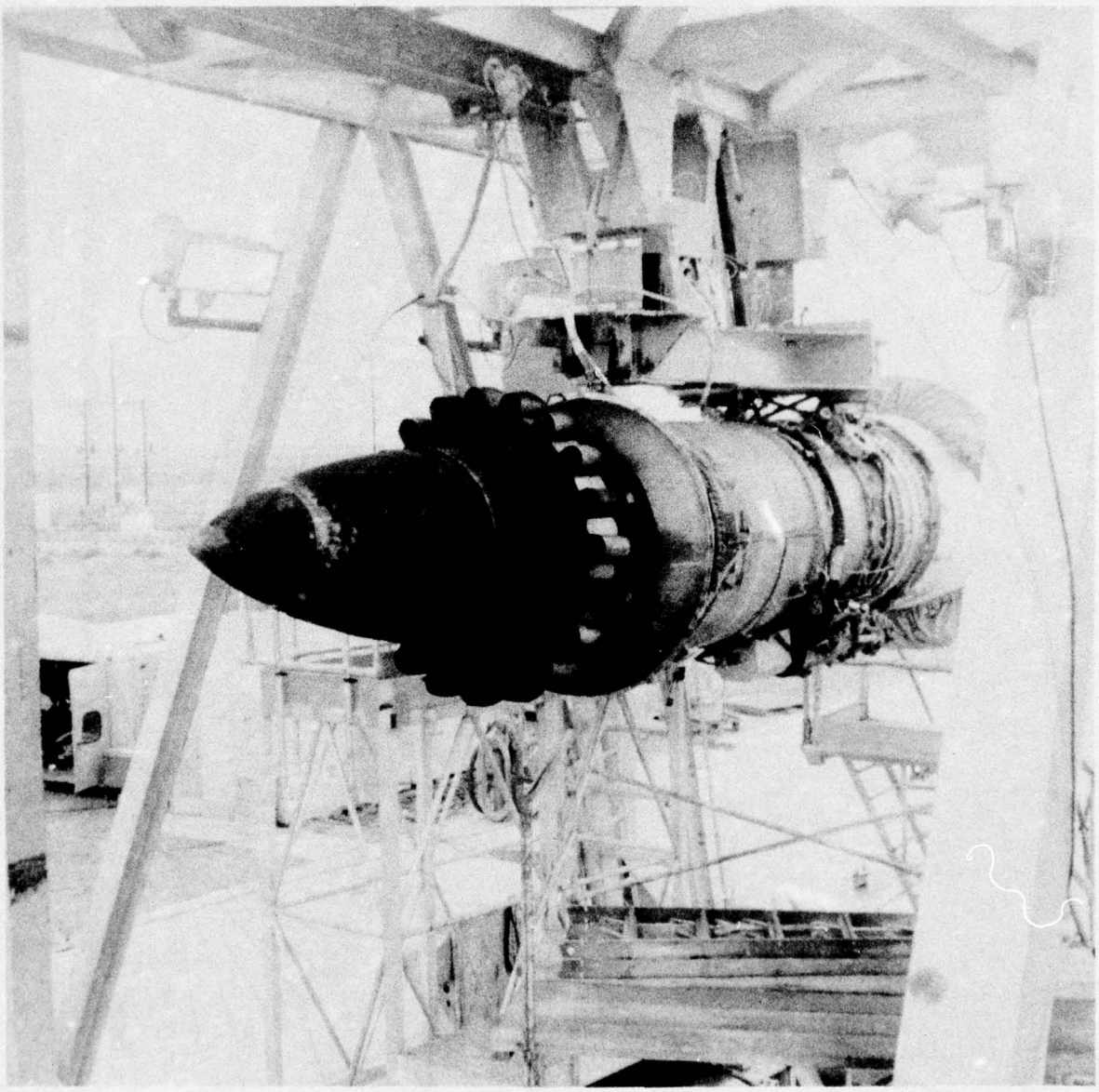

*Figure 5.—Ejector Suppressor Configuration: Bare 20-Lobe Nozzle*

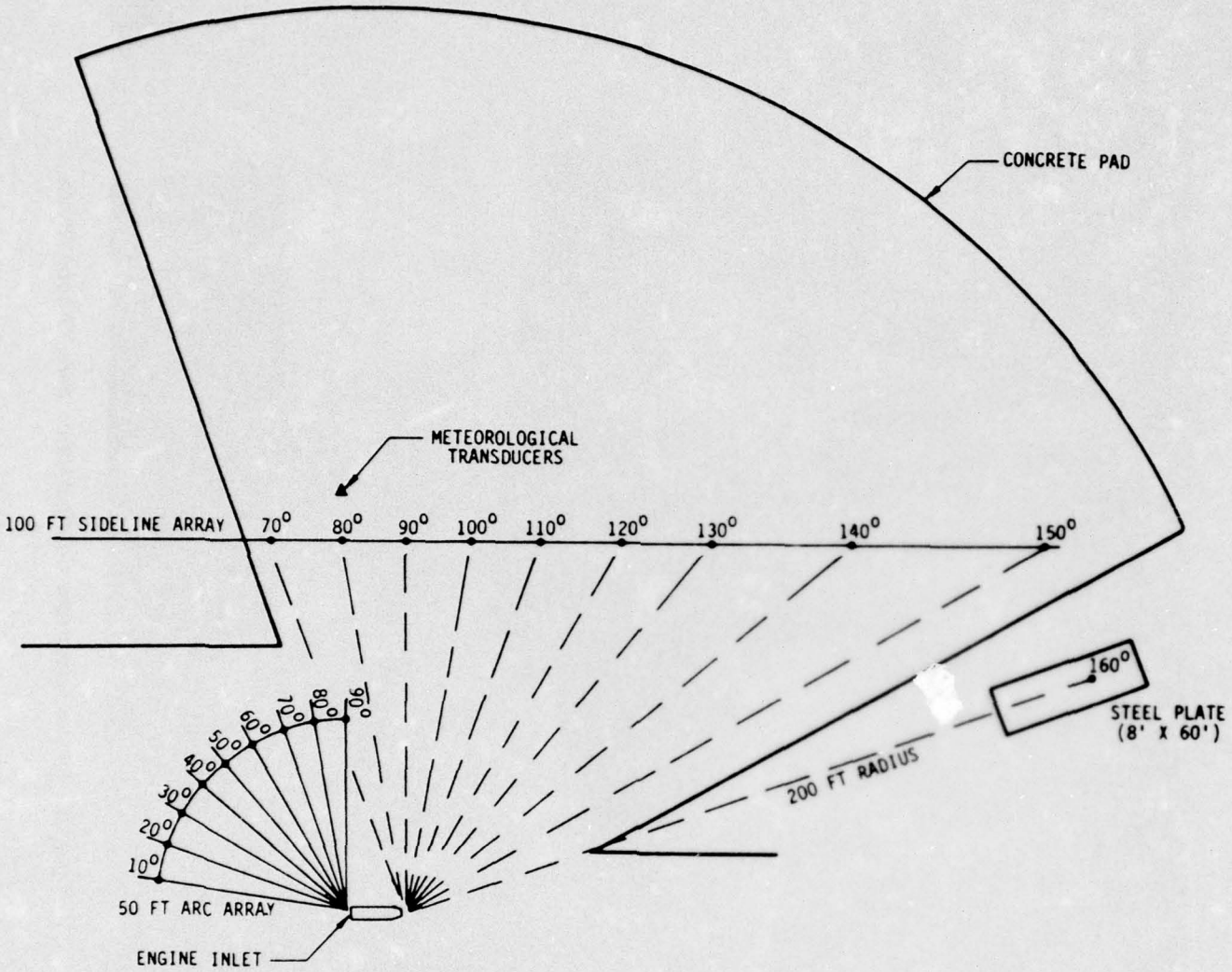


*Figure 6.—Microphone Array Layout for JT8D Retrofit Program, Boardman*

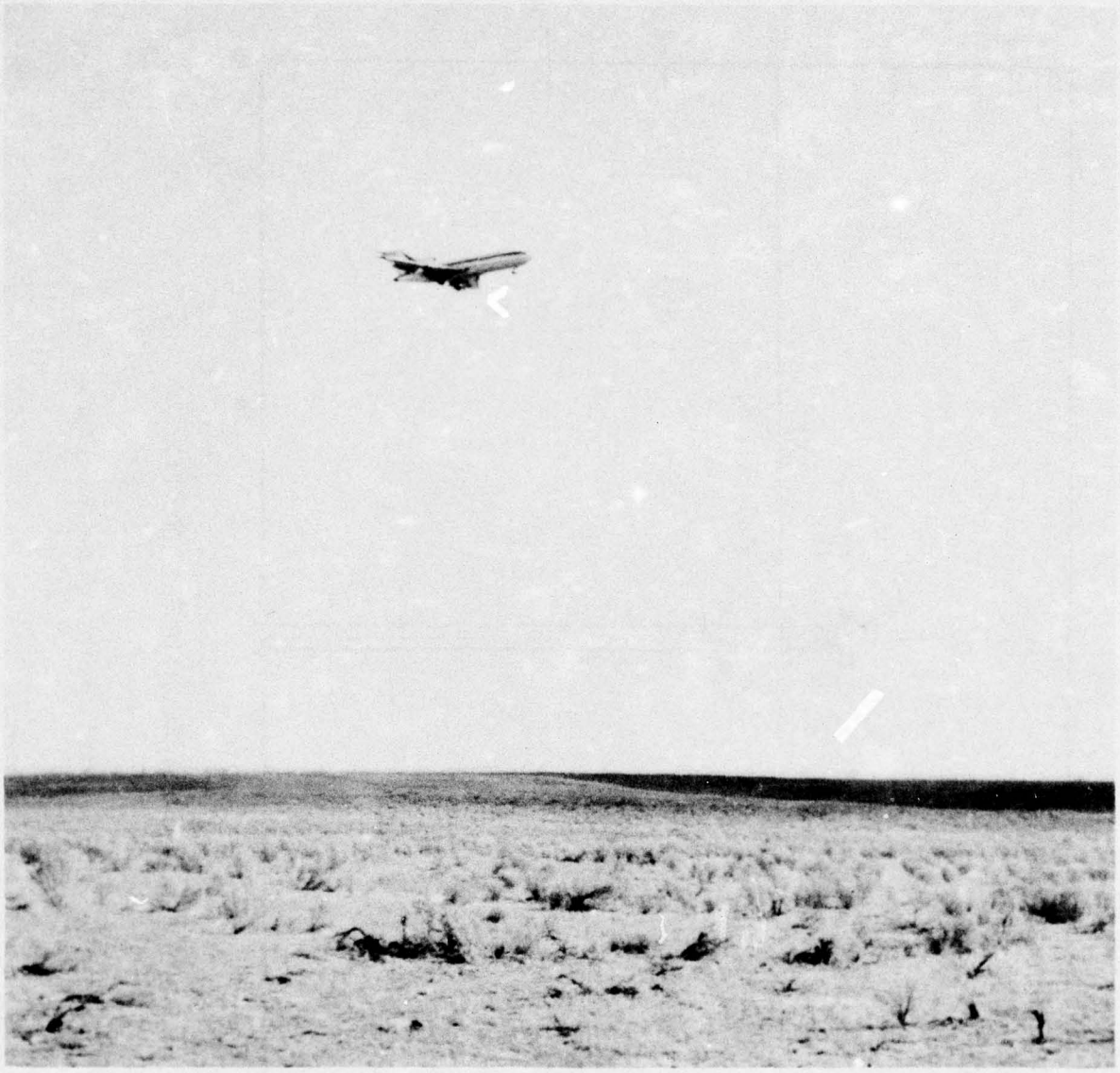

*Figure 7.—Moses Lake Test Site*

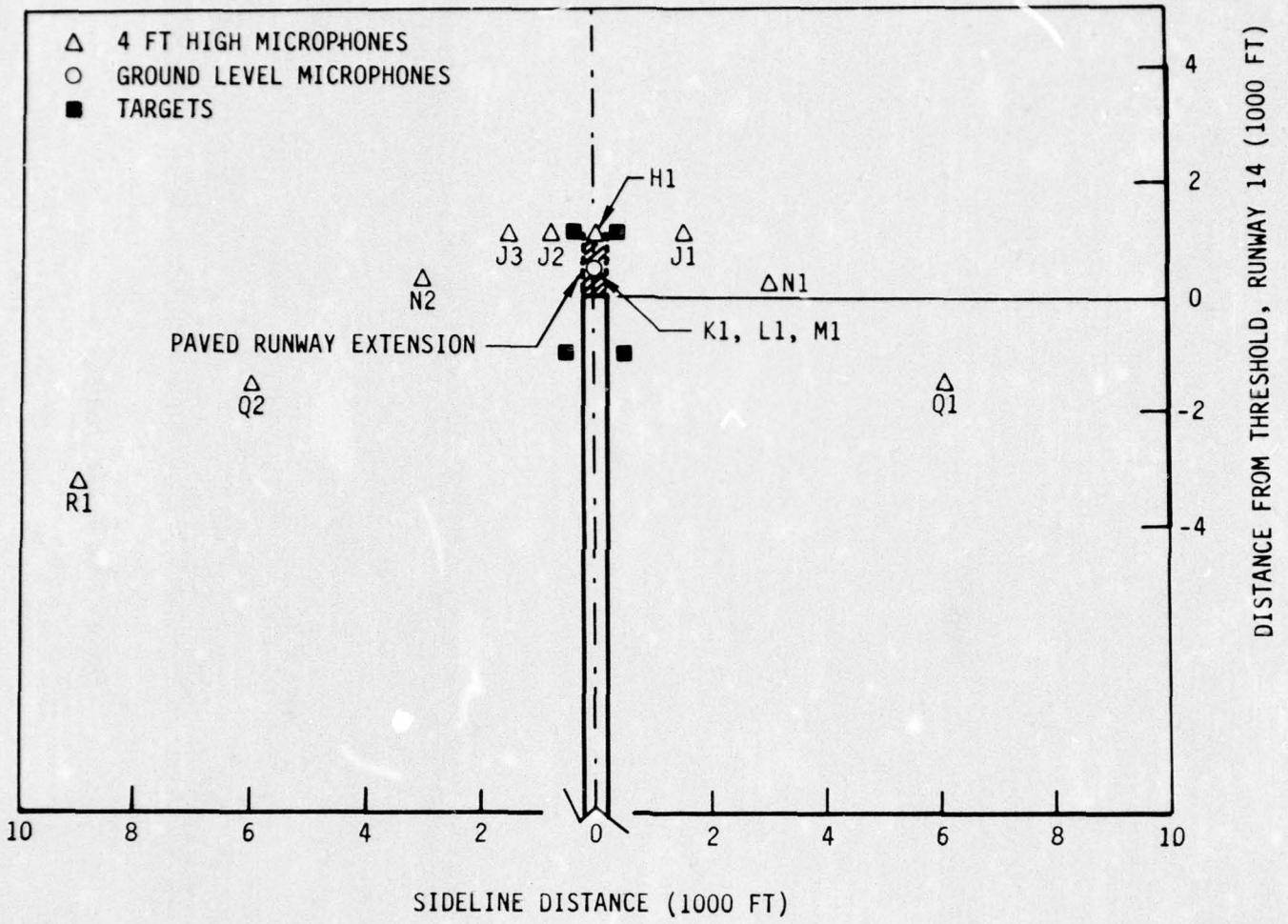


*Figure 8.—Microphone and Target Position for Level Flyover Testing*

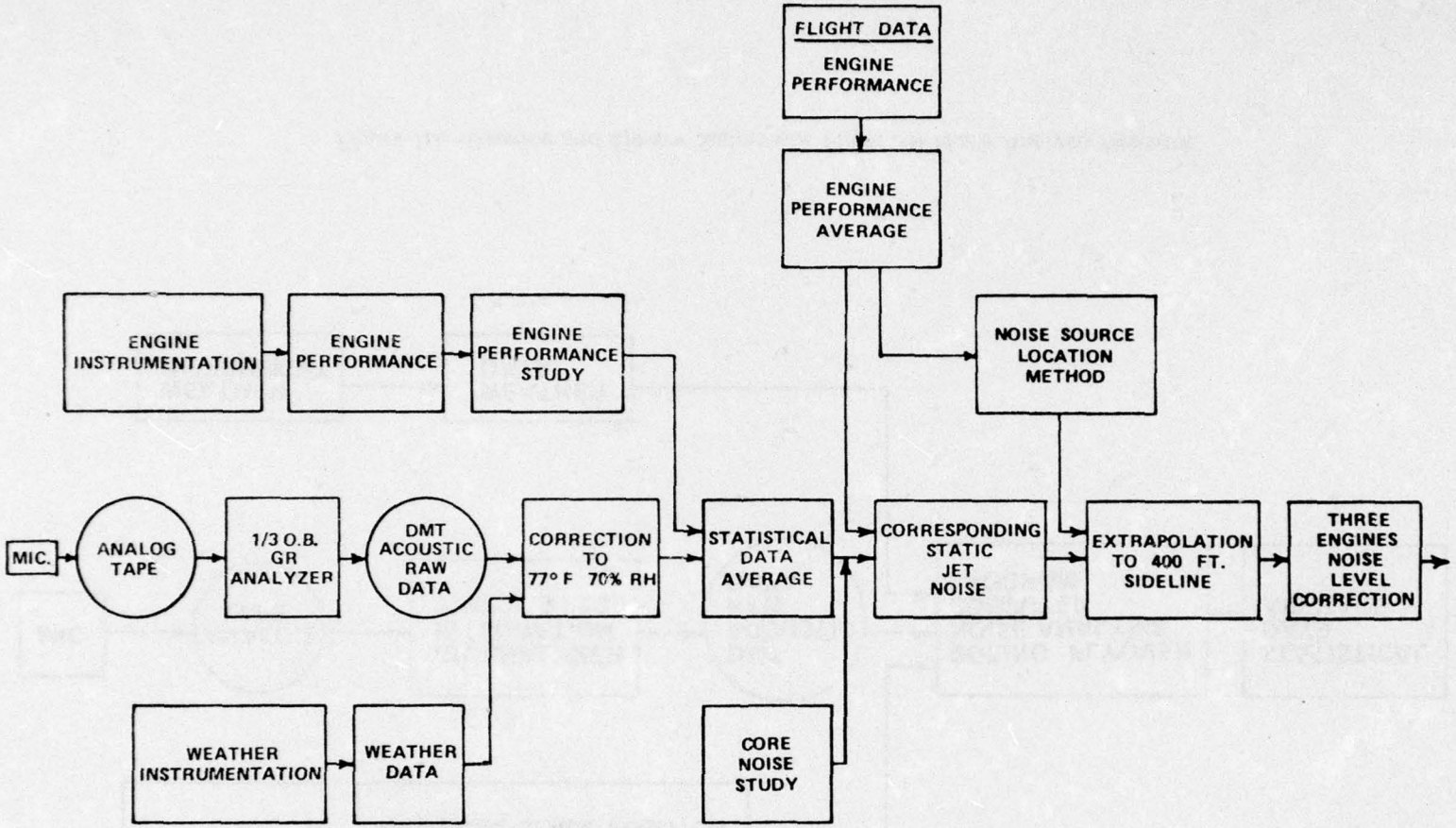


*Figure 9.—Baseline and Ejector Suppressor Static Jet Noise Analysis Network*

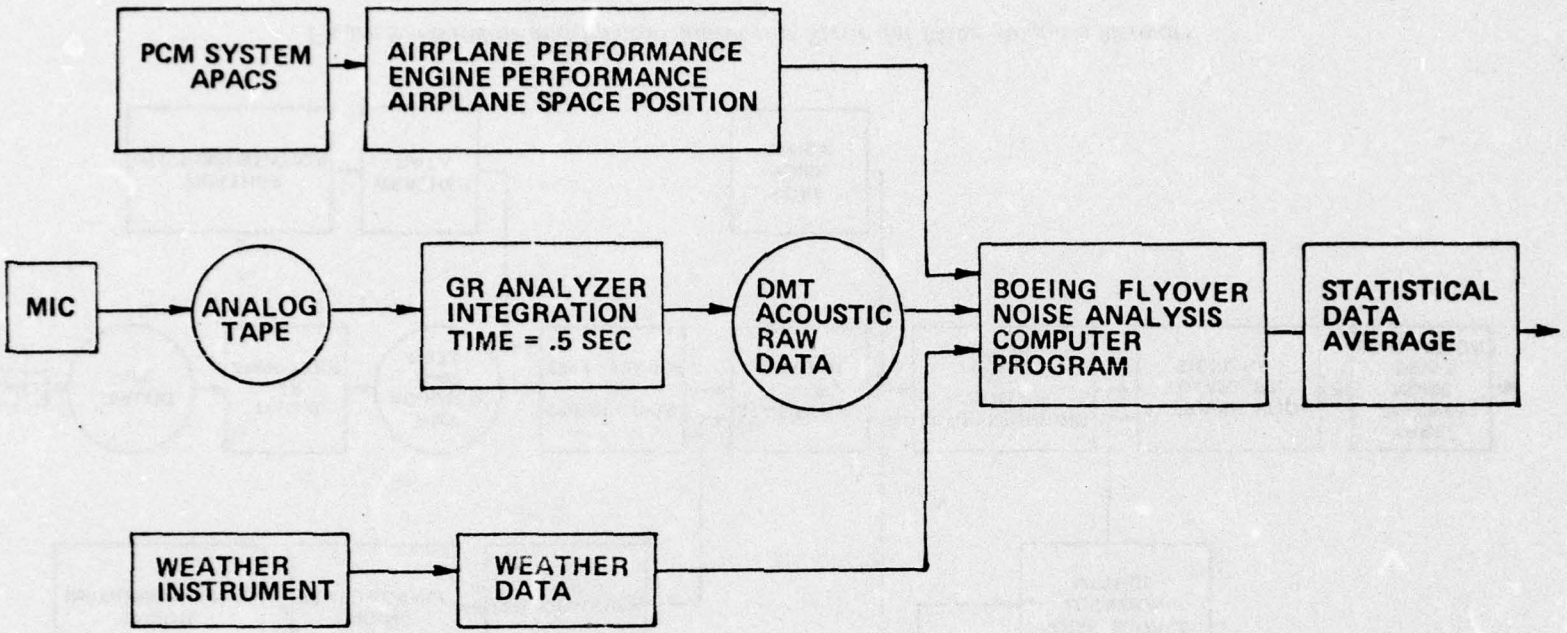


*Figure 10.—Baseline and Ejector Suppressor Flight Jet Noise Analysis Network*

## TWO - RING INLET

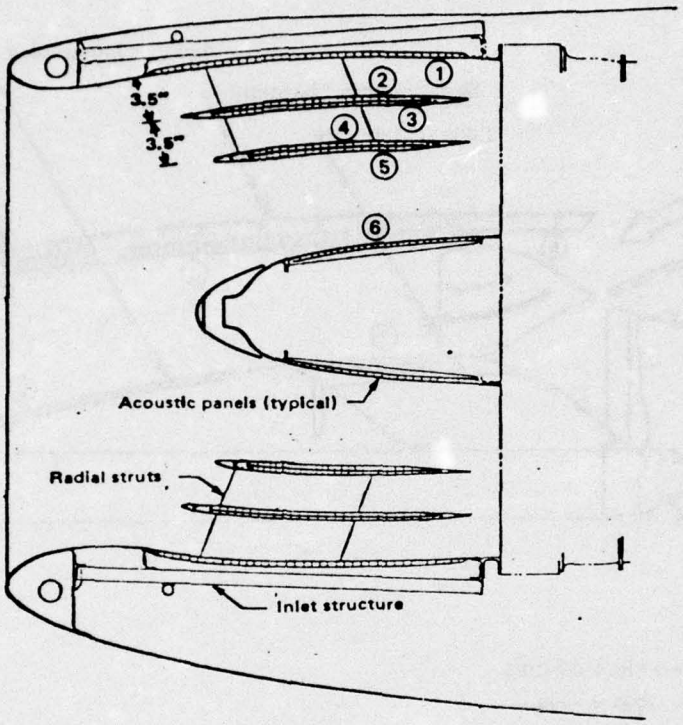


| Location | Description | Approx area ($ft^2$) | Approx length (in.) | Core size (in.) | Core depth (in.) | Flow resistance (cgs Rayls) |
|---|---|---|---|---|---|---|
| 1 | Polyimide/honeycomb | 21 | 25 | 3/8 | 0.3 | 50 at 150 dB overall sound pressure level |
| 2 | Polyimide/honeycomb | 13.5 | 19.0 | 3/8 | 0.2 | 90 at 150 dB overall sound pressure level |
| 3 | Polyimide/honeycomb | 13.5 | 19.0 | 3/8 | 0.2 | 90 at 150 dB overall sound pressure level |
| 4 | Polyimide/honeycomb | 9 | 16.3 | 3/8 | 0.3 | 50 at 150 dB overall sound pressure level |
| 5 | Polyimide/honeycomb | 9 | 16.3 | 3/8 | 0.3 | 50 at 150 dB overall sound pressure level |
| 6 | Polyimide/honeycomb | 3 | 13 | 3/8 | 0.2 | 90 at 150 dB overall sound pressure level |

Target tuning frequencies of treatments 1 through 6 are 2000 to 4000 Hz.

*Figure 11.—Schematic of the Ejector Suppressor Acoustic Treatment*

## EJECTOR SUPPRESSOR NOZZLE

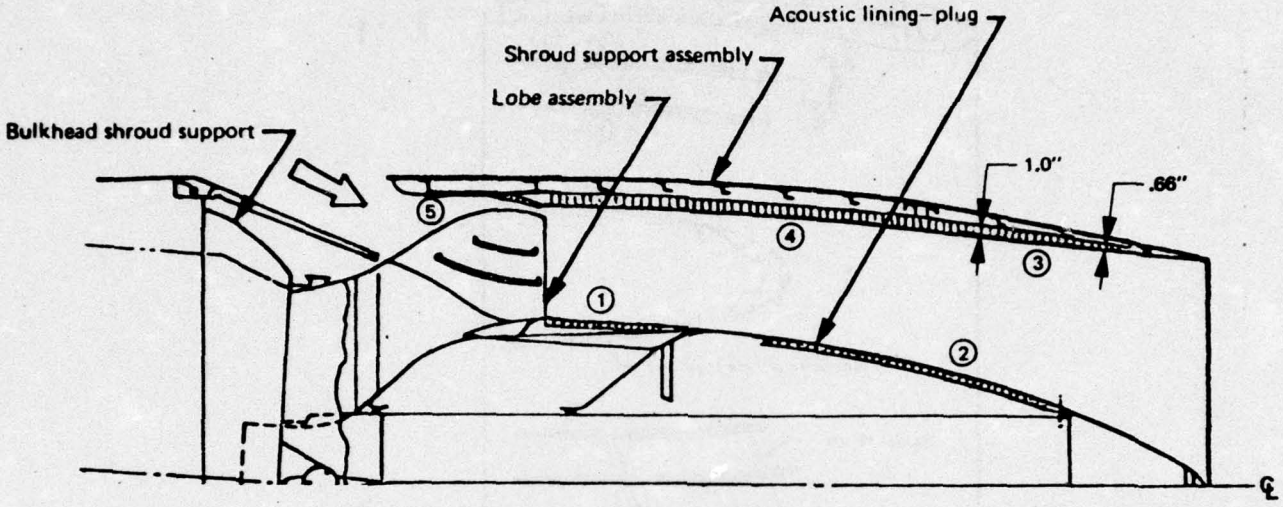


NOTE: TARGET TUNING FREQUENCIES

②,③,④,⑤ 2000 to 4000Hz

① 5000Hz

| Location | Description | Approx area ($ft^2$) | Approx length (in.) | Core size (in.) | Core depth (in.) | Hole diameter (in.) | Installed face sheet | |
|---|---|---|---|---|---|---|---|---|
| | | | | | | | Thickness (in.) | Open area (%) |
| ① | Brazed perforated sheet/honeycomb | 6 | 10 | 3/8 | 0.5 | 0.05 | 0.02 | 16 |
| ② | Brazed perforated sheet/honeycomb | 17 | 26 | 3/8 | 0.8 | 0.06 | 0.02 | 16 |
| ③ | Brazed perforated sheet/honeycomb | 20 | 19 | 3/8 | Tapered | 0.06 | 0.02 | 16 |
| ④ | Brazed perforated sheet/honeycomb | 34 | 34 | 3/8 | 1.0 | 0.06 | 0.02 | 16 |
| ⑤ | Polyimide/honeycomb | 10 | 11 | 3/8 | 0.25 | 35 cgs Rayls at 150 dB overall sound pressure level | | |

*Figure 11.—(Concluded)*

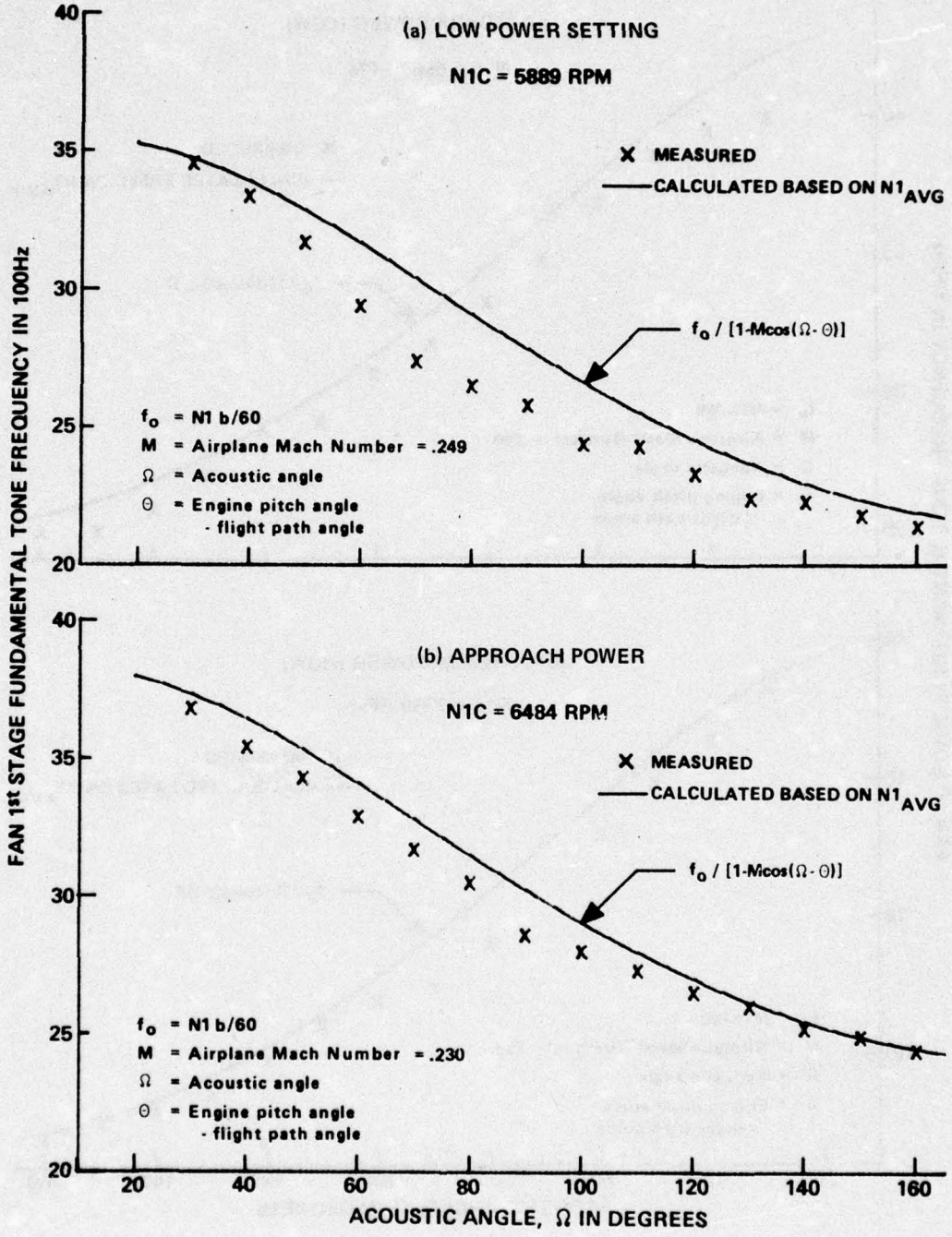


*Figure 12.—Comparison of Calculated and Measured Doppler Frequency Shift*

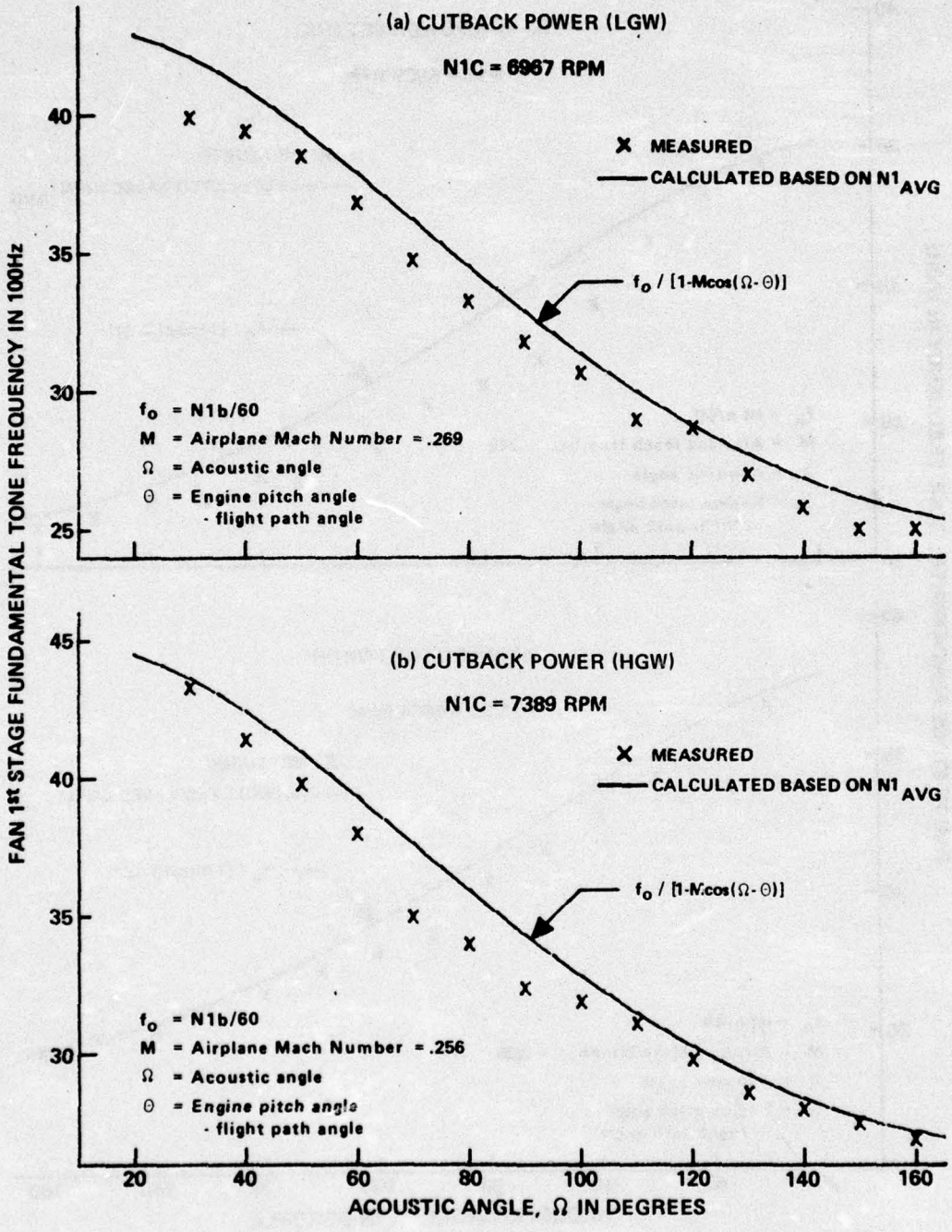


*Figure 12.—(Concluded)*

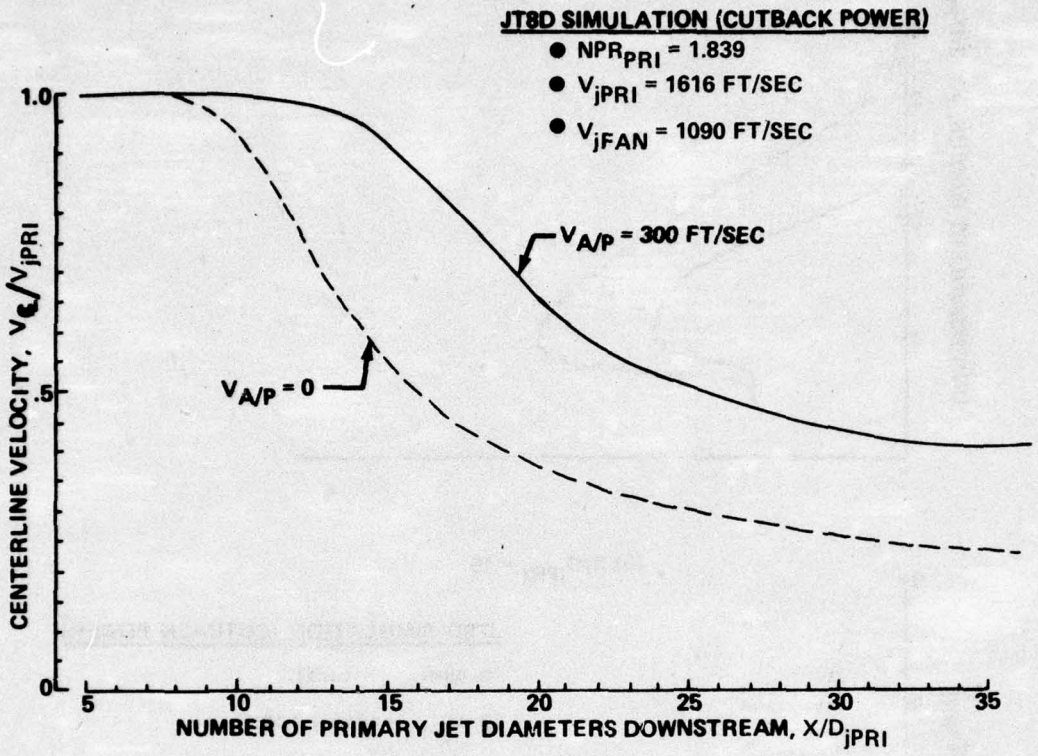


*Figure 13.—Analytical Prediction of the Centerline Velocity Decay of a Dual-Flow Jet (Lu/Flow Computer Program)*

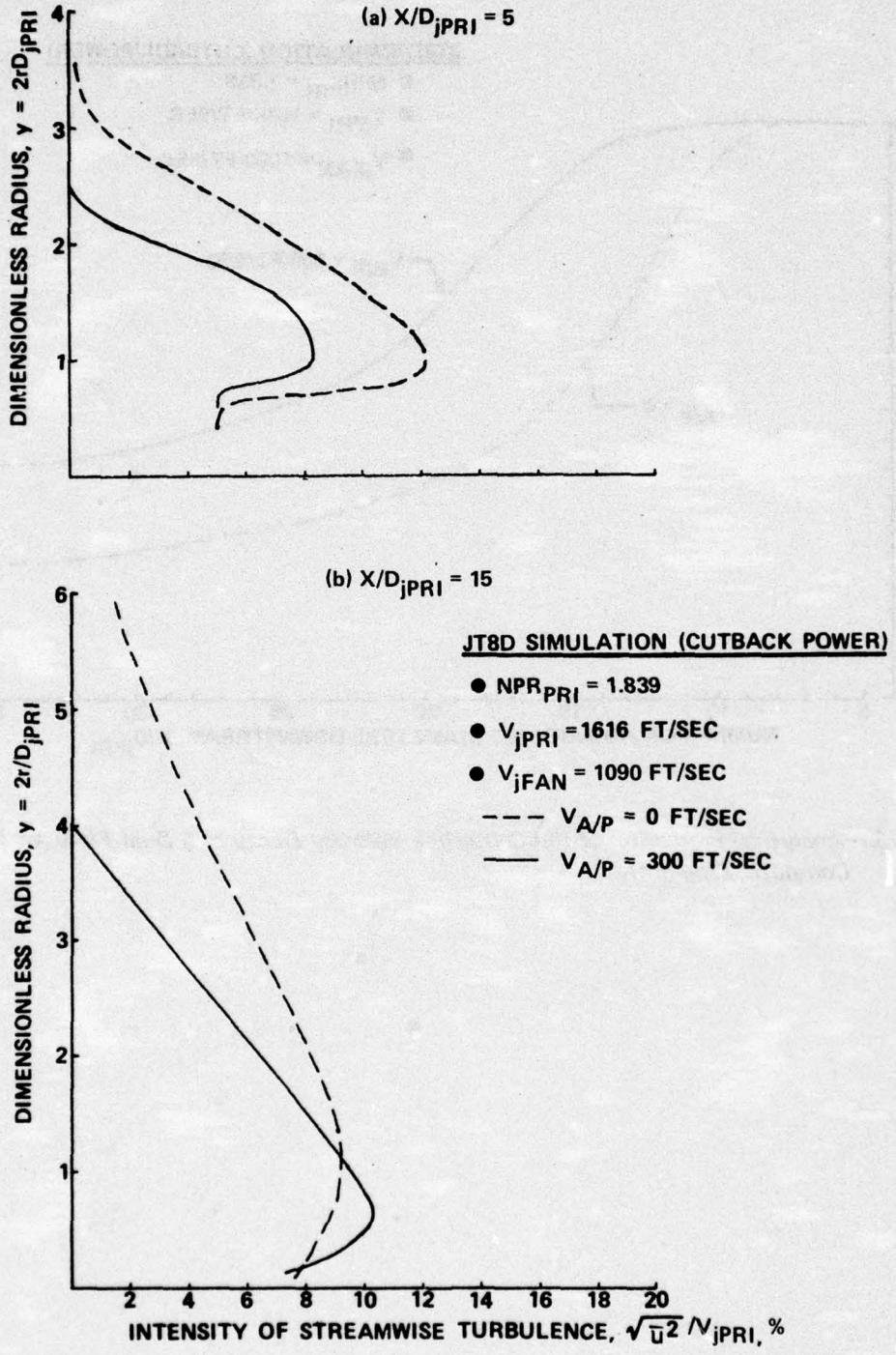


*Figure 14.—Analytical Prediction of the Radial Distribution of the Turbulence Intensity of a Dual-Flow Jet (Lu/Flow Computer Program)*

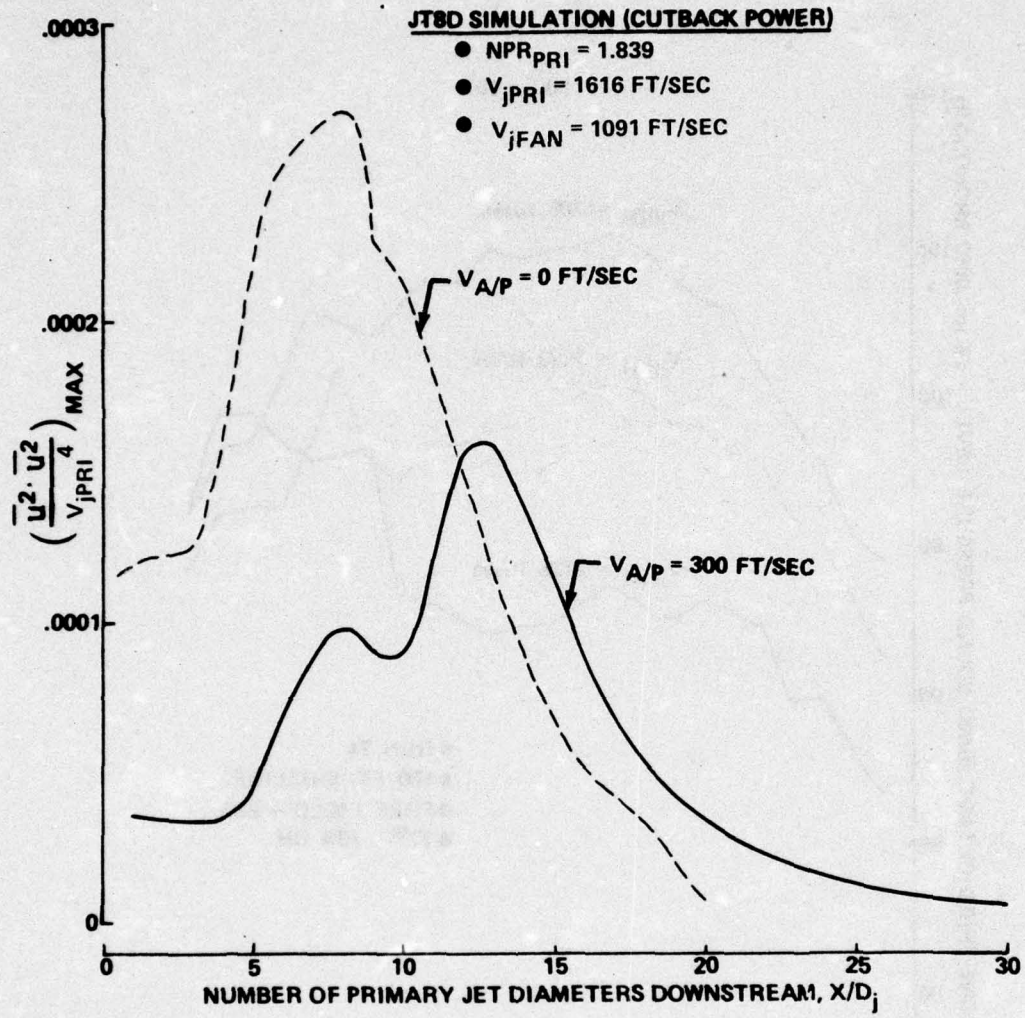


*Figure 15.—Analytical Prediction of the Distribution Along the Jet Axis of the Maximum Value of the Noise-Turbulence Correlating Parameter (Lu/Flow Computer Program)*

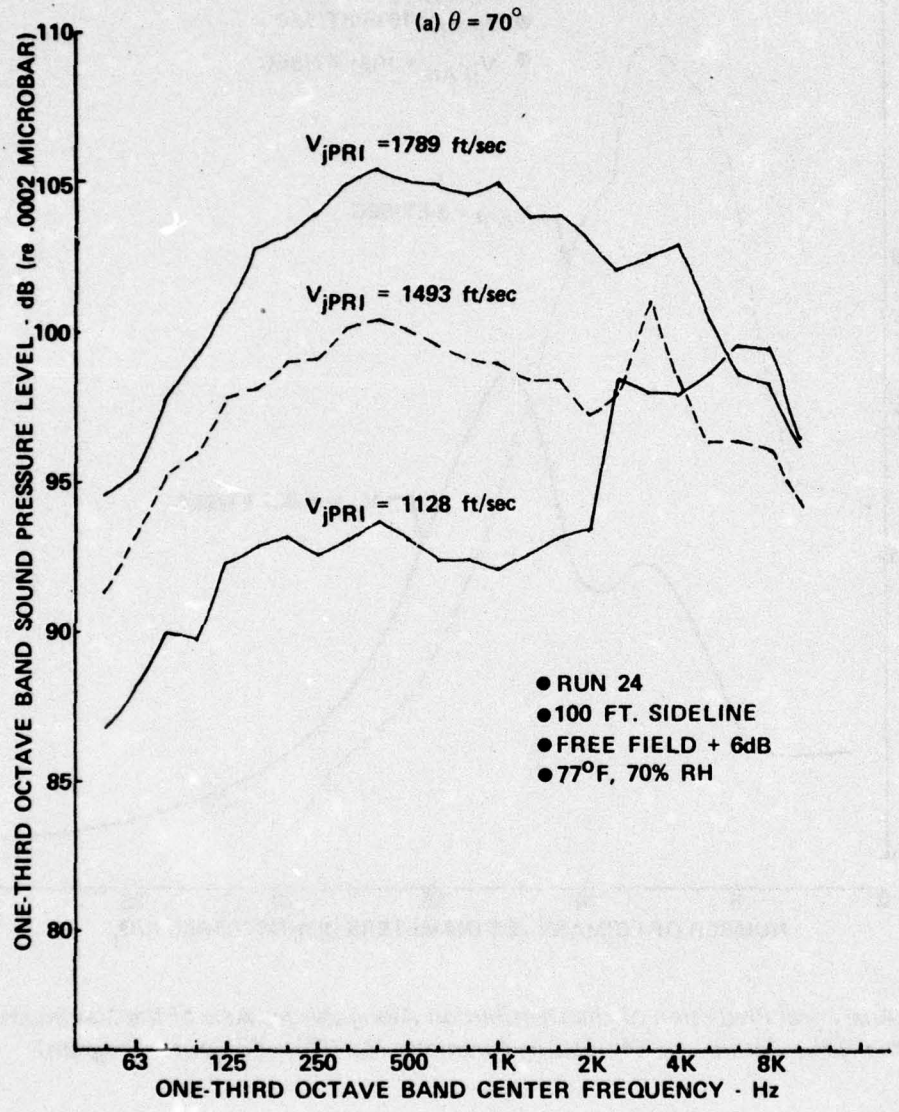


*Figure 16.—Baseline Static Noise Spectra*

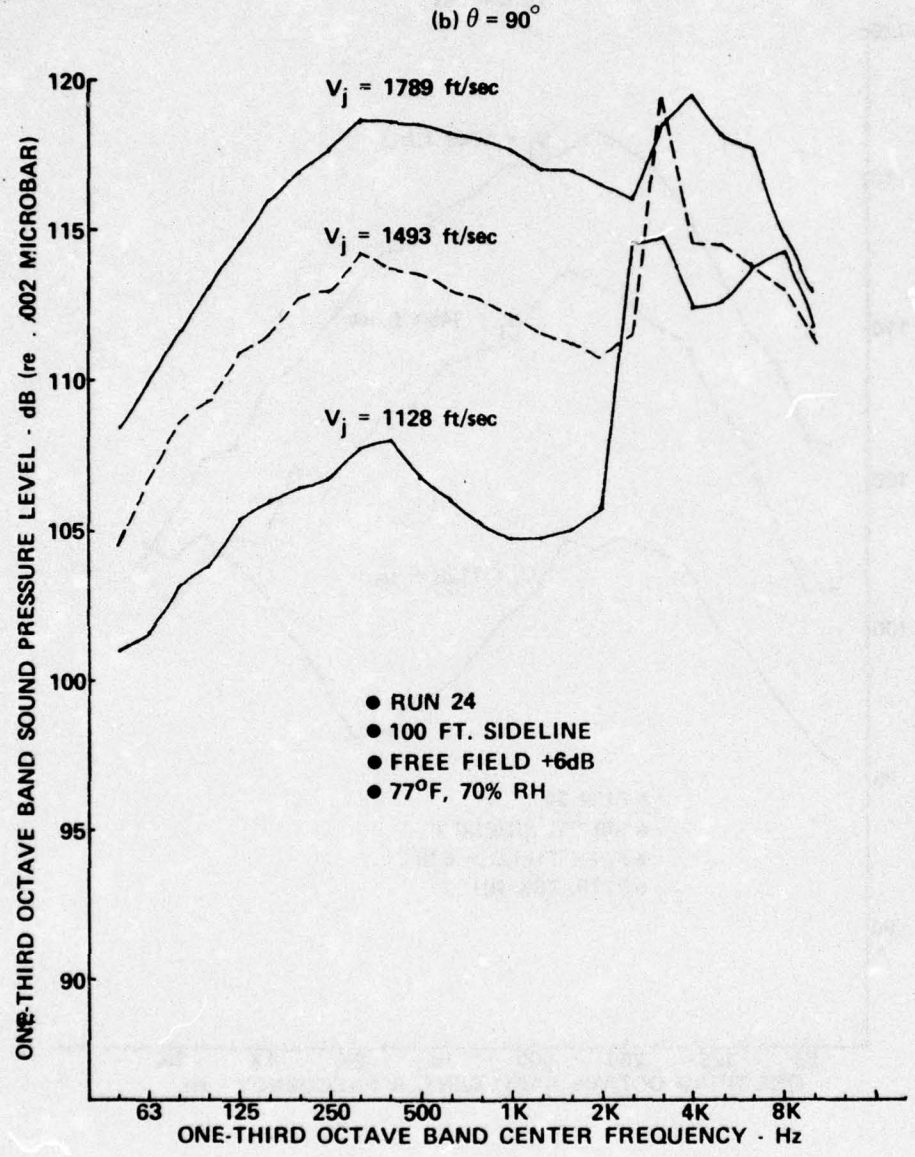


*Figure 16.—(Continued)*

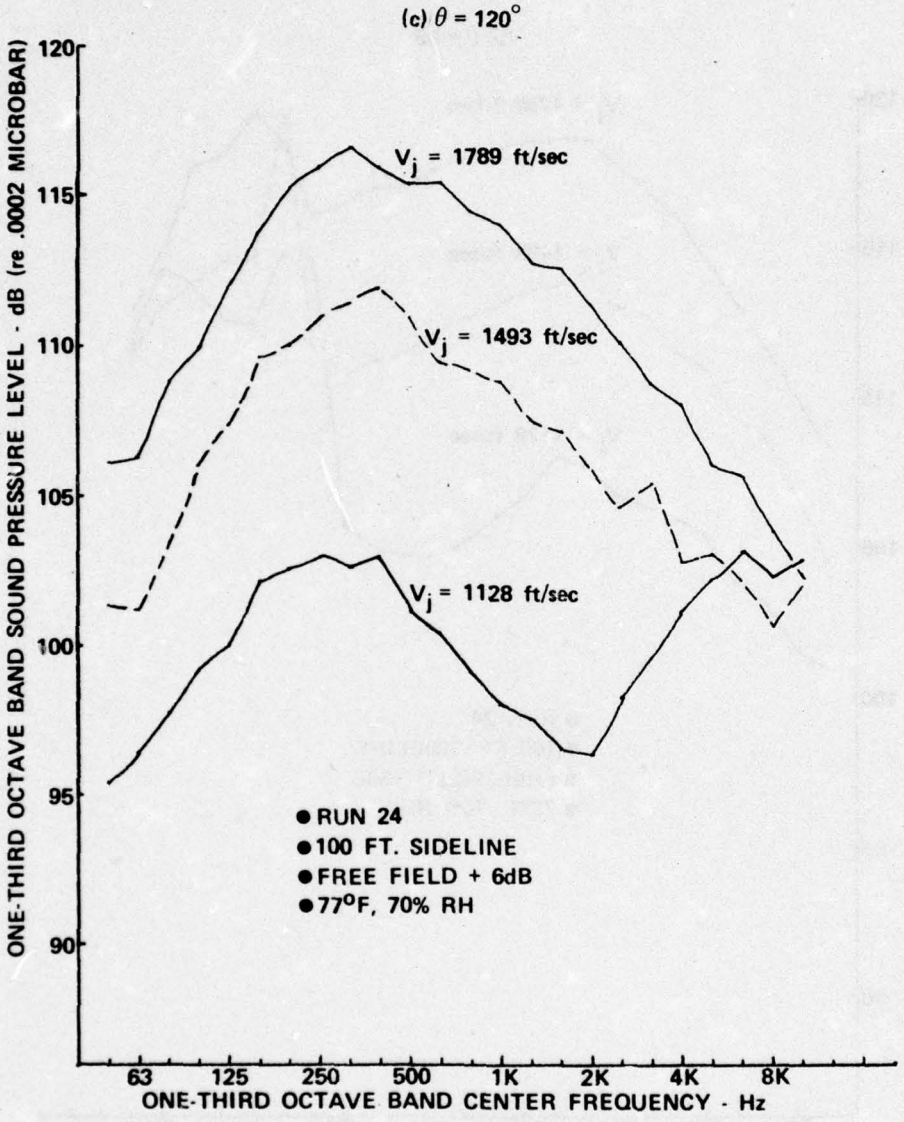


*Figure 16.—(Continued)*

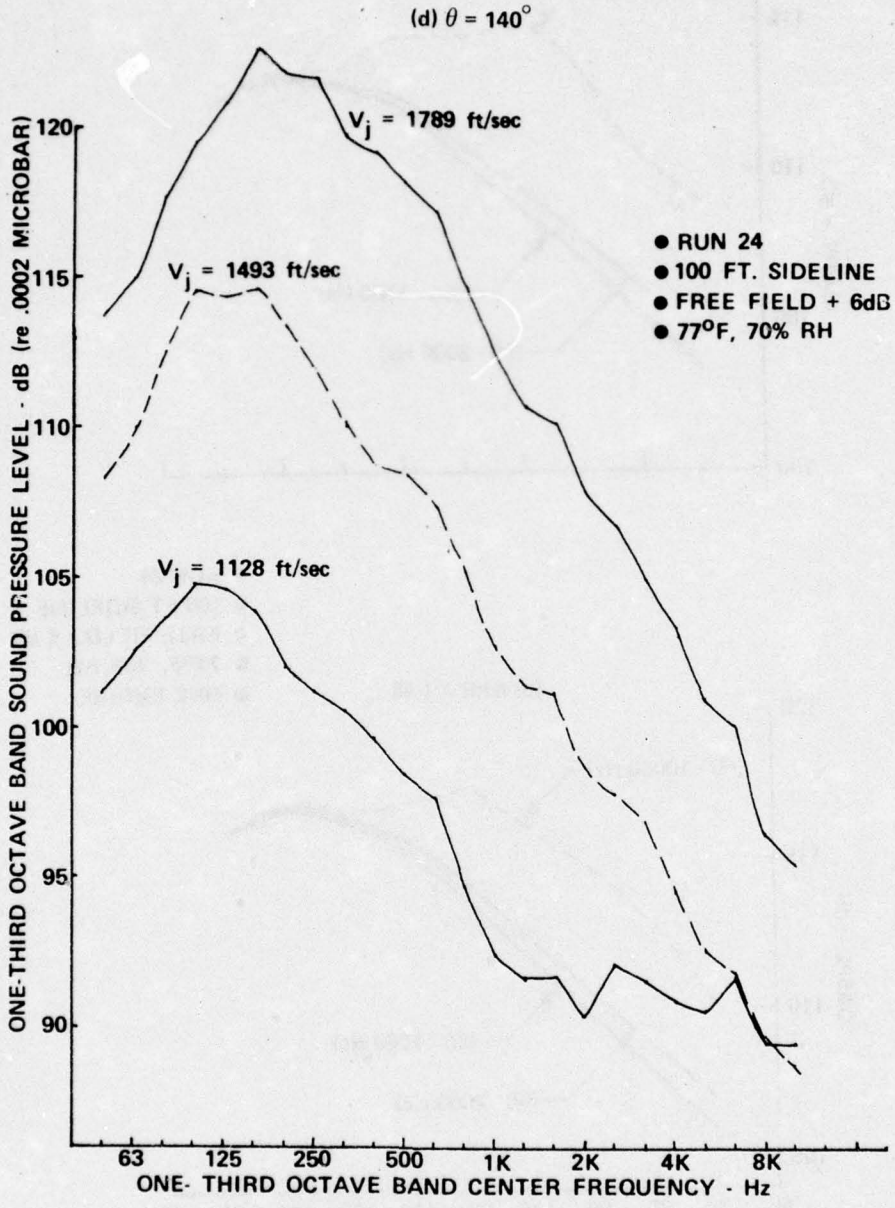


*Figure 16.—(Concluded)*

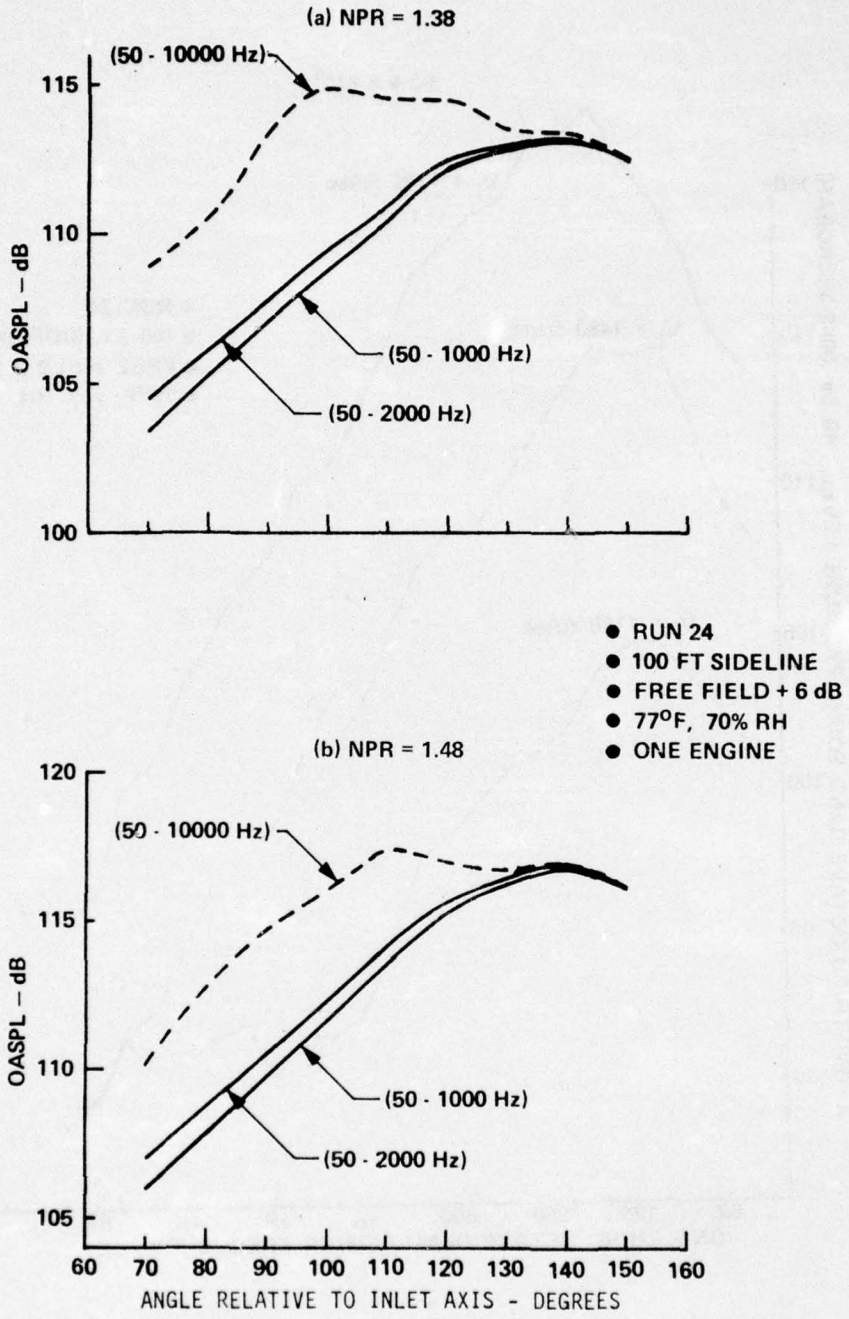


*Figure 17.—Baseline Static OASPL (50 to 1000 Hz), OASPL (50 to 2000 Hz) and OASPL (50 to 10 000 Hz) Directivities*

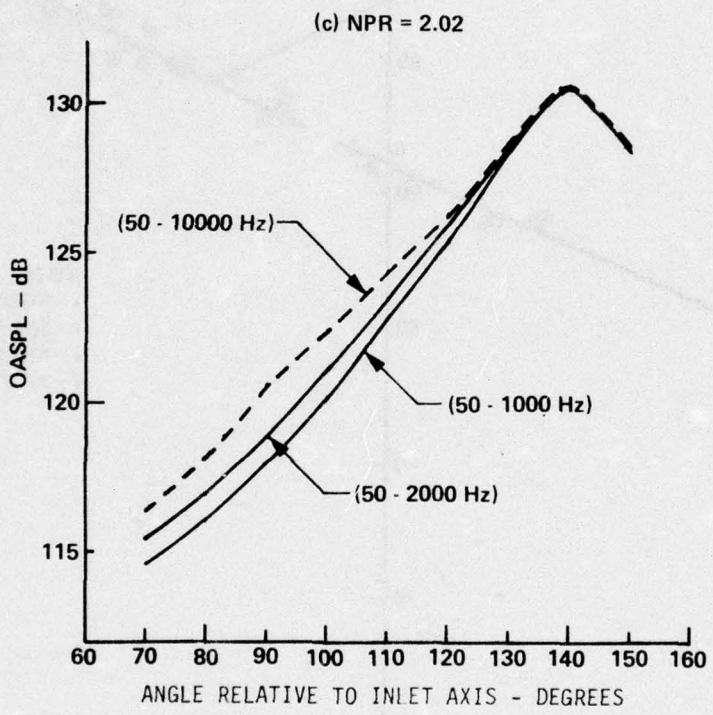


*Figure 17.—(Concluded)*

- RUN 24
- 100 FT SIDELINE
- FREE FIELD + 6 dB
- 77°F, 70% RH
- ONE ENGINE

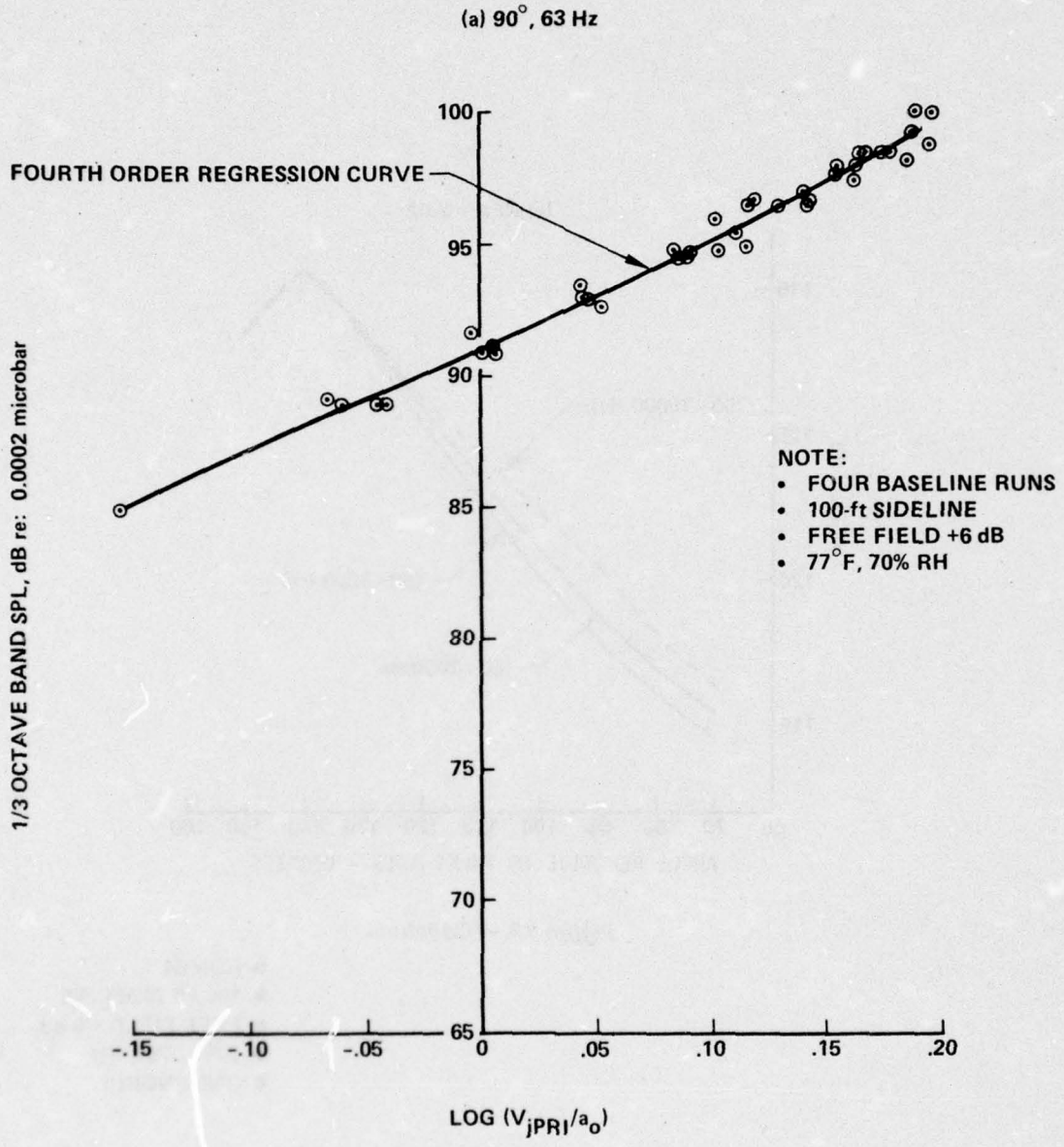


*Figure 18.—Baseline Static Noise Data Versus Engine Power Setting, $\theta = 90°$*

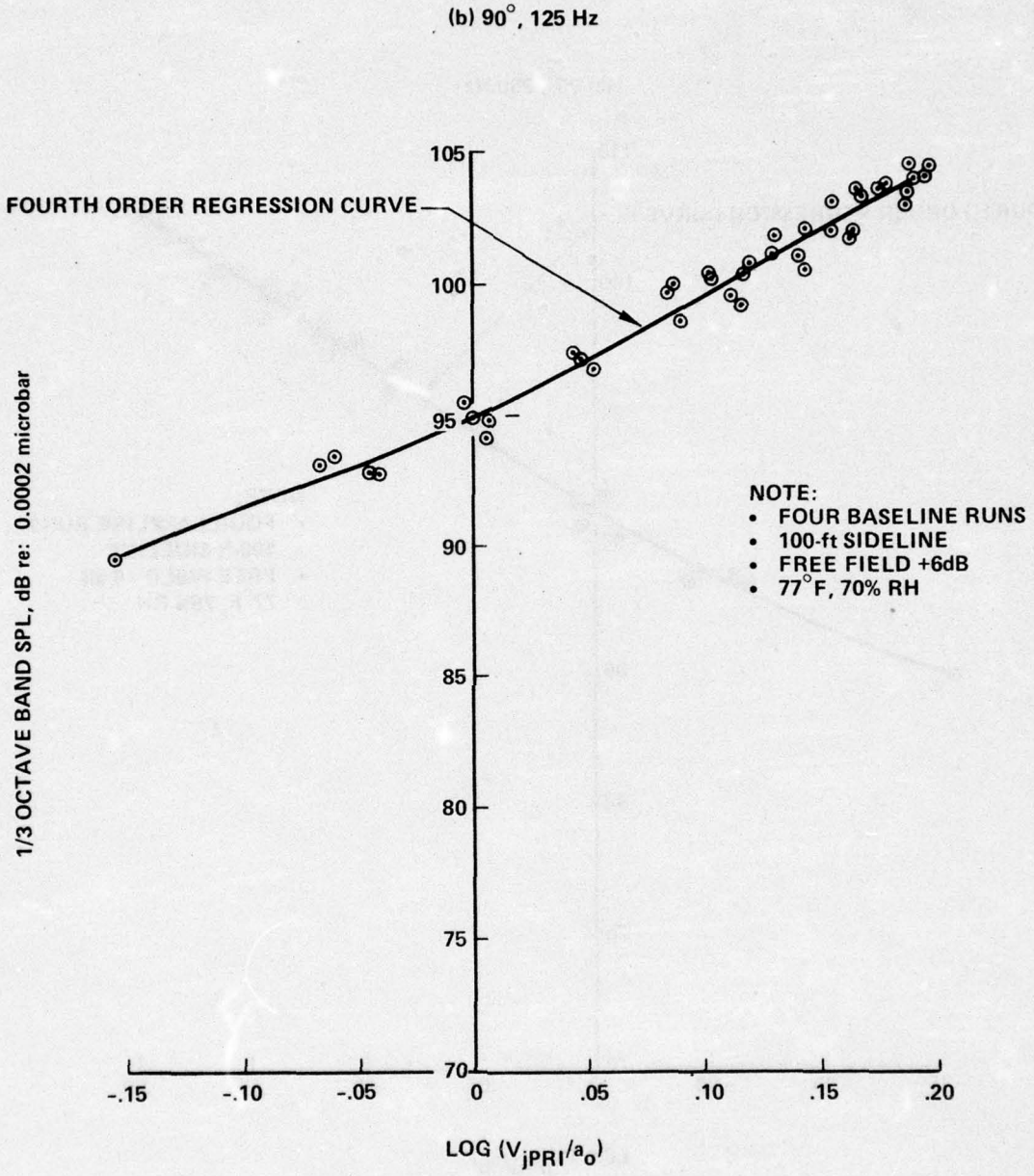


*Figure 18.—(Continued)*

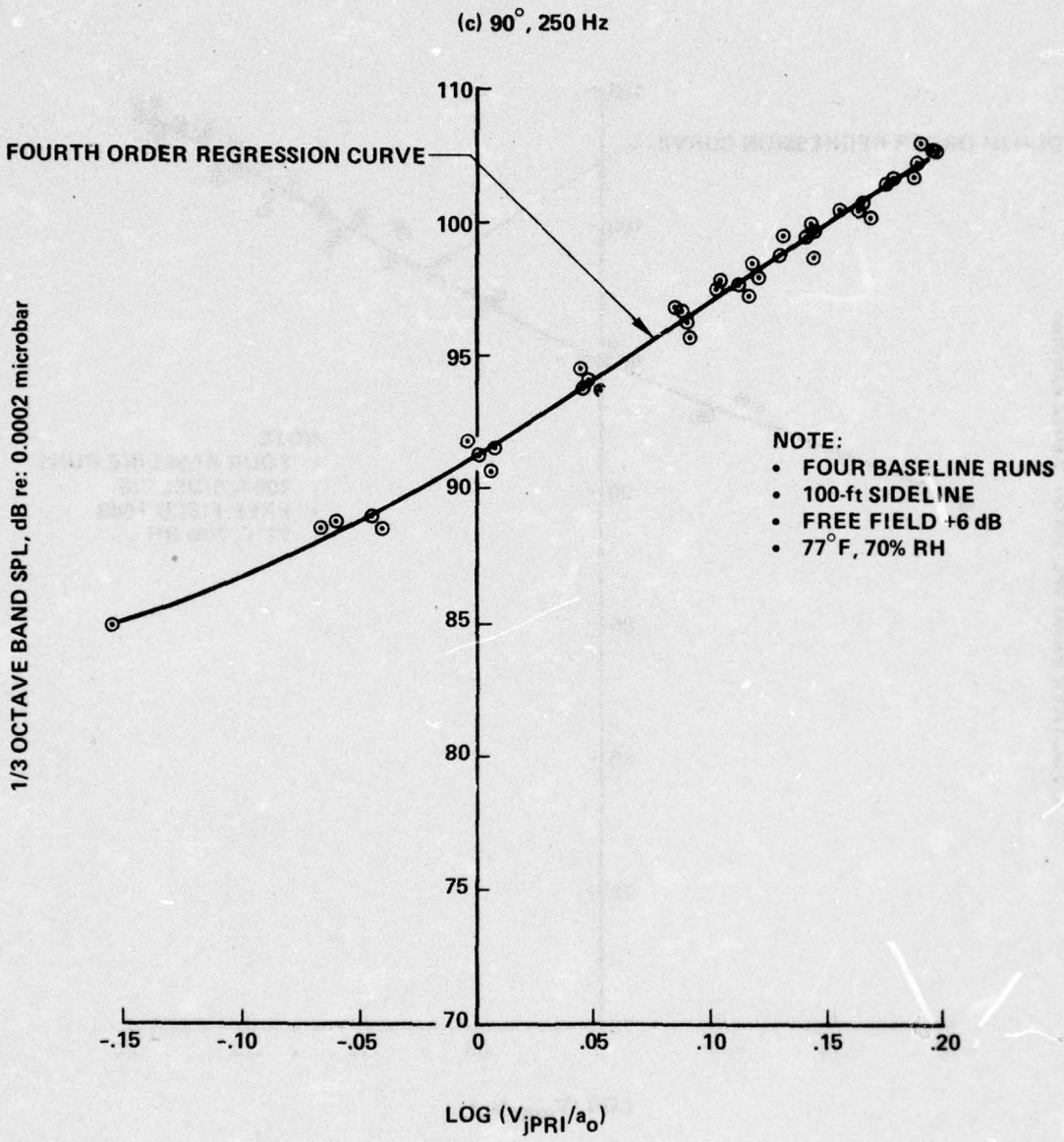


*Figure 18.—(Continued)*

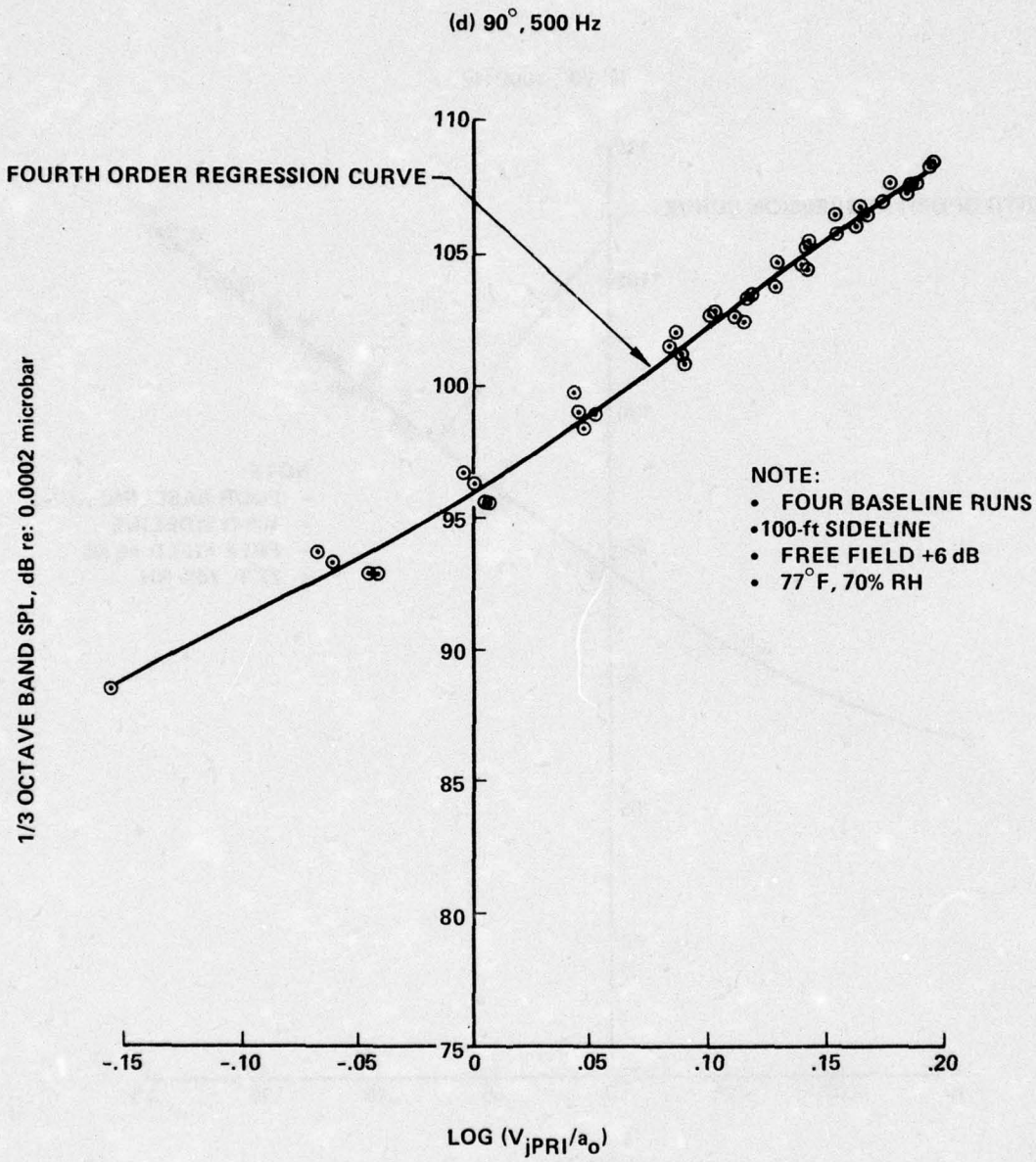


*Figure 18.—(Continued)*

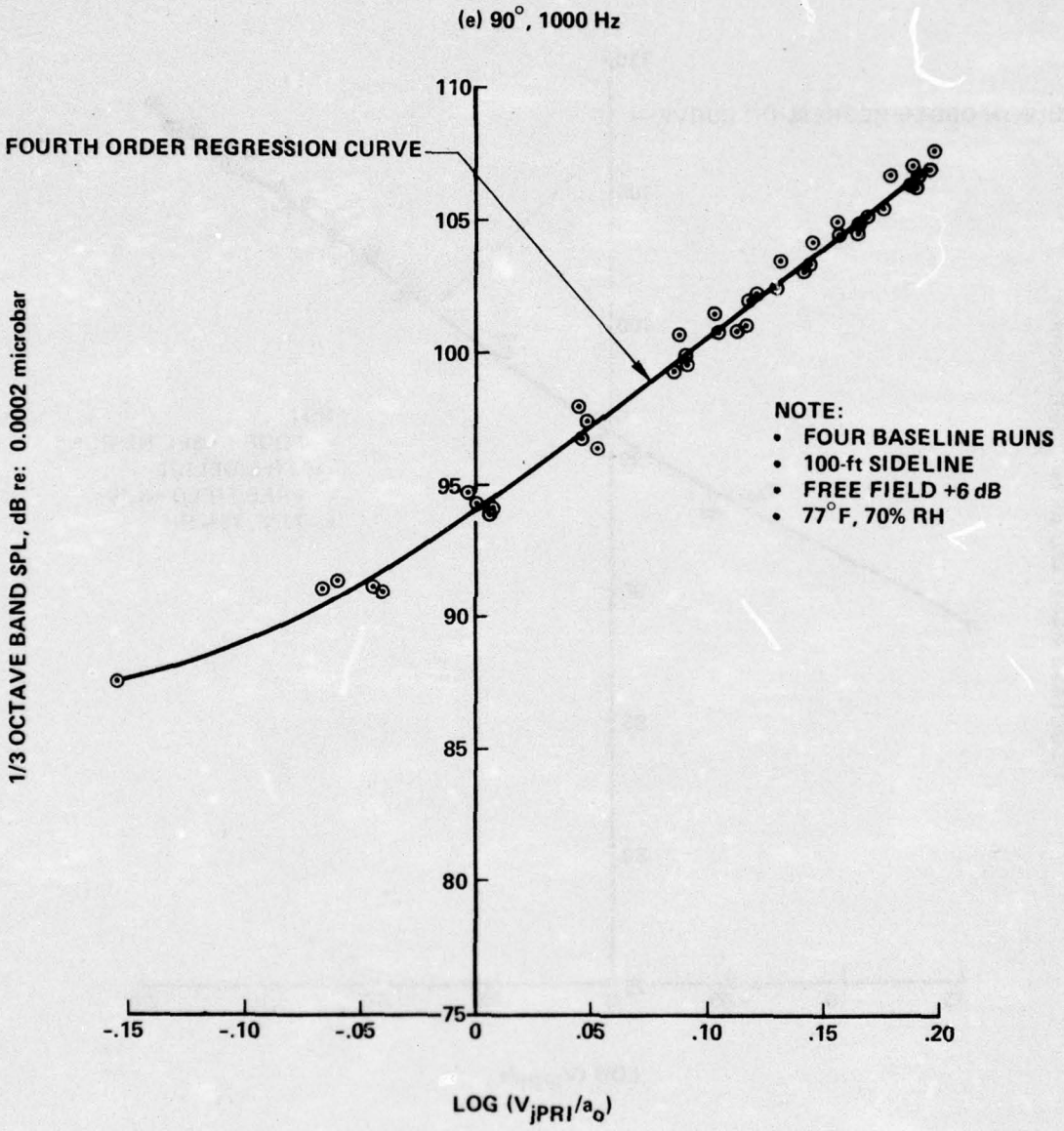


*Figure 18.—(Concluded)*

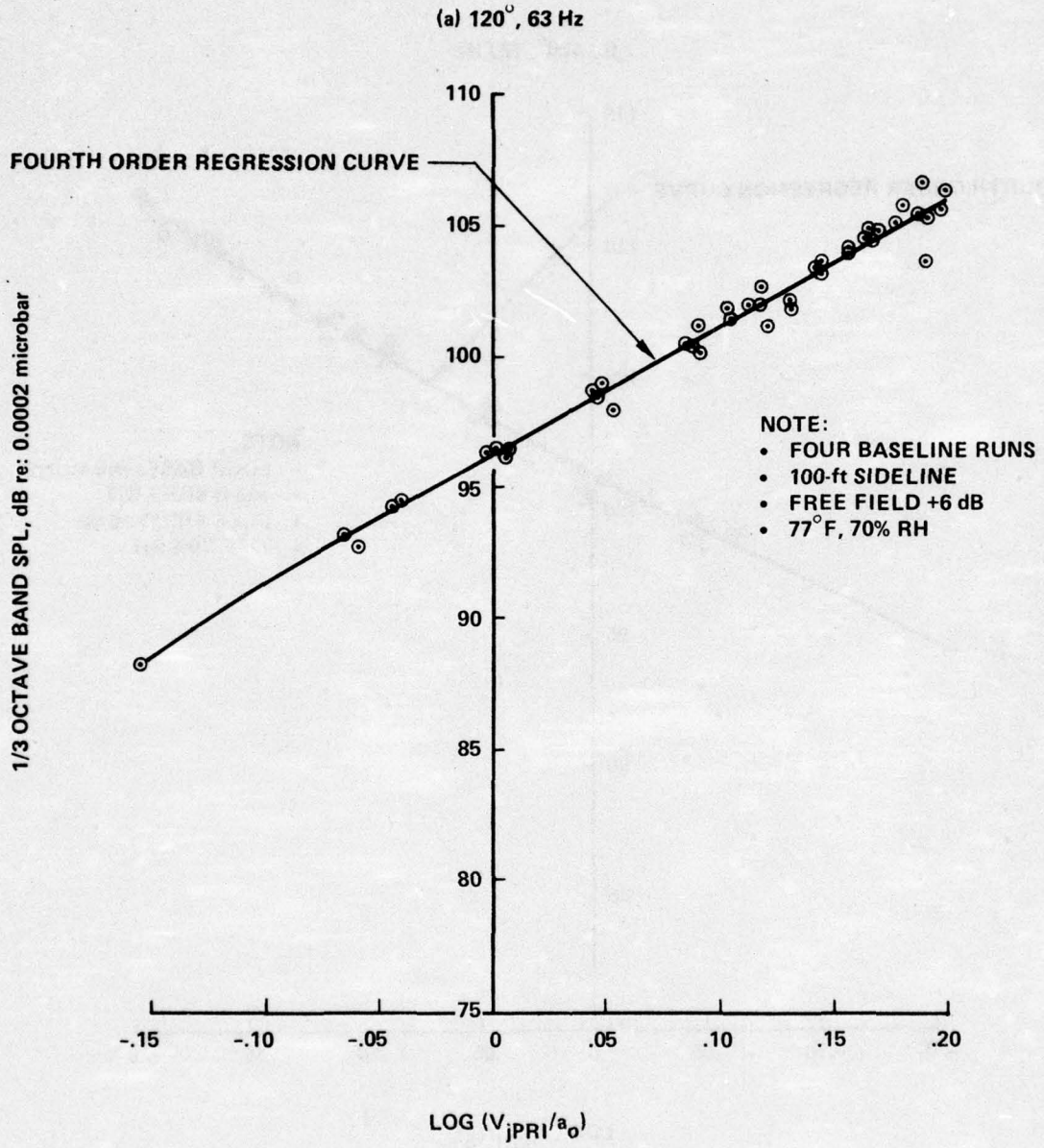


*Figure 19.—Baseline Static Noise Data Versus Engine Power Setting, $\theta = 120°$*

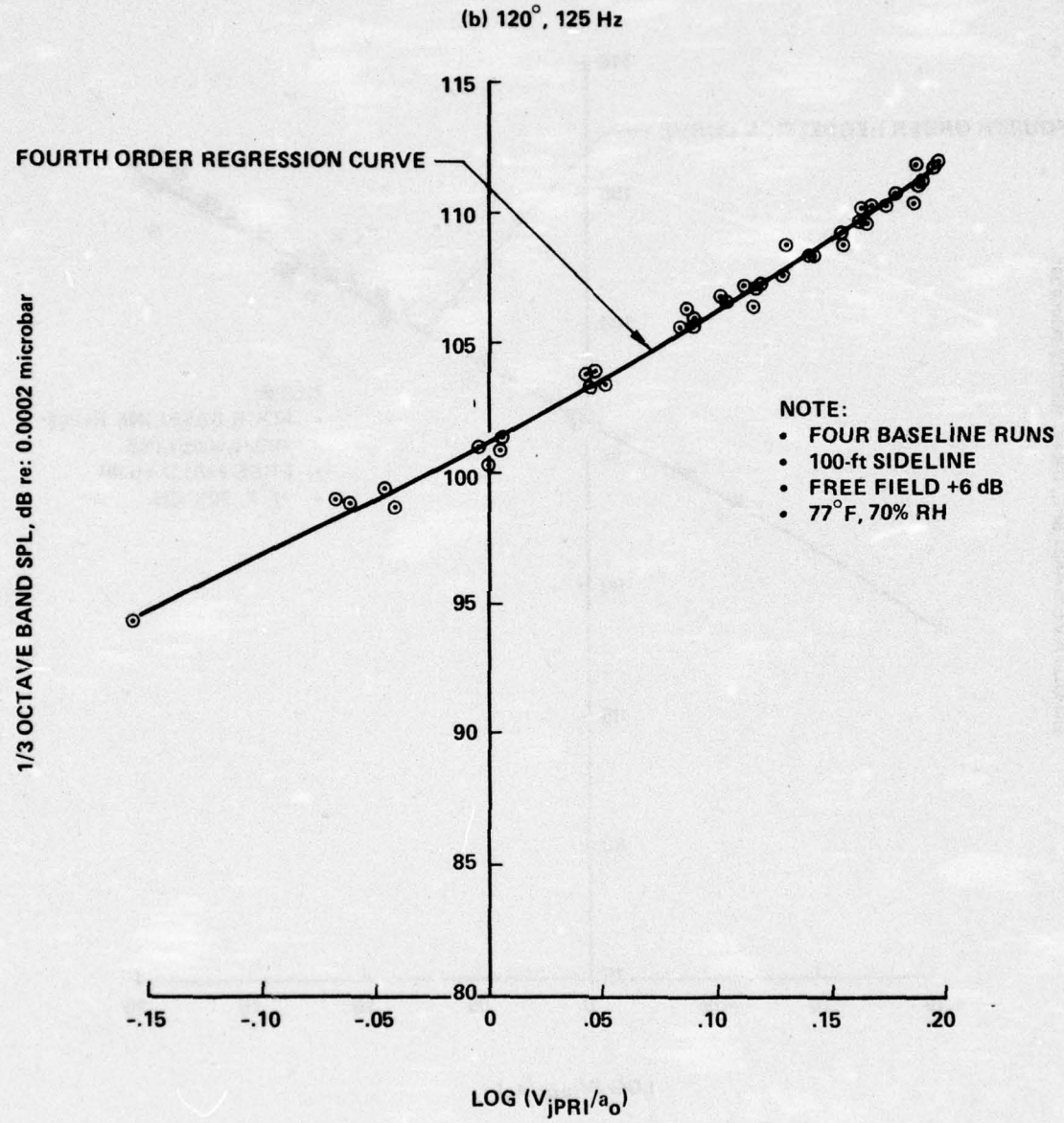


*Figure 19.—(Continued)*

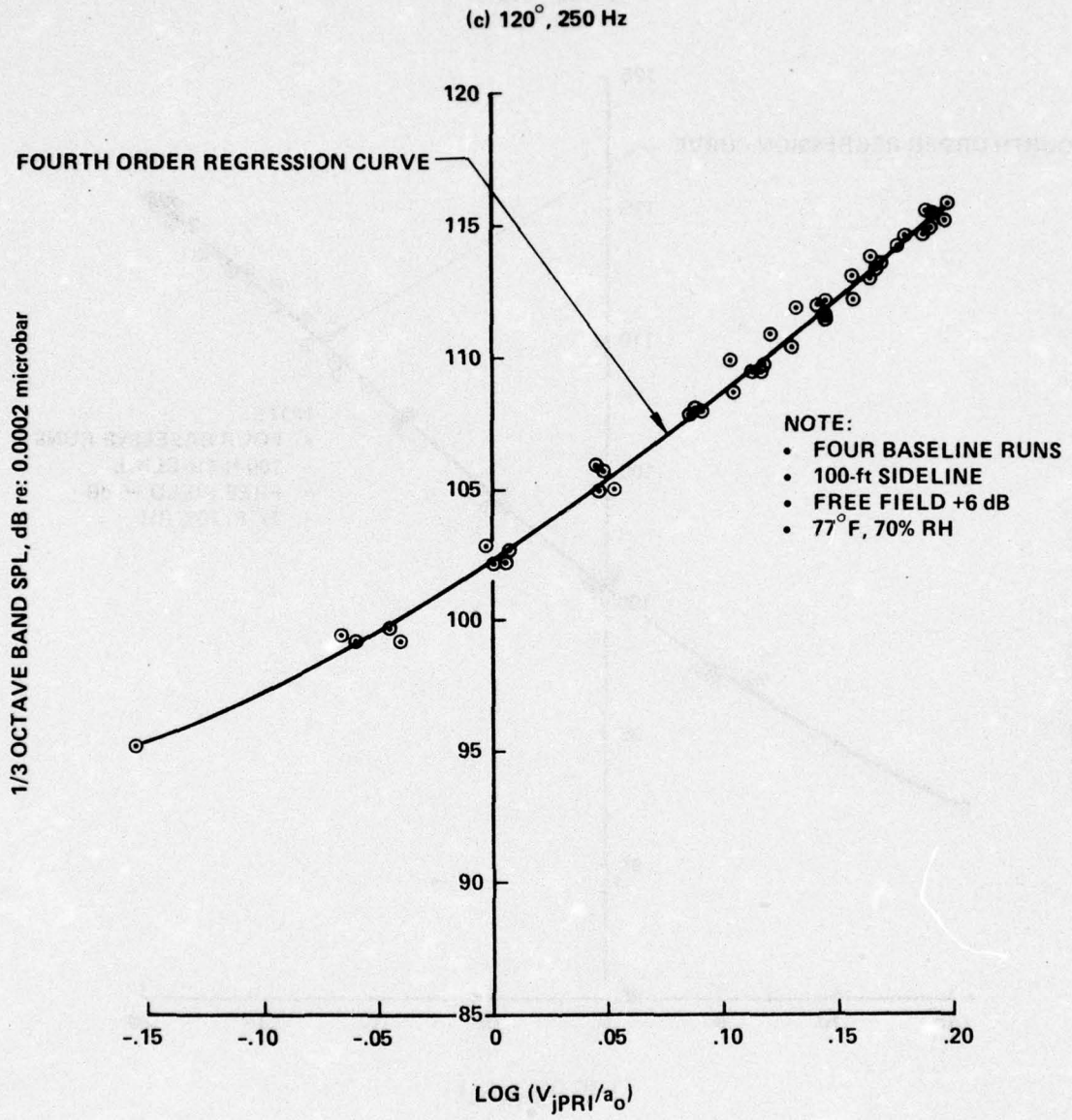


*Figure 19.—(Continued)*

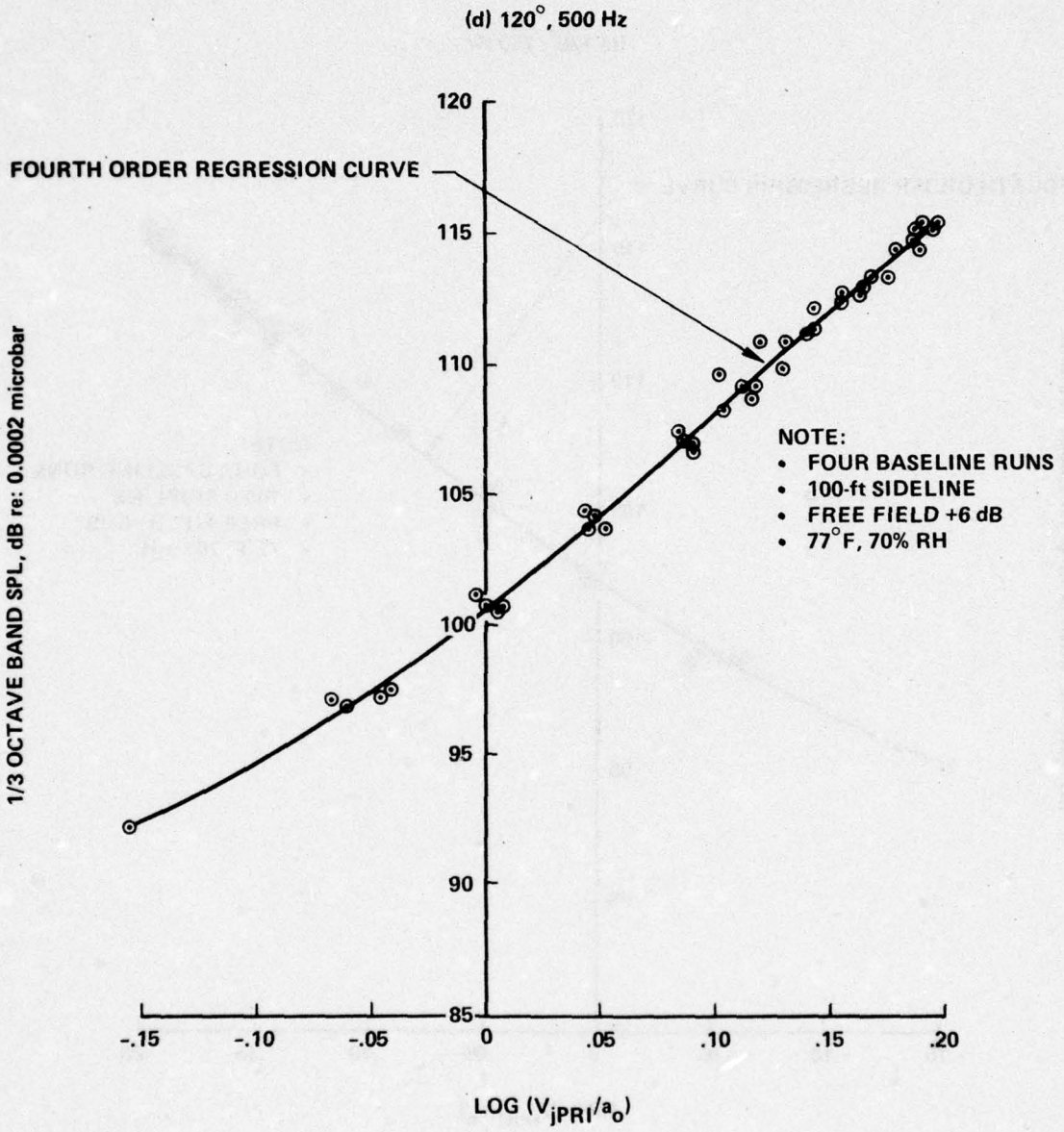


*Figure 19.—(Continued)*

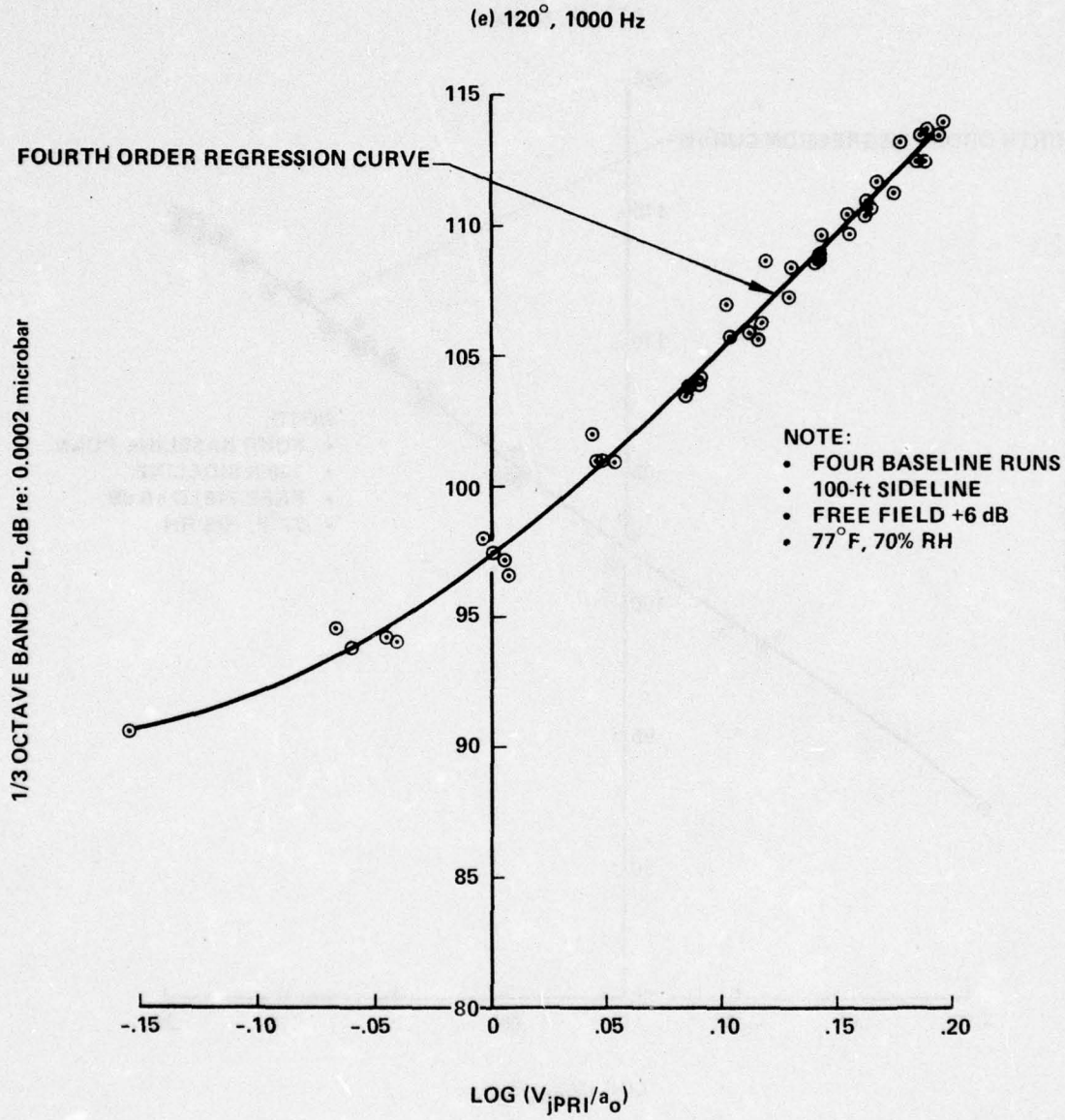


*Figure 19.—(Concluded)*

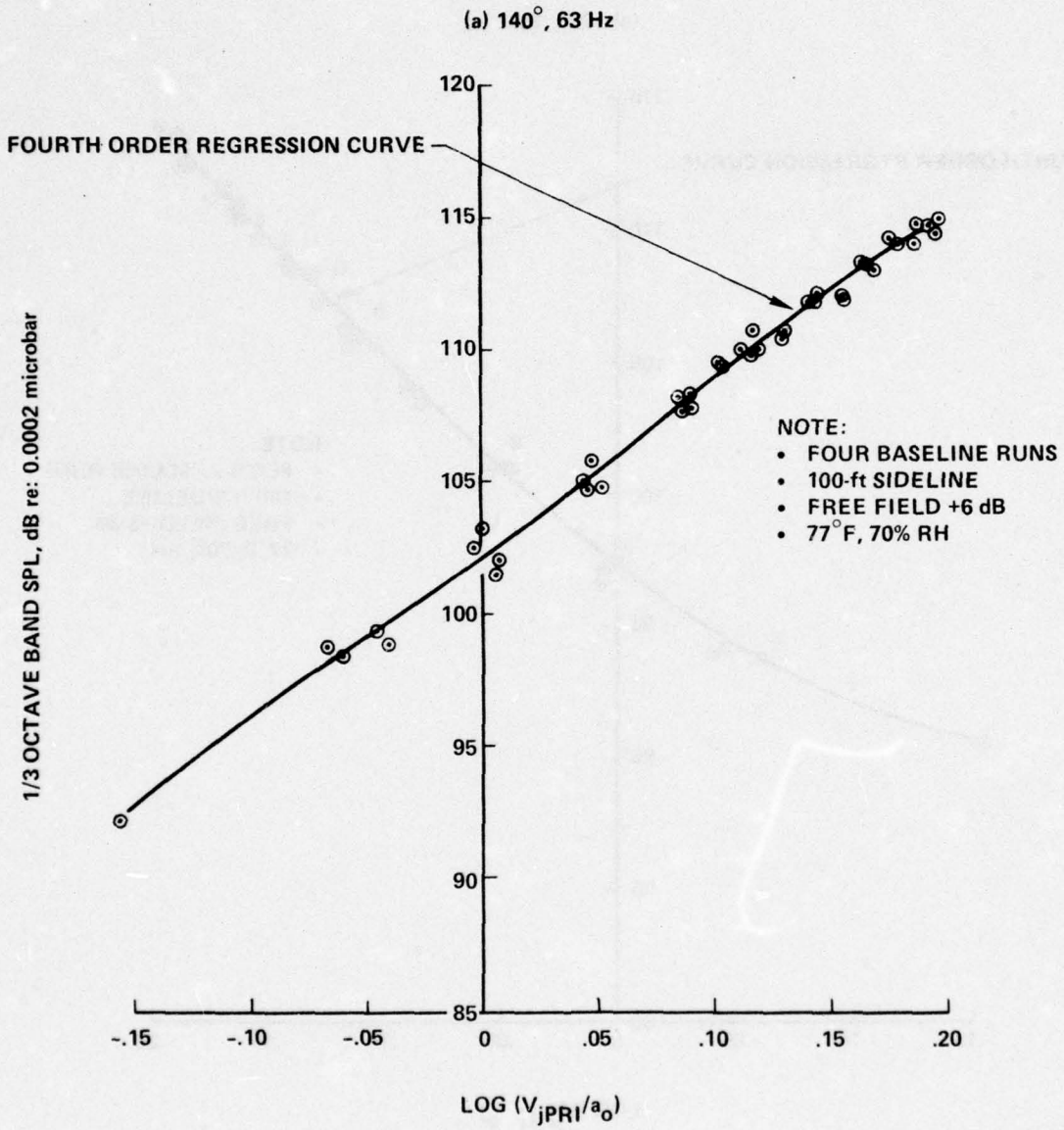


*Figure 20.—Baseline Static Noise Data Versus Engine Power Setting, $\theta = 140°$*

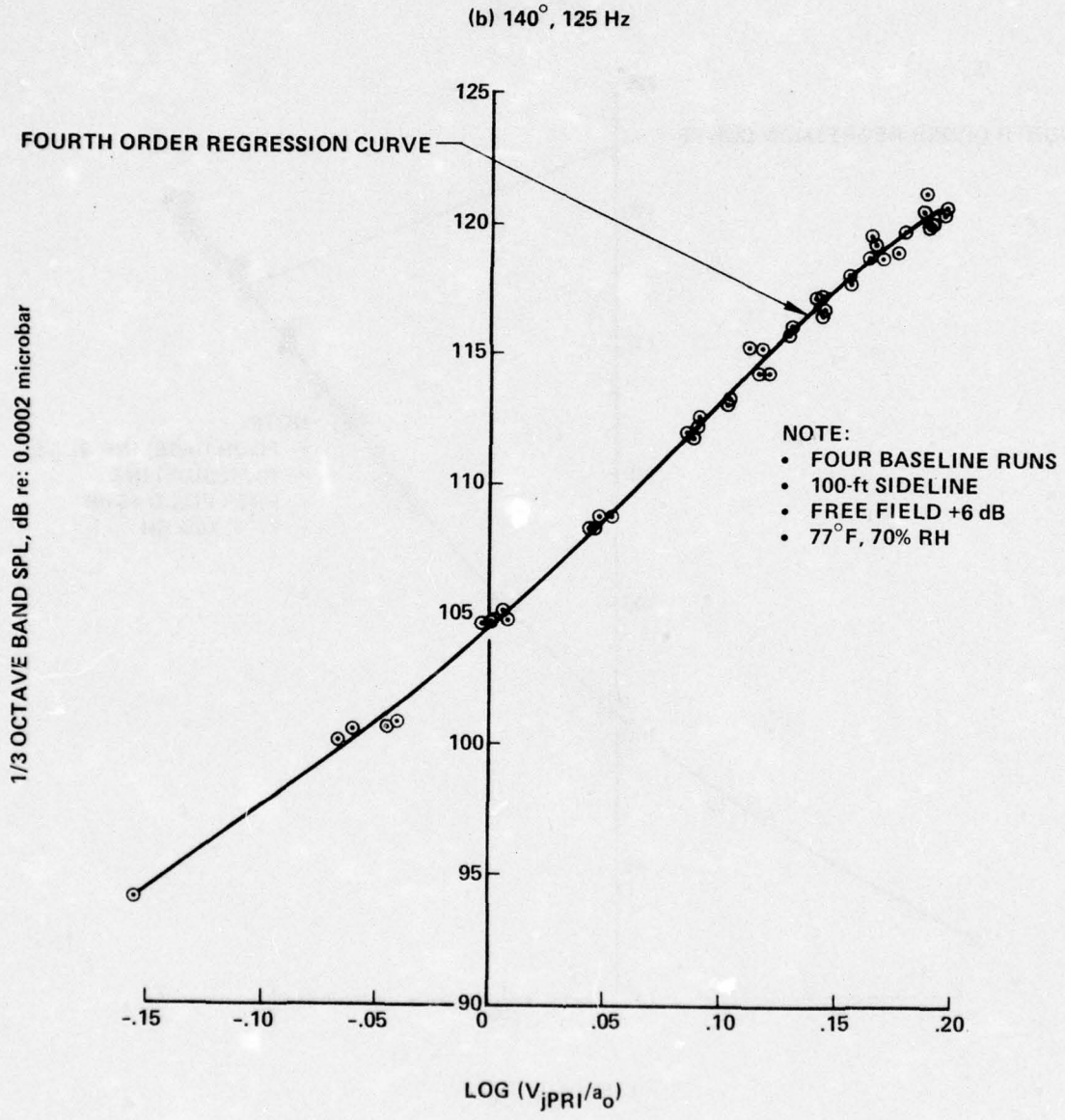


*Figure 20.—(Continued)*

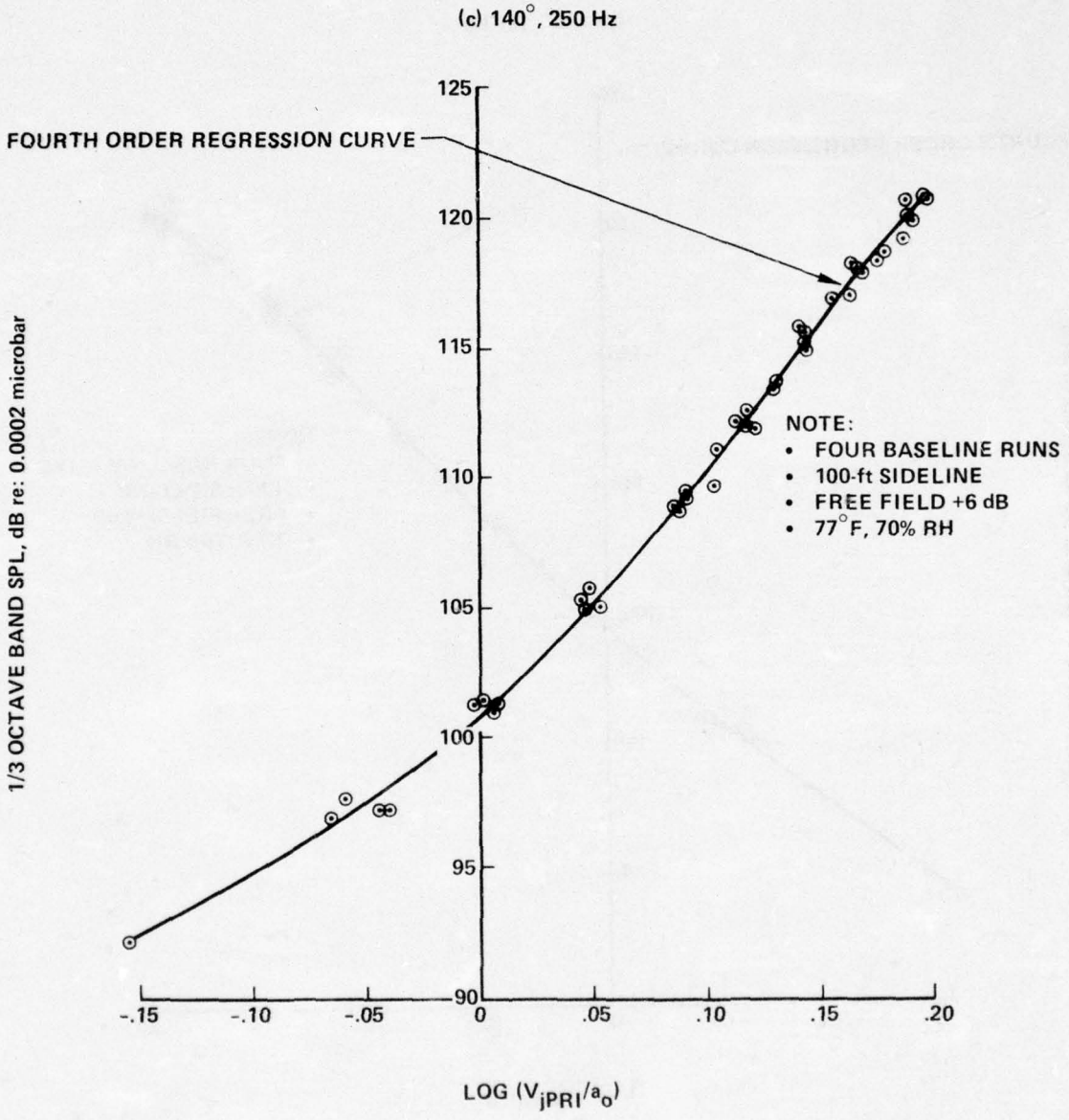


*Figure 20.—(Continued)*

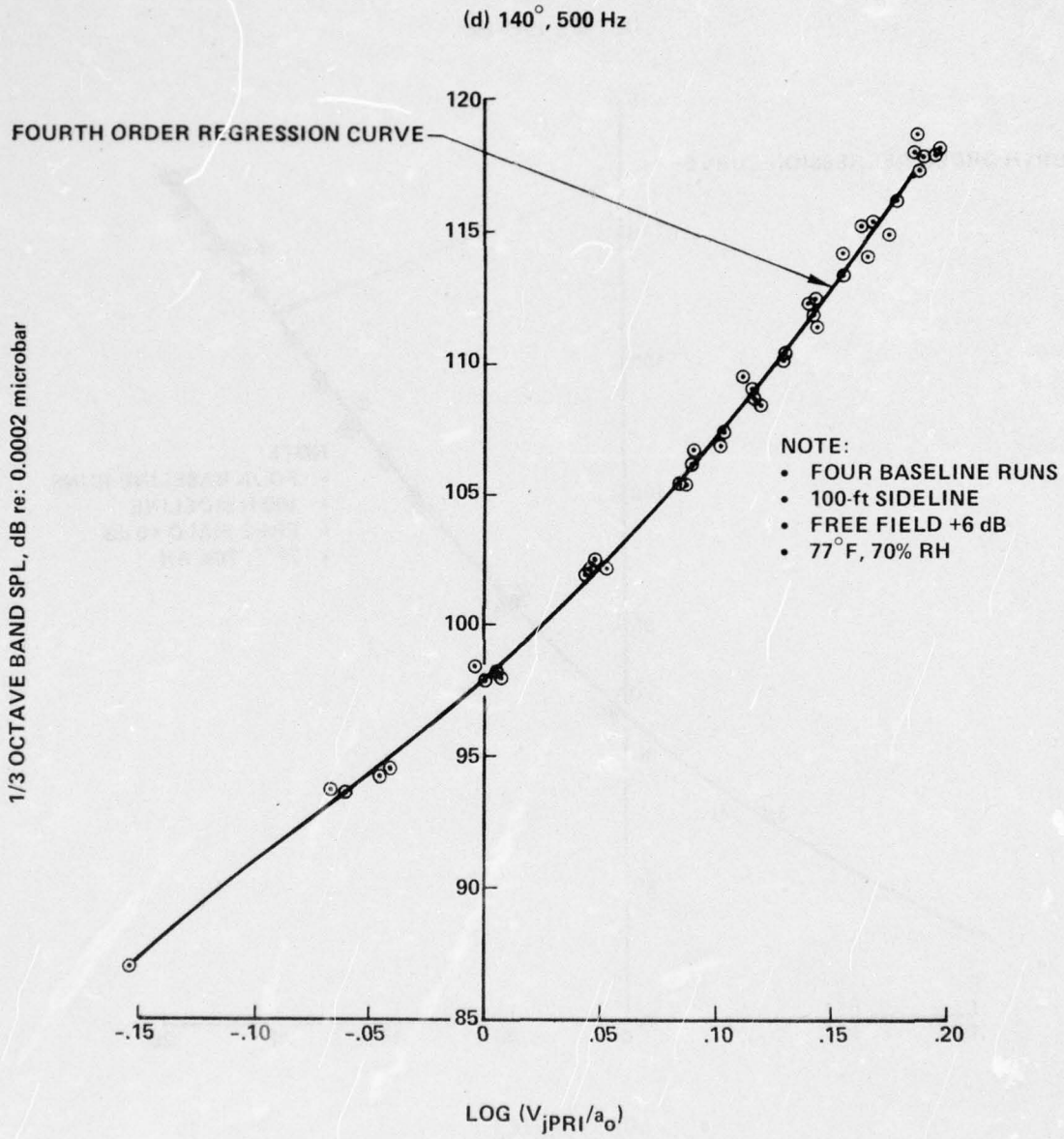


*Figure 20.—(Continued)*

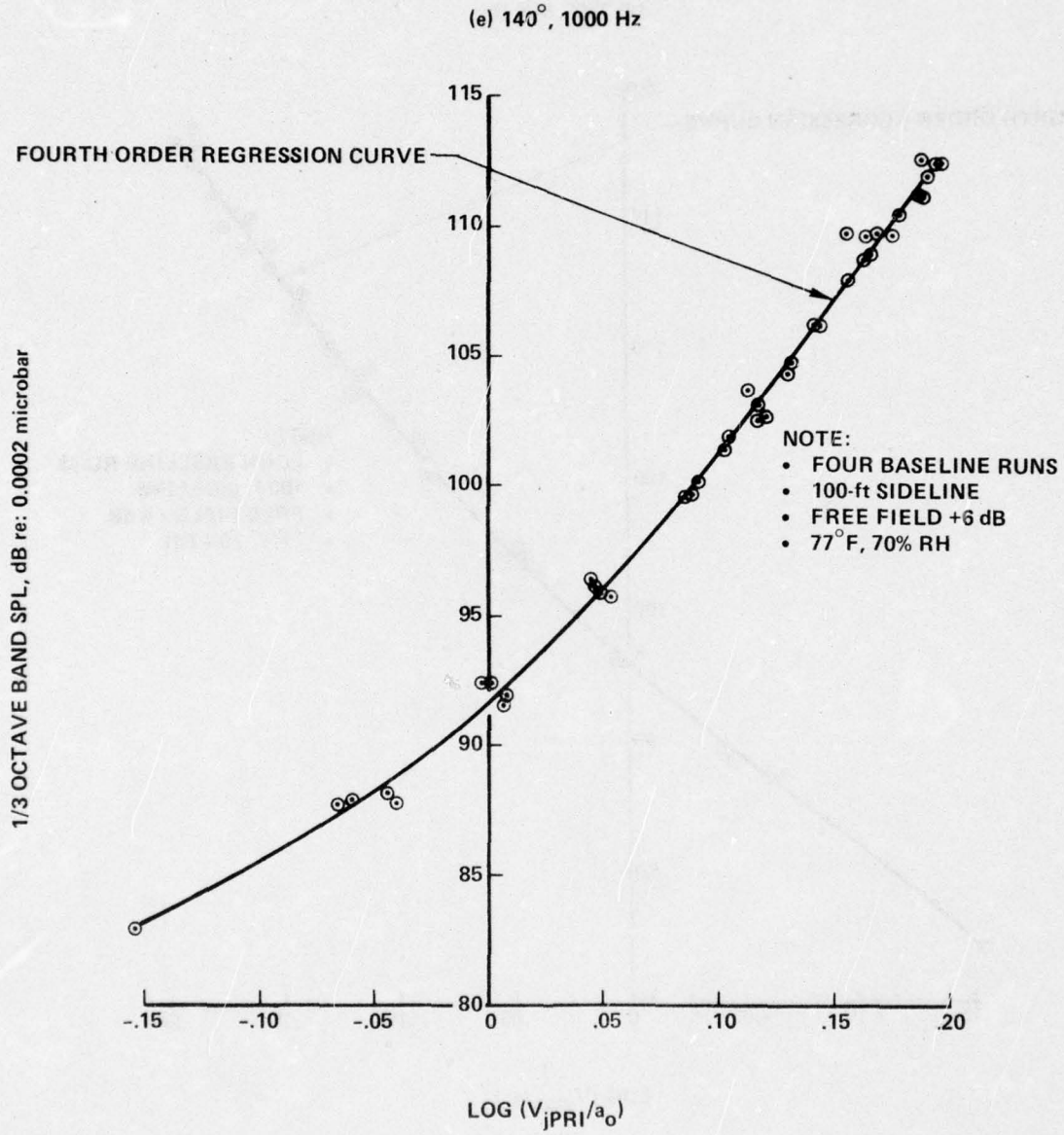


*Figure 20.—(Concluded)*

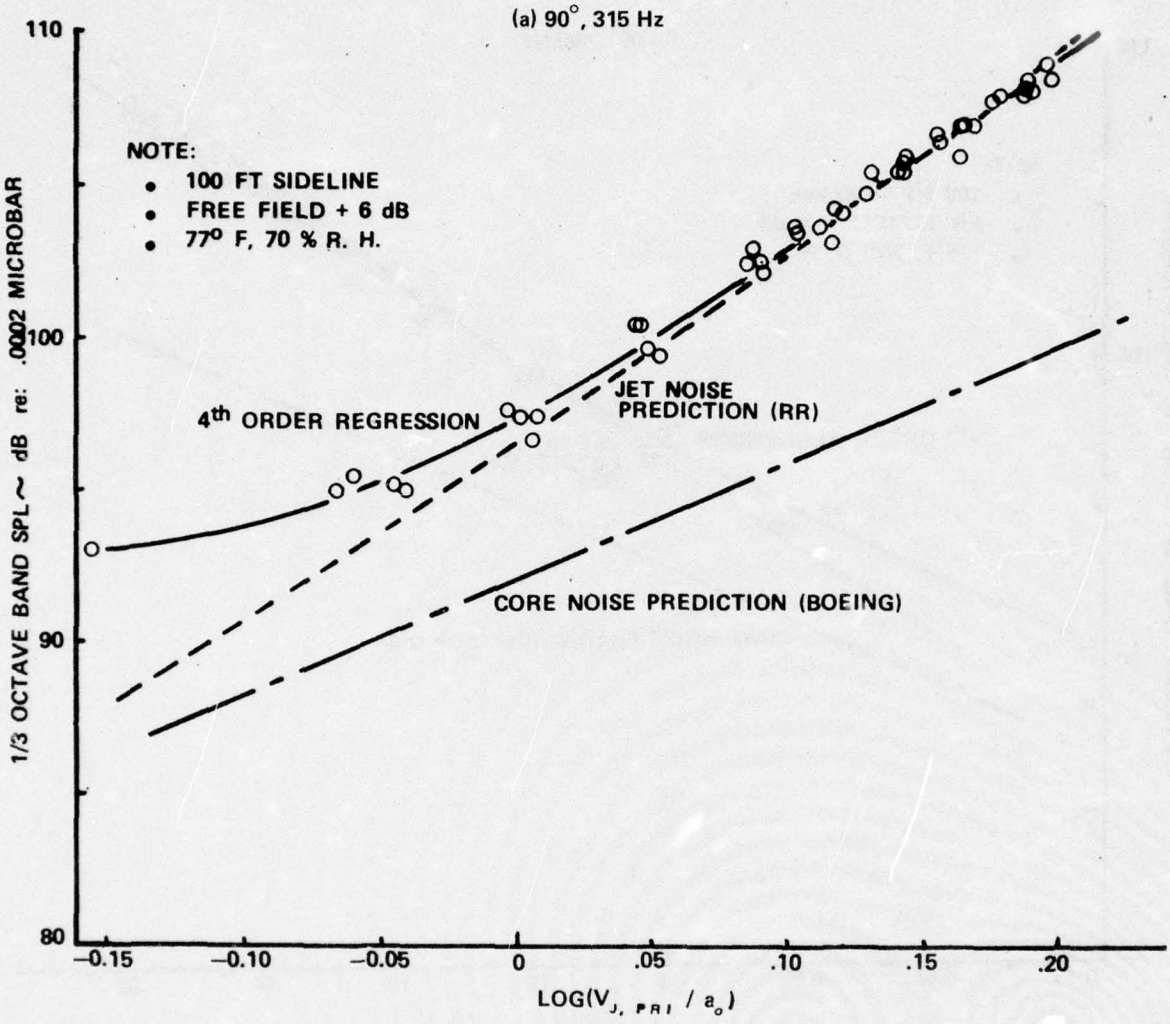


*Figure 21.—Comparison of Static Jet and Core Noise Predictions With Measured Baseline Noise Data*

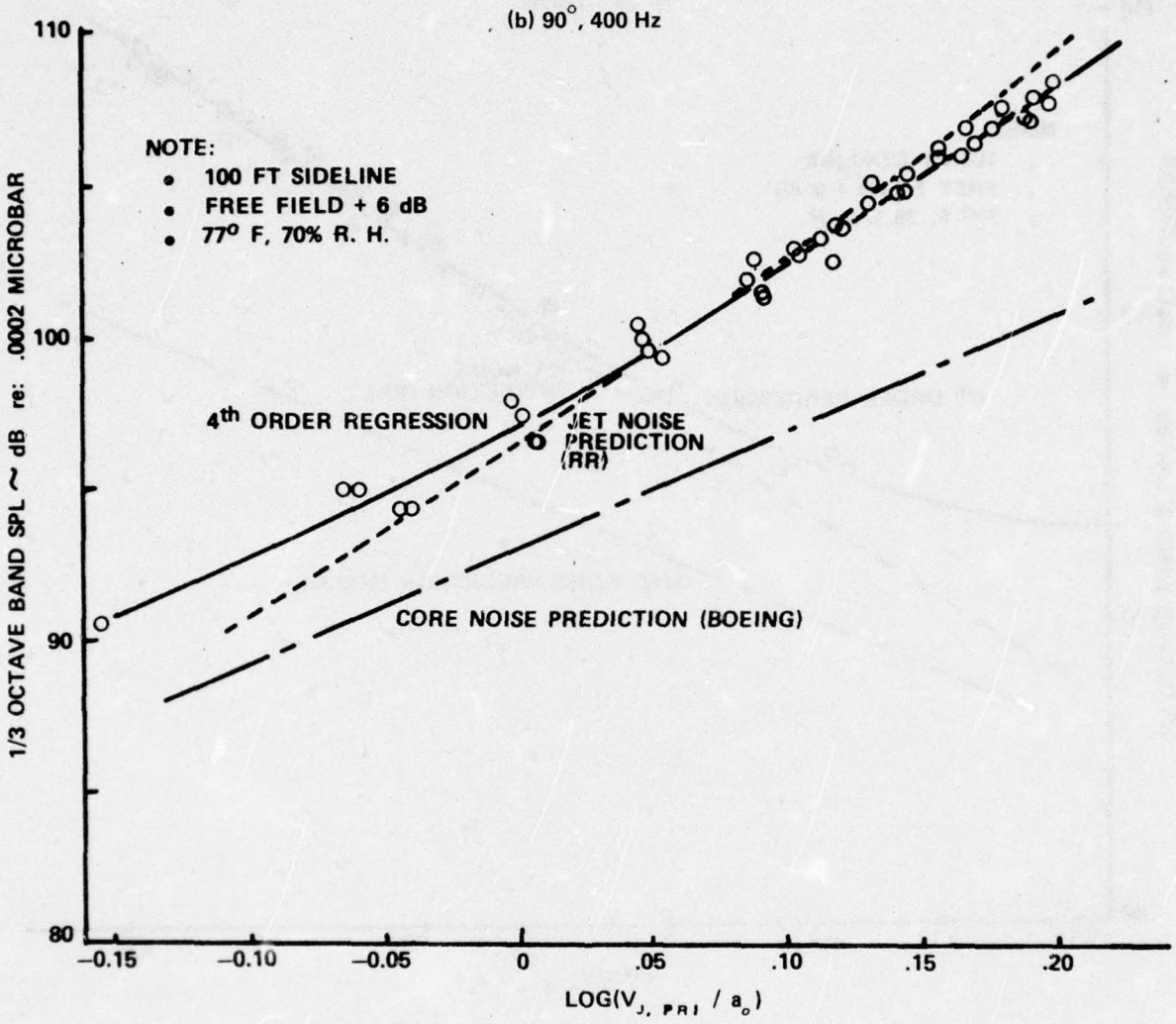


*Figure 21.—(Continued)*

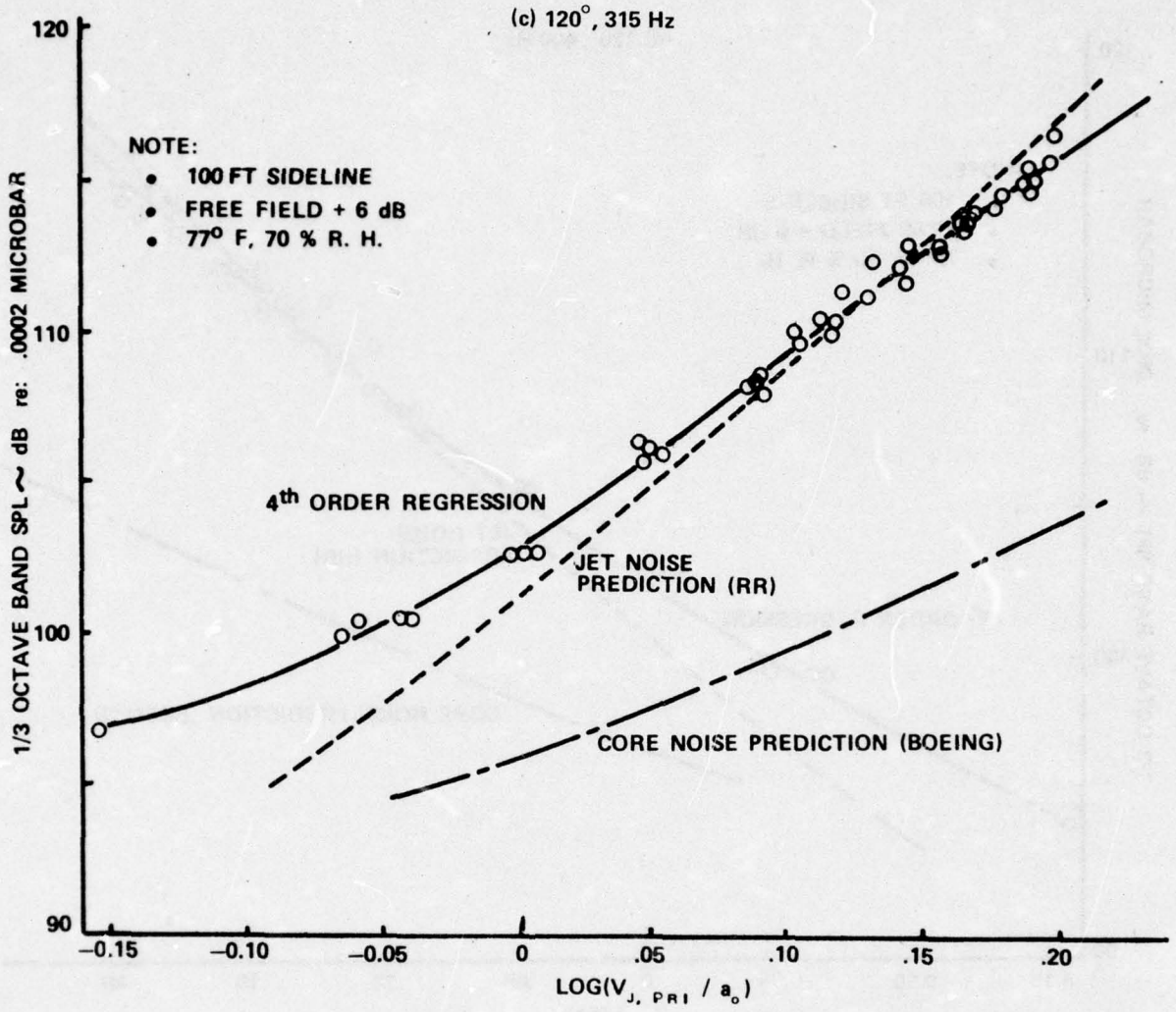


*Figure 21.—(Continued)*

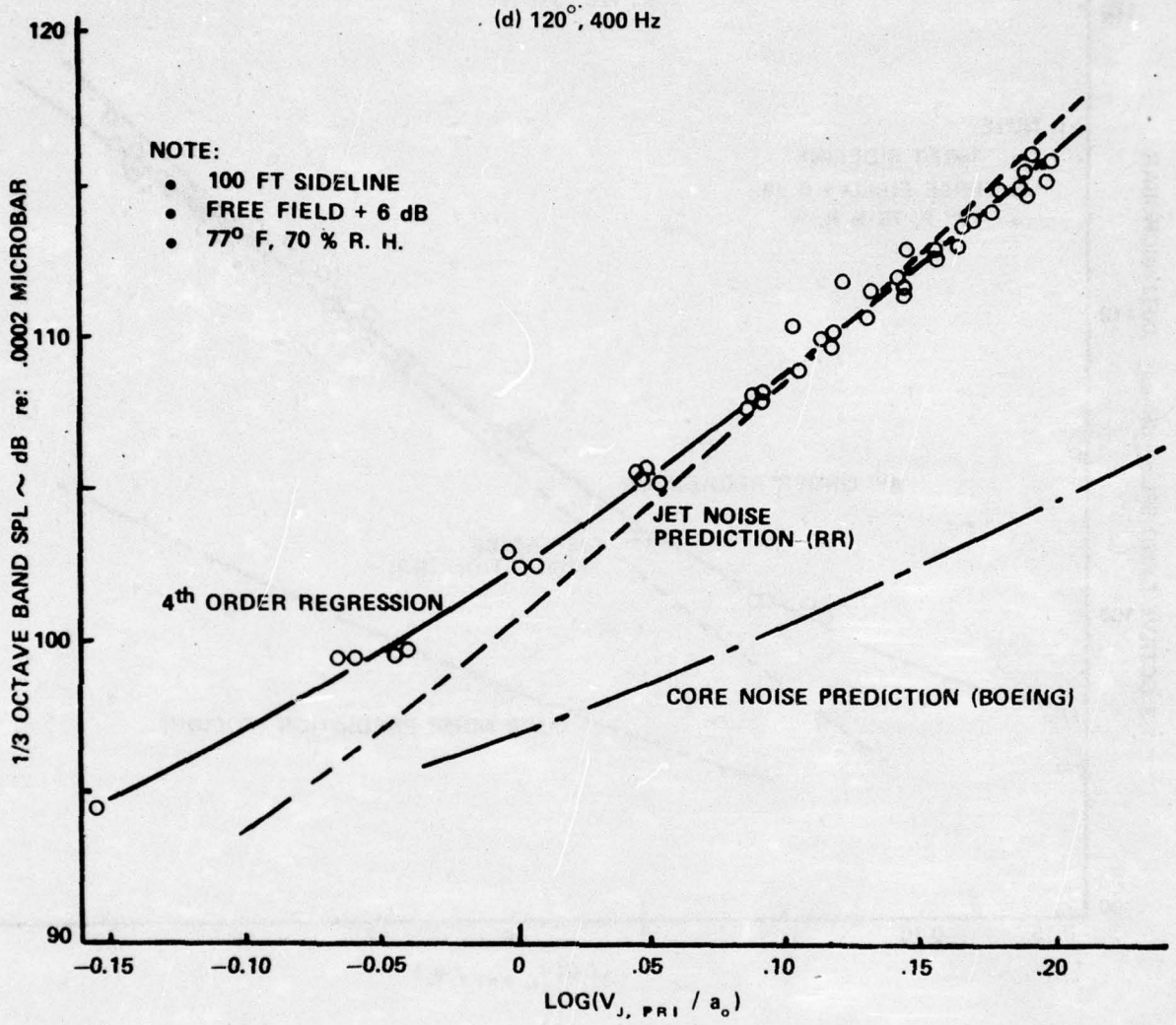


*Figure 21.—(Concluded)*

- DIRECTIVITY CHANGE $\theta = f(\theta_1, X_s)$

$$SPL(f,\theta) = SPL_{\substack{\text{MIC} \\ \text{STANDARD} \\ \text{CONDITIONS}}} (f,\theta_1) - 20 \log(d_2/d_1) - \alpha_{\substack{77^\circ \\ 70\ \text{RH}}} \times (d_2 - d_1) \times .001$$

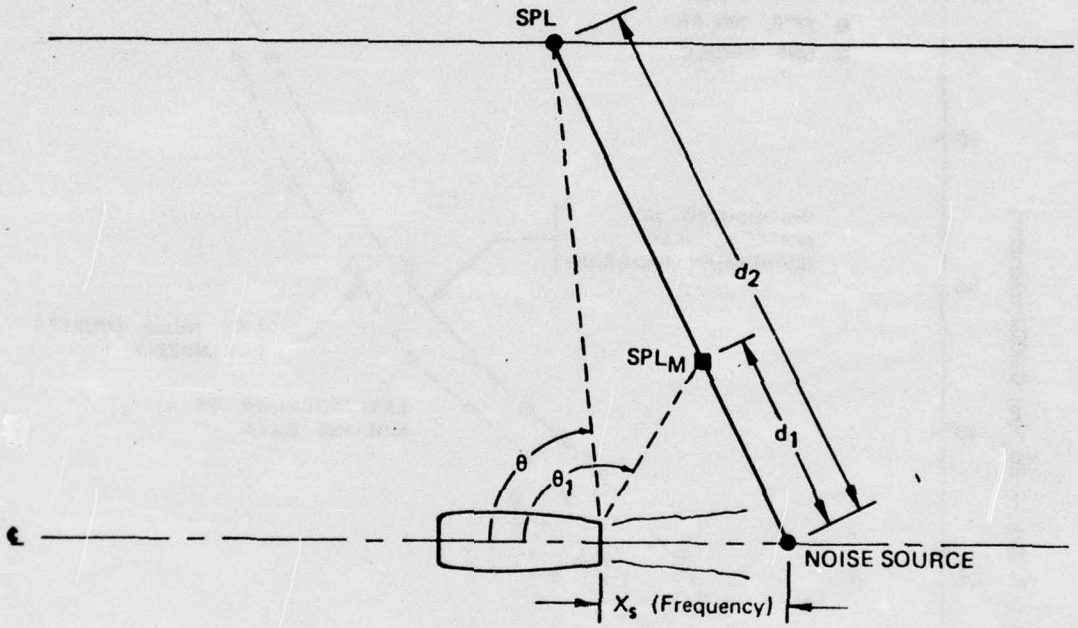


$\theta_1$ = MICROPHONE DIRECTIVITY ANGLE MEASURED FROM THE INLET

$\theta$ = NEW DIRECTIVITY ANGLE DUE TO EXTRAPOLATION FROM NOISE SOURCE

$d_1$ = MICROPHONE DISTANCE TO NOISE SOURCE

$d_2$ = EXTRAPOLATION DISTANCE FROM NOISE SOURCE LOCATION

*Figure 22.—Extrapolation Geometry*

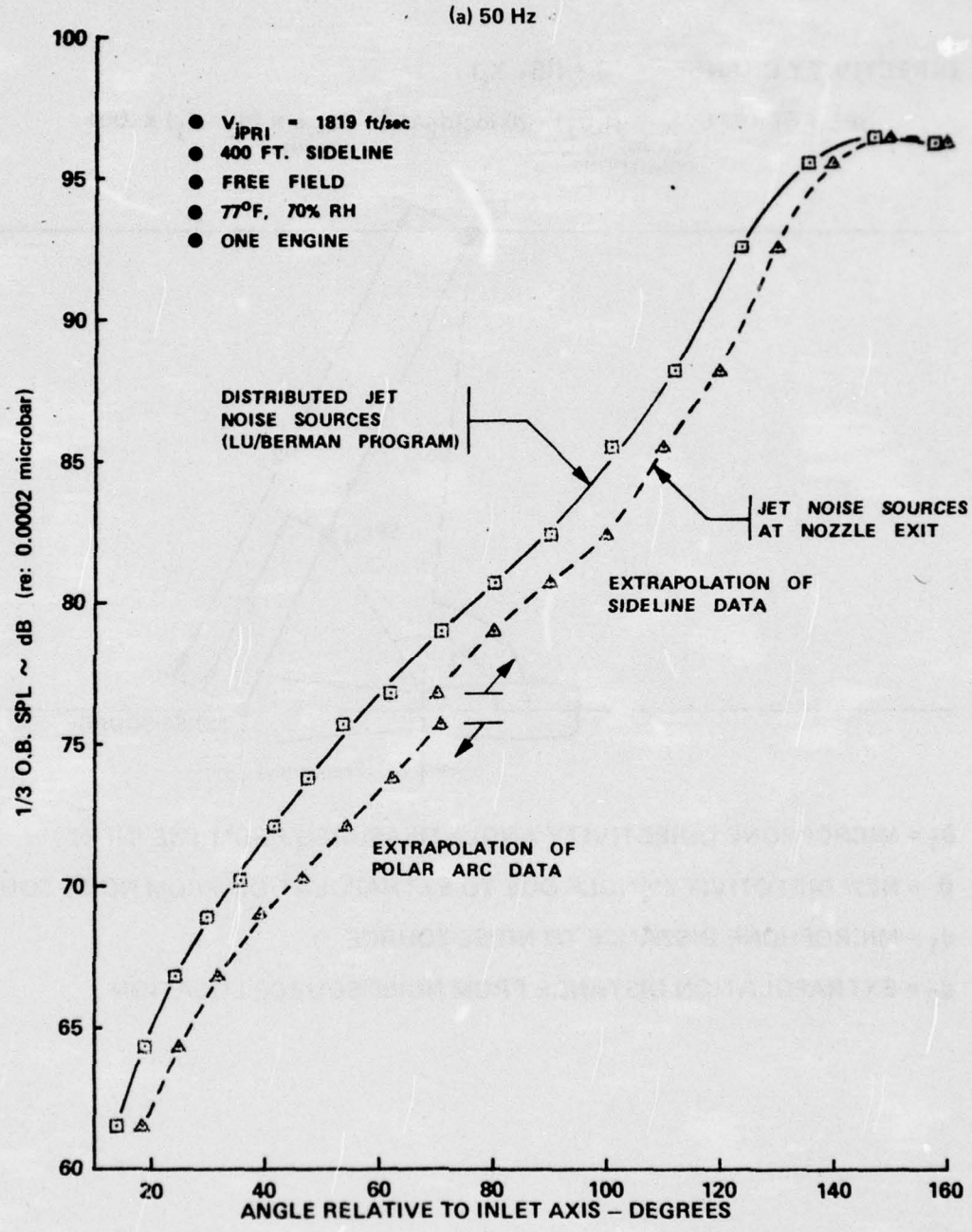


*Figure 23.—Effect of Noise Source Location Correction in the Extrapolation Results at Takeoff Power*

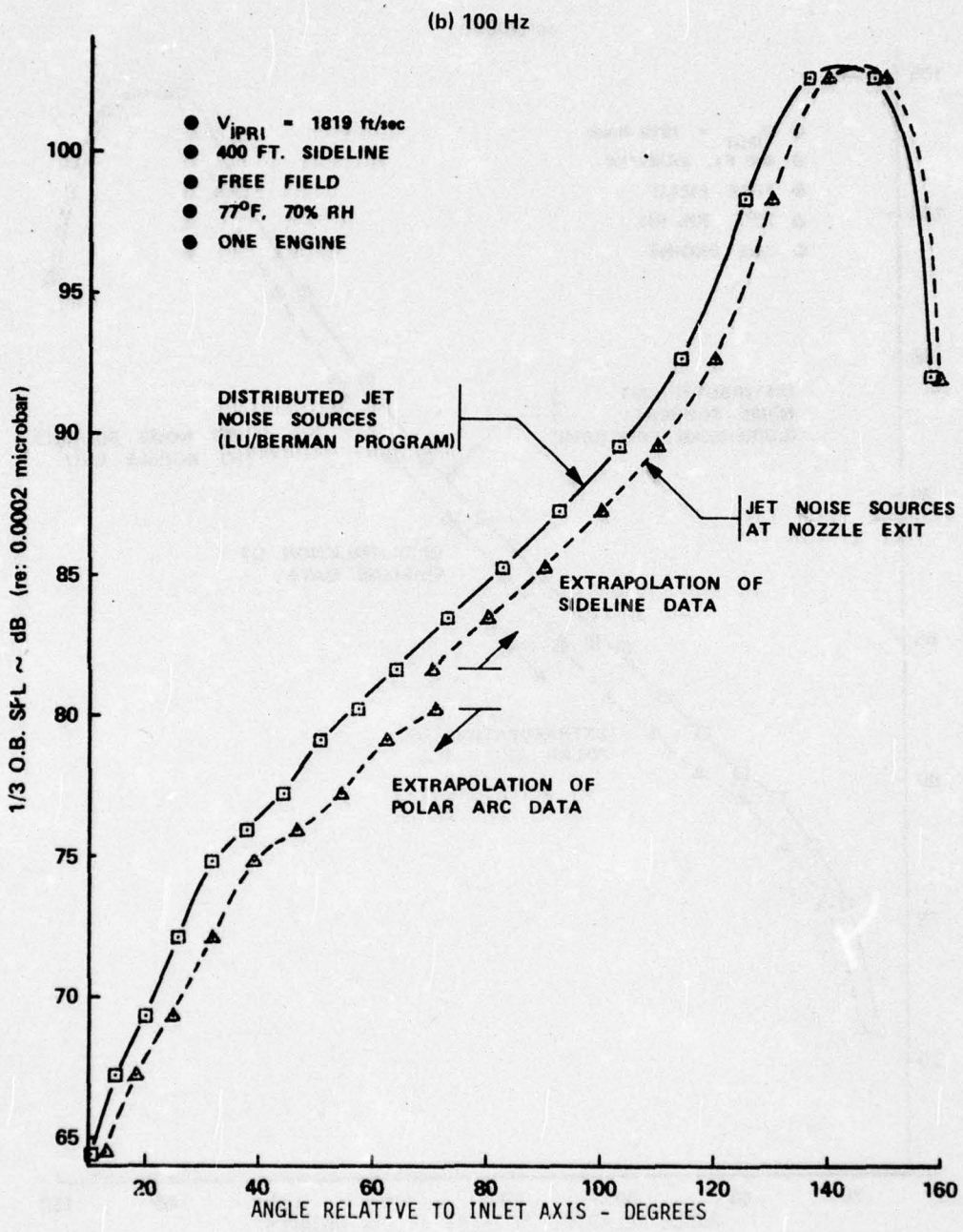


*Figure 23.—(Continued)*

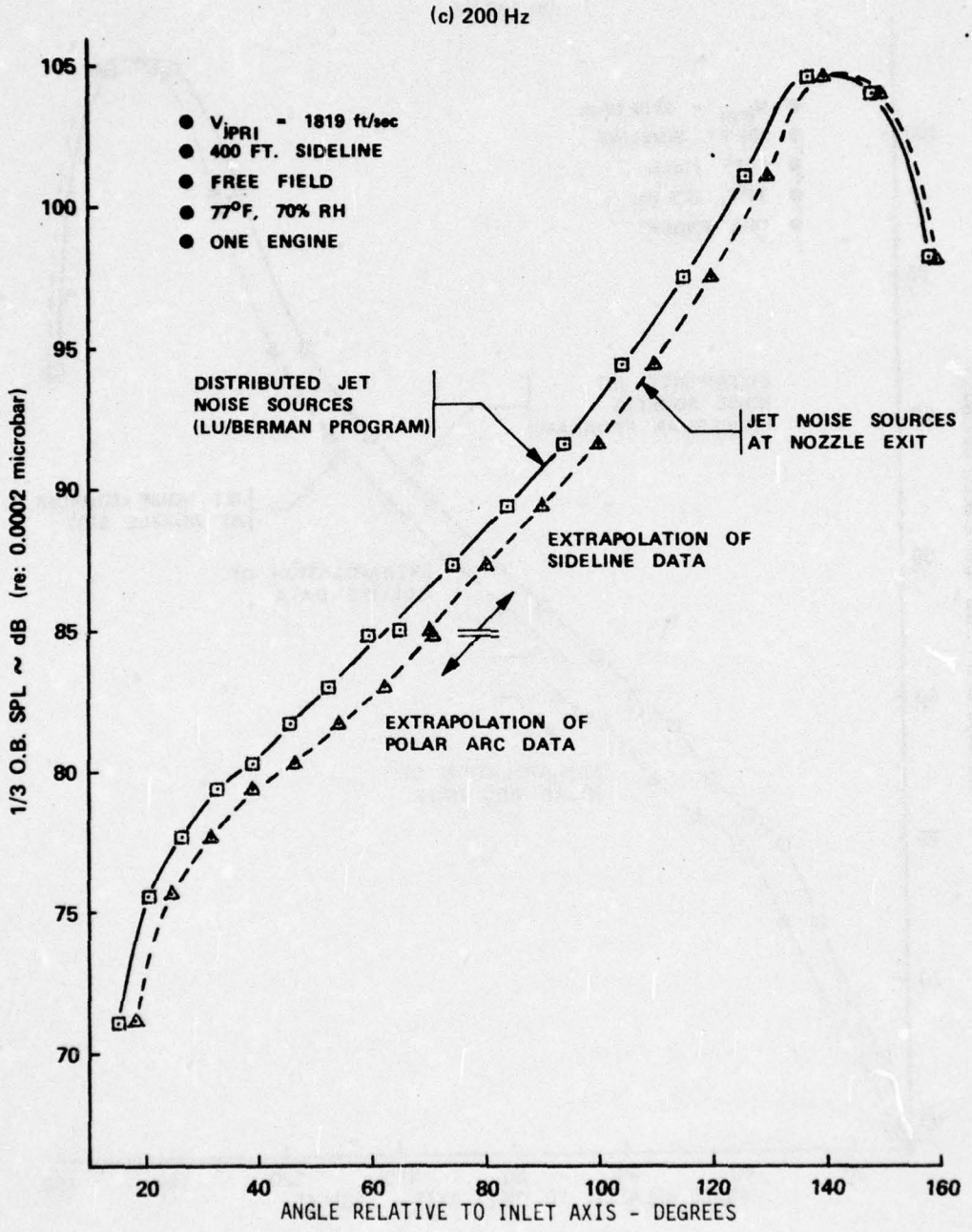


*Figure 23.—(Continued)*

(d) 400 Hz

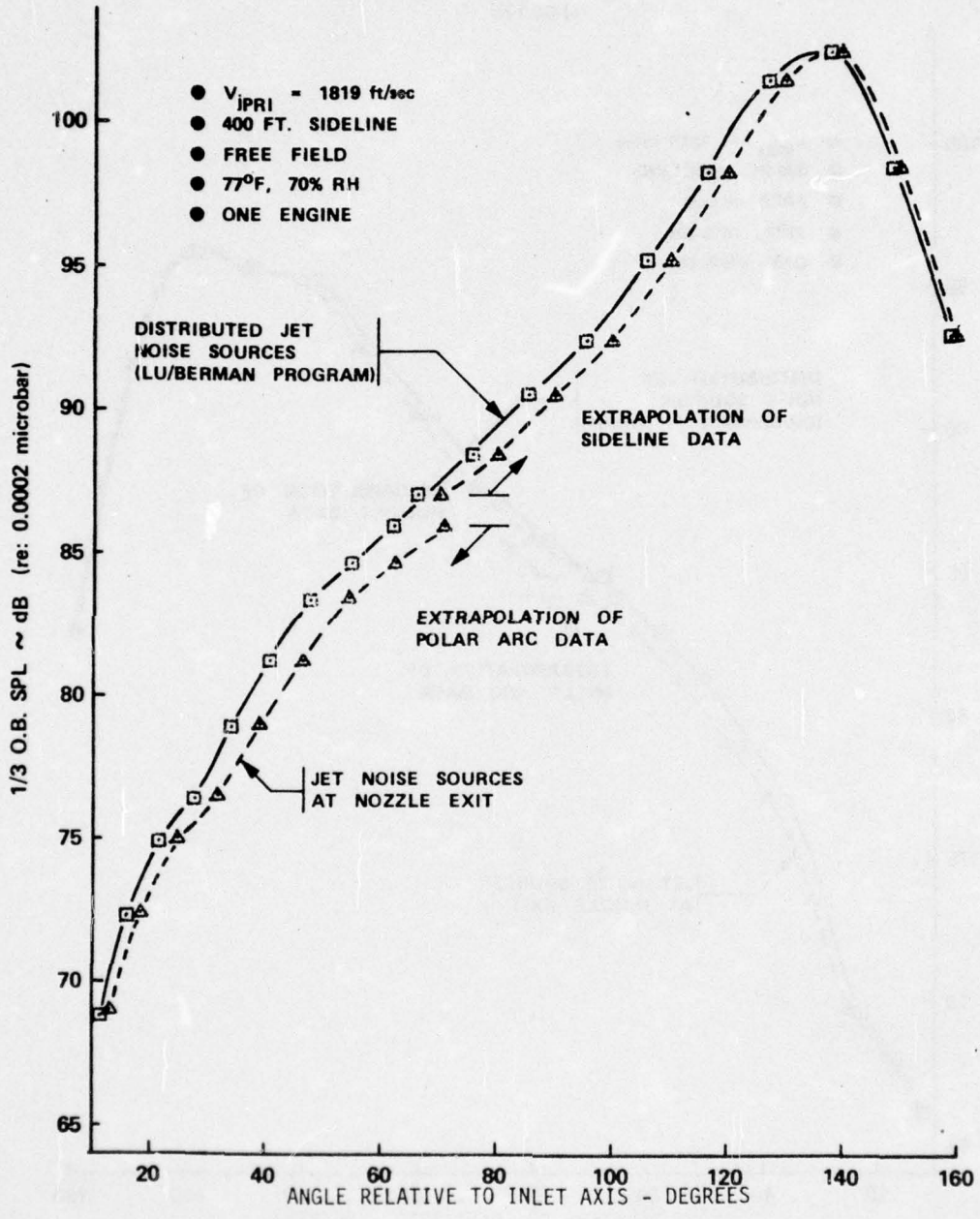


*Figure 23.—(Continued)*

(e) 800 Hz

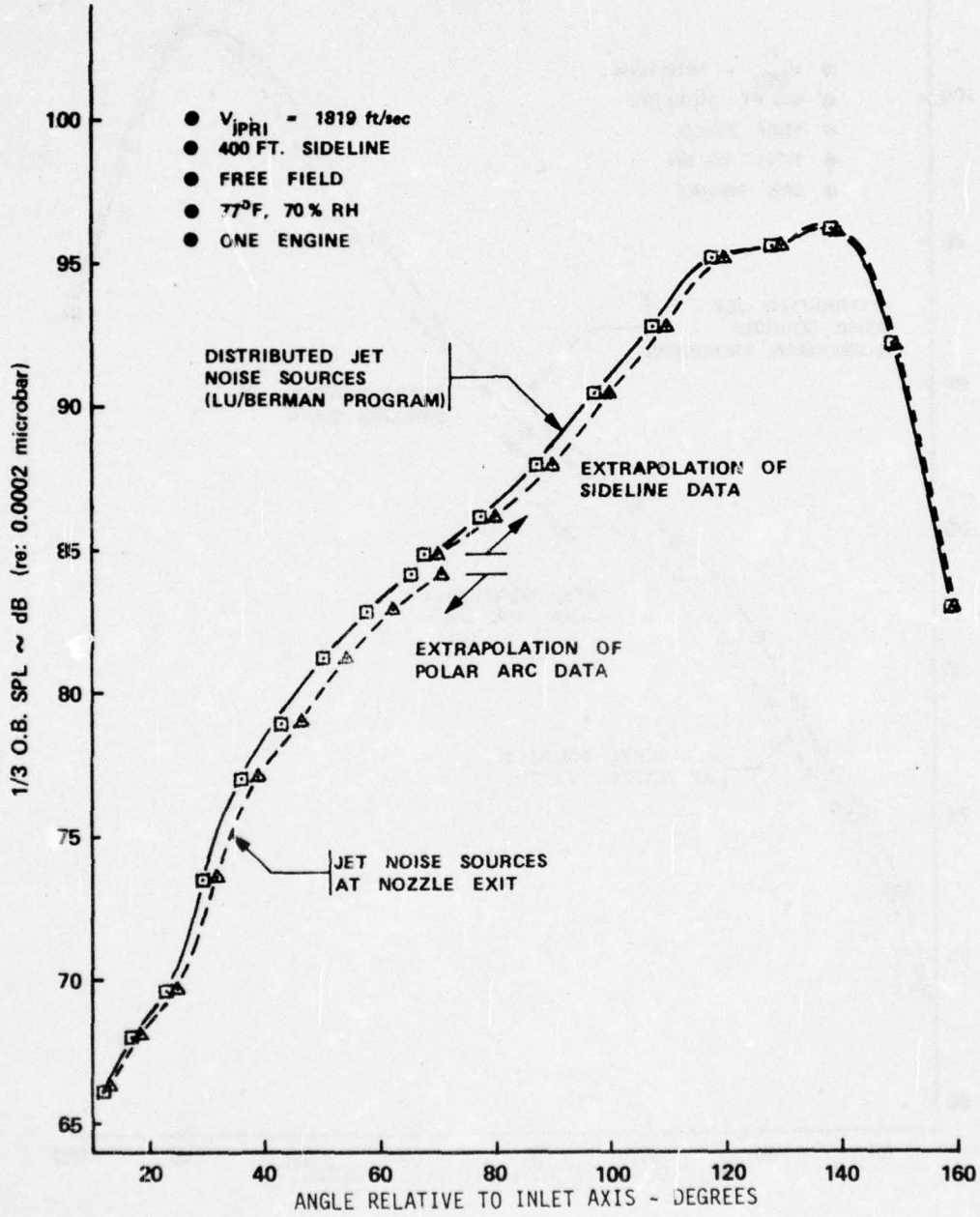


*Figure 23.—(Concluded)*

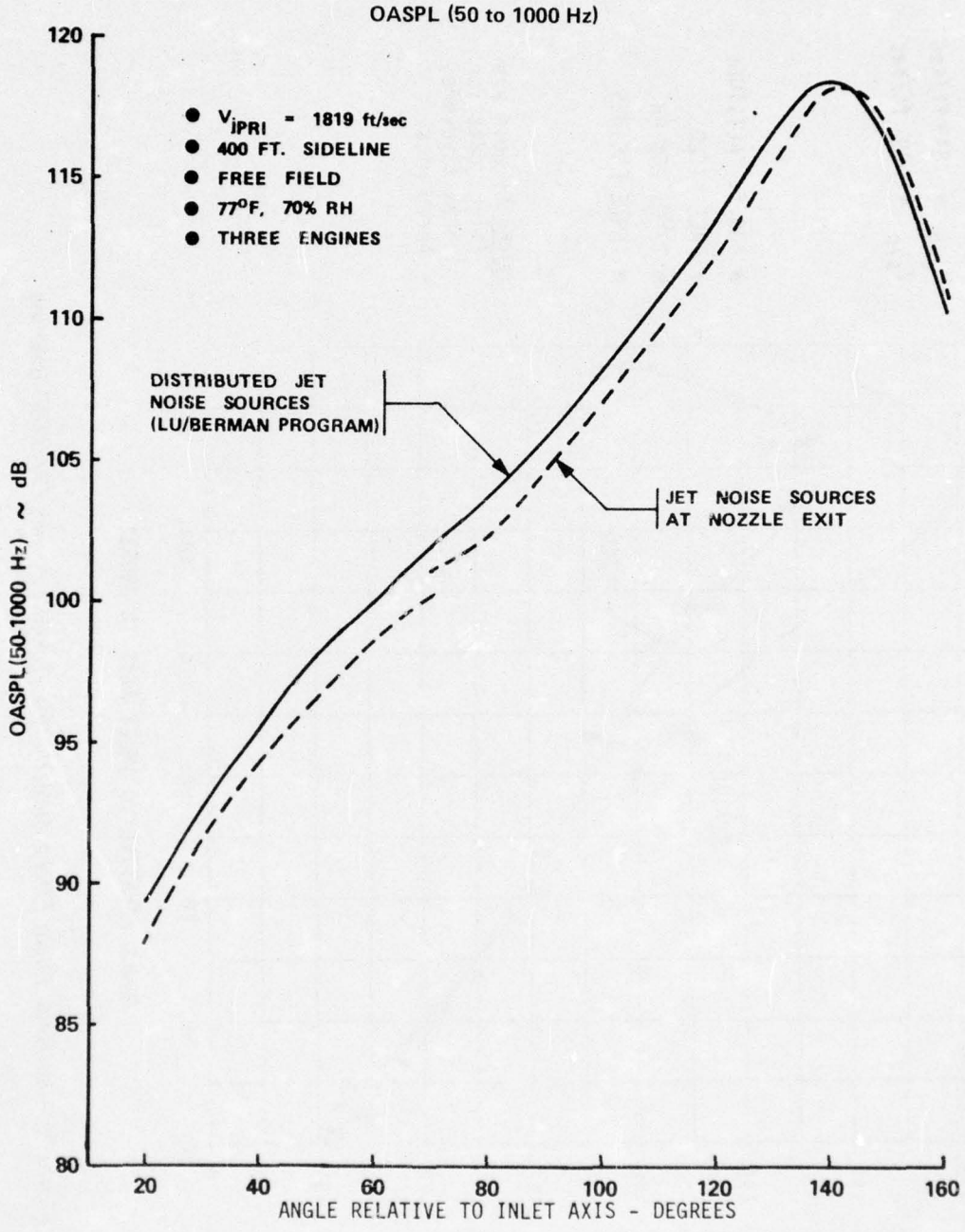


*Figure 24.—Effect of Noise Source Location Correction in the OASPL (50 to 1000-Hz) Extrapolated Directivity*

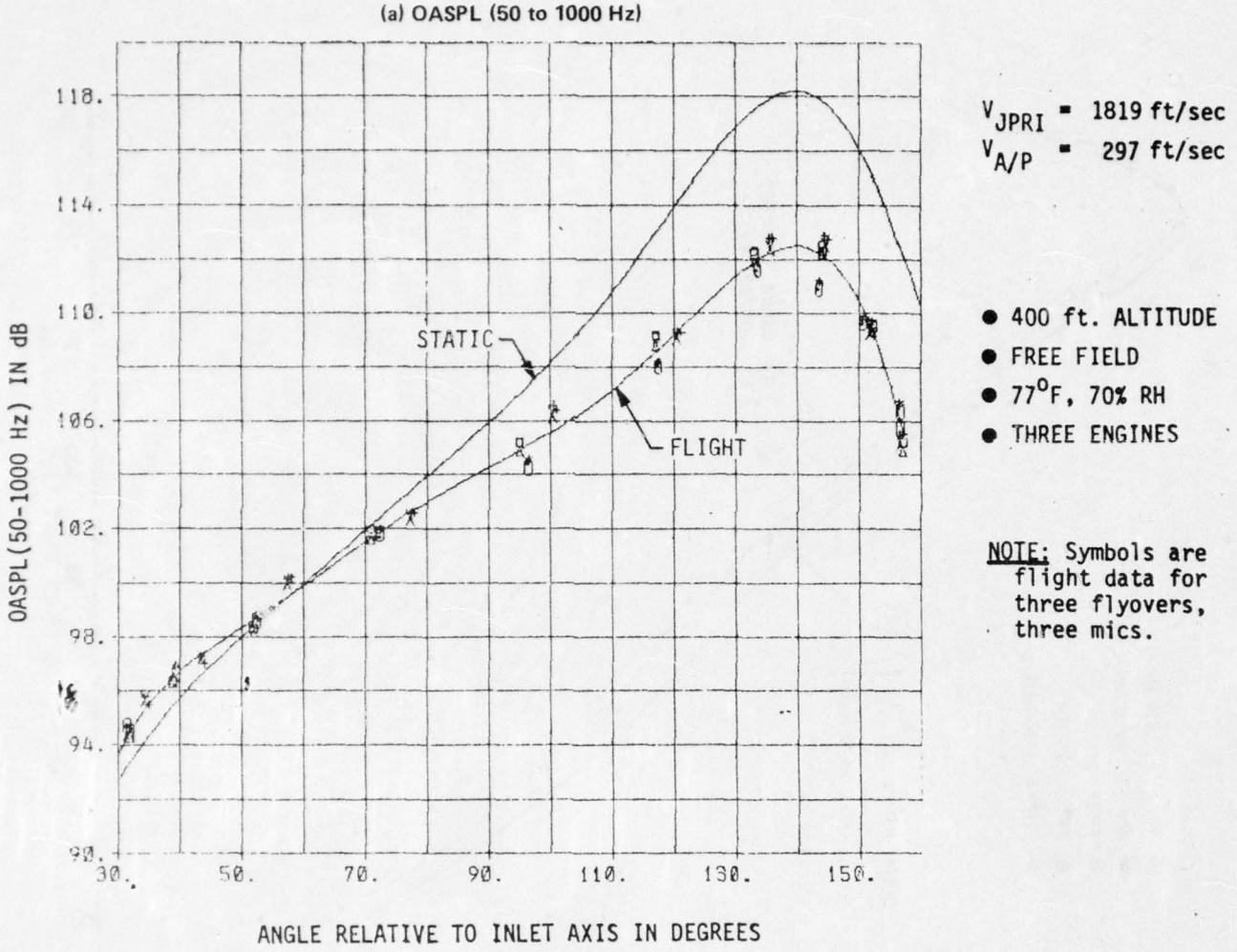


*Figure 25.—Jet Noise Flight Effects Directivity at Takeoff Power, 727/JT8D Baseline*

AD-A031 877 BOEING COMMERCIAL AIRPLANE CO SEATTLE WASH F/G 21/5
727/JT8D JET AND FAN NOISE FLIGHT EFFECTS STUDY.(U)
AUG 76 L F MUNOZ DOT-FA71WA-2637
UNCLASSIFIED D6-44145 FAA-RD-76-110 NL

2 OF 4
AD
AD31877

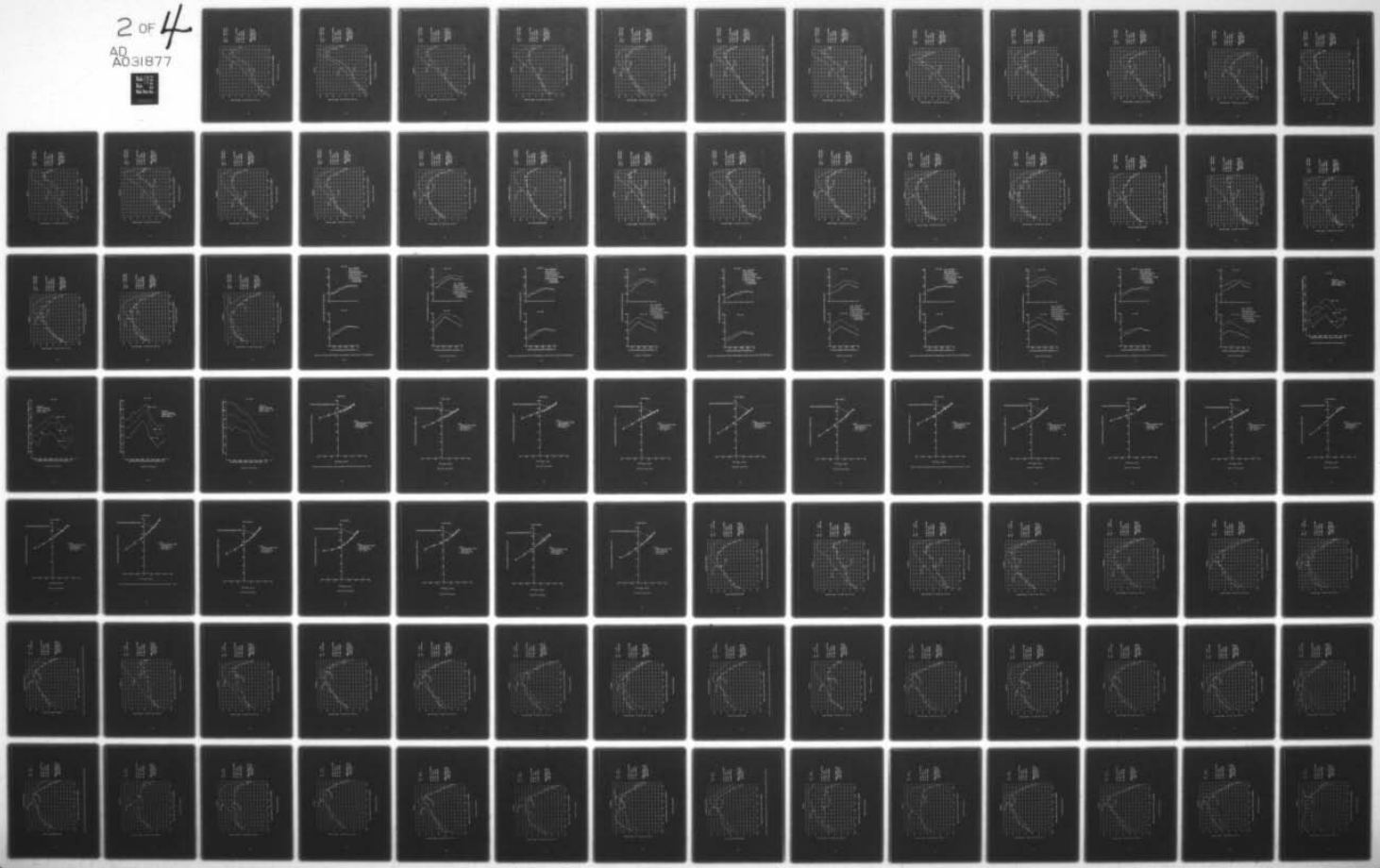

(b) 63 Hz

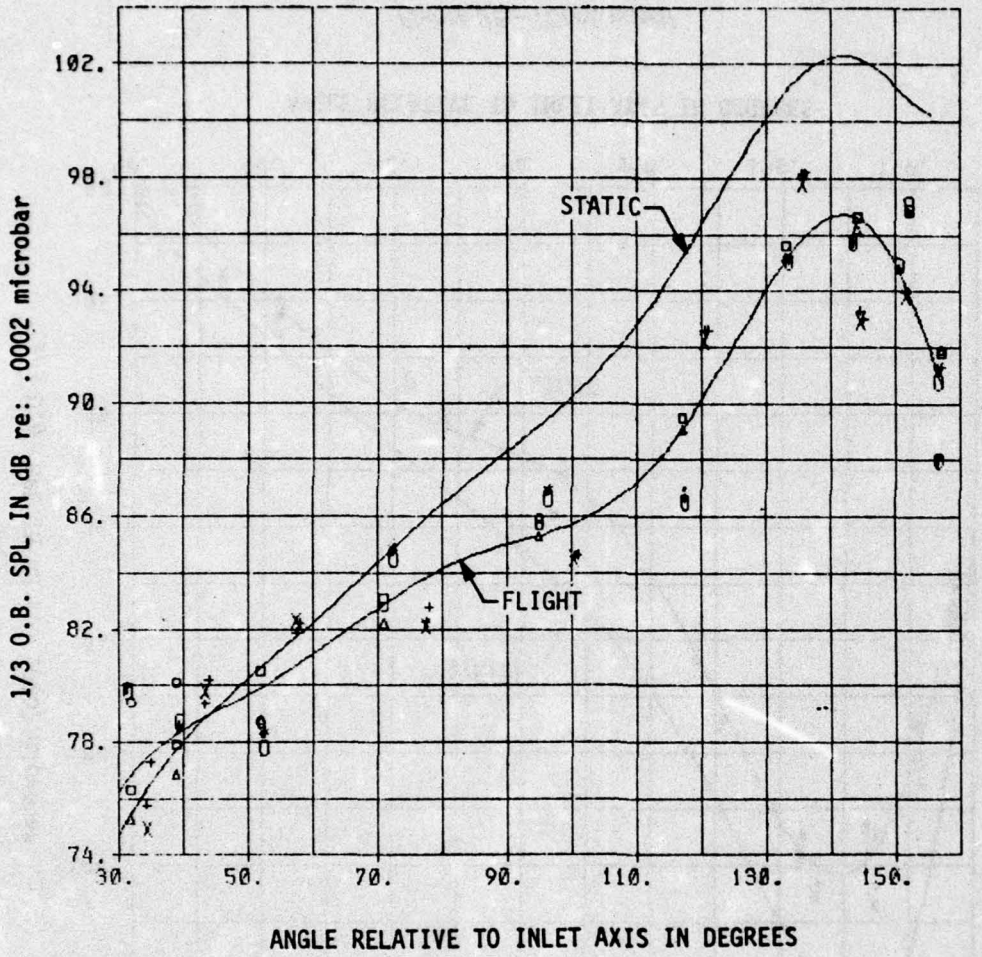


$V_{JPRI}$ = 1819 ft/sec
$V_{A/P}$ = 297 ft/sec

- 400 ft. ALTITUDE
- FREE FIELD
- 77°F, 70% RH
- THREE ENGINES

NOTE: Symbols are flight data for three flyovers, three mics.

*Figure 25.—(Continued)*

(c) 125 Hz

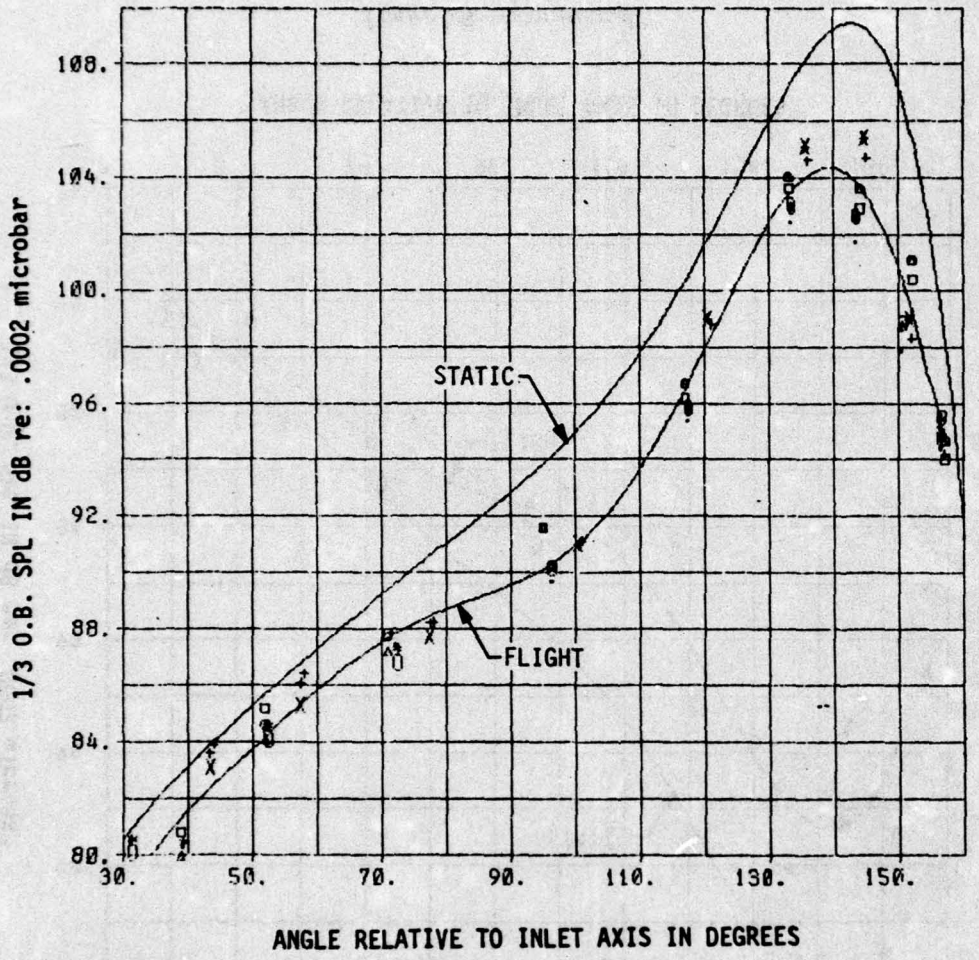


$V_{JPRI}$ = 1819 ft/sec
$V_{A/P}$ = 297 ft/sec

- 400 ft. ALTITUDE
- FREE FIELD
- 77°F, 70% RH
- THREE ENGINES

NOTE: Symbols are flight data for three flyovers, three mics.

*Figure 25.—(Continued)*

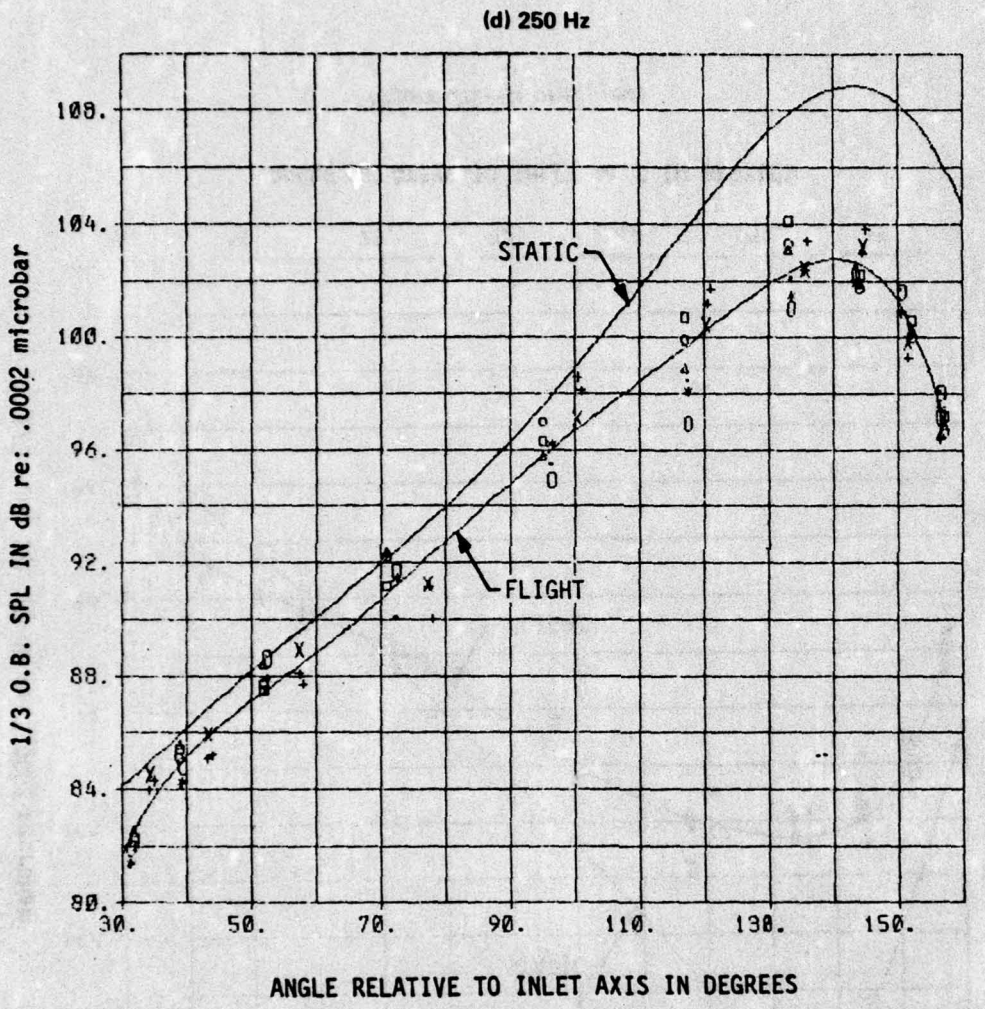


$V_{JPRI}$ = 1819 ft/sec
$V_{A/P}$ = 297 ft/sec

- 400 ft. ALTITUDE
- FREE FIELD
- 77°F, 70% RH
- THREE ENGINES

NOTE: Symbols are flight data for three flyovers, three mics.

*Figure 25.—(Continued)*

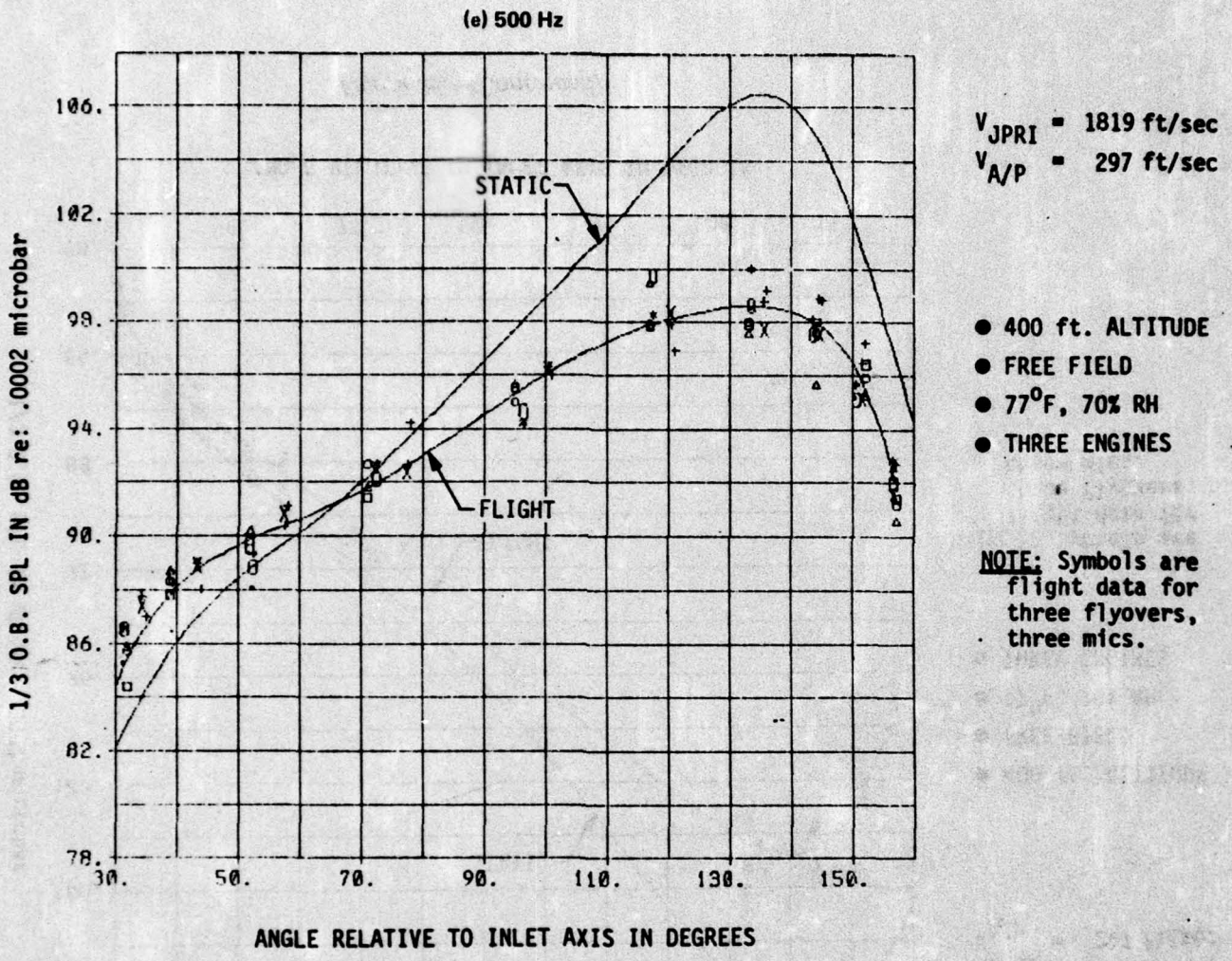


*Figure 25.—(Continued)*

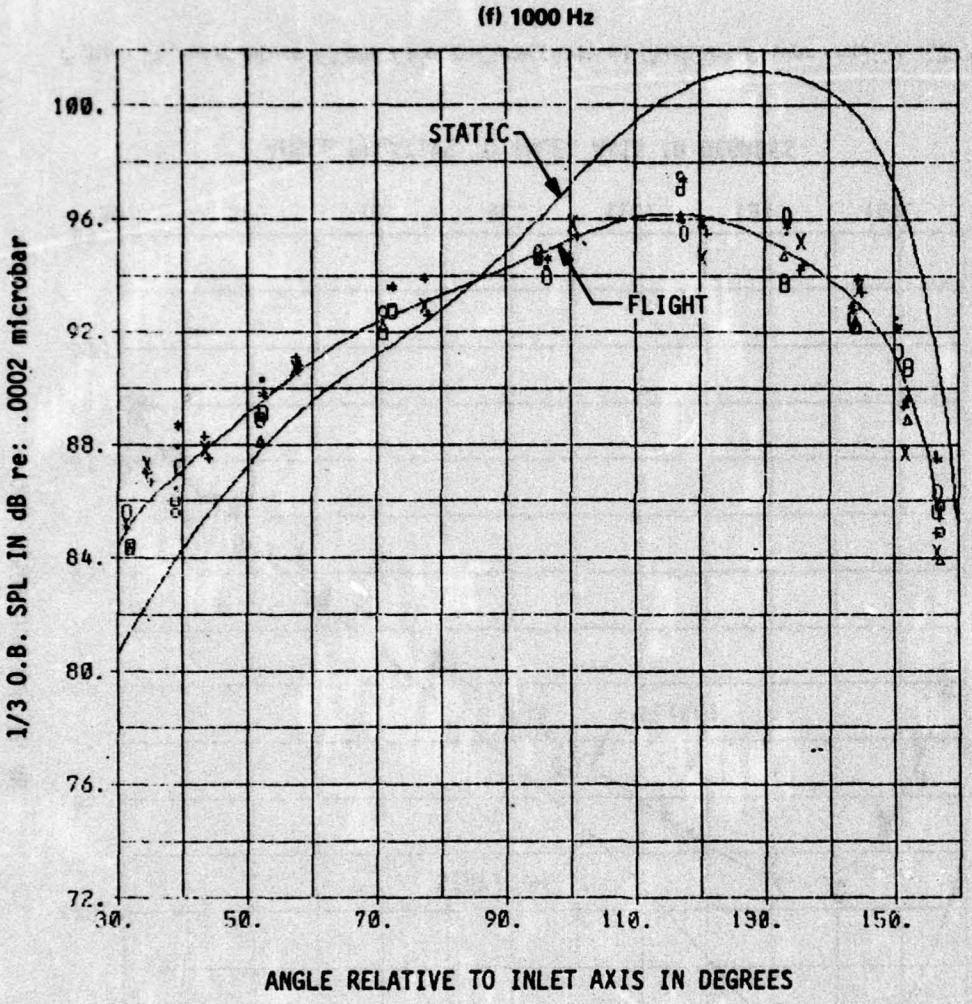


$V_{JPRI}$ = 1819 ft/sec
$V_{A/P}$ = 297 ft/sec

- 400 ft. ALTITUDE
- FREE FIELD
- 77°F, 70% RH
- THREE ENGINES

NOTE: Symbols are flight data for three flyovers, three mics.

*Figure 25.—(Concluded)*

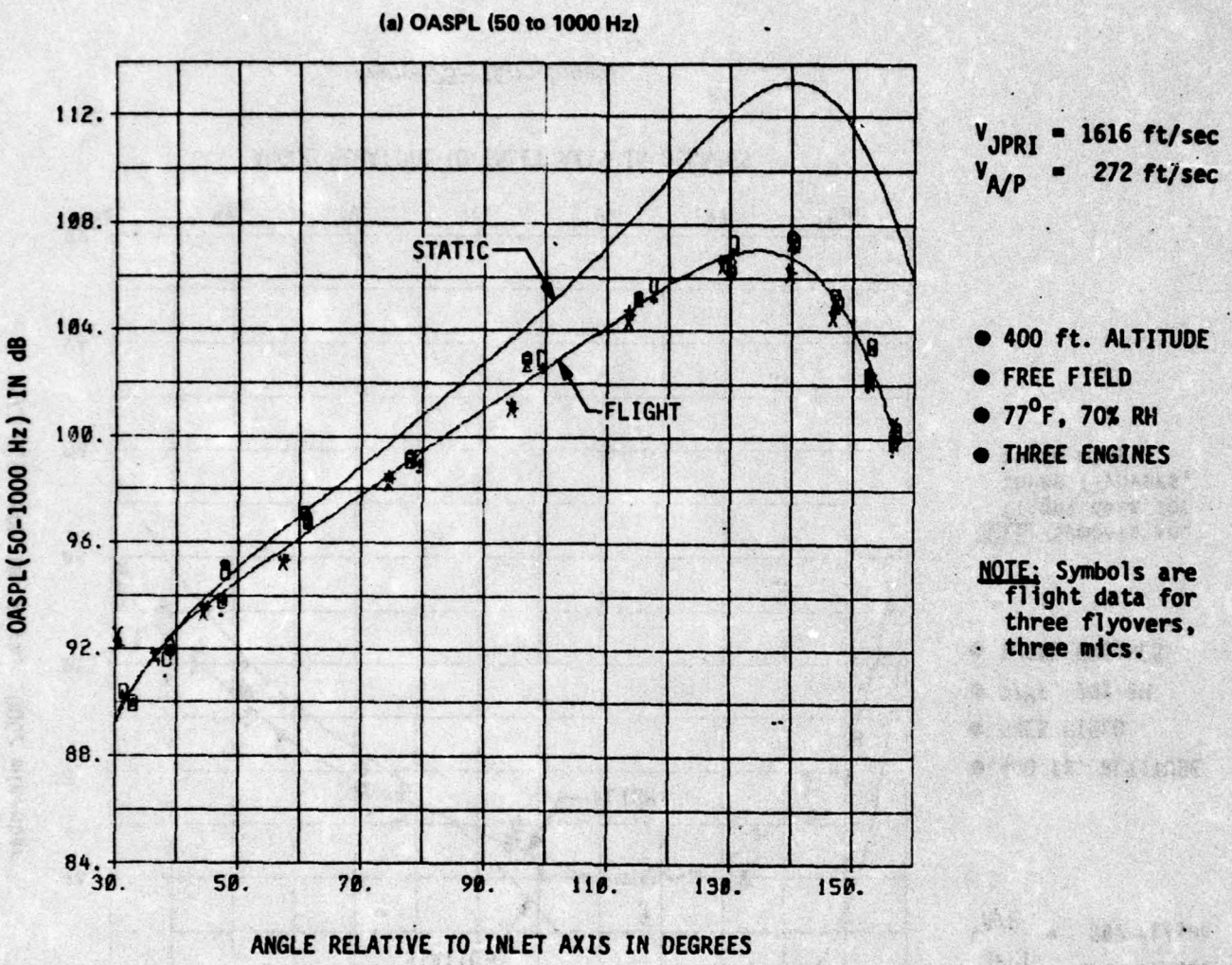


*Figure 26.—Jet Noise Flight Effects Directivity at Cutback Power (HGW), 727/JT8D Baseline*

(b) 63 Hz

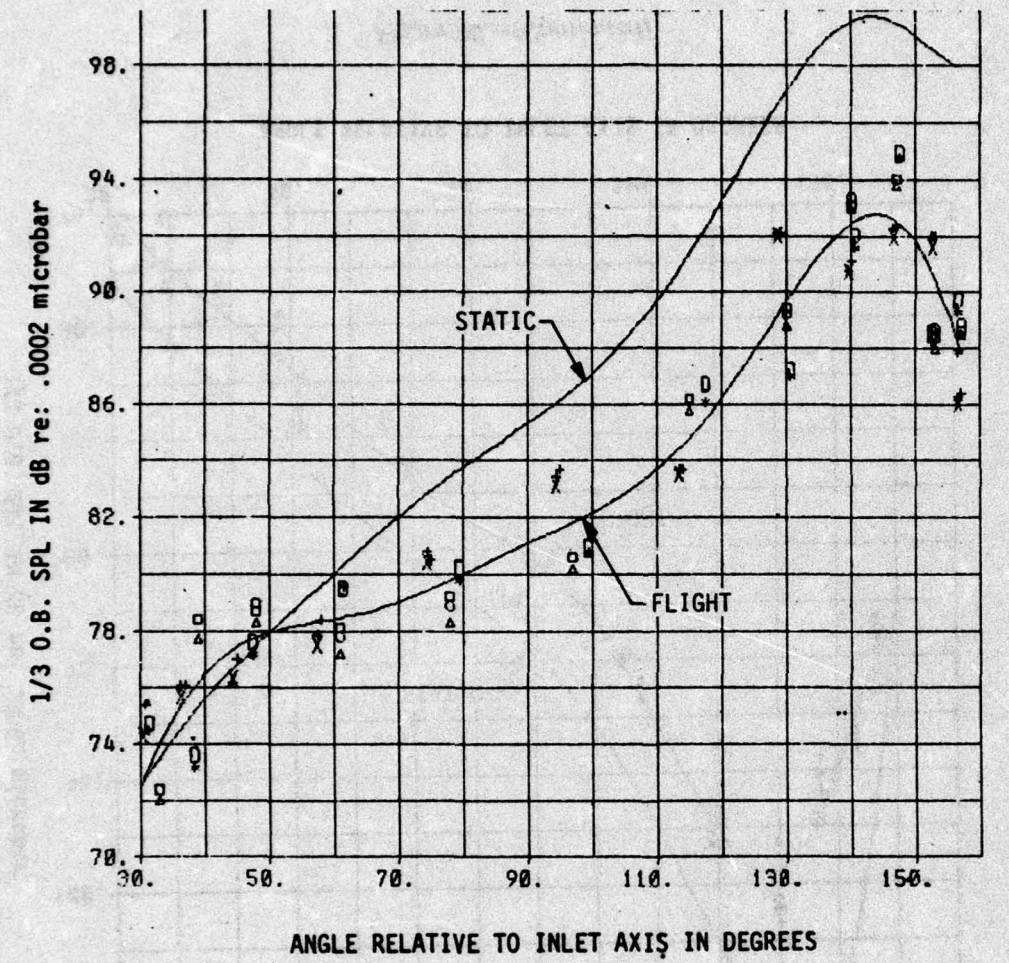


$V_{JPRI}$ = 1616 ft/sec
$V_{A/P}$ = 272 ft/sec

- 400 ft. ALTITUDE
- FREE FIELD
- 77°F, 70% RH
- THREE ENGINES

NOTE: Symbols are flight data for three flyovers, three mics.

*Figure 26.—(Continued)*

(c) 125 Hz

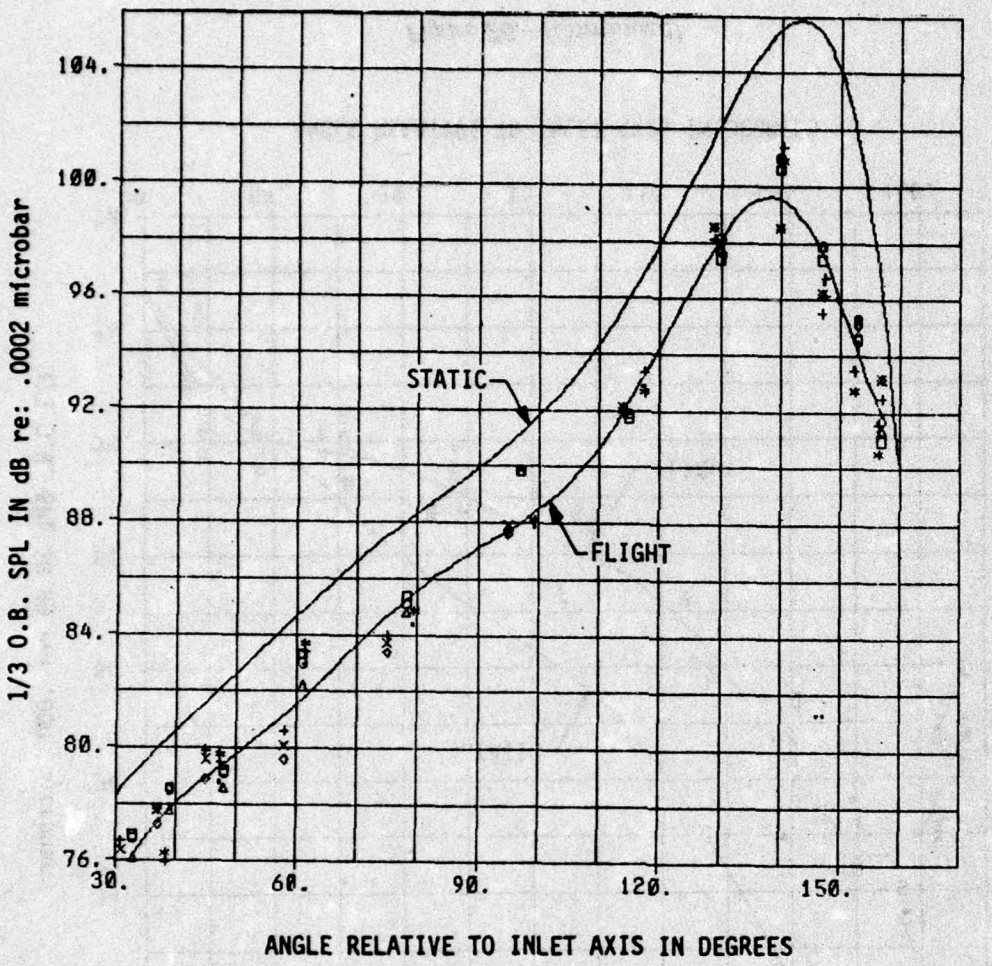


$V_{JPRI}$ = 1616 ft/sec
$V_{A/P}$ = 272 ft/sec

- 400 ft. ALTITUDE
- FREE FIELD
- 77°F, 70% RH
- THREE ENGINES

NOTE: Symbols are flight data for three flyovers, three mics.

*Figure 26.—(Continued)*

(d) 250 Hz

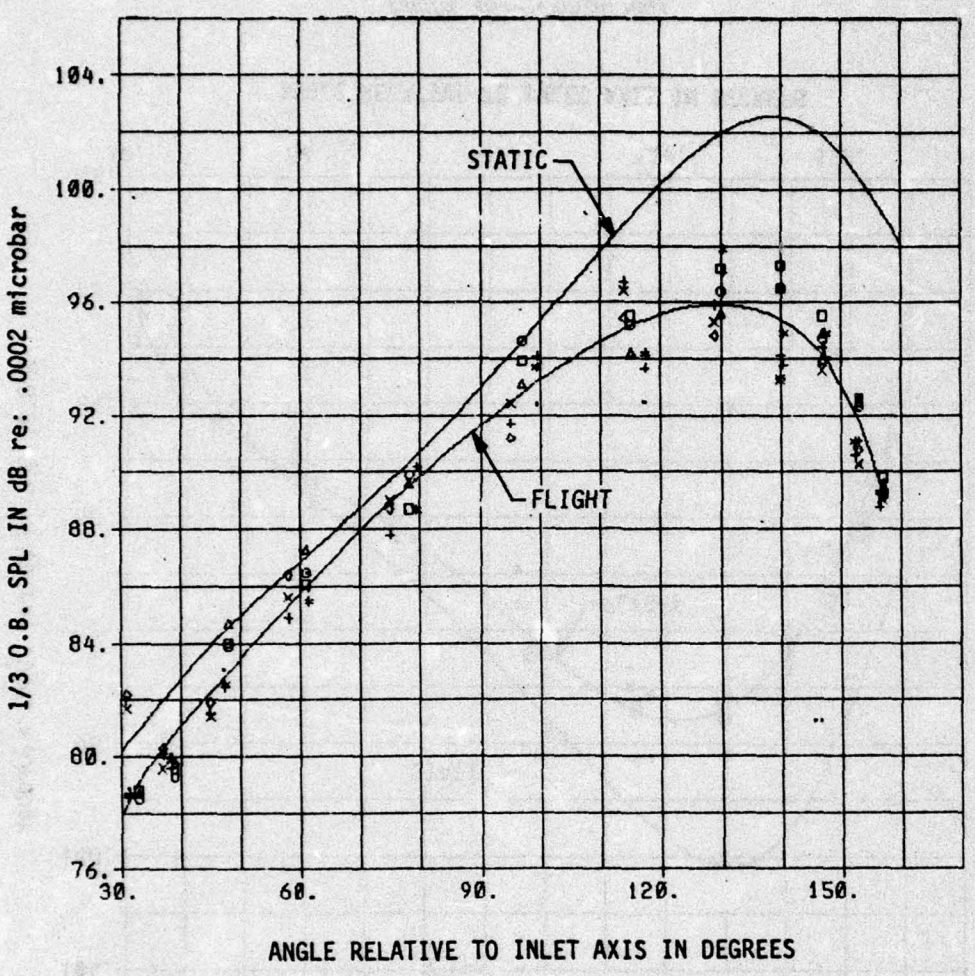


$V_{JPRI}$ = 1616 ft/sec
$V_{A/P}$ = 272 ft/sec

- 400 ft. ALTITUDE
- FREE FIELD
- 77°F, 70% RH
- THREE ENGINES

NOTE: Symbols are flight data for three flyovers, three mics.

*Figure 26.—(Continued)*

(e) 500 Hz

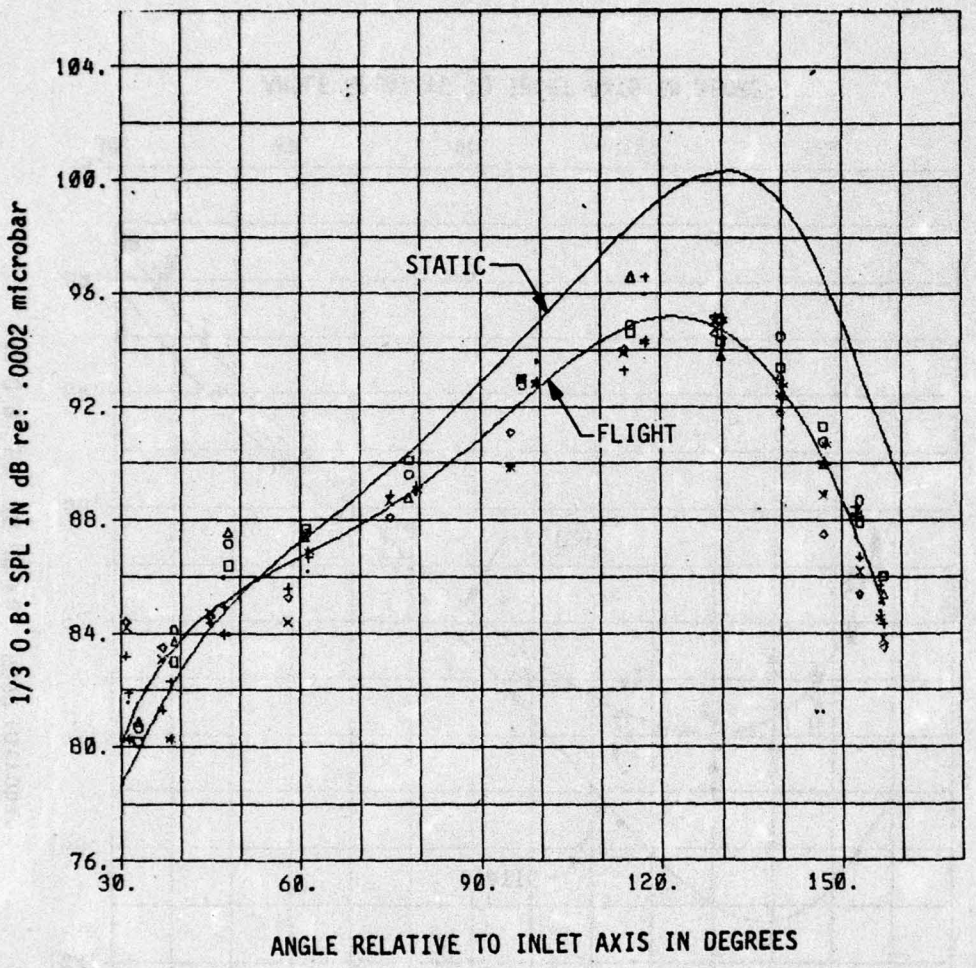


$V_{JPRI}$ = 1616 ft/sec
$V_{A/P}$ = 272 ft/sec

- 400 ft. ALTITUDE
- FREE FIELD
- 77°F, 70% RH
- THREE ENGINES

NOTE: Symbols are flight data for three flyovers, three mics.

*Figure 26.—(Continued)*

(f) 1000 Hz

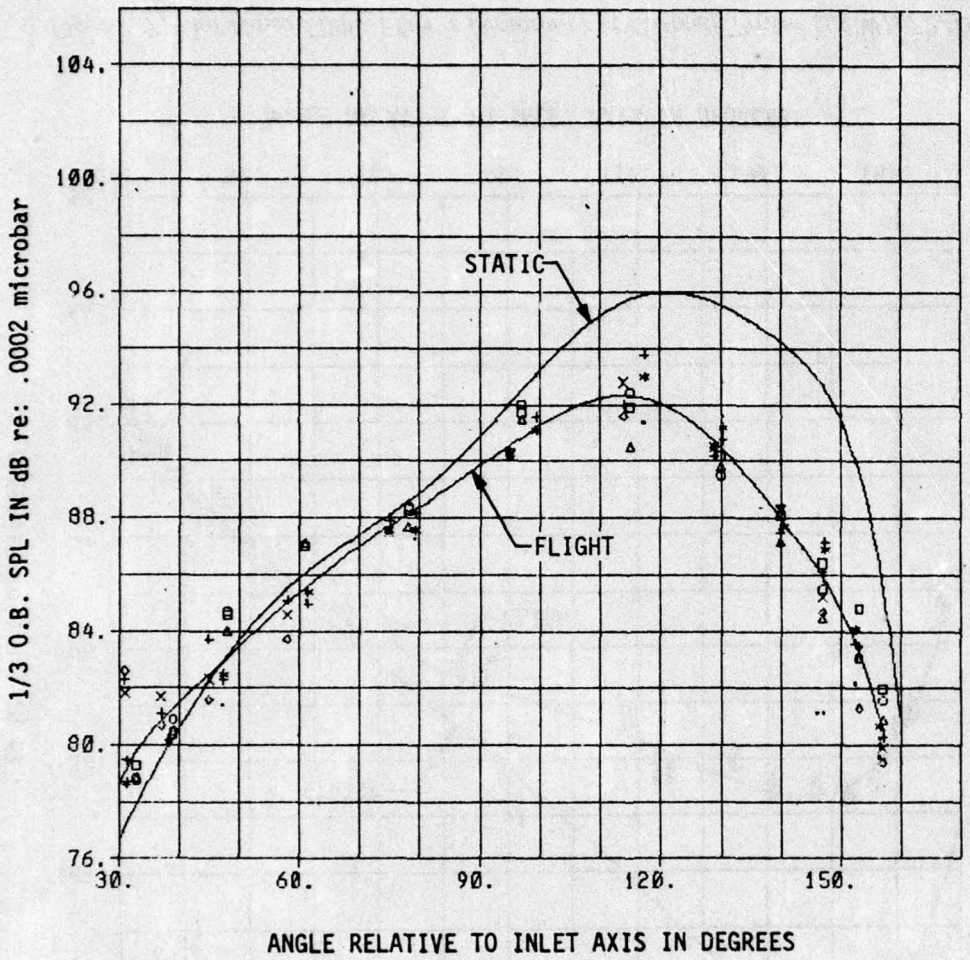


$V_{JPRI}$ = 1616 ft/sec
$V_{A/P}$ = 272 ft/sec

- 400 ft. ALTITUDE
- FREE FIELD
- 77°F, 70% RH
- THREE ENGINES

NOTE: Symbols are flight data for three flyovers, three mics.

*Figure 26.—(Concluded)*

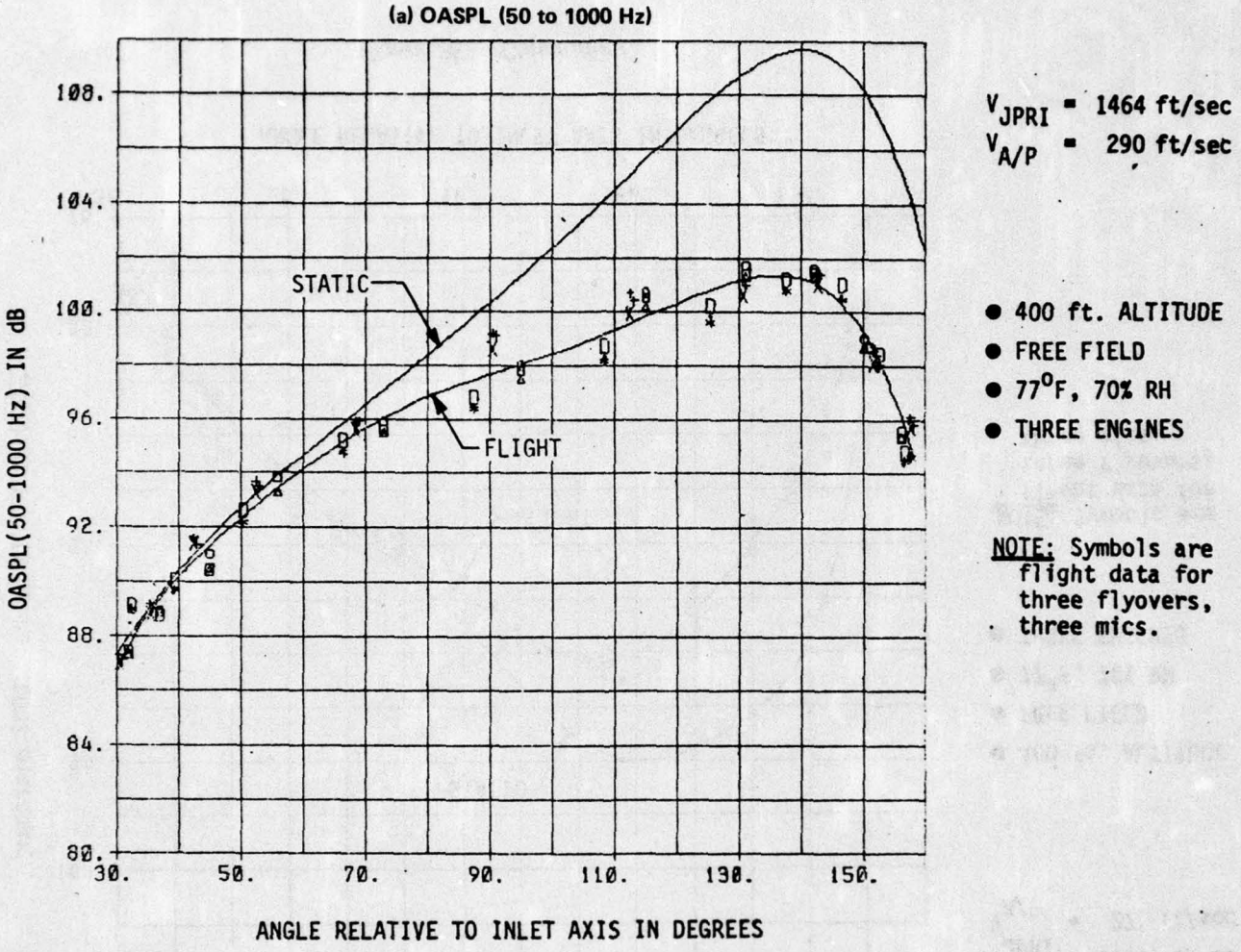


*Figure 27.—Jet Noise Flight Effects Directivity at Cutback Power (LGW), 727/JT8D Baseline*

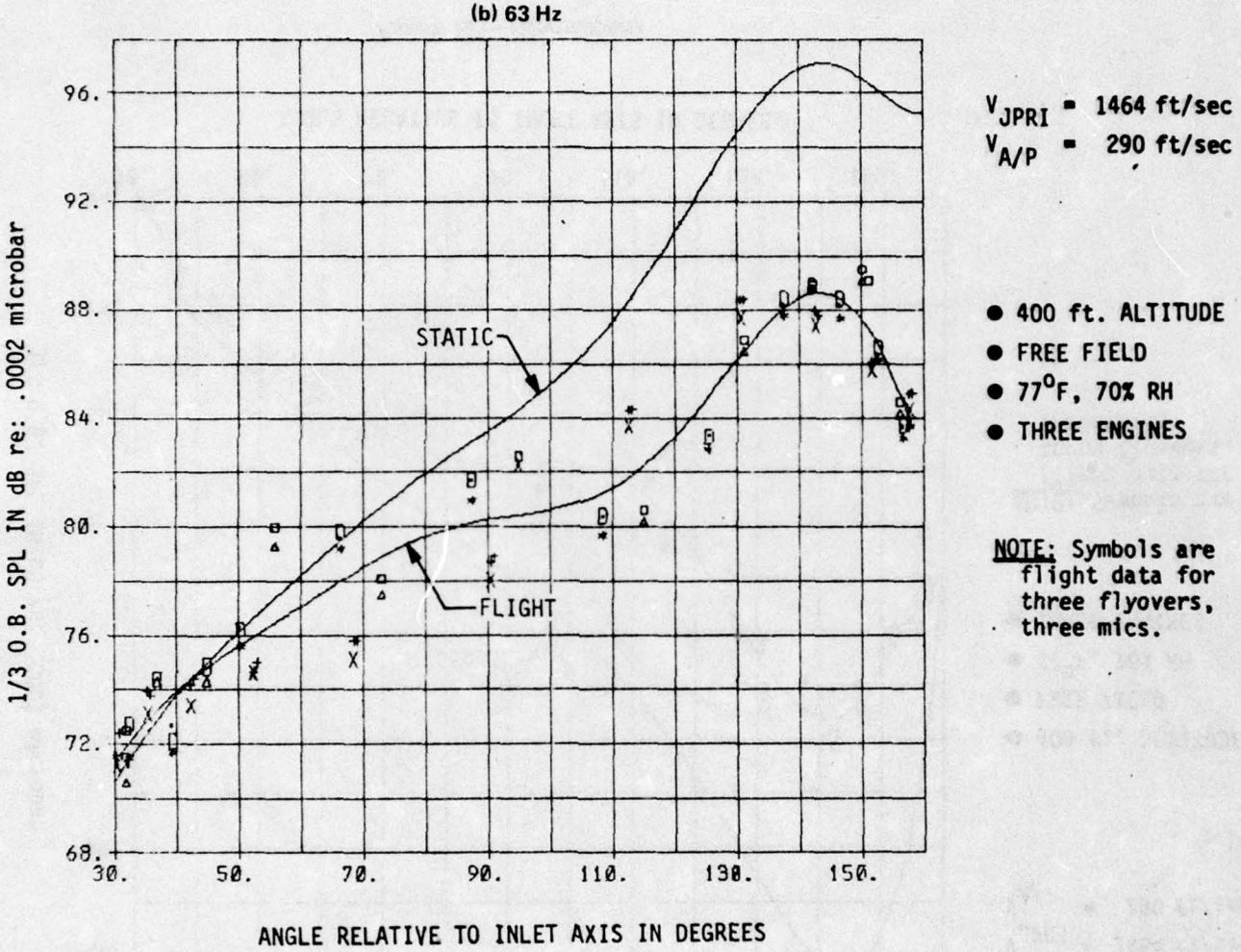


*Figure 27.—(Continued)*

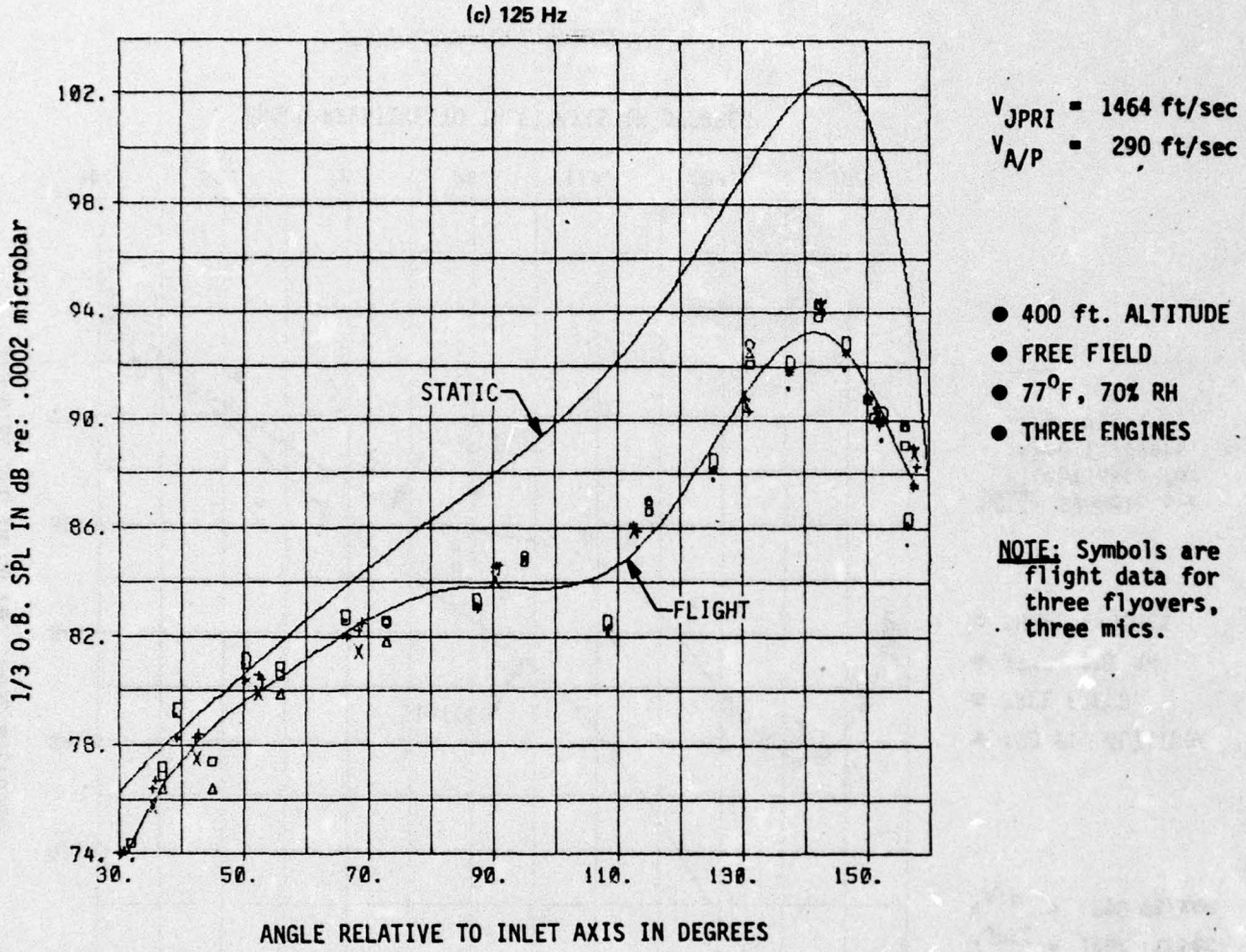


*Figure 27.—(Continued)*

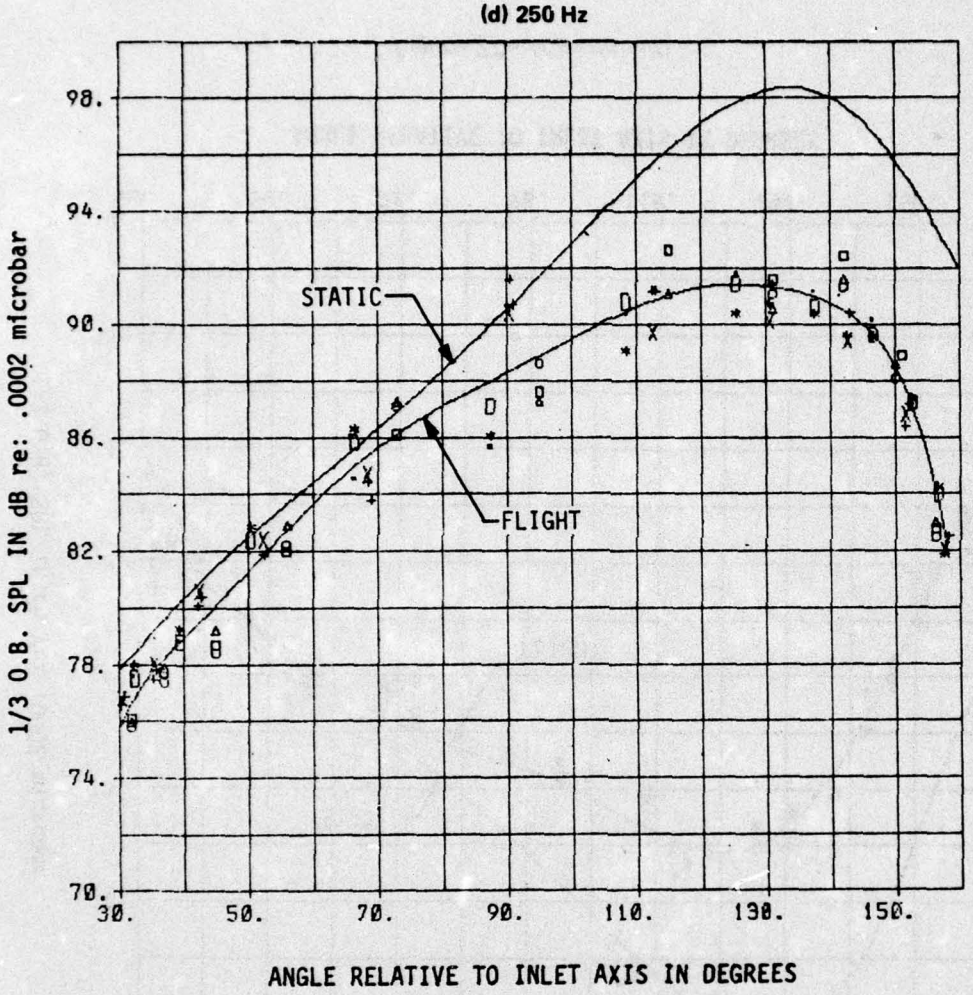


$V_{JPRI}$ = 1464 ft/sec
$V_{A/P}$ = 290 ft/sec

- 400 ft. ALTITUDE
- FREE FIELD
- 77°F, 70% RH
- THREE ENGINES

NOTE: Symbols are flight data for three flyovers, three mics.

*Figure 27.—(Continued)*

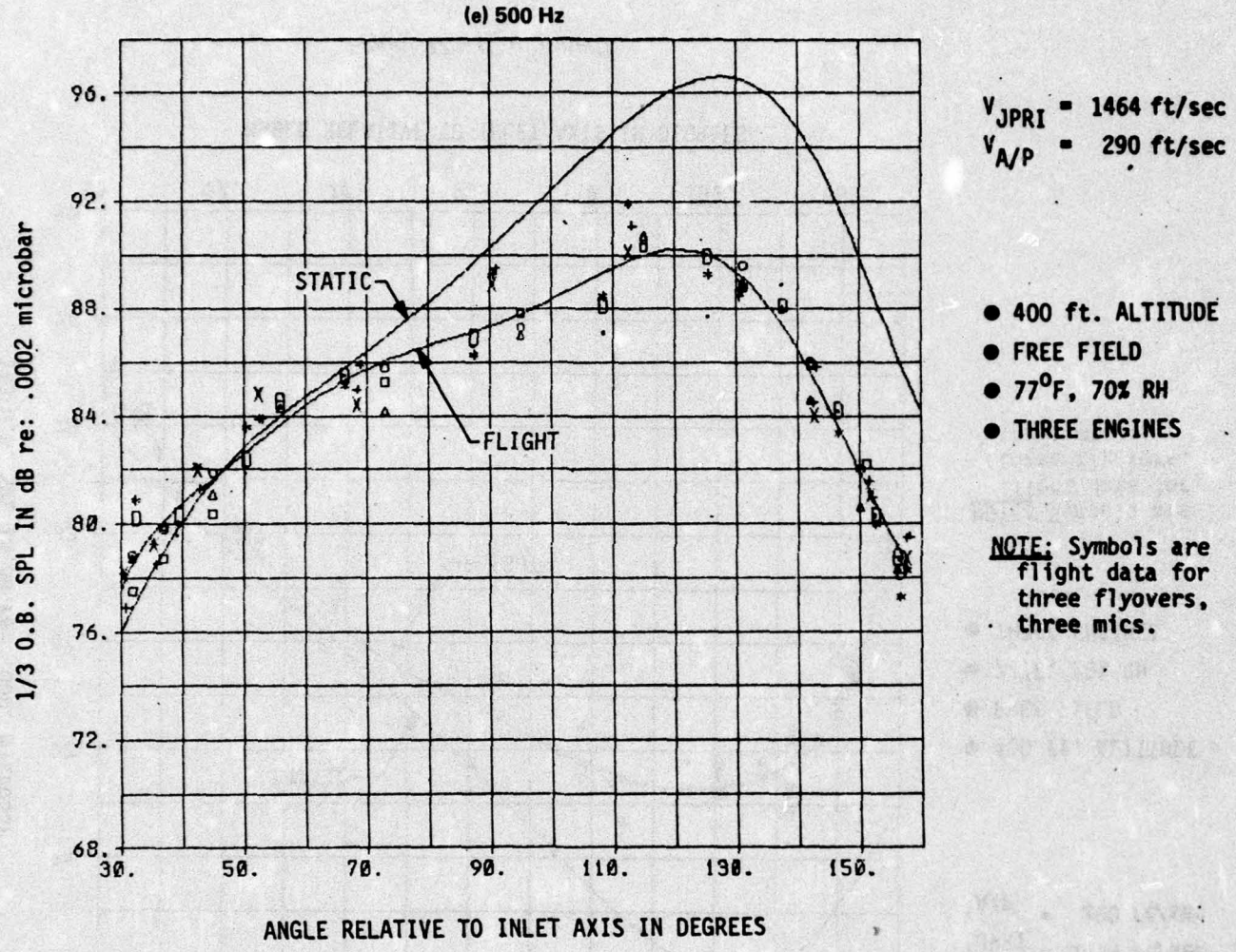


$V_{JPRI}$ = 1464 ft/sec
$V_{A/P}$ = 290 ft/sec

- 400 ft. ALTITUDE
- FREE FIELD
- 77°F, 70% RH
- THREE ENGINES

NOTE: Symbols are flight data for three flyovers, three mics.

*Figure 27.—(Continued)*

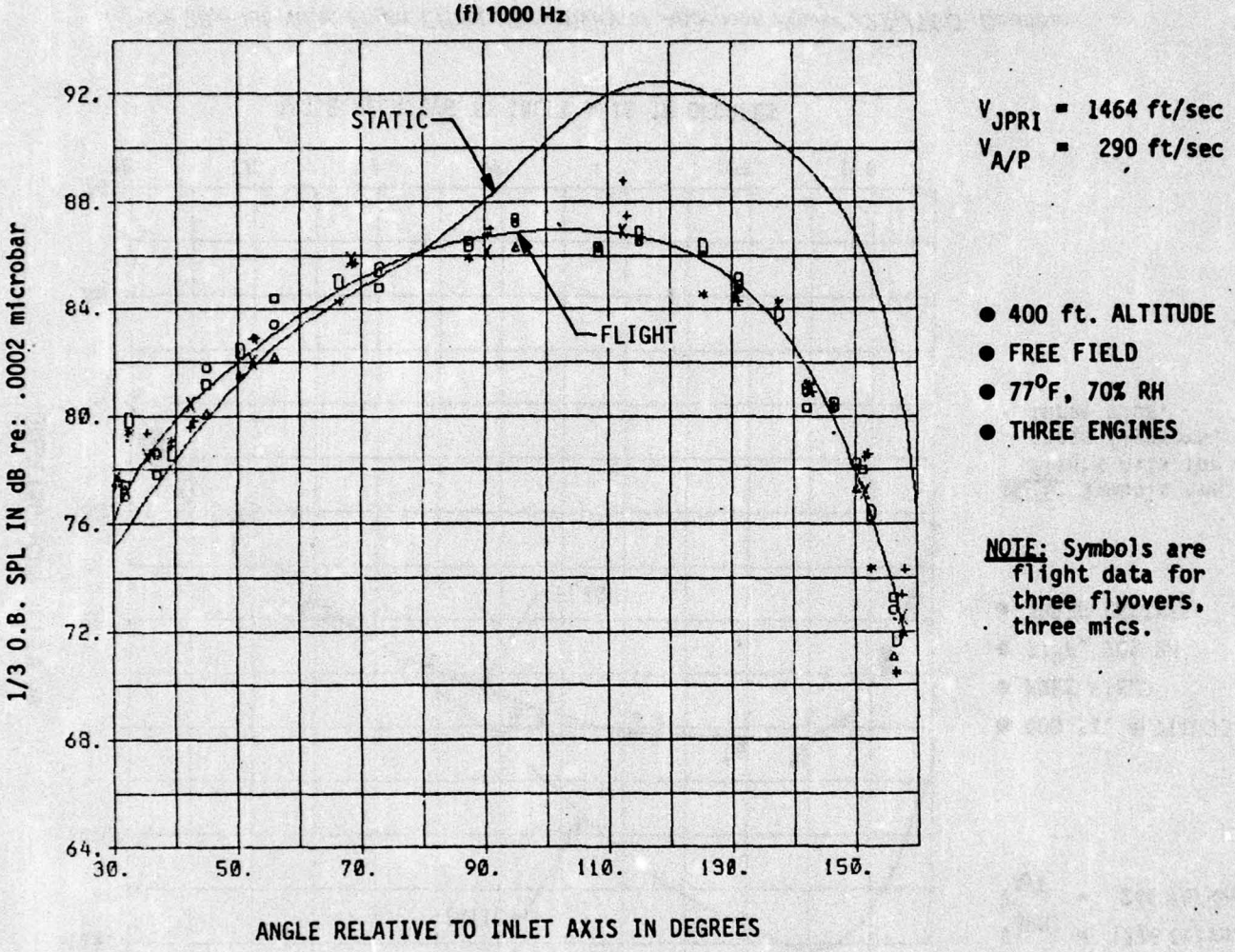


*Figure 27.—(Concluded)*

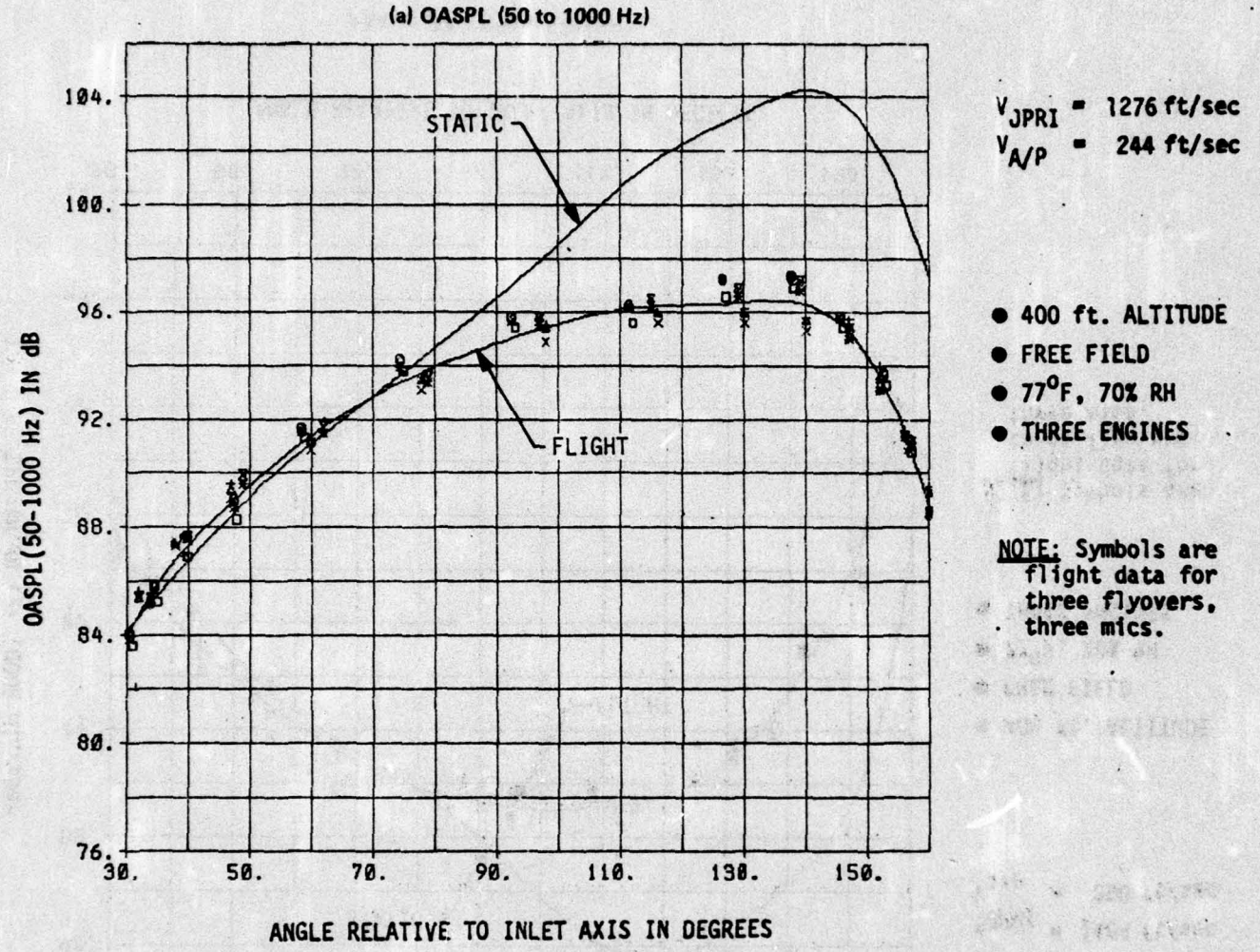


*Figure 28.—Jet Noise Flight Effects Directivity at Approach Power 727/JT8D Baseline*

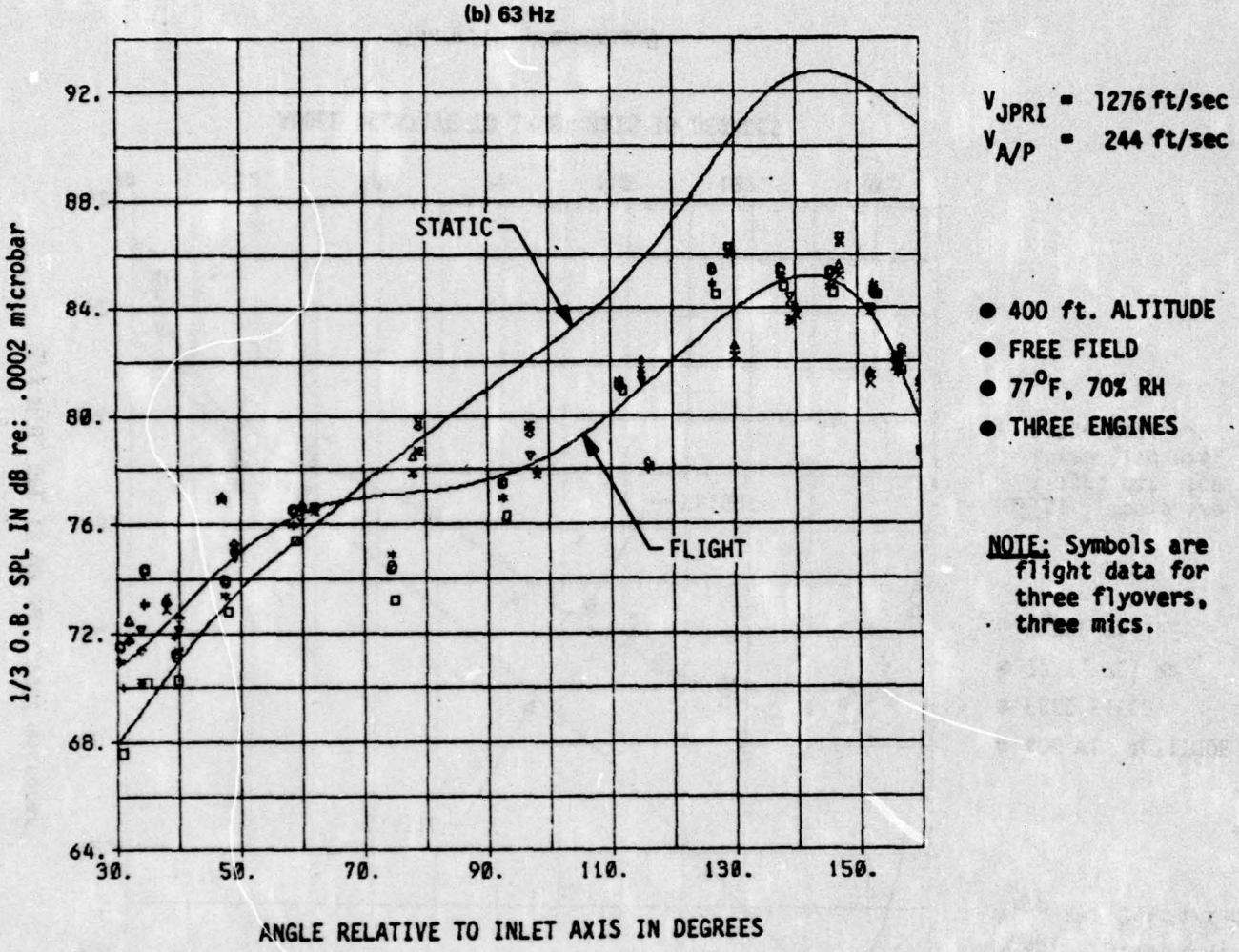


*Figure 28.—(Continued)*

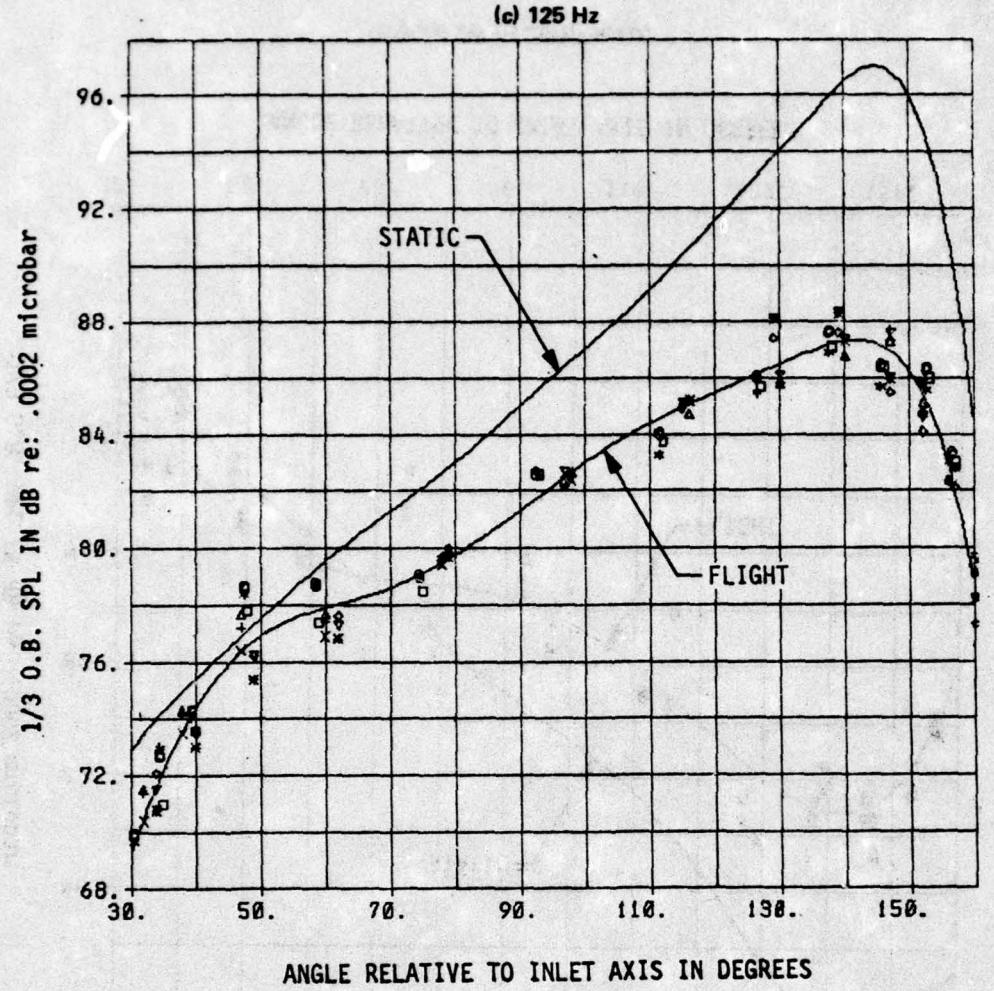


$V_{JPRI}$ = 1276 ft/sec
$V_{A/P}$ = 244 ft/sec

- 400 ft. ALTITUDE
- FREE FIELD
- 77°F, 70% RH
- THREE ENGINES

NOTE: Symbols are flight data for three flyovers, three mics.

*Figure 28.—(Continued)*

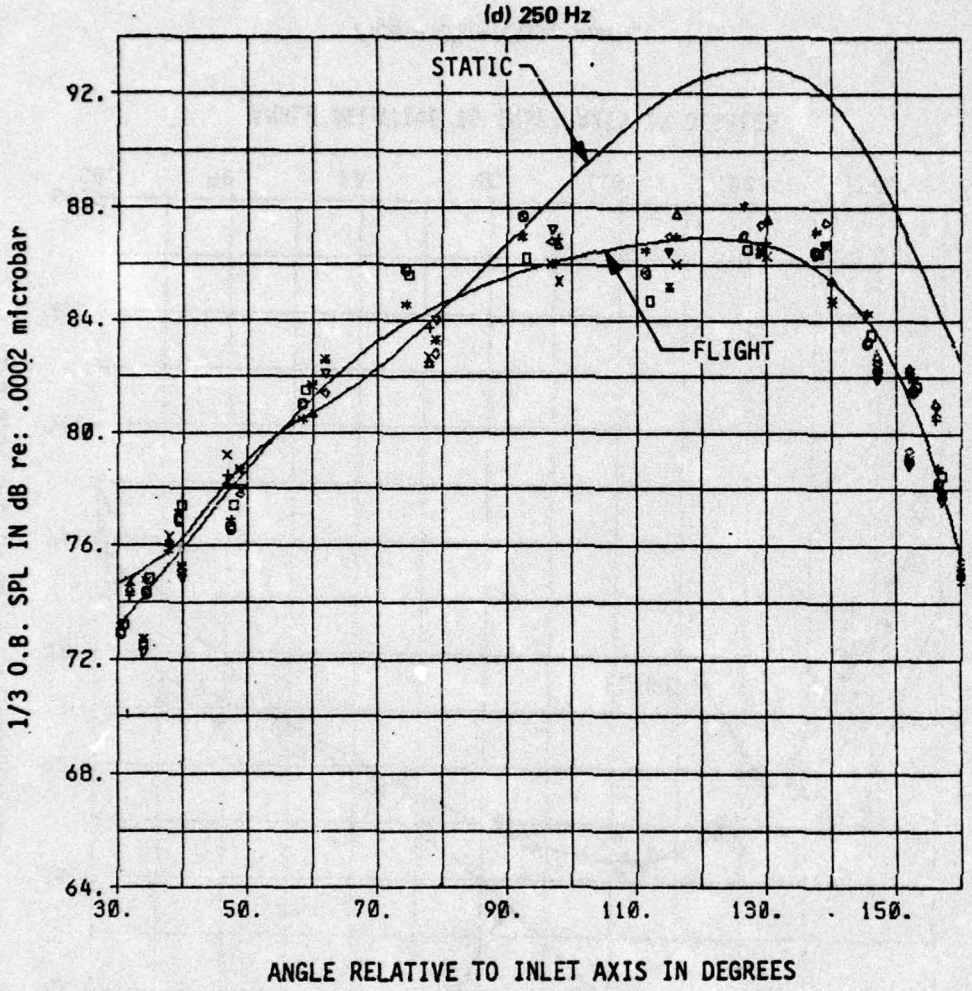


$V_{JPRI}$ = 1276 ft/sec
$V_{A/P}$ = 244 ft/sec

- 400 ft. ALTITUDE
- FREE FIELD
- 77°F, 70% RH
- *THREE ENGINES*

NOTE: Symbols are flight data for three flyovers, three mics.

*Figure 28.—(Continued)*

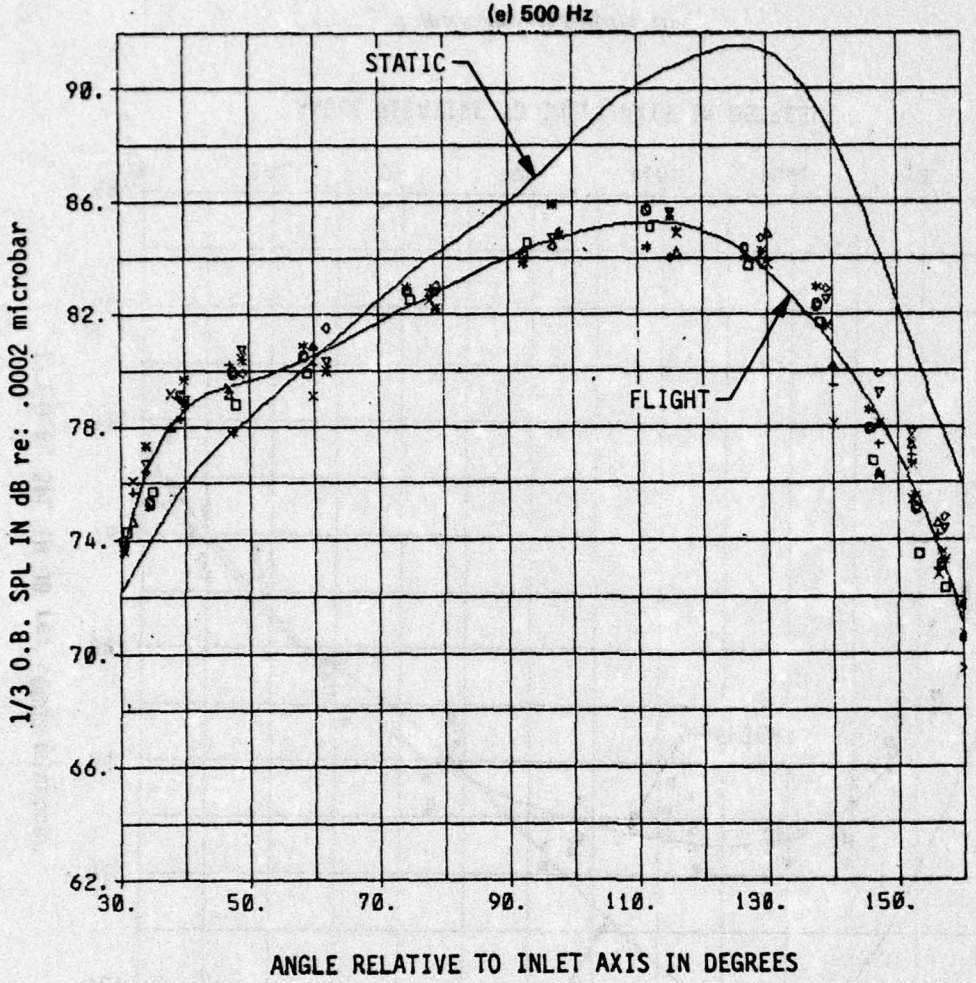


$V_{JPRI}$ = 1276 ft/sec
$V_{A/P}$ = 244 ft/sec

- 400 ft. ALTITUDE
- FREE FIELD
- 77°F, 70% RH
- THREE ENGINES

NOTE: Symbols are flight data for three flyovers, three mics.

*Figure 28.—(Continued)*

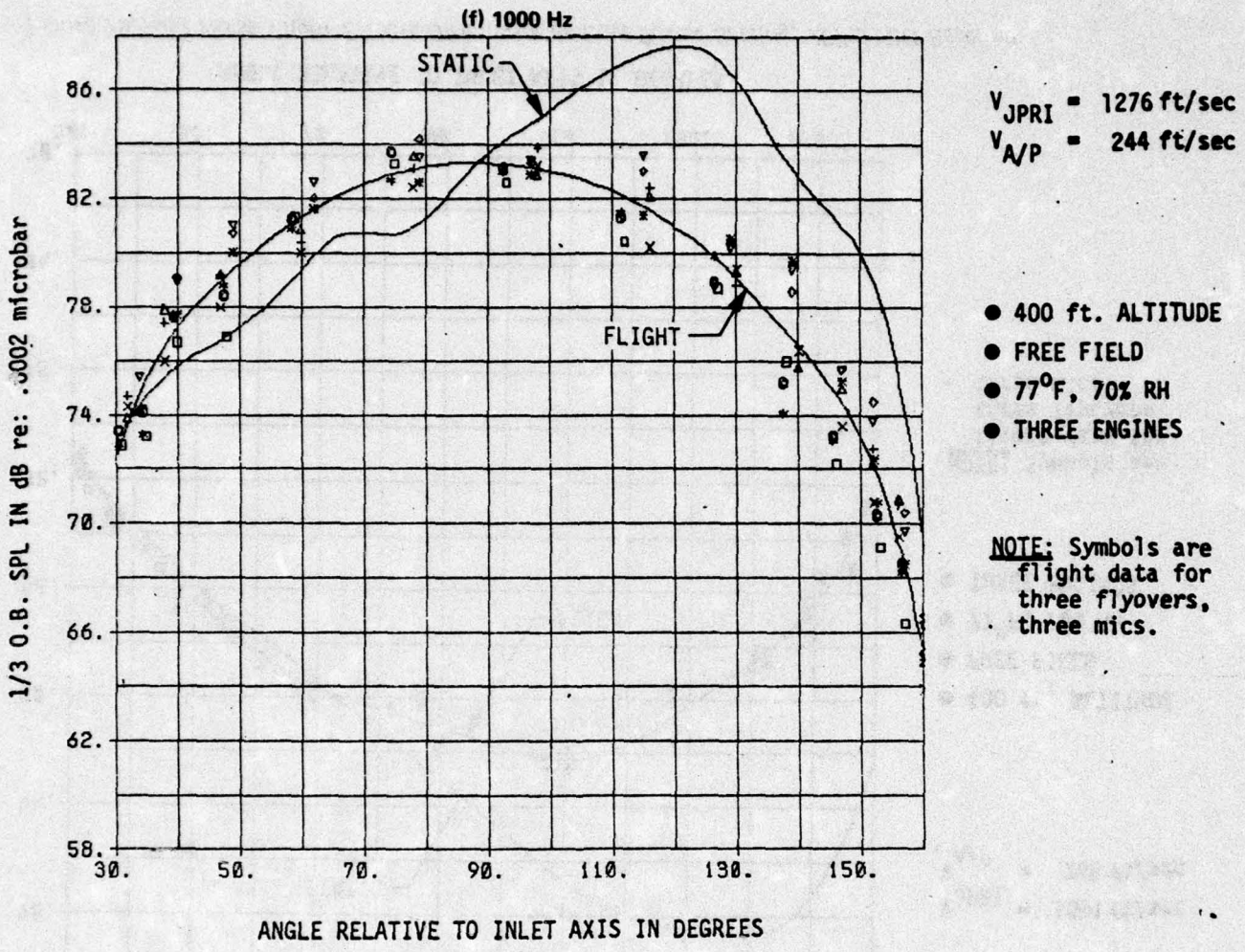


*Figure 28.—(Concluded)*

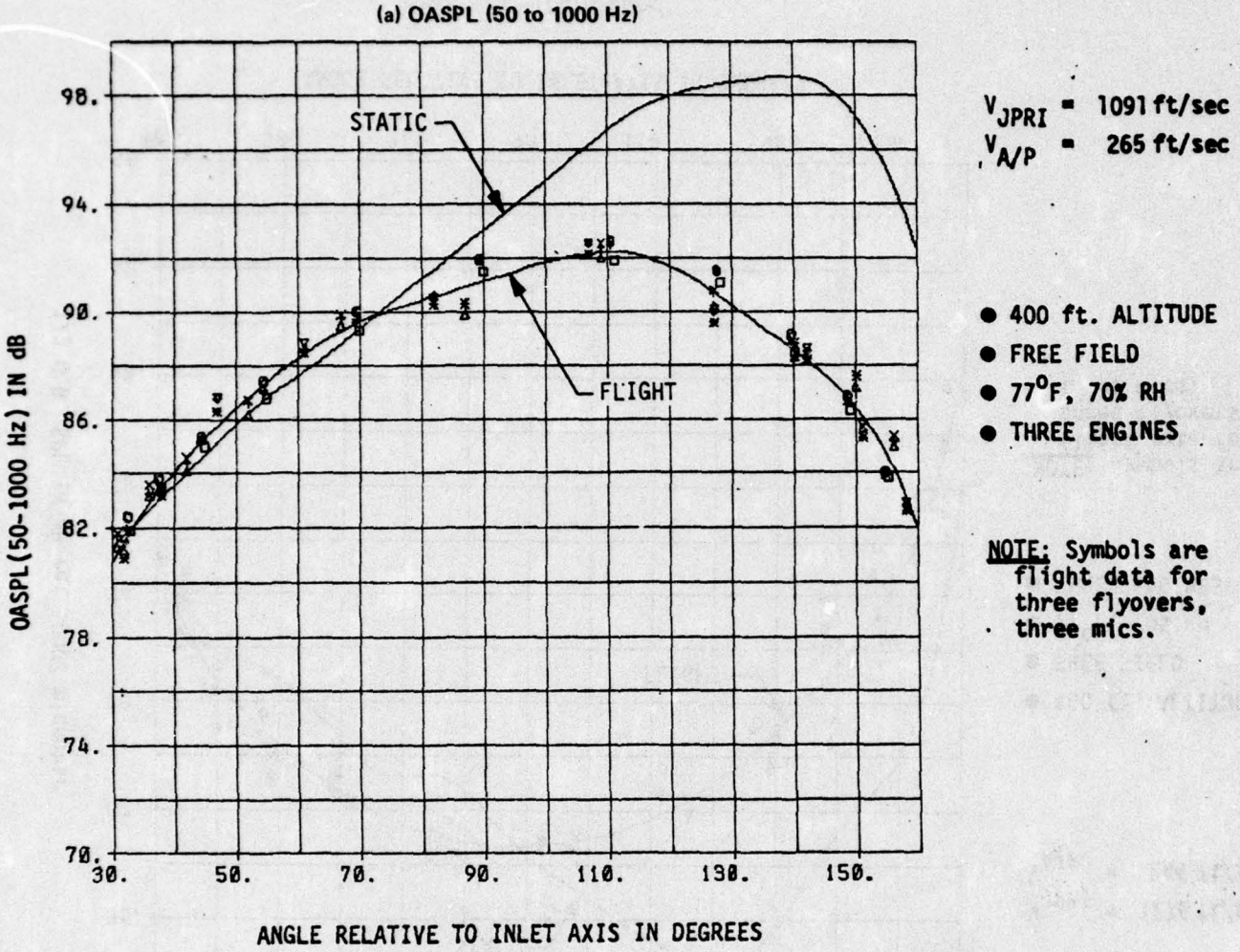


*Figure 29.—Jet Noise Flight Effects Directivity at Low Power Setting, 727/JT8D Baseline*

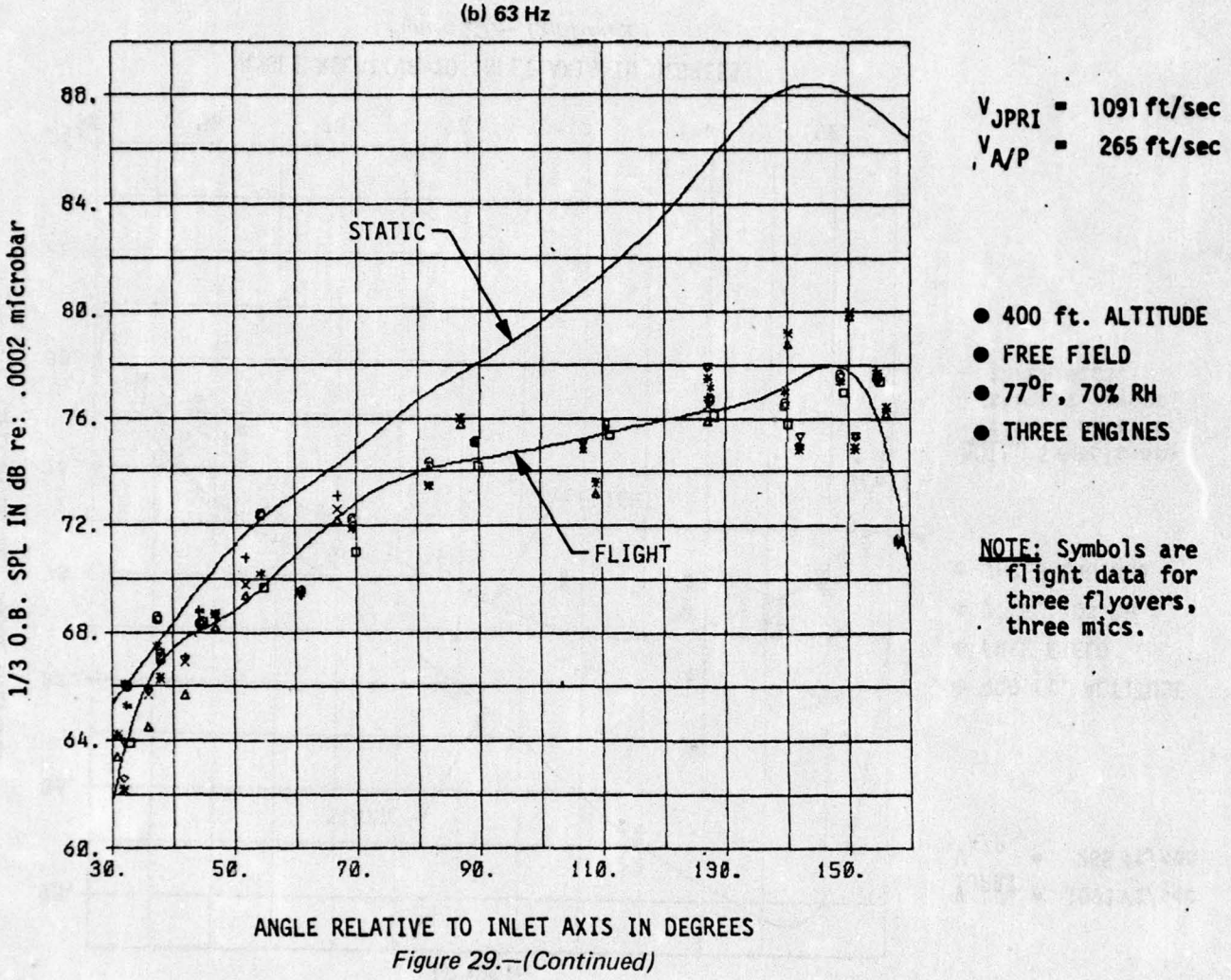


*Figure 29.—(Continued)*

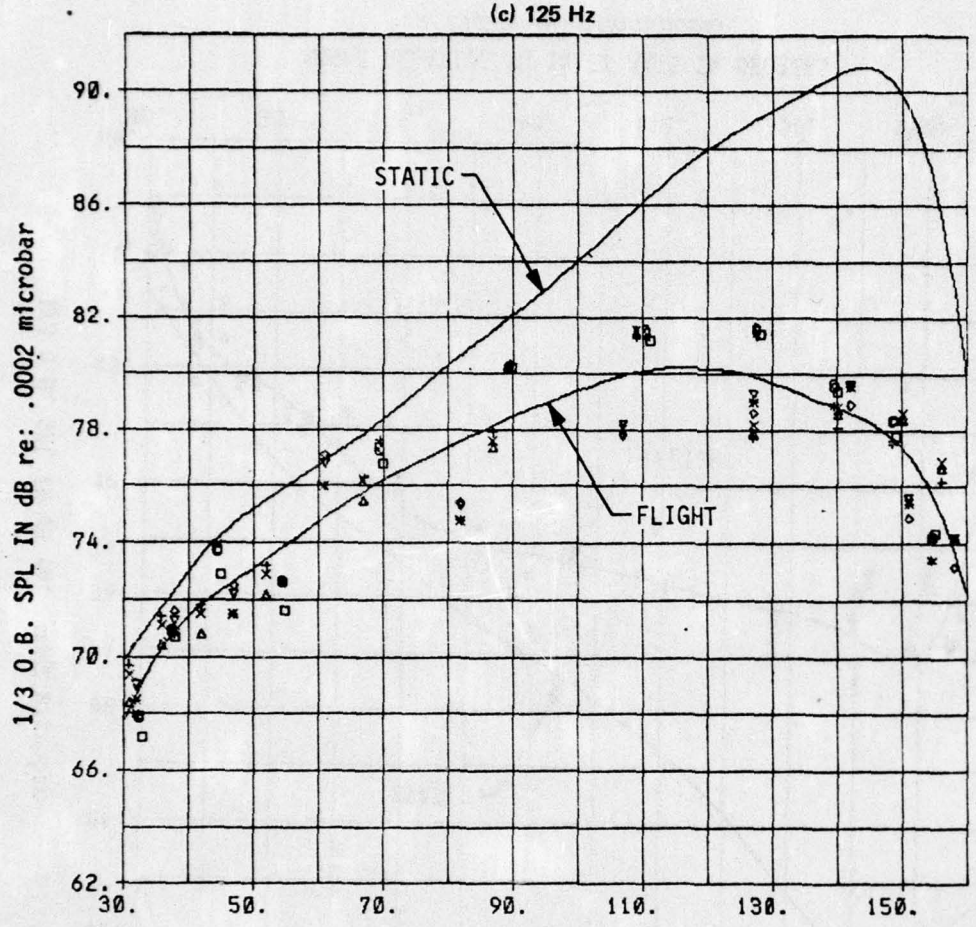


$V_{JPRI}$ = 1091 ft/sec
$V_{A/P}$ = 265 ft/sec

- 400 ft. ALTITUDE
- FREE FIELD
- 77°F, 70% RH
- THREE ENGINES

NOTE: Symbols are flight data for three flyovers, three mics.

*Figure 29.—(Continued)*

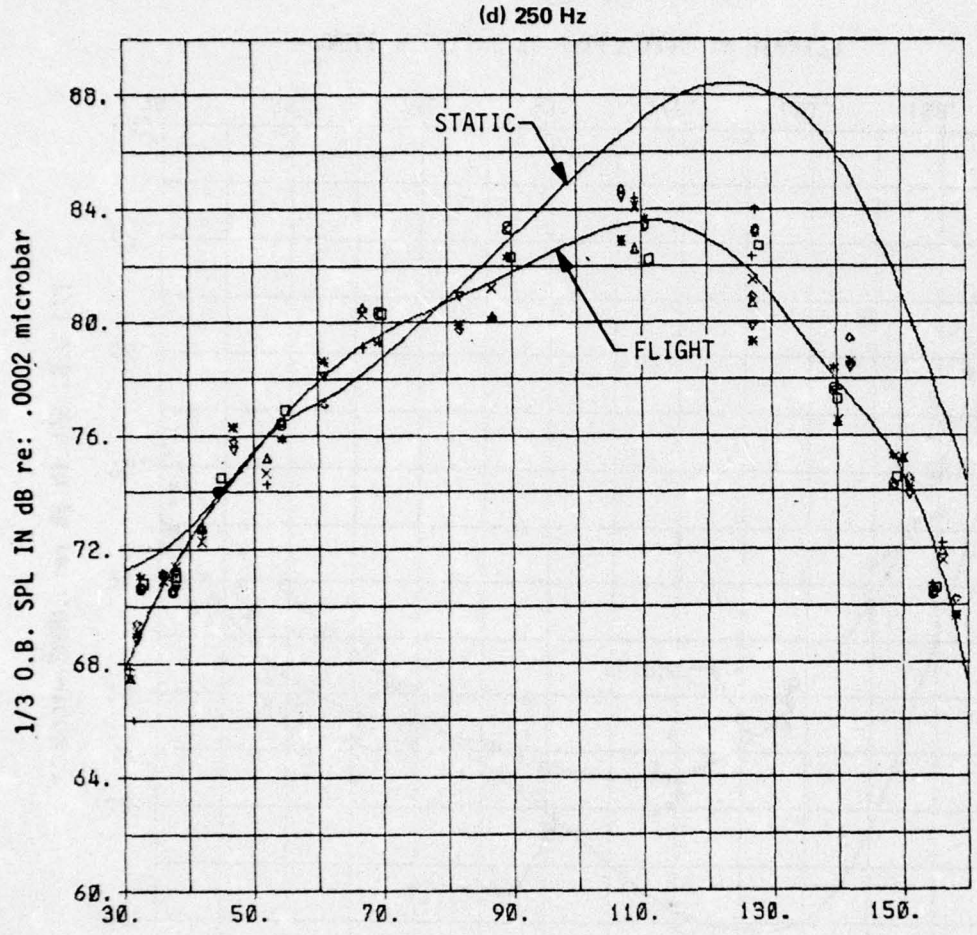


$V_{JPRI}$ = 1091 ft/sec
$V_{A/P}$ = 265 ft/sec

- 400 ft. ALTITUDE
- FREE FIELD
- 77°F, 70% RH
- THREE ENGINES

NOTE: Symbols are flight data for three flyovers, three mics.

*Figure 29.—(Continued)*

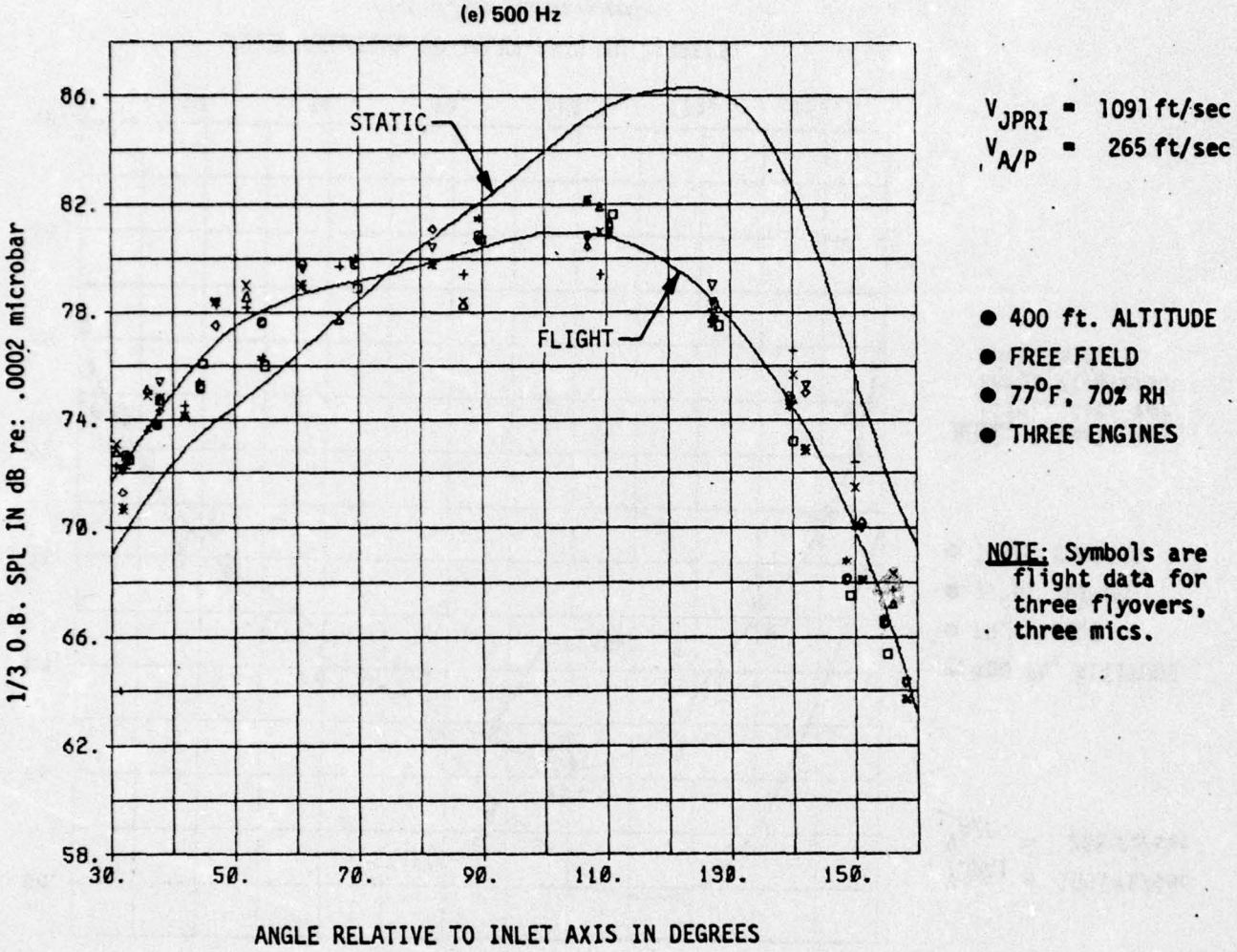


*Figure 29.—(Continued)*

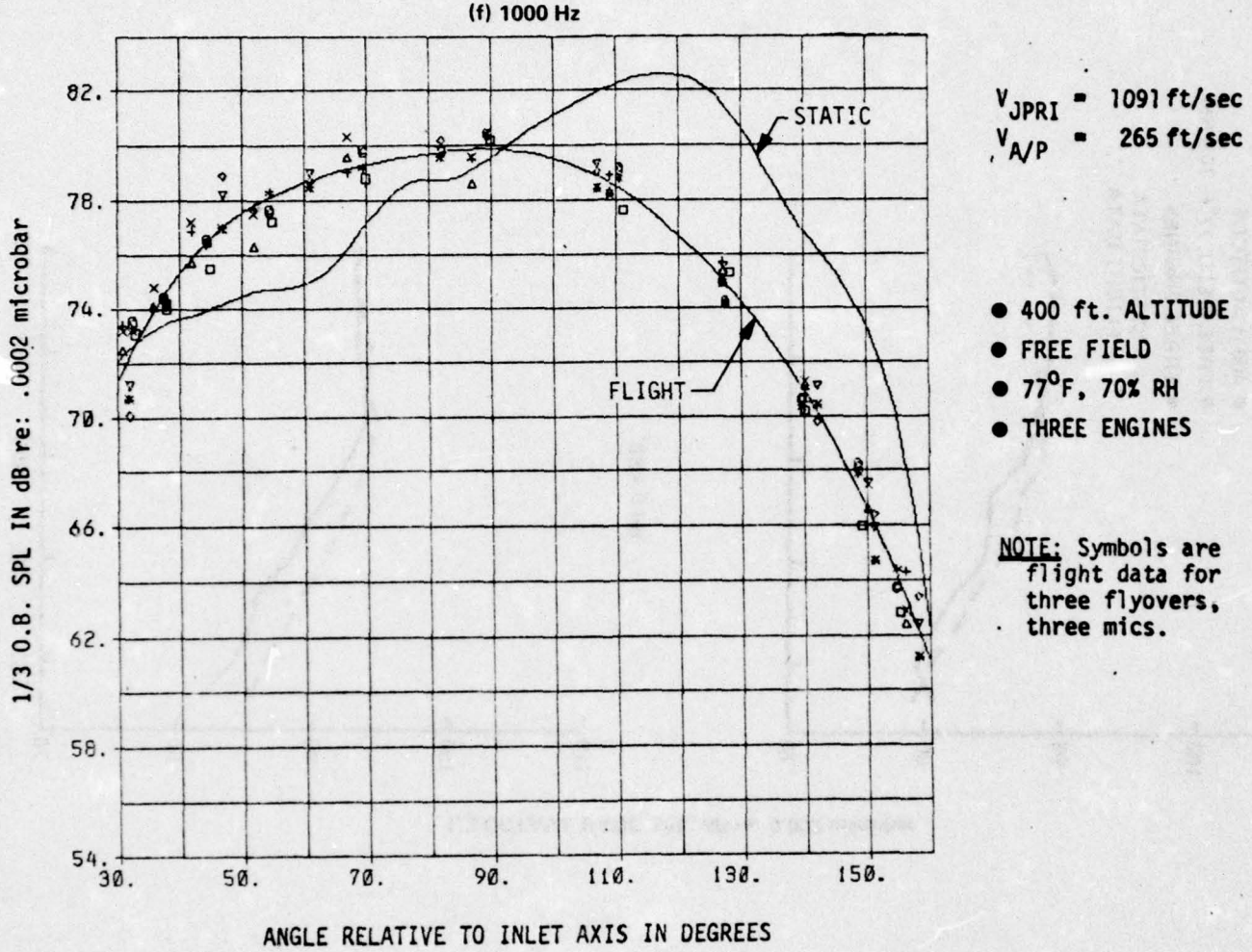


*Figure 29.—(Concluded)*

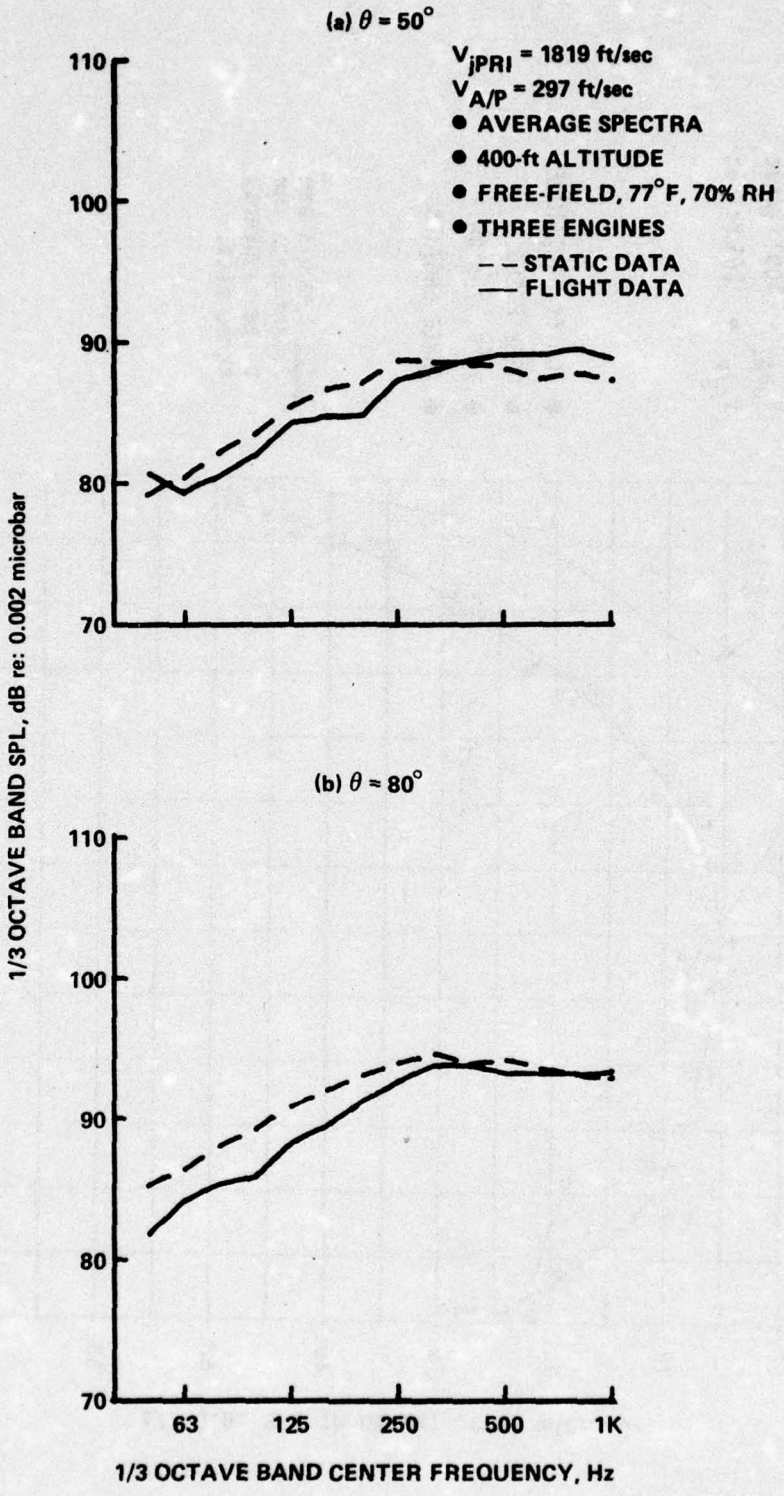


*Figure 30.—Jet Noise Flight Effects, Average Spectra, Takeoff Power, 727/JT8D Baseline*

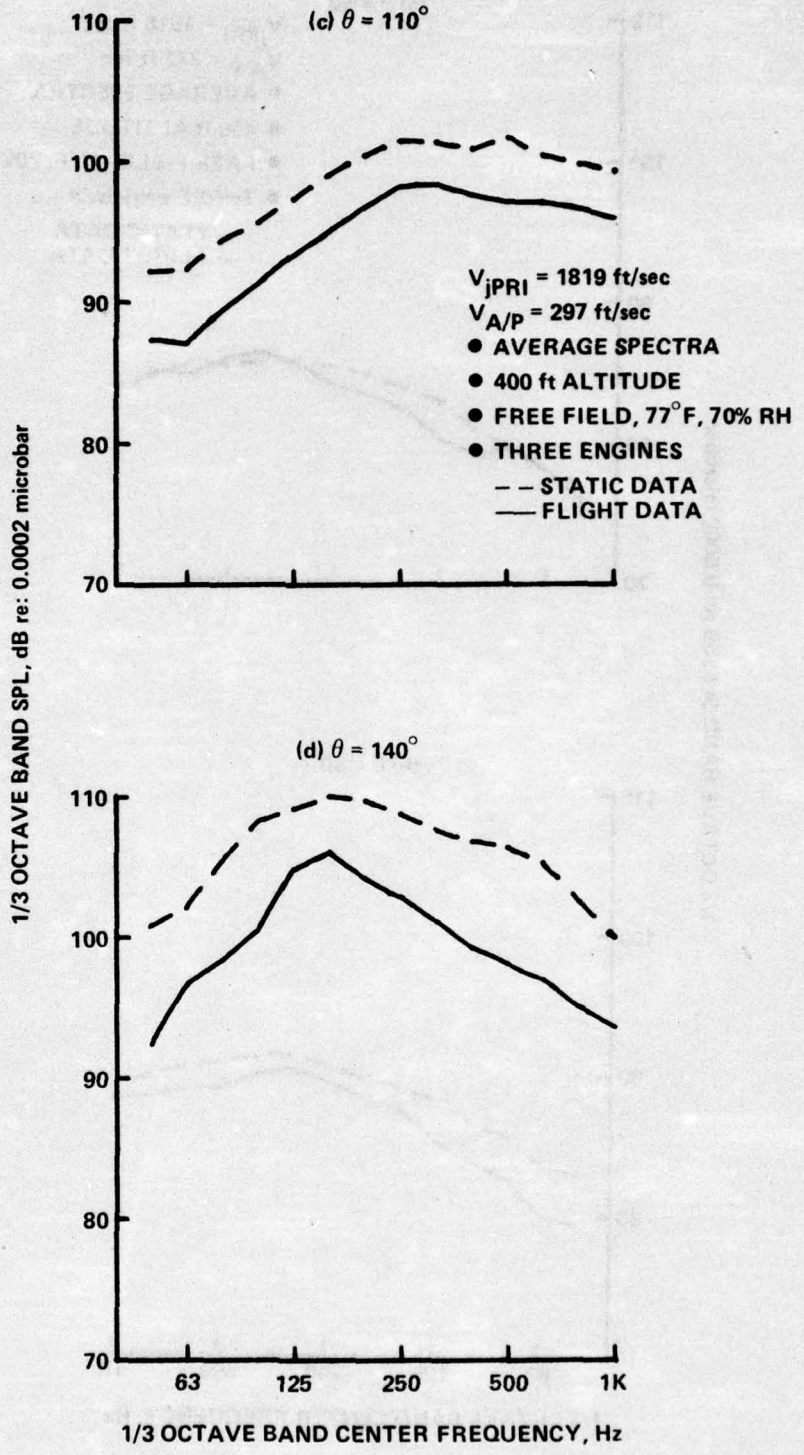


*Figure 30.—(Concluded)*

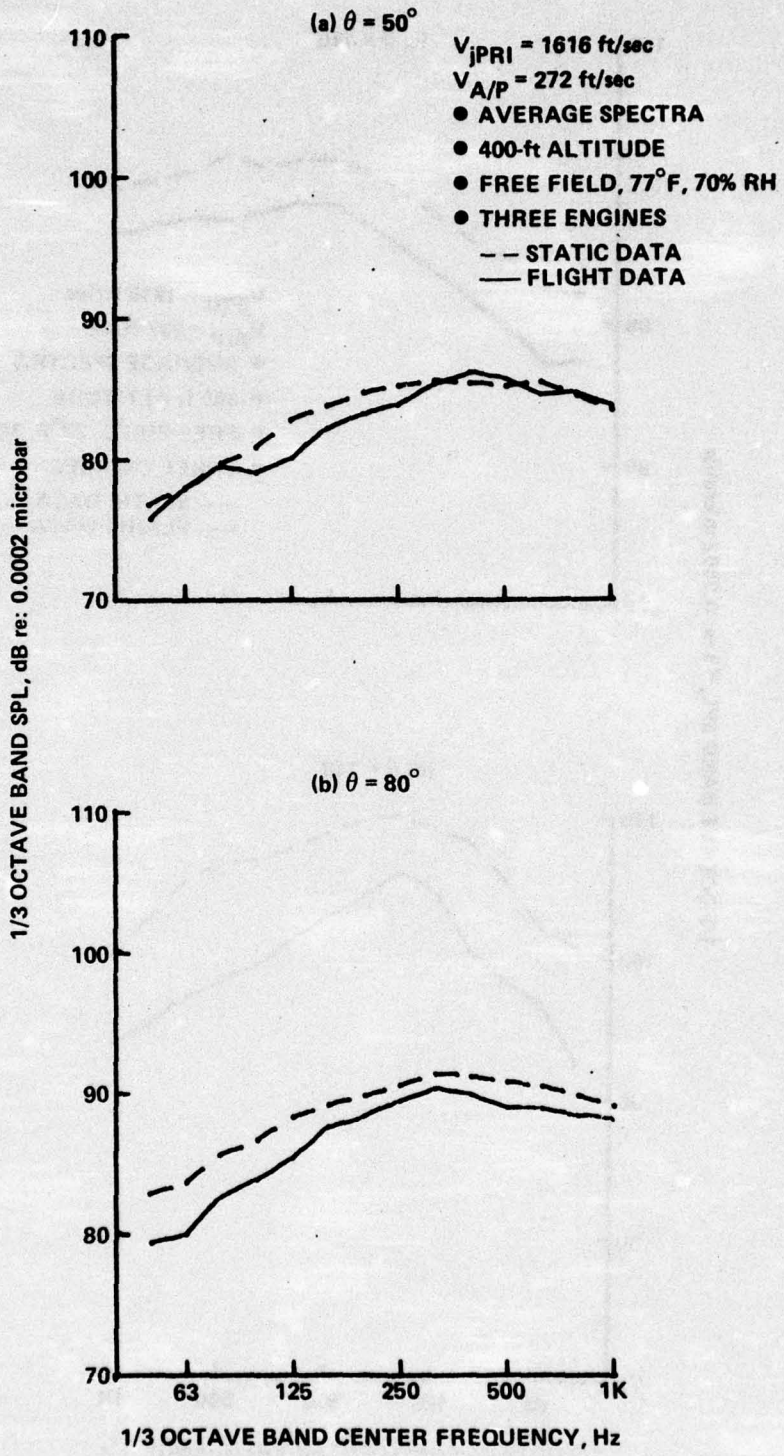


*Figure 31.—Jet Noise Flight Effects, Average Spectra, Cutback Power (HGW), 727/JT8D Baseline*

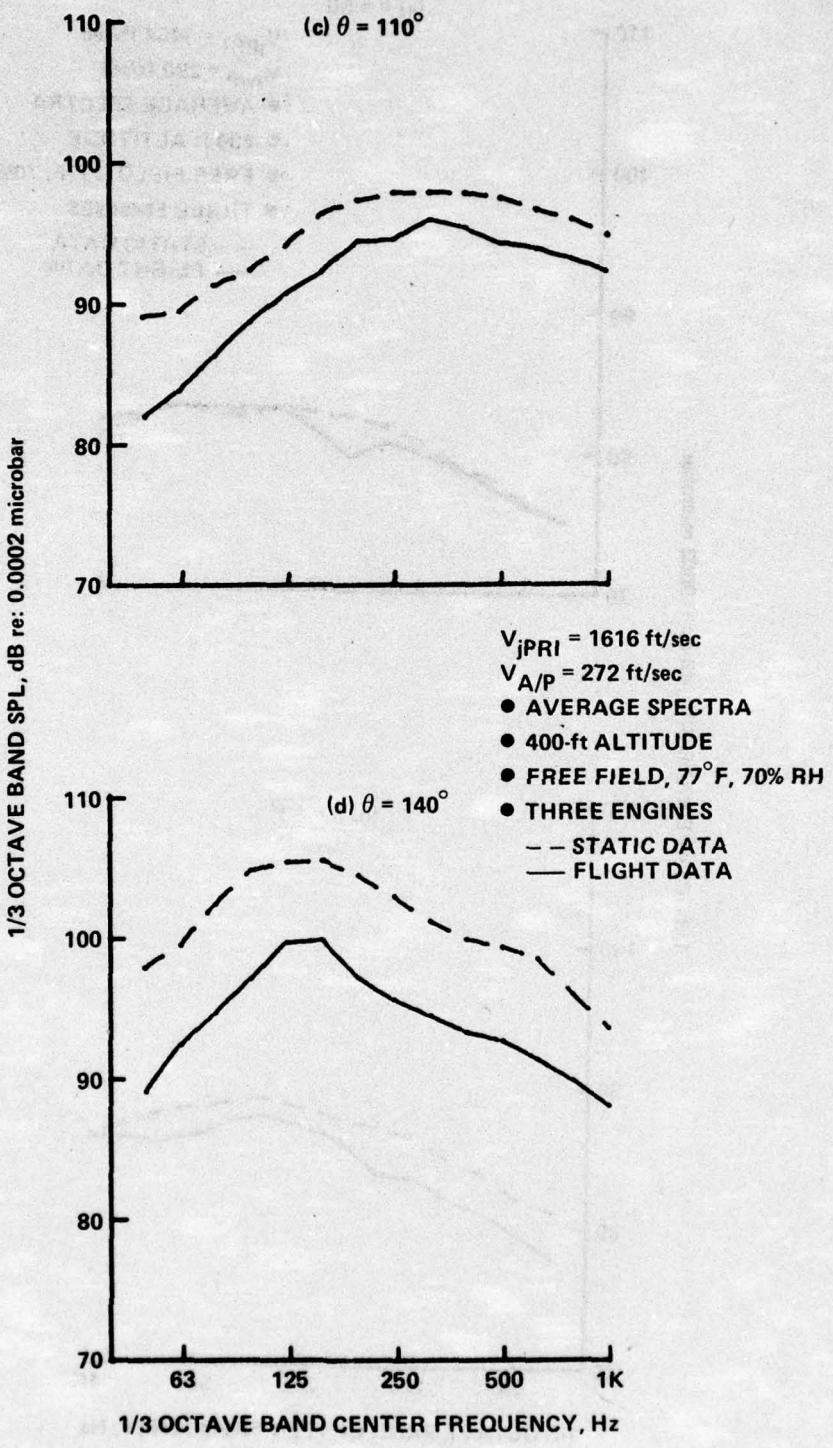


*Figure 31.—(Concluded)*

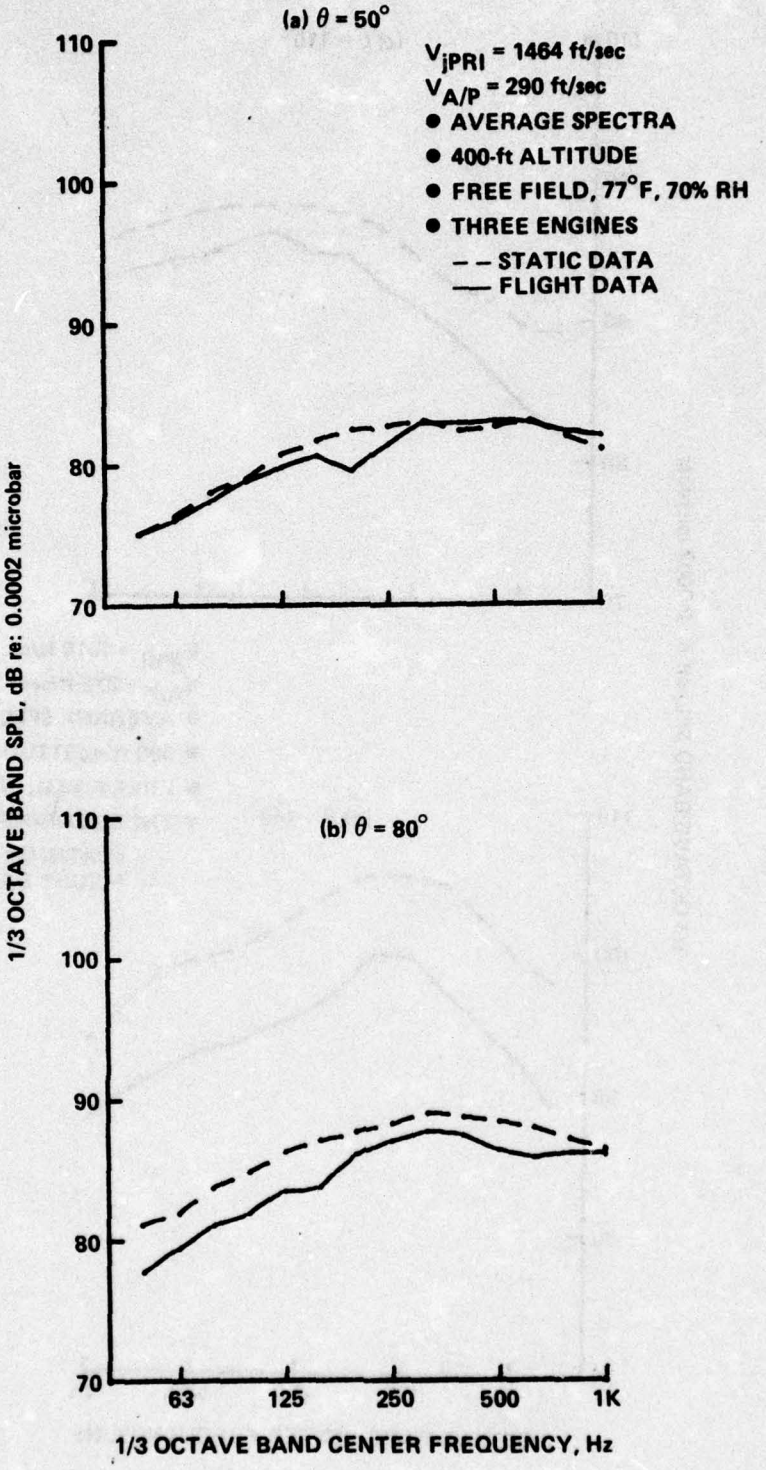


*Figure 32.—Jet Noise Flight Effects, Average Spectra, Cutback Power (LGW), 727/JT8D Baseline*

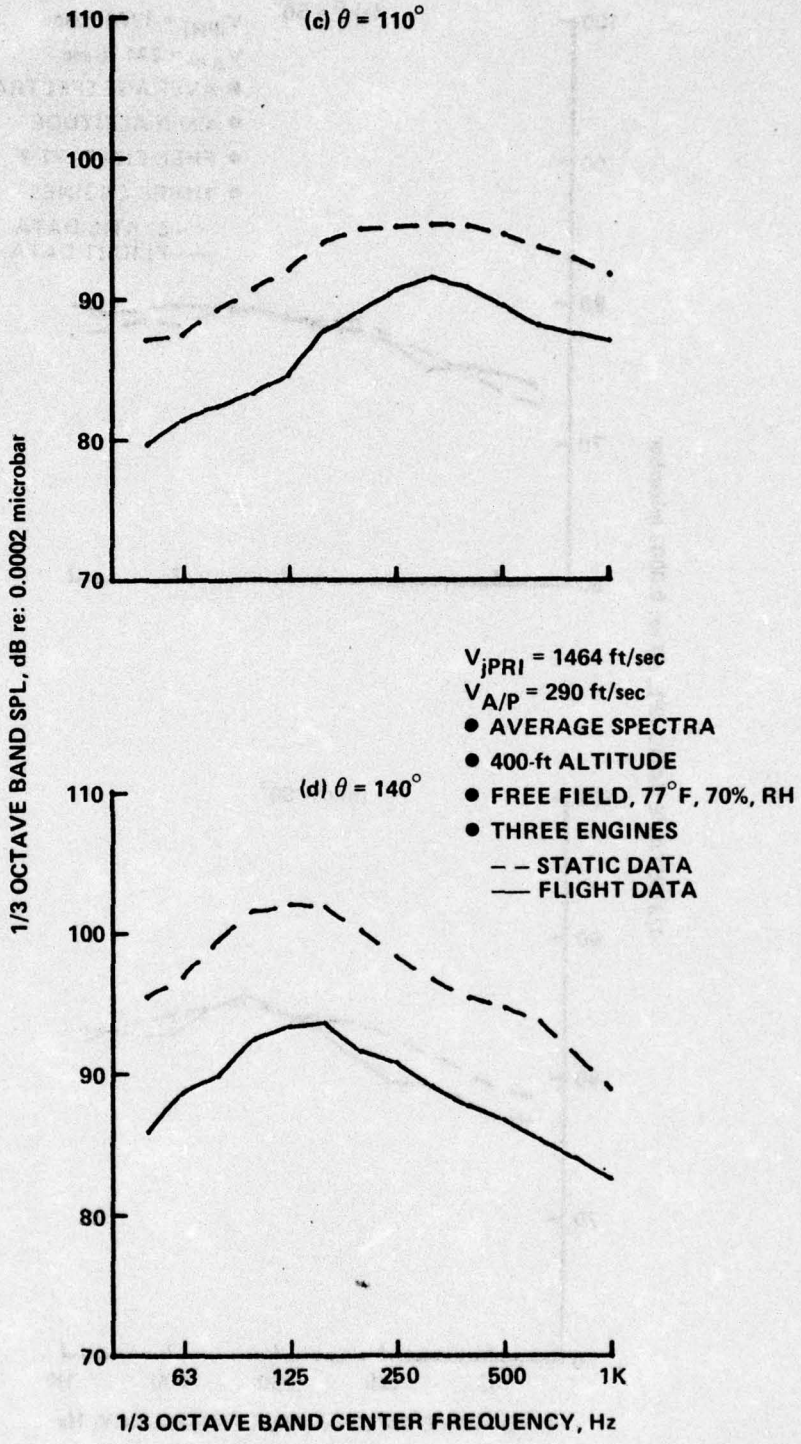


*Figure 32.—(Concluded)*

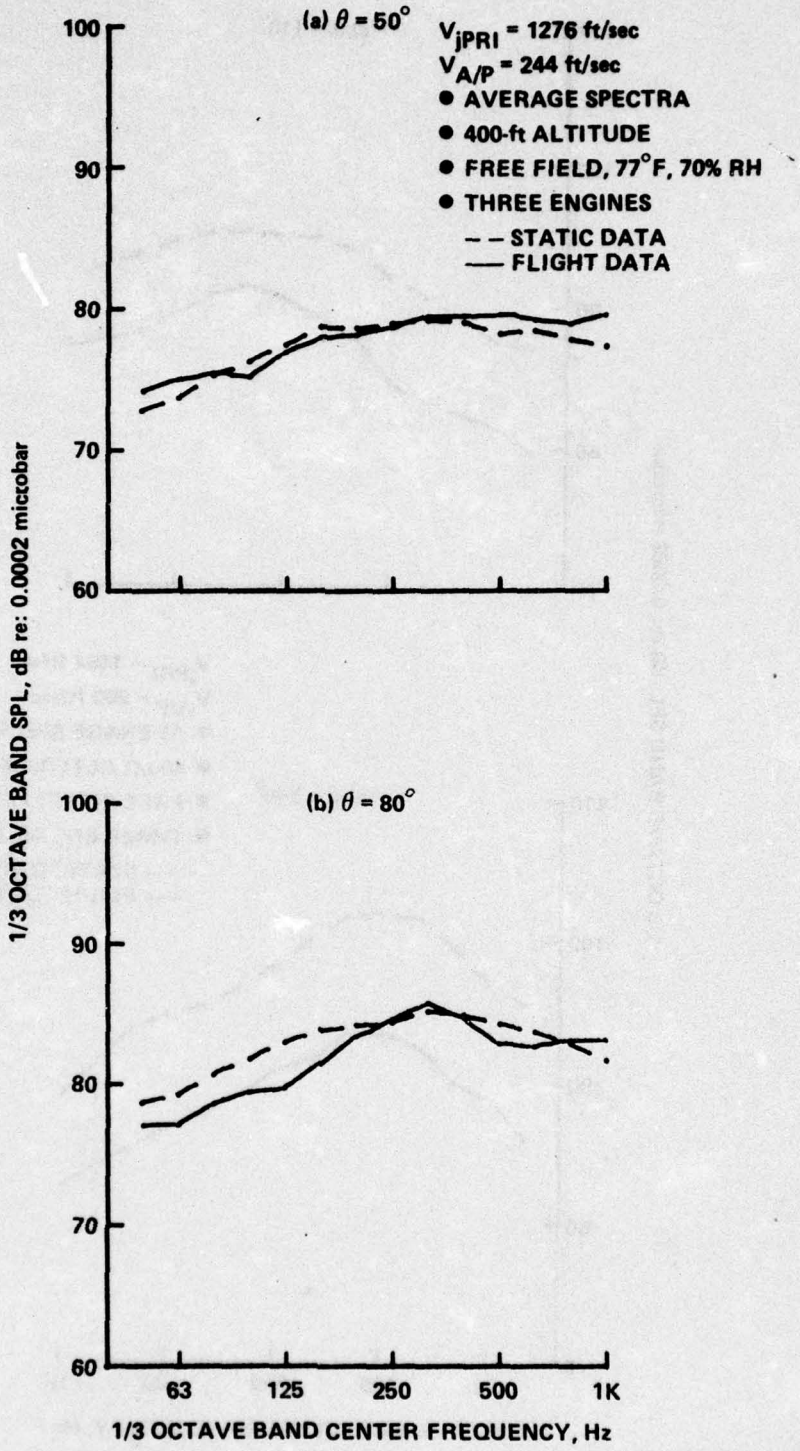


*Figure 33.—Jet Noise Flight Effects, Average Spectra, Approach Power, 727/JT8D Baseline*

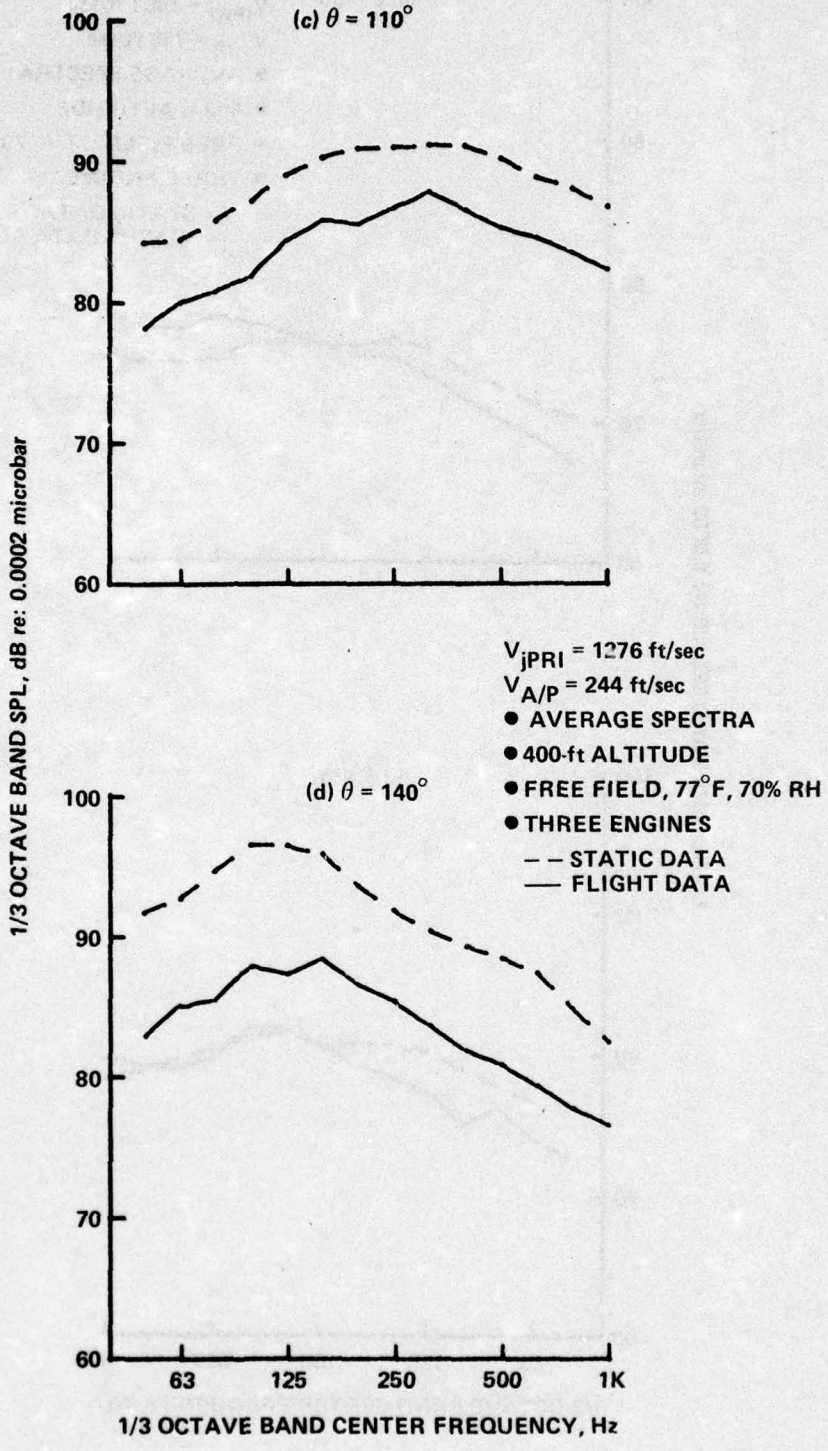


*Figure 33.—(Concluded)*

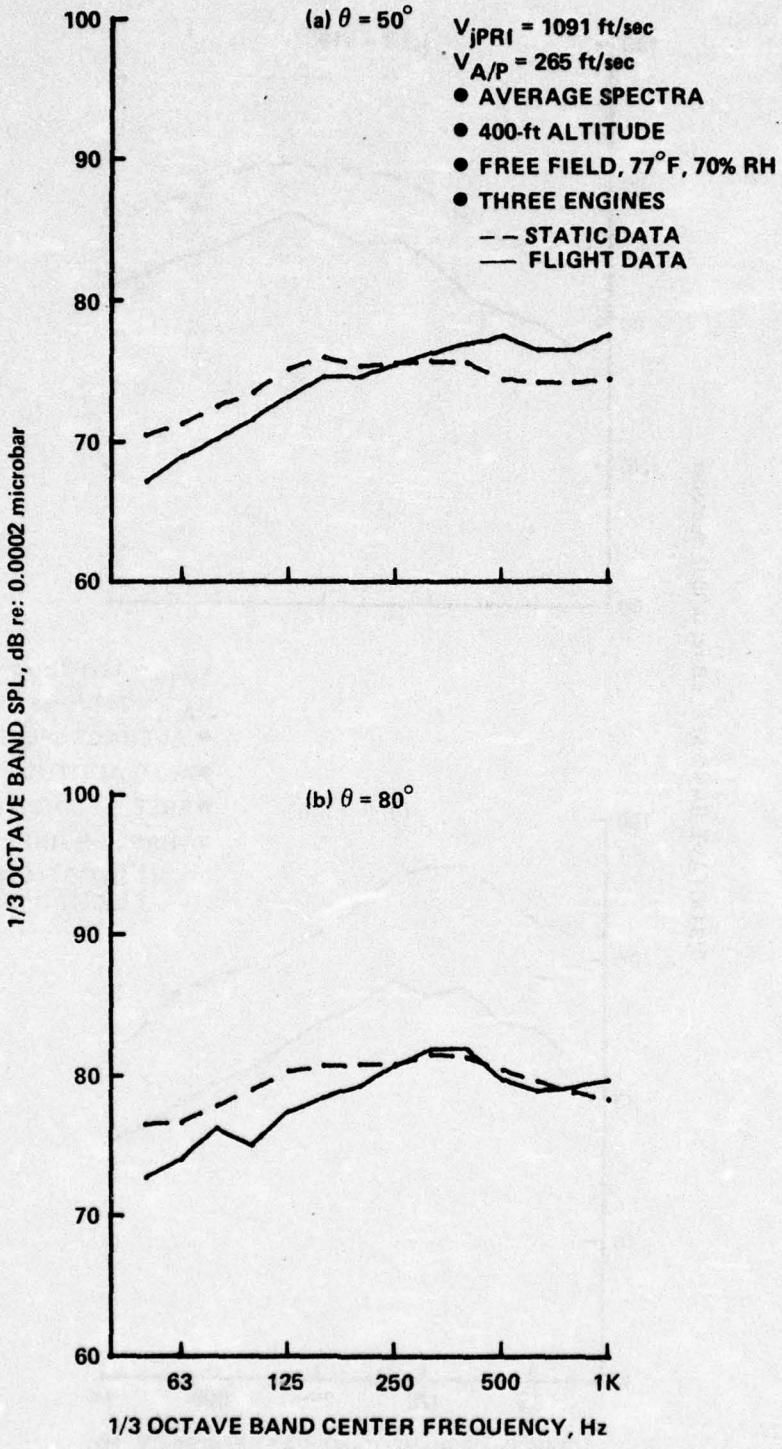


*Figure 34.—Jet Noise Flight Effects, Average Spectra, Low Power Setting, 727/JT8D Baseline*

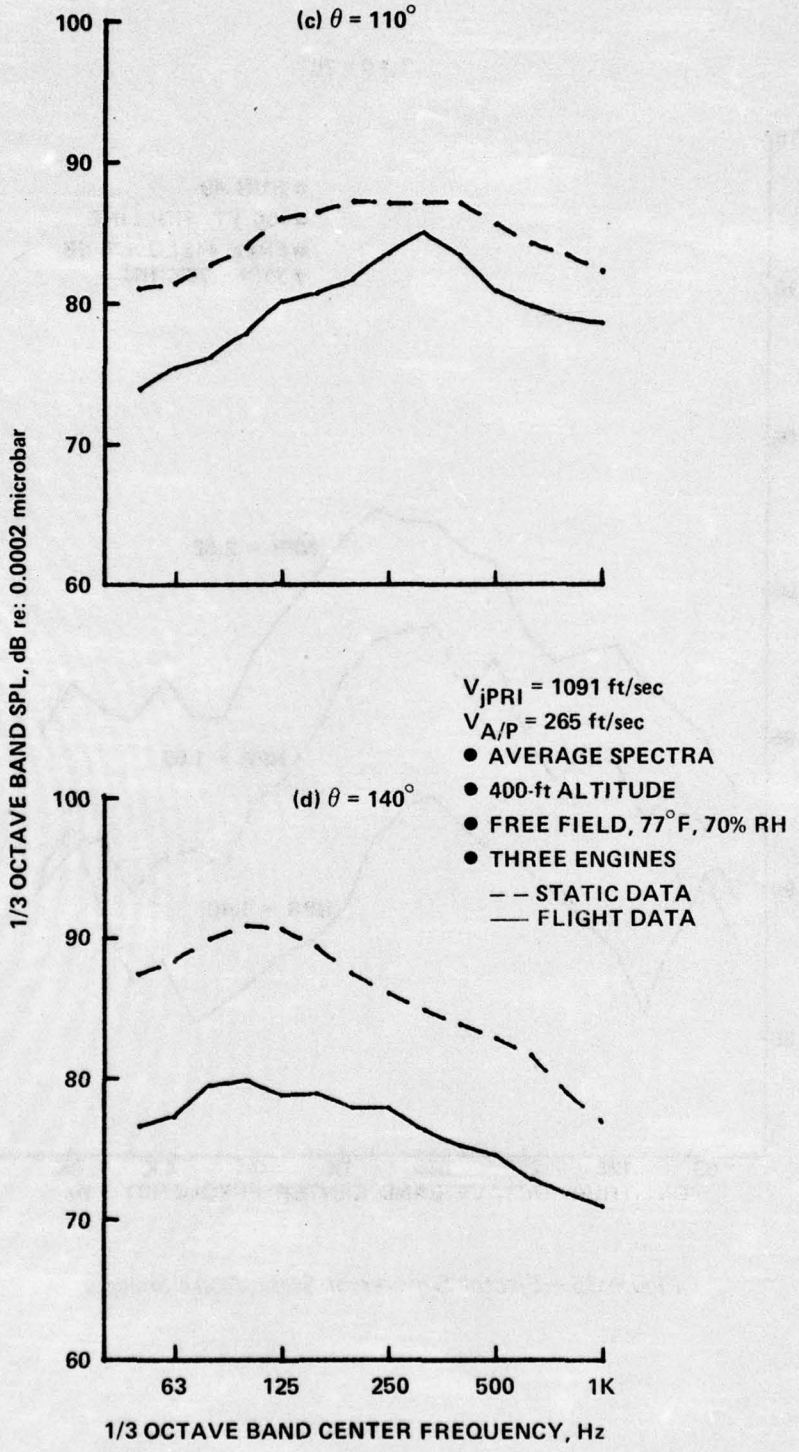


*Figure 34.—(Concluded)*

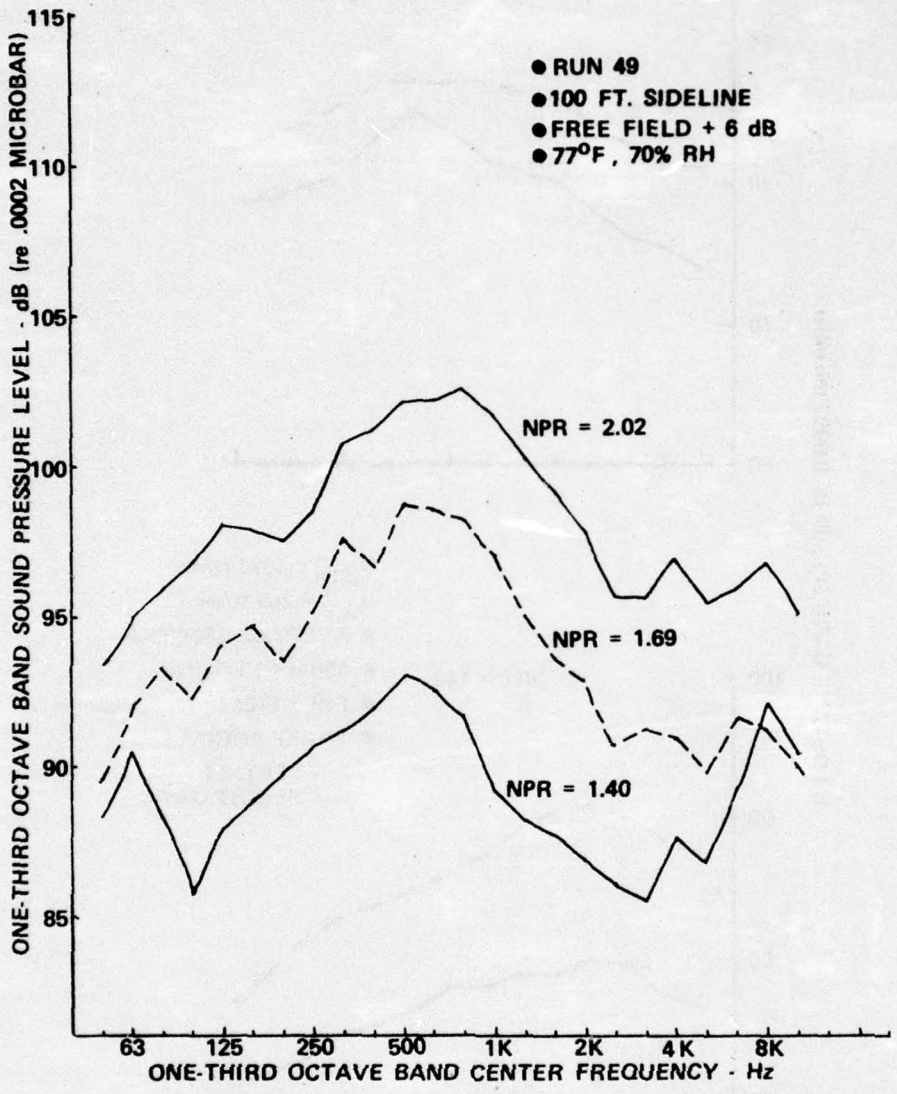


*Figure 35.—Ejector Suppressor Static Noise Spectra*

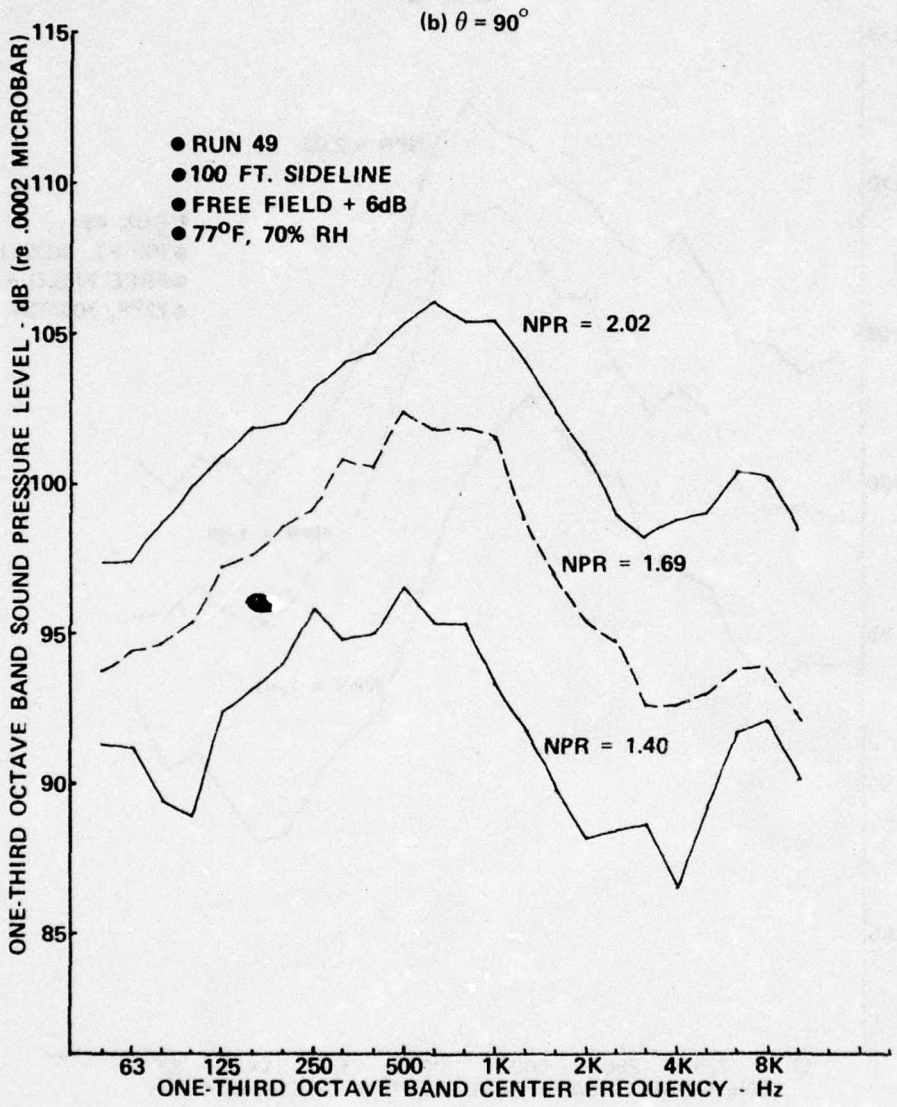


*Figure 35.—(Continued)*

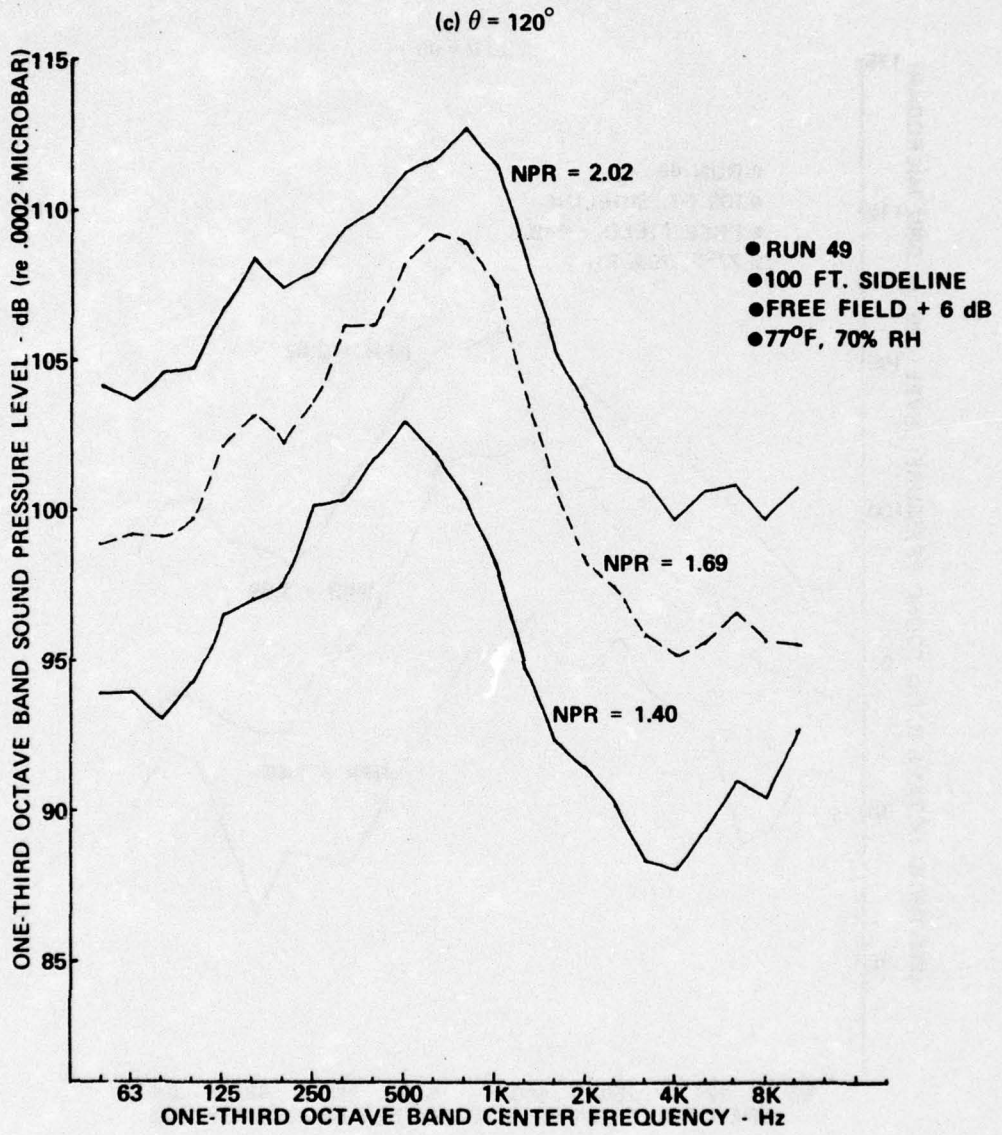


*Figure 35.—(Continued)*

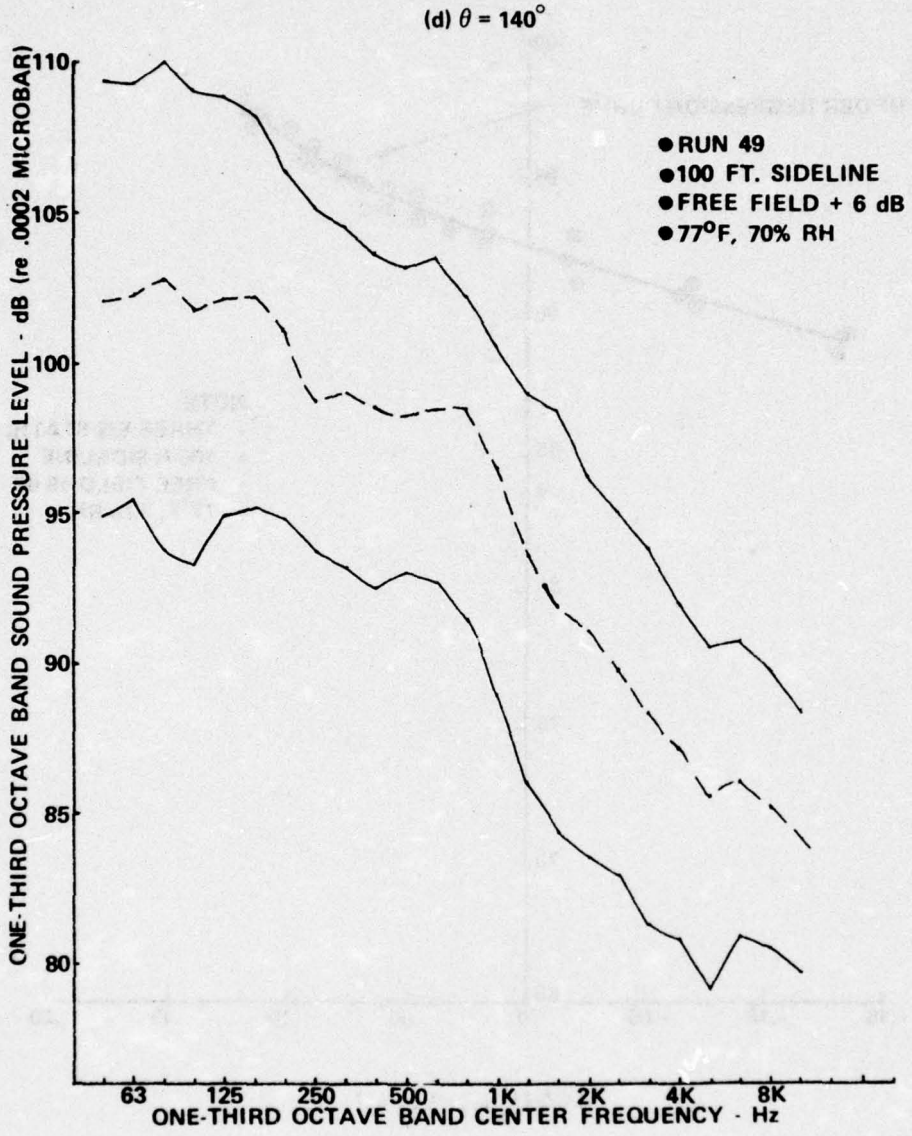


*Figure 35.—(Concluded)*

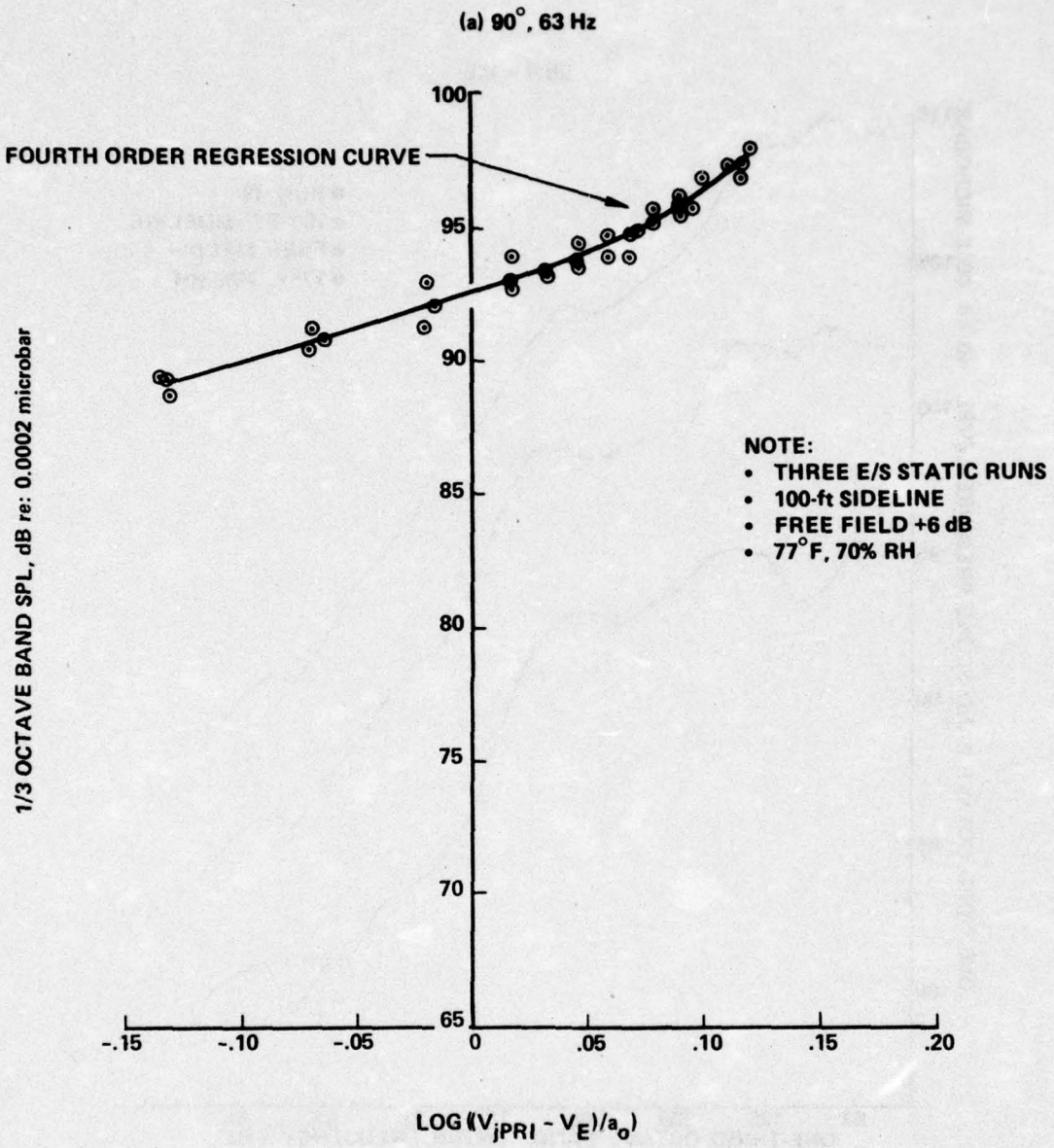


*Figure 36.—Ejector Suppressor Static Noise Data Versus Engine Power Setting, $\theta = 90°$*

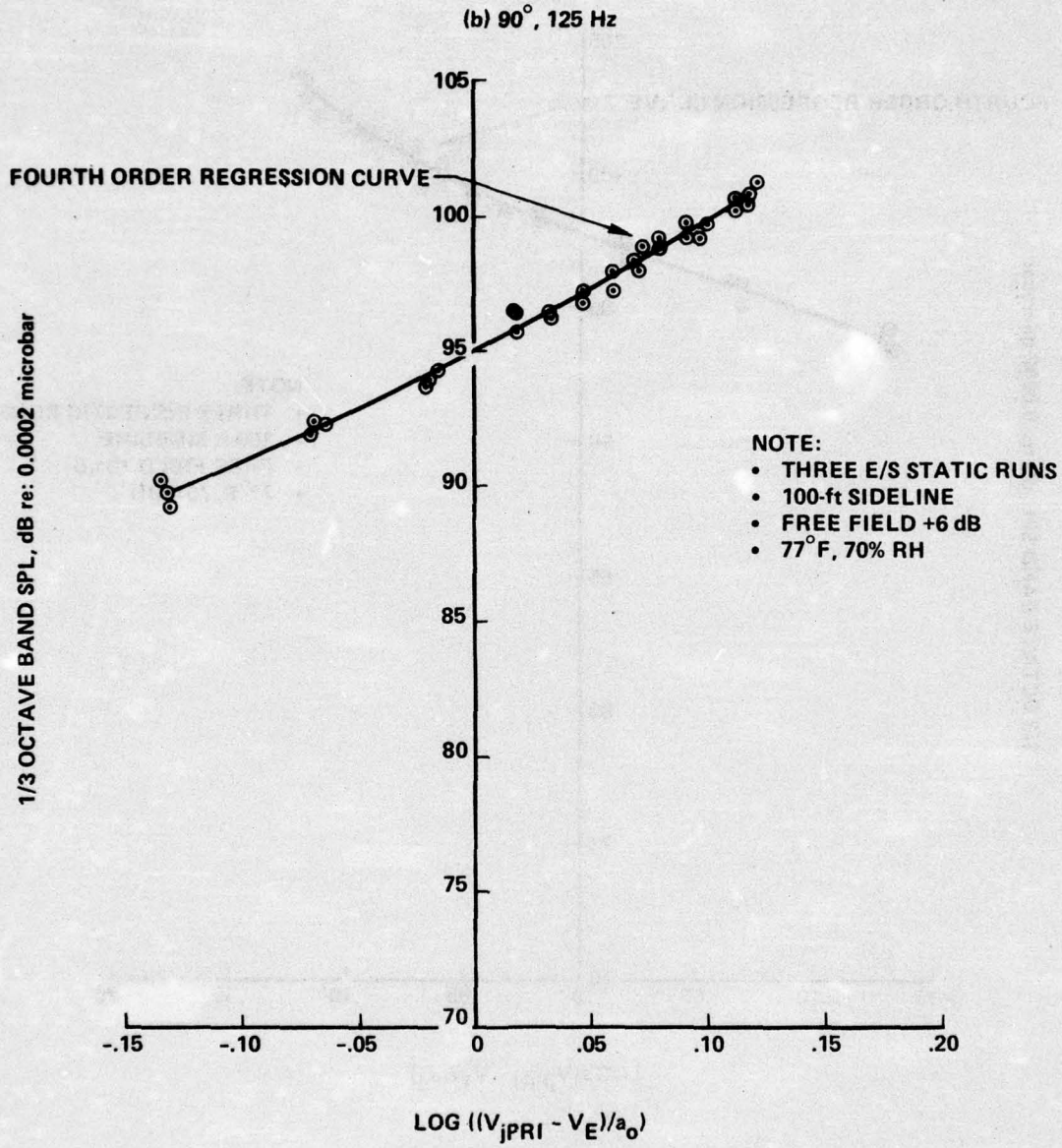


*Figure 36.—(Continued)*

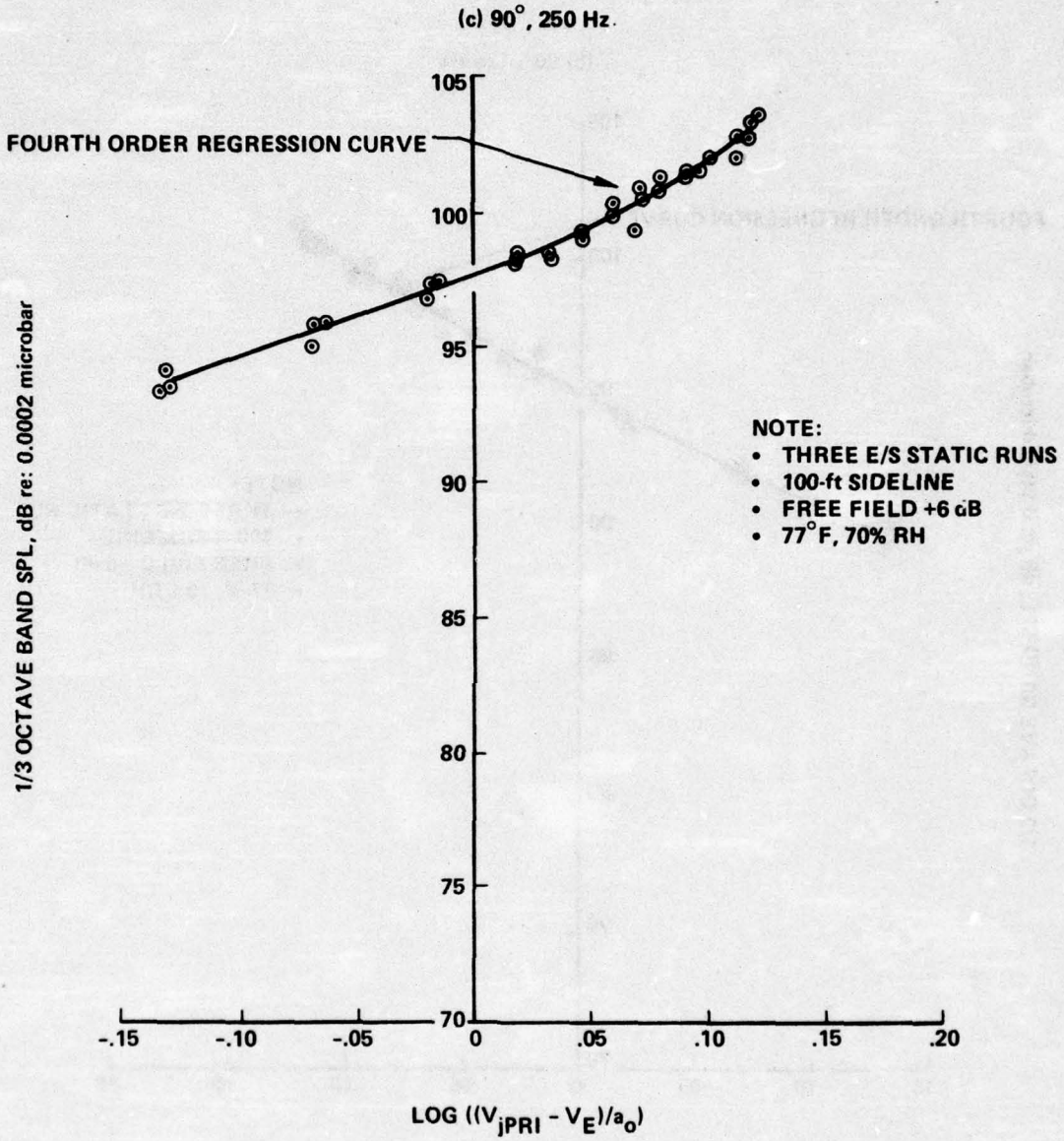


*Figure 36.—(Continued)*

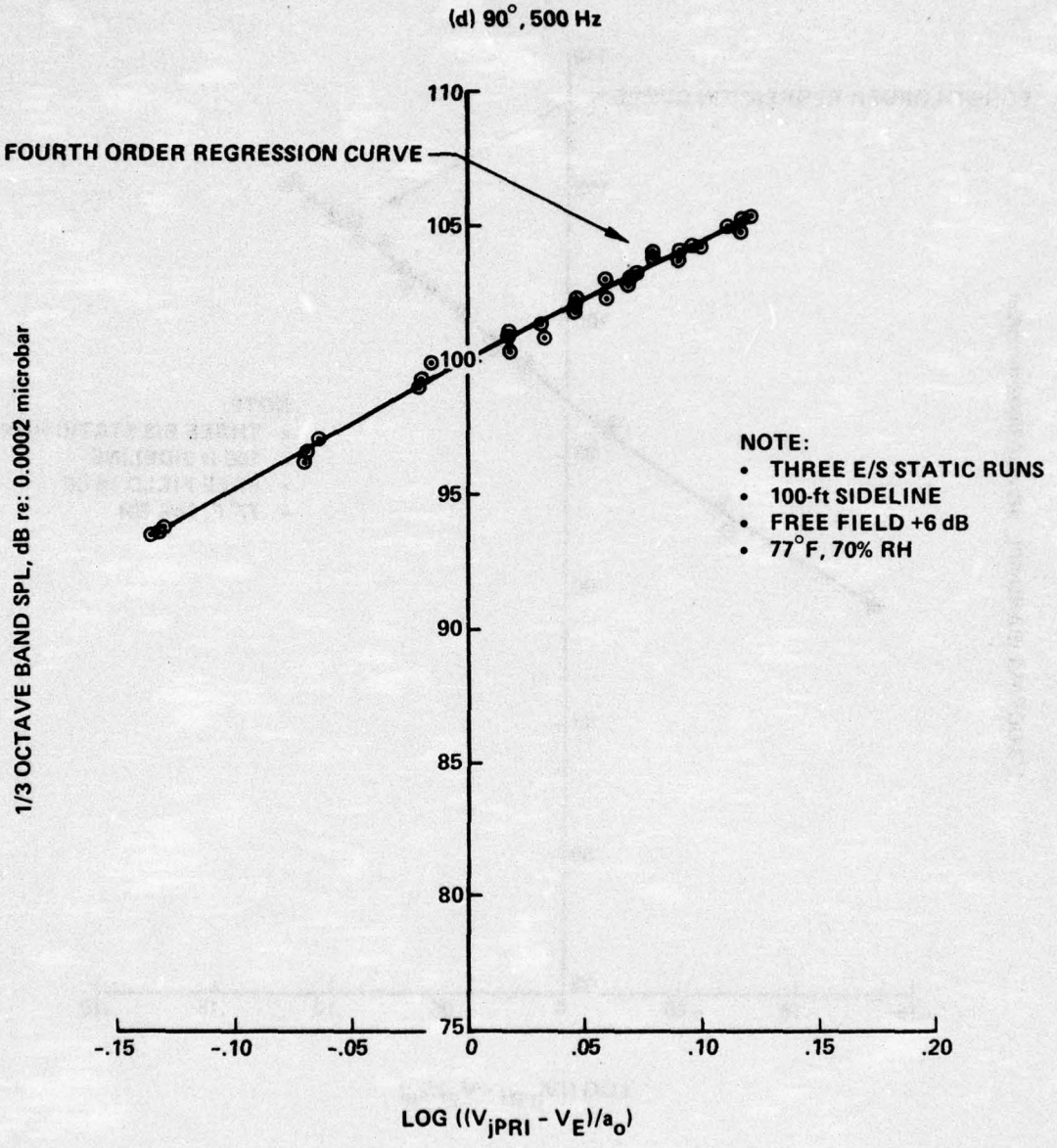


*Figure 36.—(Continued)*

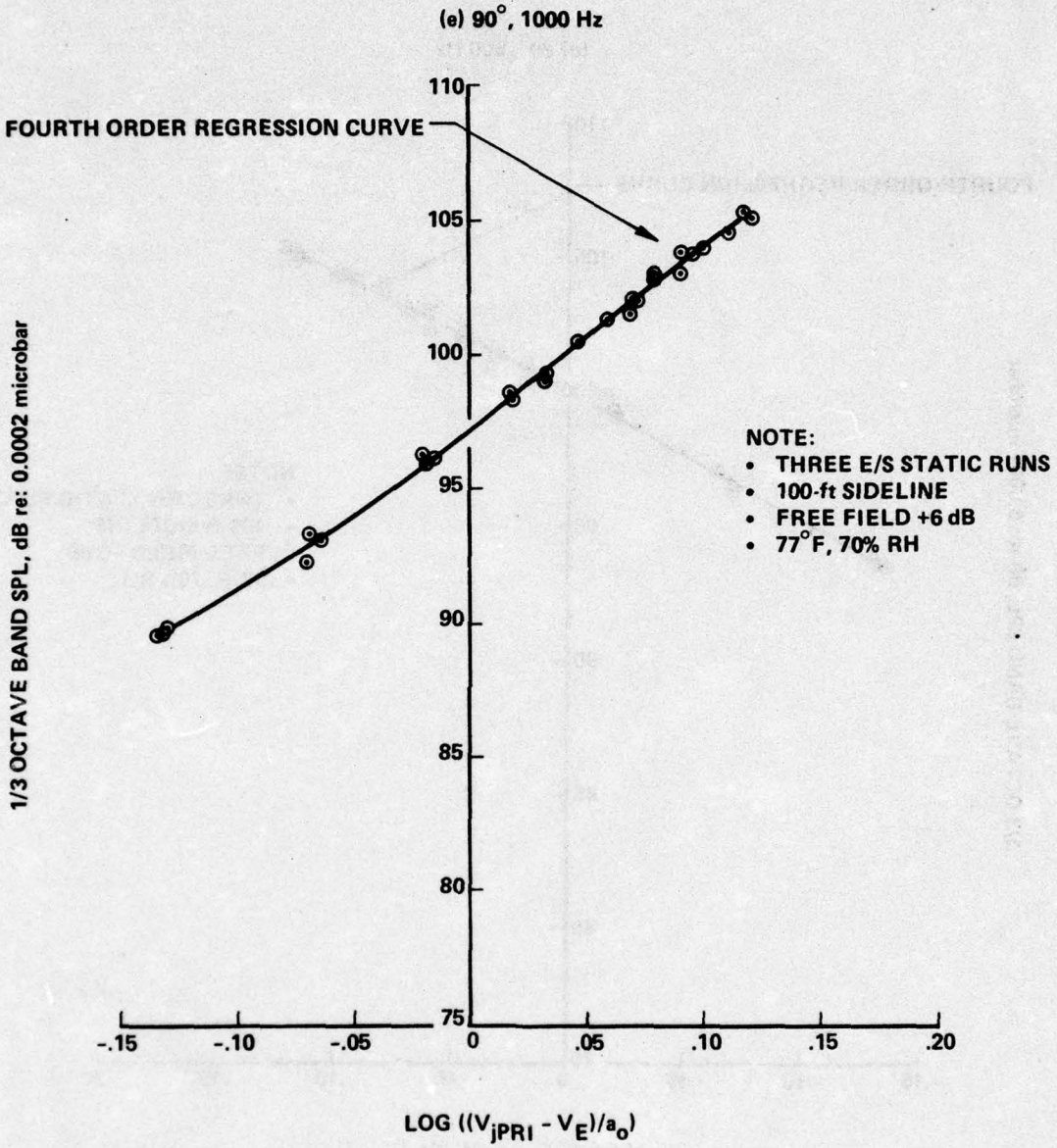


*Figure 36.—(Continued)*

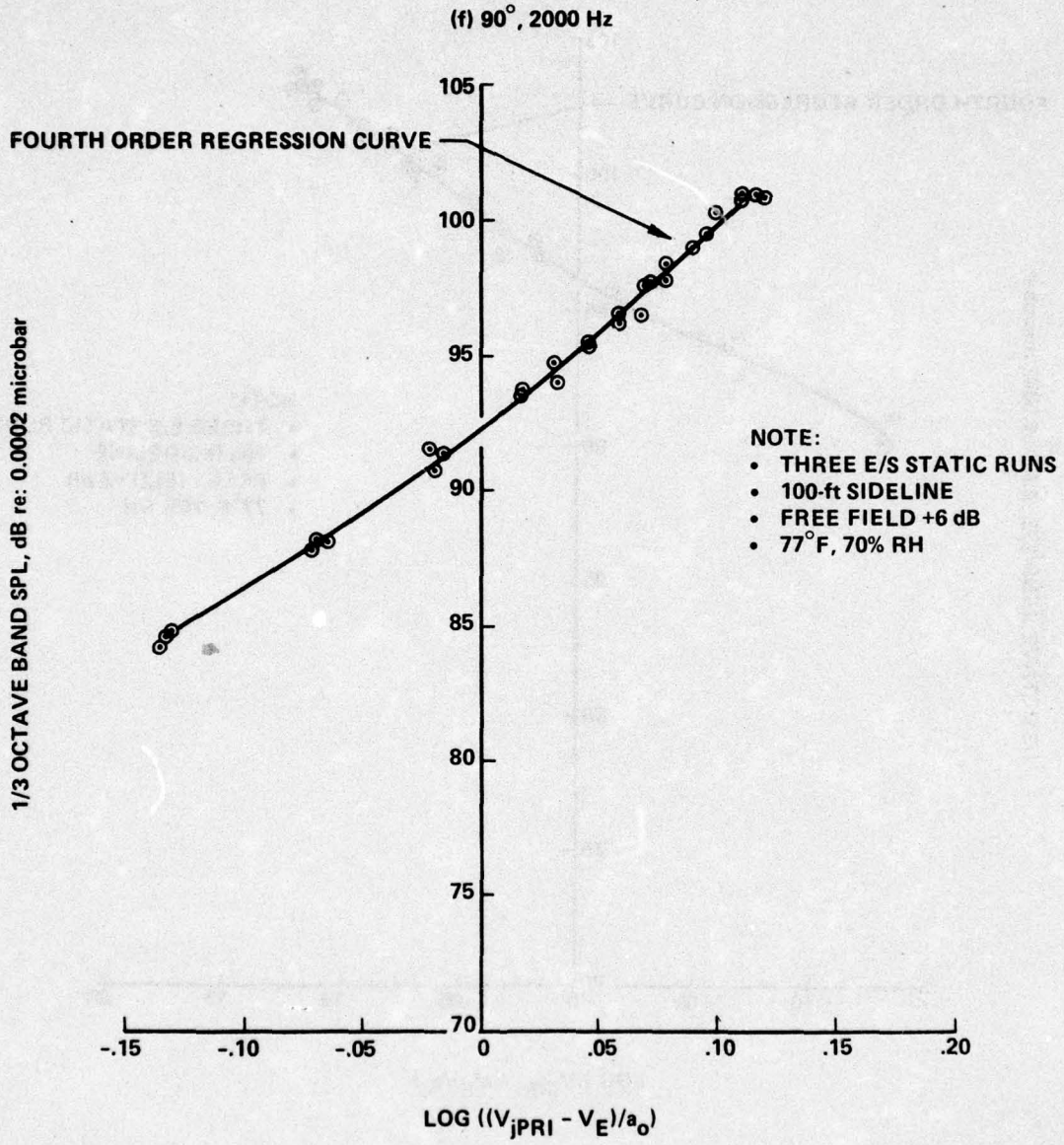


*Figure 36.—(Concluded)*

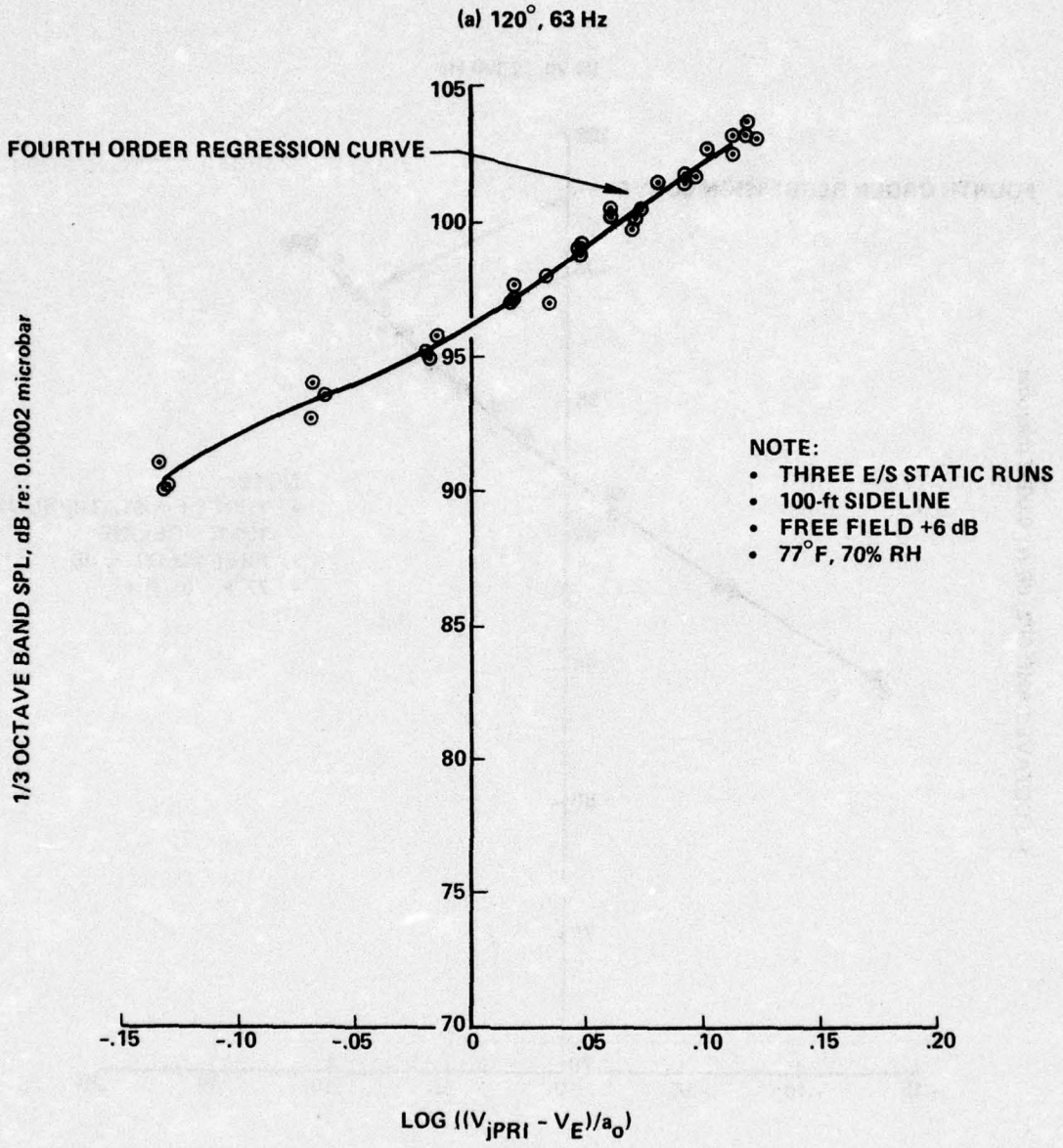


*Figure 37.—Ejector Suppressor Static Noise Data Versus Engine Power Setting, $\theta = 120°$*

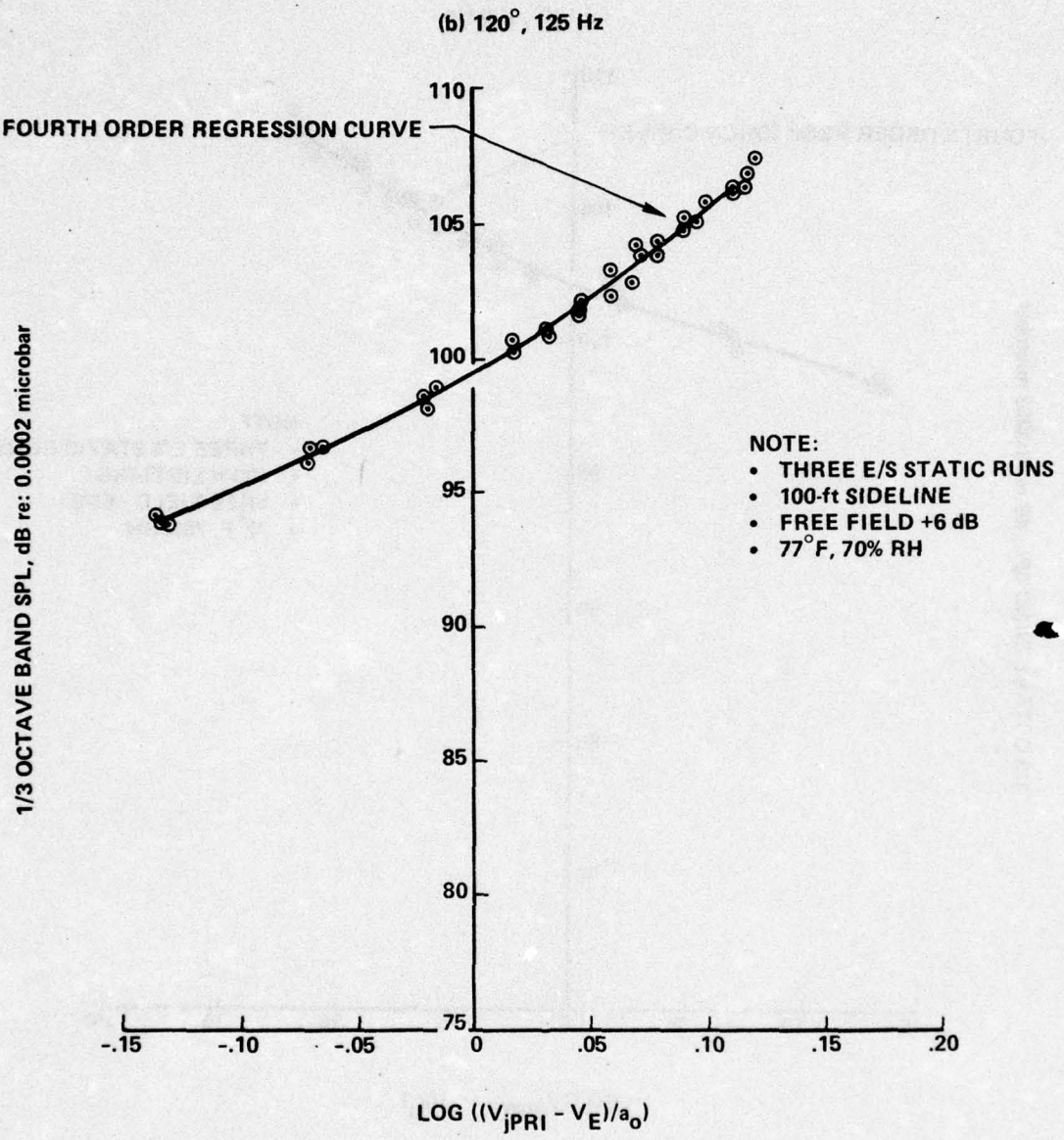


*Figure 37.—(Continued)*

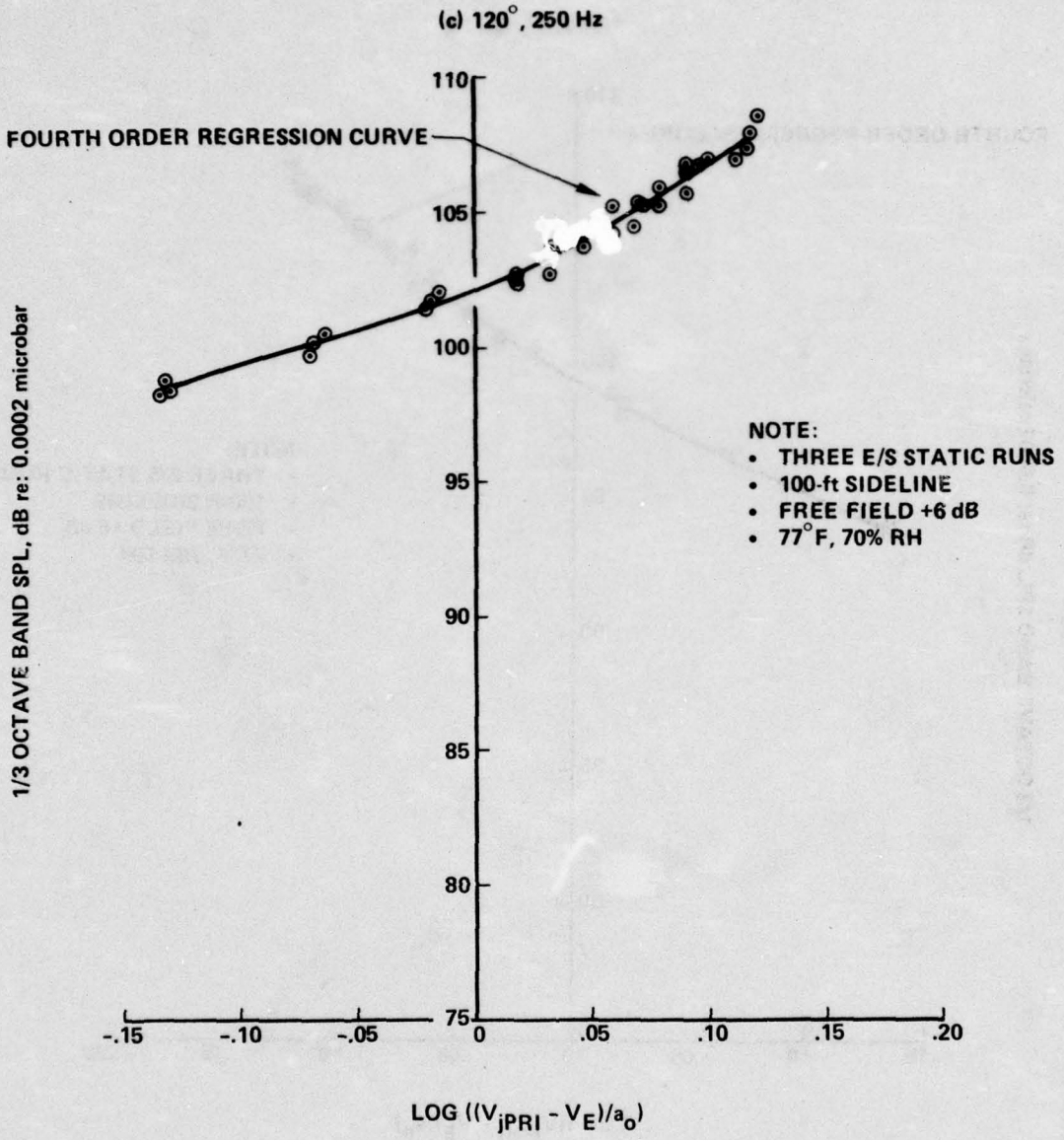


*Figure 37.—(Continued)*

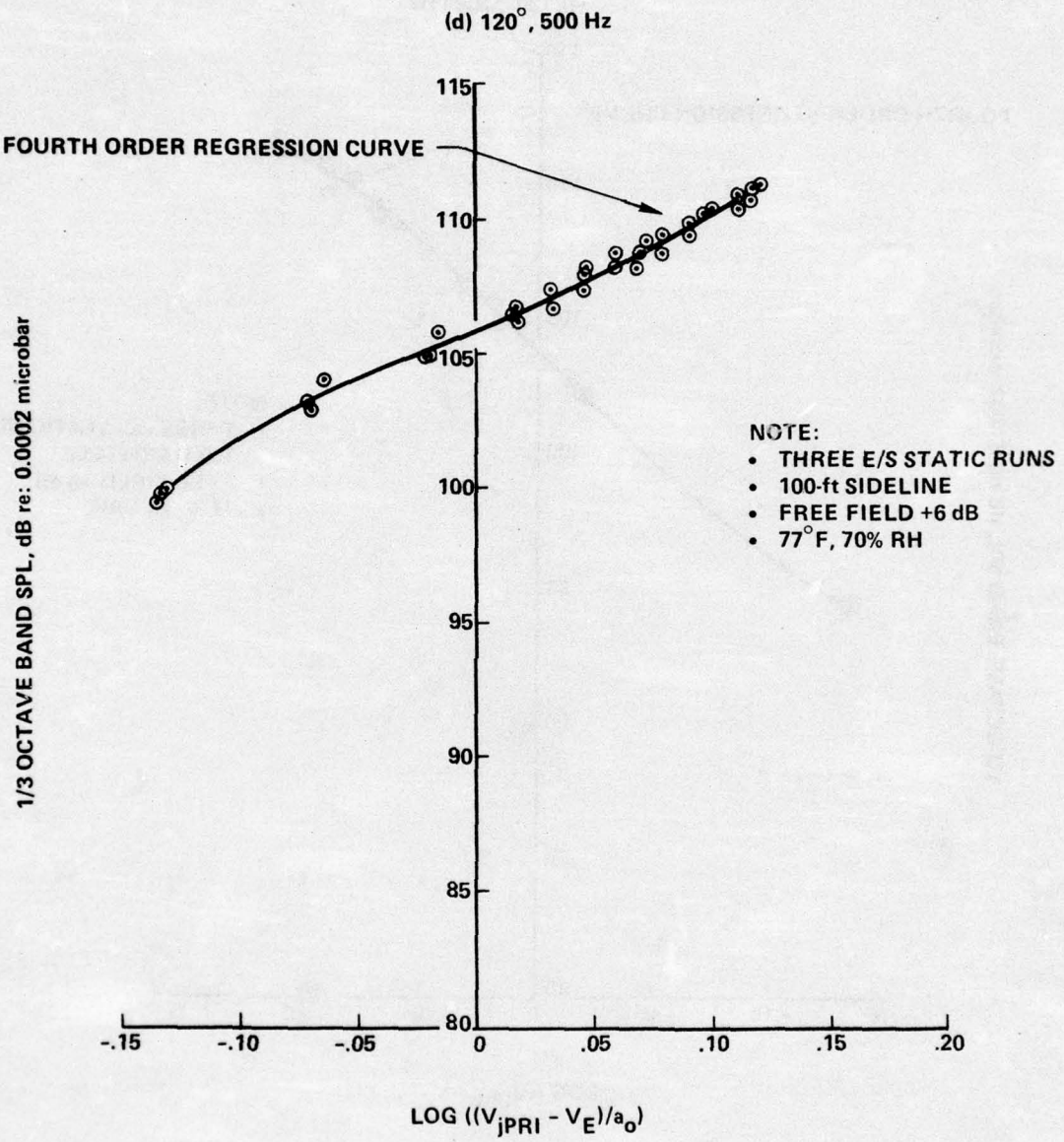


*Figure 37.—(Continued)*

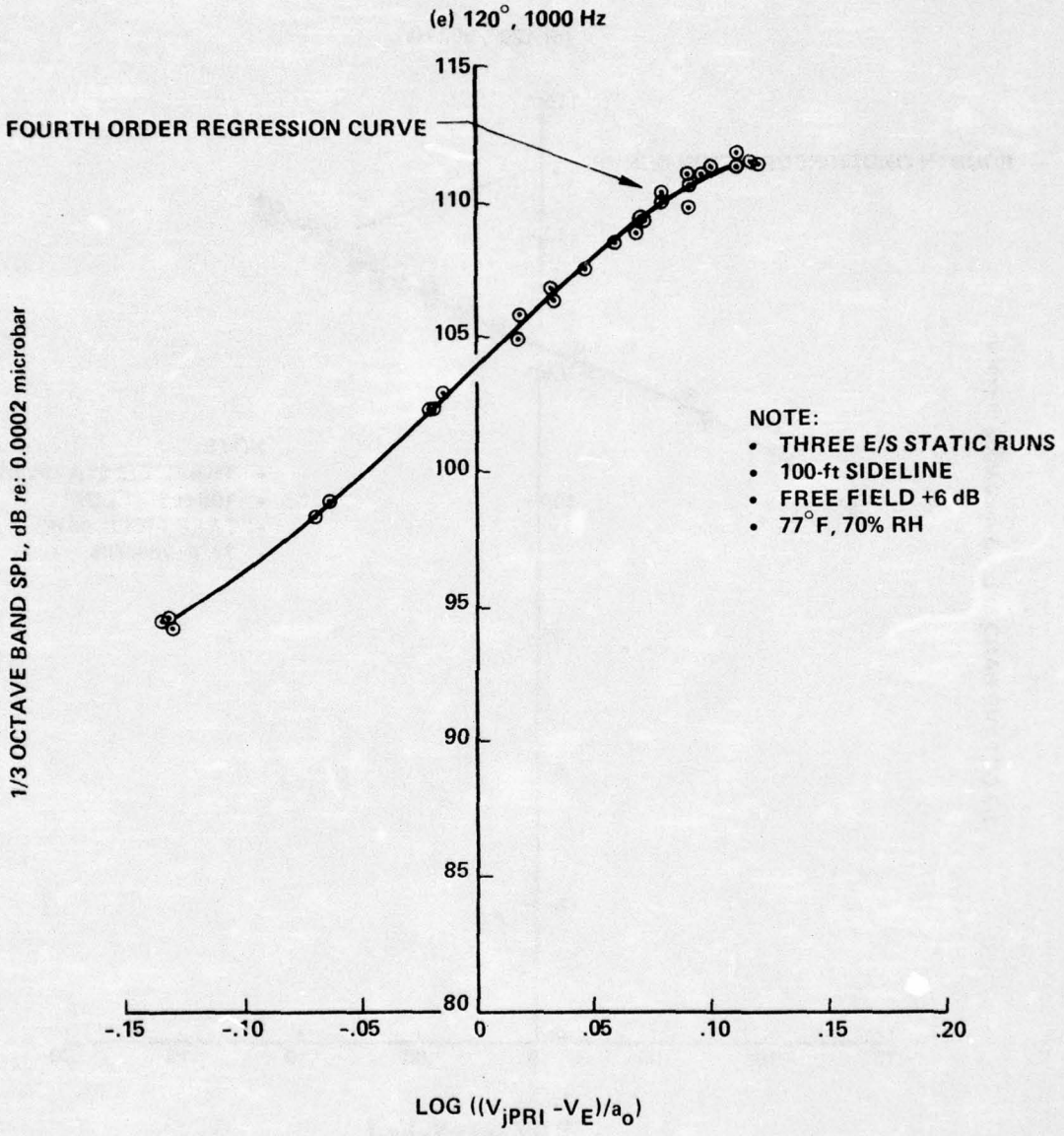


*Figure 37.—(Continued)*

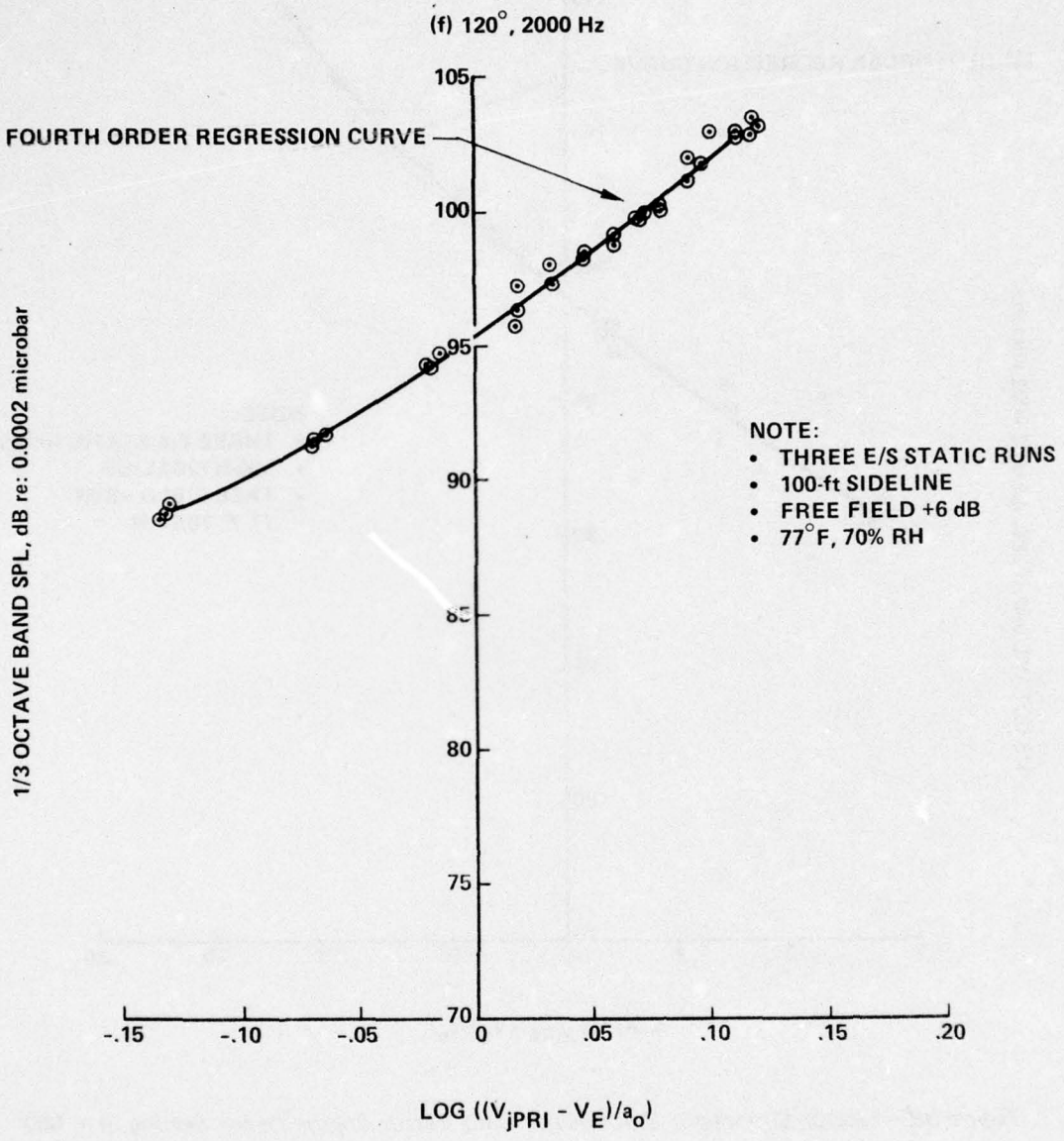


*Figure 37.—(Concluded)*

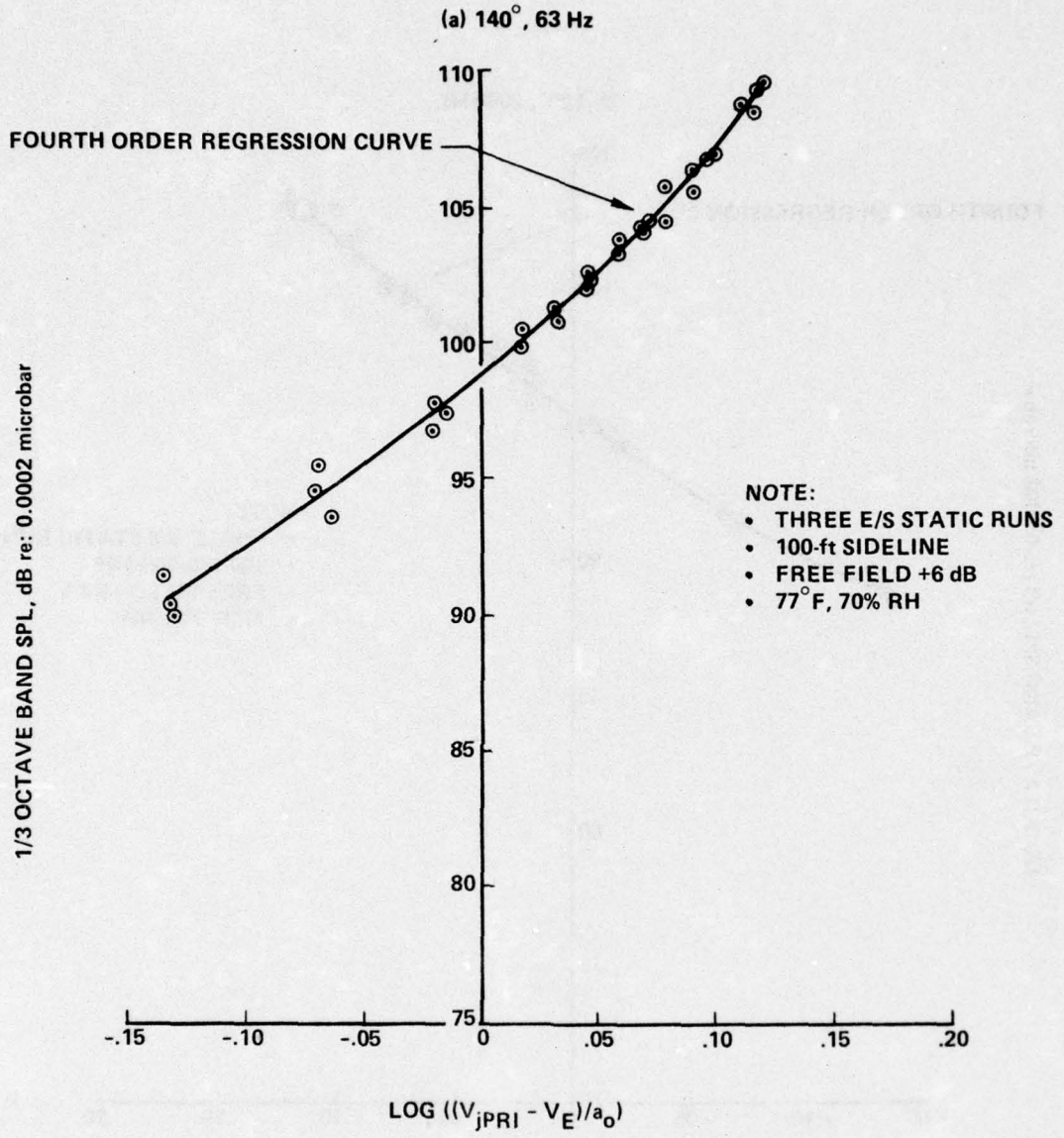


*Figure 38.—Ejector Suppressor Static Noise Data Versus Engine Power Setting, $\theta = 140^{\circ}$*

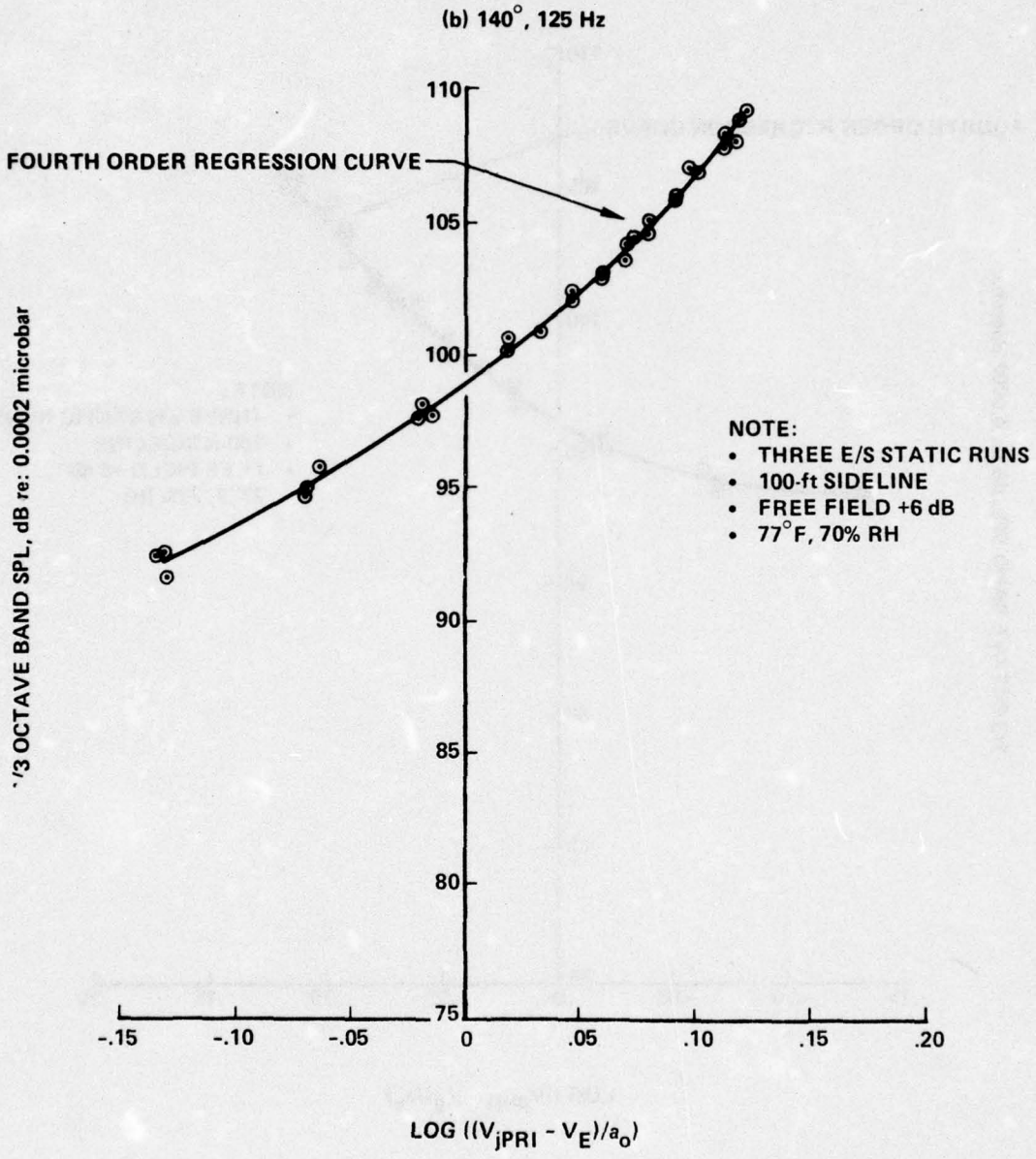


*Figure 38.—(Continued)*

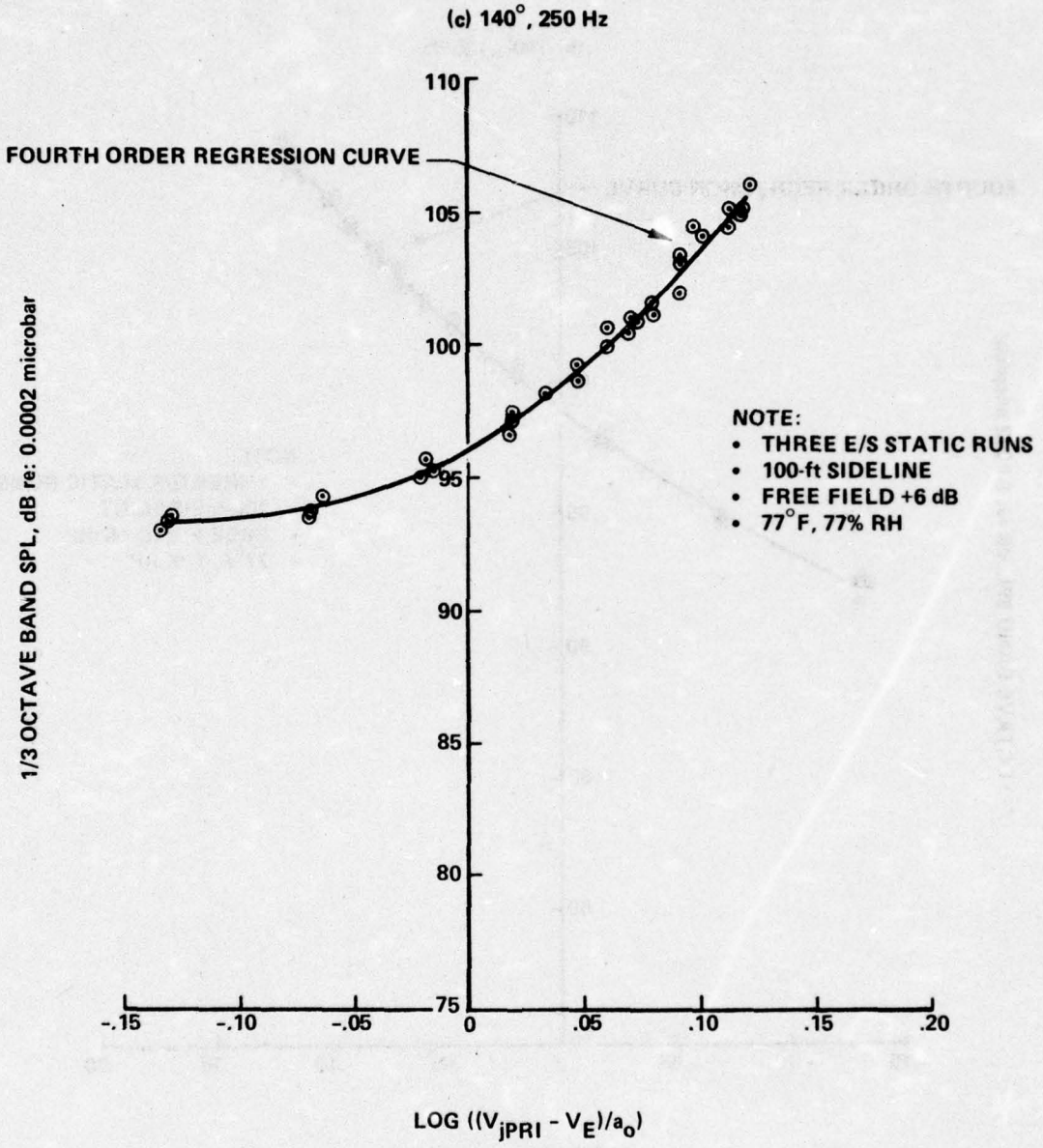


*Figure 38.—(Continued)*

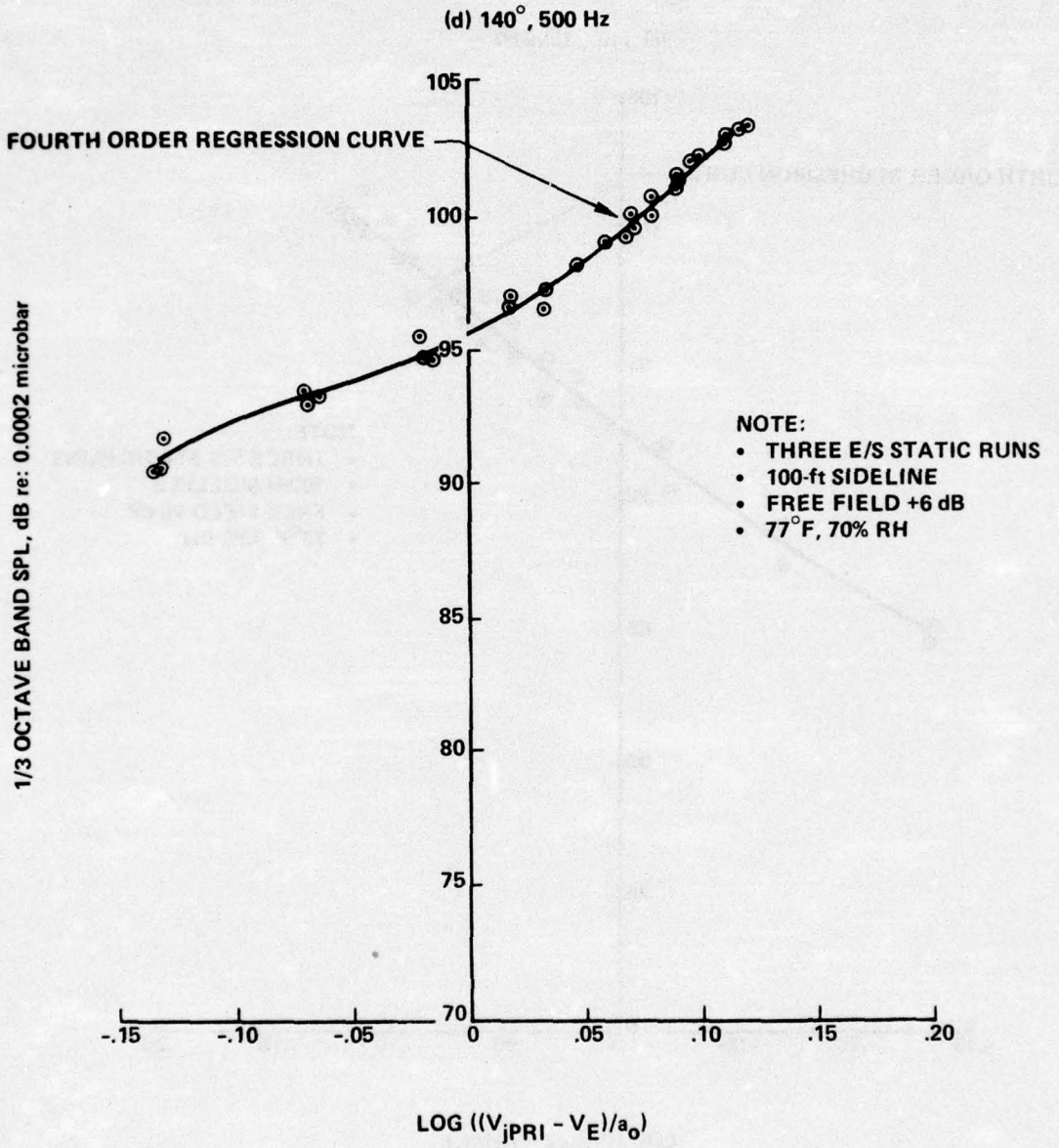


*Figure 38.—(Continued)*

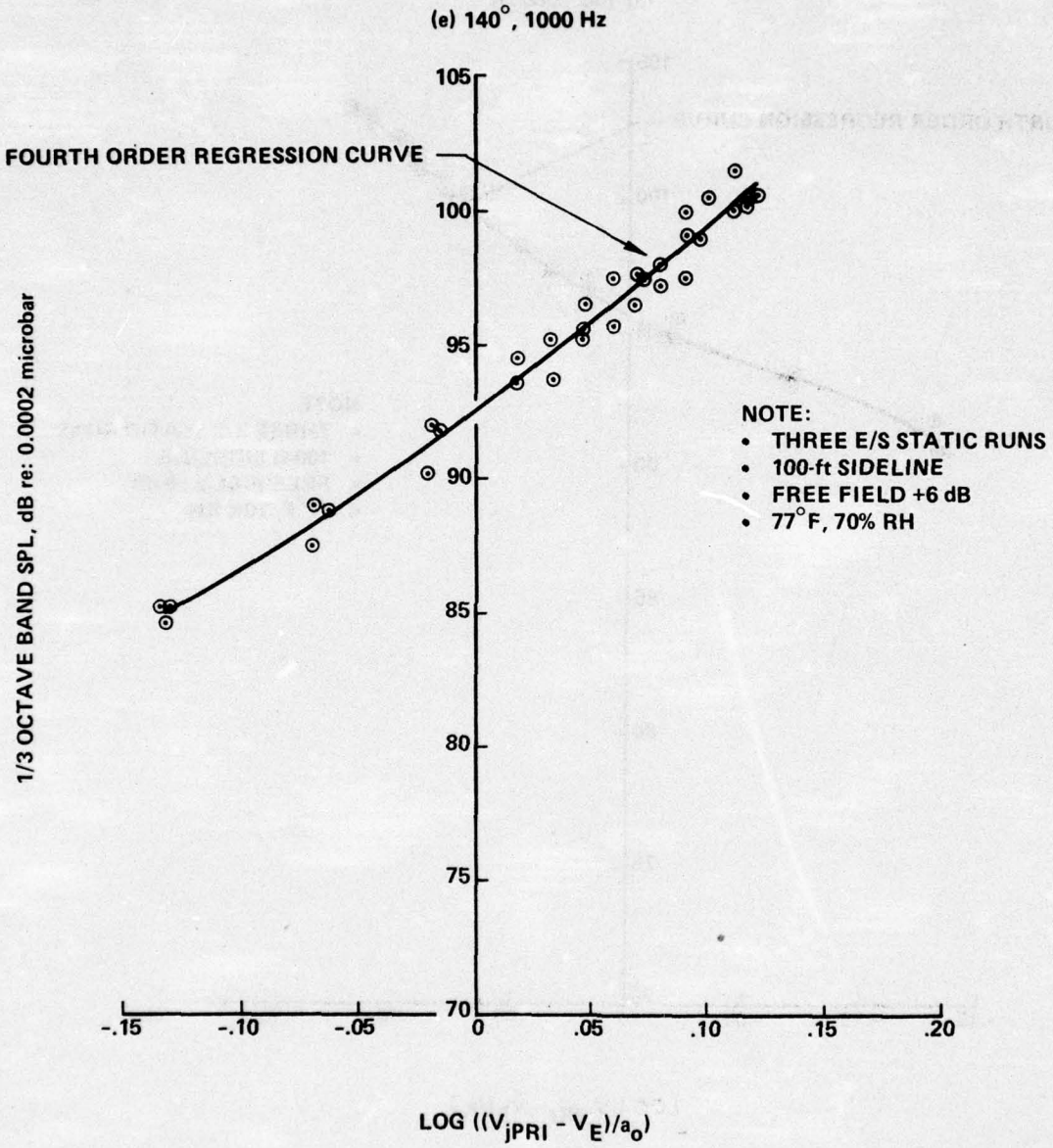


*Figure 38.—(Continued)*

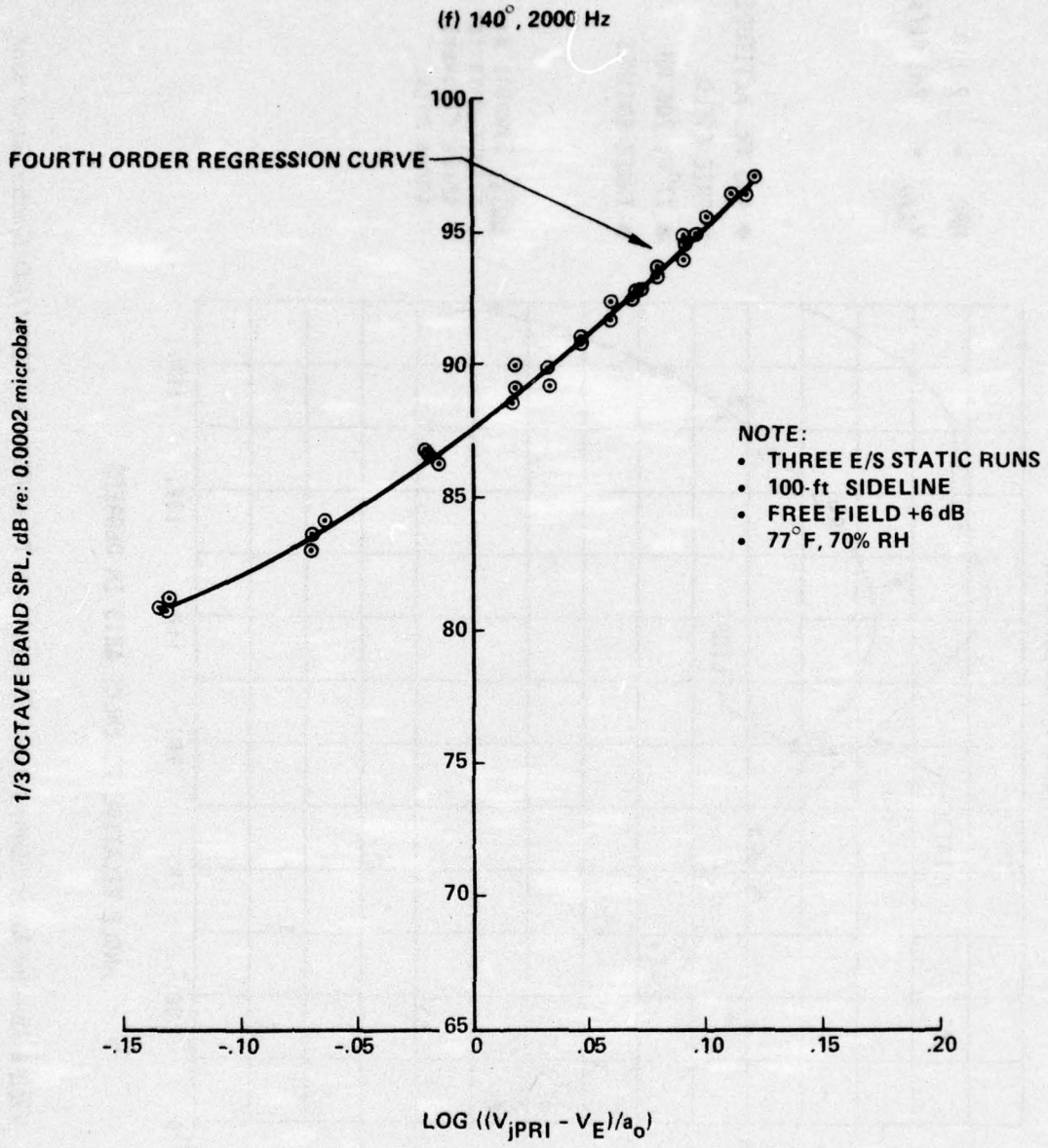


*Figure 38.—(Concluded)*

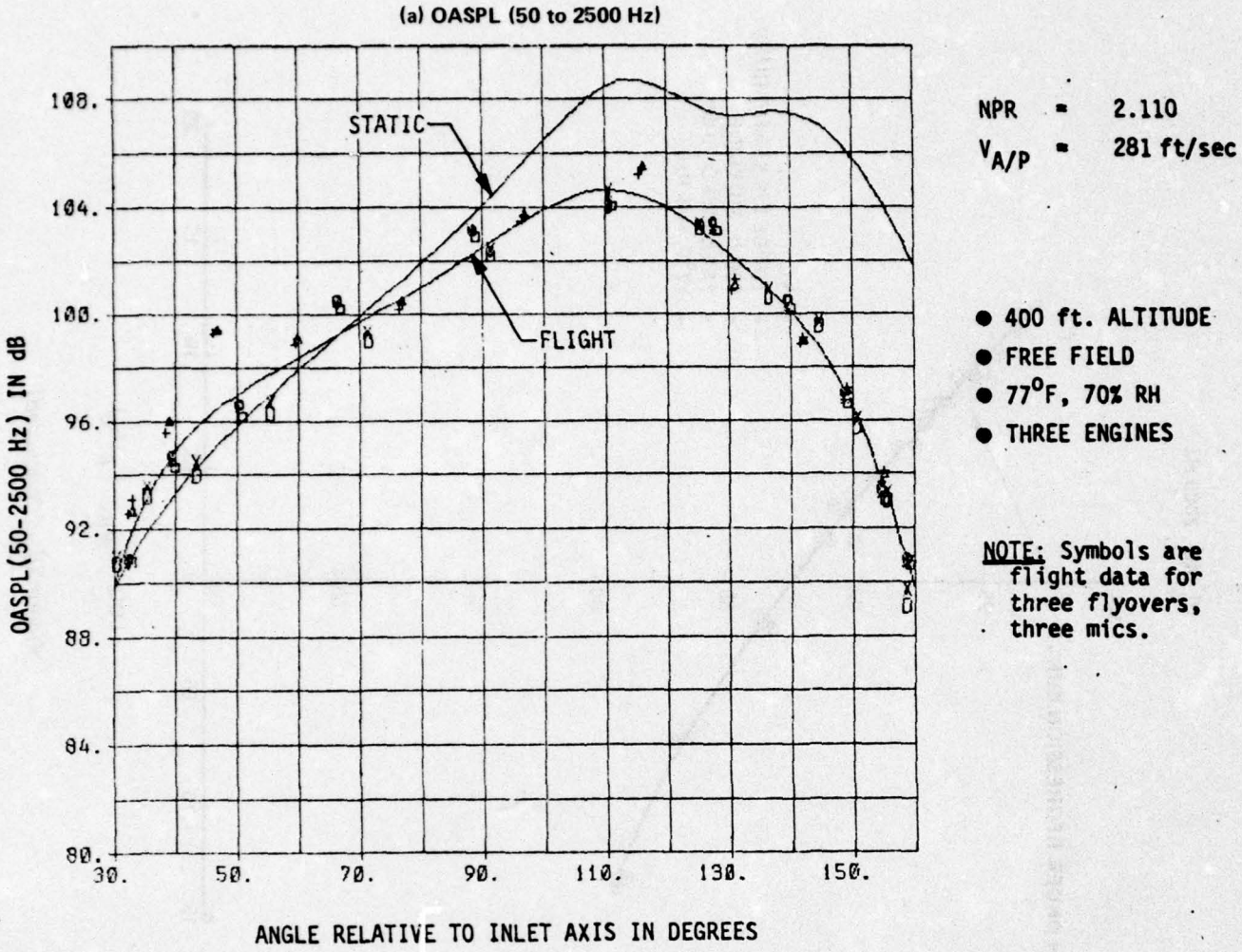


*Figure 39.—Jet Noise Flight Effects Directivity at Takeoff Power, 727/JT8D Ejector Suppressor*

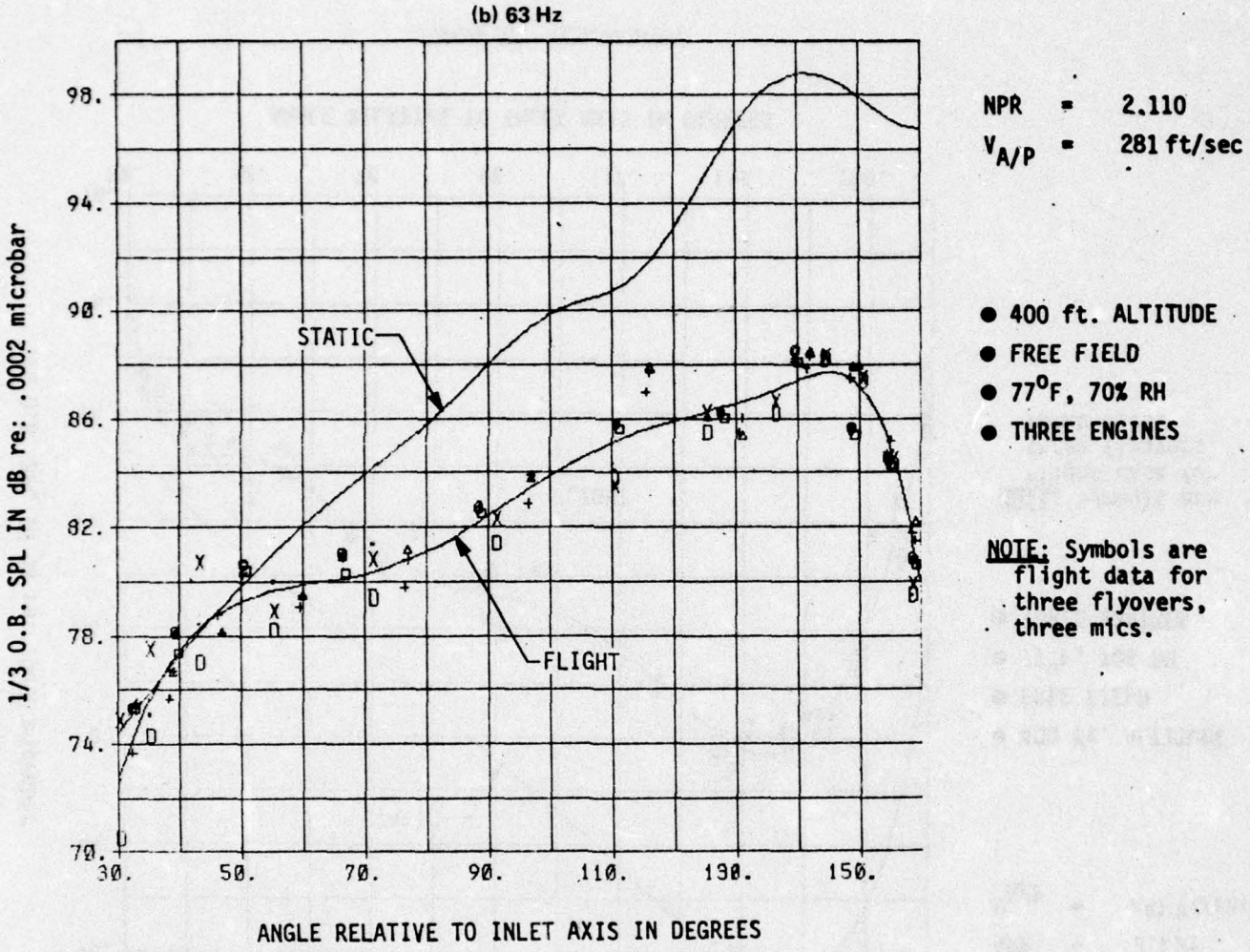


*Figure 39.—(Continued)*

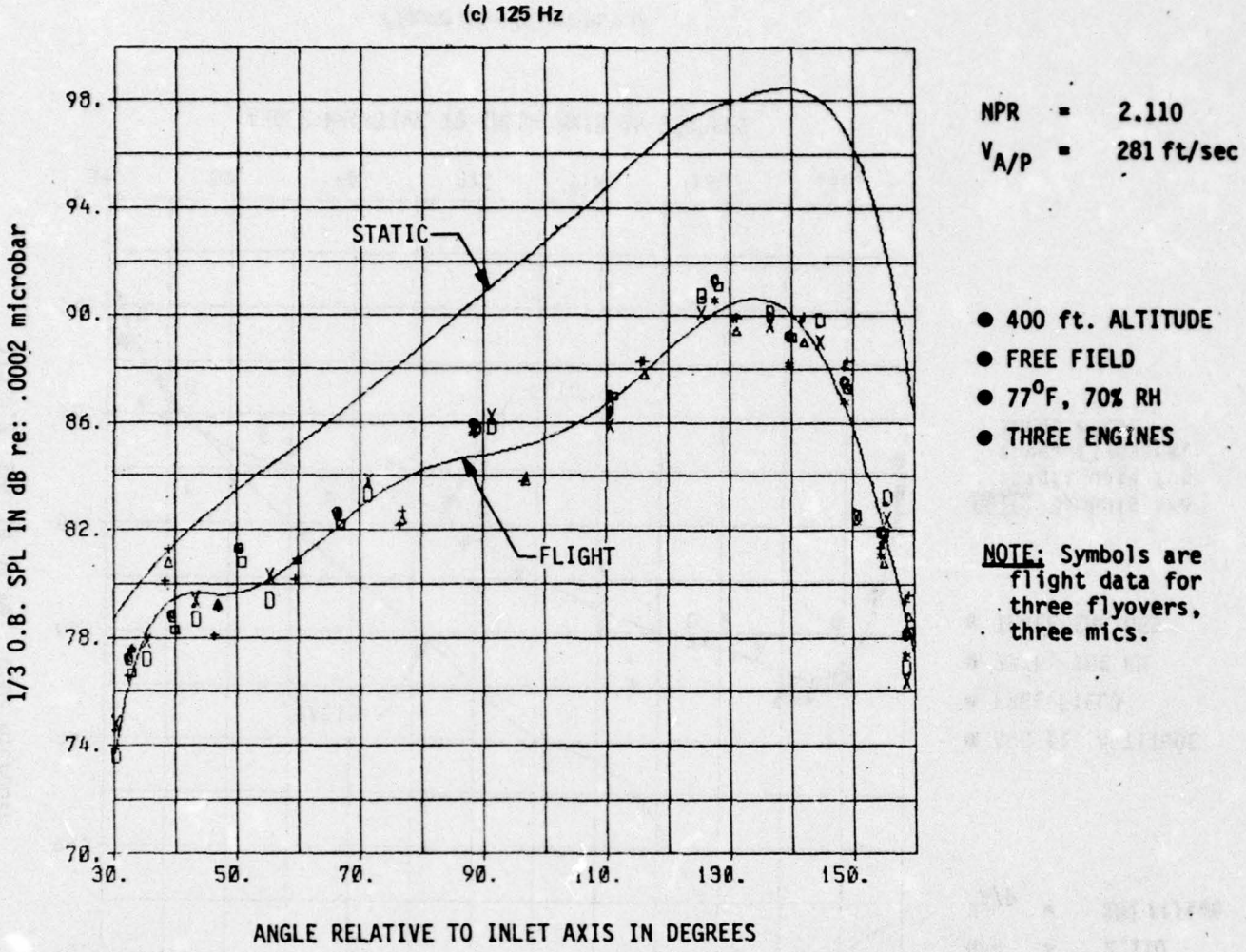


*Figure 39.—(Continued)*

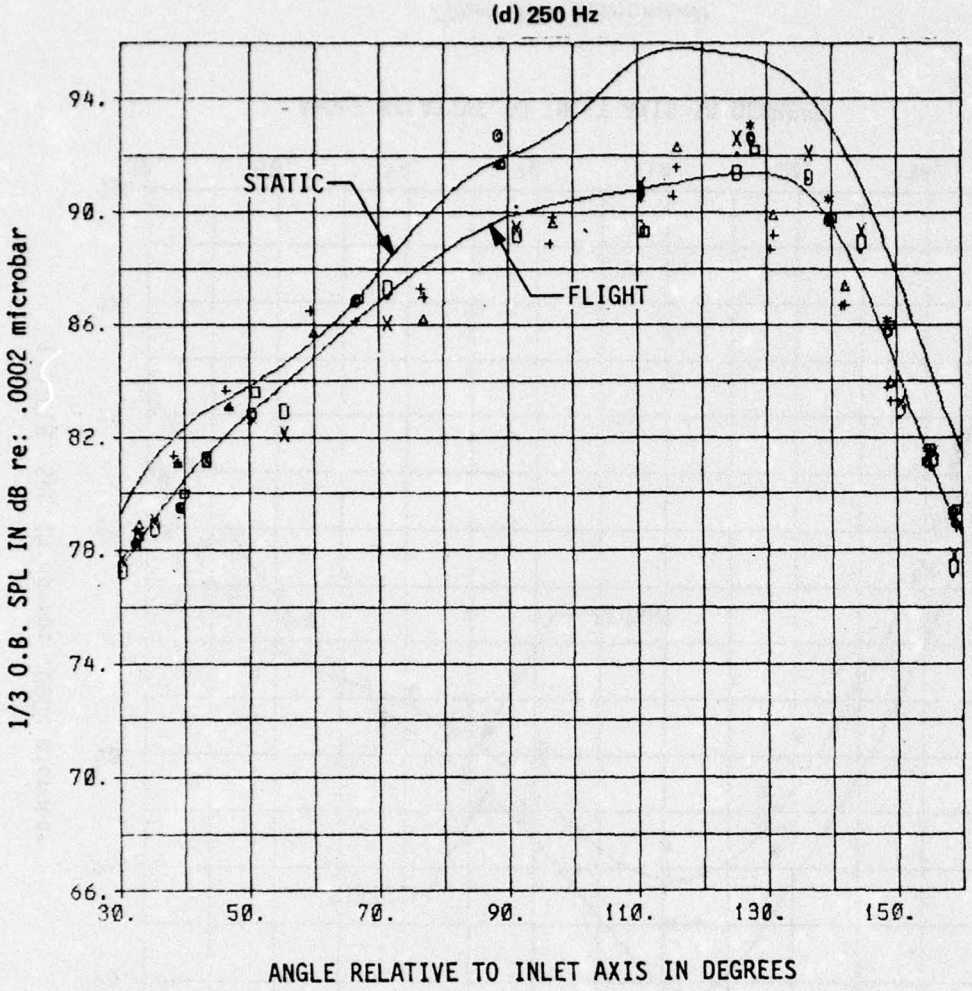


NPR = 2.110

$V_{A/P}$ = 281 ft/sec

- 400 ft. ALTITUDE
- FREE FIELD
- 77°F, 70% RH
- THREE ENGINES

NOTE: Symbols are flight data for three flyovers, three mics.

*Figure 39.—(Continued)*

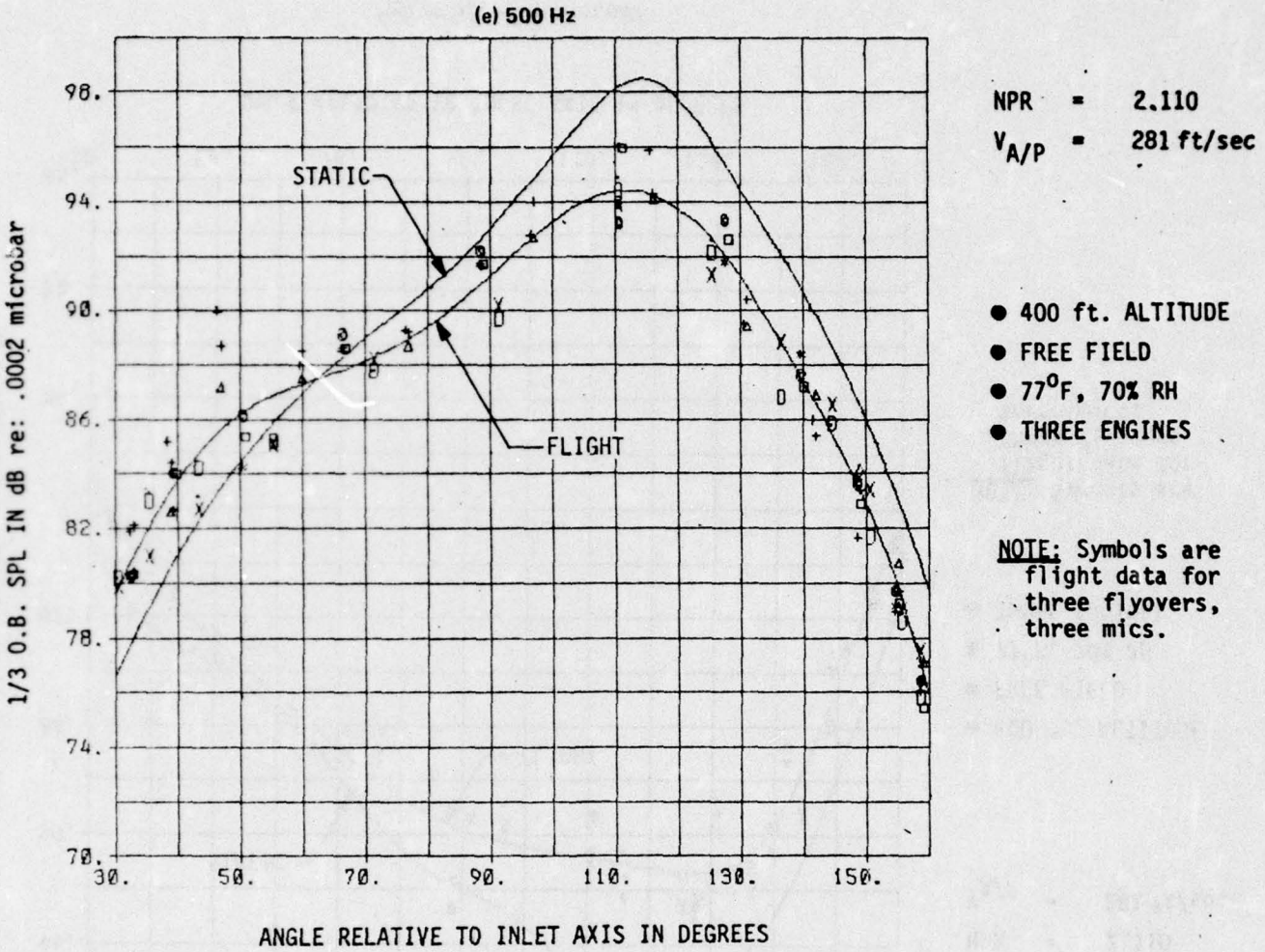


*Figure 39.—(Continued)*

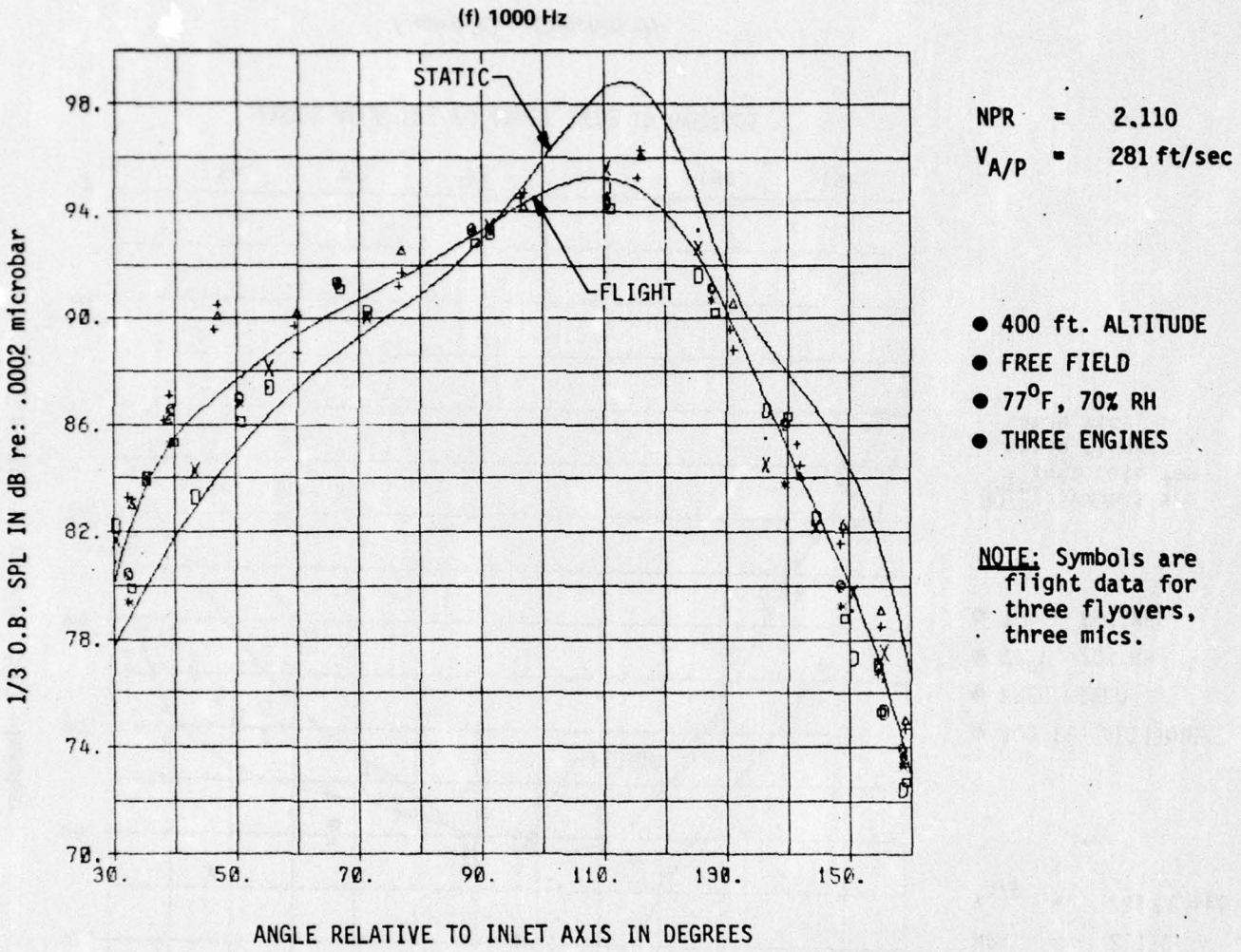


*Figure 39.—(Continued)*

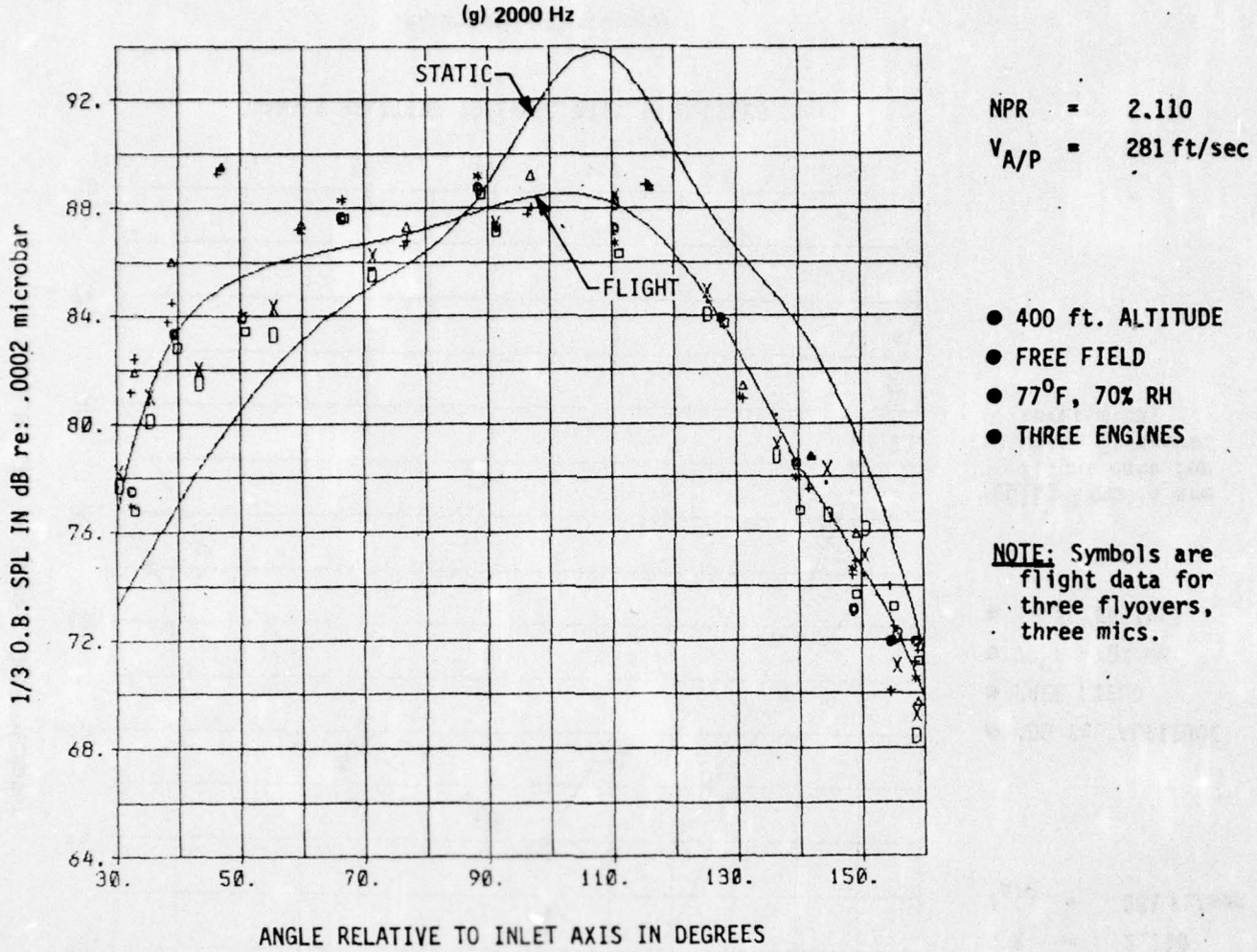


*Figure 39.—(Concluded)*

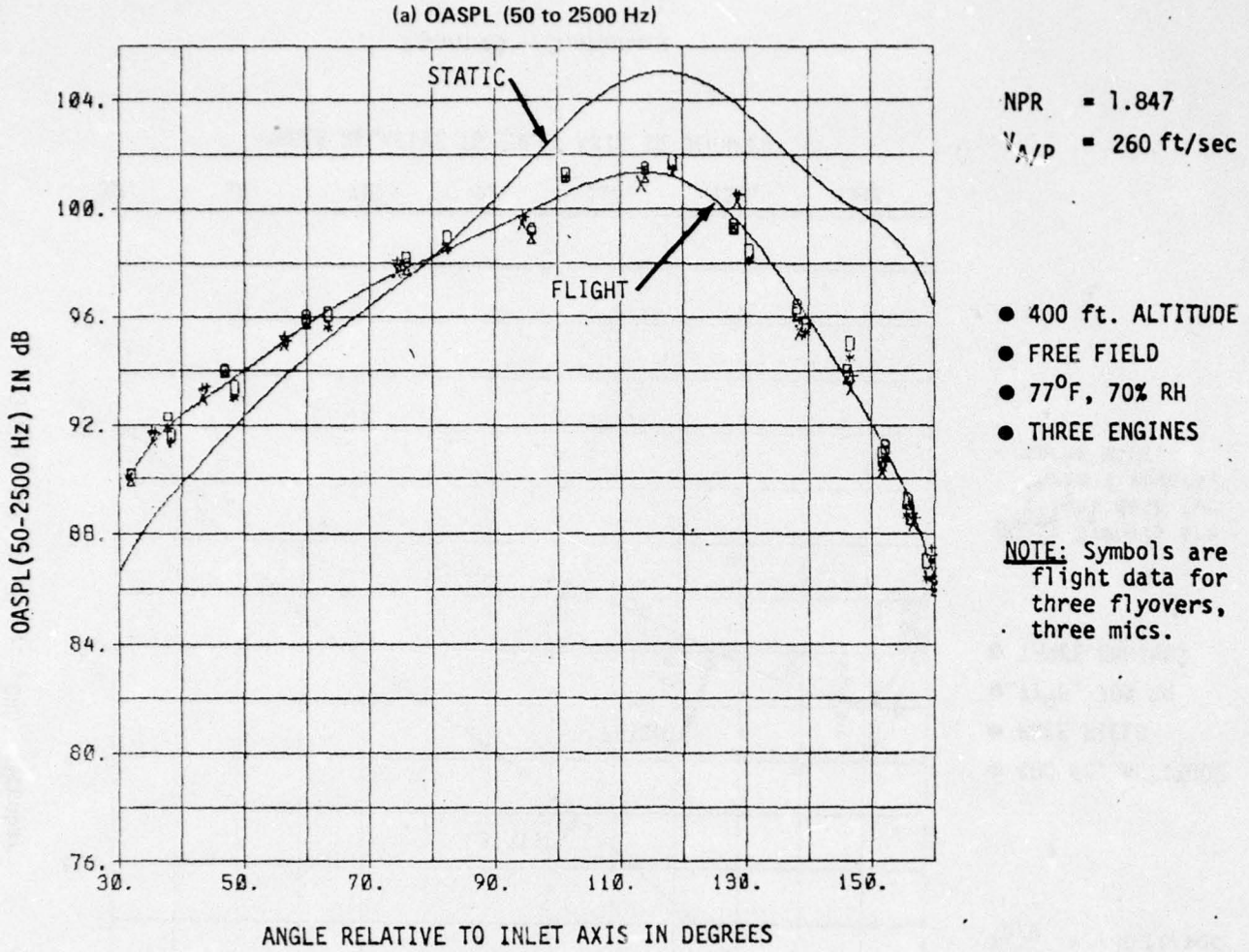


*Figure 40.—Jet Noise Flight Effects Directivity at Cutback Power (HGW), 727/JT8D Ejector Suppressor*

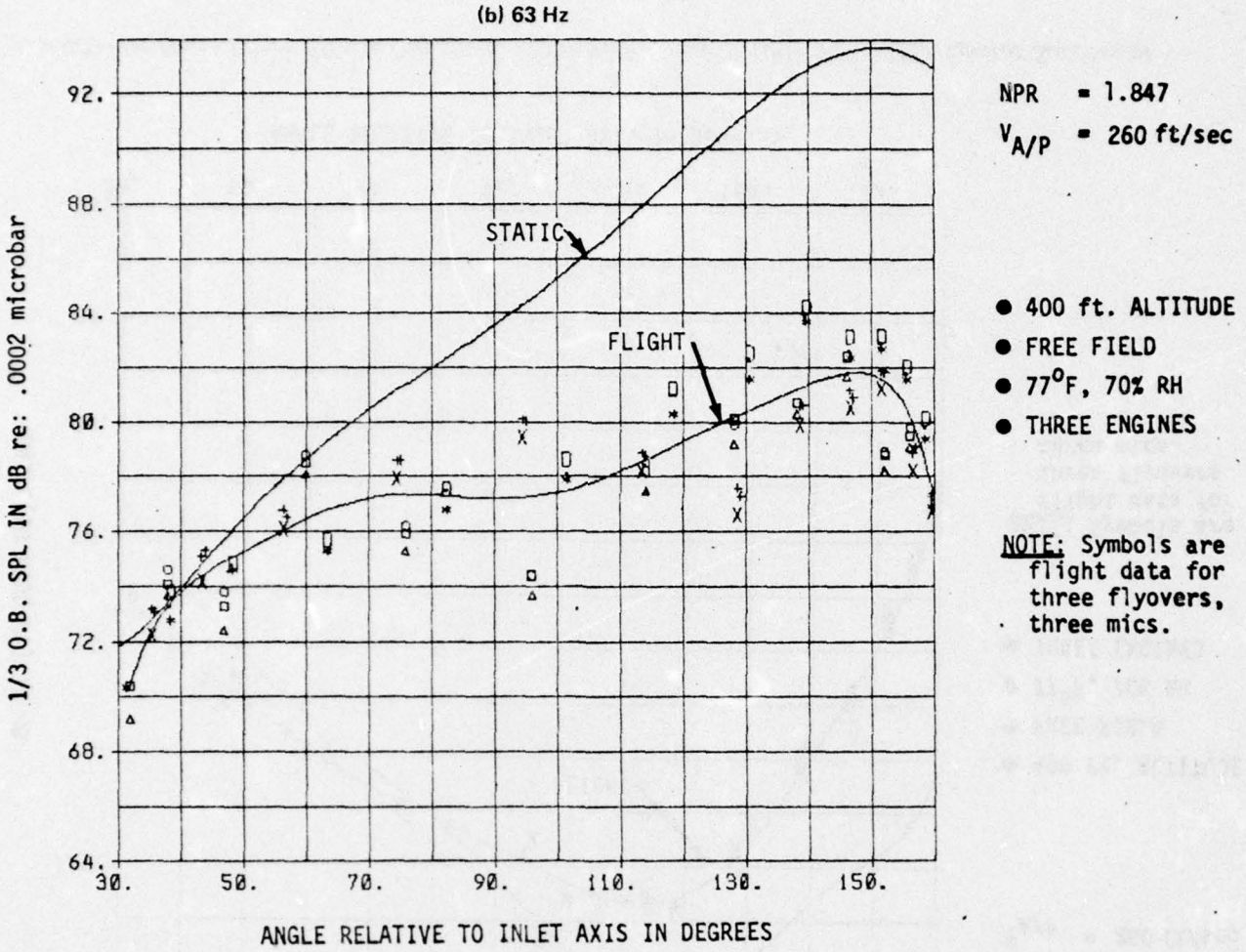


*Figure 40.—(Continued)*

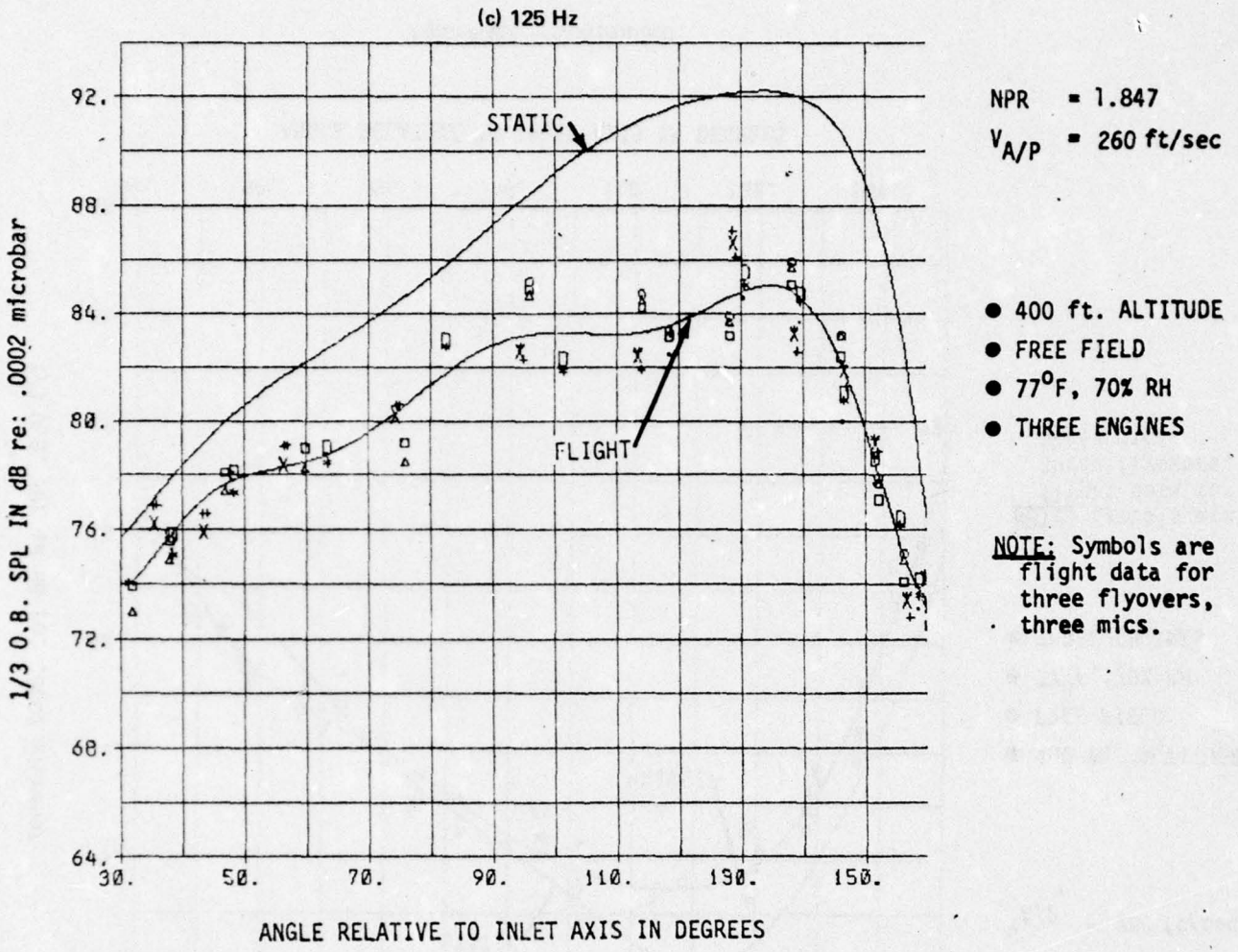


*Figure 40.—(Continued)*

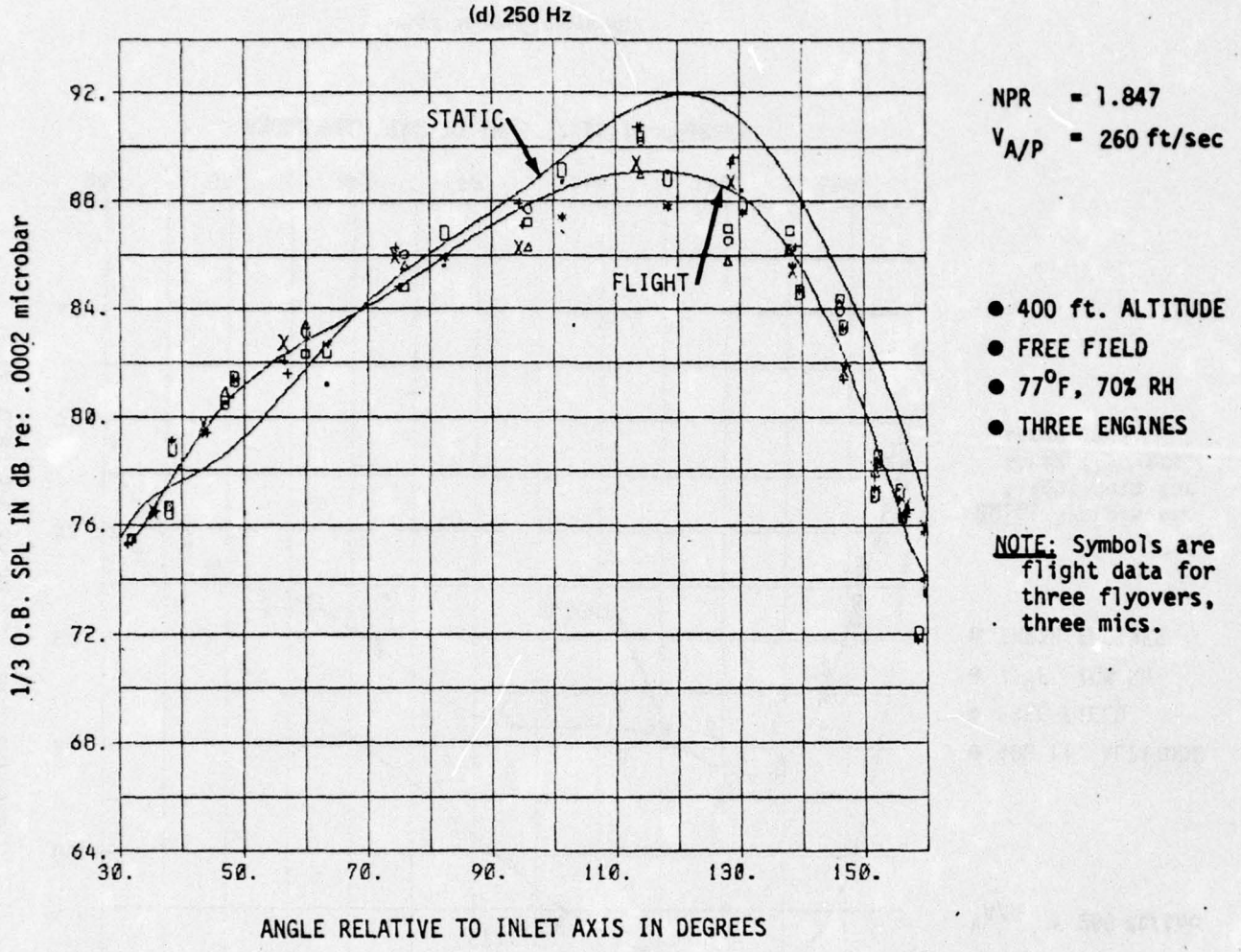


*Figure 40.—(Continued)*

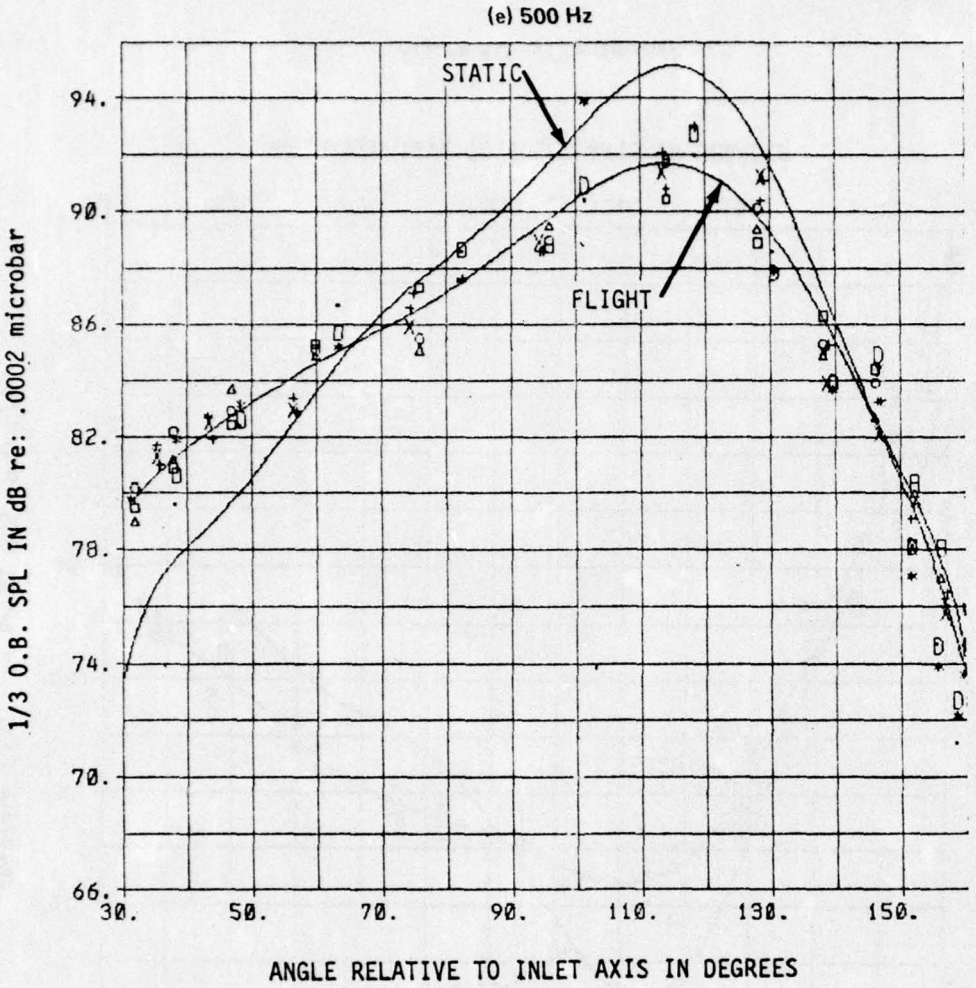


NPR = 1.847

$V_{A/P}$ = 260 ft/sec

- 400 ft. ALTITUDE
- FREE FIELD
- 77°F, 70% RH
- THREE ENGINES

NOTE: Symbols are flight data for three flyovers, three mics.

*Figure 40.—(Continued)*

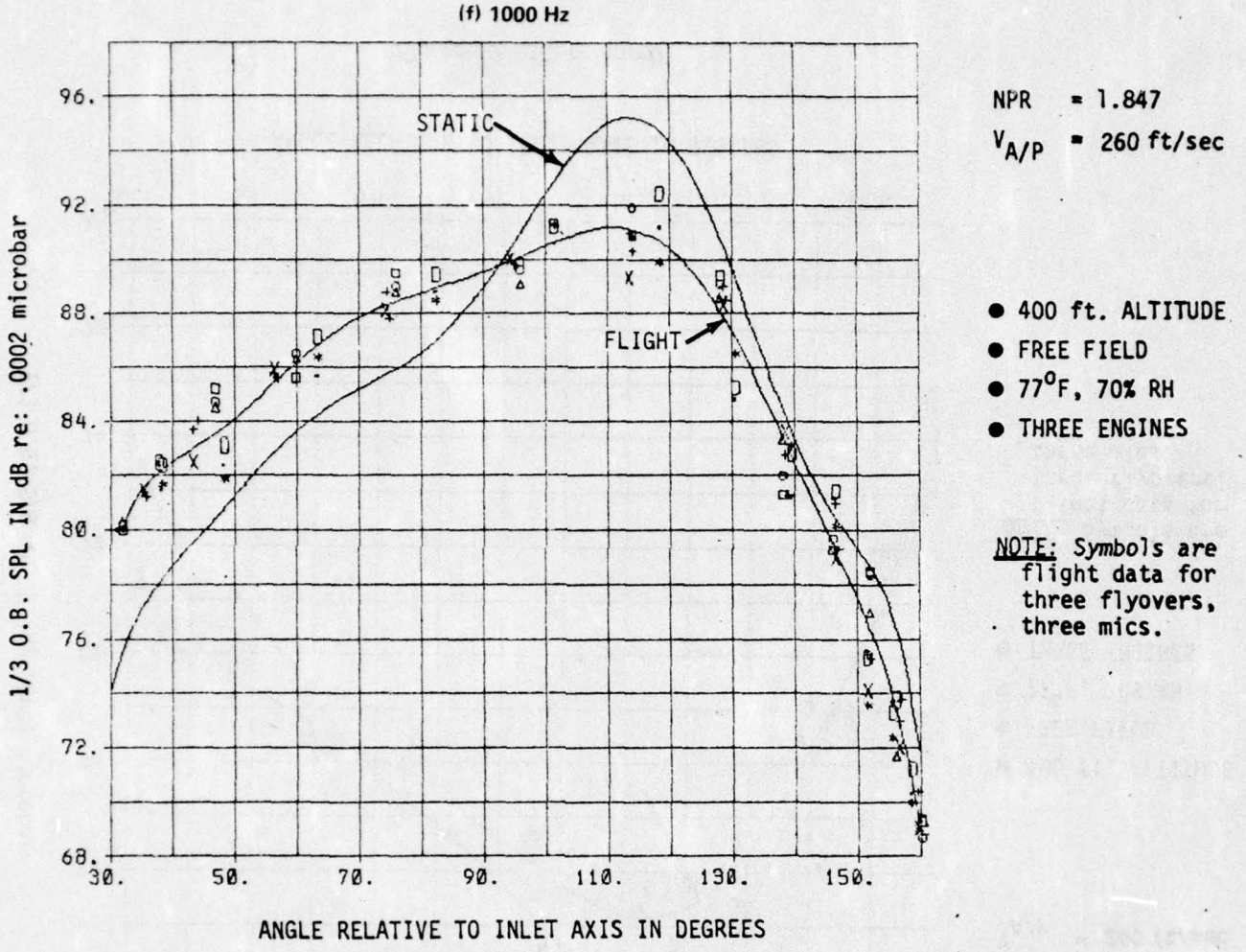


*Figure 40.—(Continued)*

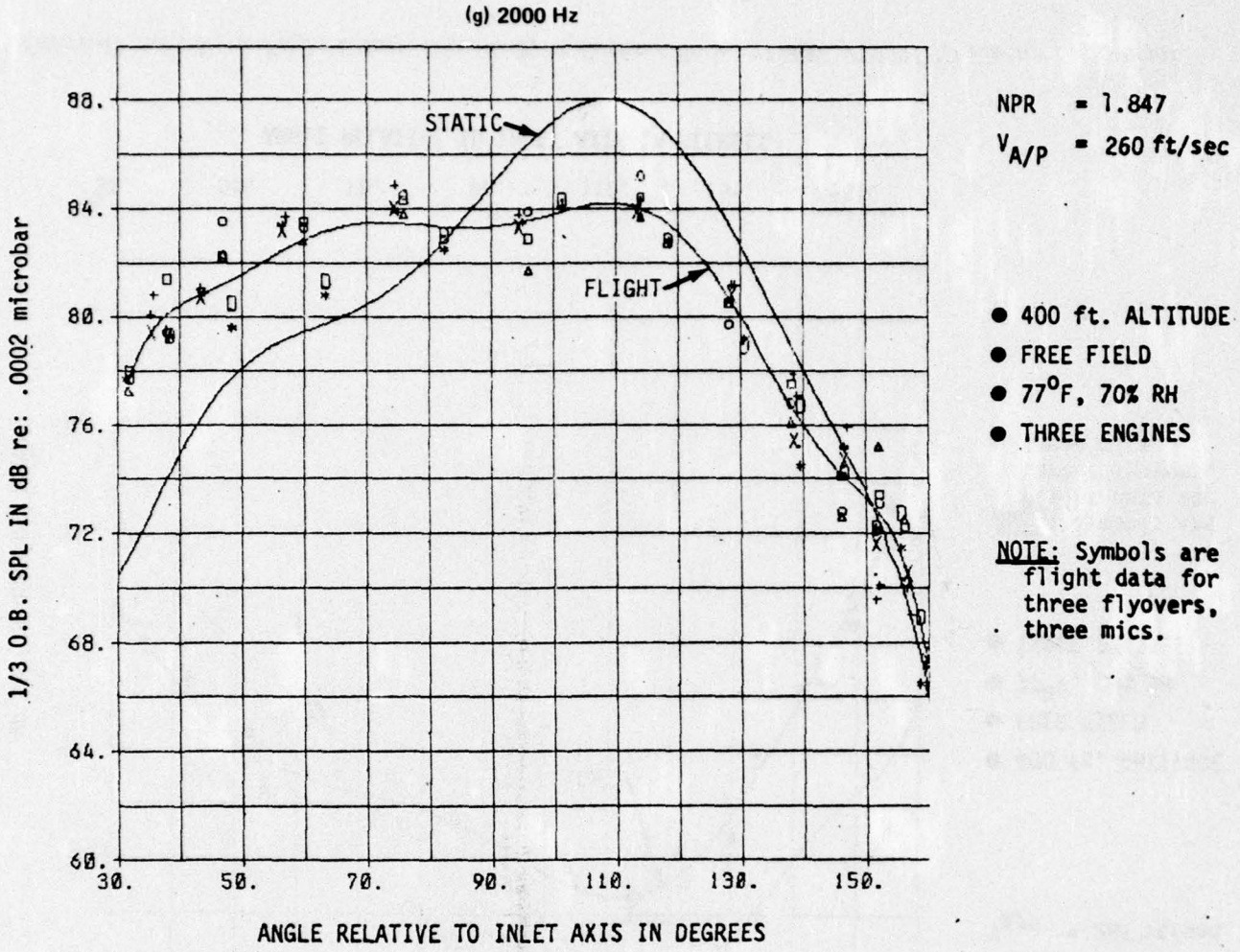


NPR = 1.847

$V_{A/P}$ = 260 ft/sec

- 400 ft. ALTITUDE
- FREE FIELD
- 77°F, 70% RH
- THREE ENGINES

NOTE: Symbols are flight data for three flyovers, three mics.

*Figure 40.—(Concluded)*

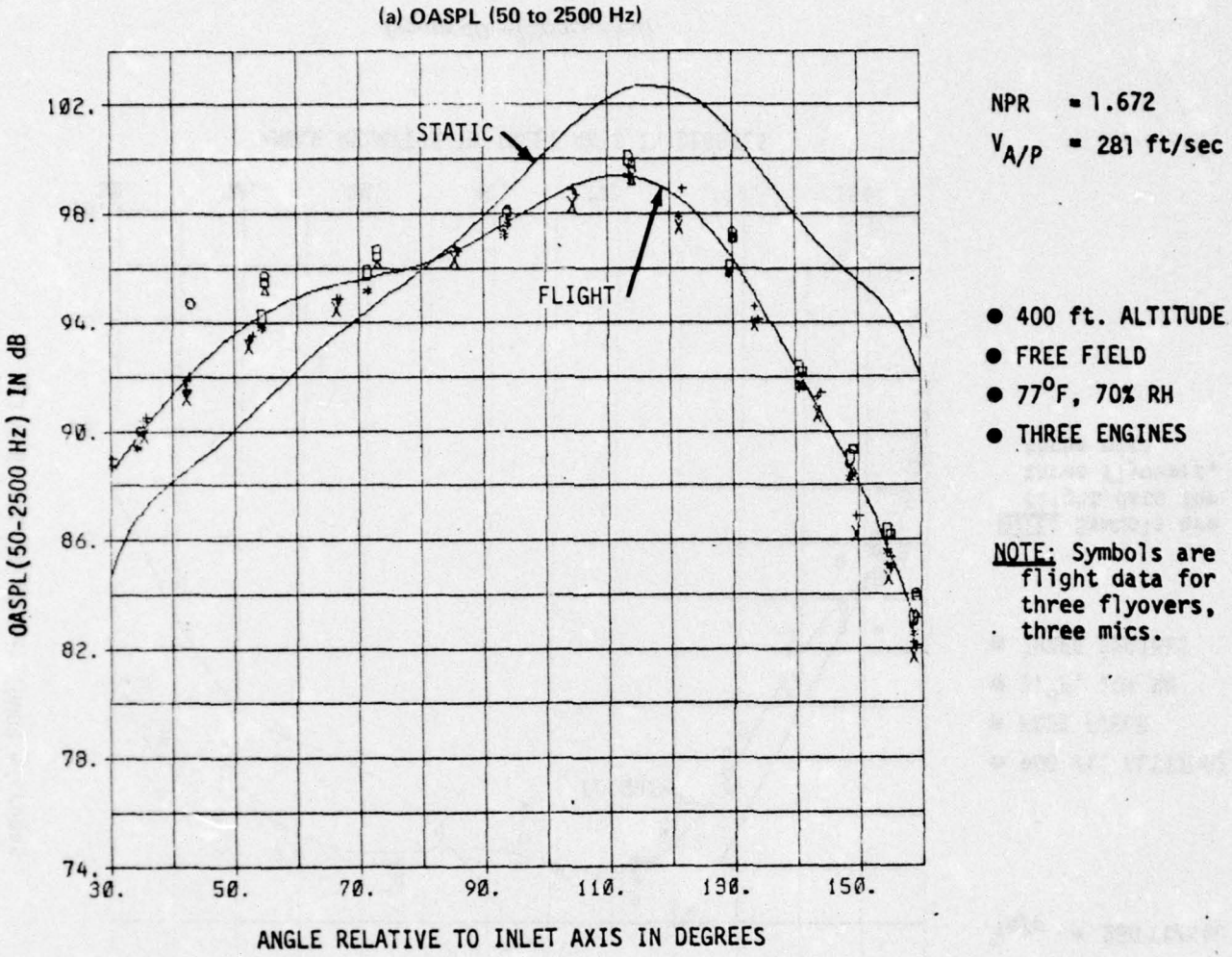


*Figure 41.—Jet Noise Flight Effects Directivity at Cutback Power (LGW), 727/JT8D Ejector Suppressor*

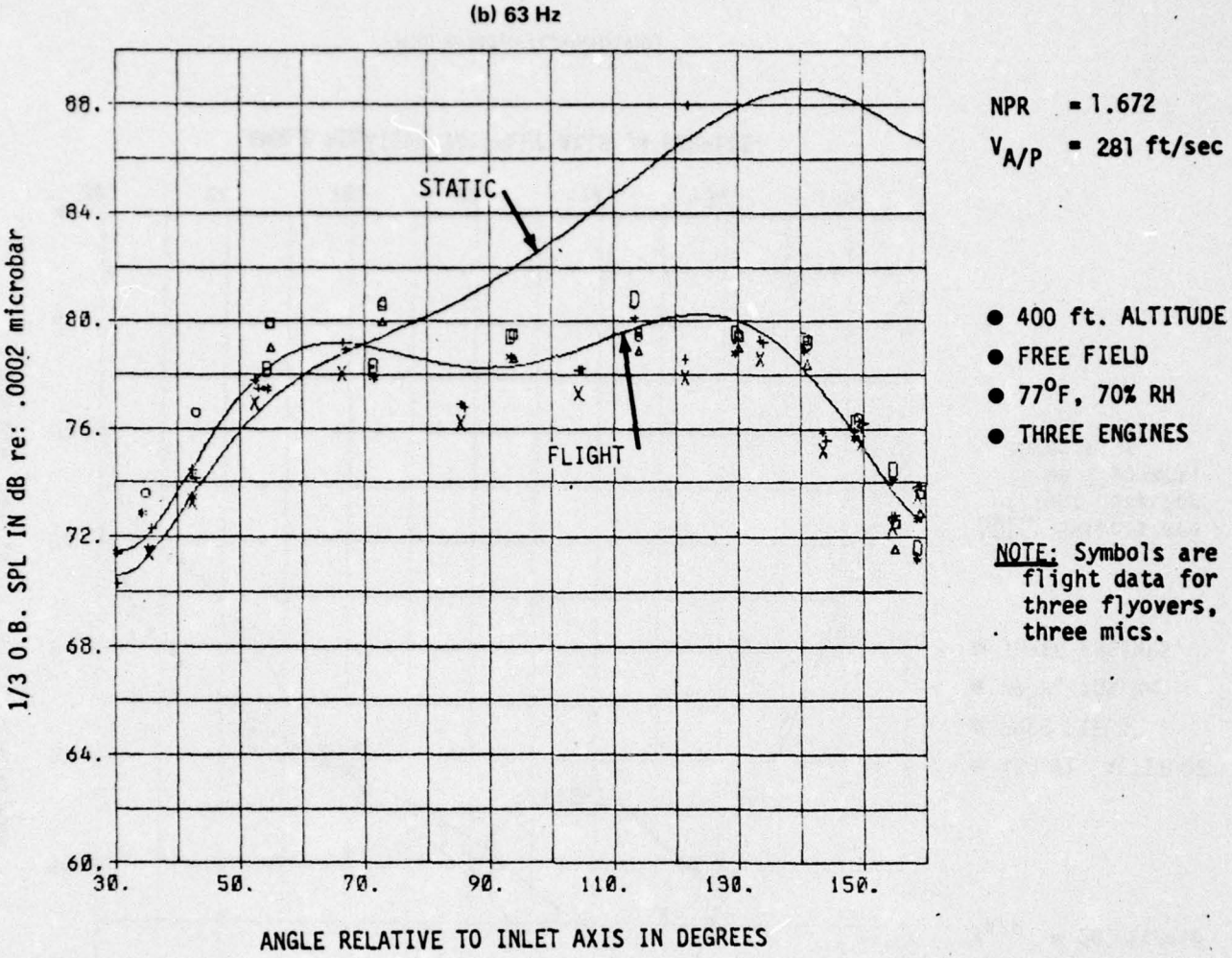


*Figure 41.—(Continued)*

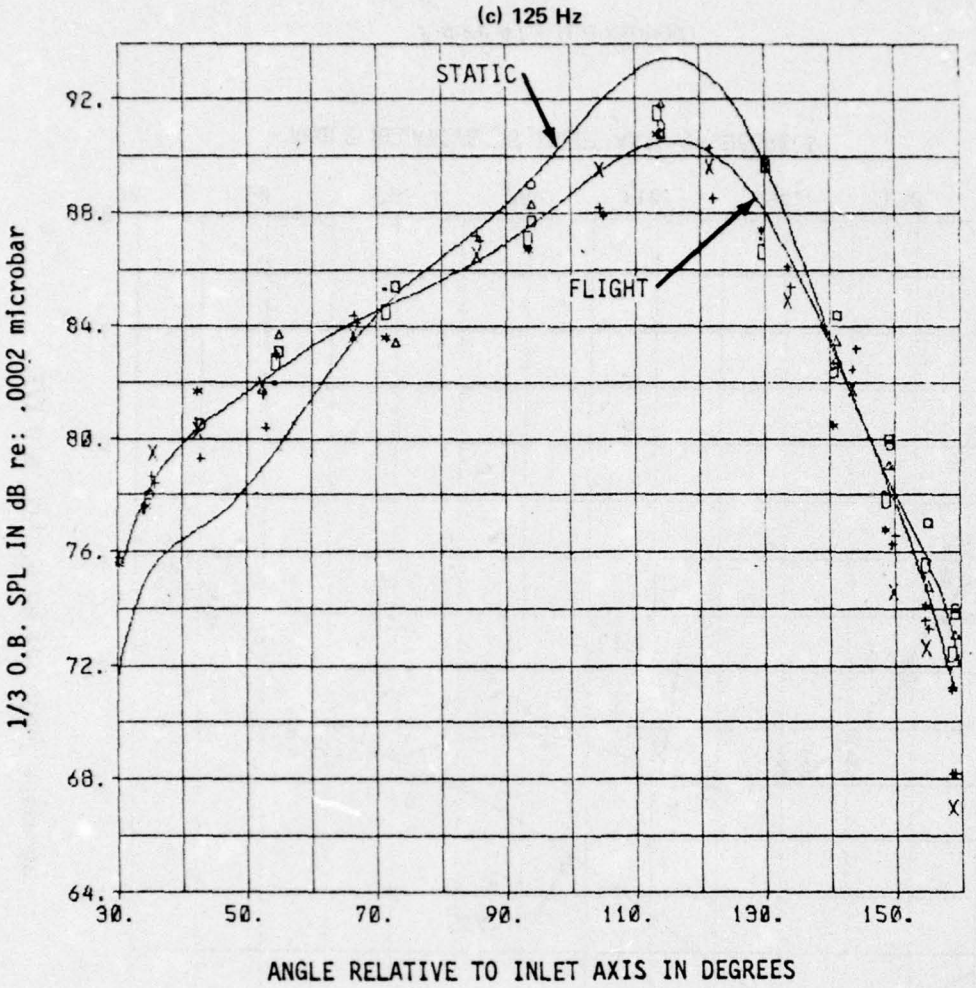


NPR = 1.672

$V_{A/P}$ = 281 ft/sec

- 400 ft. ALTITUDE
- FREE FIELD
- 77°F, 70% RH
- THREE ENGINES

NOTE: Symbols are flight data for three flyovers, three mics.

*Figure 41.—(Continued)*

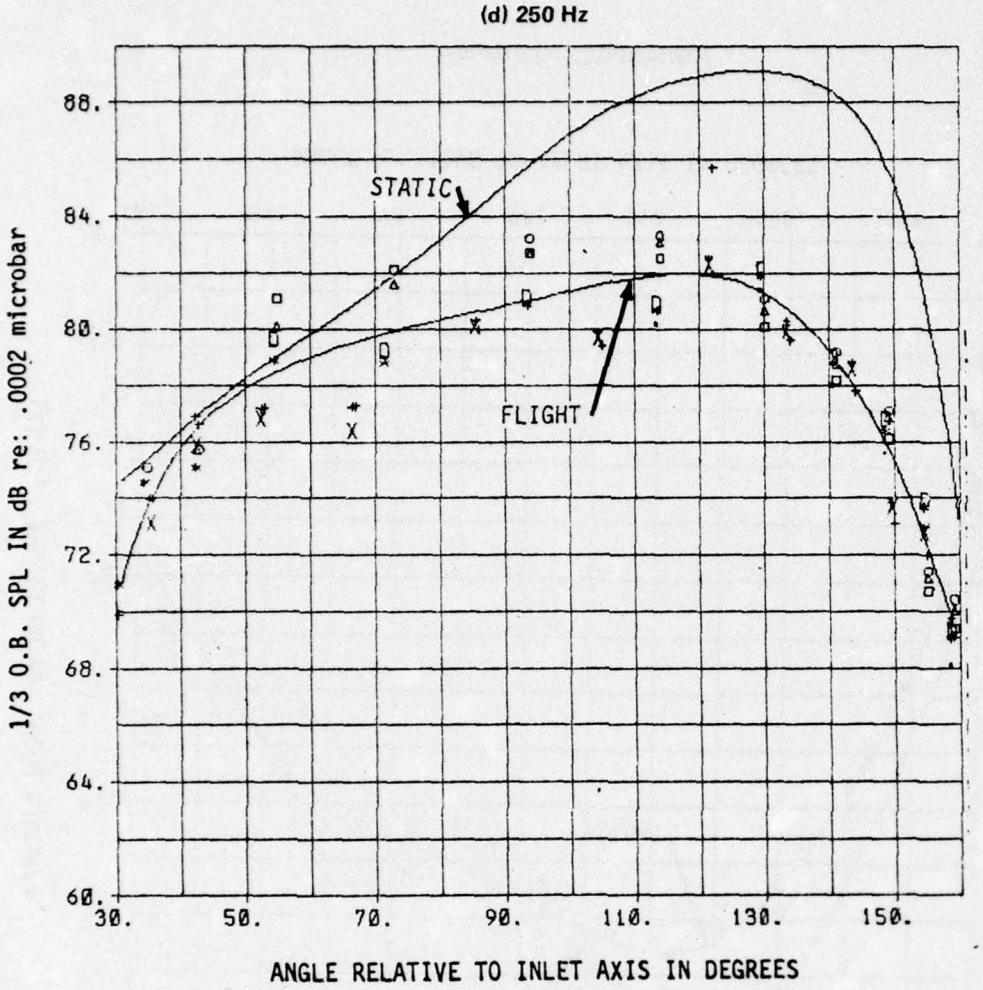


NPR = 1.672

$V_{A/P}$ = 281 ft/sec

- 400 ft. ALTITUDE
- FREE FIELD
- 77°F, 70% RH
- THREE ENGINES

NOTE: Symbols are flight data for three flyovers, three mics.

*Figure 41.—(Continued)*

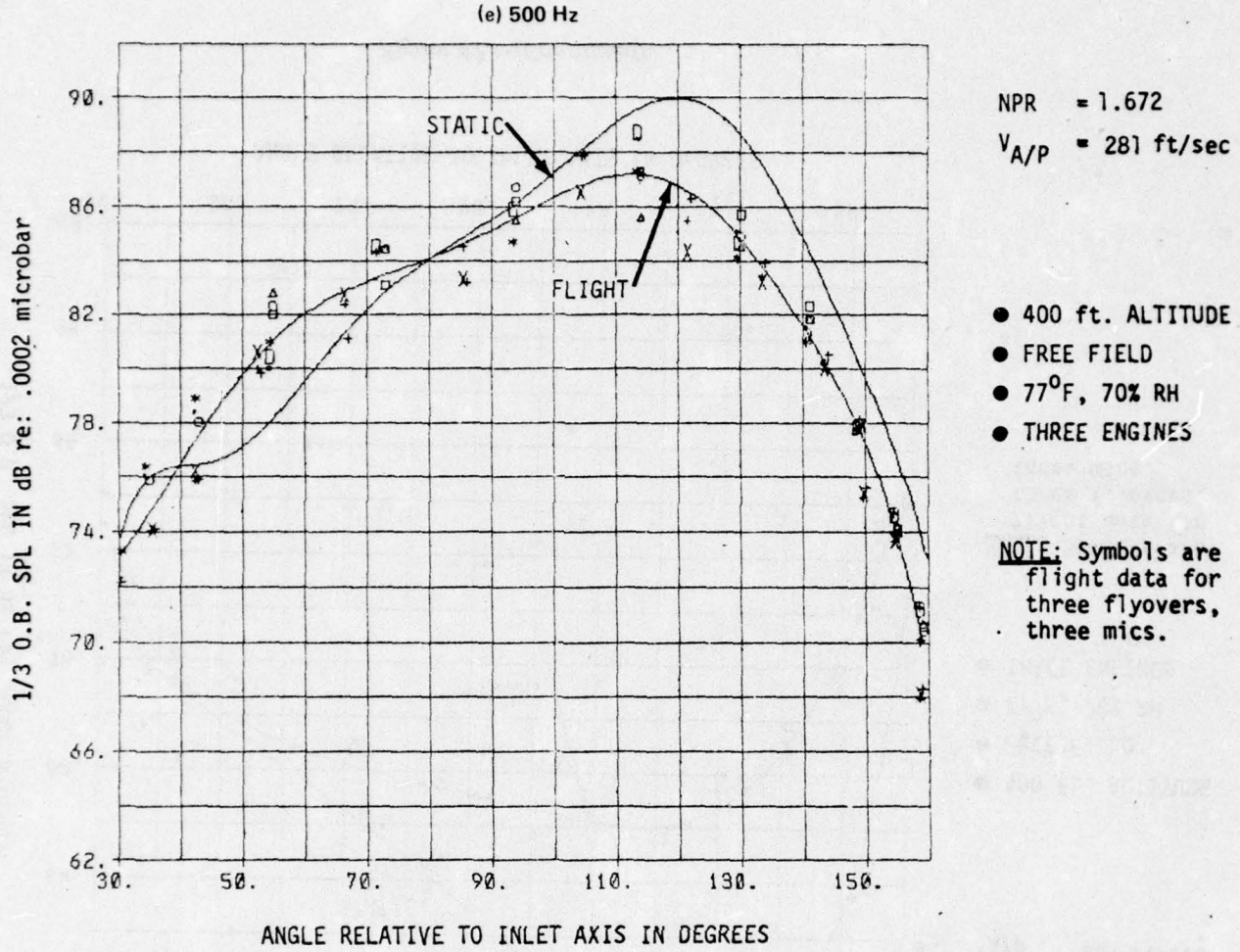


*Figure 41.—(Continued)*

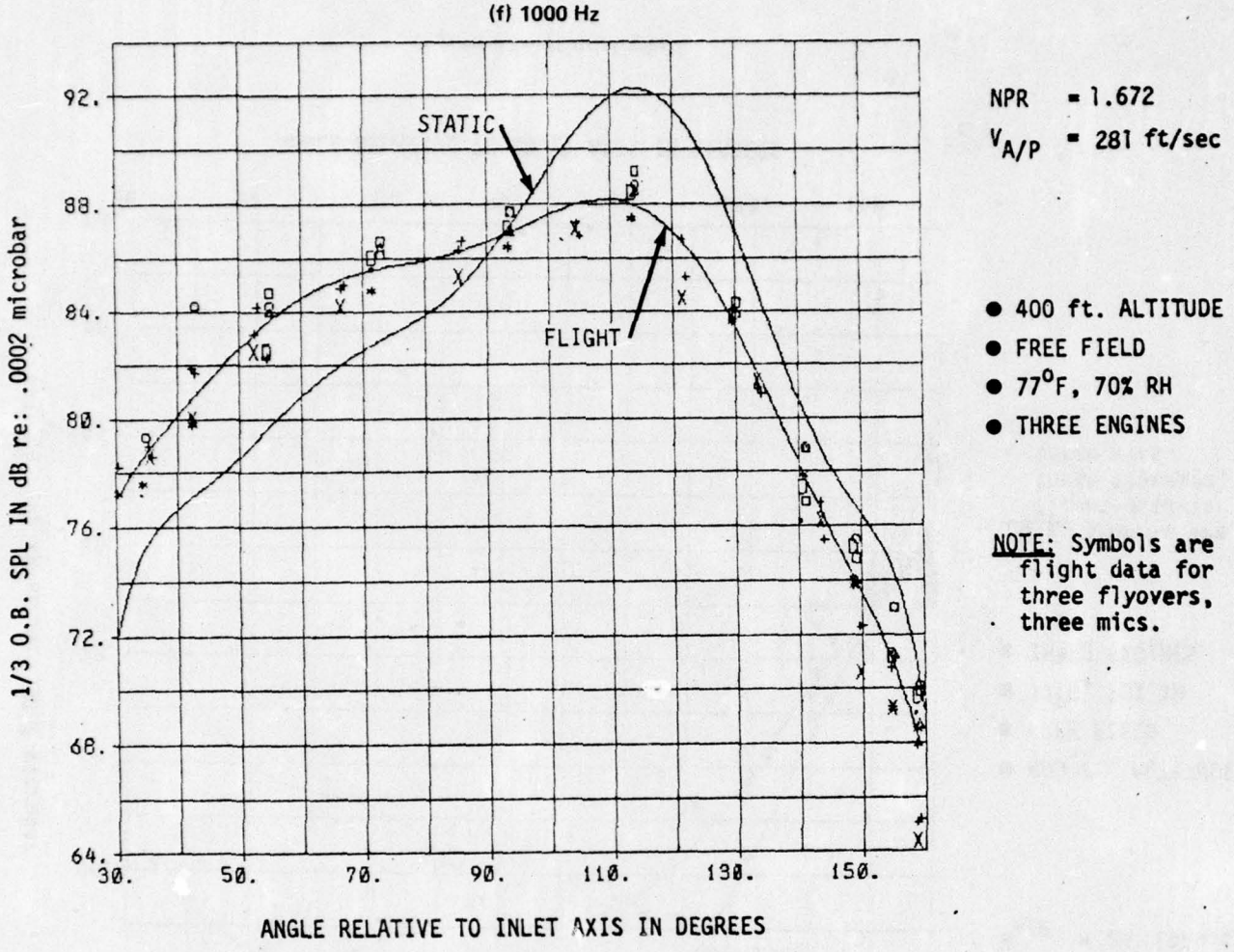


*Figure 41.—(Continued)*

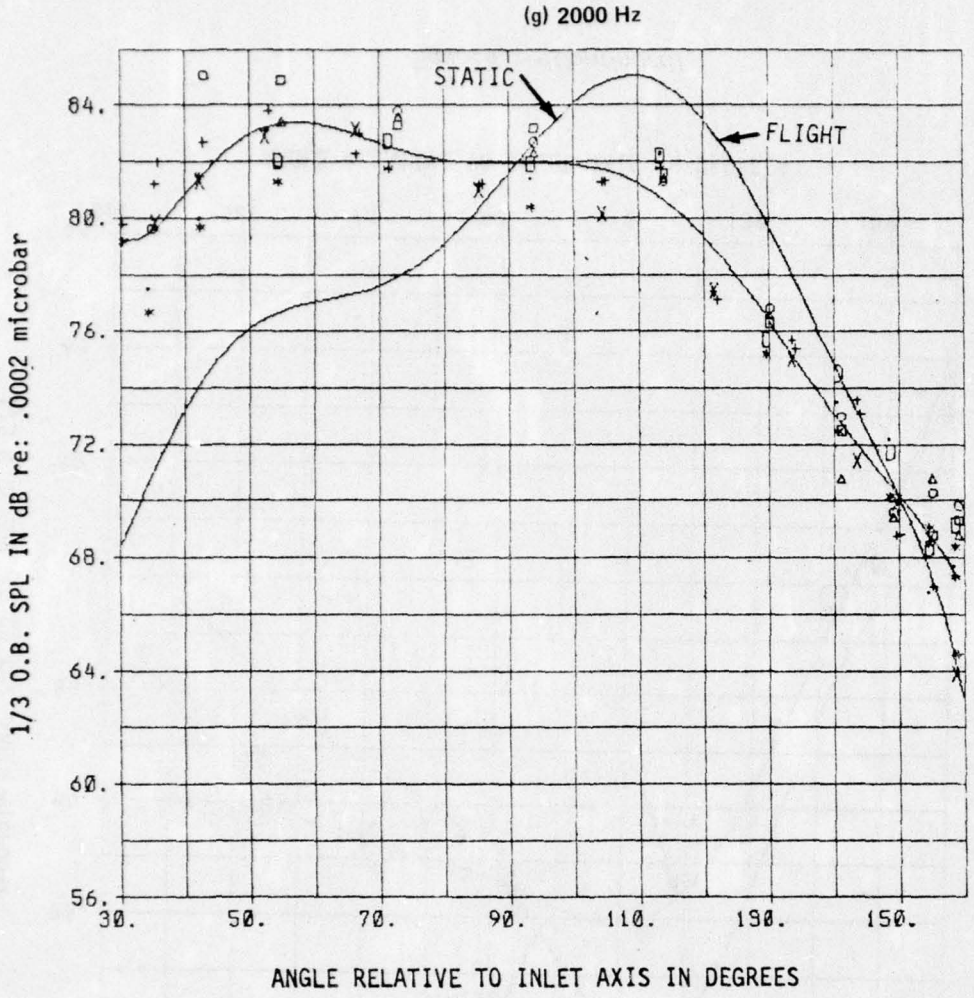


NPR = 1.672

$V_{A/P}$ = 281 ft/sec

- 400 ft. ALTITUDE
- FREE FIELD
- 77°F, 70% RH
- THREE ENGINES

NOTE: Symbols are flight data for three flyovers, three mics.

*Figure 41.—(Concluded)*

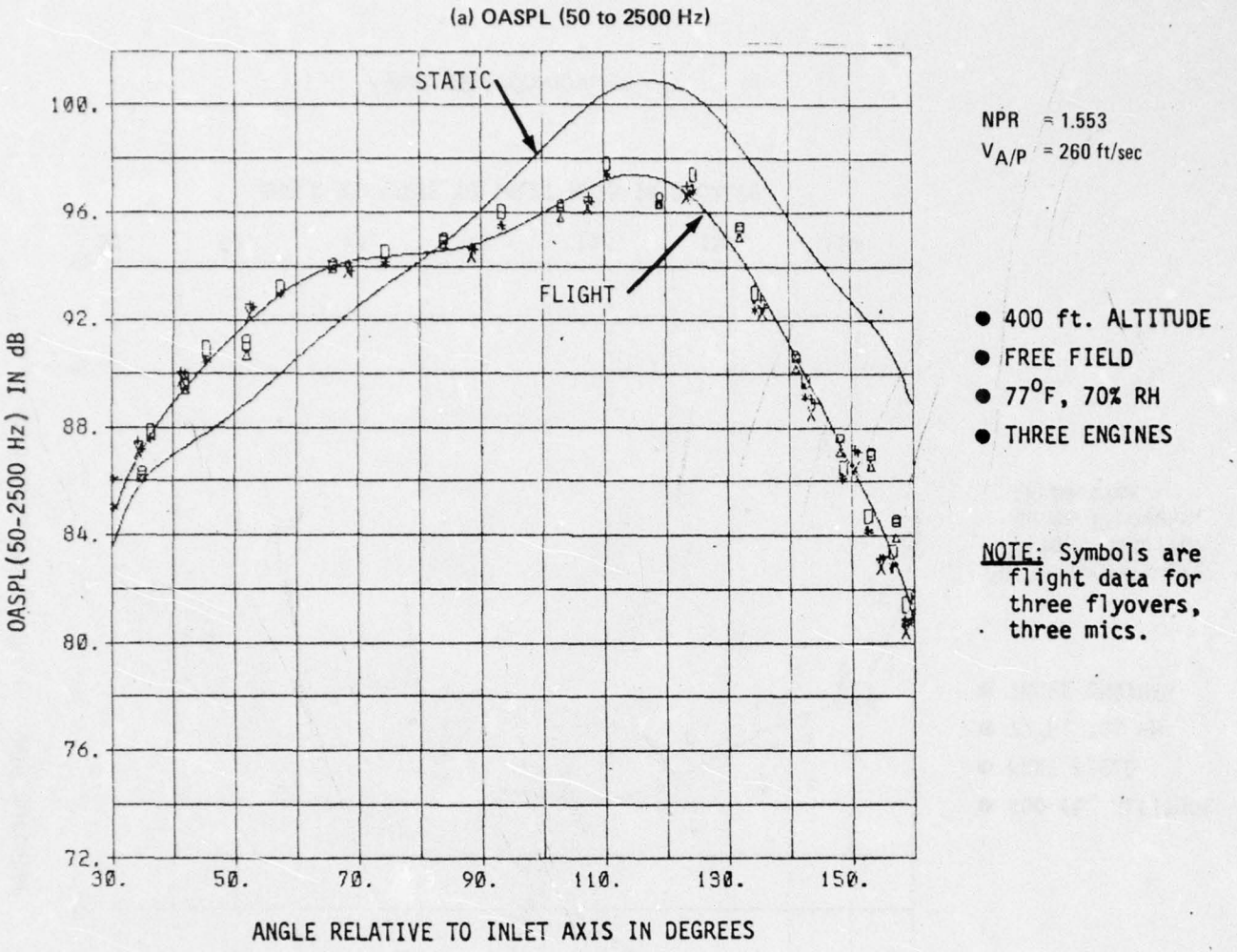


*Figure 42.—Jet Noise Flight Effects Directivity at Approach Power, 727/JT8D Ejector Suppressor*

(b) 63 Hz

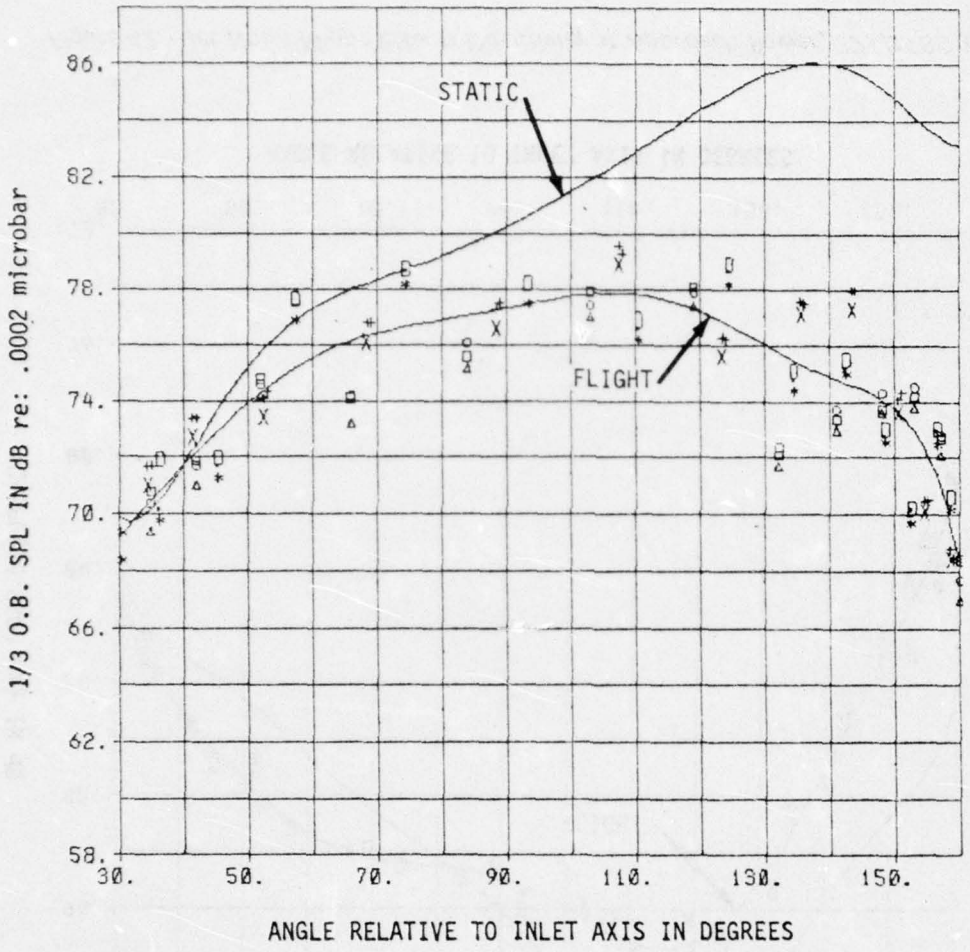


NPR = 1.553
$V_{A/P}$ = 260 ft/sec

- 400 ft. ALTITUDE
- FREE FIELD
- 77°F, 70% RH
- THREE ENGINES

NOTE: Symbols are flight data for three flyovers, three mics.

*Figure 42.—(Continued)*

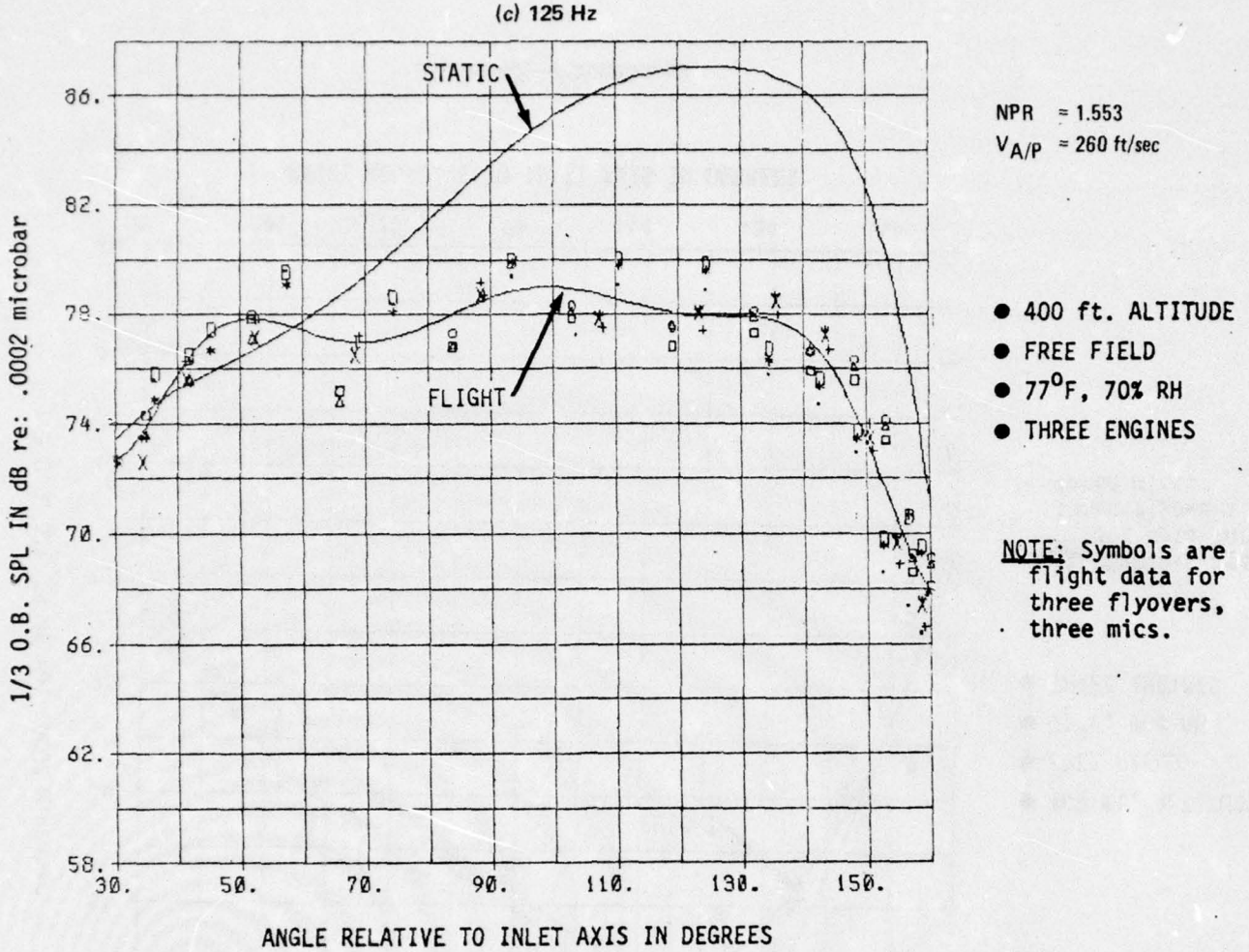


*Figure 42.—(Continued)*

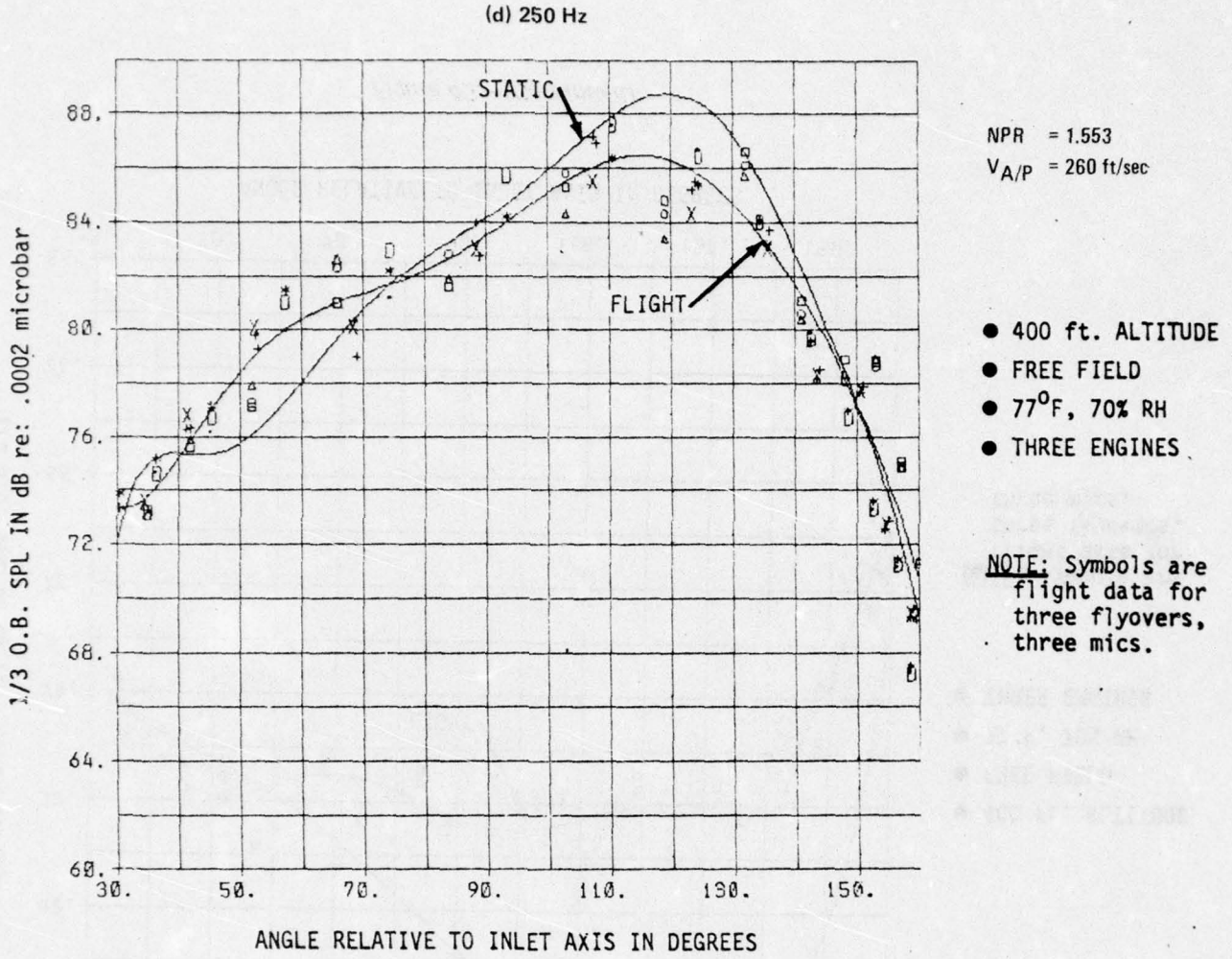


*Figure 42.—(Continued)*

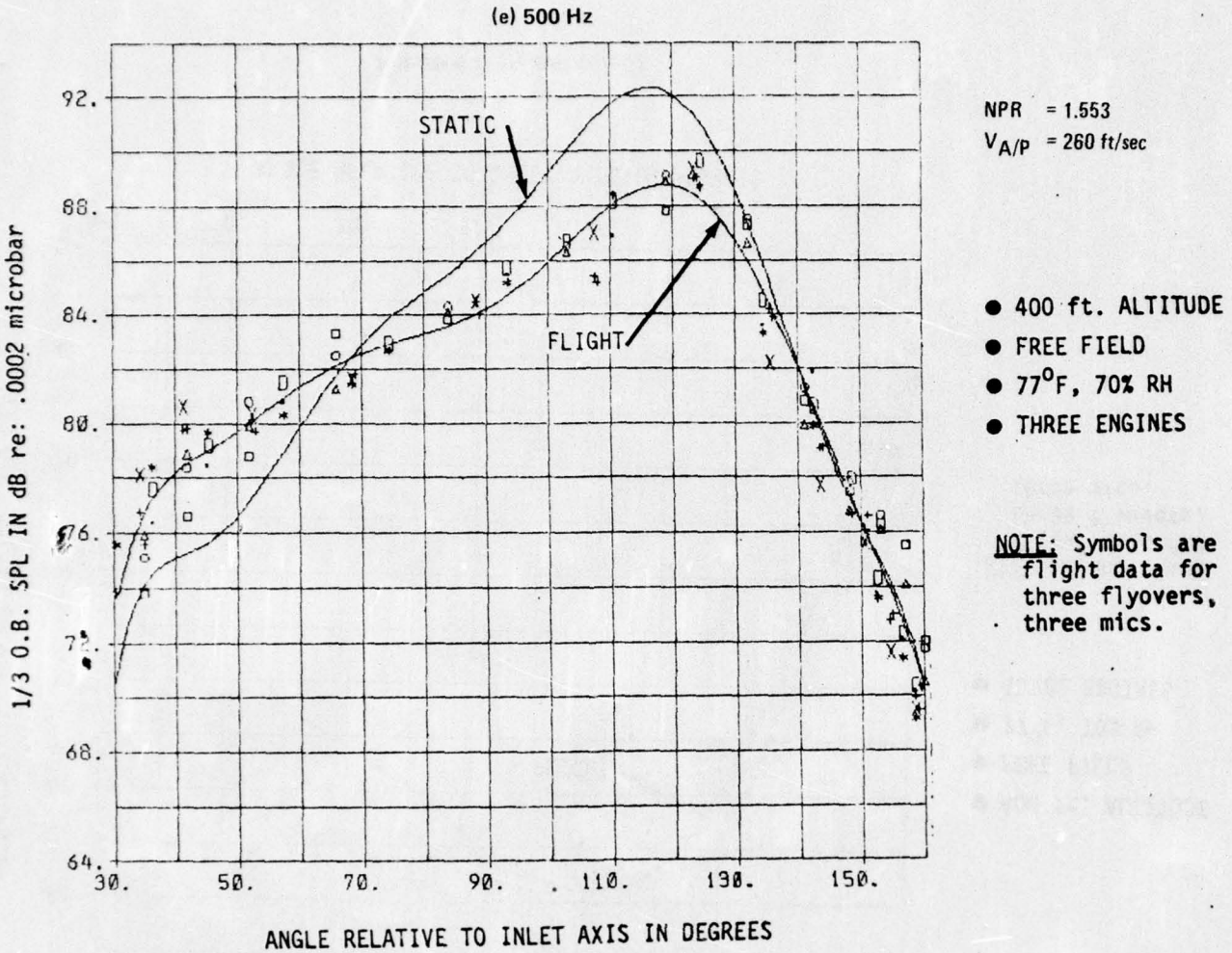


*Figure 42.—(Continued)*

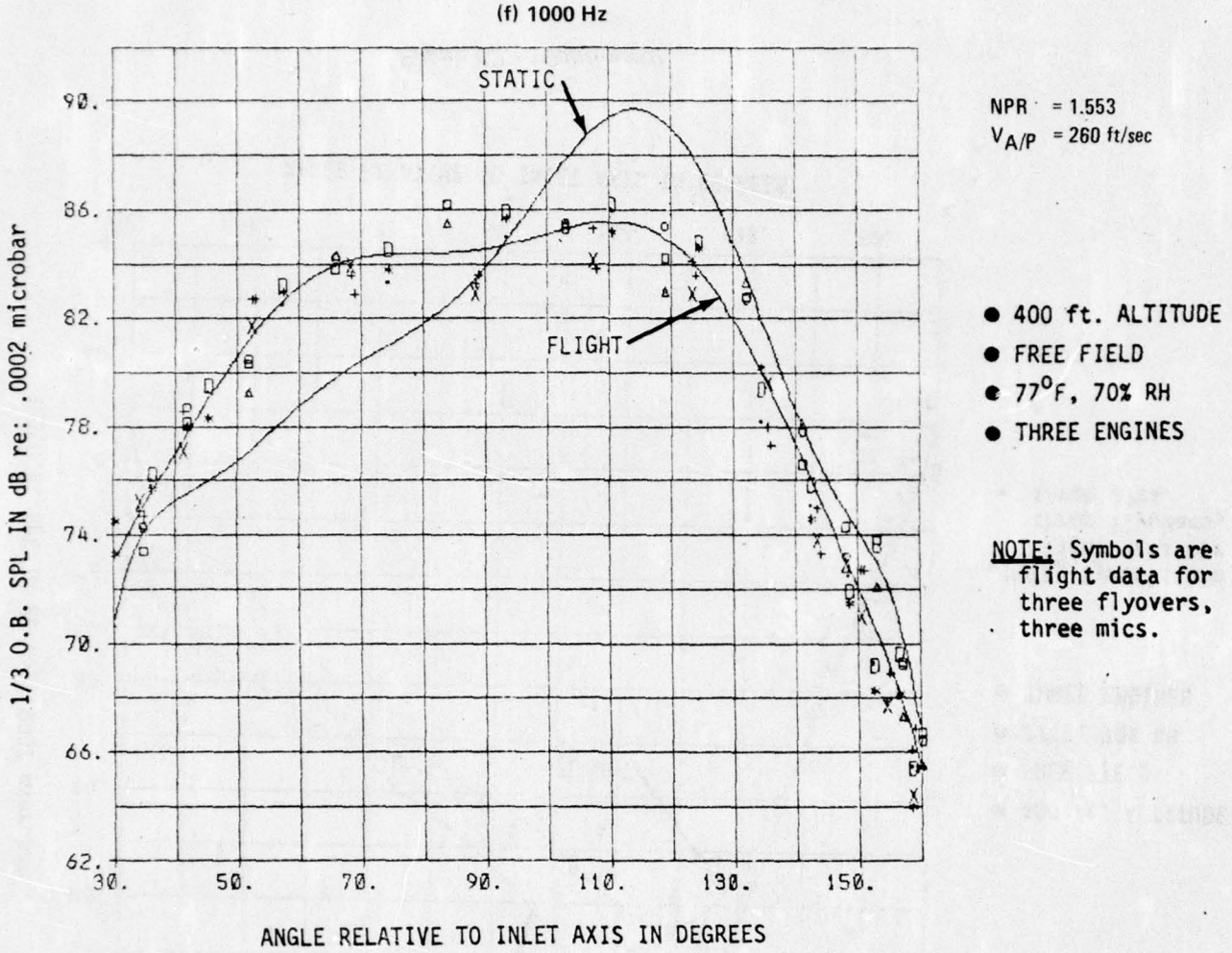


*Figure 42.—(Continued)*

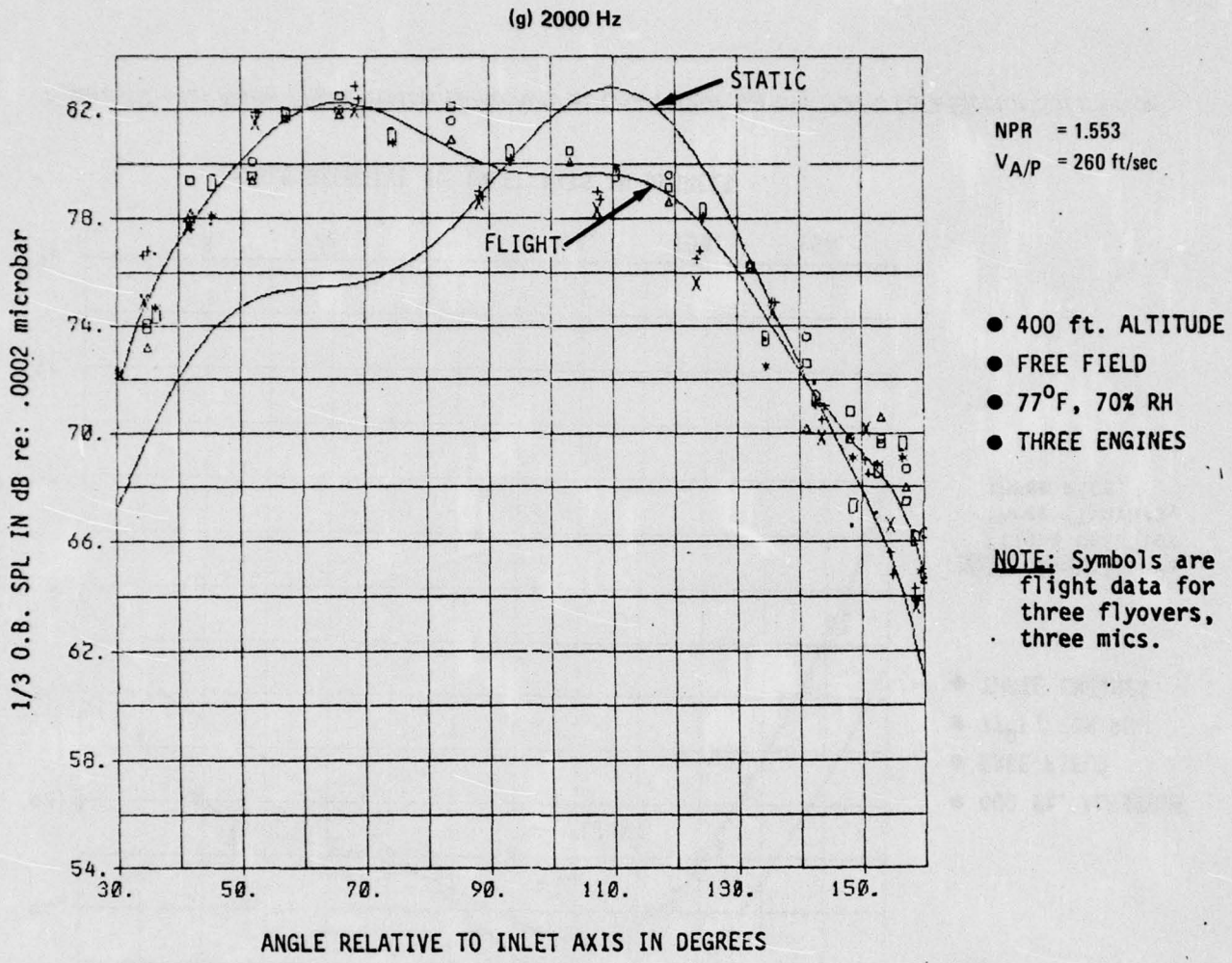


*Figure 42.—(Concluded)*

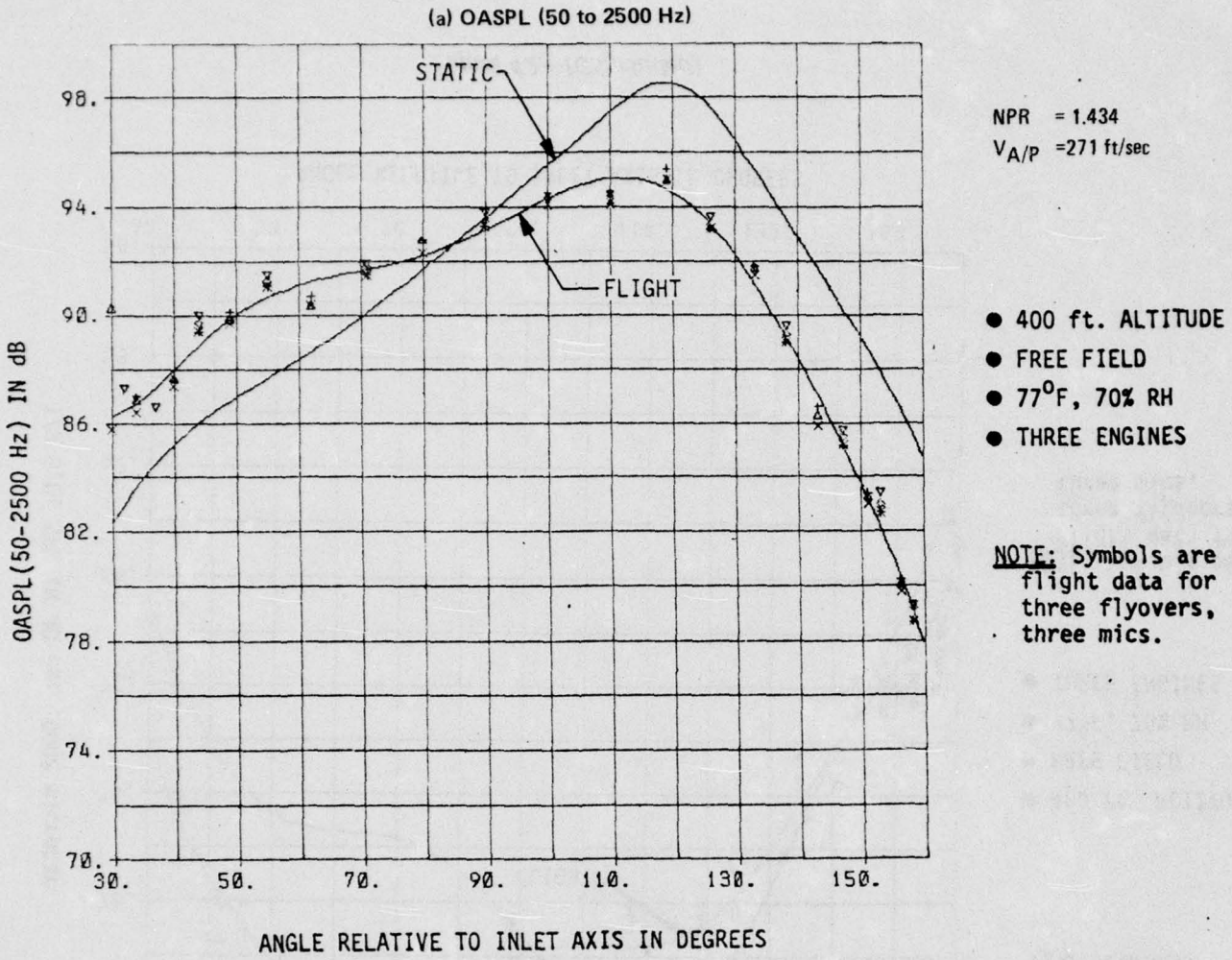


*Figure 43.—Jet Noise Flight Effects Directivity at Low Power Setting, 727/JT8D Ejector Suppressor*

(b) 63 Hz

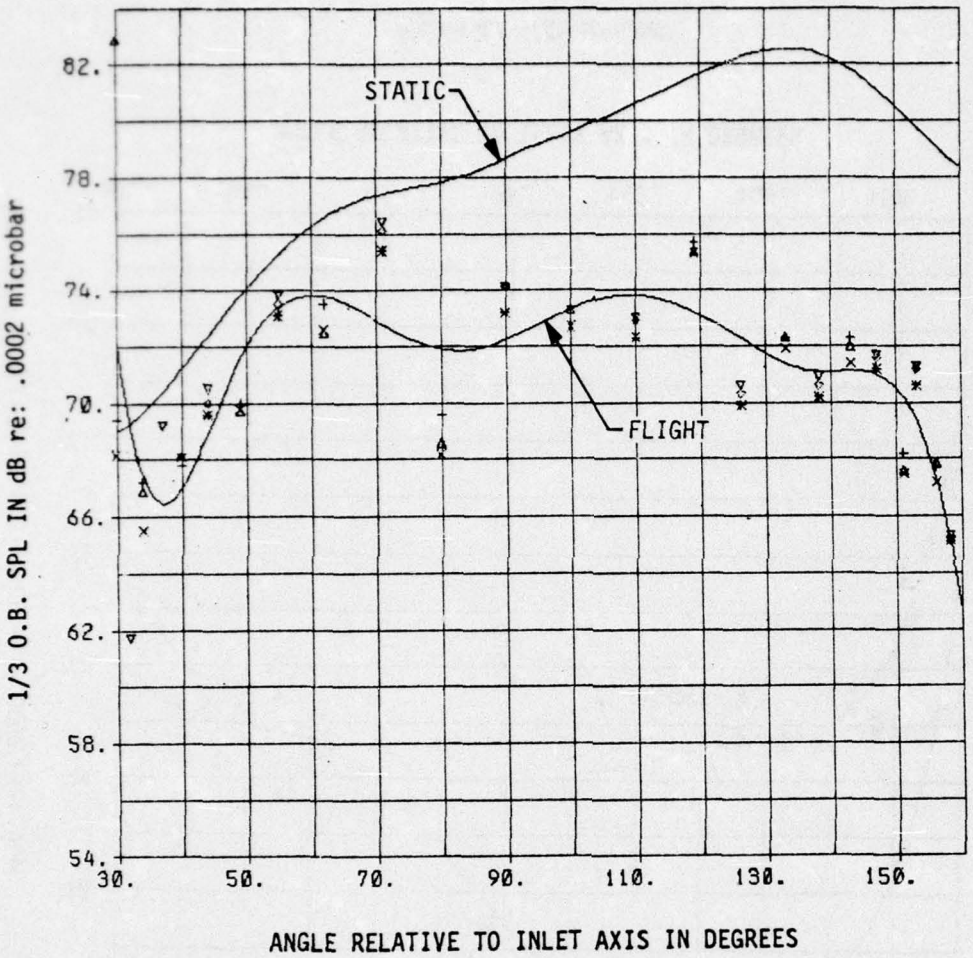


NPR = 1.434
$V_{A/P}$ = 271 ft/sec

- 400 ft. ALTITUDE
- FREE FIELD
- 77°F, 70% RH
- THREE ENGINES

NOTE: Symbols are flight data for three flyovers, three mics.

*Figure 43.—(Continued)*

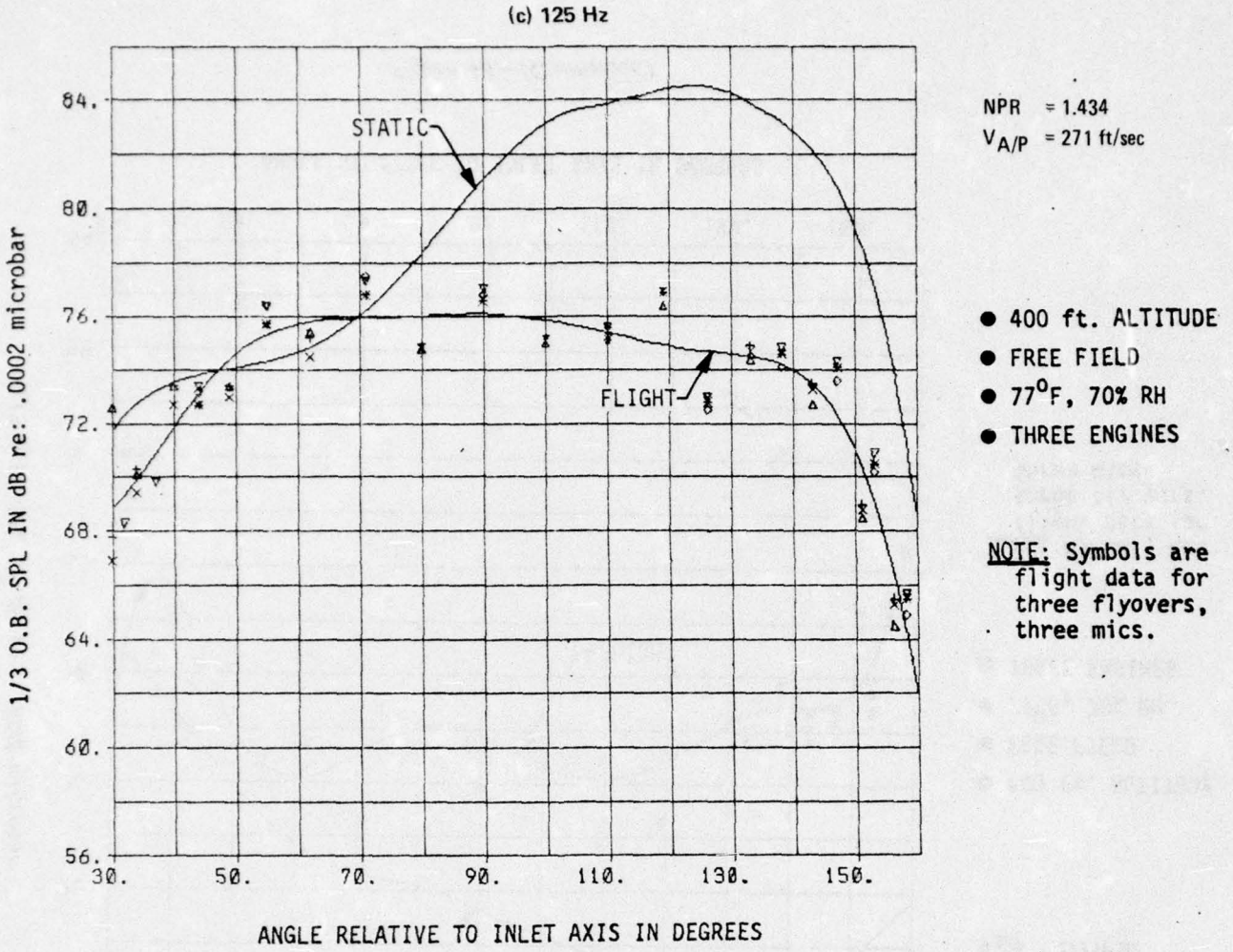


*Figure 43.—(Continued)*

(d) 250 Hz

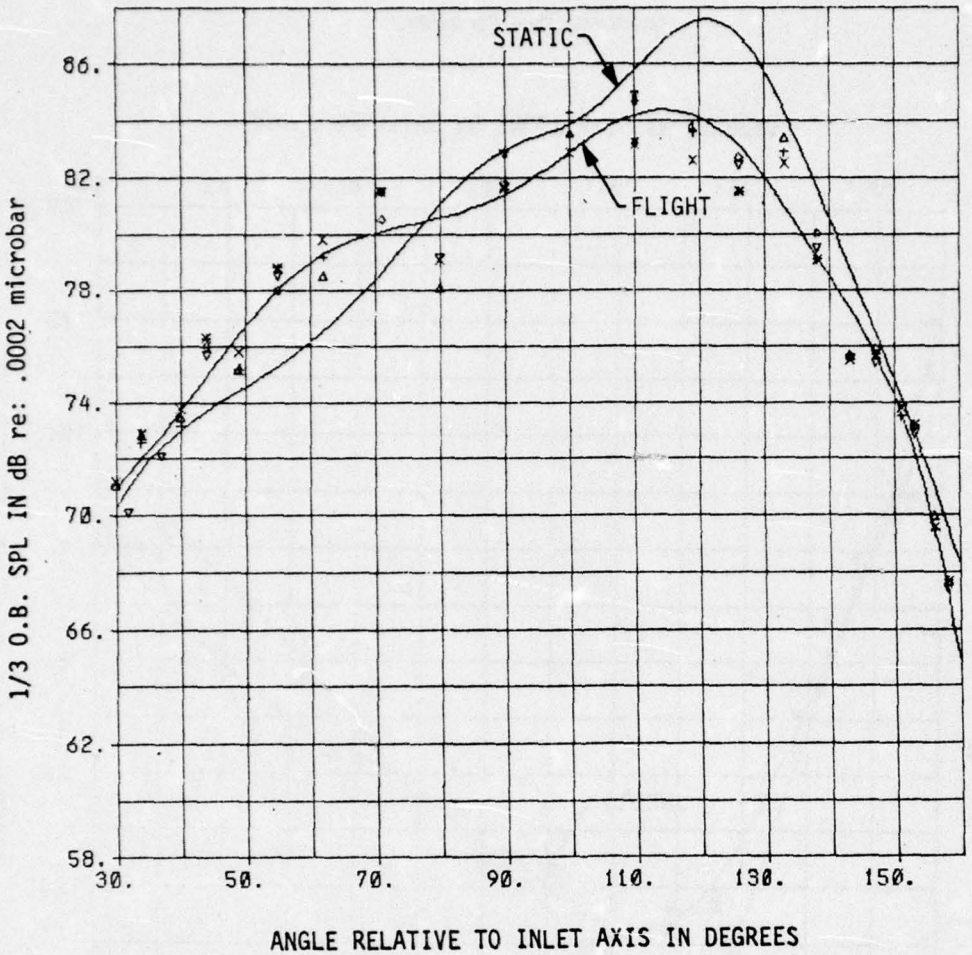


NPR = 1.434
$V_{A/P}$ = 271 ft/sec

- 400 ft. ALTITUDE
- FREE FIELD
- 77°F, 70% RH
- THREE ENGINES

NOTE: Symbols are flight data for three flyovers, three mics.

*Figure 43.—(Continued)*

(e) 500 Hz

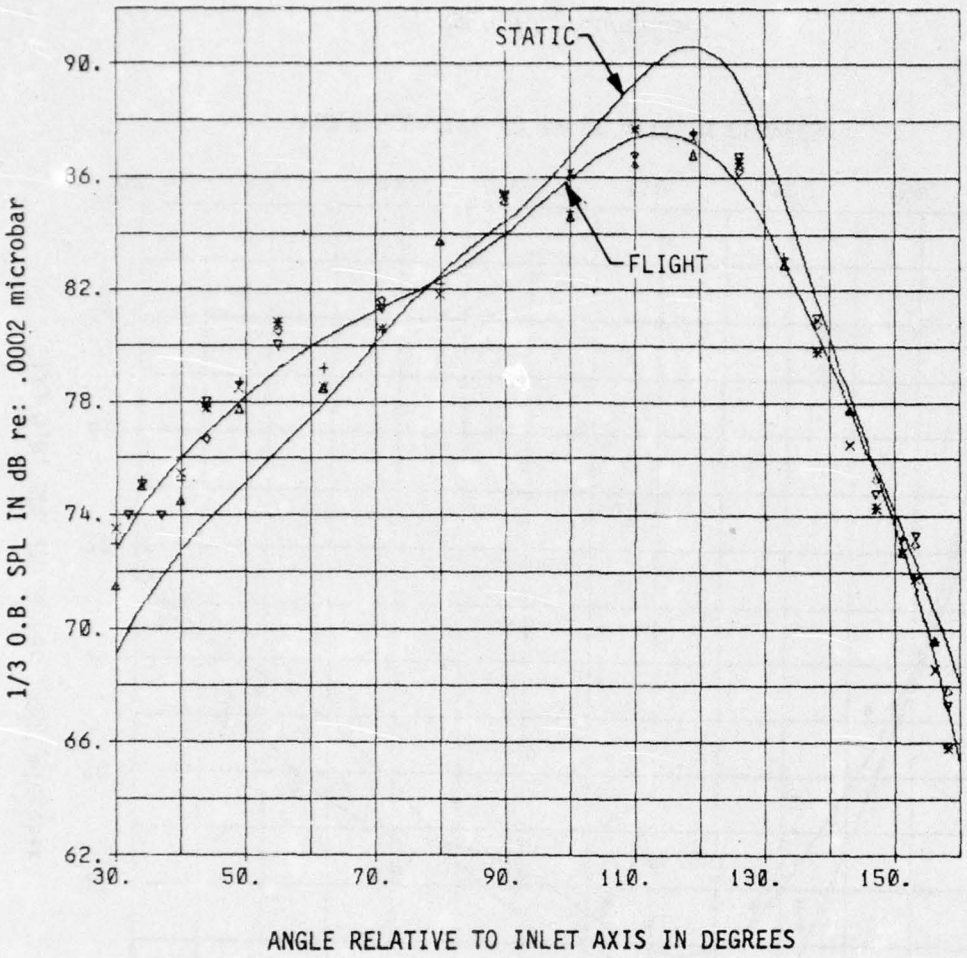


NPR = 1.434
$V_{A/P}$ = 271 ft/sec

- 400 ft. ALTITUDE
- FREE FIELD
- 77°F, 70% RH
- THREE ENGINES

NOTE: Symbols are flight data for three flyovers, three mics.

*Figure 43.—(Continued)*

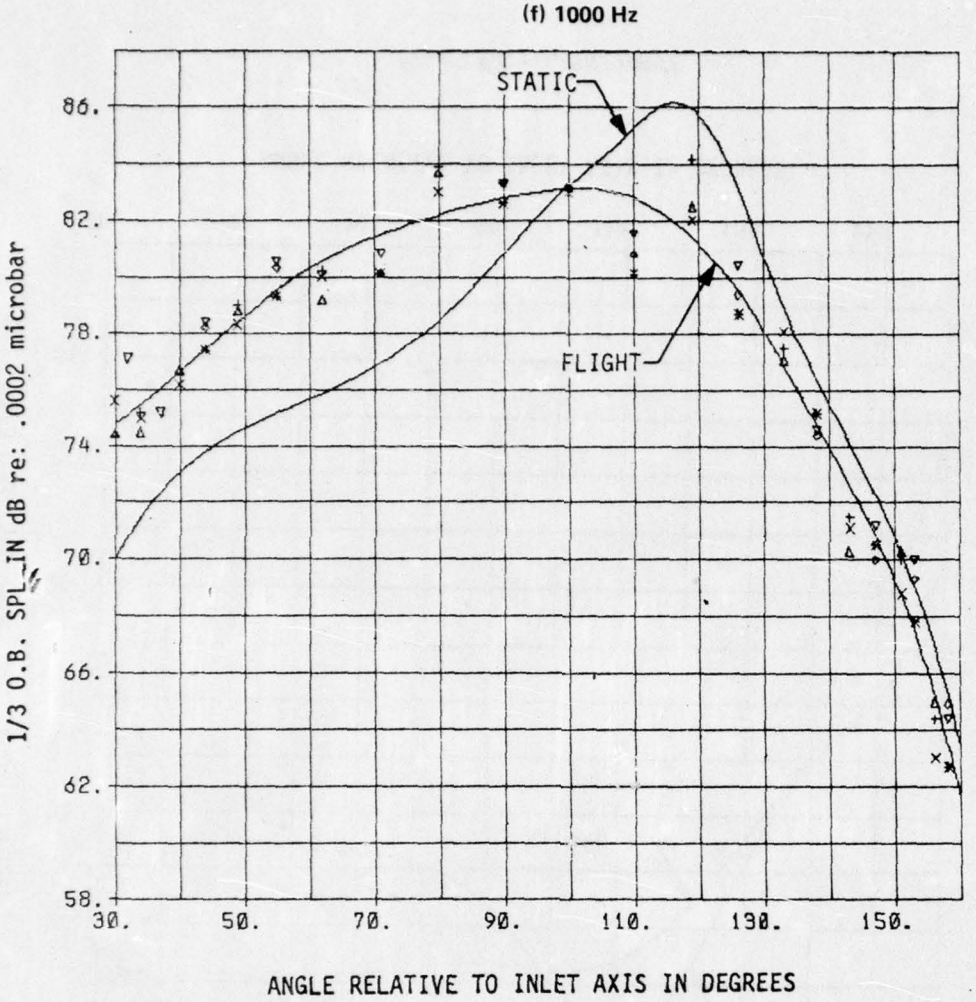


NPR = 1.434
$V_{A/P}$ = 271 ft/sec

- 400 ft. ALTITUDE
- FREE FIELD
- 77°F, 70% RH
- THREE ENGINES

NOTE: Symbols are flight data for three flyovers, three mics.

*Figure 43.—(Continued)*

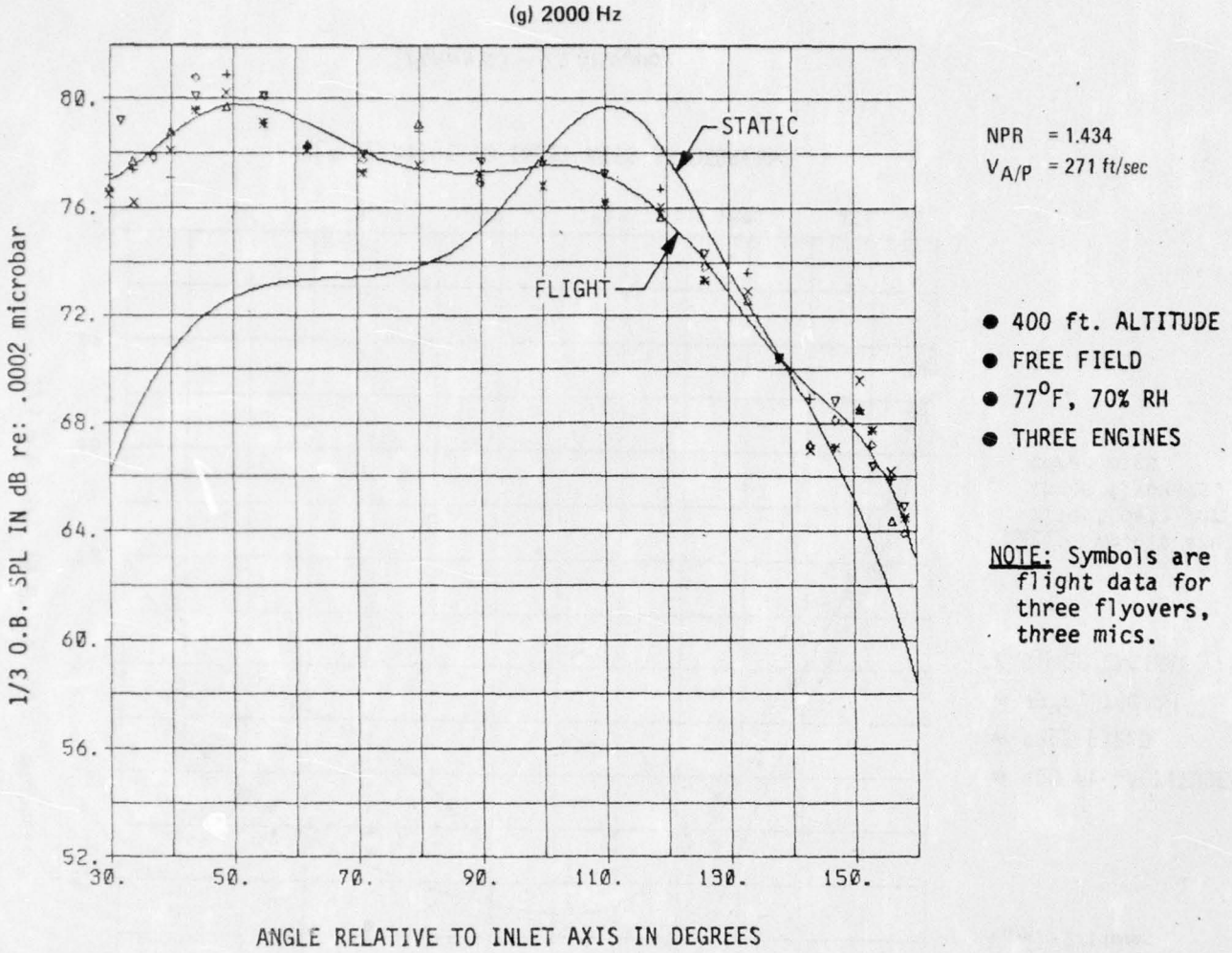


*Figure 43.—(Concluded)*

AD-A031 877 BOEING COMMERCIAL AIRPLANE CO SEATTLE WASH F/G 21/5
727/JT8D JET AND FAN NOISE FLIGHT EFFECTS STUDY.(U)
AUG 76 L F MUNOZ DOT-FA71WA-2637
UNCLASSIFIED D6-44145 FAA-RD-76-110 NL

3 OF 4
AD
A031877

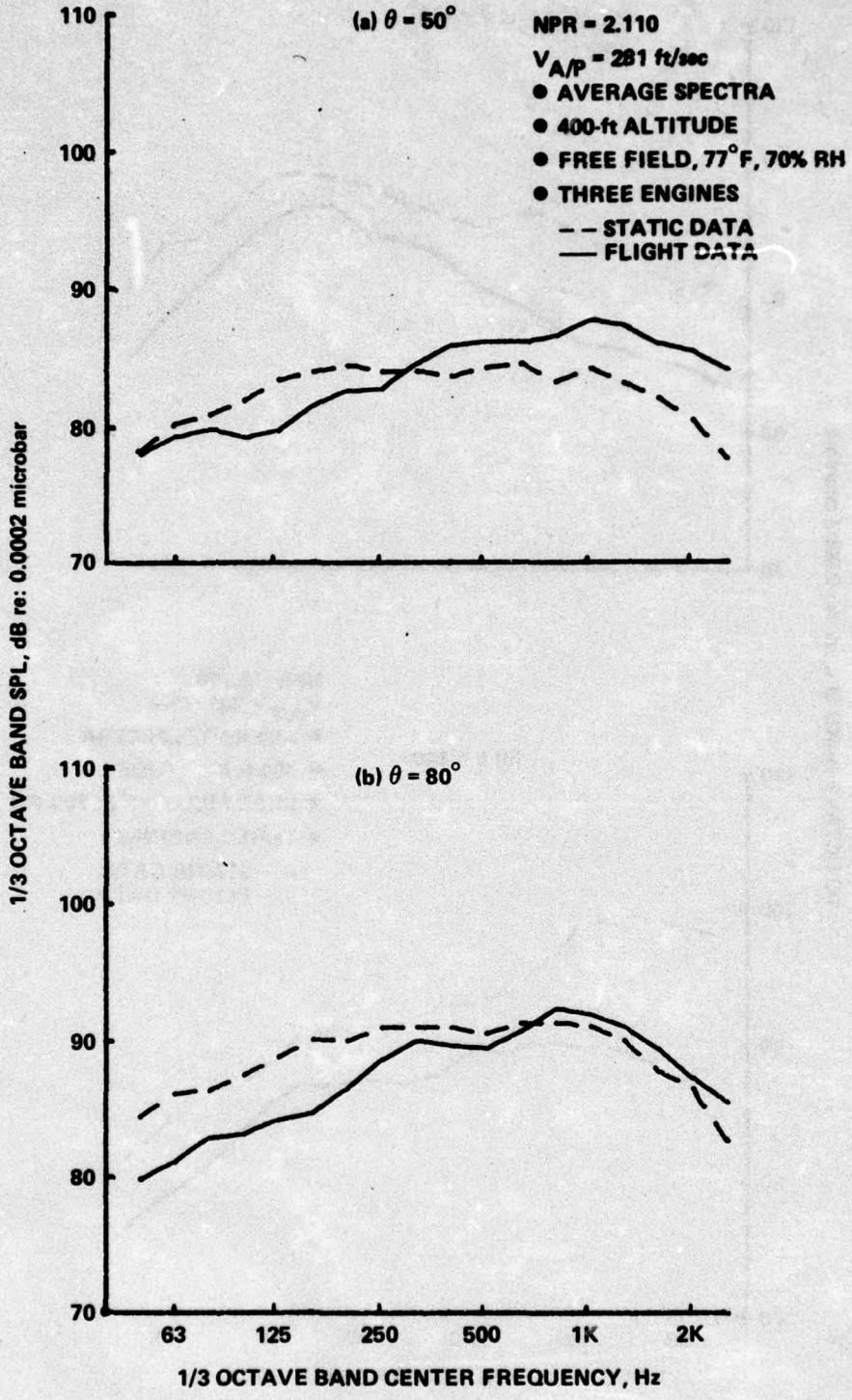


*Figure 44.—Jet Noise Flight Effects, Average Spectra, Takeoff Power, 727/JT8D Ejector Suppressor*

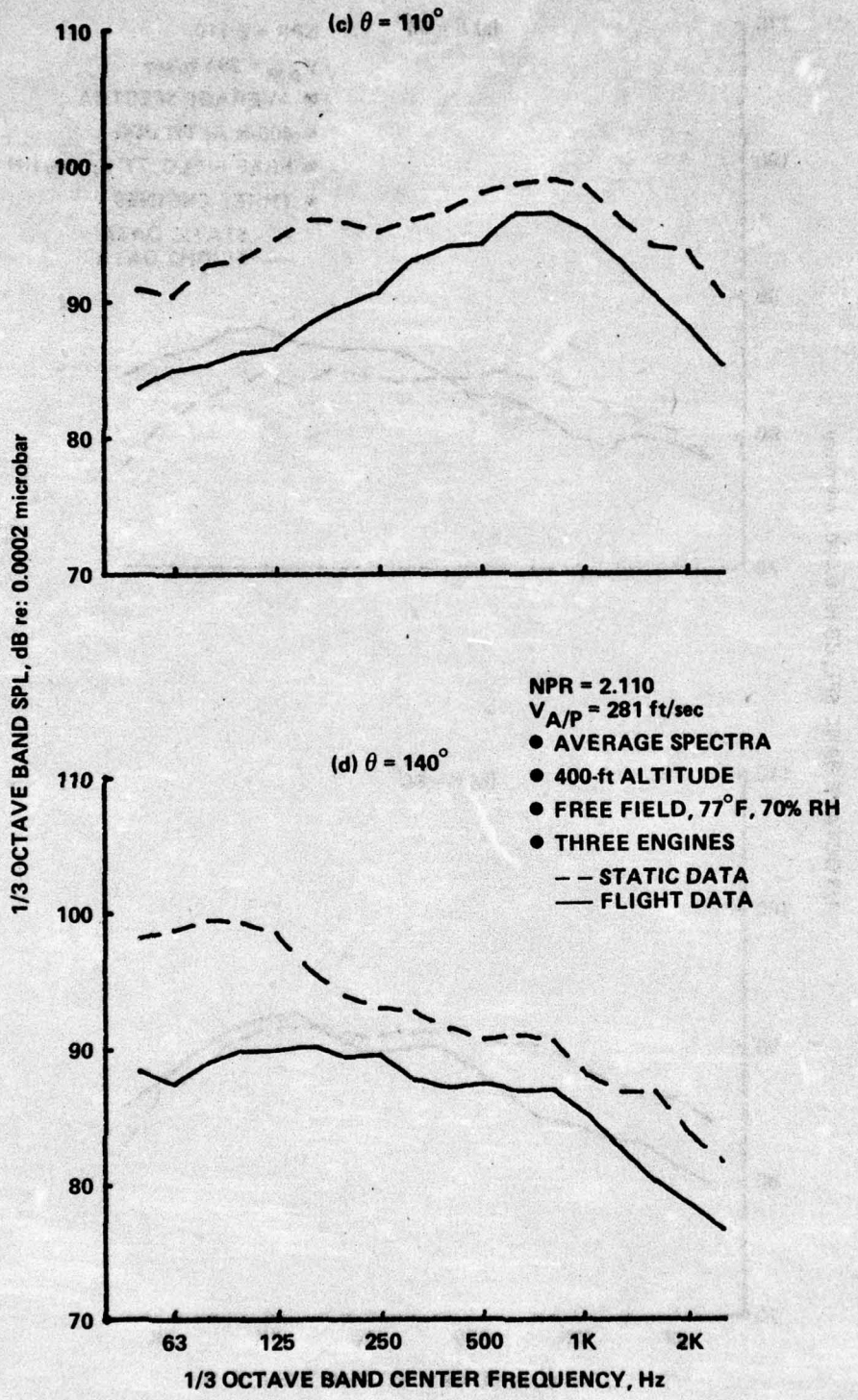


*Figure 44.—(Concluded)*

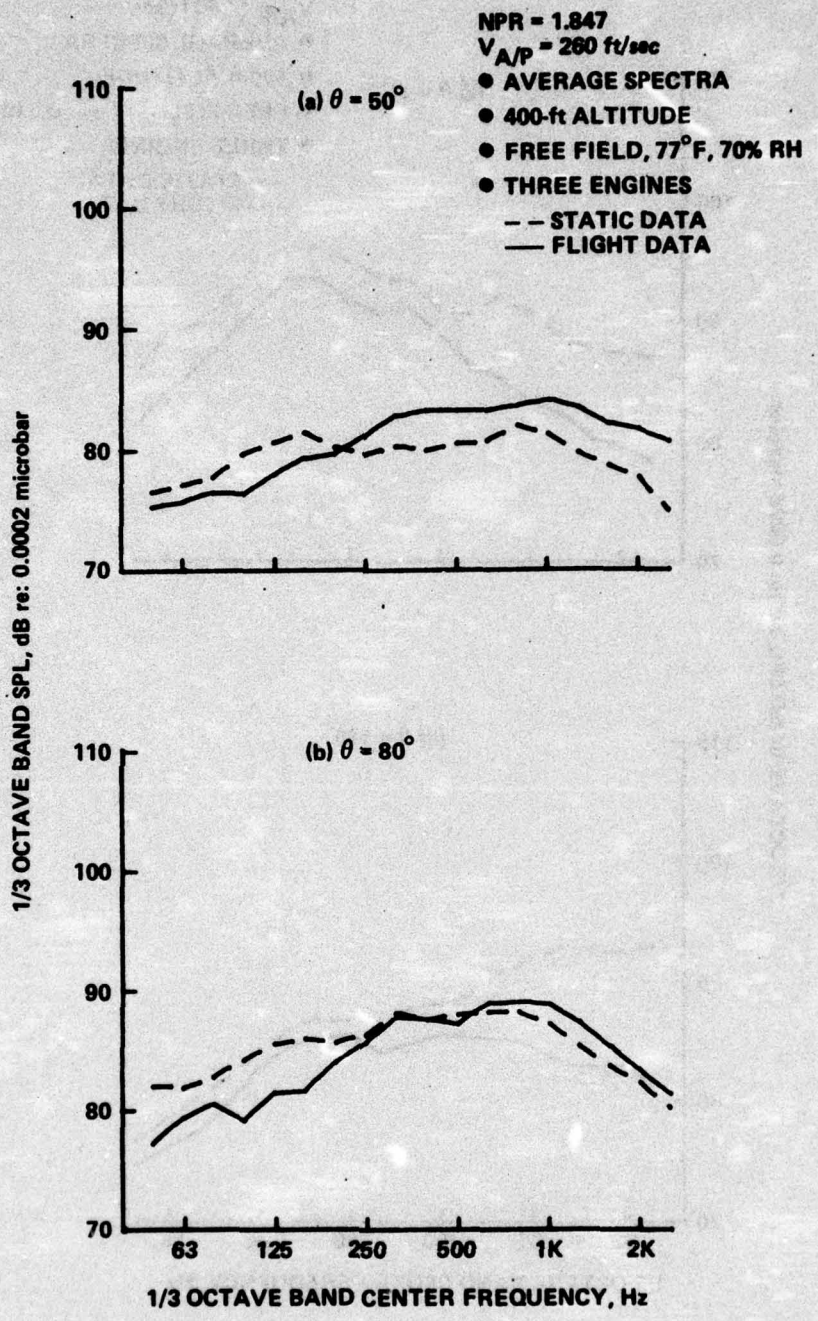


*Figure 45.—Jet Noise Flight Effects, Average Spectra, Cutback Power (HGW), 727/JT8D Ejector Suppressor*

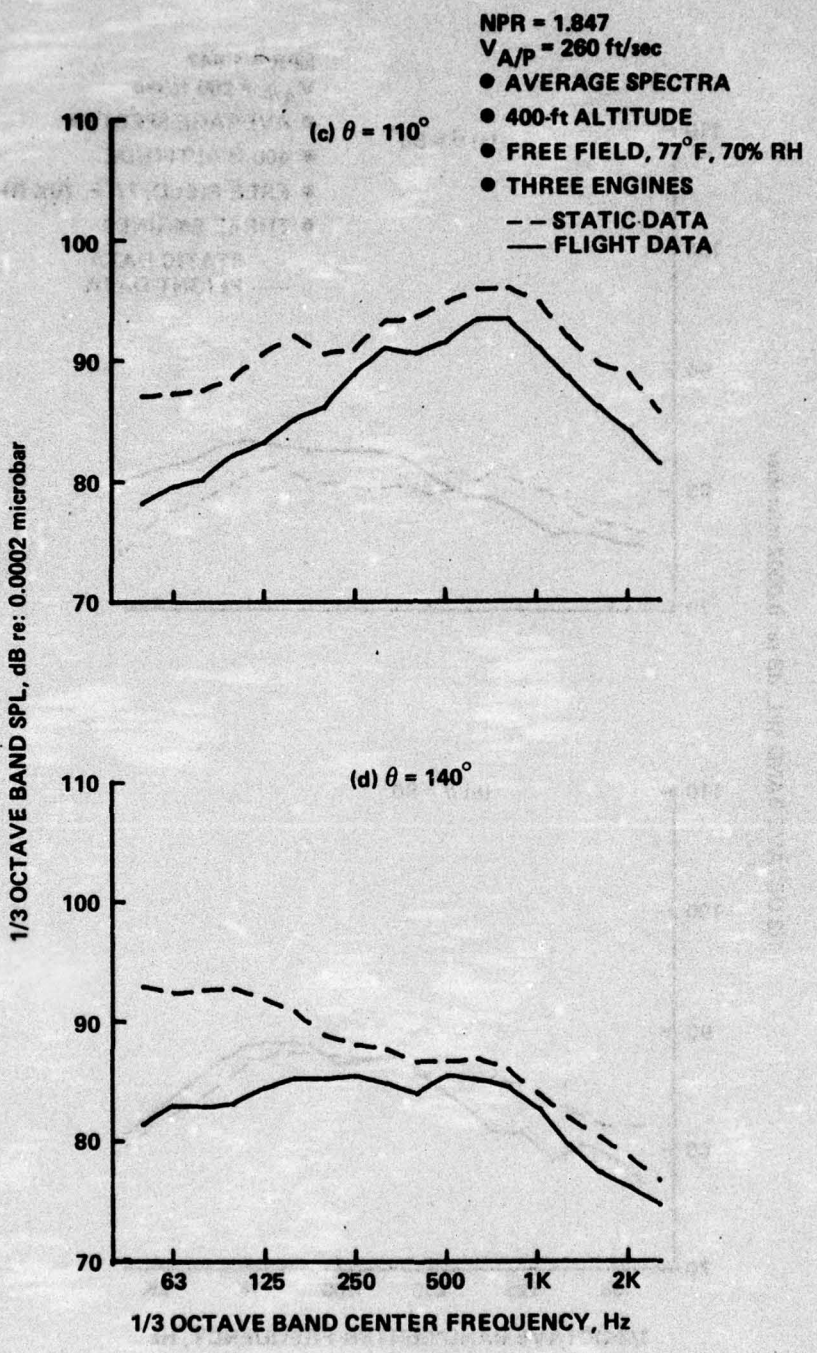


*Figure 45.—(Concluded)*

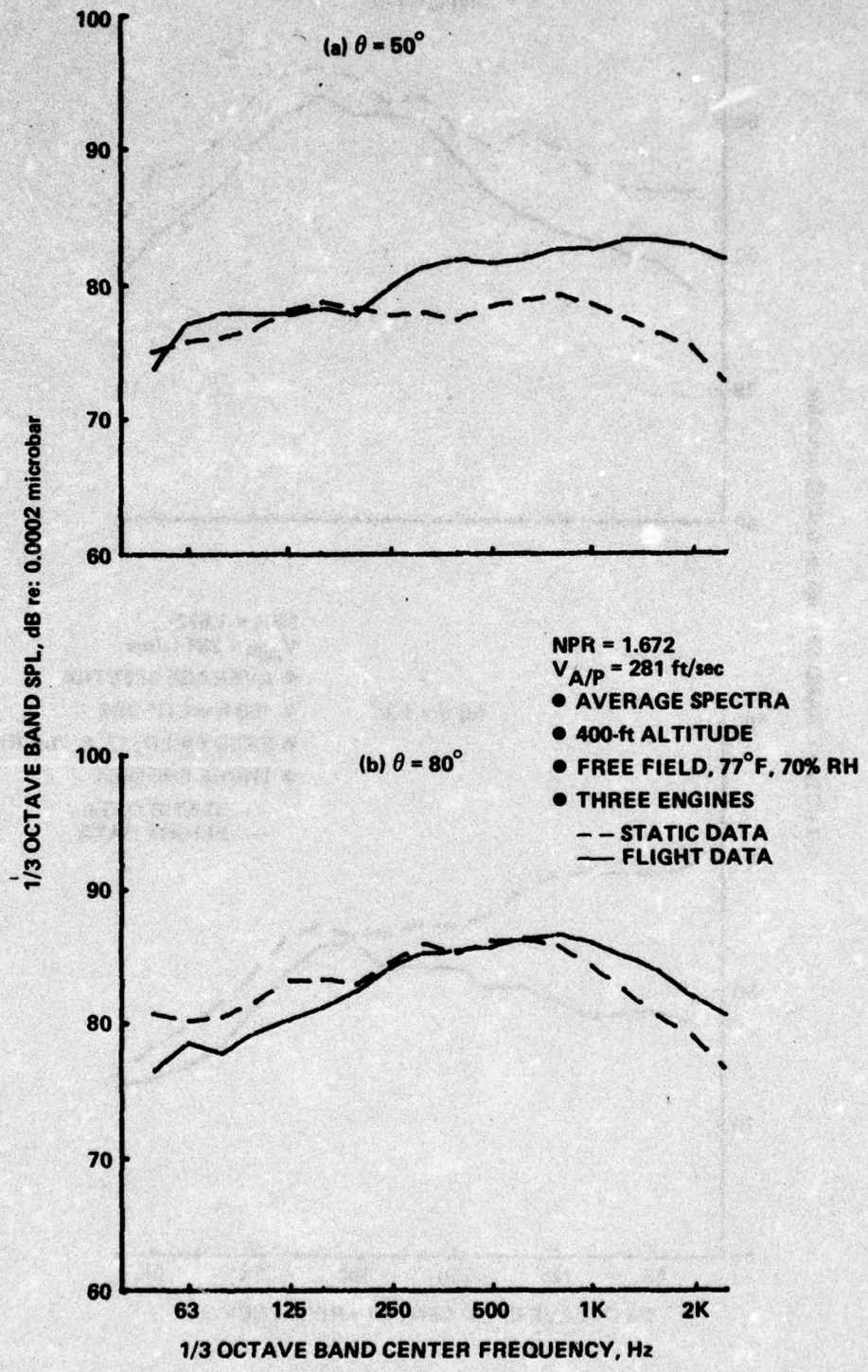


*Figure 46.—Jet Noise Flight Effects, Average Spectra, Cutback Power (LGW), 727/JT8D Ejector Suppressor*

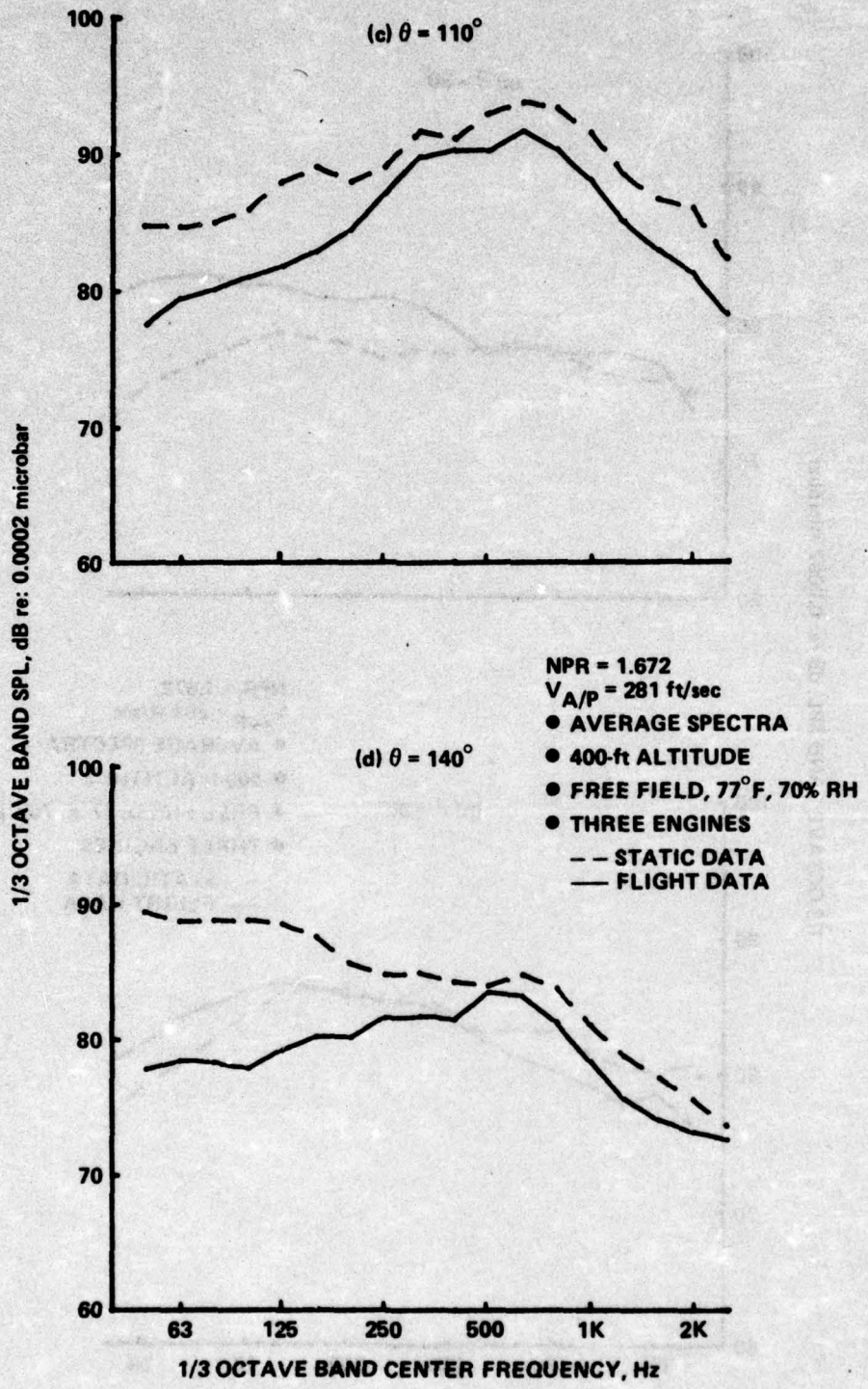


*Figure 46.—(Concluded)*

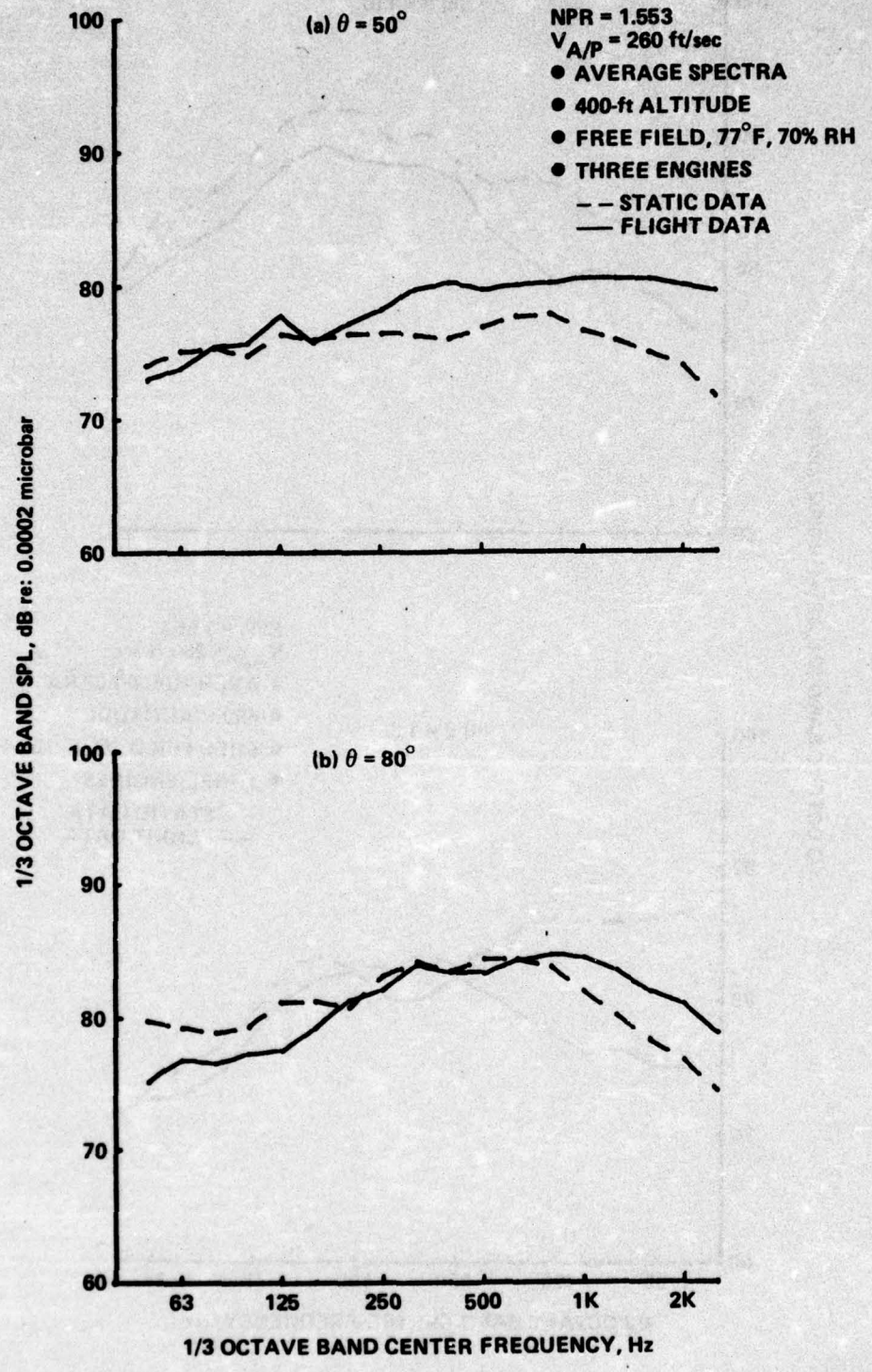


*Figure 47.—Jet Noise Flight Effects, Average Spectra, Approach Power, 727/JT8D Ejector Suppressor*

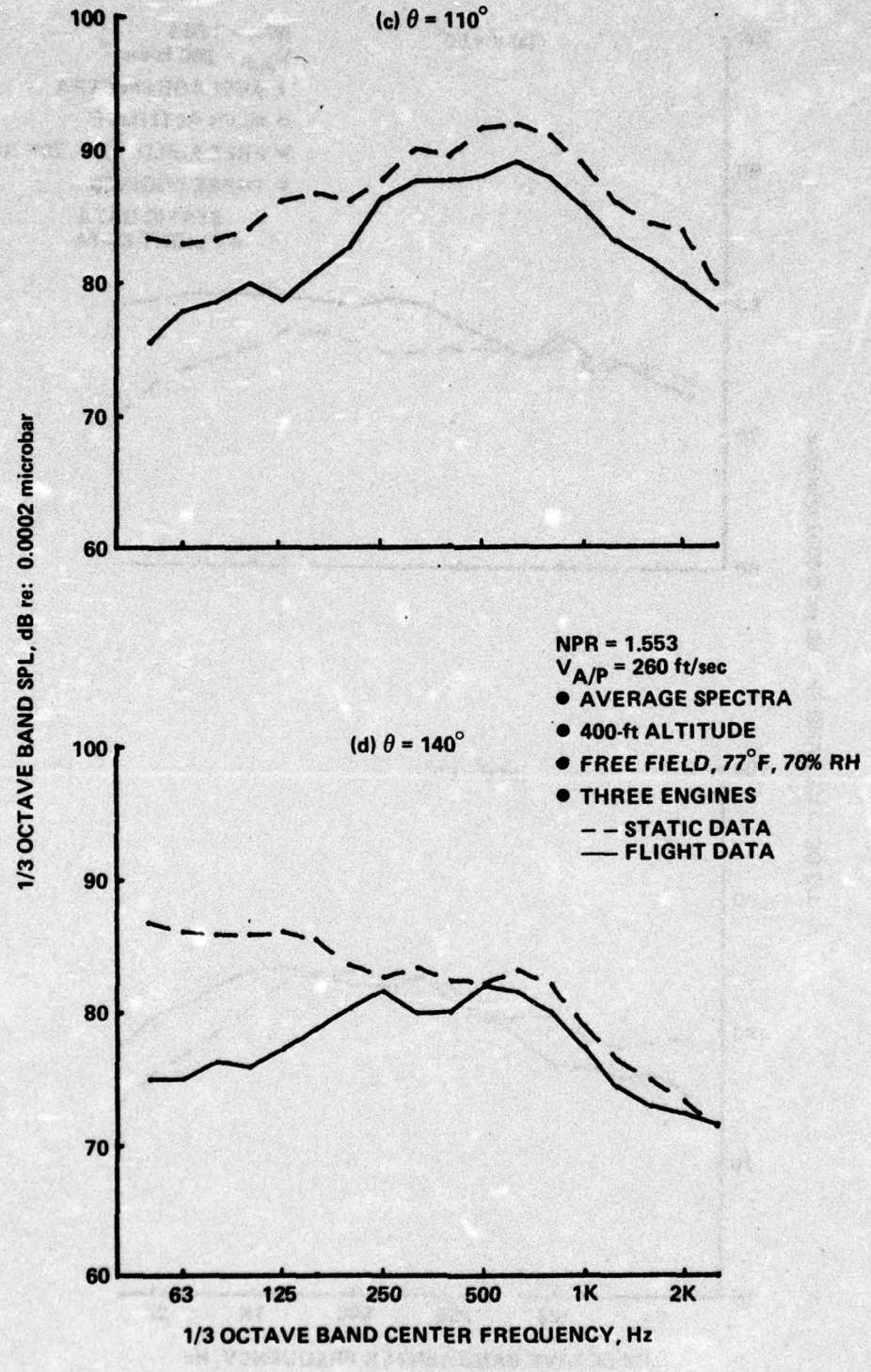


*Figure 47.—(Concluded)*

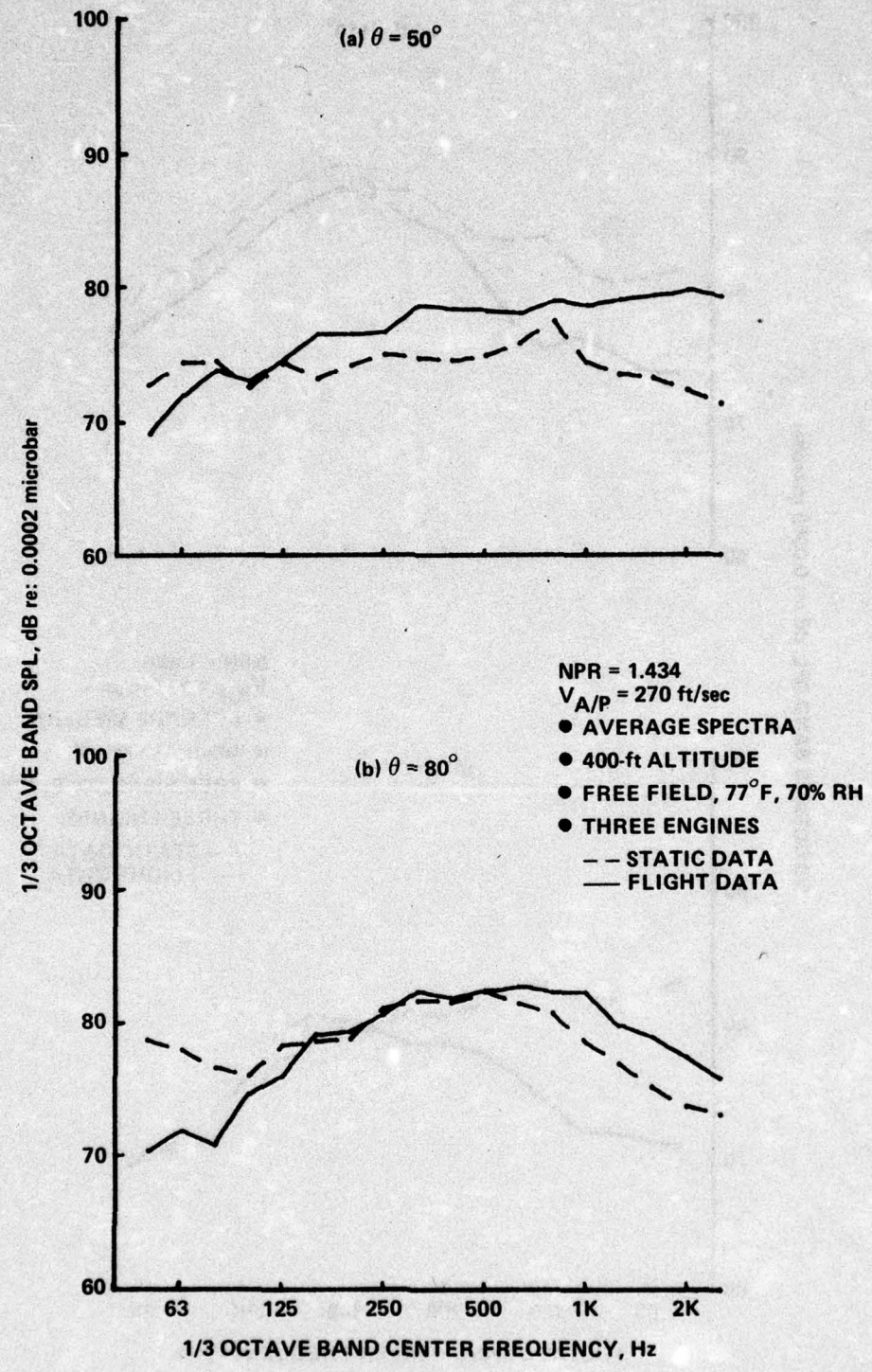


*Figure 48.—Jet Noise Flight Effects, Average Spectra, Low Power Setting, 727/JT8D Ejector Suppressor*

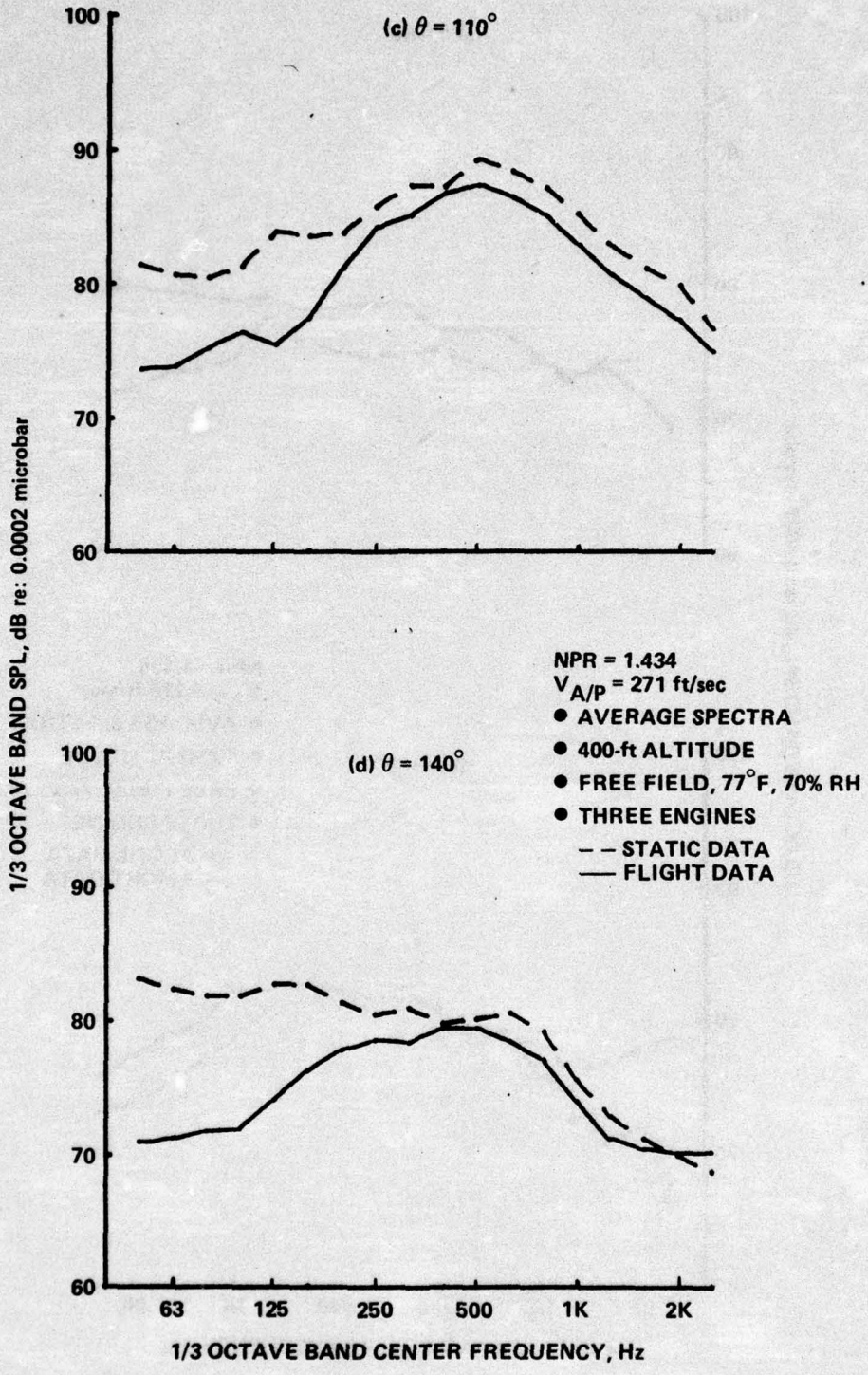


*Figure 48.—(Concluded)*

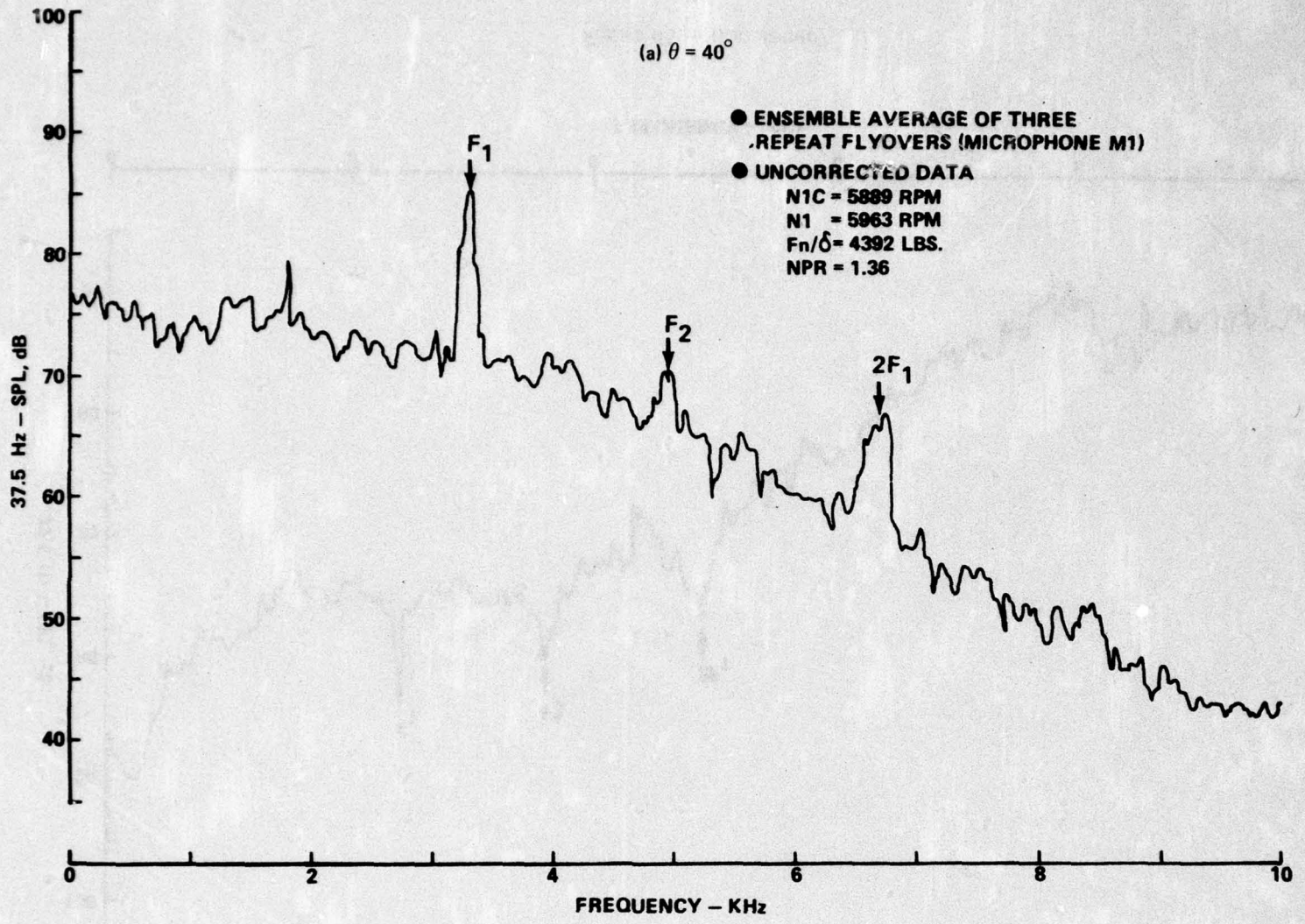


*Figure 49.—Flight Narrowband Spectra, Low Power Setting, 727/JT8D Baseline*

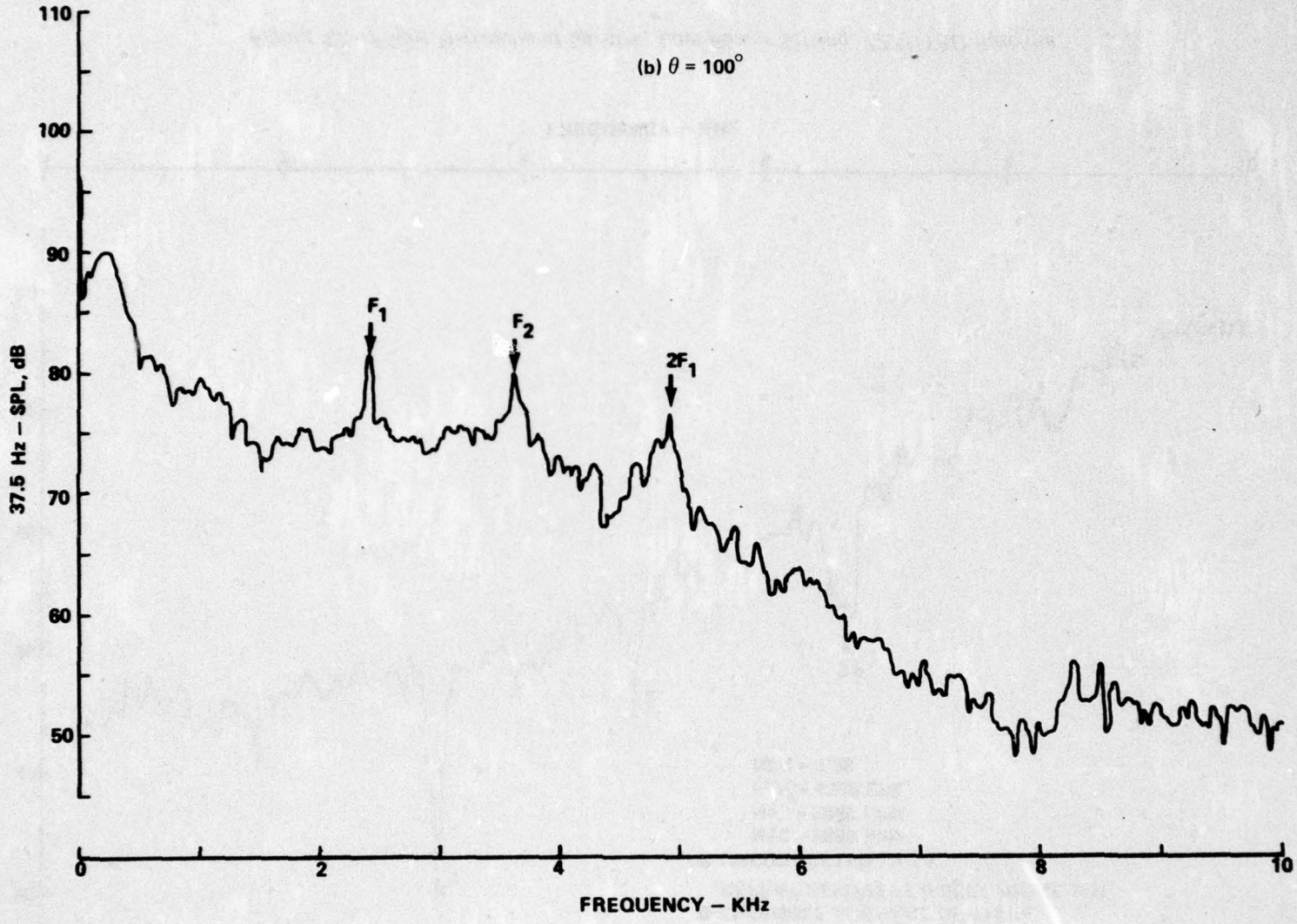


*Figure 49.—(Concluded)*

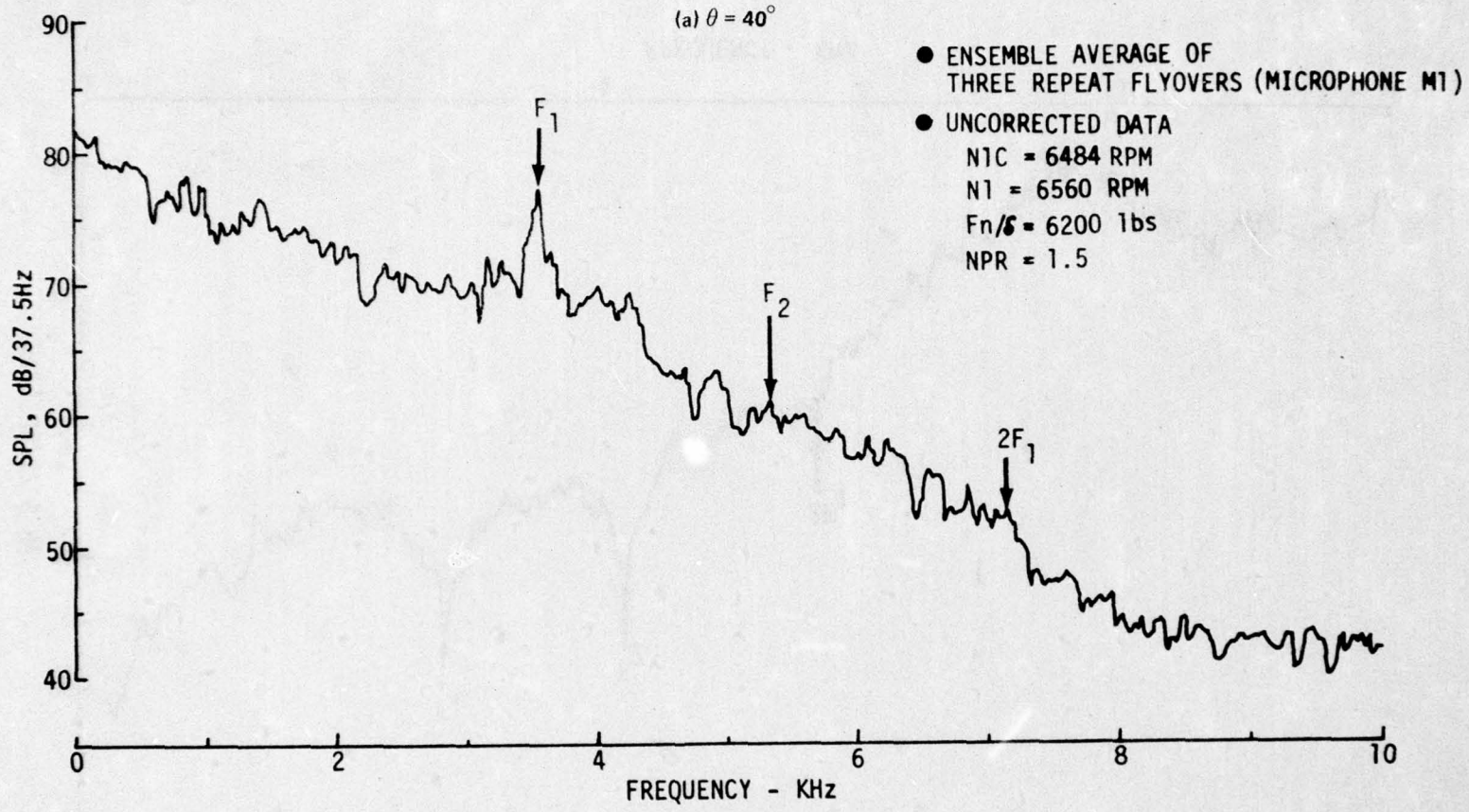


*Figure 50.—Flight Narrowband Spectra, Approach Power, 727/JT8D Baseline*

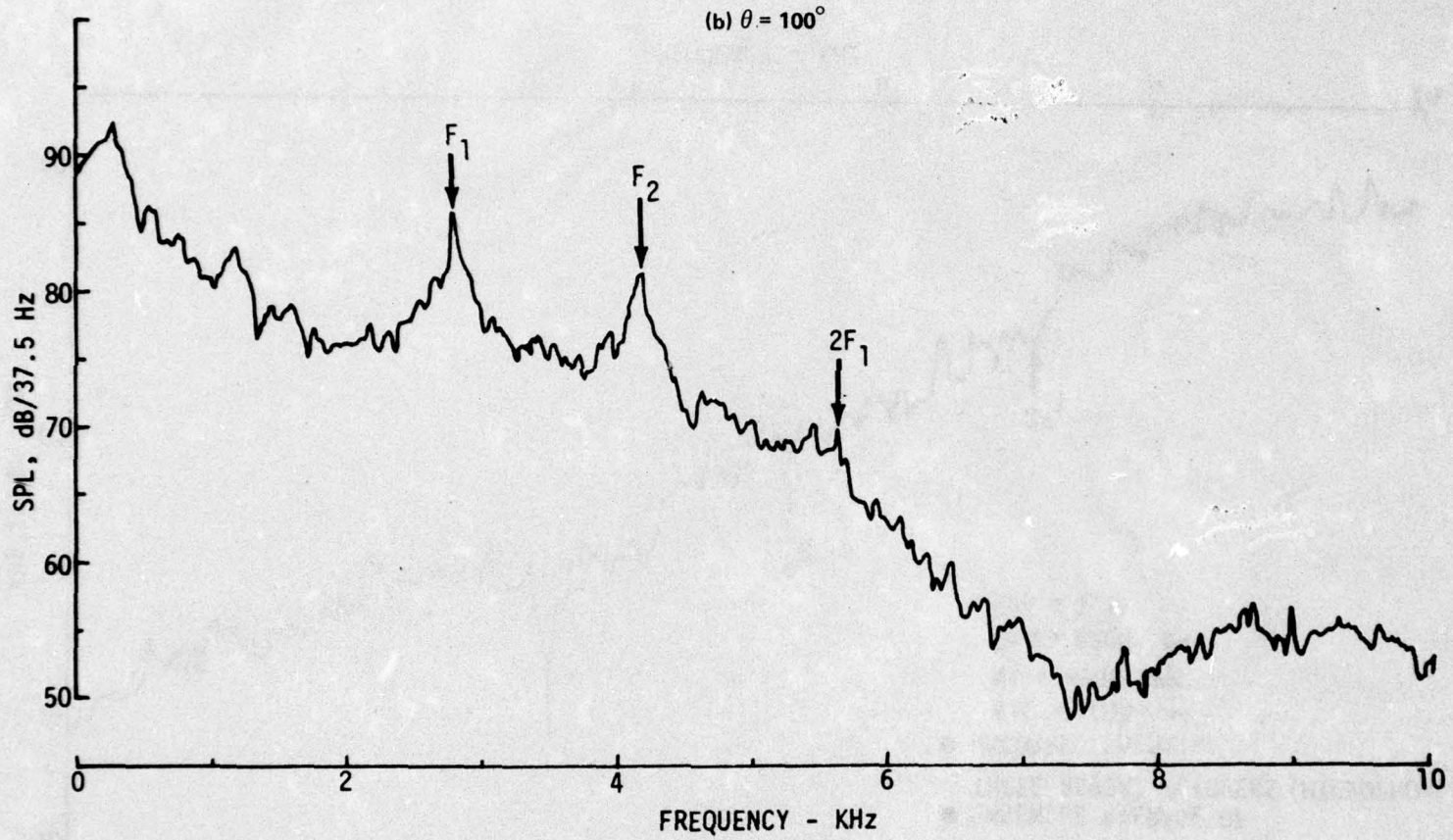


*Figure 50.—(Concluded)*

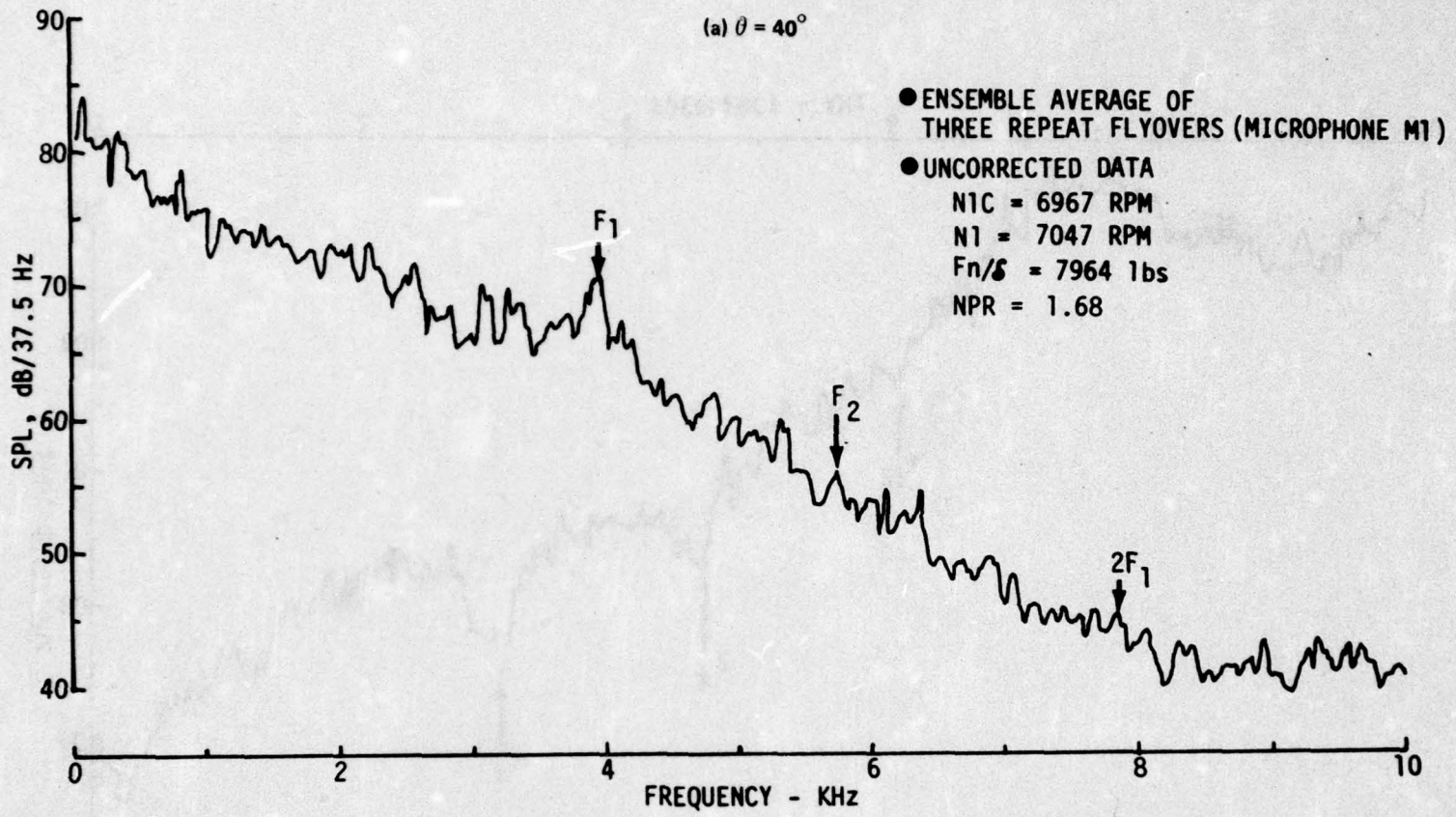


*Figure 51.—Flight Narrowband Spectra, Cutback Power (LGW), 727/JT8D Baseline*

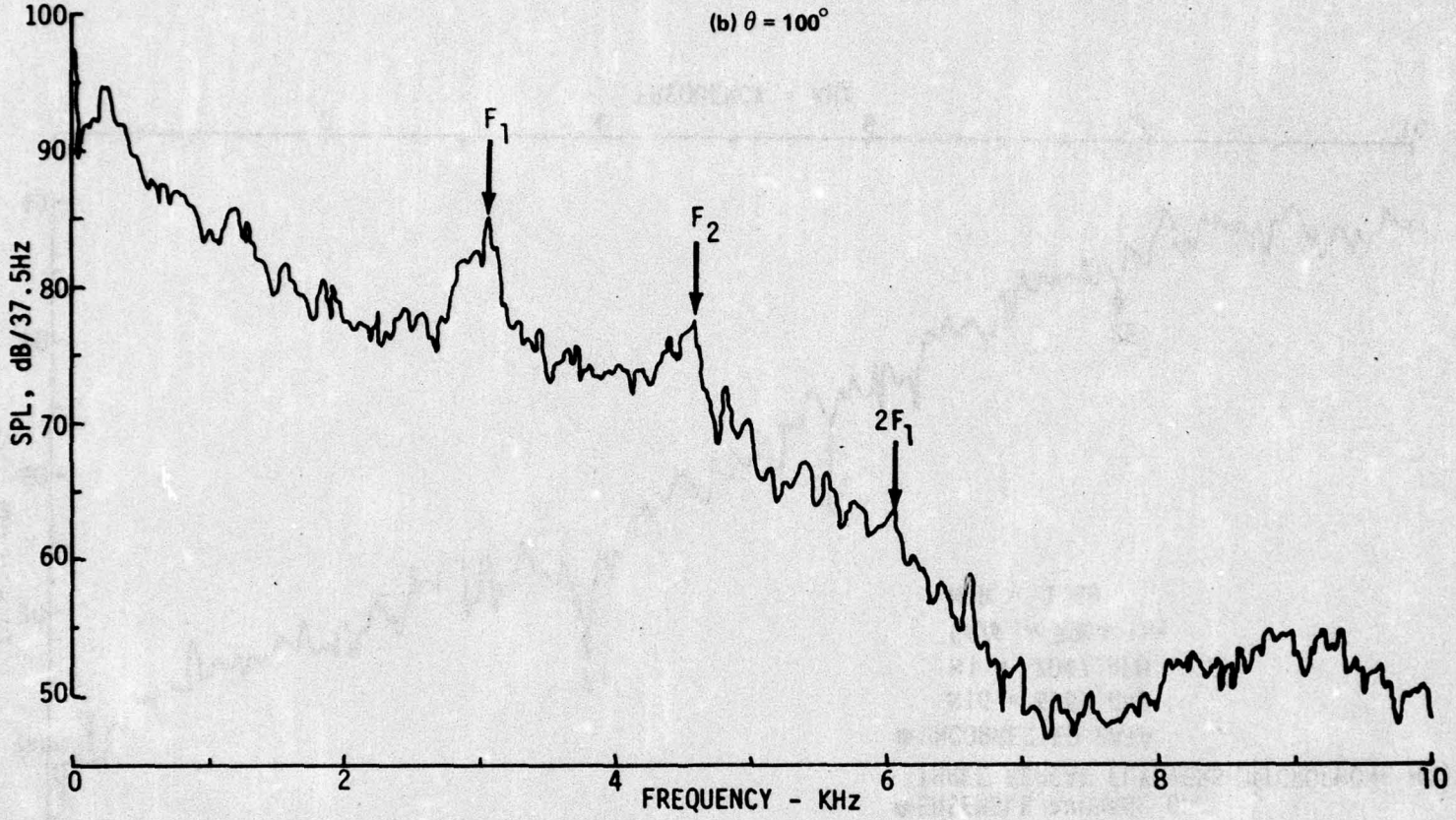


*Figure 51.—(Concluded)*

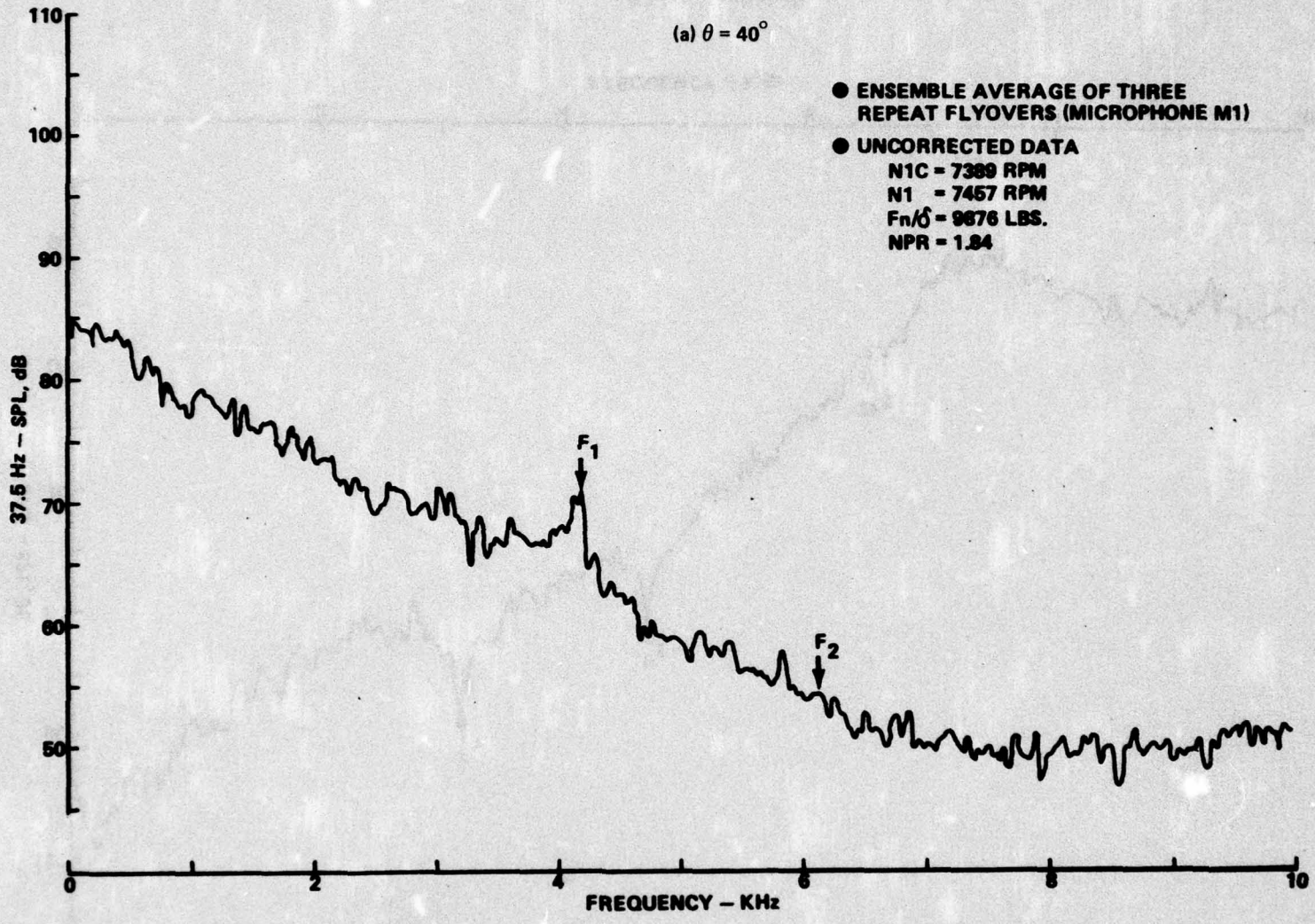


*Figure 52.—Flight Narrowband Spectra, Cutback Power (HGW), 727/JT8D Baseline*

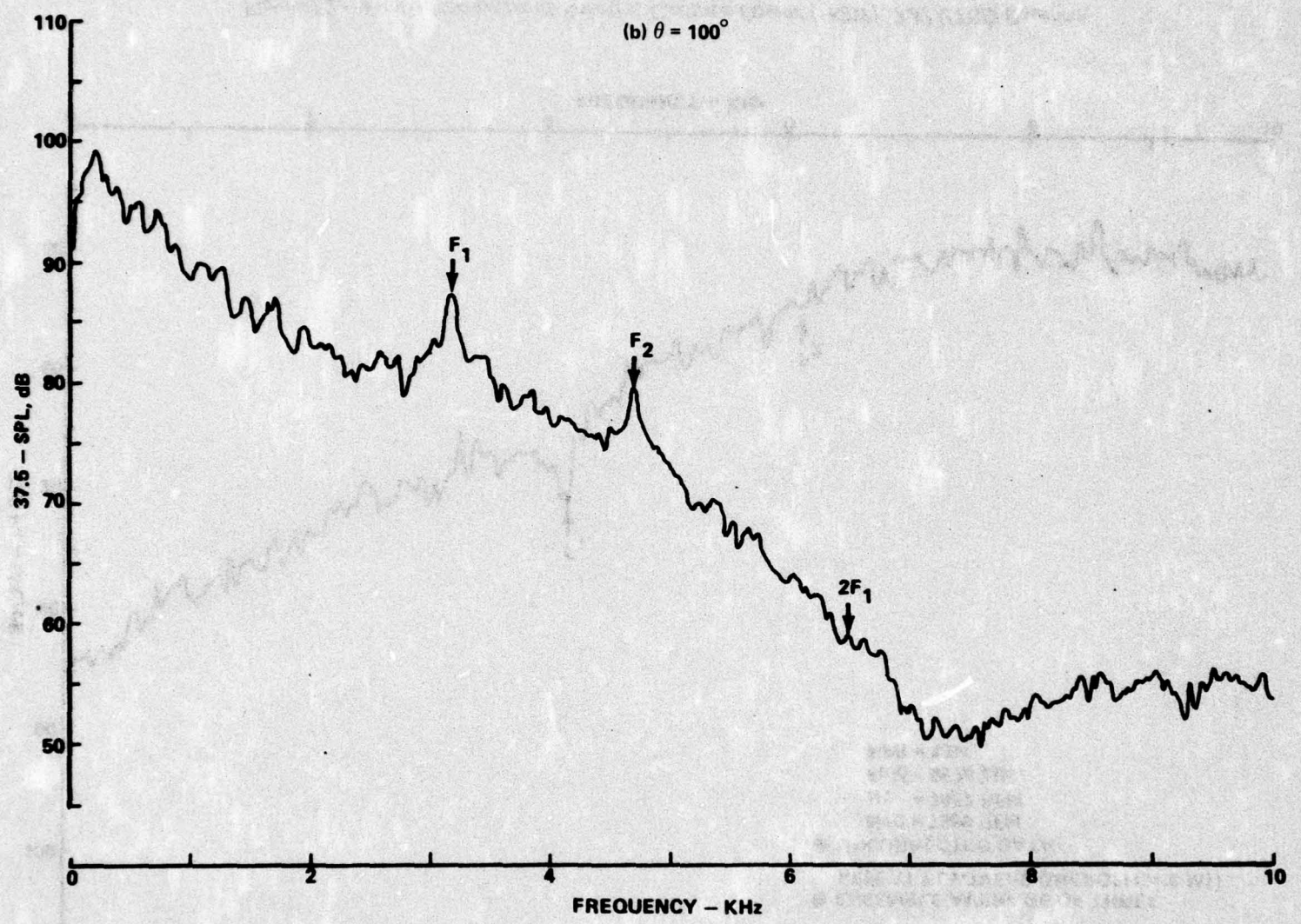


*Figure 52.—(Concluded)*

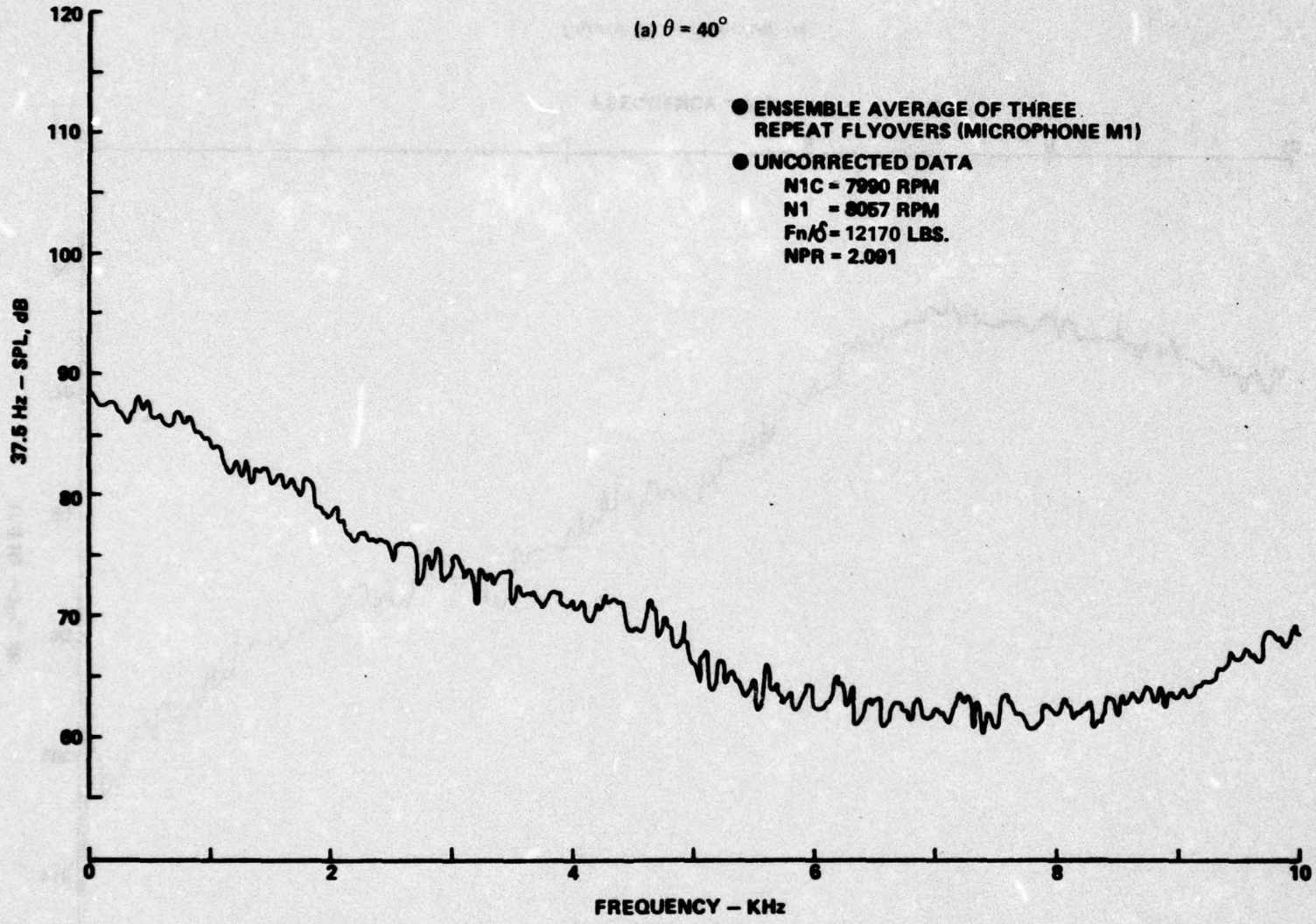


*Figure 53.—Flight Narrowband Spectra, Takeoff Power, 727/JT8D Baseline*

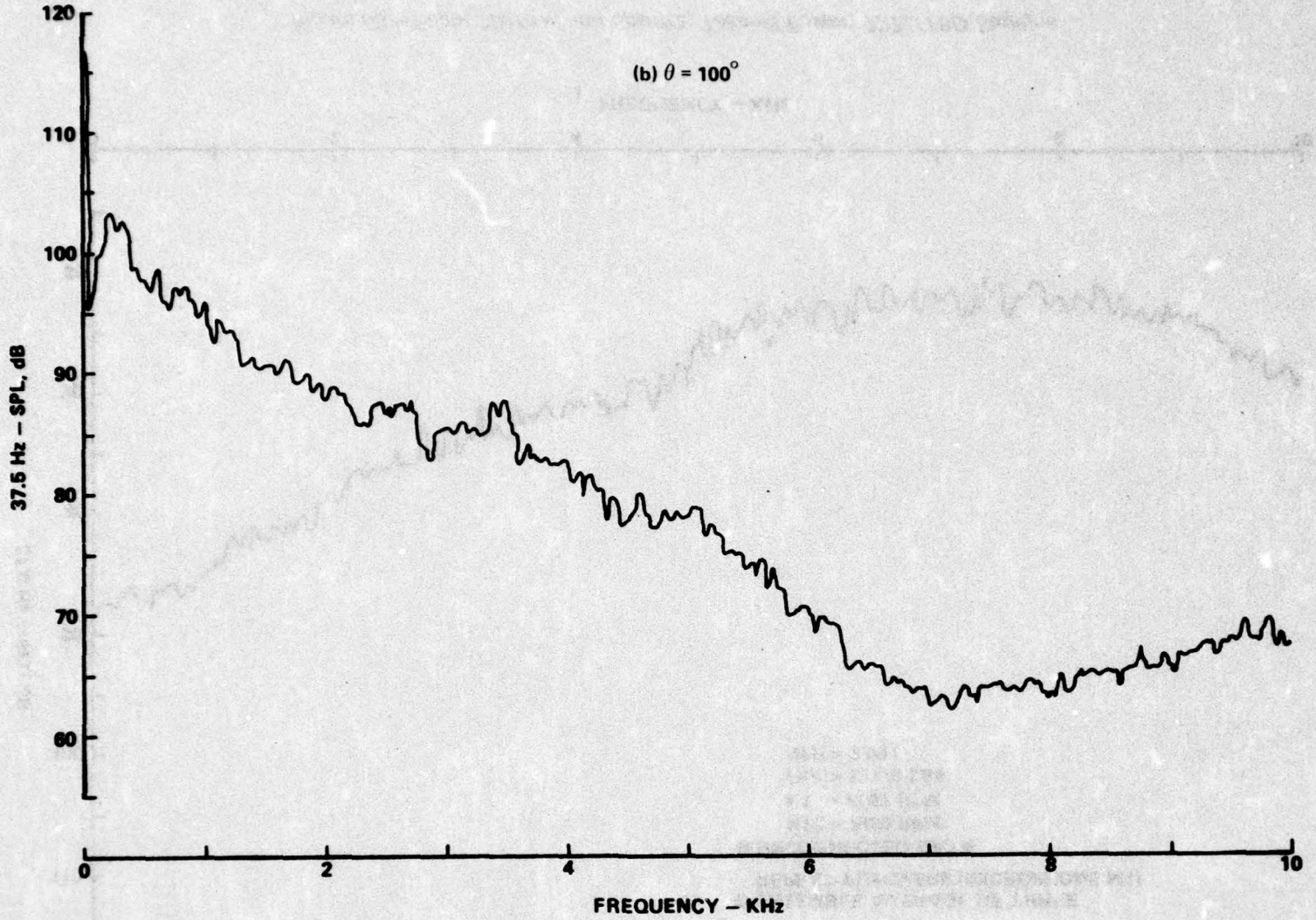


*Figure 53.—(Concluded)*

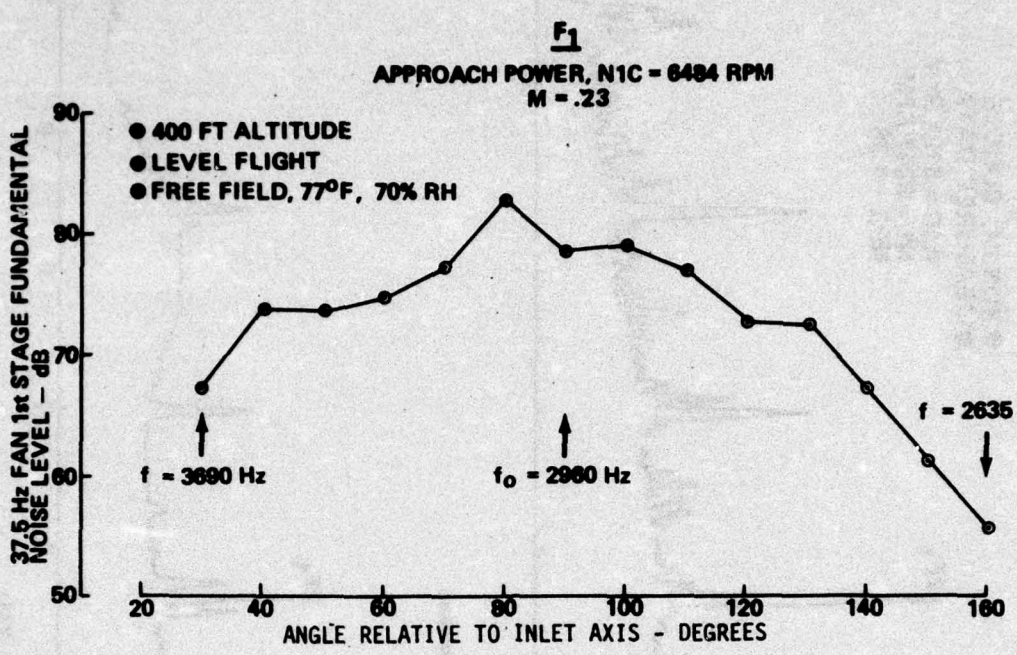


*Figure 54.—Flight Fan Noise Directivity, First-Stage Fundamental Tone, 727/JT8D Baseline*

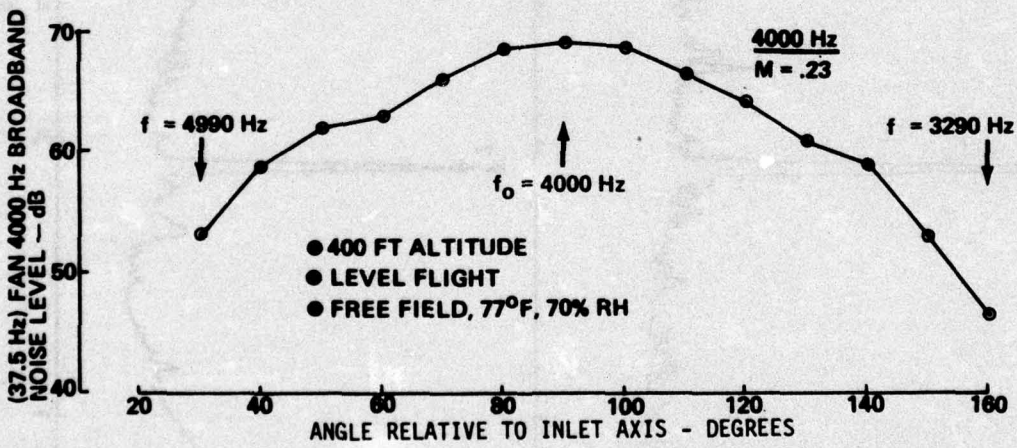


*Figure 55.—Flight Fan Noise Directivity, 4000-Hz Broadband, 727/JT8D Baseline*

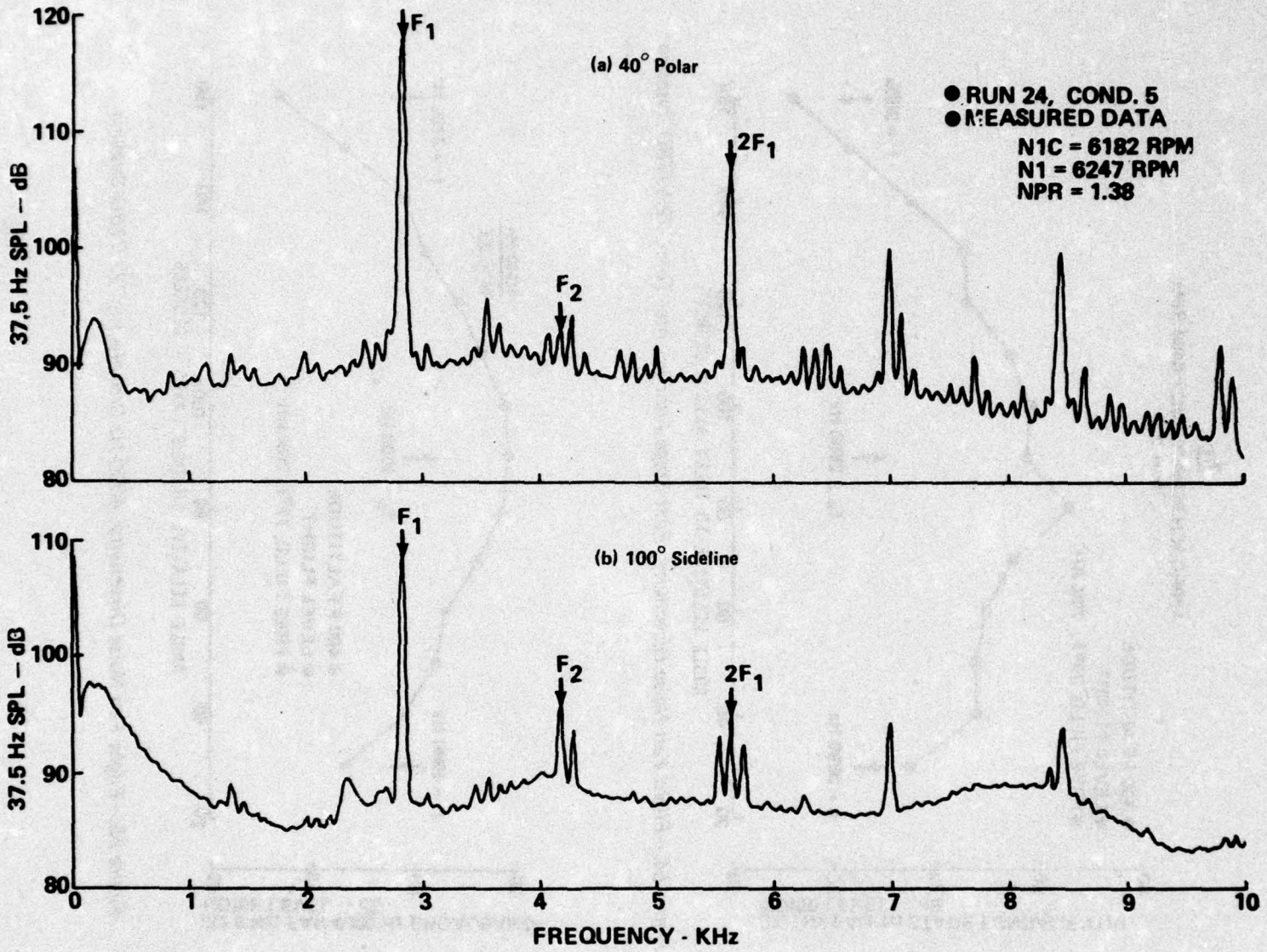


*Figure 56.—Static Narrowband Spectra, Approach Power, JT8D-9 Baseline*

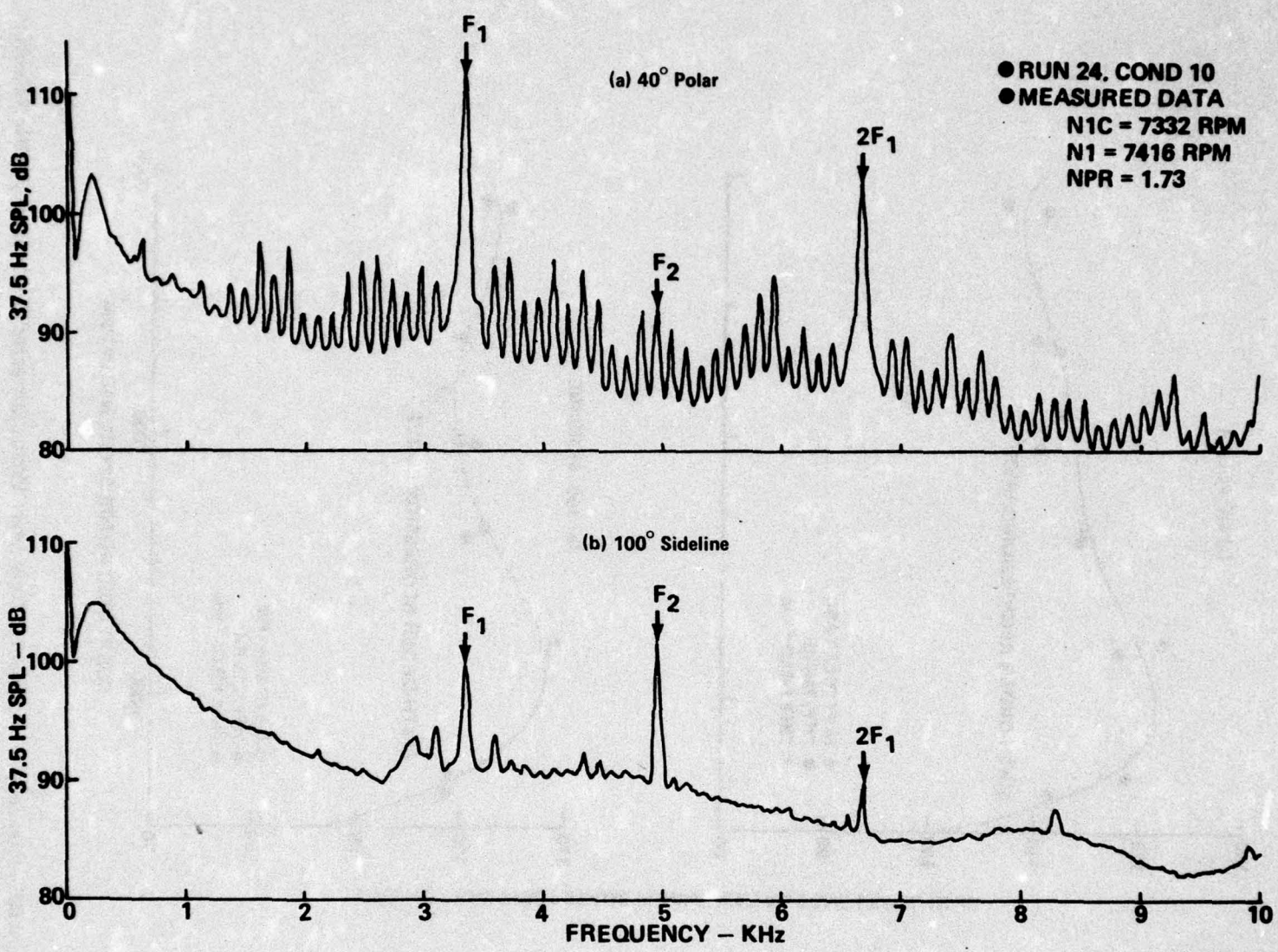


*Figure 57.—Static Narrowband Spectra, Cutback Power, JT8D-9 Baseline*

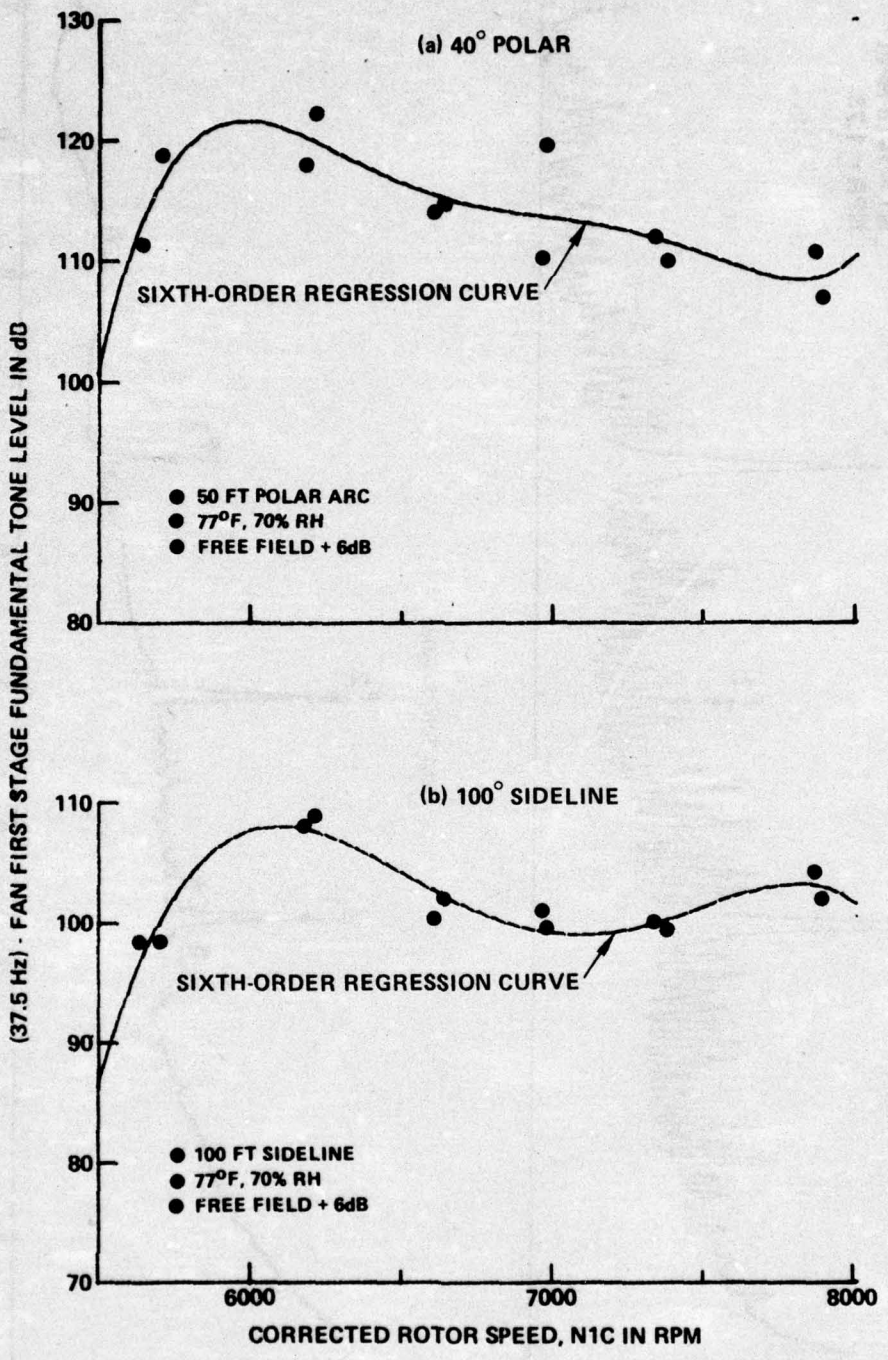


*Figure 58.—First-Stage Fundamental Tone Level Versus Corrected Rotor Speed, JT8D-9 Baseline Static Test*

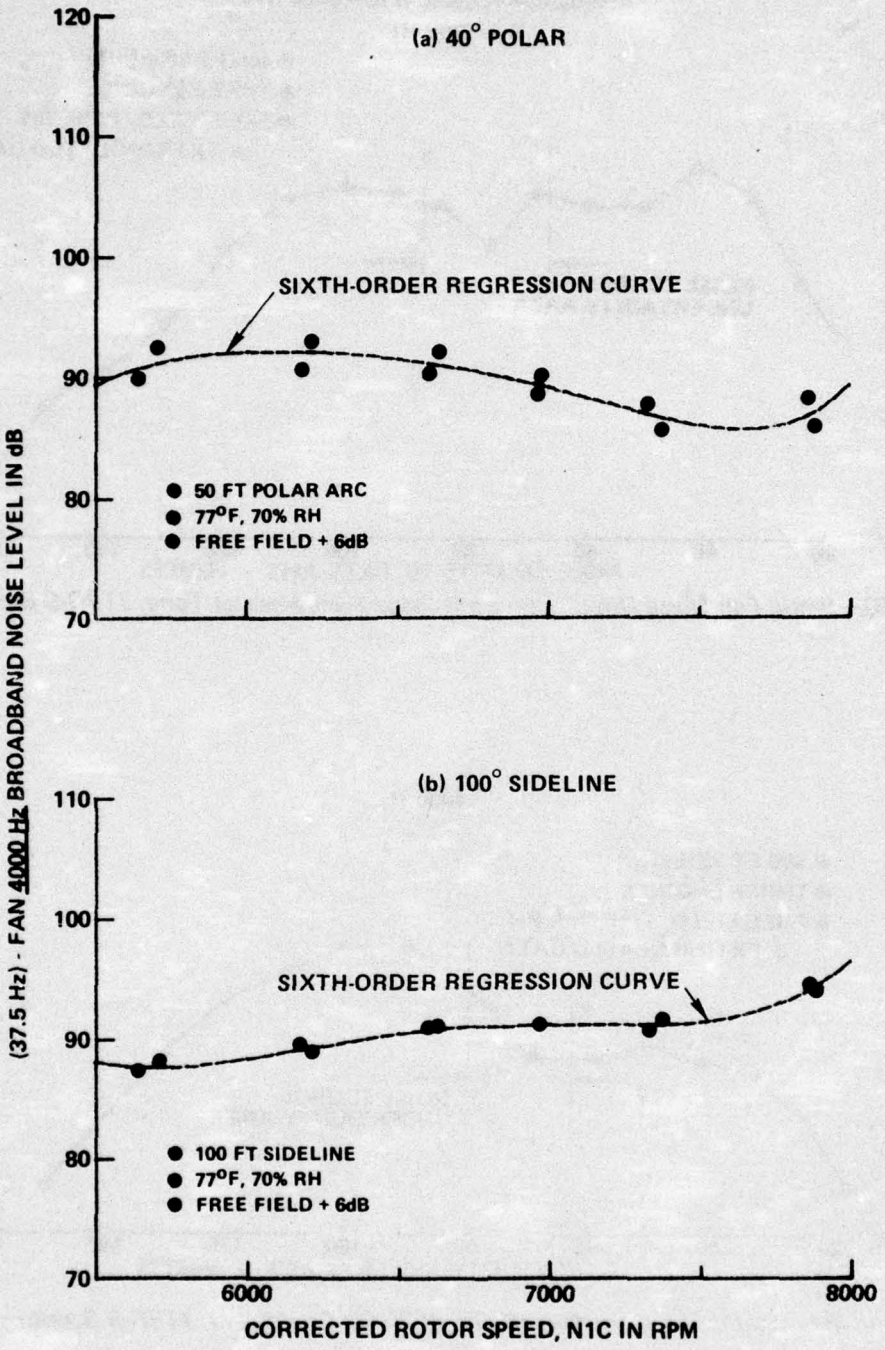


*Figure 59.—Fan 4000-Hz Broadband Noise Level Versus Corrected Rotor Speed, JT8D-9 Baseline Static Test*

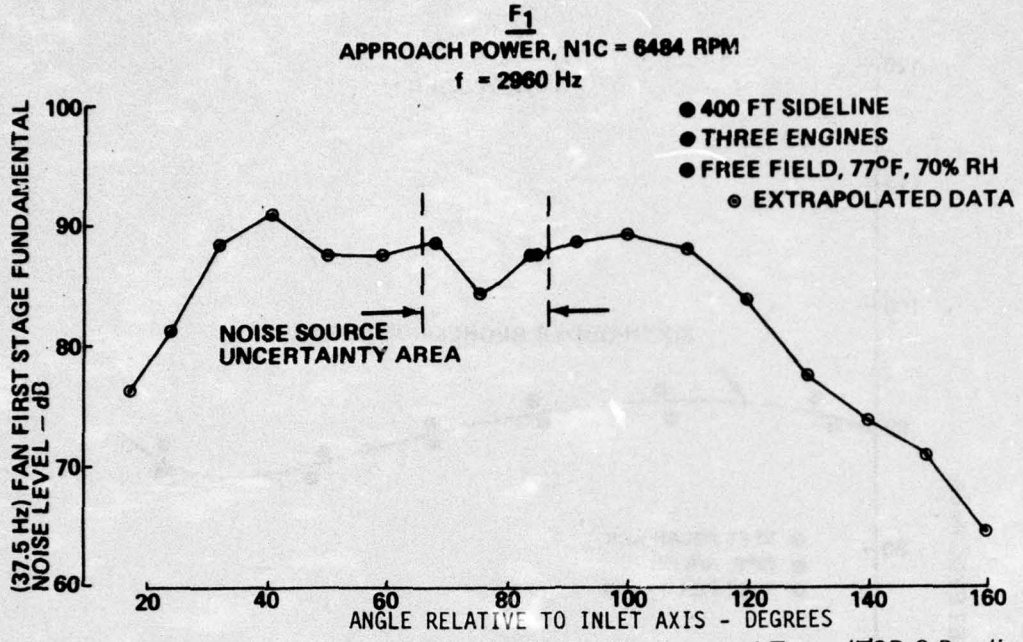


*Figure 60.—Static Fan Noise Directivity, First-Stage Fundamental Tone, JT8D-9 Baseline*

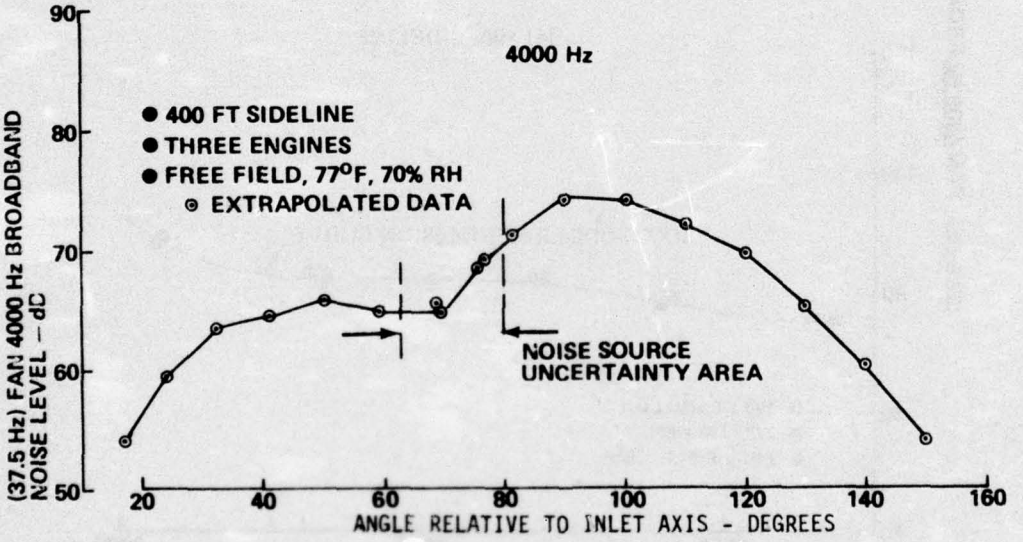


*Figure 61.—Static Fan Noise Directivity, 4000-Hz Broadband, JT8D-9 Baseline*

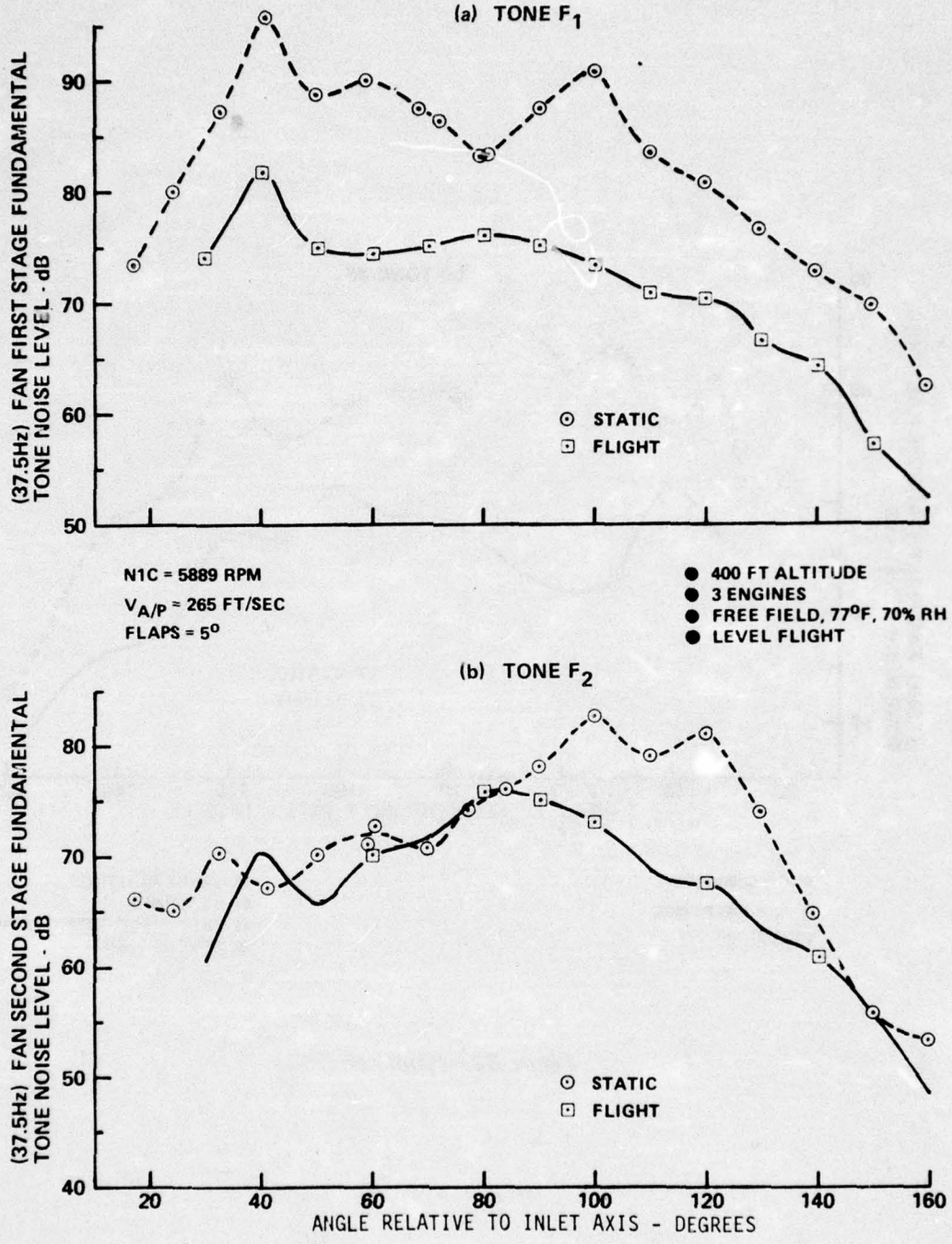


*Figure 62.—Fan Noise Flight Effects Directivity, Low Power Setting, 727/JT8D Baseline*

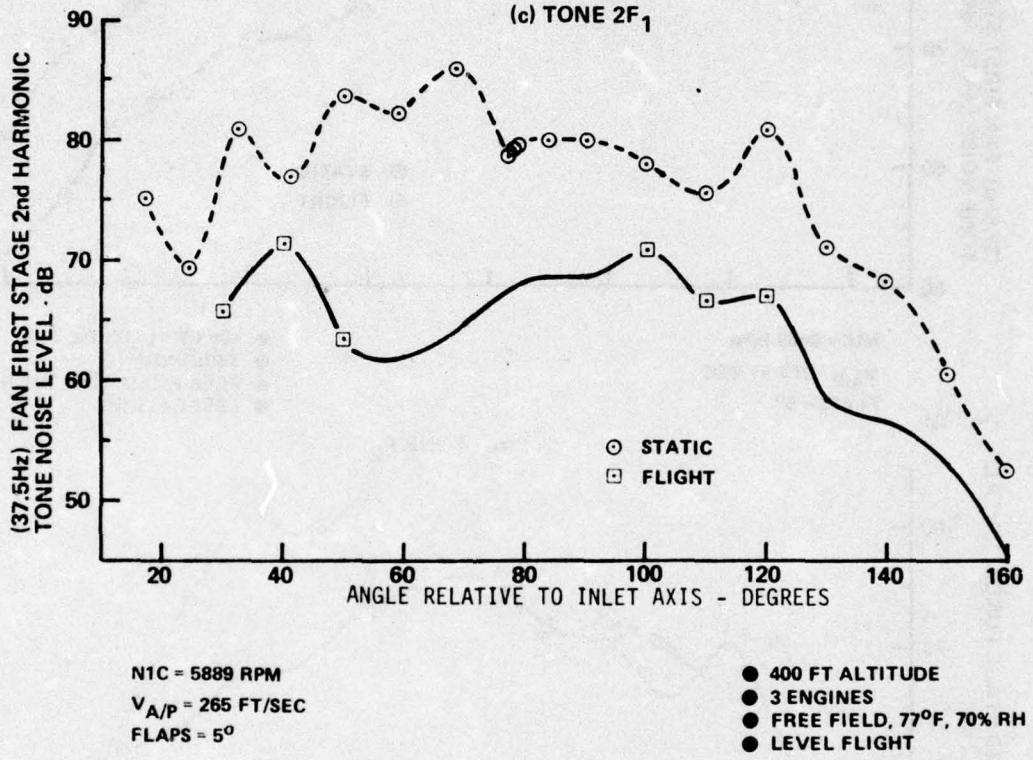


*Figure 62.—(Continued)*

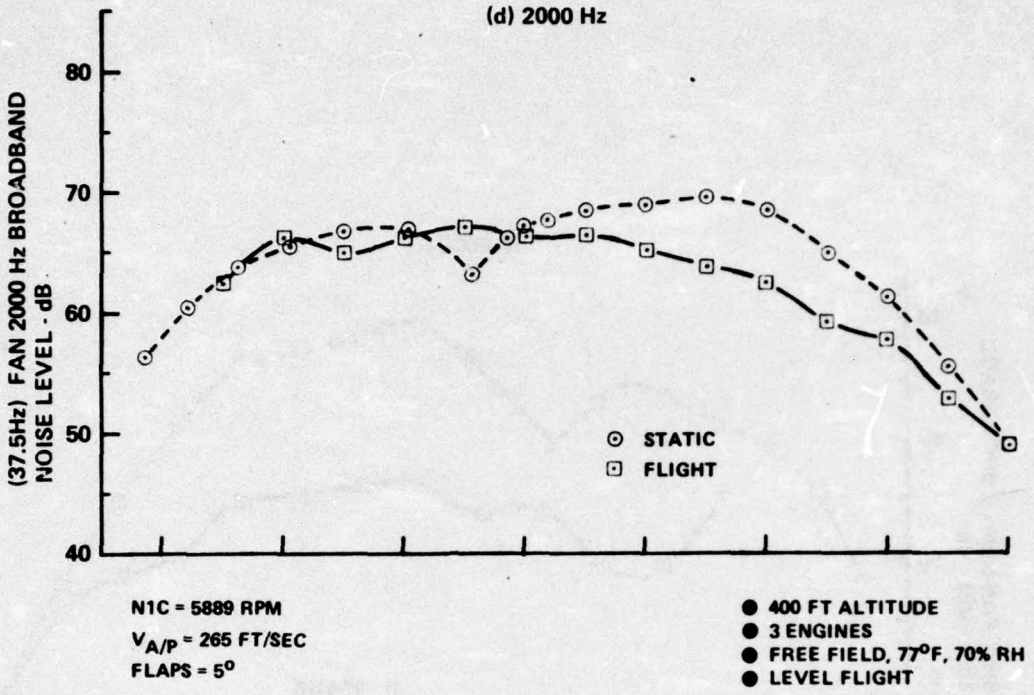


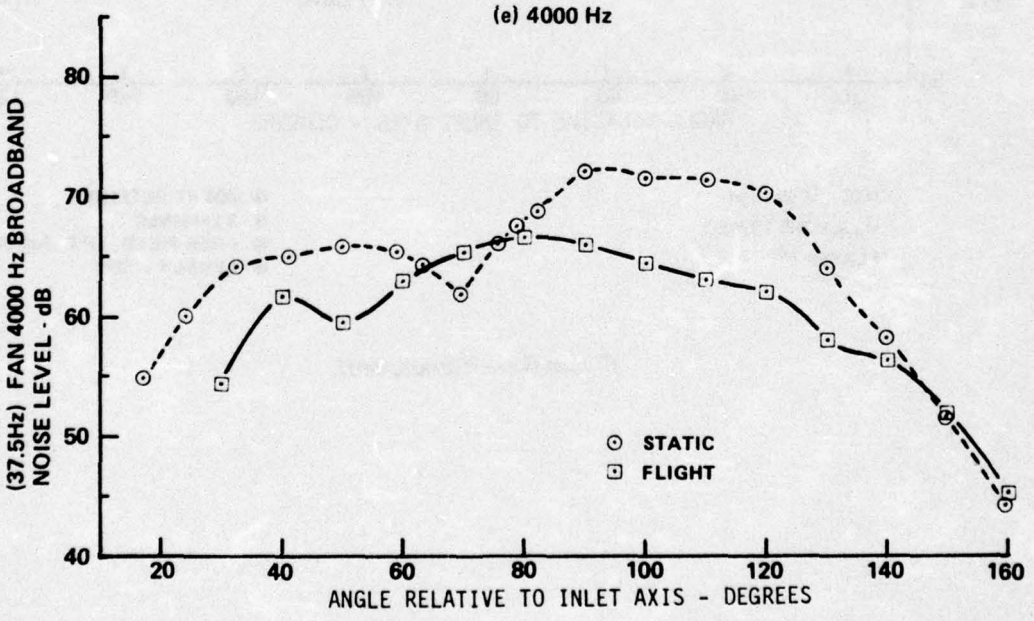


*Figure 62.—(Continued)*

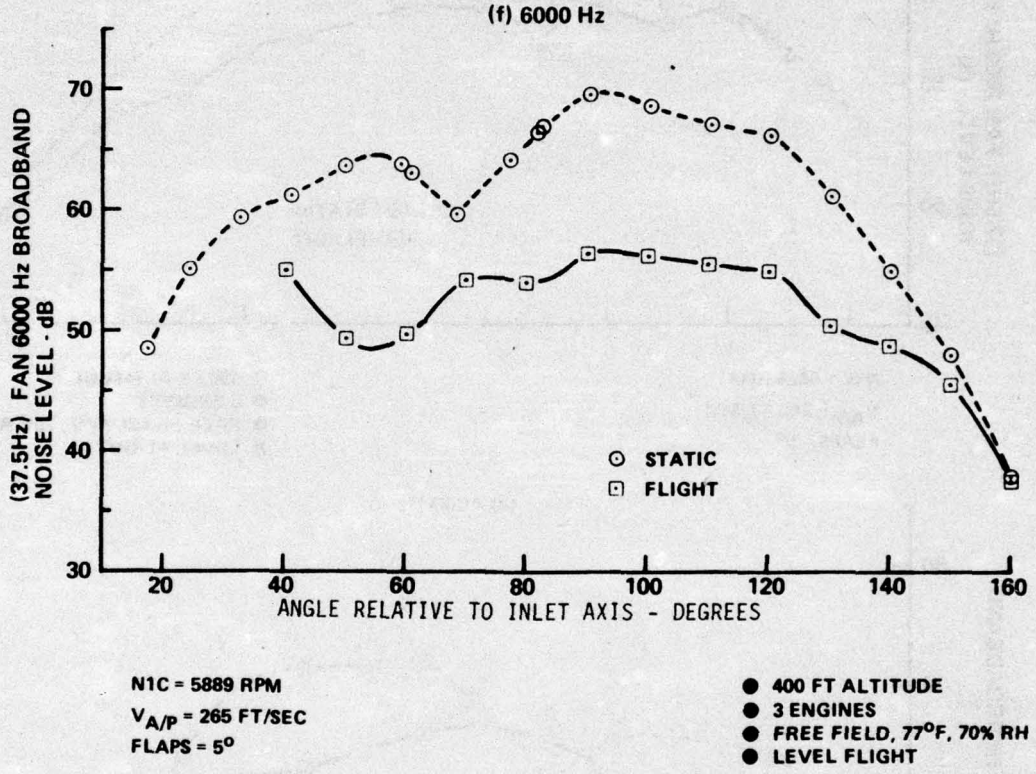


*Figure 62.—(Concluded)*

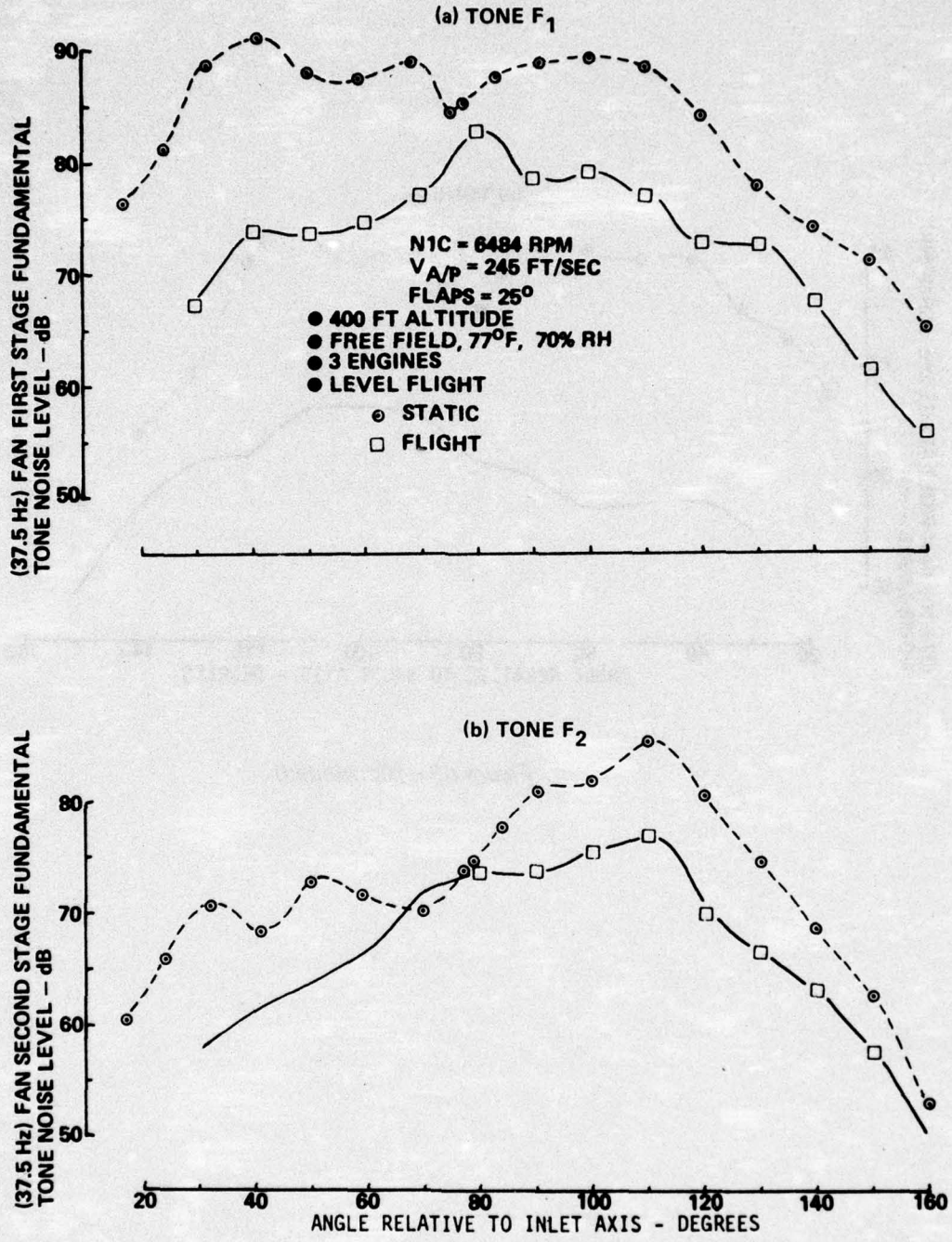


*Figure 63.—Fan Noise Flight Effects Directivity, Approach Power, 727/JT8D Baseline*

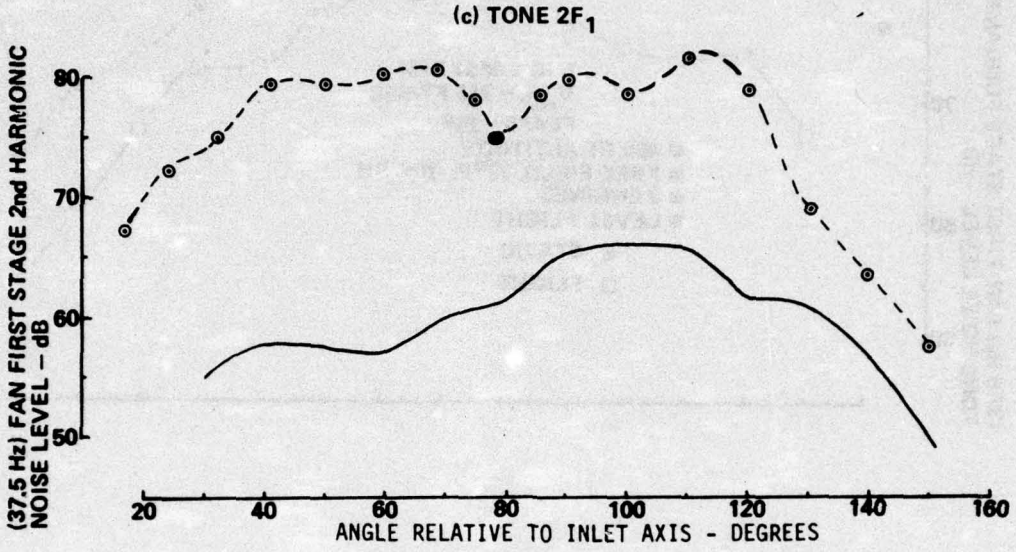


*Figure 63.—(Continued)*

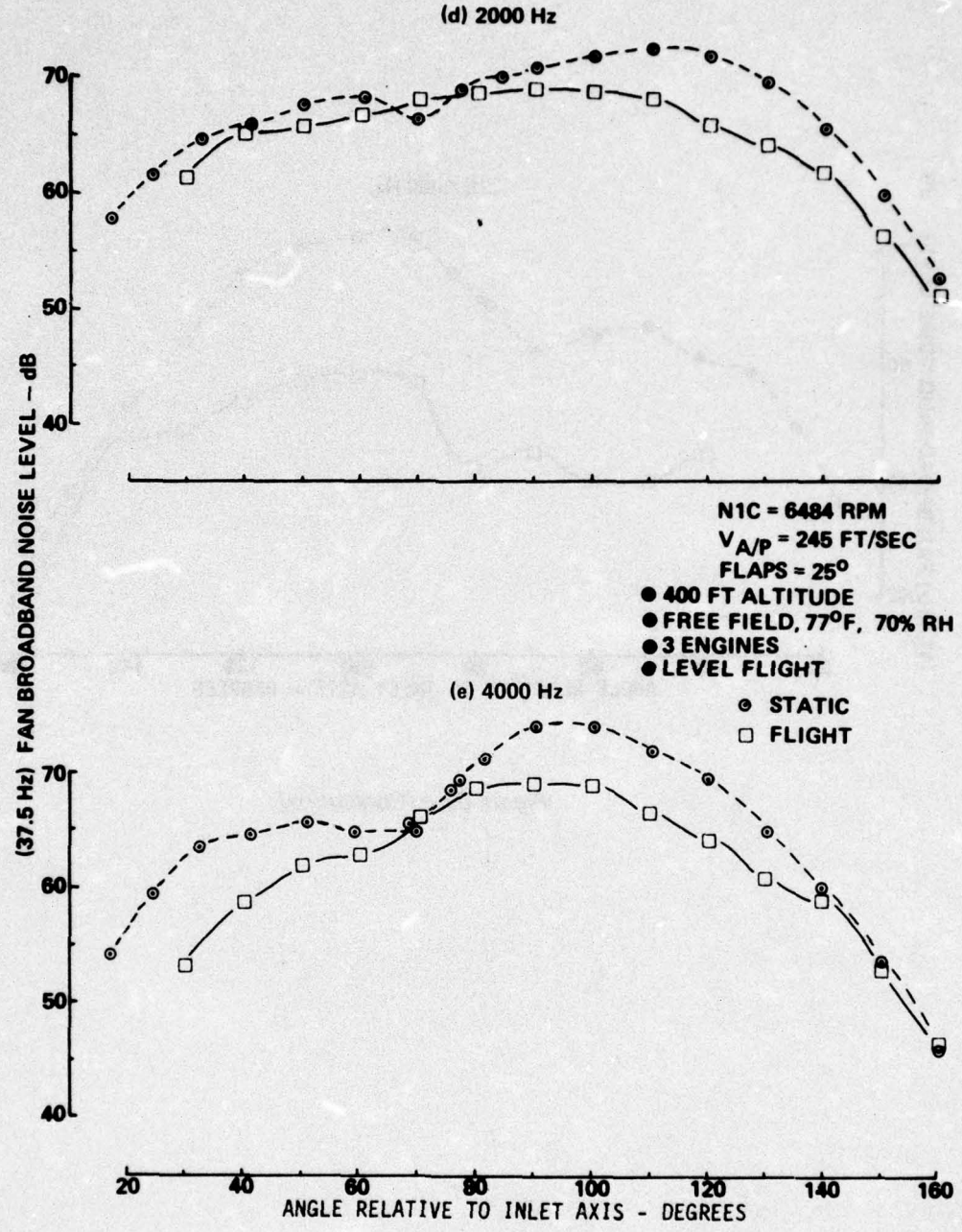


*Figure 63.—(Continued)*

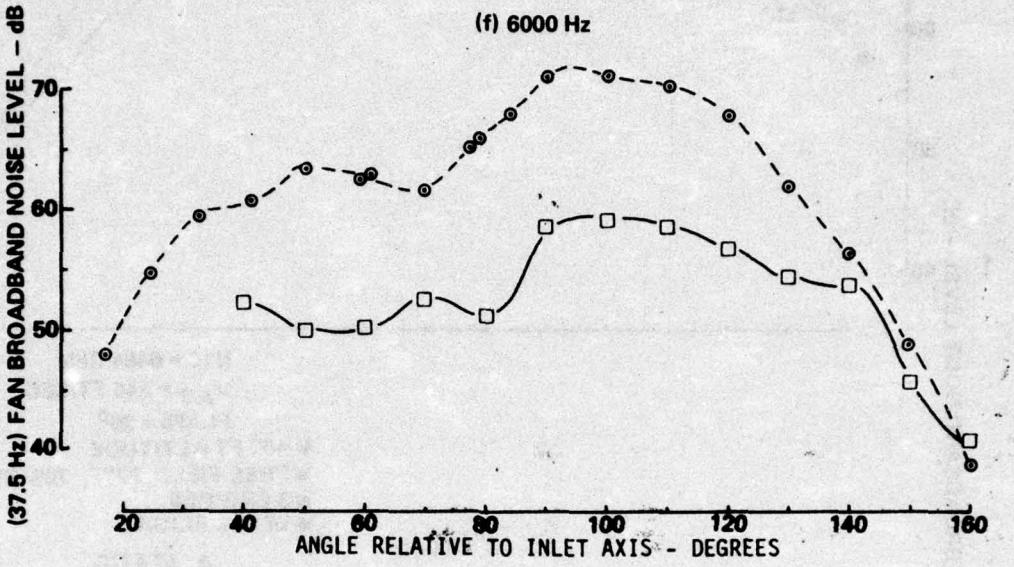


*Figure 63.—(Concluded)*

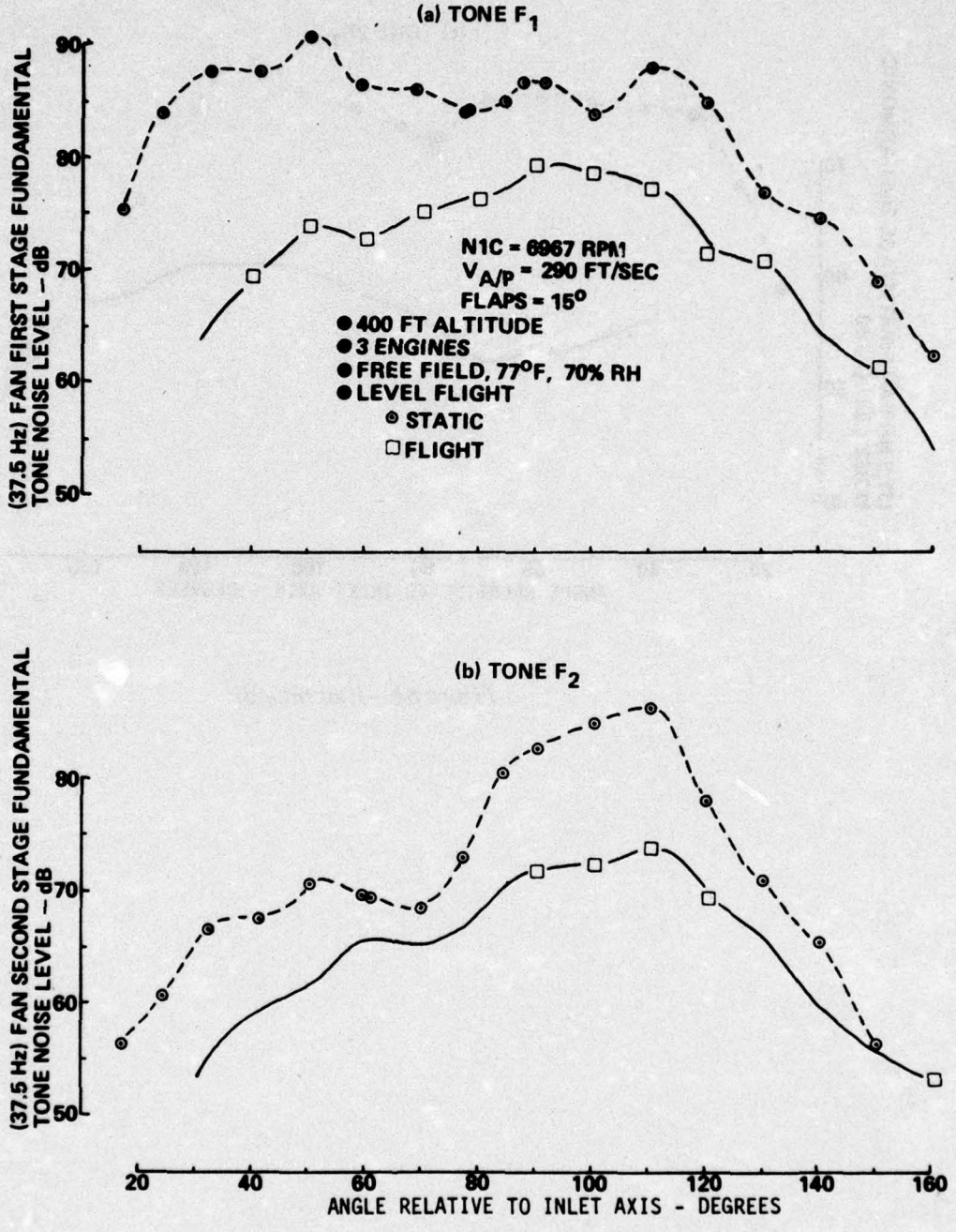


*Figure 64.—Fan Noise Flight Effects Directivity, Cutback Power (LGW), 727/JT8D Baseline*

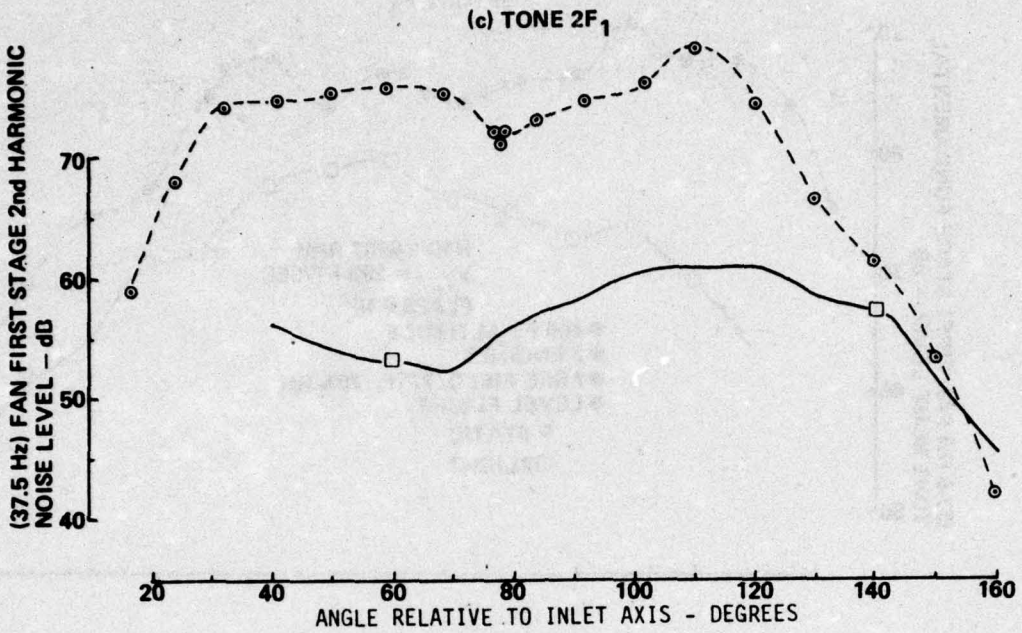


*Figure 64.—(Continued)*

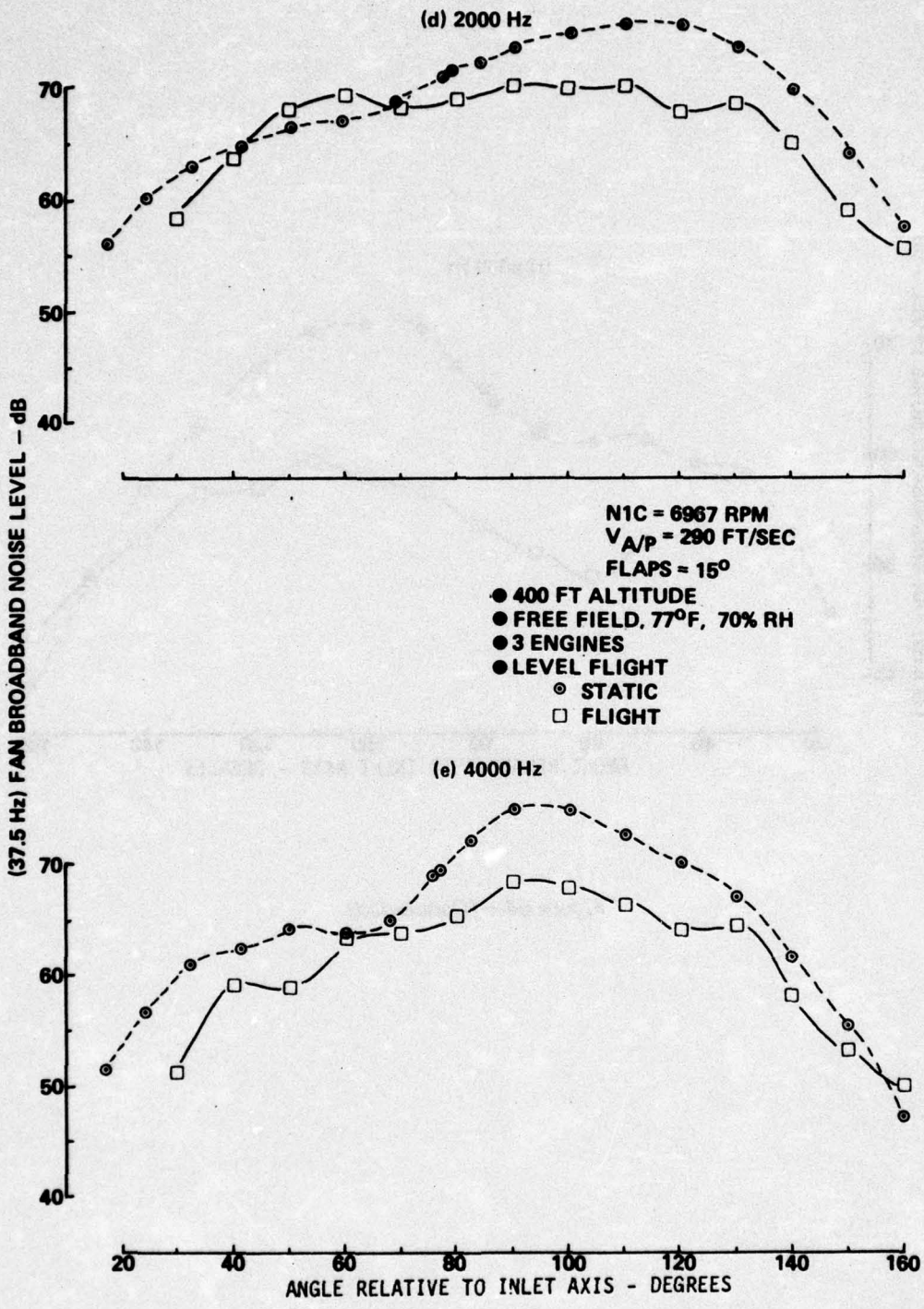


*Figure 64.—(Continued)*

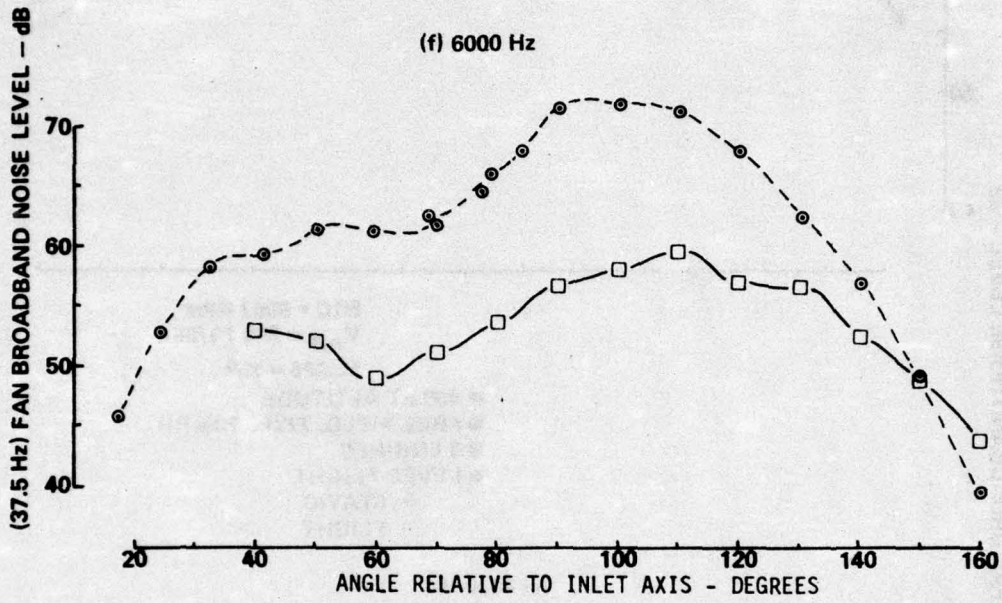


*Figure 64.—(Concluded)*

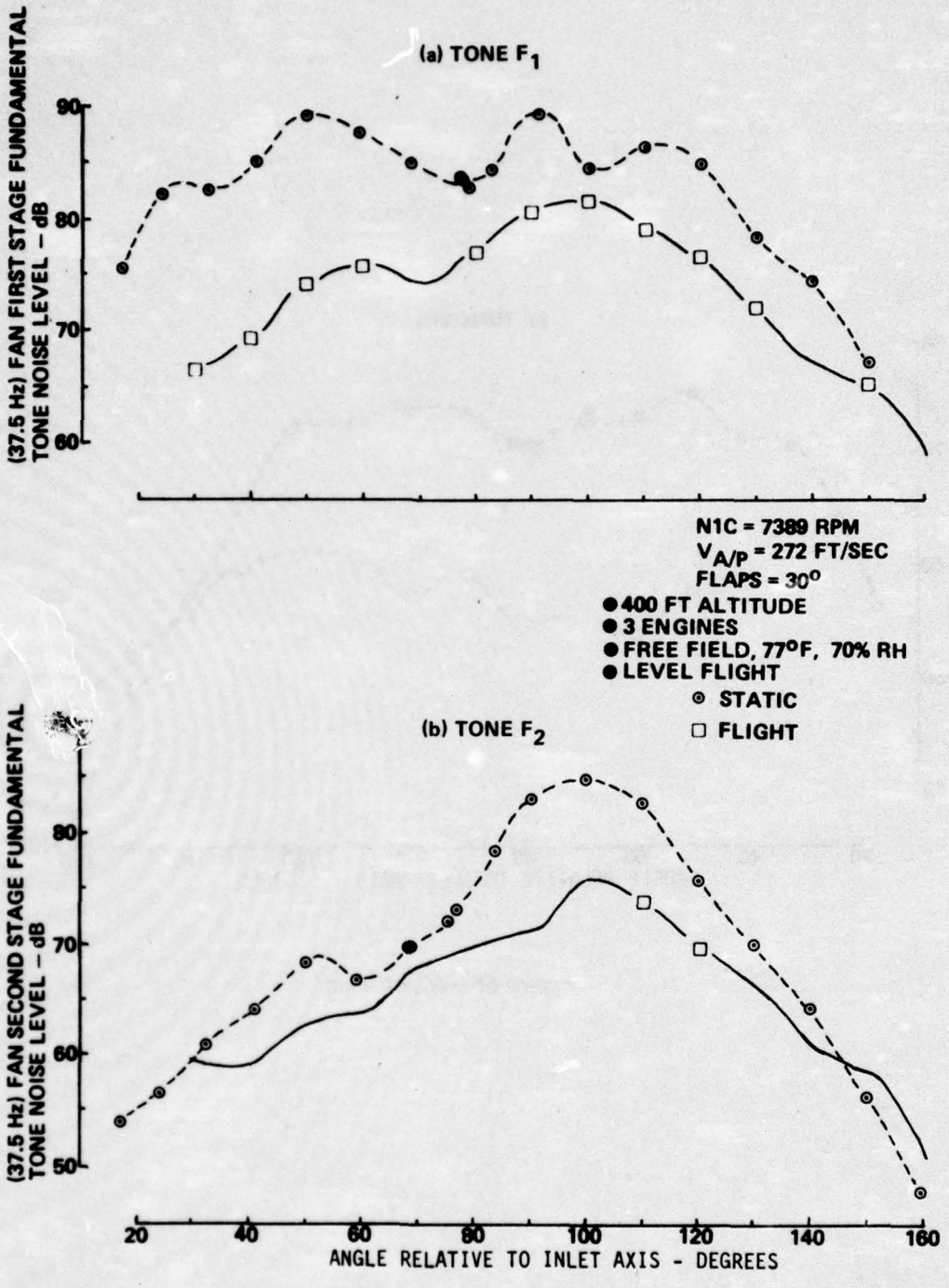


*Figure 65.—Fan Noise Flight Effects Directivity, Cutback Power (HGW), 727/JT8D Baseline*

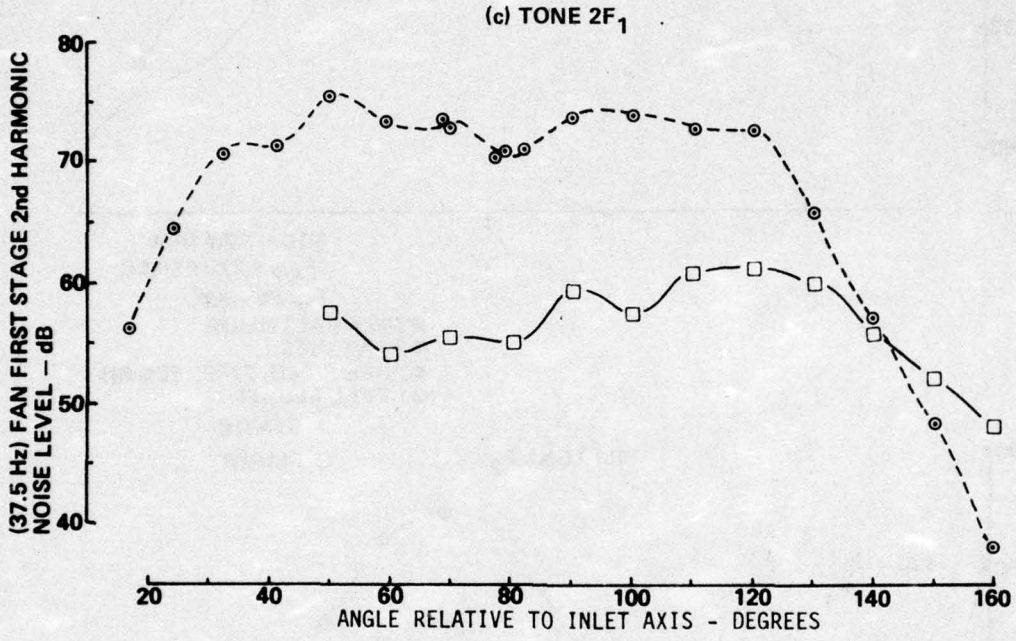


*Figure 65.—(Continued)*

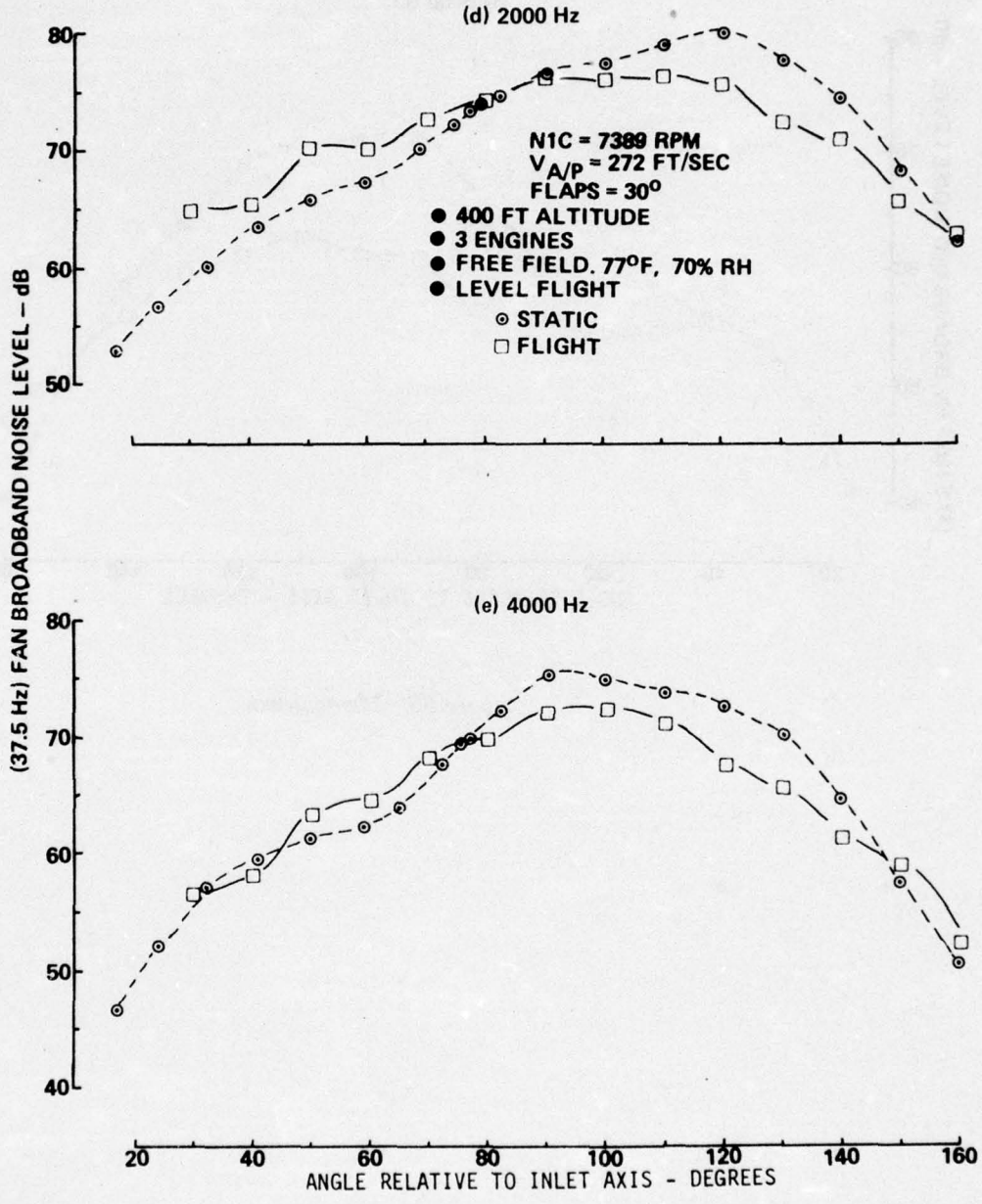


*Figure 65.—(Continued)*

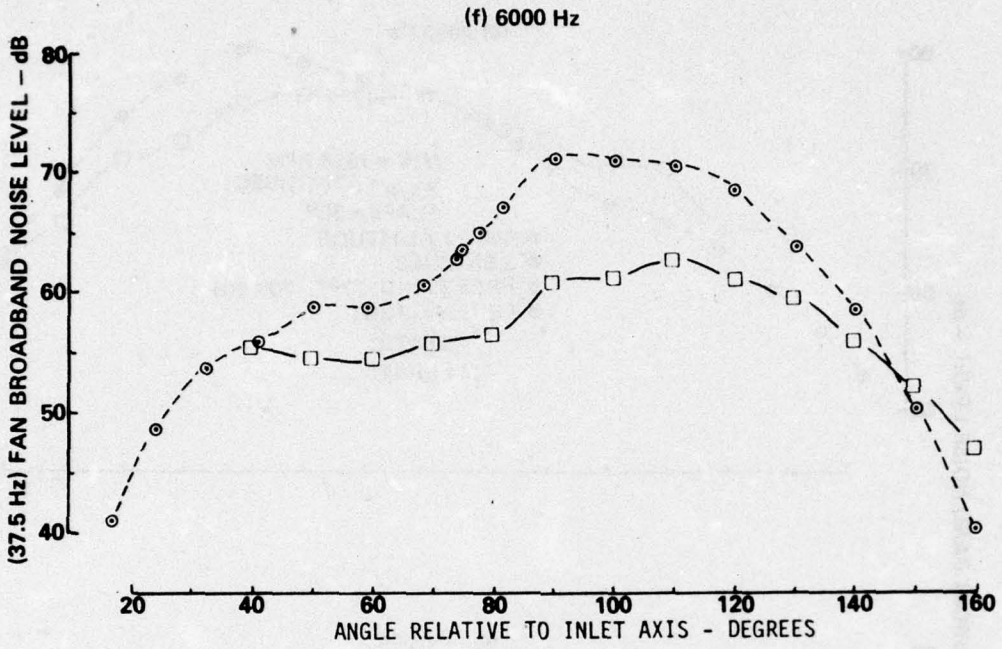


*Figure 65.—(Concluded)*

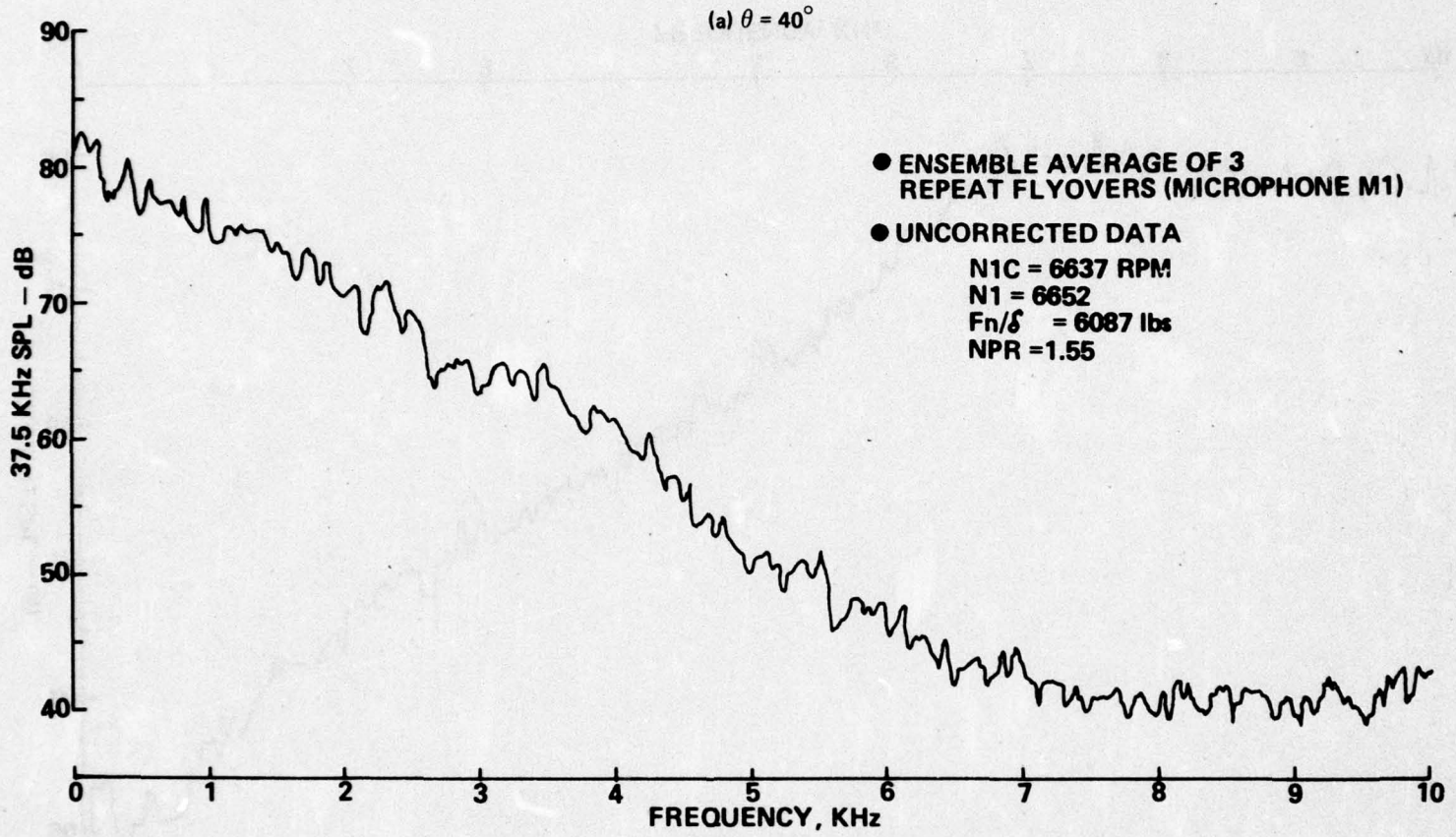


*Figure 66.—Flight Narrowband Spectra, Approach 727/JT8D Ejector Suppressor*

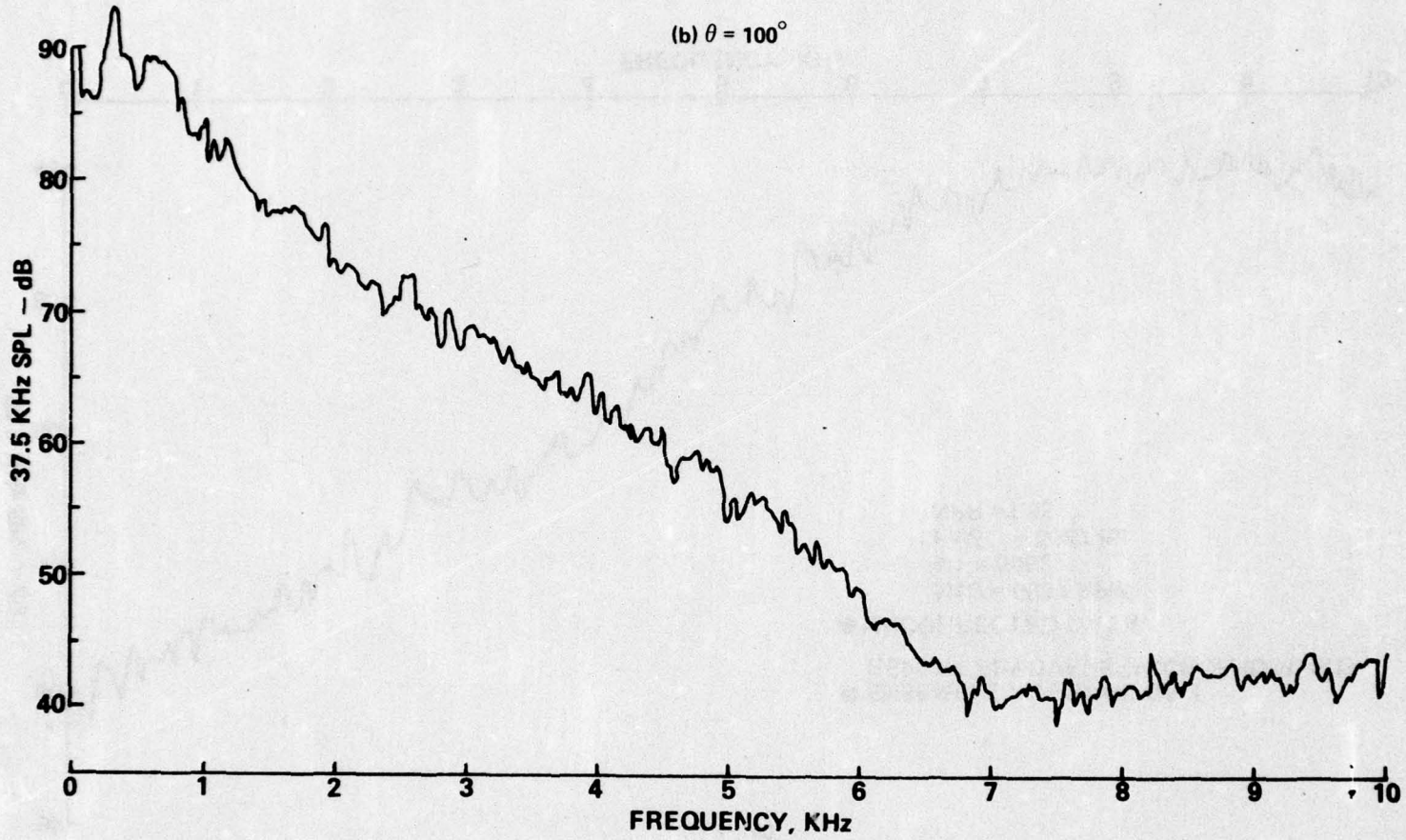


*Figure 66.—(Concluded)*

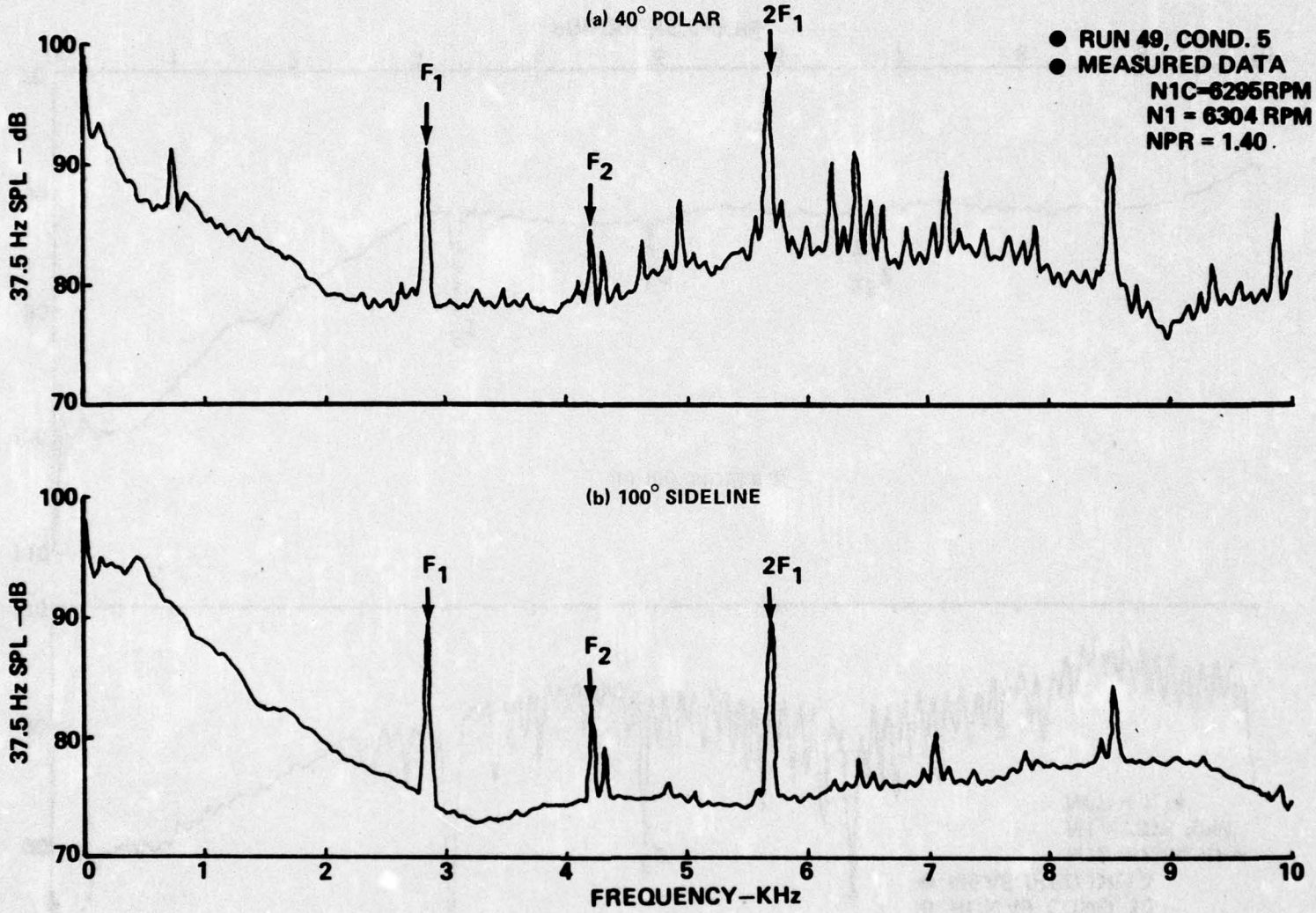


*Figure 67.—Static Narrowband Spectra, Approach Power, JT8D-9 Ejector Suppressor*

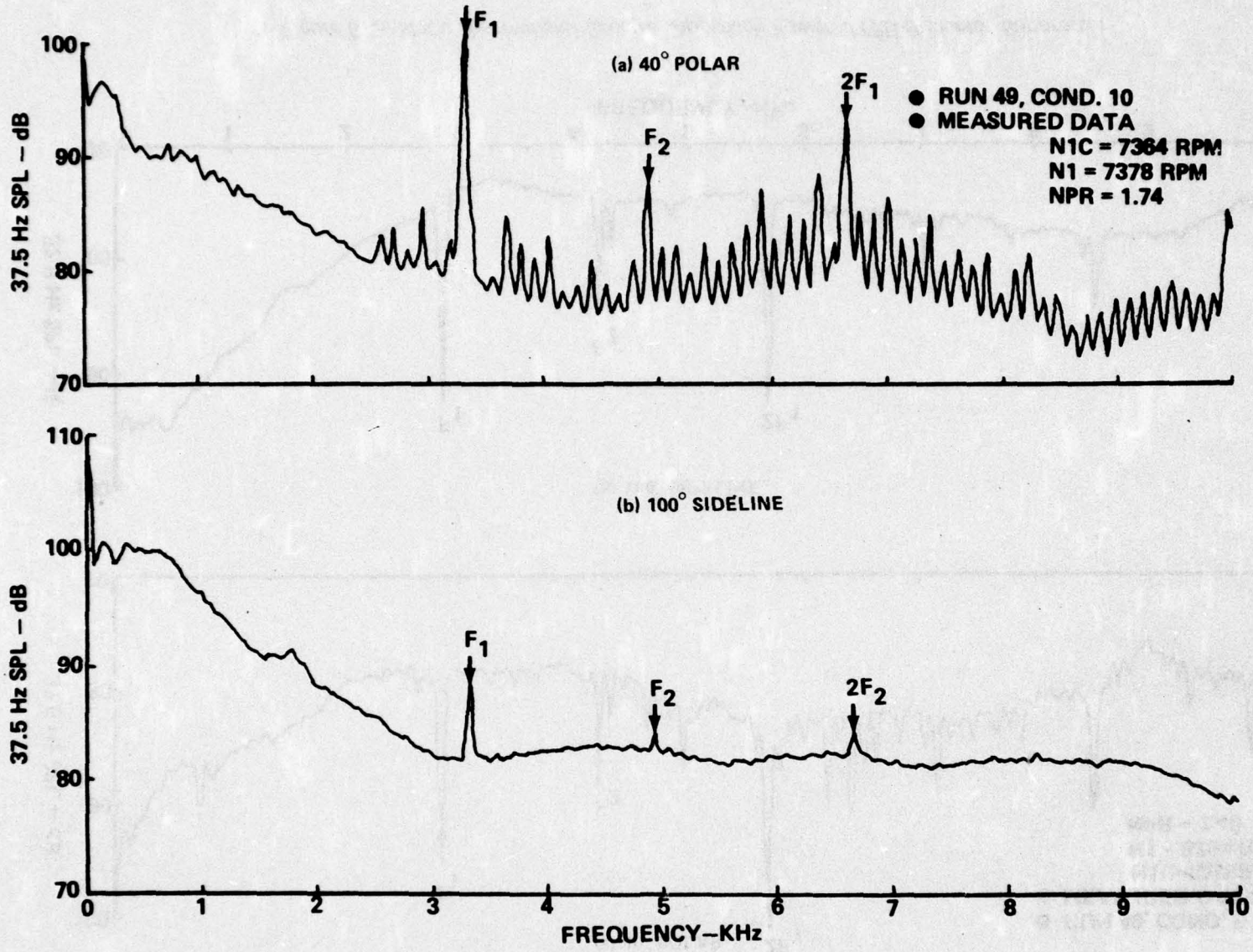


*Figure 68.—Static Narrowband Spectra, Cutback Power, JT8D-9 Ejector Suppressor*

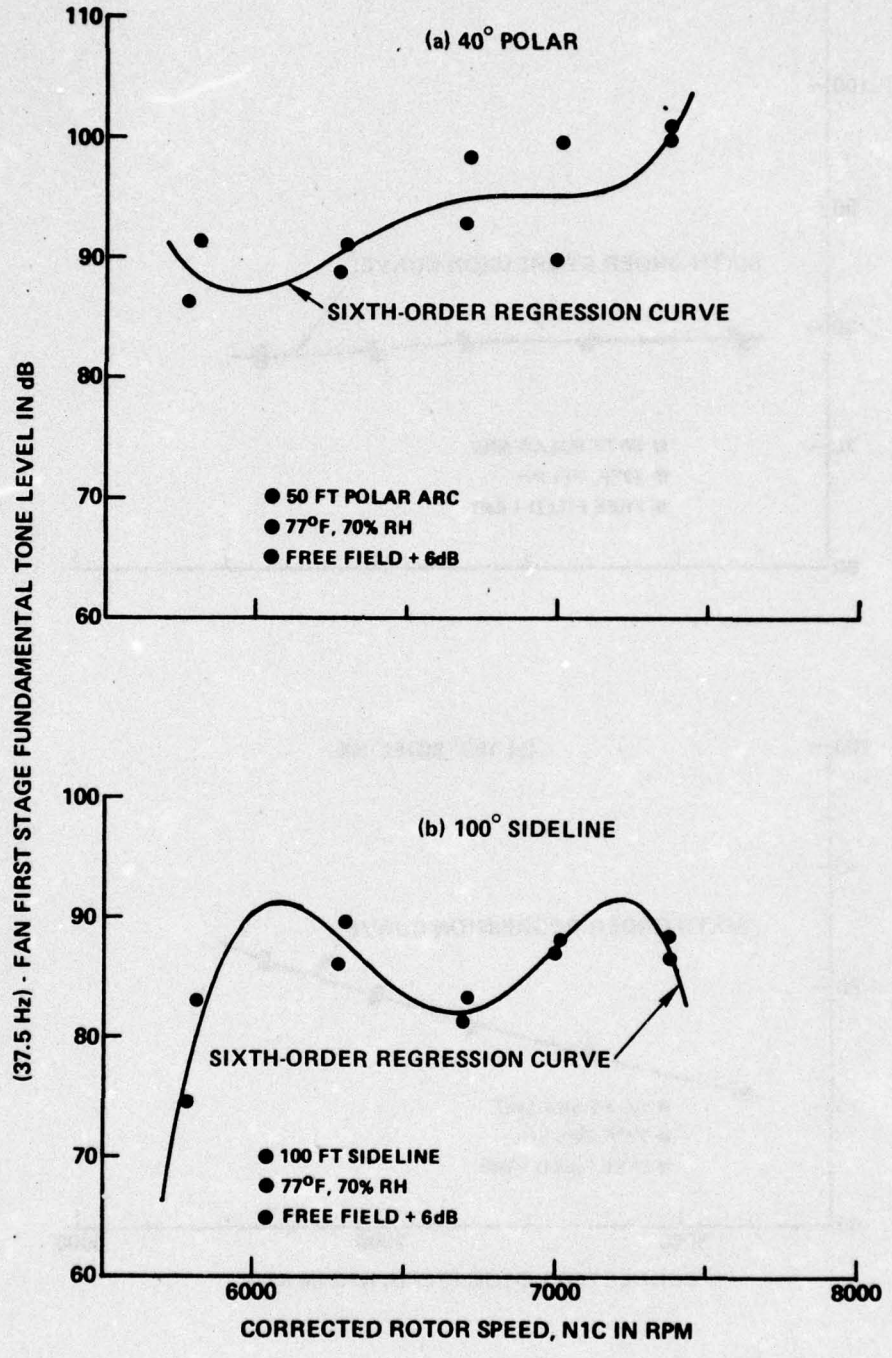


*Figure 69.—Fan First-Stage Fundamental Tone Level Versus Corrected Rotor Speed, JT8D-9 Ejector Suppressor Static Test*

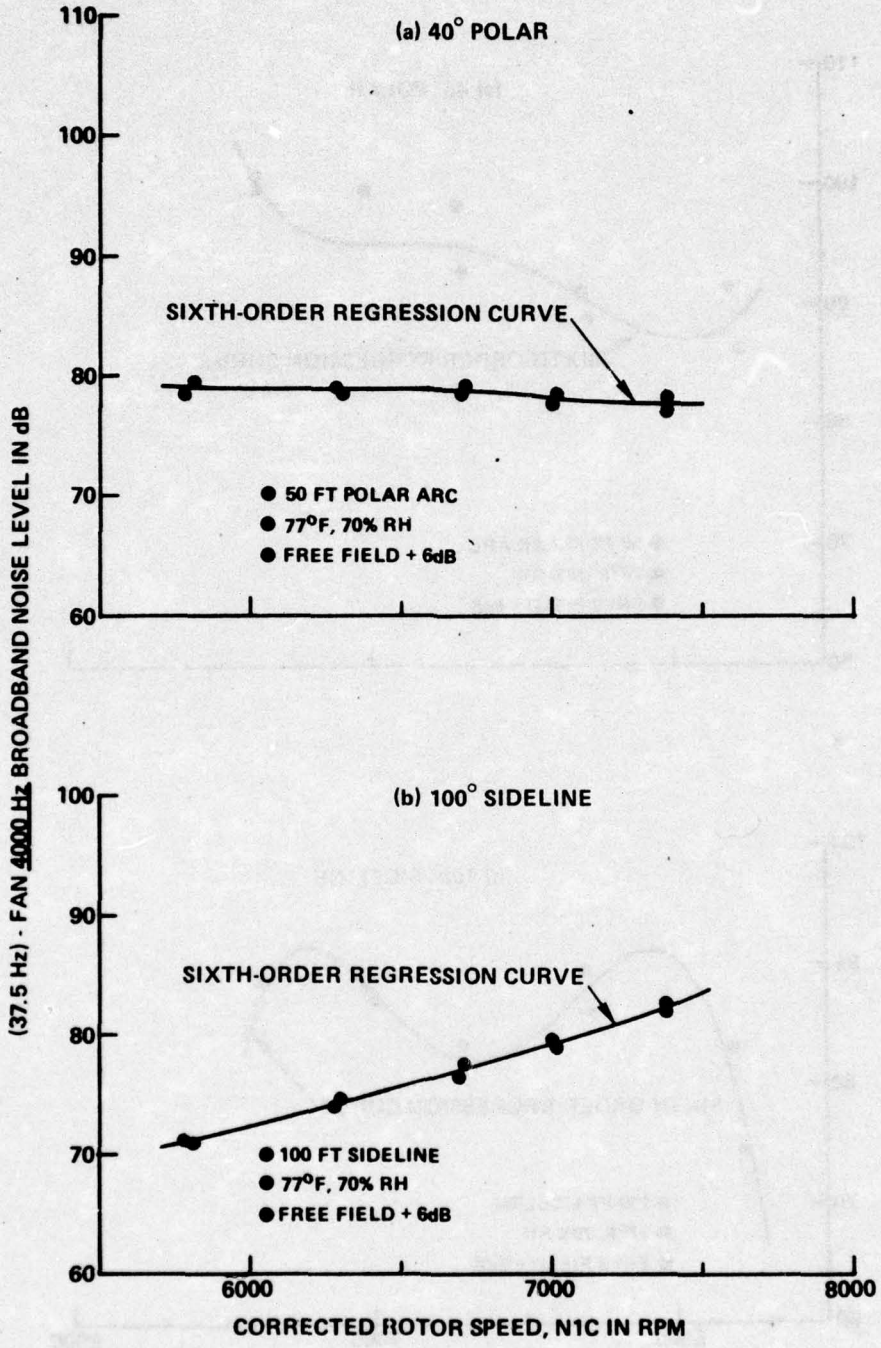


*Figure 70.—Fan 4000-Hz Broadband Noise Level Versus Corrected Rotor Speed, JT8D-9 Ejector Suppressor Static Test*

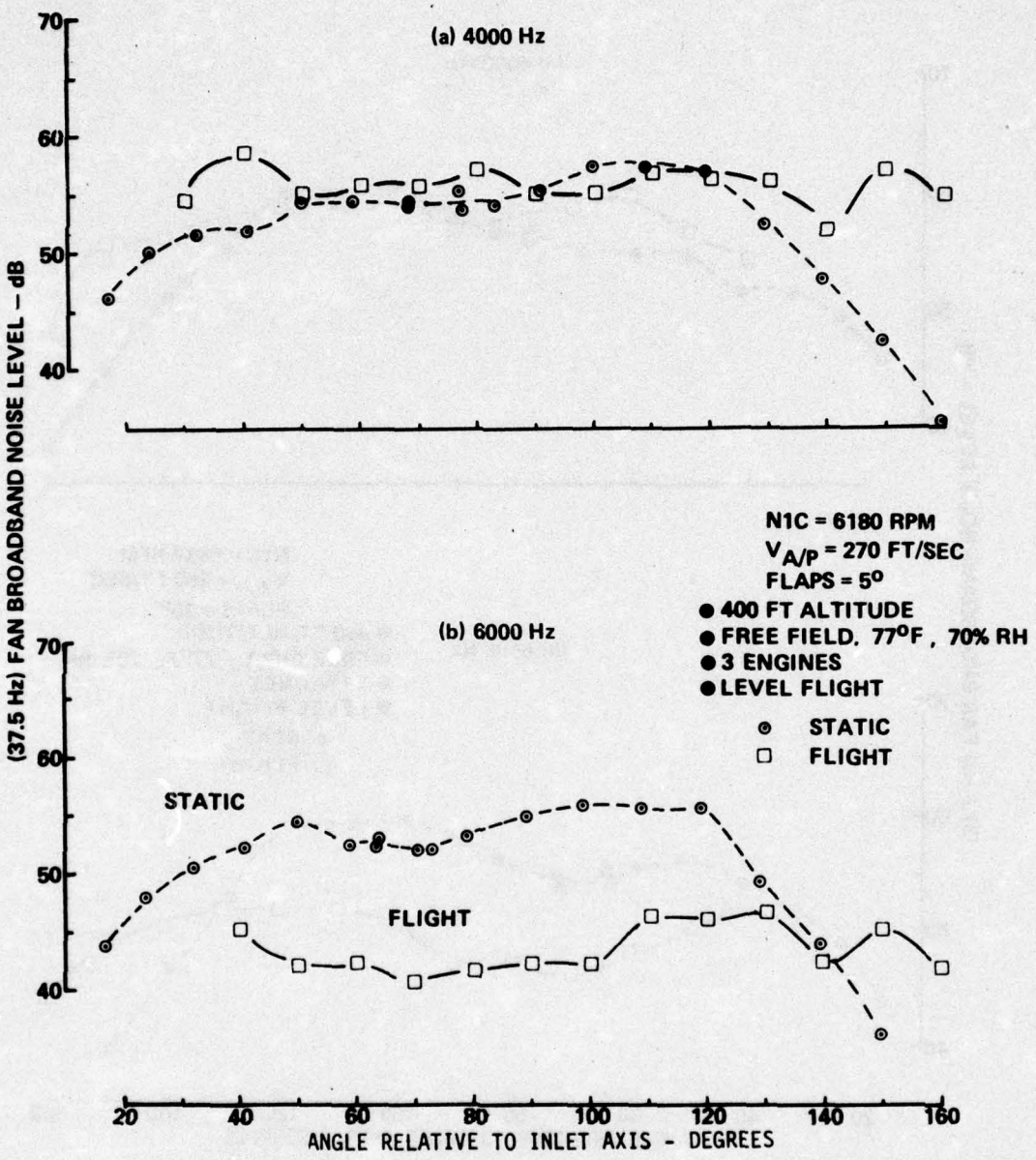


*Figure 71.—Fan Noise Flight Effects Directivity, Low Power Setting, 727/JT9D Ejector Suppressor*

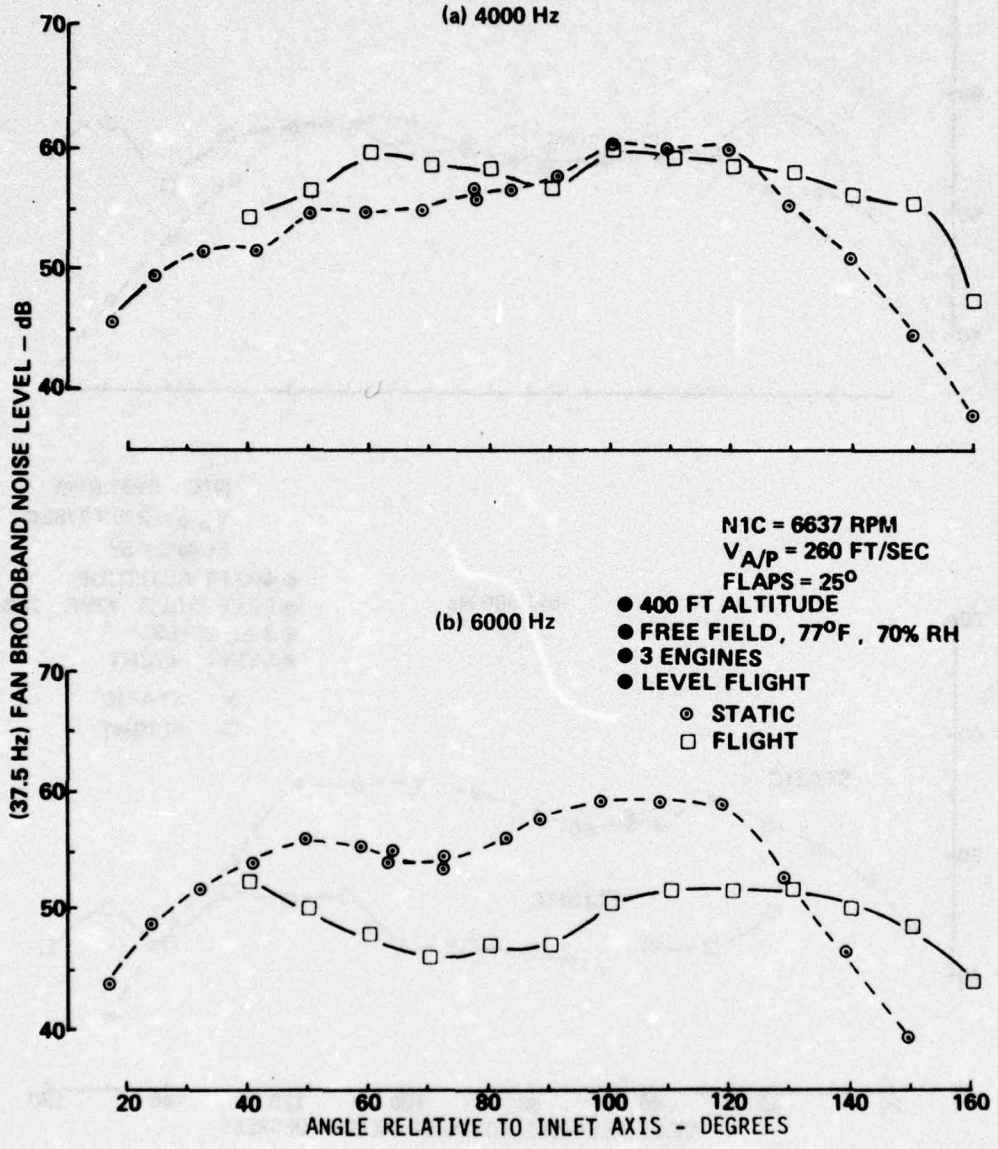


*Figure 72.—Fan Noise Flight Effects Directivity, Approach Power, 727/JT8D Ejector Suppressor*

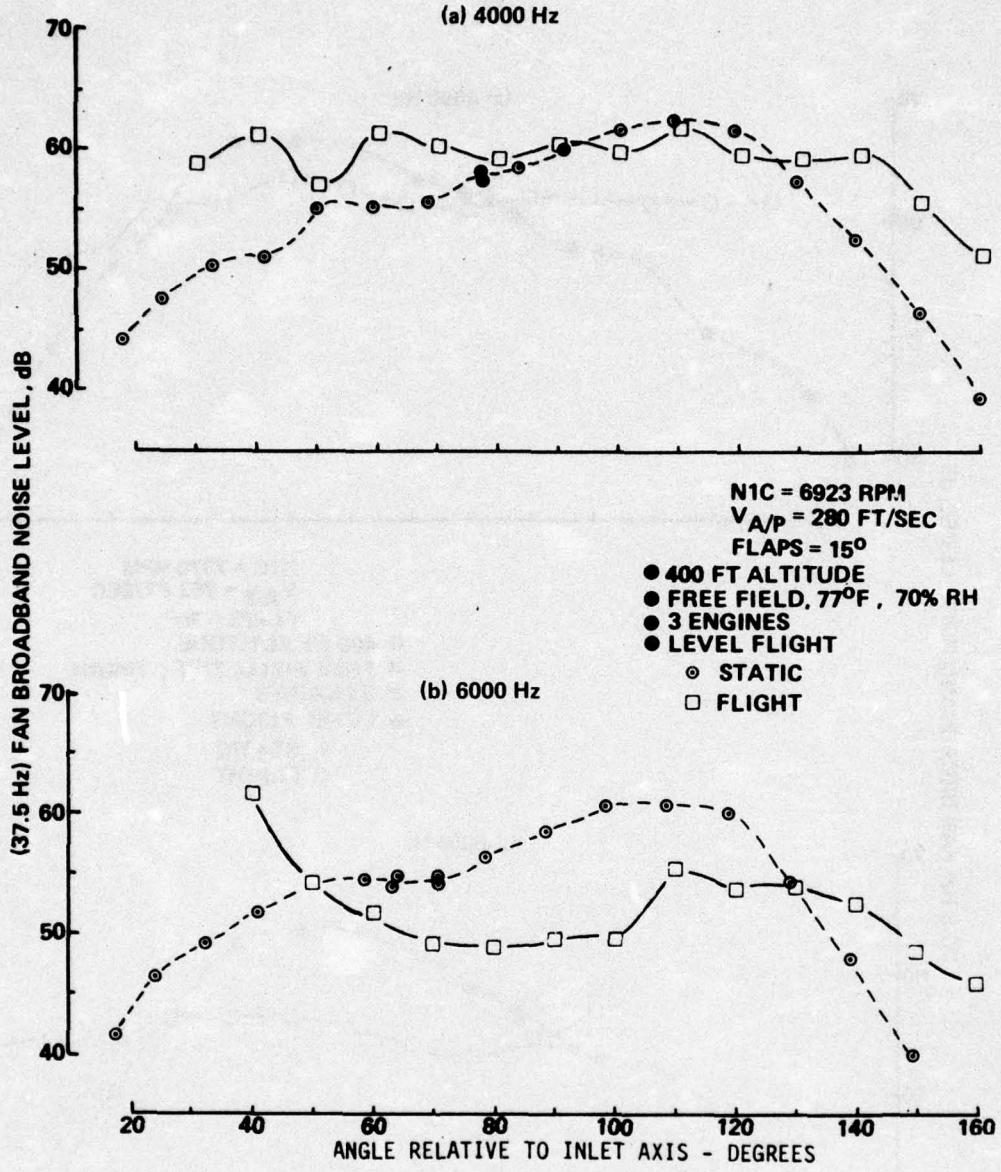


*Figure 73.—Fan Noise Flight Effects Directivity, Cutback Power (LGW), 727/JT8D Ejector Suppressor*

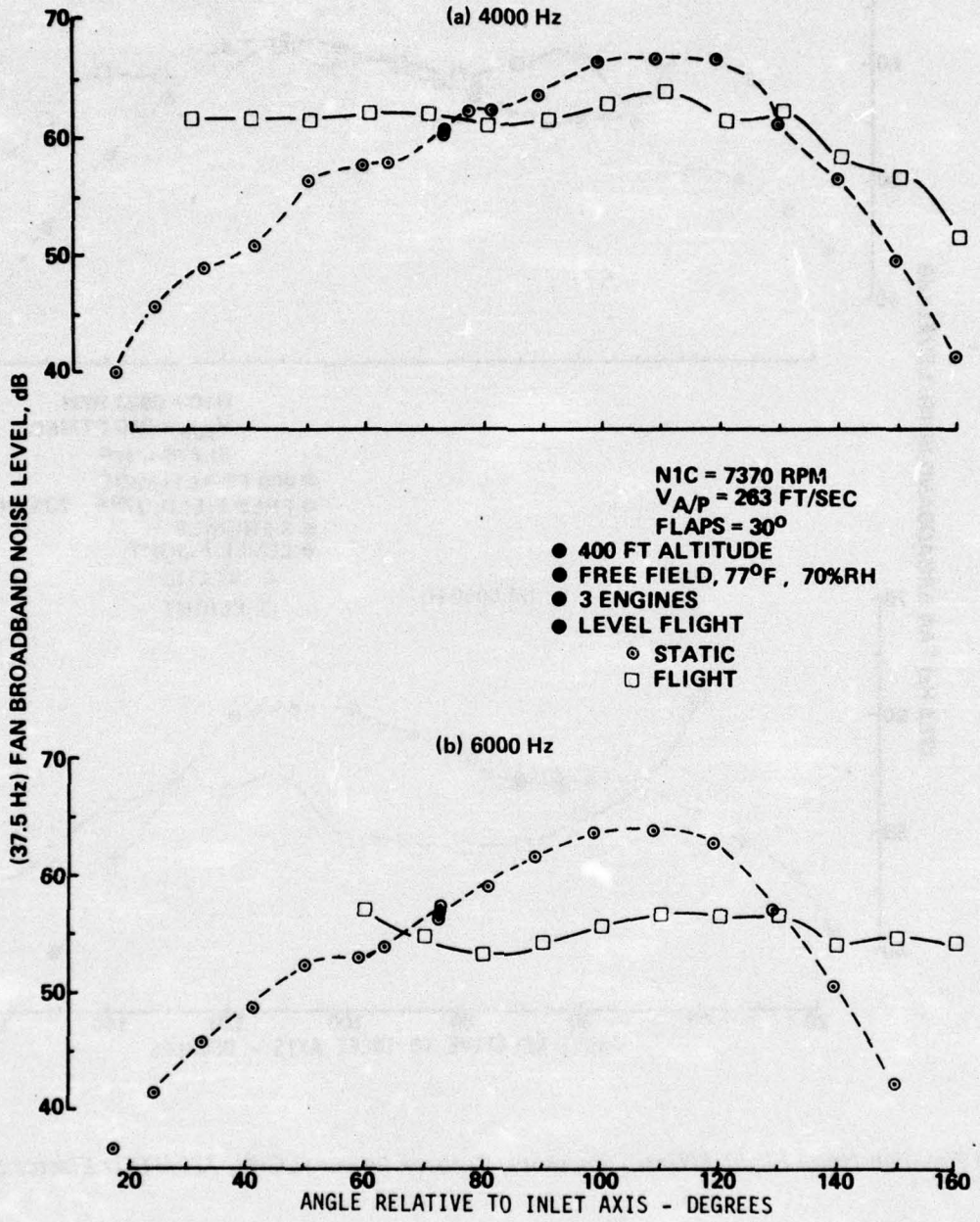


*Figure 74.—Fan Noise Flight Effects Directivity, Cutback Power (HGW), 727/JT8D Ejector Suppressor*

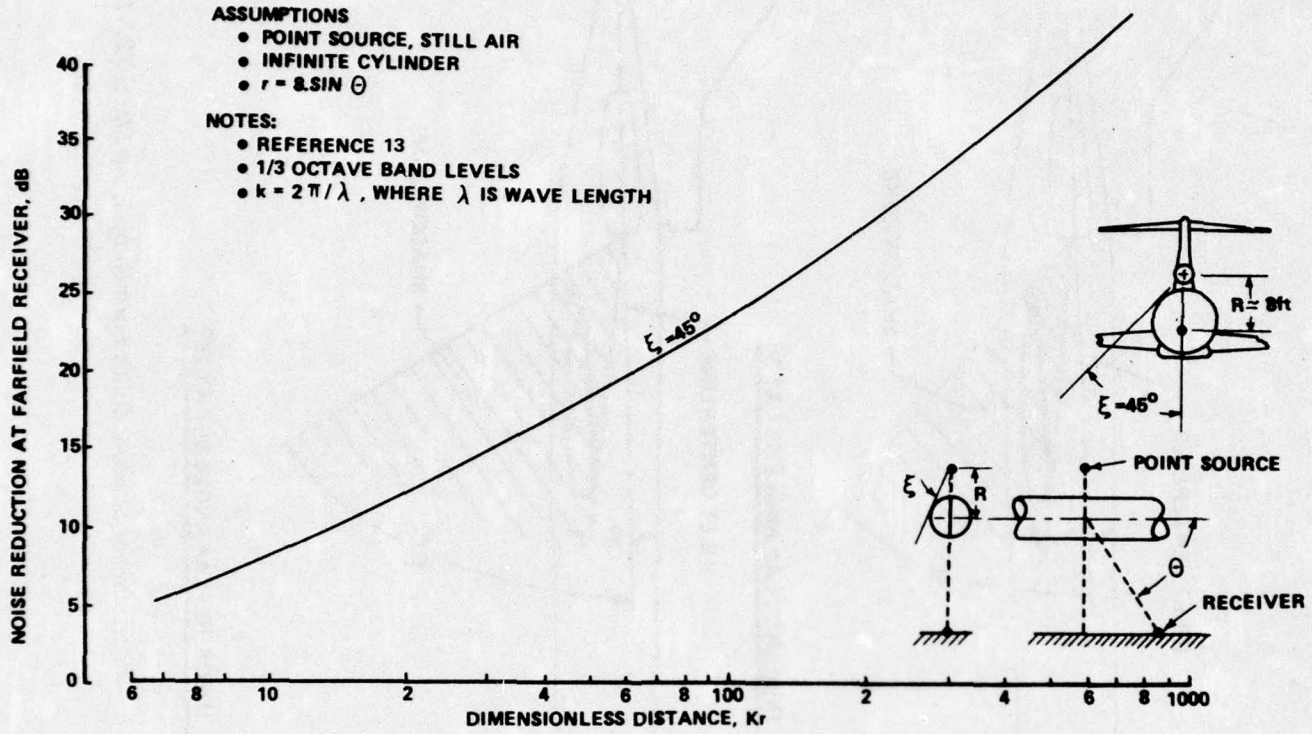


*Figure 75.—Center Engine Fuselage Noise Shielding, 727-100 Airplane*

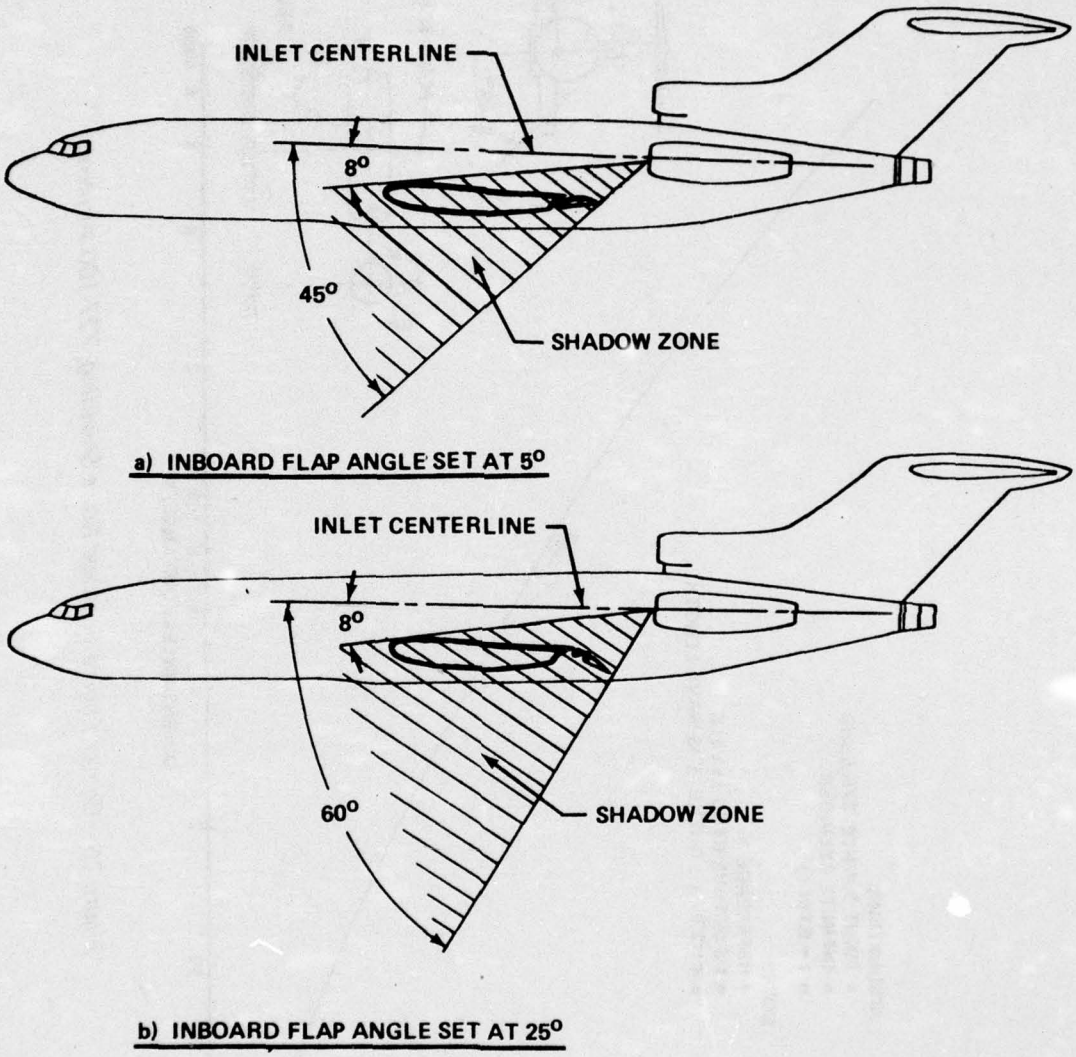


*Figure 76.—Approximate Shadow Zones Formed by Wing Flaps, 727-100 Airplane*

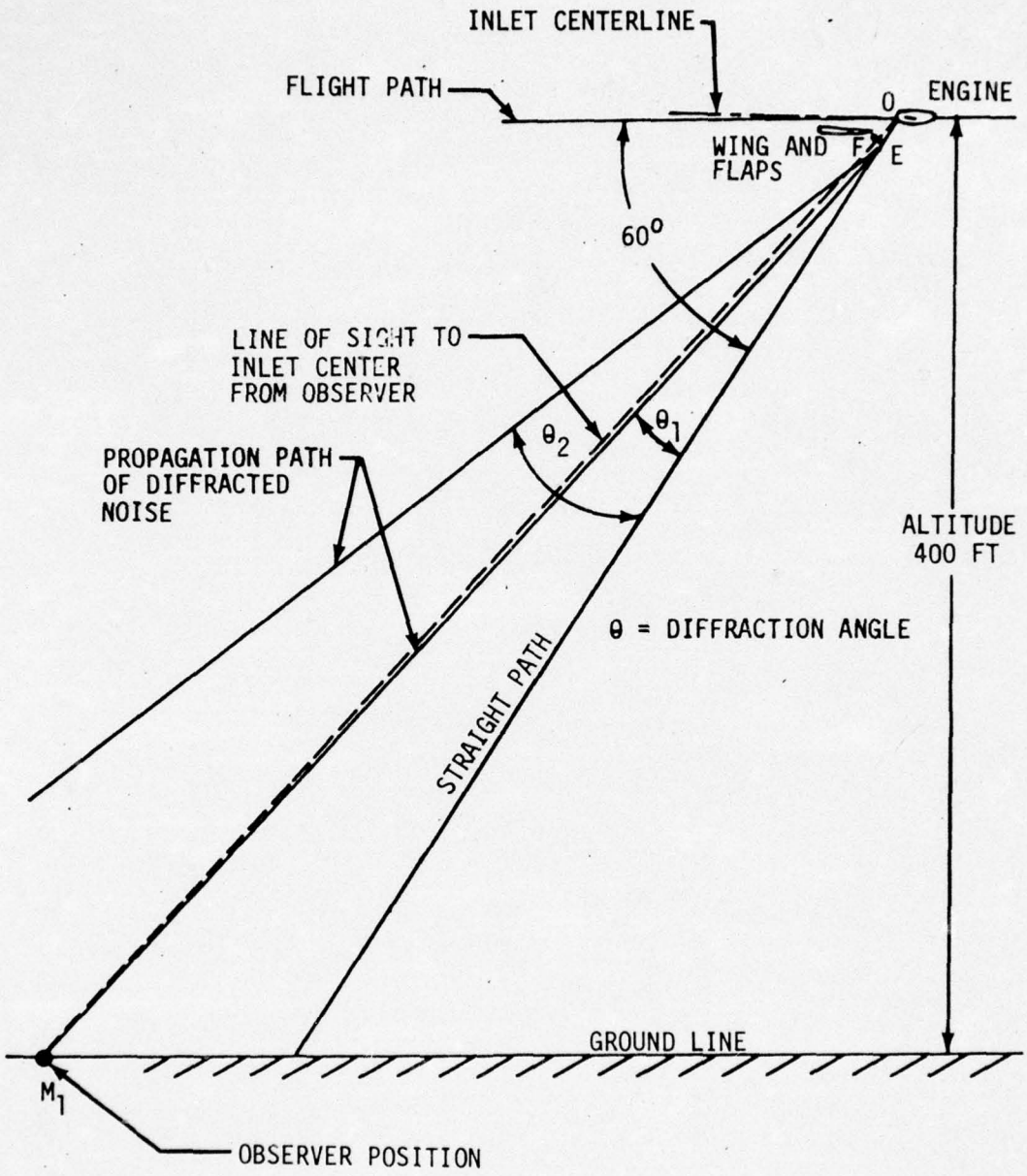


*Figure 77.—Scale Drawing Showing Flap Trailing-Edge Sound Wave Diffraction Paths (Flap Setting = 25°)*

# APPENDIX A
# AIRPLANE AND ENGINE PERFORMANCE DATA

This appendix includes airplane and engine performance data used in the jet and fan noise flight effects study.

## A.1 BASELINE CONFIGURATION

The JT8D baseline engines were instrumented in the static and flight tests to measure performance parameters required to define engine operating conditions.

Figures A-1 and A-2 show static engine performance for the selected acoustic runs. Nondimensional ideal primary jet velocity ($V_{jPRI}/a_o$) is shown as a function of primary nozzle pressure ratio ($P_{T7}/P_{amb}$) in figure A-1 and as a function of corrected low-pressure compressor rotor speed ($N1/\sqrt{\theta_{t2}}$) in figure A-2. The unique dependence between these parameters can be seen from the figures.

Flight effects on the engine performance are shown in figures A-3 and A-4, where the flight and static engine data are compared.

The static and flight baseline engine operating conditions were matched for the jet noise study using the nondimensional ideal primary jet velocity, and for the fan noise study using the corrected low-pressure rotor speed. The mismatch between the jet and fan noise corresponding engine operating conditions can be seen in figure A-4.

Average engine and airplane performance parameters for the baseline configuration selected flyovers are summarized in table A-1.

## A.2 EJECTOR SUPPRESSOR CONFIGURATION

The ejector suppressor nacelle, in the suppression mode, forces the engine airflow (primary and fan) to exit through the 20-lobe nozzle. The blow-in doors are also open, and free-stream air is entrained inside the ejector. The primary and fan streams, partially mixed with the entrained air, are expanded to ambient through the shroud exit nozzle.

In addition to the engine performance parameters measured to define engine operating conditions, the ejector suppressor tailpipe was instrumented with static pressure tabs on plug and ejector surfaces, as well as with total pressure and temperature rakes at the shroud exit. Entrained airflow total pressures were measured with a probe located at the 20-lobe nozzle exit station and directed to the incoming entrained flow.

Jet noise is generated inside the ejector by the mixing of the entrained air and engine airflow, and downstream of the shroud nozzle exit by the mixing of the exhaust flow and the surrounding air.

The engine performance scaling parameter for the jet noise generated inside the ejector was assumed to be the corrected lobe primary relative velocity $(V_{jPRI} - V_E)/\sqrt{\theta_{amb}}$. Figure A-5 shows this parameter as a function of primary nozzle pressure ratio, $P_{T7}/P_{amb}$. The ideal expanded primary jet velocity at lobe exit, $V_{jPRI}$, was calculated using the primary flow conditions measured behind the turbine, $P_{T7}$ and $T_{T7}$, and the measured static pressure values at the lobe exit. The ideal entrained velocity, $V_E$, was calculated using the measured total pressure at the lobe exit, the ambient temperature condition, and the internal static pressure values.

The scaling parameter for the jet noise generated downstream of the shroud exit was assumed to be the maximum shroud exit velocity. Exit velocity profiles were calculated from the total pressures and temperature measurements at the shroud exit. Velocity profiles for two power settings are shown in figure A-6. Maximum exit velocities are shown as a function of primary nozzle pressure ratio in figure A-7. Shroud exit conditions were measured with a bellmouth inlet instead of the two-ring acoustic inlet. Effects on the shroud exit conditions were estimated negligible for acoustic purposes (about 1%).

Static and flight engine performances are compared in figure A-8, where corrected low-pressure rotor speed is shown plotted against primary nozzle pressure ratio.

Static and flight engine operating conditions for the ejector suppressor configuration were matched for the jet noise study using the primary nozzle pressure ratio, and for the fan noise study using the corrected low-pressure rotor speed. The mismatch between the jet and fan noise corresponding engine operating conditions can be seen in figure A-8. Average engine and airplane performance parameters in flight for the ejector suppressor configuration are summarized in table A-2.

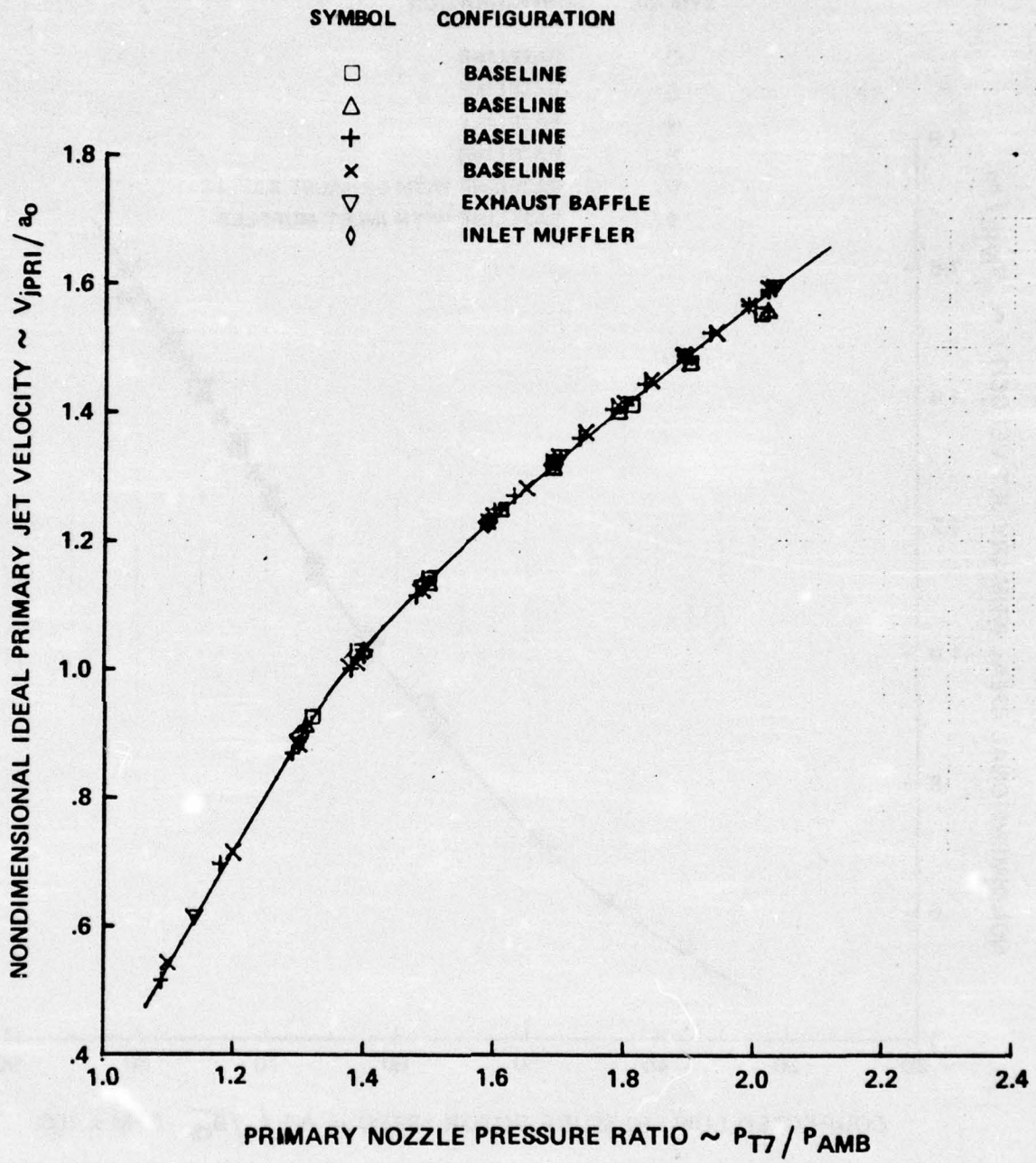


*Figure A-1.—Ideal Primary Jet Velocity Versus Nozzle Pressure Ratio, JT8D-9 Baseline Static Engine Performance Data*

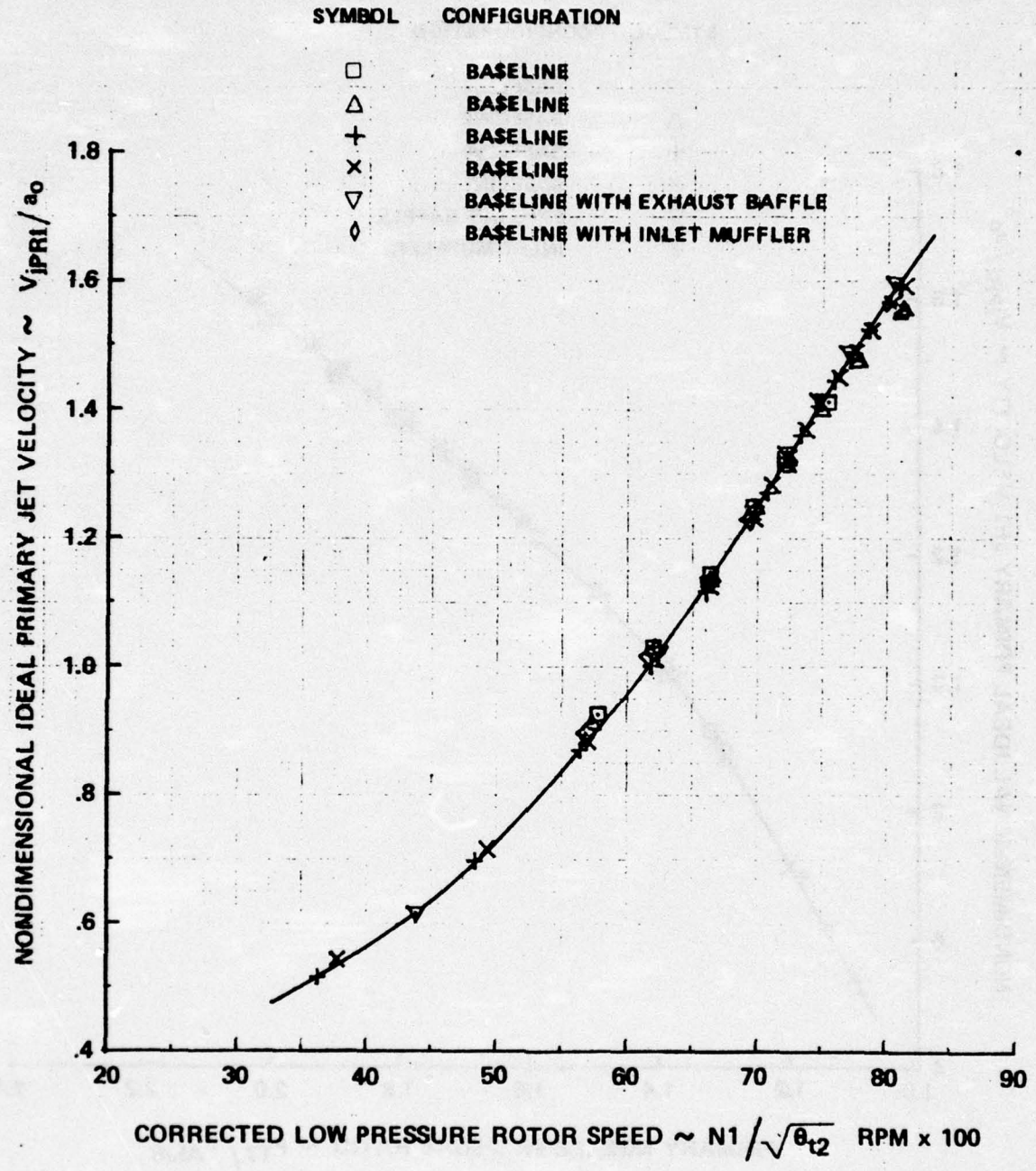


*Figure A-2.—Ideal Primary Jet Velocity Versus Corrected Low-Pressure Rotor Speed, JT8D-9 Baseline Static Engine Performance Data*

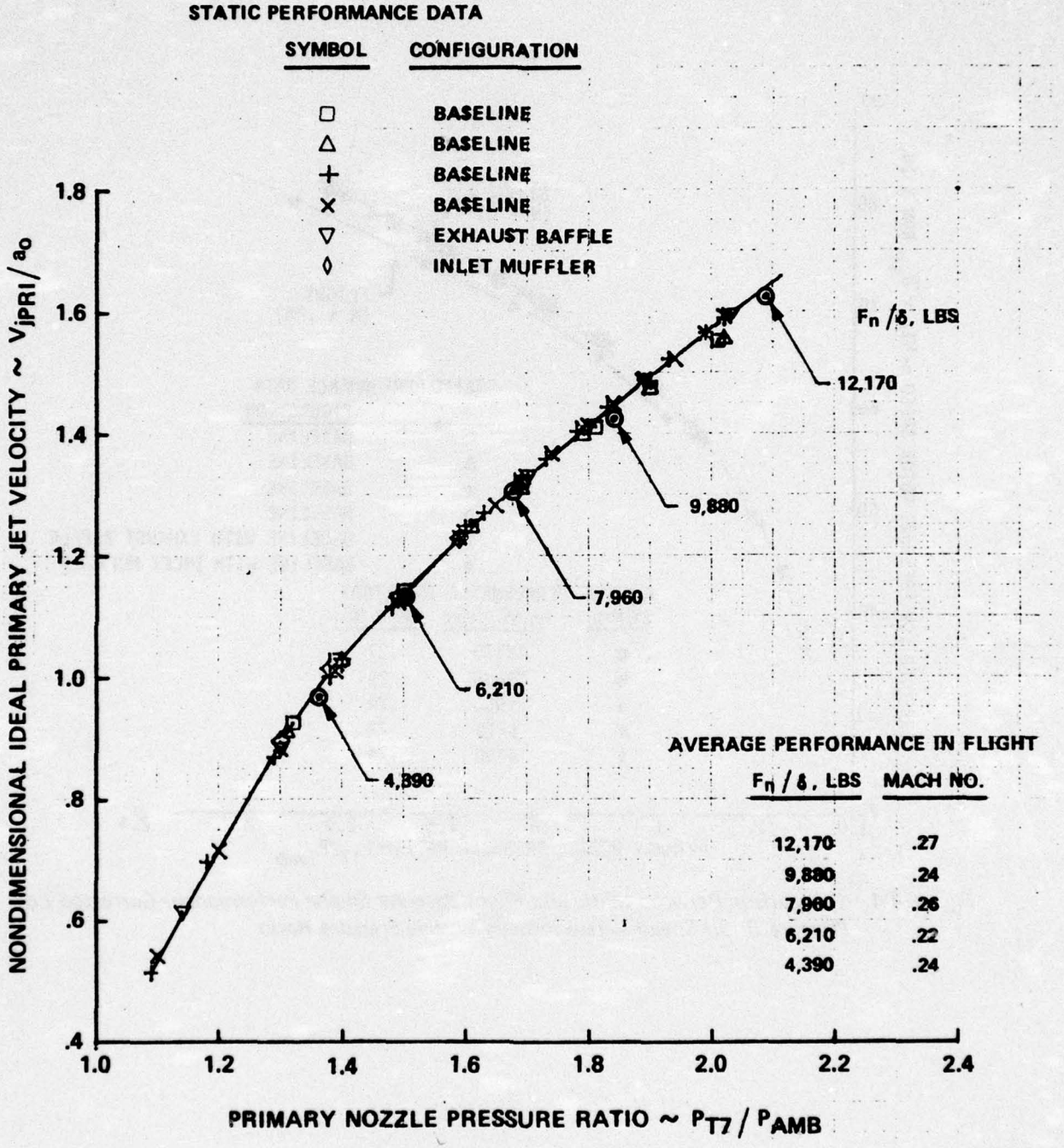


*Figure A-3.—Comparison Between Static and Flight Baseline Engine Performance—Ideal Primary Jet Velocity Versus Primary Nozzle Pressure Ratio*

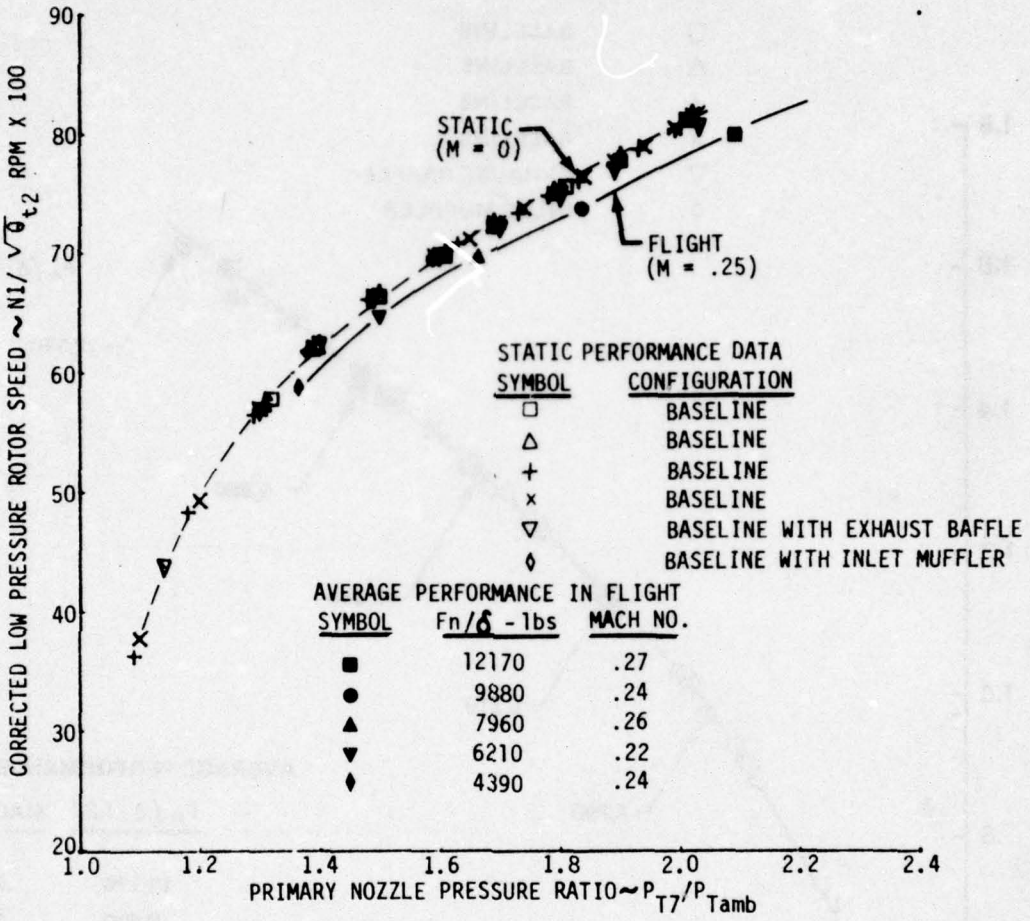


*Figure A-4.—Comparison Between Static and Flight Baseline Engine Performance—Corrected Low-Pressure Rotor Speed Versus Primary Nozzle Pressure Ratio*

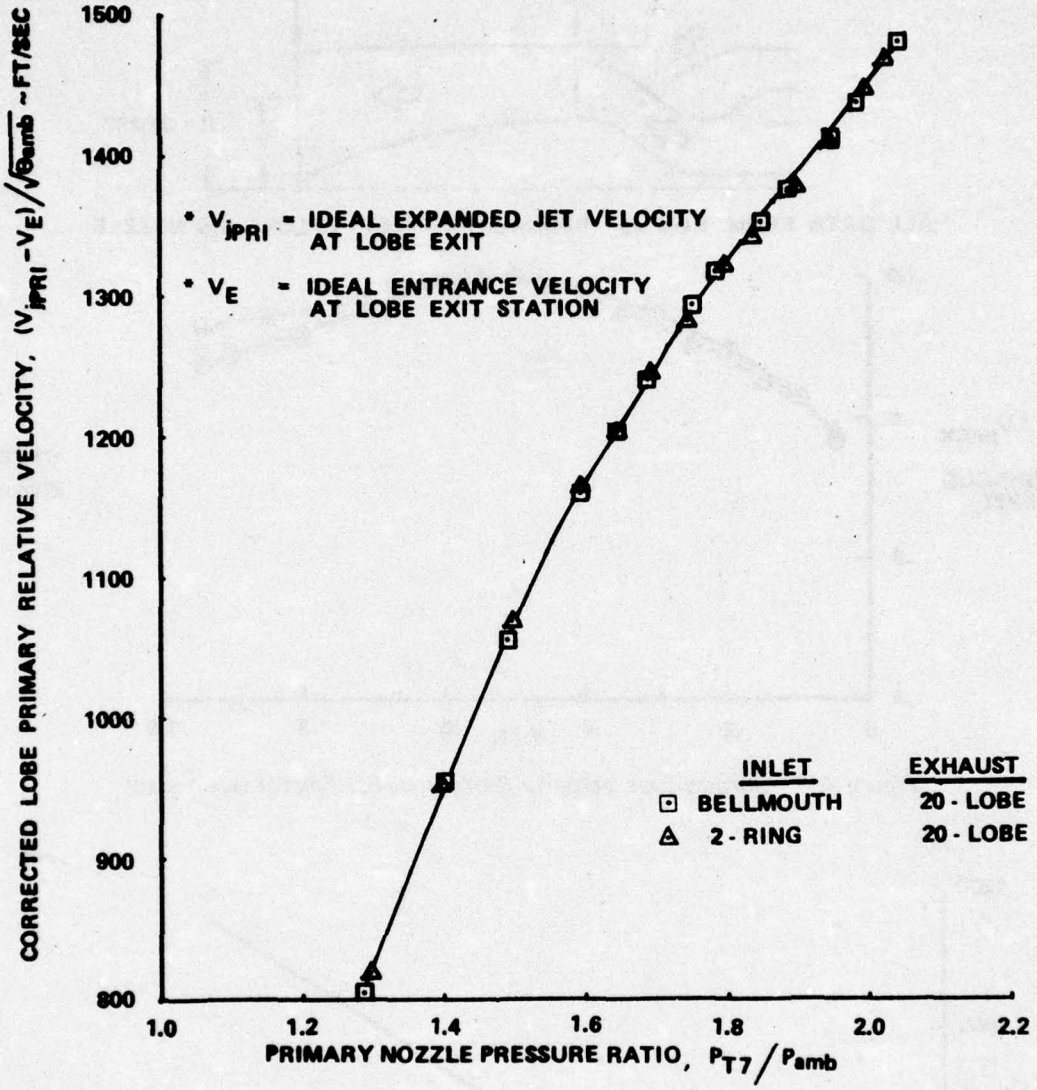


*Figure A-5.—Corrected Lobe Primary Jet Relative Velocity, JT8D Ejector Suppressor*

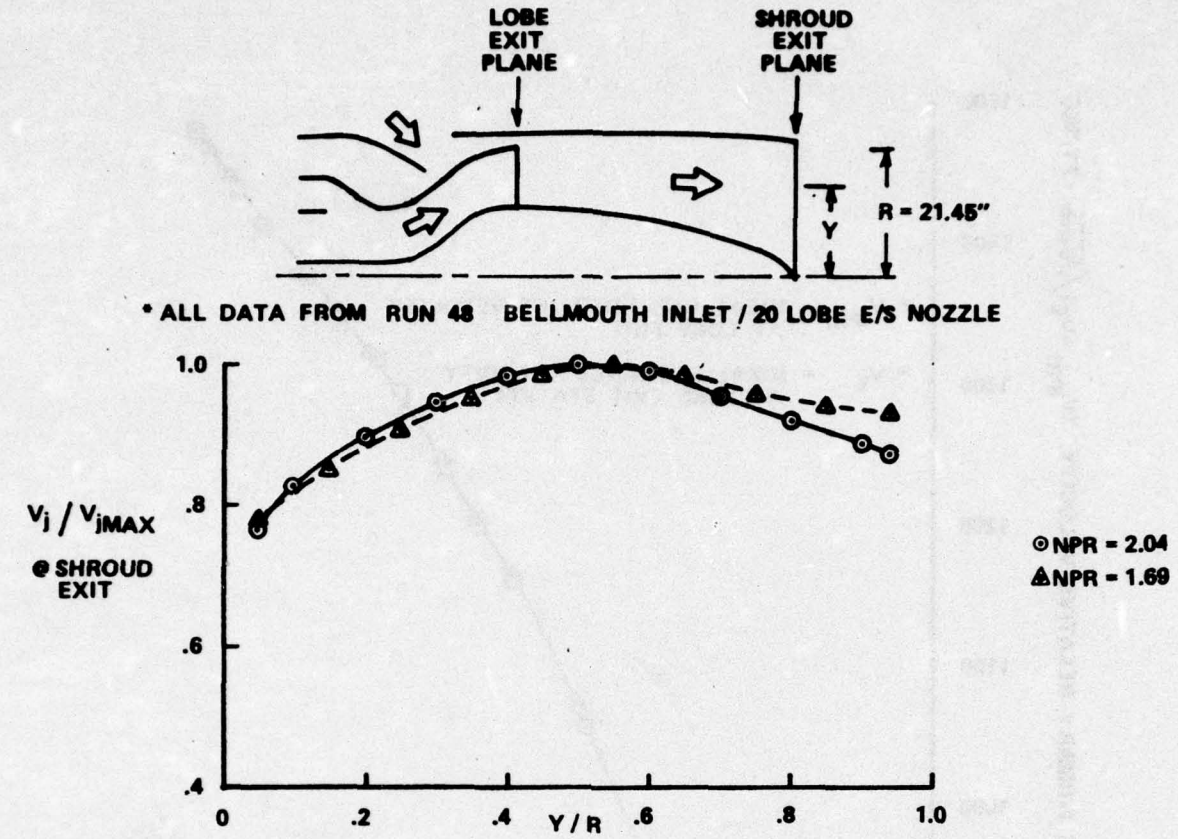


*Figure A-6.—Shroud Exit Velocity Profiles, JT8D Ejector Suppressor*

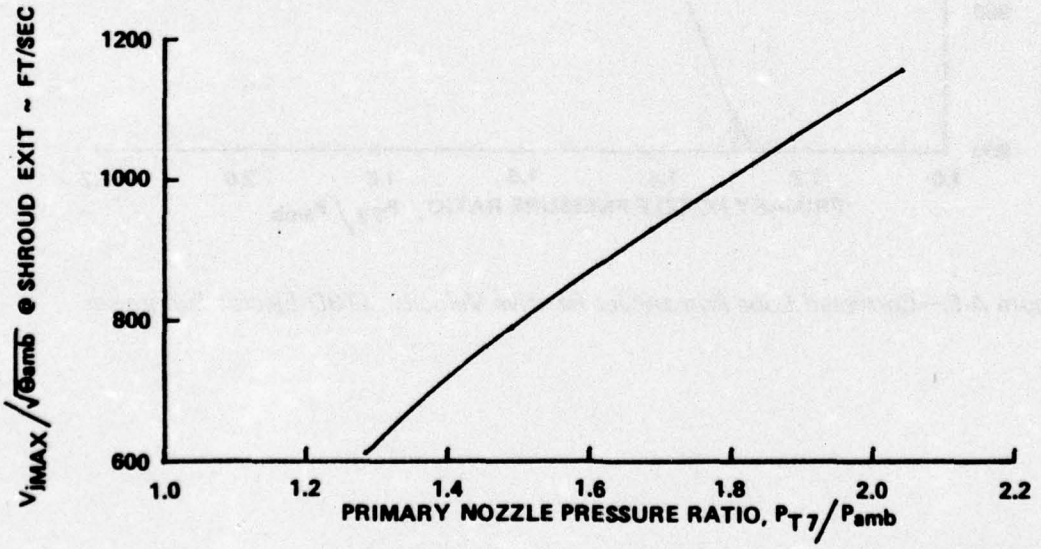


*Figure A-7.—Maximum Shroud Exit Velocity as a Function of Power Setting*

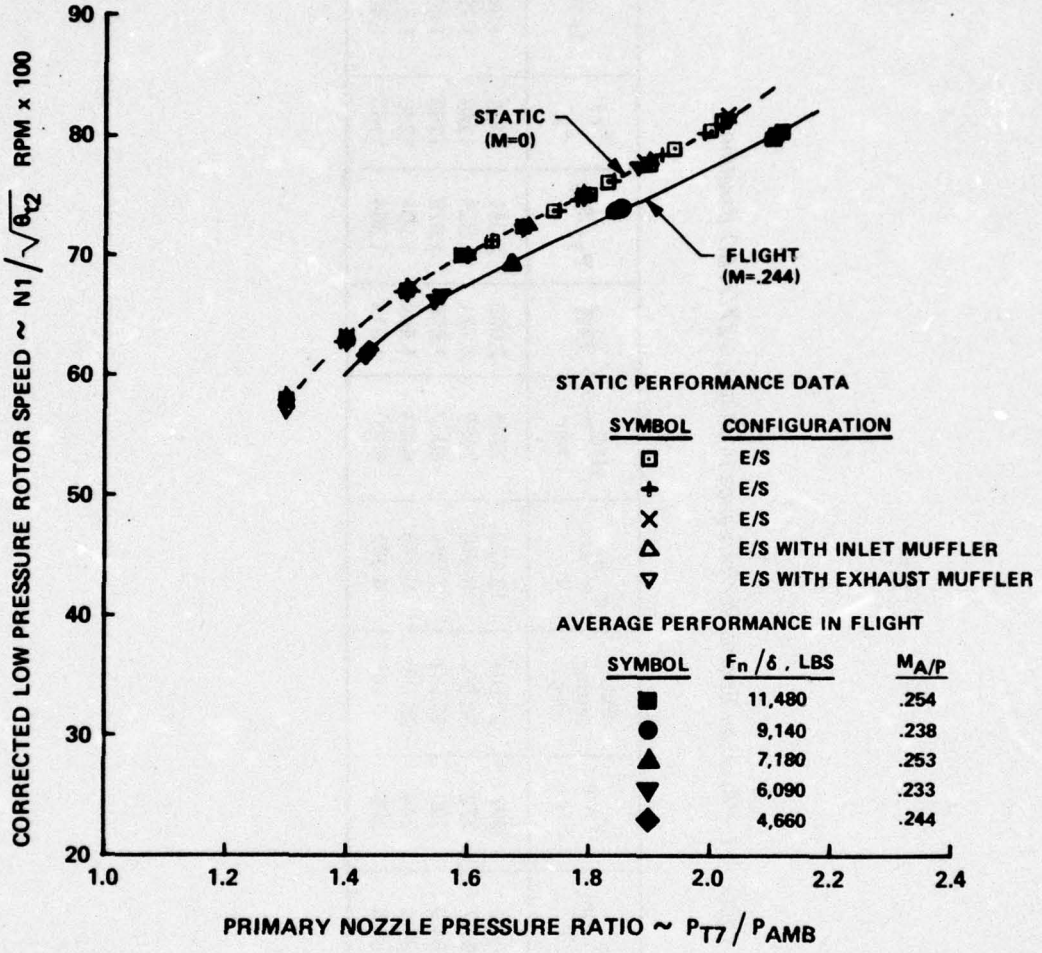


*Figure A-8.—Comparison of JT8D Ejector Suppressor Static and Flight Engine Performance*

*Table A-1.—Average Engine Performance in Flight, 727/JT8D Baseline*

| $F_n/\delta$, target lb | Operational power setting | $T_{amb}$, °F | $V_{A/P}$ ft/sec | Flap setting, deg | $F_n/\delta_{ave}$, lb | $N1C_{ave}$, rpm | EPR | $P_{T7}/P_\infty$ | $T_{T7}$ °R | $P_{TF7}/P_\infty$ | $T_{TF7}$, °R |
|---|---|---|---|---|---|---|---|---|---|---|---|
| 12 000 | Takeoff | 60.2 | 297 | 30 DN* | 12 170 | 7990 | 2.000 | 2.091 | 1434 | 1.968 | 663 |
| 10 000 | Cutback (HGW) | 62.7 | 272 | 30 DN | 9 876 | 7389 | 1.771 | 1.839 | 1349 | 1.799 | 640 |
| 8 000 | Cutback (LGW) | 63.9 | 290 | 15 DN | 7 964 | 6967 | 1.606 | 1.678 | 1289 | 1.676 | 627 |
| 6 000 | Approach | 66.4 | 244 | 25 DN | 6 215 | 6484 | 1.454 | 1.501 | 1230 | 1.519 | 612 |
| 4 000 | Low power | 66.3 | 265 | 5 UP** | 4 392 | 5889 | 1.314 | 1.364 | 1163 | 1.403 | 595 |

*DN = gear down
**UP = gear up

*Table A-2.—Average Engine Performance in Flight, 727/JT8D Ejector Suppressor*

| $F_n/\delta$ target, lb | Operational power setting | $T_{amb}$, °F | $V_{A/P}$, ft/sec | Flap setting deg | $F_N/\delta_{ave}$, lb | $N1C_{ave}$, rpm | EPR | $P_{T7}/P_\infty$ | $T_{T7}$, °R | $P_{TF7}/P_\infty$ | $T_{TF7}$, °R |
|---|---|---|---|---|---|---|---|---|---|---|---|
| 12 000 | Takeoff | 49.6 | 281 | 30 DN* | 11 480 | 8000 | 2.017 | 2.110 | 1417 | 1.959 | 651 |
| 10 000 | Cutback (HGW) | 51.0 | 263 | 30 DN | 9 140 | 7370 | 1.776 | 1.847 | 1324 | 1.788 | 623 |
| 8 000 | Cutback (LGW) | 52.7 | 281 | 15 DN | 7 180 | 6923 | 1.599 | 1.672 | 1262 | 1.660 | 608 |
| 6 000 | Approach | 56.1 | 260 | 25 DN | 6 090 | 6637 | 1.496 | 1.553 | 1222 | 1.557 | 600 |
| 4 000 | Low power | 55.5 | 271 | 5 UP** | 4 660 | 6180 | 1.373 | 1.434 | 1164 | 1.462 | 586 |

*DN = gear down
**UP = gear up

# APPENDIX B
# JET AND FAN NOISE SOURCE LOCATION

## B.1 INTRODUCTION

Total engine noise is the combination of several noise components which differ in their characteristics (spectrum, directivity). Under certain engine operating conditions, some of these components dominate the total noise, while others could become dominant at other operating conditions. Three noise components–jet noise, core noise, and turbomachinery noise–have been identified in today's aircraft engines. Jet noise is generated by the mixing process between the turbulent jet and the surrounding air. Turbomachinery noise is associated with the engine airflow interaction with the rotor-stator blade system. Core noise consists of such noise components as combustion noise, entropy noise, swirl noise, etc.

Turbomachinery noise and core noise are generated by sources located inside the engine. The corresponding acoustic energy is transmitted mainly along the engine ducts toward the inlet and/or exhaust, where it is radiated outward. Jet noise, however, is generated downstream of the nozzle exit, where the mixing process occurs, by noise sources spatially distributed in the turbulent efflux.

Therefore, a microphone located close to the engine (near field) will receive sound signals from each of these sources. The noise intensity would be dominated by one of the noise components depending upon the microphone position and the relative strength of the noise sources. When these near-field data are extrapolated to farther distances, knowledge of the location of the dominant noise source is required.

If the microphone is located far enough from the engine (far field), the distributed noise sources will appear concentrated in a single-point source. Then, noise extrapolation can be readily done by assuming straight line noise propagation.

## B.2 JET NOISE SOURCE LOCATIONS

As the jet noise is generated by the mixing process between the jet flow and the surrounding air, the actual noise source generation occurs downstream of the nozzle exit. Experiments to isolate these noise sources have been conducted by several investigators. MacGregor and Simcox (ref. 15) used the so-called "wall isolation technique," where the jet is retracted into a sound-isolated test cell in incremental steps, allowing only part of the jet to radiate outwards. Grosche, Jones, and Wilhold (ref. 16) used a concave mirror-microphone system. More recently, Strout (ref. 9) and Jaeck (ref. 17) used the multiple sideline technique to obtain information on the location of jet noise sources. Since the experiments had inherent jet refraction effects, apparent noise sources were determined.

The experimental data show that noise source location is a function of frequency, directivity angle, power setting, and nozzle type. The frequency dependence is such that low frequencies are generated far downstream, and the high frequencies are generated closer to the nozzle exit. This is in agreement with the turbulence structure along the jet.

The methods used in this study to determine the location of the jet noise sources for the baseline and ejector suppressor configurations are discussed in the following paragraphs.

### B.2.1 BASELINE

The Boeing Lu/Berman flow/noise analytical computer program was used to obtain the baseline jet noise source locations. This computer program (ref. 8 and 18) calculates the fluid mechanics of a multiannular flow turbulent jet, divides the jet in slices or segments one jet diameter long, computes the noise generated by each slice, and finally adds the sound power from all the segments to obtain the noise from the entire jet (fig. B-1). The information on noise source location provided by this computer program is shown in figures B-2 and B-3. Two cases simulating a low power and high power setting for the baseline engines are shown. The figures display the noise contribution of each segment of the jet to the 50-, 200-, and 800-Hz frequencies, at 90° directivity angle and at 100-ft sideline. The maximum of each curve indicates the axial region contributing the most to the noise at the selected frequency and at the selected observer location. The second derivative of these curves near the maximum is very small, showing that a number of segments contribute with similar noise intensity strength. Although this indicates that the assumption of a point source is not rigorously correct, jet noise can be thought, as a first approximation, to be generated by acoustic point sources distributed along the jet axis. In this study, the point source is associated with the segment corresponding to the maximum of curves similar to those shown in figures B-2 and B-3.

Comparison of the extrapolation results using the noise source locations, provided by the analytical program and those obtained from two empirical methods is presented in figures B-4 through B-6. The figures show the analytical method to represent an average of the two empirical methods at low frequencies, and to agree well with them at high frequencies.

The noise source locations used in the extrapolation of the baseline jet noise data are plotted versus Strouhal number in figure B-7.

### B.2.2 EJECTOR SUPPRESSOR

Noise source locations for the ejector suppressor configurations were determined from experimental data obtained with a model scale ejector suppressor, using a multiple sideline technique. The 20-lobe model scale ejector suppressor was tested in the Boeing anechoic chamber under NASA-sponsored contract NAS2-8213. The simulation differed from the full scale in that a single flow was used instead of the full-scale dual flow. Noise was recorded by three parallel sideline microphone arrays.

Two jet noise generation regions are distinguished in this configuration. The premerging noise region is located inside the shroud and the postmerging noise region is located downstream of the shroud exit. Noise sources of the premerging noise regions are located inside the shroud and therefore would appear to an observer as being located at the shroud exit plane. Noise sources of the postmerging region, however, are distributed downstream of the shroud exit plane. In reality, the ejector suppressor noise generation mechanism includes complex interaction of the internal sound field with both the nozzle and the internal and

external flows. This greatly complicates the determination of noise source locations for this configuration.

Although the flow/noise analytical computer program does not have the capability of studying ejector suppressor type nozzles, it was used to obtain information on the postmerging jet noise source locations. The postmerging jet was simulated as a low-velocity single jet. Velocity and total temperature profiles at the shroud exit were used as inputs to the computer program. These flow parameters were obtained from the static propulsion data.

Comparison of the experimental noise source location data (anechoic chamber) and the analytical simulation is shown in figure B-8. The experimental and the analytical results show that noise sources are not located far downstream of the nozzle exit (shroud exit) except for the high power settings. This indicates that the noise source location correction effect on the extrapolation of the low power settings will be small.

Differences between the experimental and analytical results are evident at high power settings. These differences are thought to be due to the ejector suppressor complex noise generation mechanism which the analytical computer program is not able to simulate. In order to account for the effects associated with the more complex ejector suppressor noise generation mechanism, the curves derived from the experimental data were used in the extrapolation of the ejector suppressor static jet noise data.

## B.3 FAN NOISE SOURCE LOCATIONS

Fan noise is generated inside the engine and propagates forward (inlet fan noise) and aft (aft fan noise). This characteristic has an important effect on the fan noise directivity pattern and thus in the extrapolation of the fan noise data. Fan noise sources are assumed to be located at the inlet plane for inlet fan noise and at the fan exhaust plane for aft fan noise.

To determine the range of angles dominated by the inlet fan noise and exhaust fan noise, a study was conducted with both baseline and ejector suppressor static 1/3-octave-band noise data. Acoustic data corresponding to the inlet and/or exhaust muffler runs were compared with those of a bare engine. Results of these comparisons are presented in figure B-9 for the baseline configuration and in figure B-10 for the ejector suppressor nacelle. These results indicate that inlet fan noise dominates the forward arc angles from 10° to 60°, and the aft fan noise dominates the aft sideline angles of 100° and higher. Consequently, fan noise sources were assumed located at the inlet for microphone angles from 10° to 60° polar arc and at the exhaust for microphone angles from 100° to 160° sideline. (See fig. 6 for static test microphone array layout.) No clear separation of inlet and aft fan noise is possible for the microphone angles 70°, 80°, and 90° polar and 70°, 80°, and 90° sideline. For this study, however, apparent noise sources, located in the engine centerline between the inlet and exhaust planes, were defined for each of these microphone angles. The location of these sources was determined so that the extrapolated polar and sideline noise data corresponding to these microphones give compatible results.

- TURBULENT JET FLUID MECHANICS
- LIGHTHILL NOISE FORMULATION
- FFOWCS WILLIAMS FLIGHT DOPPLER FACTOR

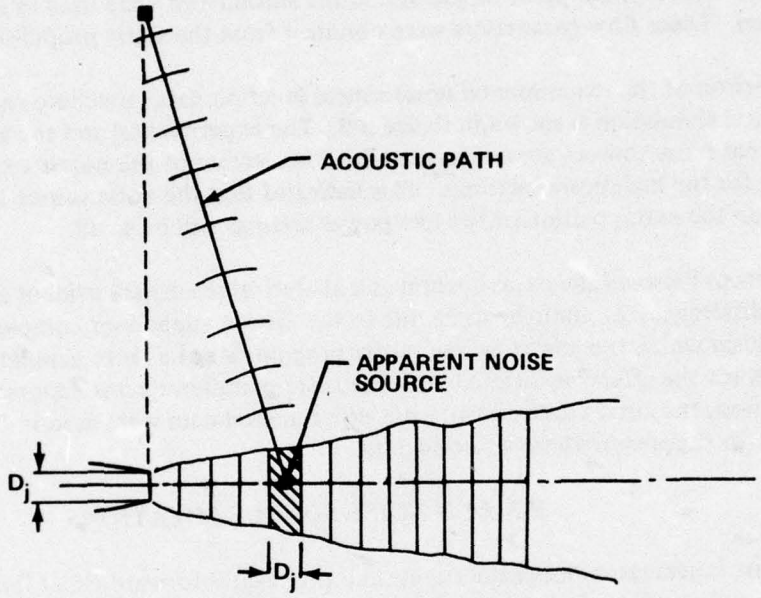


*Figure B-1.—Lu/Berman Flow/Noise Analytical Program Schematic*

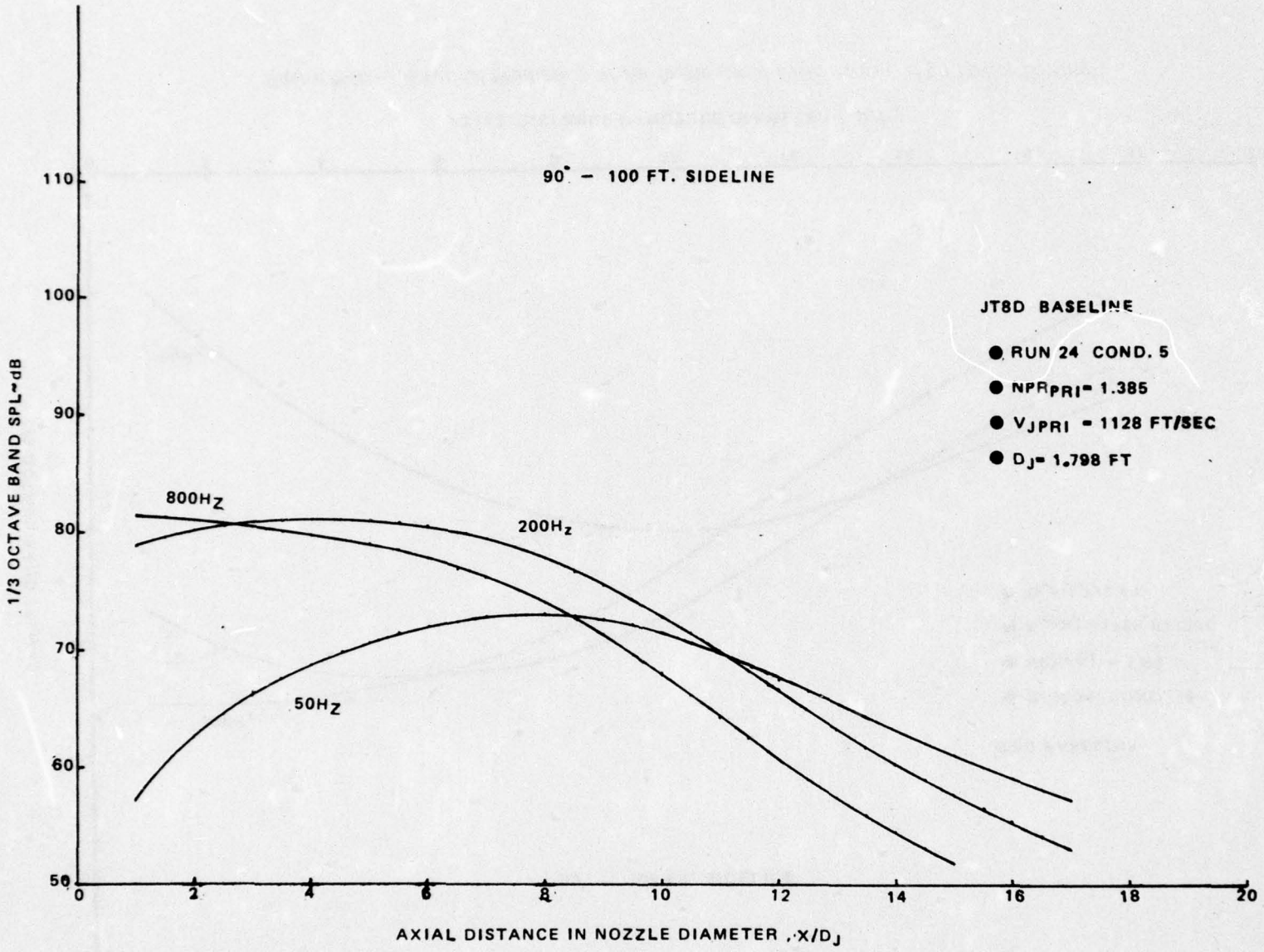


*Figure B-2.—Analytical Prediction of Jet Noise Axial Distribution, Low Power Setting*

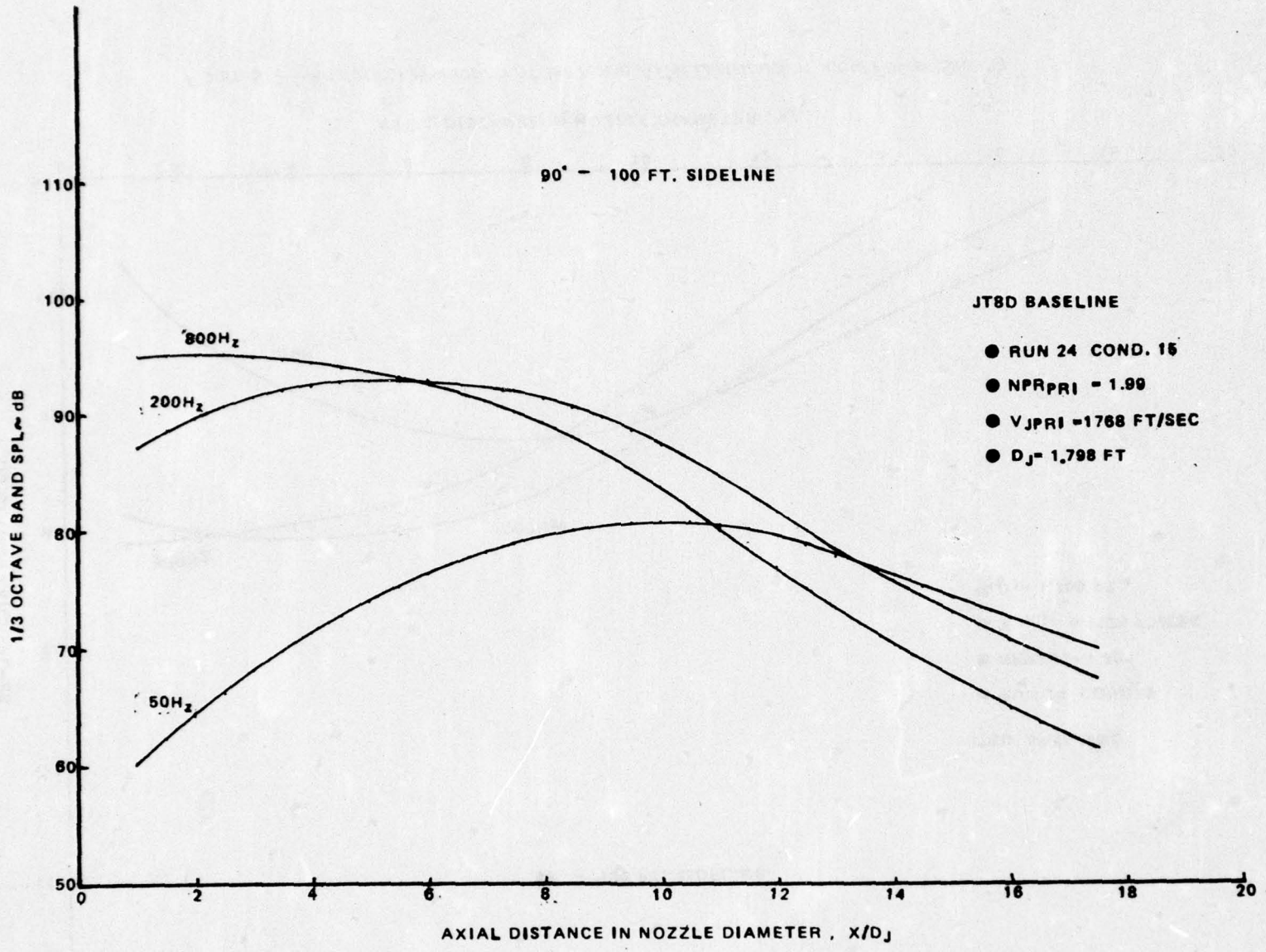


*Figure B-3.—Analytical Prediction of Jet Noise Axial Distribuiton, High Power Setting*

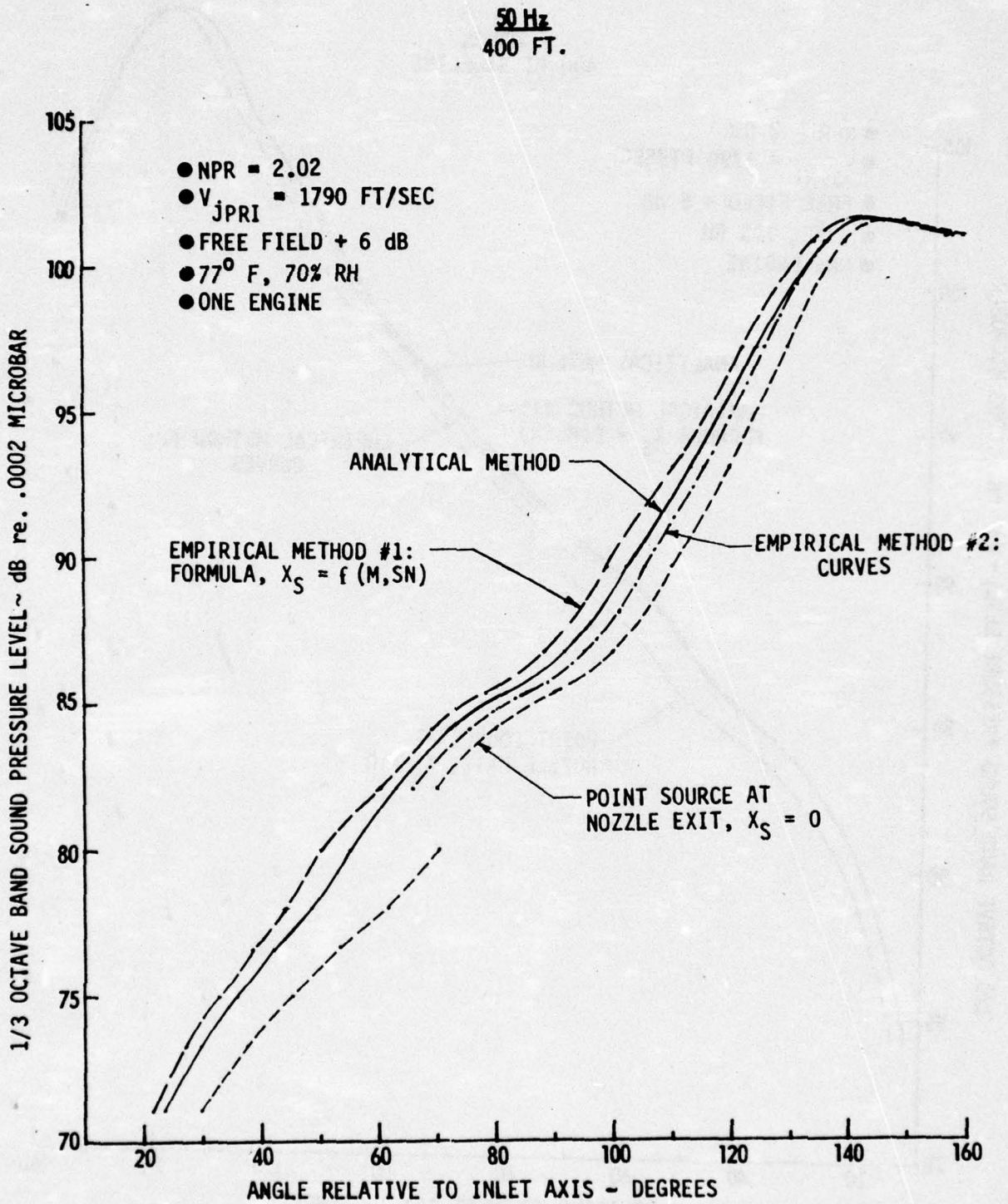


*Figure B-4.—Comparison of Extrapolation Results Using Analytical and Empirical Noise Source Location Methods, 50 Hz*

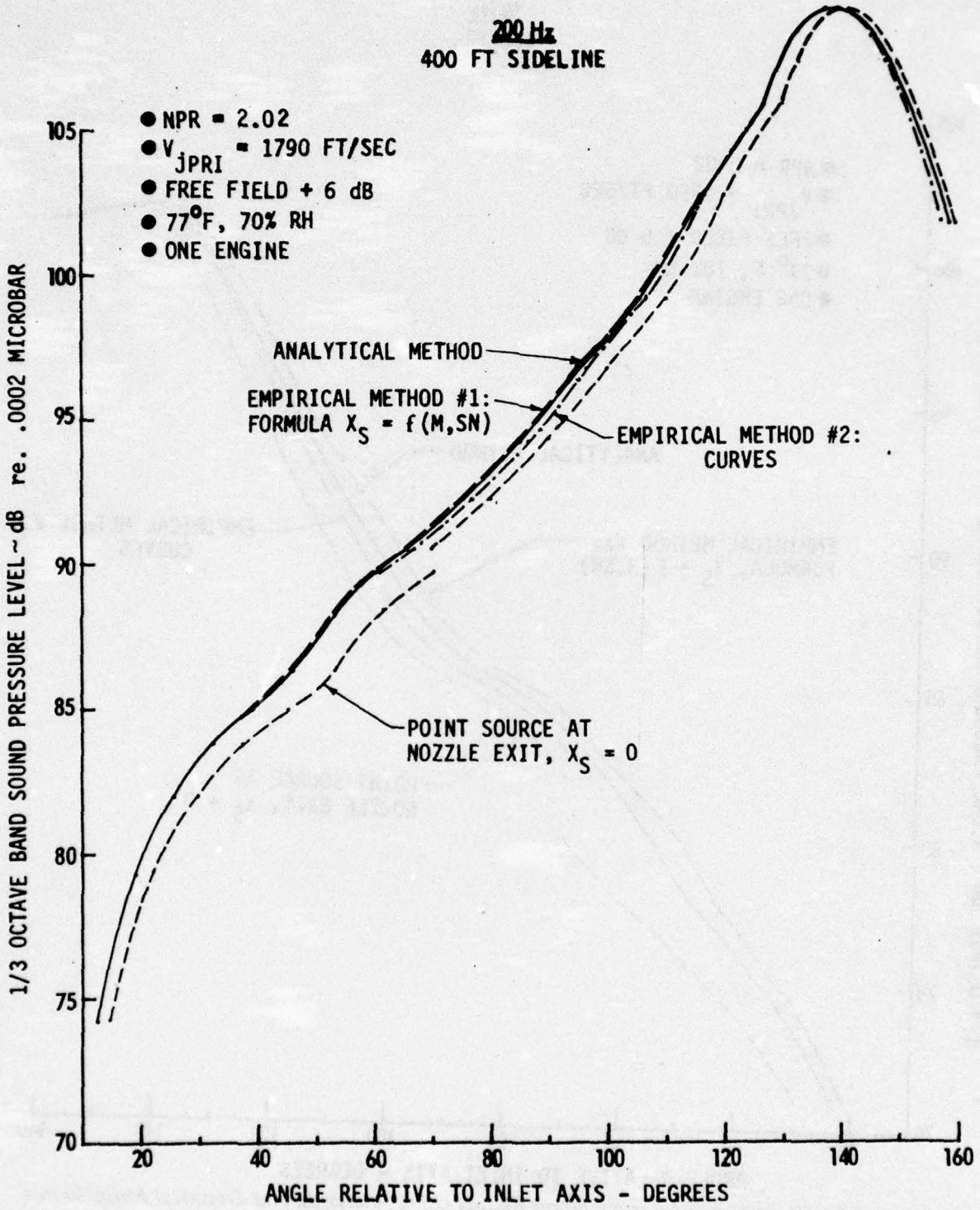


*Figure B-5.—Comparison of Extrapolation Results Using Analytical and Empirical Noise Source Location Methods, 200 Hz*

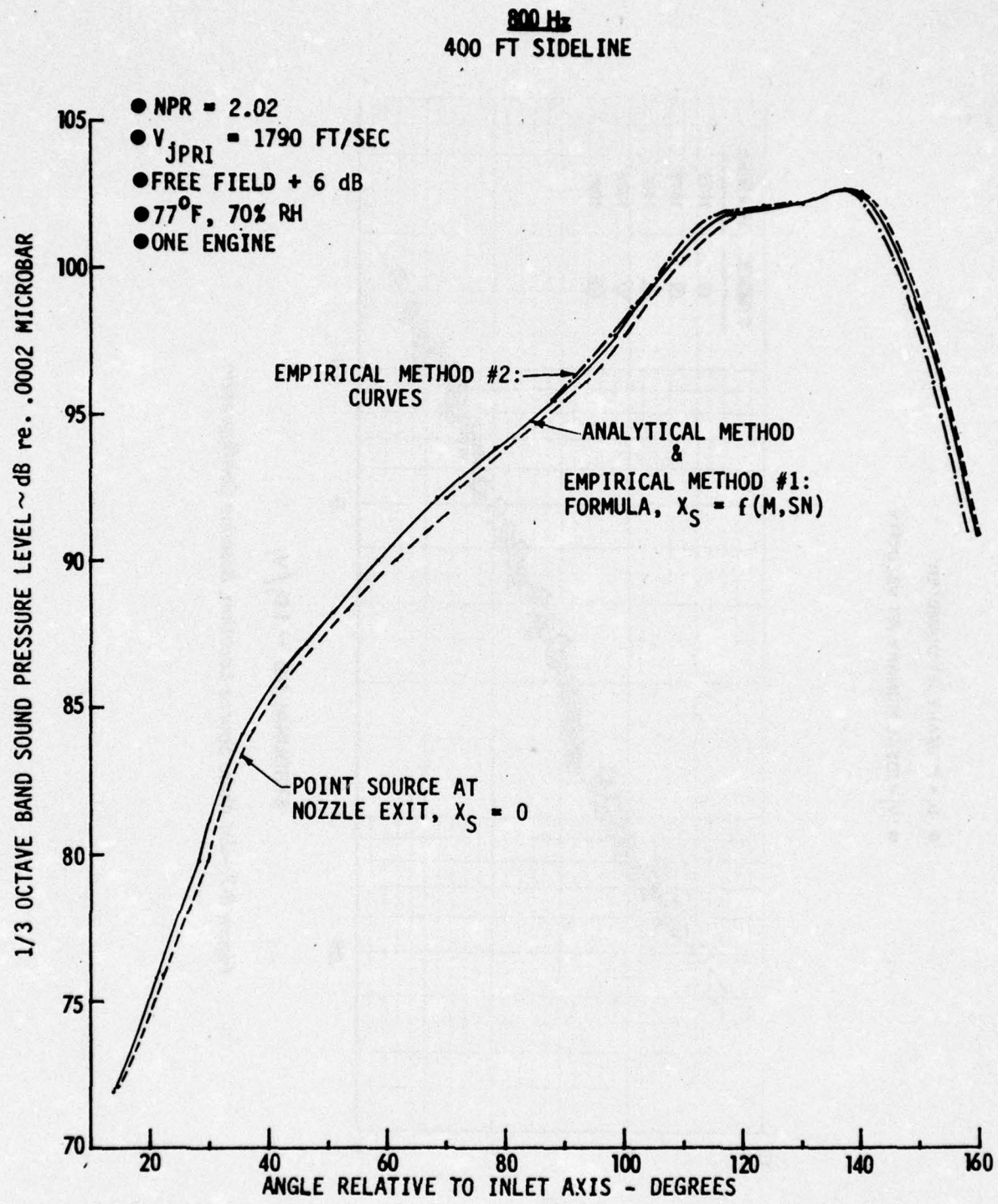


*Figure B-6.—Comparison of Extrapolation Results Using Analytical and Empirical Noise Source Location Methods, 800 Hz*

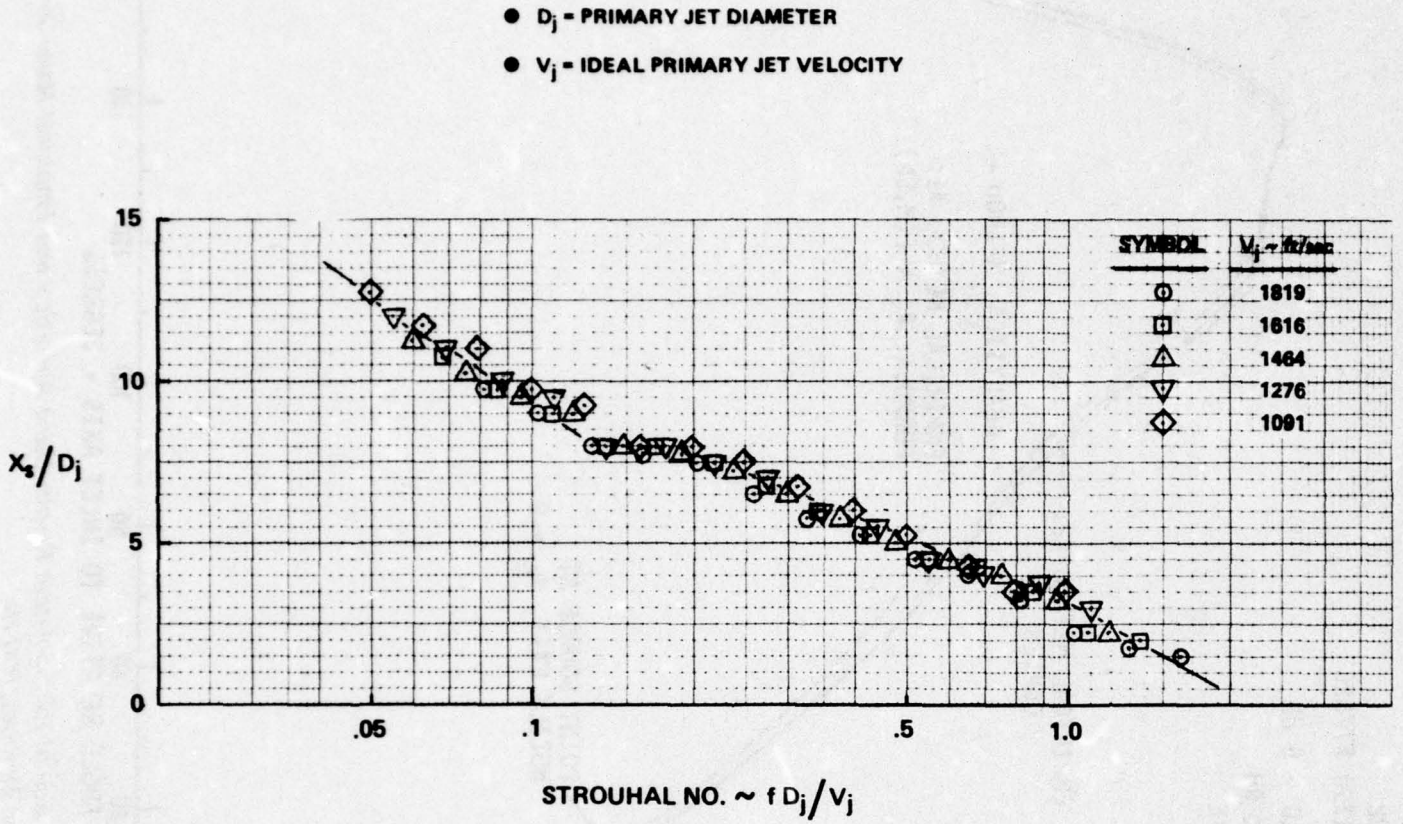


*Figure B-7.—Jet Noise Source Location, Baseline Configuration*

- $D_j$ = DIAMETER SHROUD EXIT = 3.58 FT.
- $V_j$ = IDEAL JET VELOCITY AT SHROUD EXIT ~ FT/SEC

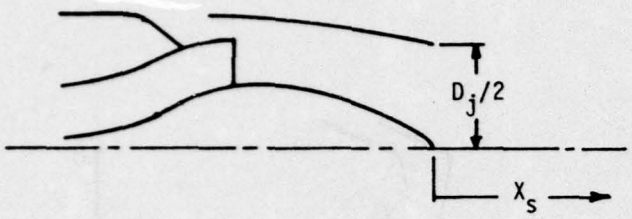


OPEN SYMBOLS ~ MULTIPLE SIDELINE TECHNIQUE *

| | $P_{T_7}/P_{am}$ | $T_T$ ~ °R (SHROUD EXIT) |
|---|---|---|
| ▲ | 2.25 | 1180° |
| ⊡ | 1.75 | 1175° |
| ⊙ | 1.44 | 1160° |

CLOSED SYMBOLS ~ ANALYTICAL PREDICTIONS (LU/BERMAN)

| | | |
|---|---|---|
| ● | 1.885 | 1060° |
| ■ | 1.687 | 1010° |

* NOTE: LTC DATA, SINGLE FLOW

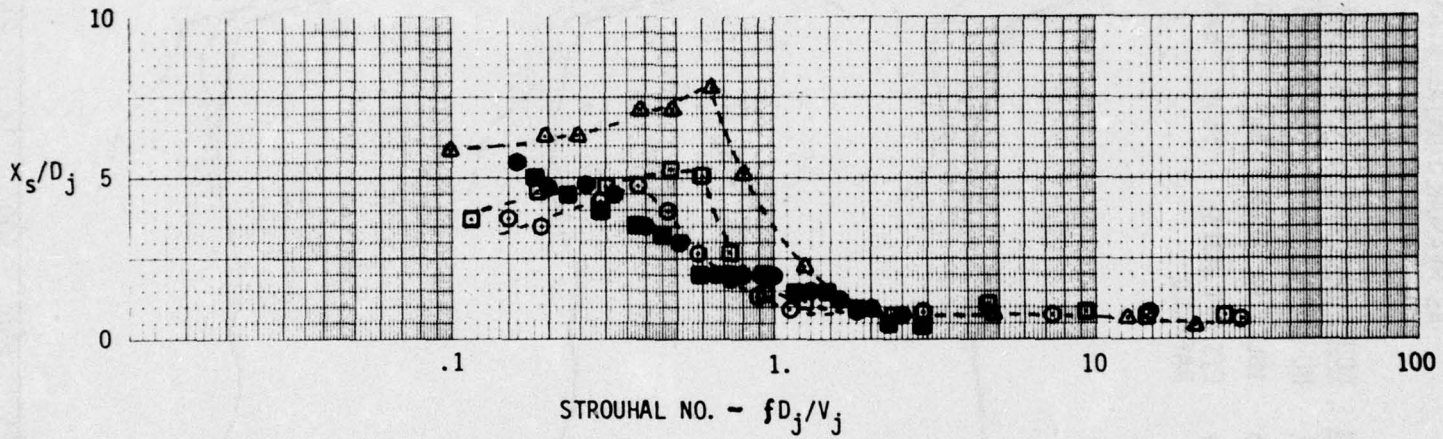


*Figure B-8.—Noise Source Location, 20-Lobe/Ejector Suppressor*

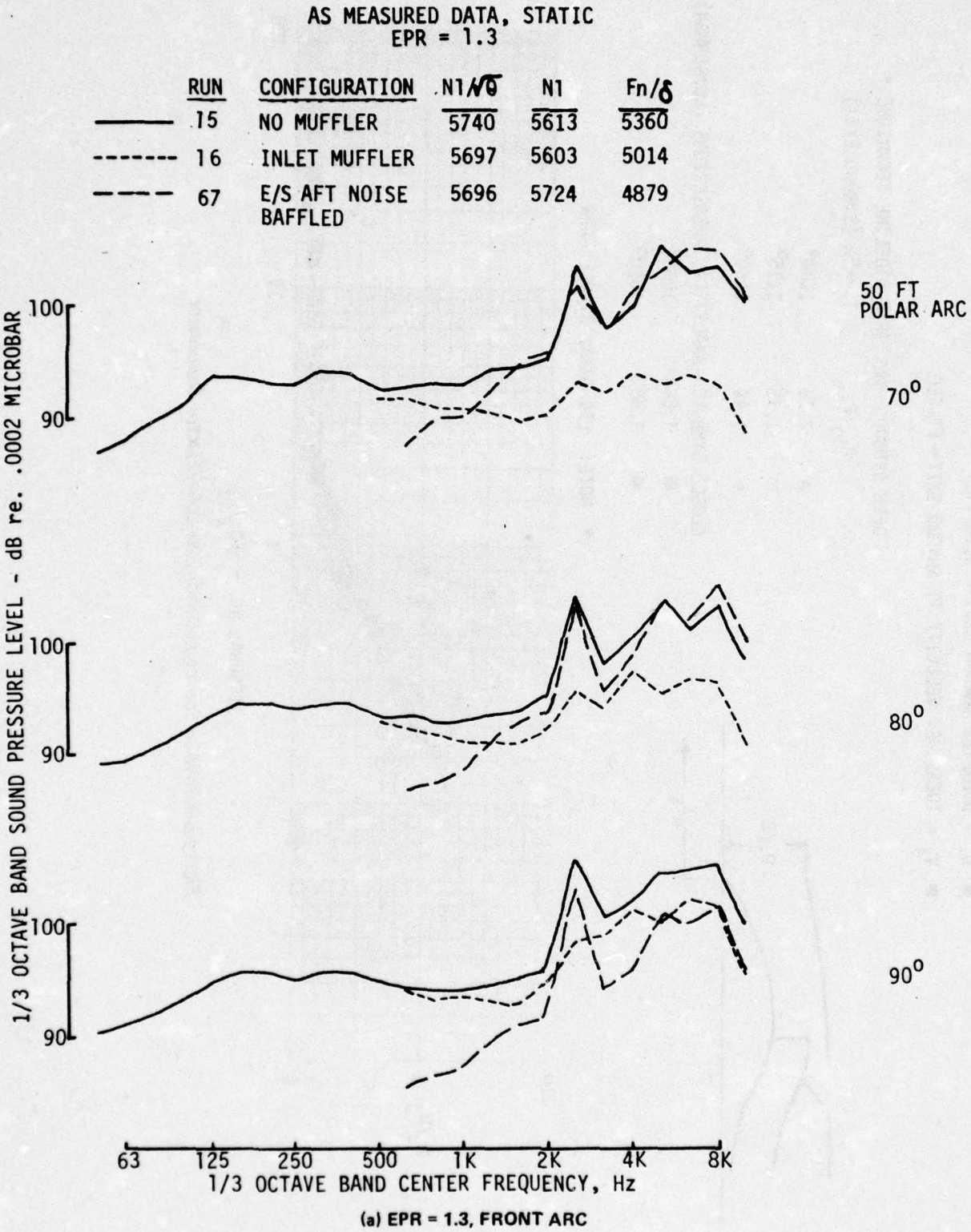


(a) EPR = 1.3, FRONT ARC

*Figure B-9.—Baseline Configuration Static Test Results*

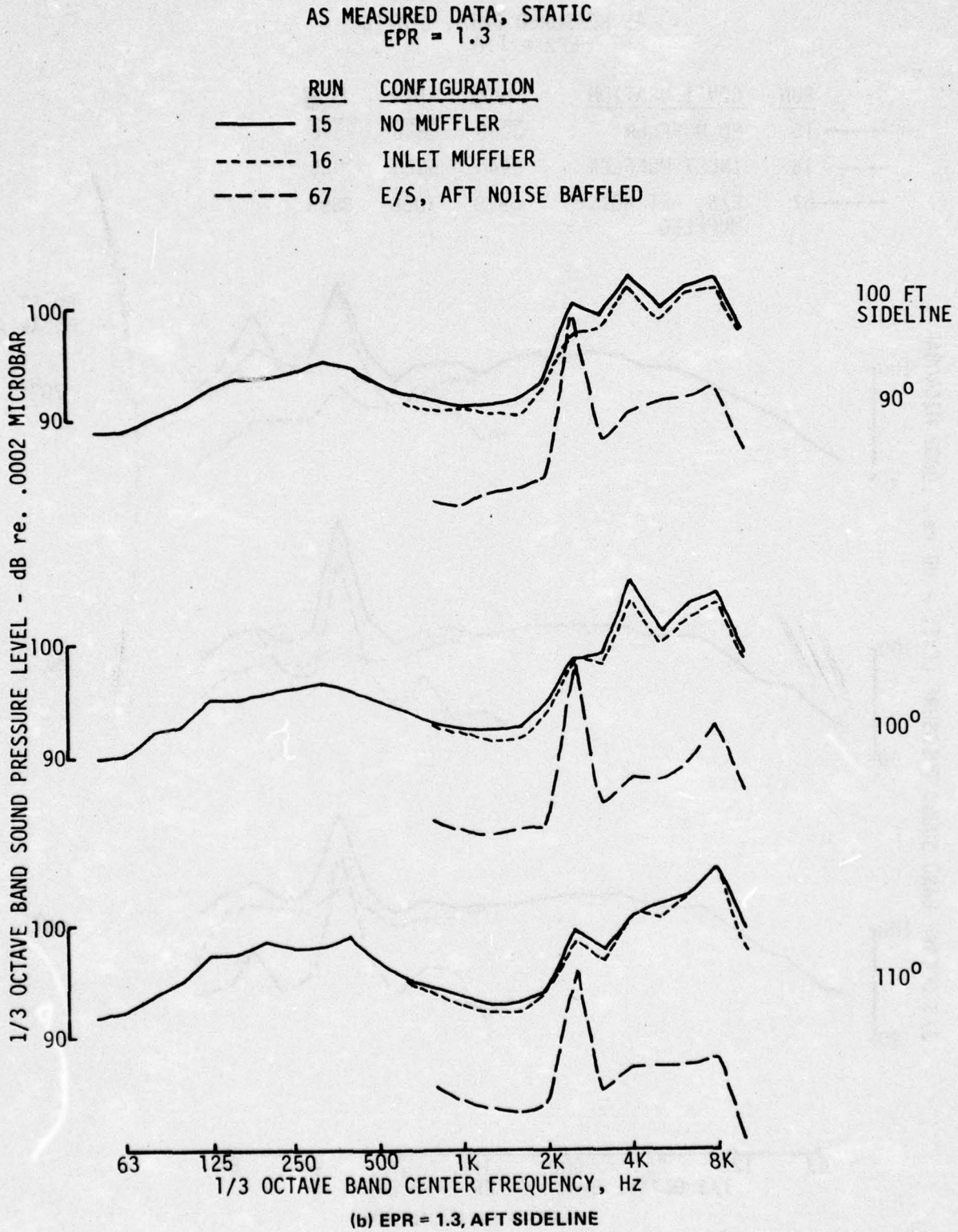


**(b) EPR = 1.3, AFT SIDELINE**

*Figure B-9.—(Continued)*

AS MEASURED DATA, STATIC
EPR = 1.6

| | RUN | CONFIGURATION | $N1/\sqrt{\theta}$ | N1 | Fn/δ |
|---|---|---|---|---|---|
| ——— | 15 | NO MUFFLER | 6985 | 6836 | 9598 |
| - - - - - | 16 | INLET MUFFLER | 6940 | 6826 | 9026 |
| — — — | 67 | E/S, AFT NOISE MUFFLED | 6978 | 7006 | 8893 |

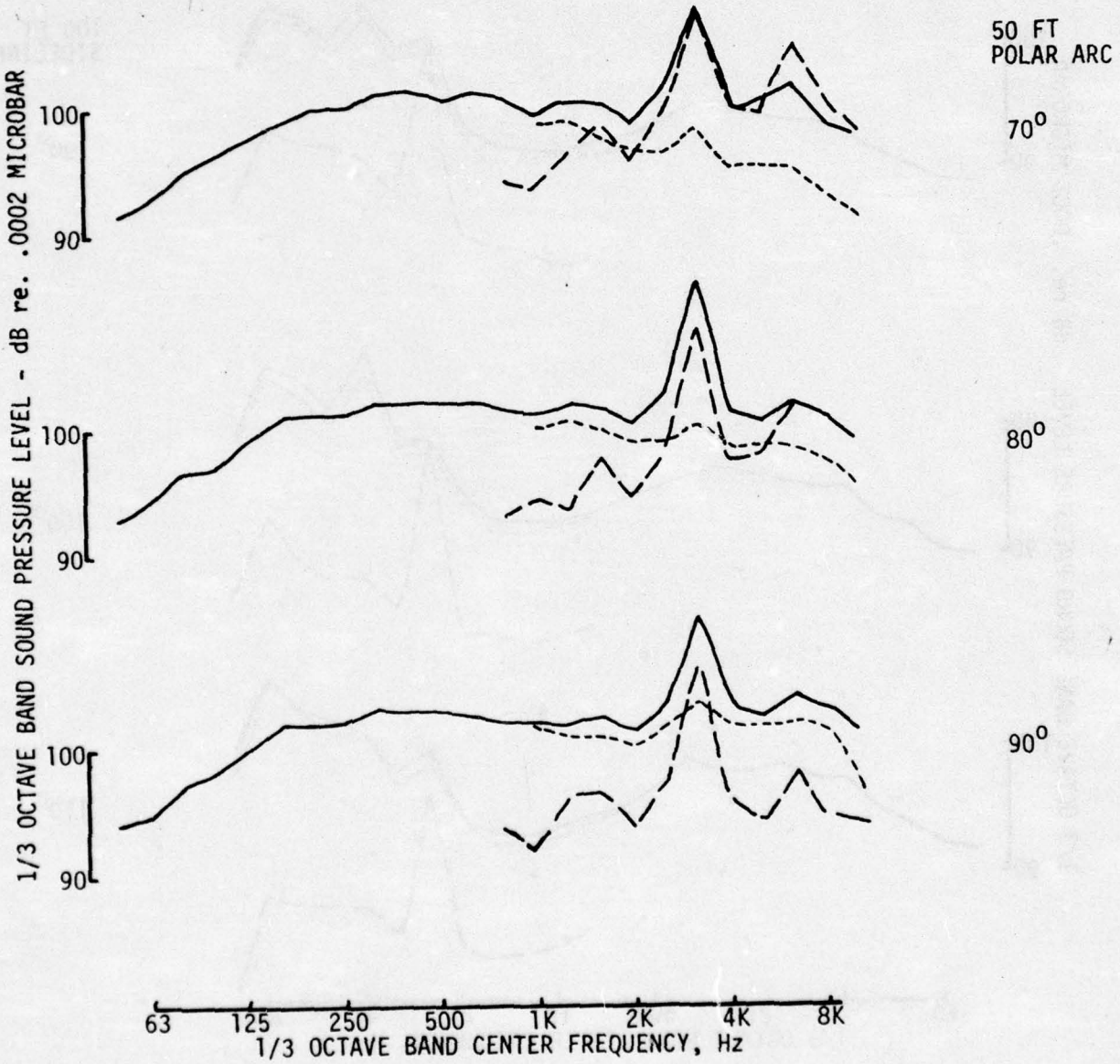


(c) EPR = 1.6, FRONT ARC

*Figure B-9.—(Continued)*

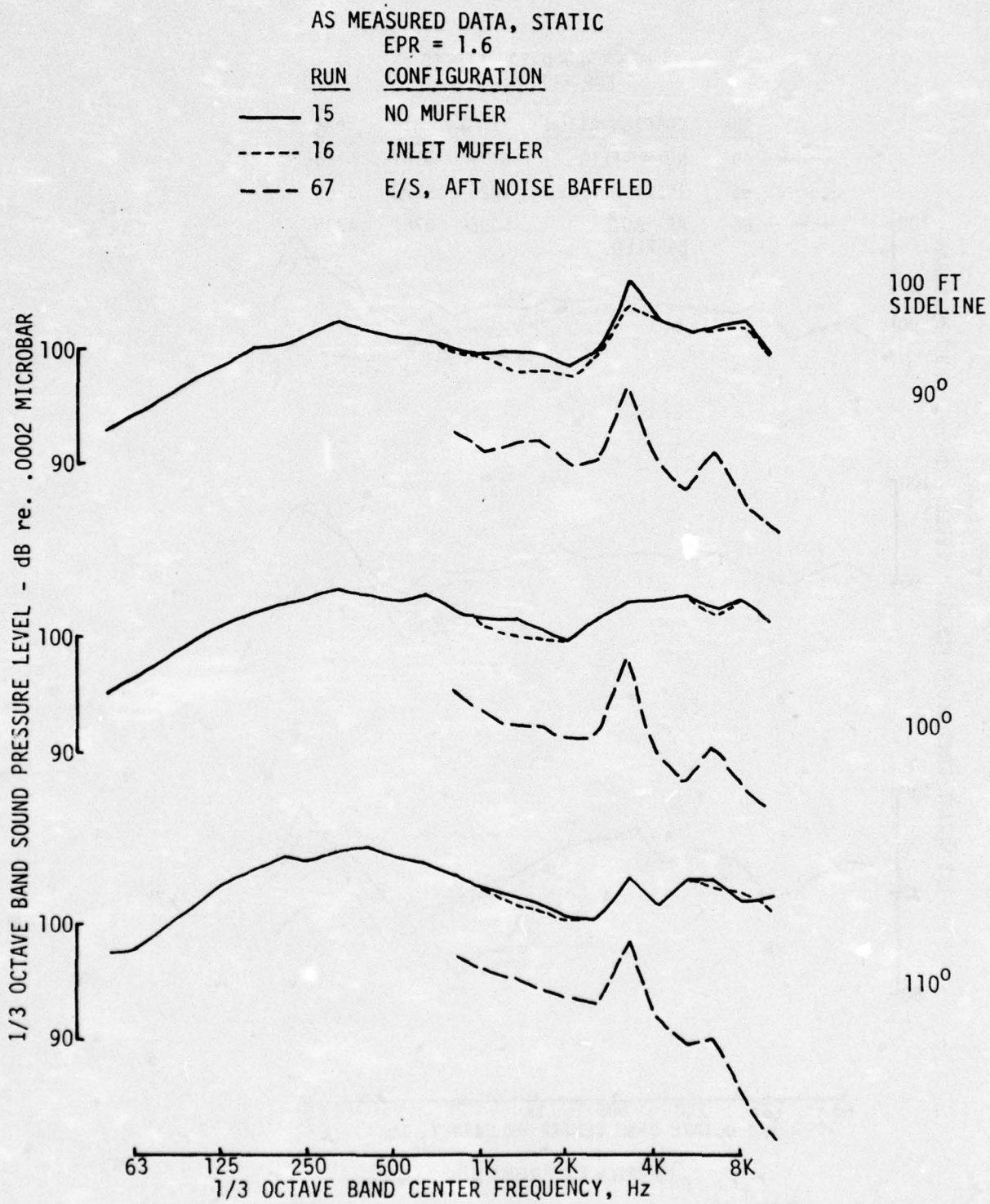


**(d) EPR = 1.6, AFT SIDELINE**

*Figure B-9.—(Concluded)*

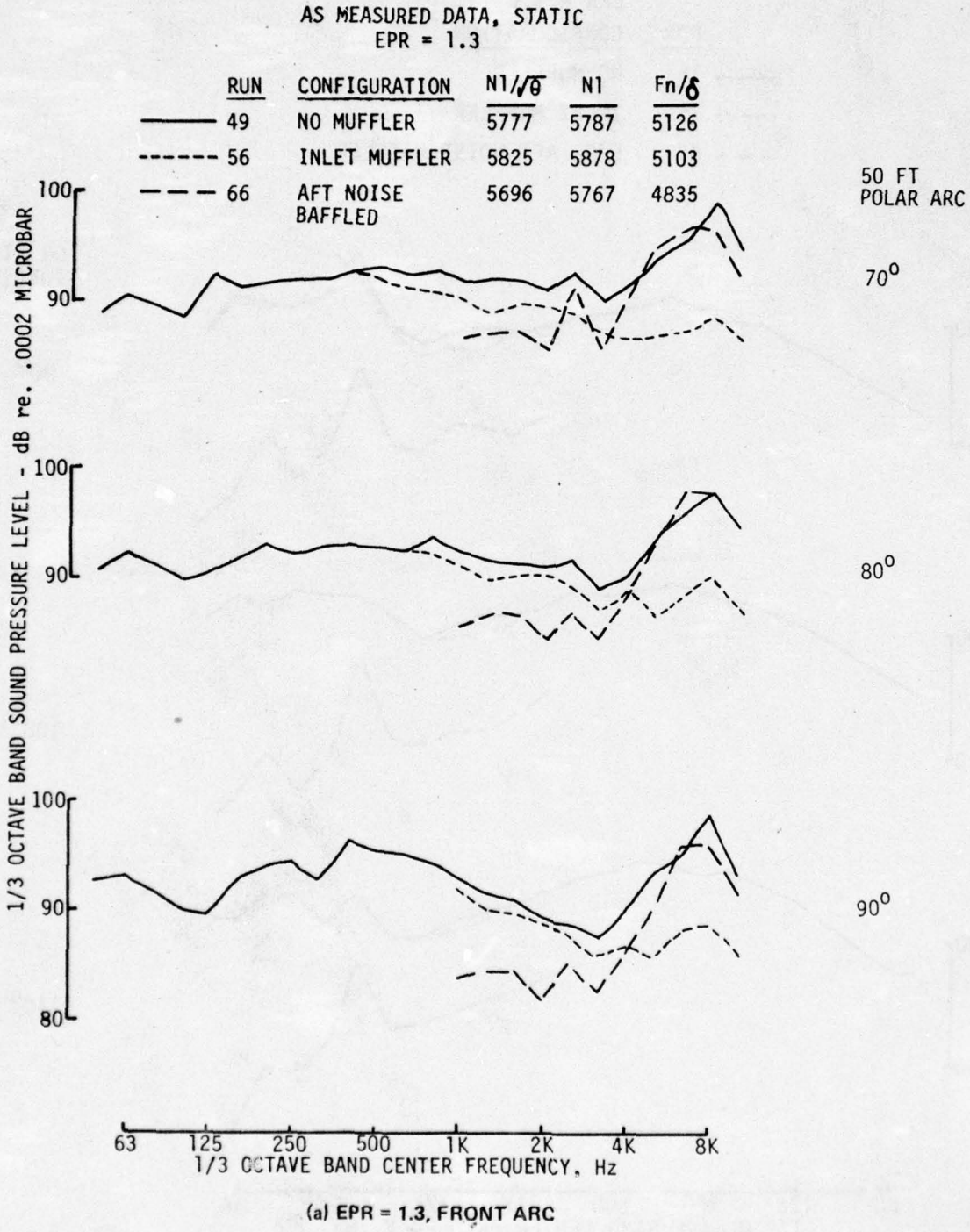


(a) EPR = 1.3, FRONT ARC

*Figure B-10.—Ejector Suppressor Configuration Static Test Results*

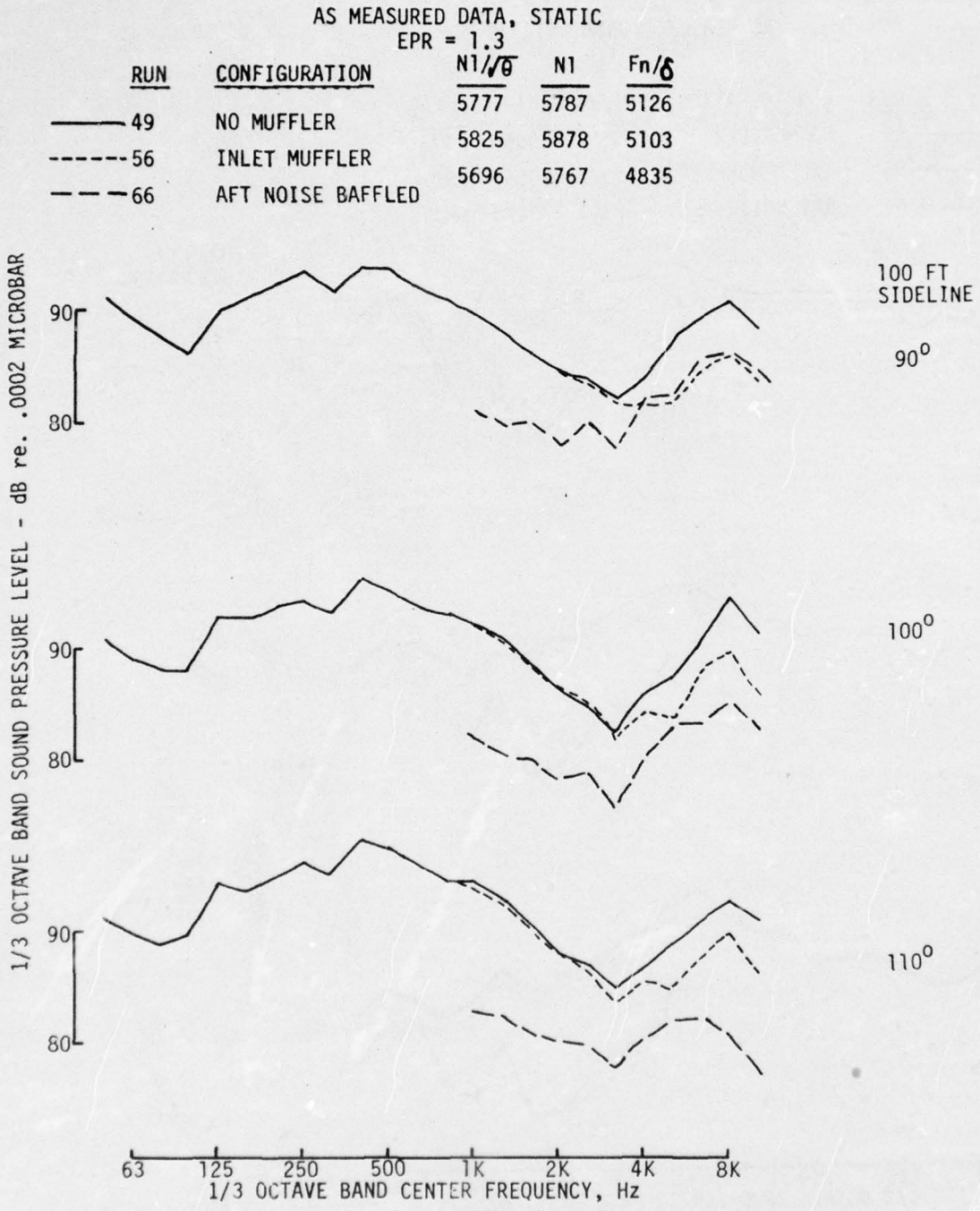


**(b) EPR = 1.3, AFT SIDELINE**

*Figure B-10.—(Continued)*

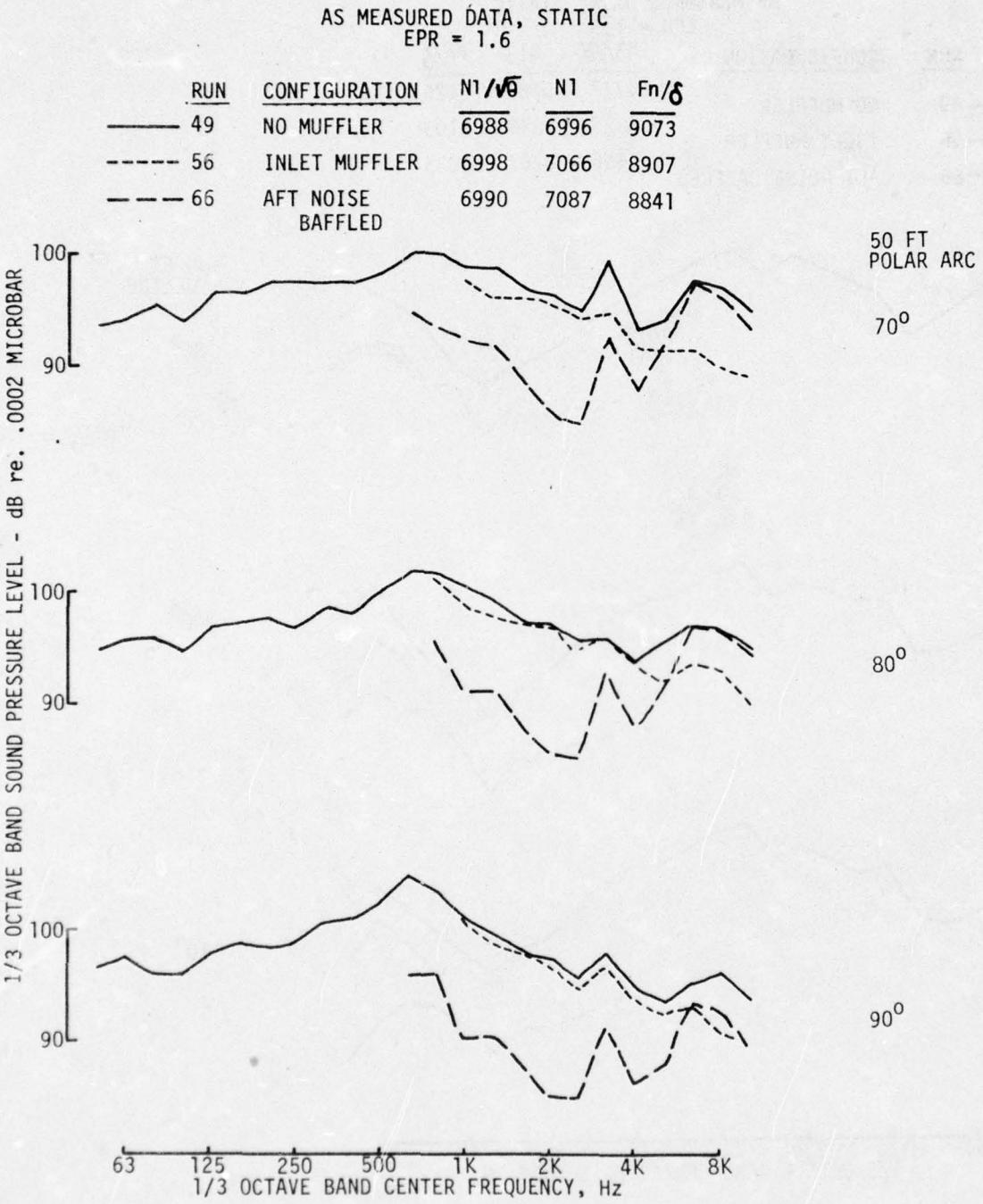


(c) EPR = 1.6, FRONT ARC

*Figure B-10.—(Continued)*

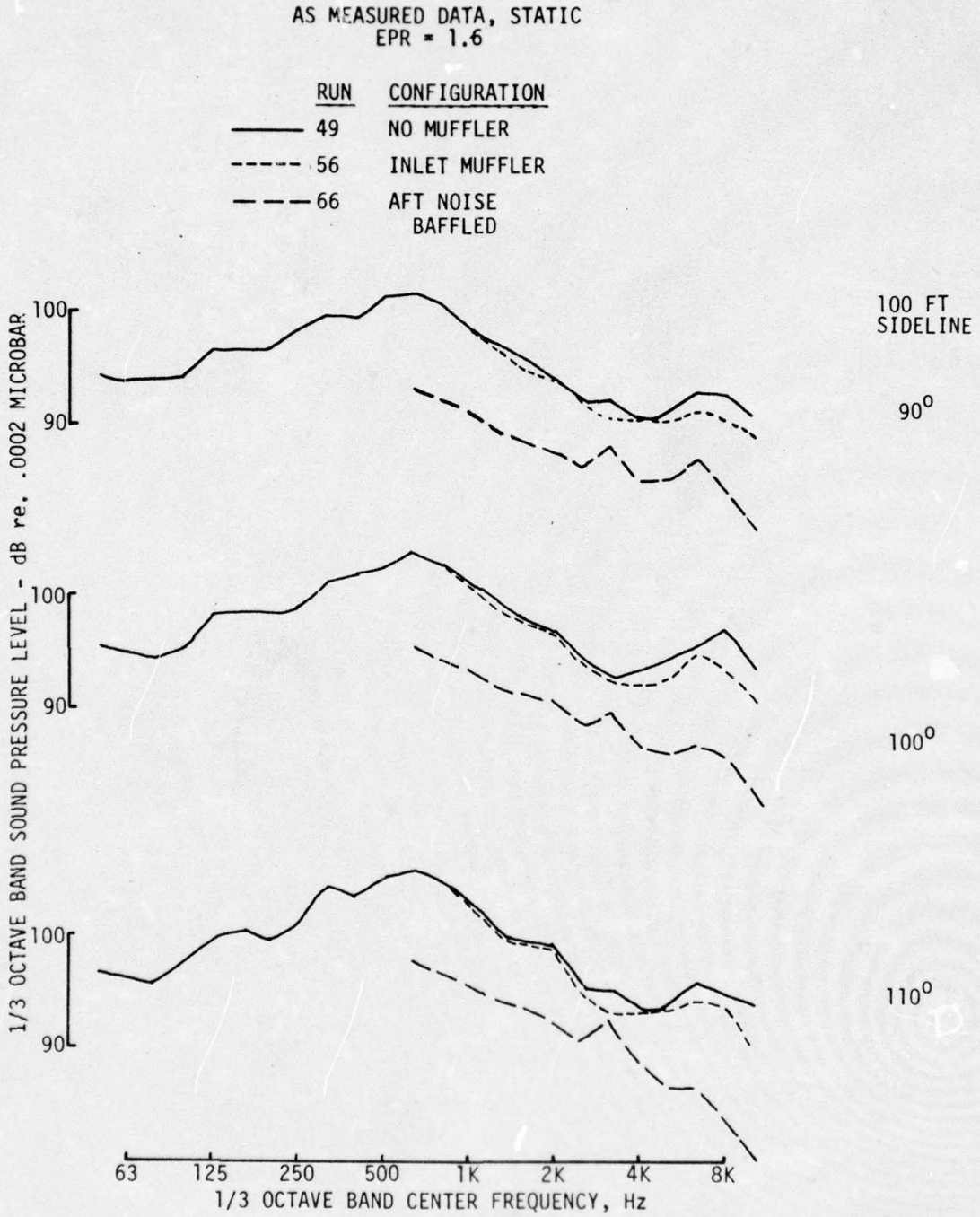


**(d) EPR = 1.6, AFT SIDELINE**

*Figure B-10.—(Concluded)*

# APPENDIX C
# JET AND FAN NOISE STATISTICAL ANALYSIS

The recorded noise signals represent a finite time history or sample record of a random physical phenomenon (pressure fluctuations created by sound waves). The properties of random data are described by using statistical functions. The intensity of a random signal is described by a mean square value which is simply the average of the squared values of the time history during a certain time period T. The goodness of the intensity estimate (i.e., how close the estimate is to the true value of the population) depends on such factors as the length of the averaging period and the type of random signal, stationary or nonstationary, under study.

In a static test, jet and fan broadband noise are generally assumed to be the result of stationary processes. In addition, noise records can be made for a long sample time which permits good mean value estimates from each time sample. The flight noise data, however, are not stationary. Nevertheless, for short time intervals the airplane moves little in relation to the microphones, and the assumption that the random noise signal is stationary can be made. As a result, a compromise has to be made between the integration time required to obtain good estimates and the short time interval over which stationarity of the signal can be assumed. Another problem existing in the analysis of noise data is the unrepeatability or data scatter due to the large number of variables involved, which cannot be controlled. This causes the signal to be nonergodic, and several sample records are then required to assure good mean values estimates. As was mentioned in section 3, several repeated static and flight data were used to obtain the final noise average.

Attention in this appendix is first focused on the integration time selection for the flight data. As mentioned previously, this integration time is an important factor in the statistical quality of the flight data. The theory of uncertainty of random noise is reviewed and the results obtained by using different integration times are discussed. Later the appendix addresses an interesting aspect of fan noise analysis—that of the variation of the tone peak amplitude with time.

## C.1 INTEGRATION TIME FOR JET NOISE FLIGHT DATA ANALYSIS

A conflicting situation is found in the flight noise data analysis. Long integration times are required to statistically reduce uncertainties due to the random fluctuations of the noise signal. However, as a result of airplane motion, difficulties in correlating noise with airplane position increase with the integration time, thus giving rise to a bias error. The uncertainties of the noise signal (pressure) are generally expressed as a confidence interval. For a Gaussian noise (amplitude obeys a normal distribution), the confidence intervals are obtained by using the chi-square distribution (ref. 19 and 20) with the number of degrees of freedom, n, defined as

$$n = 2 B_e T$$

where

$B_e$ = effective frequency bandwidth
$T$ = integration time

As the integration time increases, the number of degrees of freedom increases (linearly) and the confidence intervals are reduced. Table C-1 shows the single-sample 90% confidence interval for five integration times at 200 Hz, 1/3-octave-band center frequency. Since 1/3-octave-band frequency bandwidths are a function of the band center frequency, the preceding equation indicates a dependence of n on the band center frequency.

For flight noise data, the noise levels obtained in each integration time interval were correlated with the airplane position at the time corresponding to the center of the time interval. During the integration interval, the noise level changes because of airplane motion (airplane-observer distance change) and noise directivity shape. This gives rise to a difference between the "true" noise level at the time corresponding to the center of the integration interval, and the noise level obtained from the integration. This difference or bias error is a function of the directivity angle and is always negative; the "true" noise level is lower than the integration noise level, except in some cases at the peak directivity. Consequently, the flight effect results (static levels minus flight levels) using the flight noise levels from the integration will be conservative for those cases where noise reduction occurs in flight.

Baseline and ejector suppressor (figs. C-1 and C-2) configuration flight noise data are shown plotted versus time for three different integration times, 0.1, 0.2, and 0.5 sec. The noise data shown were plotted at the center of each integration time interval. Data corresponding to the 0.5-sec integration time can be considered as an average of the others for the region of positive directivity curve slope and slightly higher than the average for the negative directivity curve slope. Based on the 200-Hz directivity slope (fig. C-1, view (C)), the bias errors at 90° directivity angle are shown in table C-2 for five integration times. Also shown are the total (uncertainty and bias error) 90% confidence intervals for each of these five integration times.

Examination of figures C-1 and C-2 and table C-2 indicates that for this study the 0.5-sec integration time gives the best tradeoff between signal fluctuation uncertainty and airplane motion.

## C.2 FAN TONE TIME HISTORY

Fan tone generation is generally associated with the pressure fluctuations caused by the rotor blades and the stator vanes of a fan. The pressure fluctuations originate from a variety of sources. Common major causes of the pressure fluctuations are wakes trailing blades and vanes, inflow turbulence and vortices, and boundary layers within the inlet. Mechanical asymmetry in the fan geometry causes modulations in the levels and frequencies of the tones being generated. It is therefore easy to realize that fan tones would not be pure tones of constant amplitudes nor fixed frequencies. Fan tones are found to be very narrow band noise (pseudo tones) concentrated near the blade passage frequency or its harmonics. The test data show that the amplitudes of the peaks of these tones vary widely as a function of time.

Figures C-3 and C-4 are examples of the fan tone noise level time histories of the baseline and ejector suppressor configurations, obtained from analyzing the static noise records. These traces were obtained by locking the narrowband analyzer on the fan first-stage fundamental blade passage frequencies and processing the sound pressure signals every 0.05 sec. The filter bandwidth used was 20 Hz nominal.

These level variations are predominantly of random nature (ref. 21), and the four time histories presented and others analyzed seem to confirm this. For the comparison studies of this contract work, time-varying tone levels were averaged for a nominal duration of 32 sec, and the resulting averages were used to represent the static tone levels. Figures C-3 and C-4 include the averaged values that correspond to the time histories shown. Since the averaging time was very long, the averaged values used in the comparison study are considered to be sufficiently close to the true averages of the static fan tone levels.

Because of the Doppler frequency shift, in-flight fan tone time histories are extremely difficult to obtain from static measurements. Reference 22 shows a decrease in the fan tone variation from static to flight for an engine without IGV's. The tone variations were measured by microphones placed inside the inlet. The observed reduction is attributed to the in-flight inlet cleanup effect. Since the tone levels are also reduced in flight by the same effect for engines with IGV's, a smaller tone variation with time is expected in flight than is seen in static data.

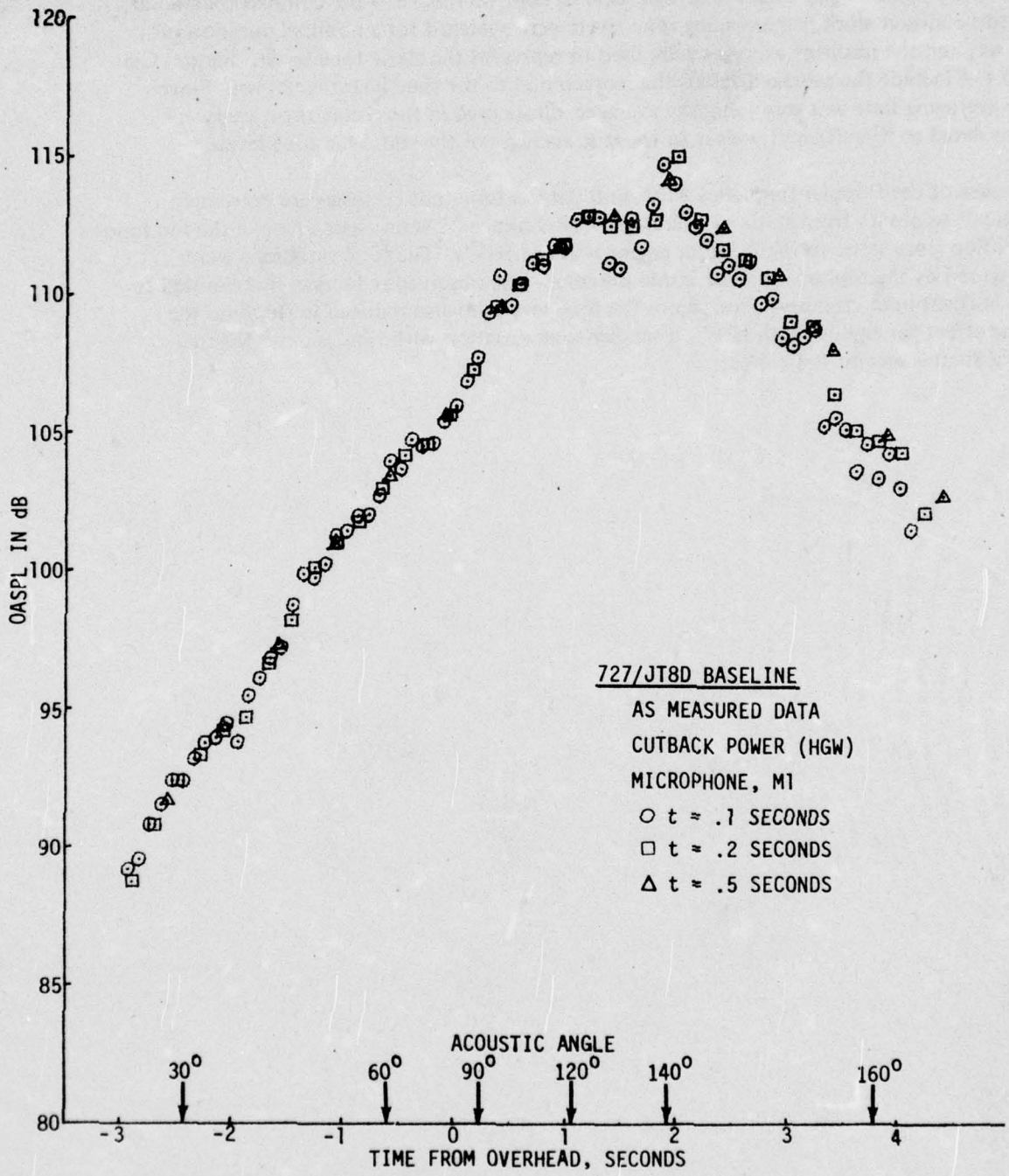


(a) INTEGRATION TIME EFFECT ON OASPL

*Figure C-1.—Baseline Configuration Flight Noise Data Analysis*

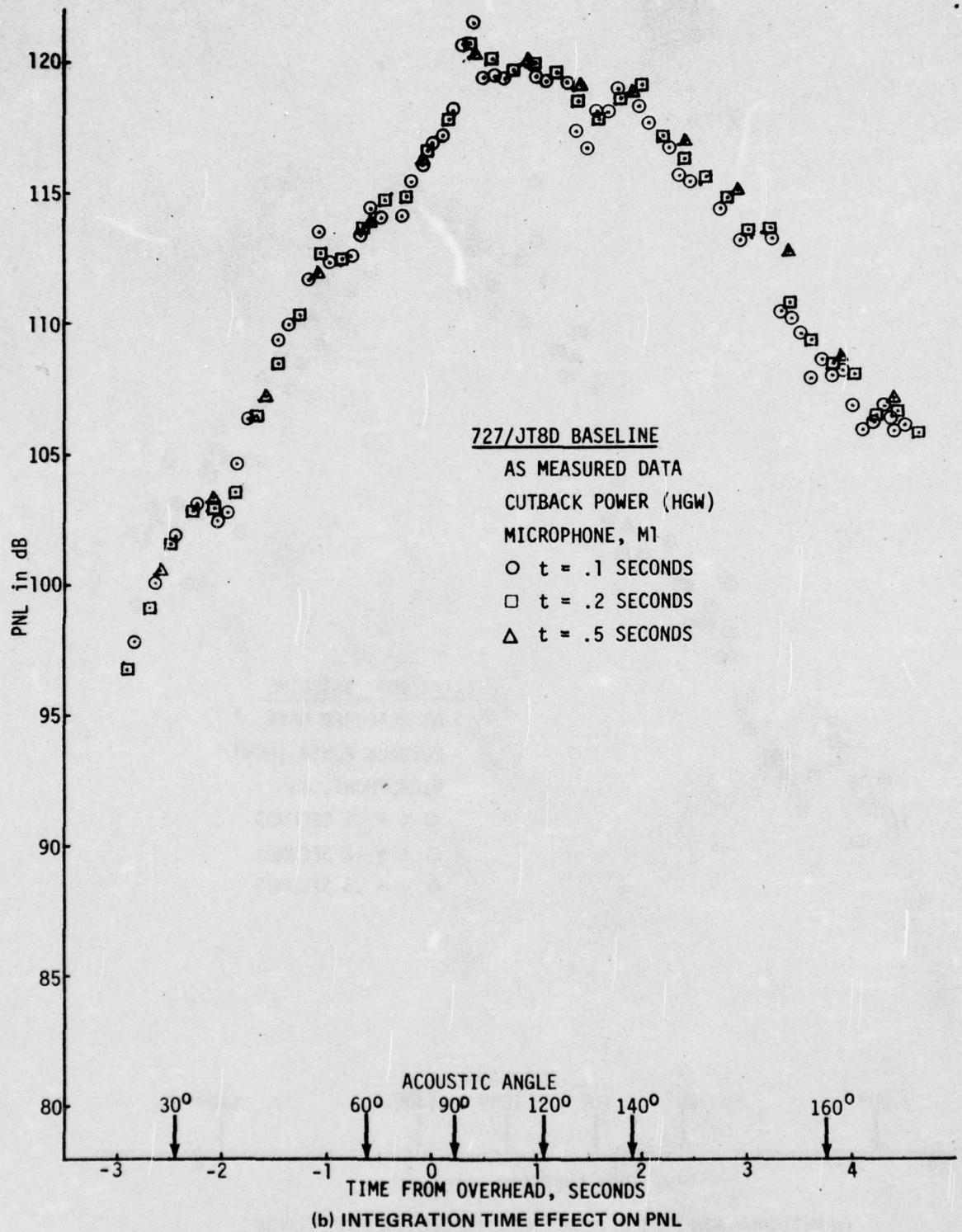


(b) INTEGRATION TIME EFFECT ON PNL

*Figure C-1.—(Continued)*

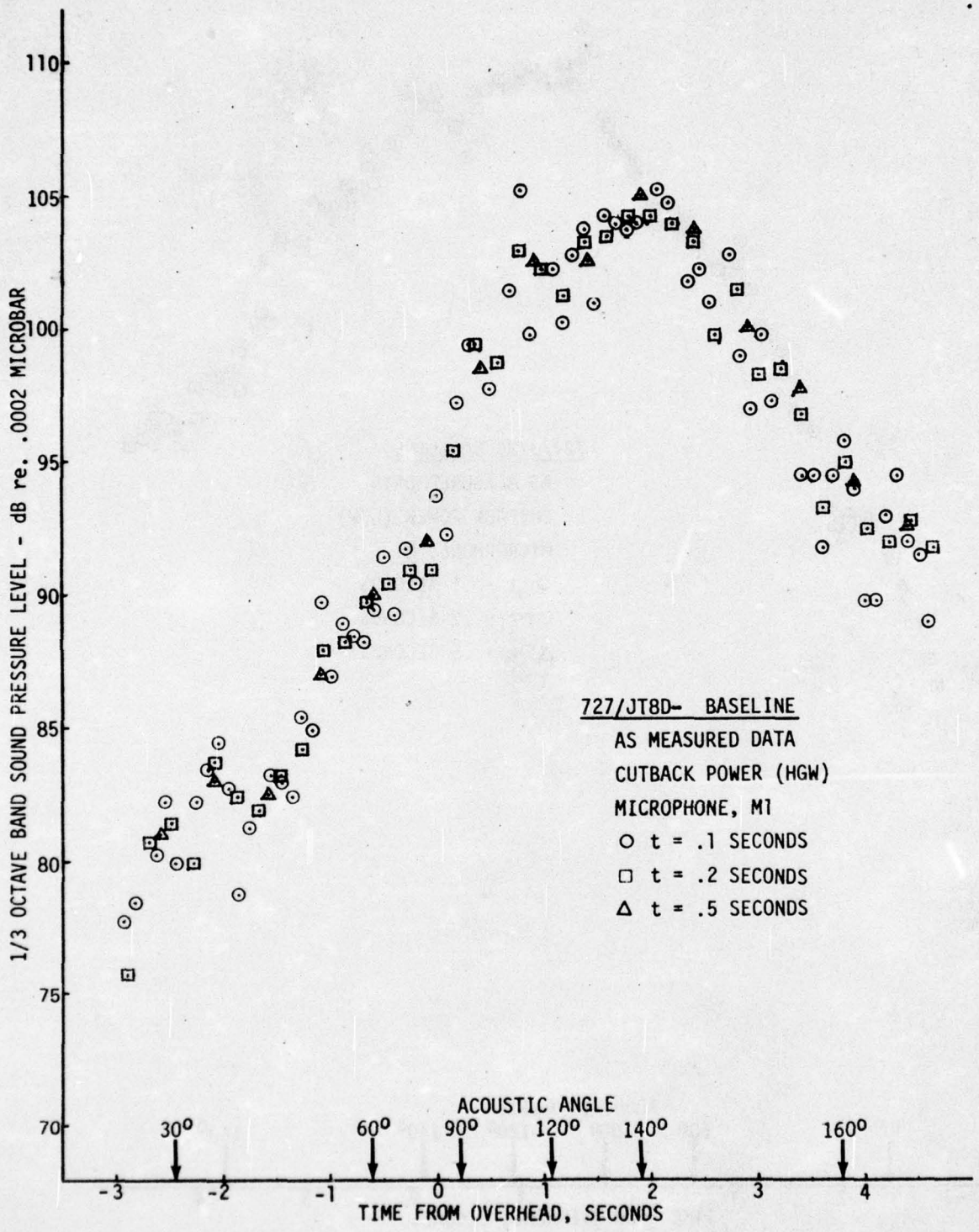


(c) INTEGRATION TIME EFFECT ON 200-Hz CENTER FREQUENCY

*Figure C-1.—(Continued)*

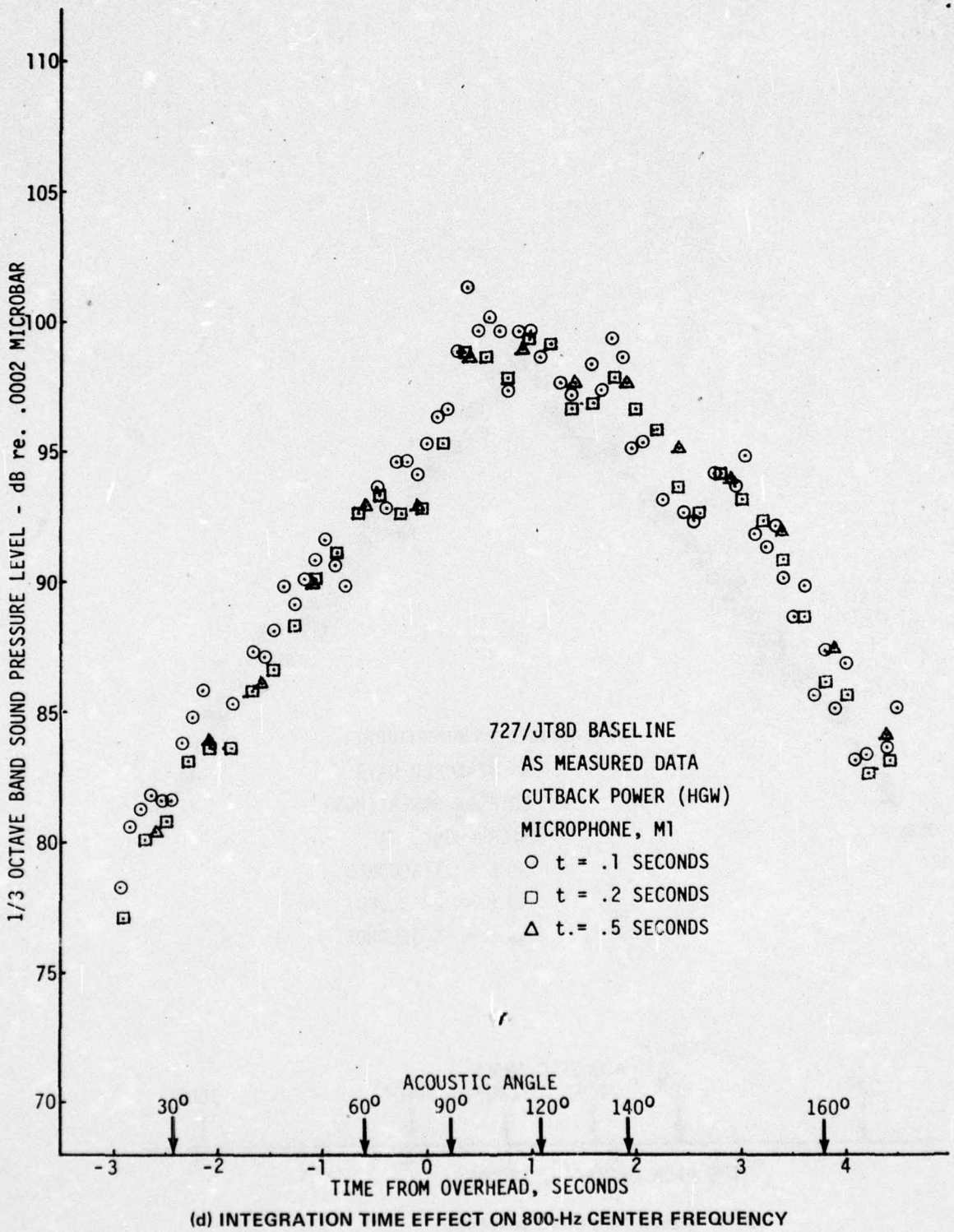


(d) INTEGRATION TIME EFFECT ON 800-Hz CENTER FREQUENCY

*Figure C-1.—(Concluded)*

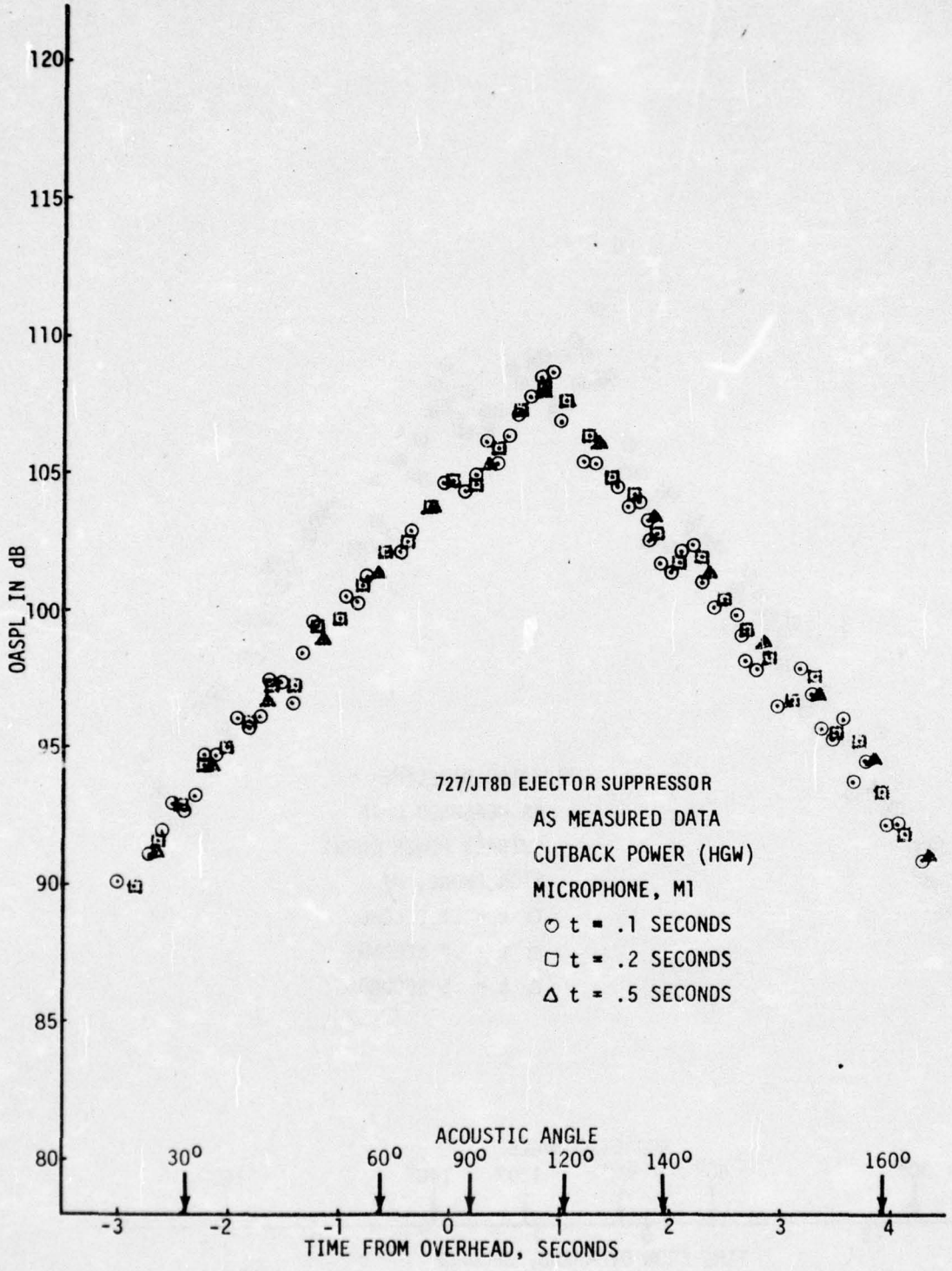


(a) Integration Time Effect on OASPL

*Figure C-2.—Ejector Suppressor Configuration Flight Noise Data Analysis*

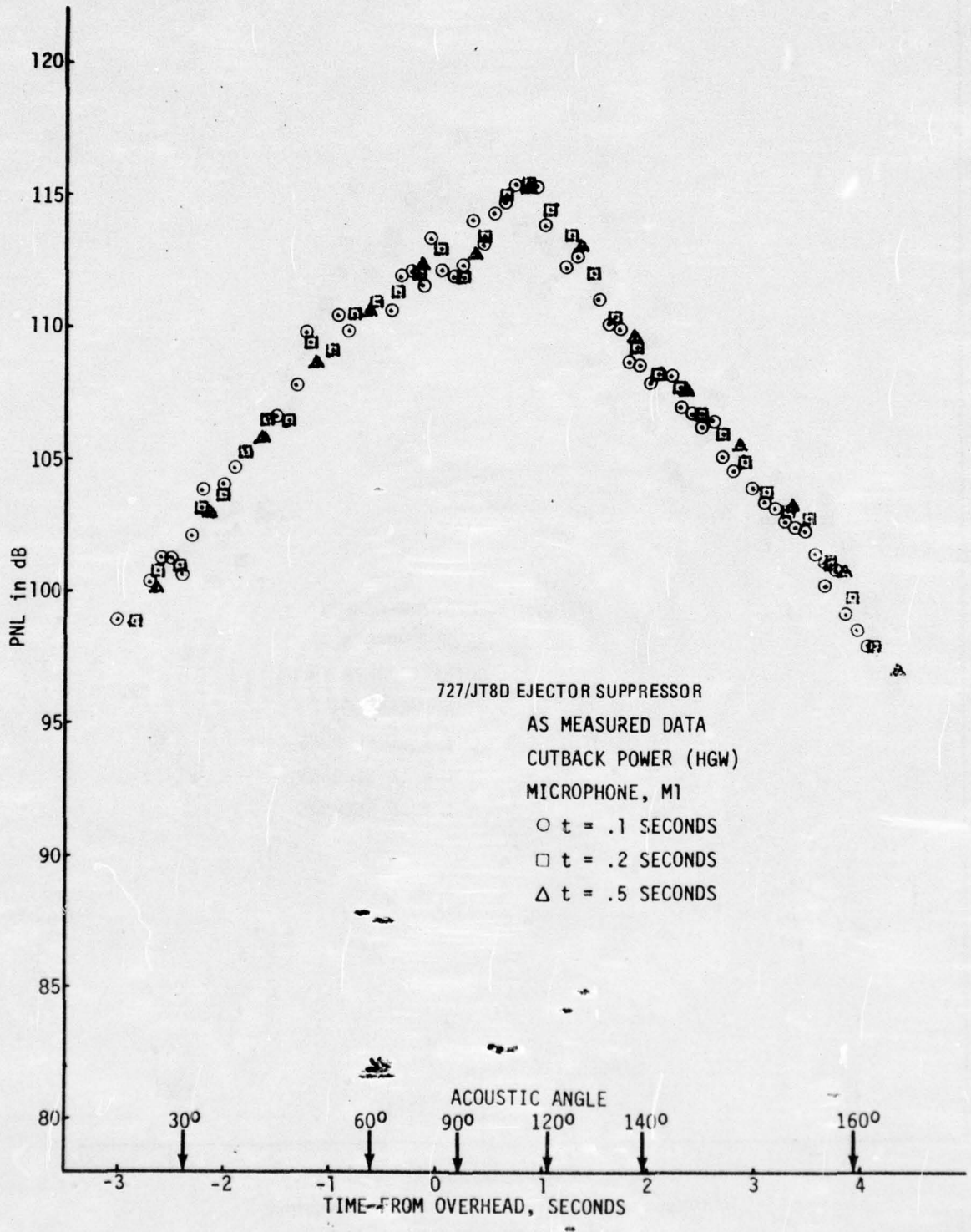


(b) Integration Time Effect on PNL

*Figure C-2.—(Continued)*

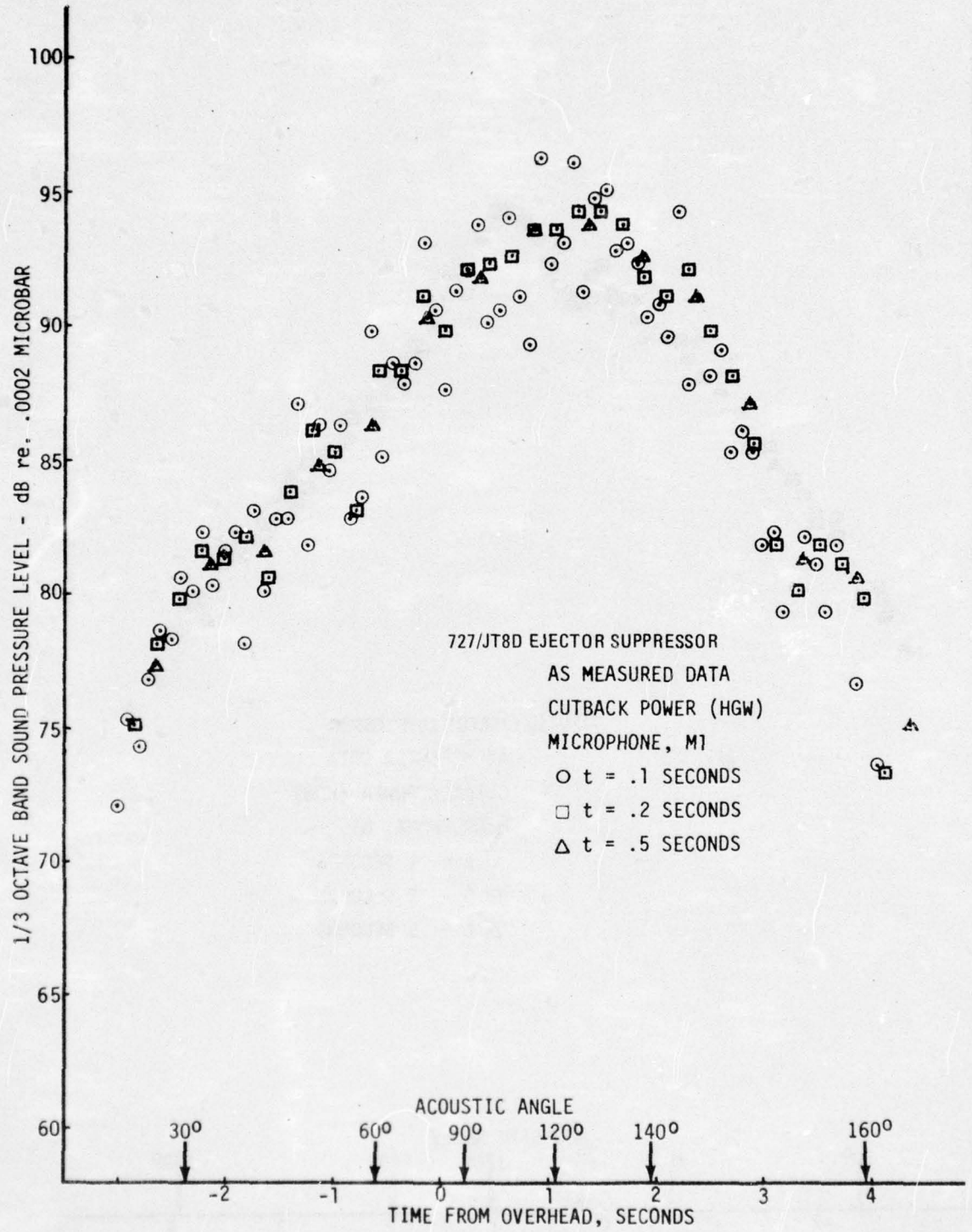


(c) Integration Time Effect on 200-Hz Center Frequency

*Figure C-2.—(Continued)*

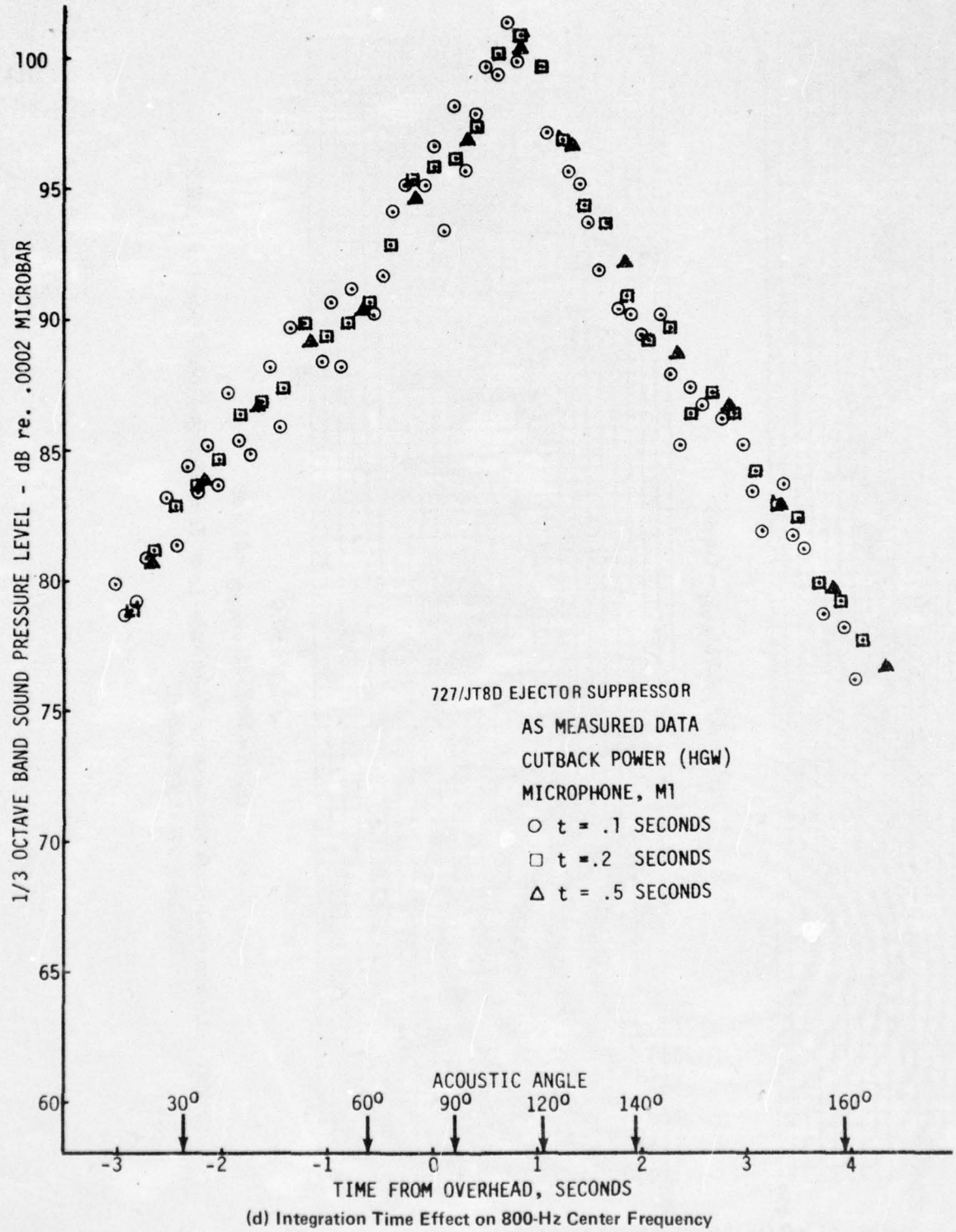


(d) Integration Time Effect on 800-Hz Center Frequency

*Figure C-2.—(Concluded)*

AD-A031 877 BOEING COMMERCIAL AIRPLANE CO SEATTLE WASH F/G 21/5
727/JT8D JET AND FAN NOISE FLIGHT EFFECTS STUDY.(U)
AUG 76 L F MUNOZ DOT-FA71WA-2637
UNCLASSIFIED D6-44145 FAA-RD-76-110 NL

4 OF 4
AD A031877

END
DATE FILMED
1-77

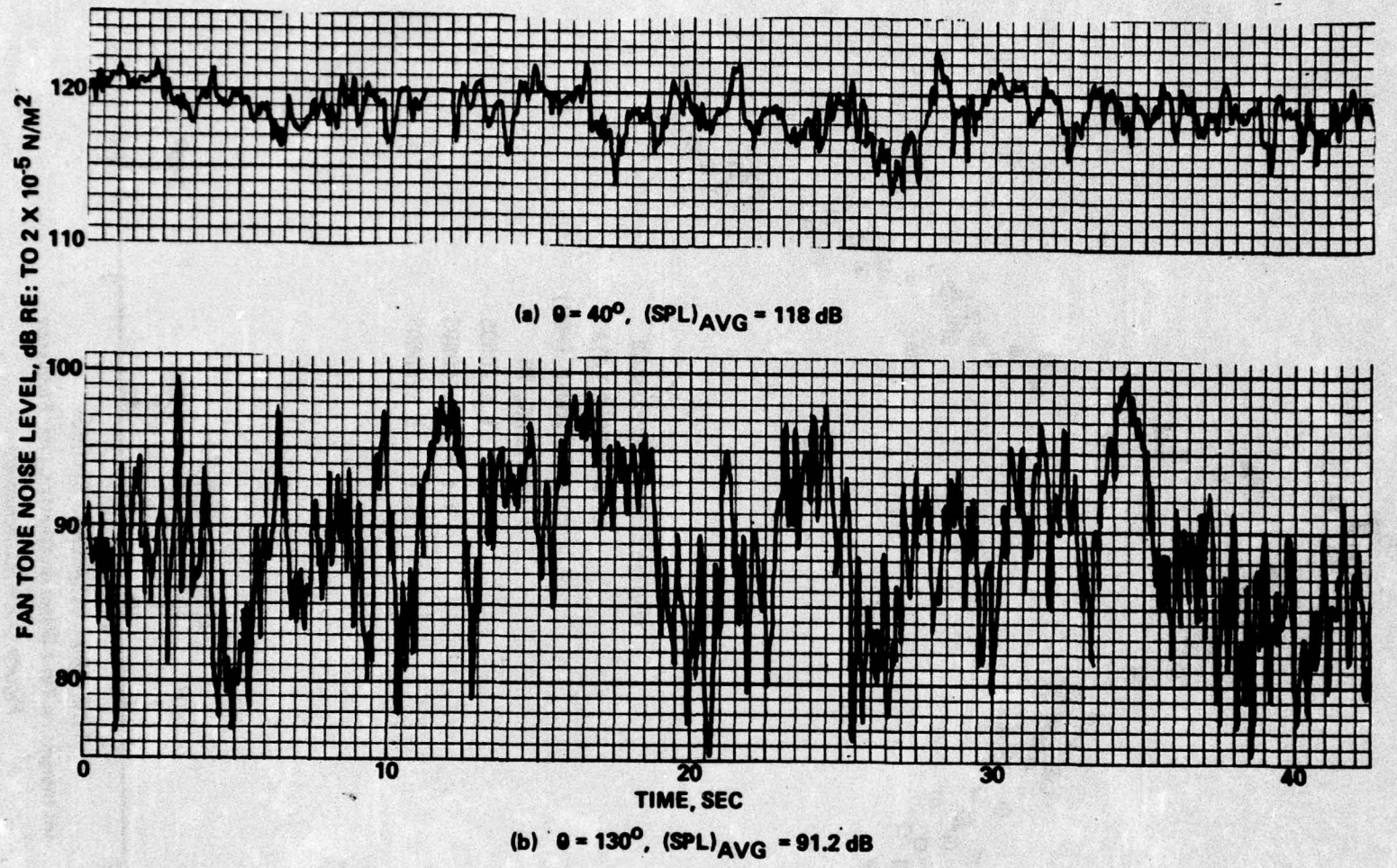


*Figure C-3.—Fan First-Stage Fundamental Tone Noise Level Time History (Tone Frequency = 2809 Hz, Run 24-5, JT8D-9 Baseline)*

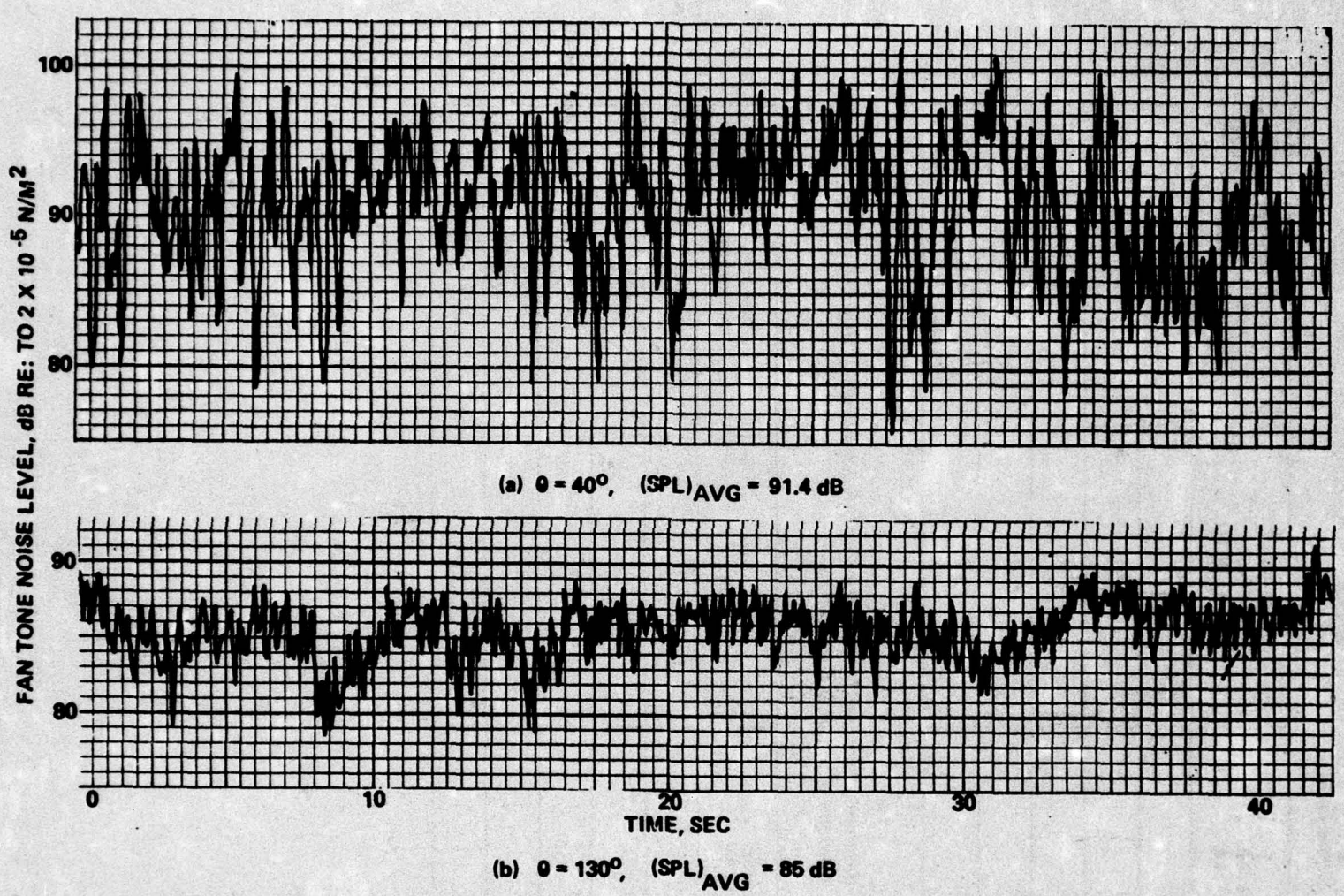


*Figure C-4.—Fan First-Stage Fundamental Tone Noise Level Time History (Tone Frequency = 2833 Hz, Run 49-5, JT8D-9 Ejector Suppressor Configuration)*

*Table C-1.—Flight Jet Noise, 90% Confidence Levels at 200-Hz Center Frequency, Single Sample*

| Integration time, T, sec | Degrees of freedom, n at 200 Hz | Random noise uncertainty; 90% confidence levels |
|---|---|---|
| 0.5 | 46 | +1.6<br>-1.5 |
| 0.4 | 36.8 | +1.8<br>-1.6 |
| 0.3 | 27.6 | +2.2<br>-1.9 |
| 0.2 | 18.4 | +2.7<br>-2.2 |
| 0.1 | 9.2 | +4.4<br>-2.7 |

*Table C-2.—Baseline Flight Jet Noise, 90% Confidence Levels at 200-Hz Center Frequency and at 90° Angle*

| Integration time, T, sec | Bias error, dB | Total 90% confidence levels |
|---|---|---|
| 0.5 | 1.4 | +0.2<br>-2.9 |
| 0.4 | 1.1 | +0.7<br>-2.7 |
| 0.3 | 0.9 | +1.3<br>-2.8 |
| 0.2 | 0.6 | +2.1<br>-2.8 |
| 0.1 | 0.3 | +4.1<br>-3.0 |

# REFERENCES


1. Tate, R. B., Ridley, H. G., and Lambert, J. A., *727 Noise Retrofit Feasibility. Volume I. Lower Goal Design, Fabrication, Ground and Flight Testing,* FAA-RD-72-40-I, March 1972.

2. Anderson, J. R., Ridley, H. G., and Smith, J. W., *727 Noise Retrofit Feasibility Program. Volume II. Upper Goal Design, Fabrication, and Ground Testing,* FAA-RD-72-40-II, November 1972.

3. Hiatt, D. L., McKaig, M. B., et al., *727 Noise Retrofit Feasibility Program. Volume III: Upper Goal Flight Testing and Program Summary,* FAA-RD-72-40-III, June 1973.

4. McKaig, M. B., "Use of Flush-Mounted Microphones To Acquire Free-Field Data," AIAA paper 74-92, January 1974.

5. *Standard Values of Atmospheric Absorption as a Function of Temperature and Humidity for Use in Evaluating Aircraft Flyover Noise,* ARP 866, August 1964.

6. Morse, P. M., and Ingard, K. O., *Theoretical Acoustics,* McGraw Hill, 1968

7. Lowson, M. V., "The Sound Field for Irregularities in Motion," Roc. Roy. Soc. (London), Vol. 286, Series A, 1965, pp 559-572.

8. Lu, H. Y., *Multiannular Axisymmetric Jet Flow Prediction Using a Two-Equation Model of Turbulence,* Boeing document D6-42606, September 1975.

9. Strout, F. G., *Flight Effects on Noise Generated by the JT8D-17 Engine in a Quiet Nacelle and a Conventional Nacelle as Measured in the NASA-Ames 40 X 80 Foot Wind Tunnel,* NASA CR-137797, January 1976.

10. "Prediction Procedure for Coaxial Jet Noise," Letter from M. J. T. Smith of Rolls-Royce to SAE Jet Noise Subcommittee, dated November 3, 1975.

11. Jaeck, C. L., *Empirical Jet Noise Predictions for Single and Dual Flow Jets With and Without Suppressor Nozzle: Volume 1. Single Flow Subsonic and Supersonic Jets,* Boeing document D6-42929-1, April 1976.

12. Savkar, S. D., and Edelfelt, I. H., *Radiation of Cylindrical Duct Acoustic Modes With Flow Mismatch,* NASA CR-132613, March 1975.

13. Dunn, D., et al., *Aircraft Configuration Noise Reduction, Vol, I,* FAA-RD-76-I, June 1976.

14. Harris, C. M. (Editor), *Handbook of Noise Control,* McGraw-Hill, 1957.

15. MacGregor, G. R., and Simcox, C. D., "Location of Acoustic Sources in Jet Flow by Means of Wall Isolation Technique," AIAA paper 73-1041, Seattle, Washington, 1973.

16. Grosche, F. R., Jones, J. H., and Wilhold, G. A., "Measurements of the Distribution of Sound Source Intensities in Turbulent Jets," AIAA paper 73-989, Seattle, Washington, 1973.

17. Jaeck, C. L., *Static and Wind Tunnel Near-Field/Far-Field Jet Noise Measurements from Model-Scale Single-Flow Baseline and Suppressor Nozzles. Vol. 1: Noise Source Locations and Extrapolation of Static Free-Field Jet Noise Data,* NASA CR-137913, September 1976.

18. Chun, K. S., Berman, C. H., and Cowan, S. J., *The Effects of Motion on Jet Exhaust Noise From Aircraft.* NASA CR-2701, June 1976.

19. Beranek, Leo L., *Noise and Vibration Control,* McGraw-Hill Co., 1971.

20. Bendat, J. S., and Piersol, A. G., *Random Data: Analysis and Measurement Procedures,* Wiley-Interscience, 1971.

21. Merriman, J. E., and Good, R. C., "Effect of Forward Motion on Fan Noise," AIAA paper 75-464, March 1975.

22 Roundhill, J. P., and Schaut, L. A., "Model and Full Scale Test Results Relating to Fan Noise In-Flight Effects," AIAA paper 75-465, March 1975.

GPO 908-552